Science and Technology of Nuclear Installations

Integral Test Facilities and Thermal–Hydraulic System Codes in Nuclear Safety Analysis

Guest Editors: Klaus Umminger and Alessandro Del Nevo

Integral Test Facilities and Thermal-Hydraulic System Codes in Nuclear Safety Analysis

Science and Technology of Nuclear Installations

Integral Test Facilities and Thermal-Hydraulic System Codes in Nuclear Safety Analysis

Guest Editors: Klaus Umminger and Alessandro Del Nevo

Editorial Board

Contents

Hindawi Publishing Corporation
Science and Technology of Nuclear Installations
Volume 2012, Article ID 826732, 3 pages
doi:10.1155/2012/826732

Editorial

Integral Test Facilities and Thermal-Hydraulic System Codes in Nuclear Safety Analysis

Klaus Umminger[1] and Alessandro Del Nevo[2]

[1] *AREVA NP GmbH, Paul-Gossen Strasse 100, 91052 Erlangen, Germany*
[2] *ENEA UTIS-TCI, C.R. Brasimone, 40032 Camugnano (Bo), Italy*

Correspondence should be addressed to Klaus Umminger, klaus.umminger@areva.com

Received 1 December 2011; Accepted 1 December 2011

A considerable amount of resources has been devoted at the international level during the past three decades for establishing and conducting experimental programmes in scaled-down integral test facilities (ITFs). These were aimed at solving open issues for current nuclear power plant (NPP), demonstrating the technical feasibility of innovative designs, and generating reference databases to support code development and assessment. Since the end of the nineties, the maintenance of the competences of experienced research teams as well as the creation of a new generation of professionals in the area of the nuclear safety is also a priority objective of operating research facilities and promoting experimental programmes.

Tens of ITFs have been built and operated so far all over the world. Few of them, related to existing water reactor technology, are currently in operation (e.g., ATLAS, PMK, PKL-III, ROSA/LSTF, INKA) or under refurbishment (e.g., PACTEL, PSB-VVER). Some others are constructed or under design and are focused on innovative water reactor concepts (e.g., MASLWR, SPES-3).

The experimental data from such facilities are applicable to full-scale nuclear plant conditions; if the test facilities and the initial and boundary conditions of experiments are properly scaled, for example, the scaling will not affect the evolution of physical processes important for the postulated accident scenario. This evaluation determines whether the data may be used in nuclear plant safety analyses of a postulated accident.

On the other side, the experimental data are fundamental for supporting the development and demonstrating the reliability of computer codes in simulating the behavior of an NPP during a postulated accident scenario: in general, this is a regulatory requirement. The reliance on computer codes, among the other things, is based on the reason that, very often, one cannot directly apply results from test facilities to a plant, including the "reference" plant of the facility design.

Applications of computer codes to accident analyses require the implicit assumptions that these codes have the capabilities to scale up phenomena and processes from test facilities to full-scale plant conditions. However, the different scale, in terms of geometry, characterizing any facility and a nuclear plant does not ensure a priori that a code, which is able to reproduce a generic transient in a scaled facility, is also able to calculate with the same accuracy the same transient in NPP.

The aforementioned topics involve a number of key activities, in which the research is taken up. This special issue documents the present scientific and technical status and recent advances in relation to the ITF, the experimental programmes, the issues connected with the code assessment, and the scaling issue, which is related both to the representativeness of the phenomena in the facilities as well as the applicability of the codes.

The special issue collects 17 papers, which are divided into 4 main groups, according to the following rationale: (1) Western PWR technology (8 papers), (2) Eastern PWR (or VVER) technology (4 papers), (3) BWR technology (3 papers), and (4) innovative, integral-type, water reactor concepts (2 papers).

The paper by K. Umminger et al. presents the *PKL-III* integral test facility and provides a survey of test objectives and programs carried out to date as well as plans for

future investigations. The authors point out important results achieved in improving the level of understanding of the PWRs system response under accident conditions as well as of the thermal-hydraulic phenomena relevant for the nuclear reactor safety and the importance for code validation.

Then, K. Y. Choi et al. describe *ATLAS* integral test facility, the main findings, and lessons learned obtained using the data of the past integral effect tests. The paper discusses also the future prospects of the application of ATLAS facility in the framework of national nuclear R&D program in Korea.

T. Takeda et al. discuss the analysis of a PWR loss of feedwater (LOFW) by means of a *ROSA/LSTF* experiment conducted for the OECD/NEA ROSA project and the application of RELAP5 code. The description of relevant phenomena of the transient and the results of assessment of the code are reported in the paper.

C. Addabbo and A. Annunziato illustrate the *LOBI* facility project. The paper provides a historical perspective and summarizes major achievements of the research programme which has represented an effective approach to international collaboration in the field of reactor safety research and development. Focus is also given to the issue of the management of research data.

The paper of J. Freixa and A. Manera addresses the issue of the validation process of system codes for the transient analyses of PWR. Five posttest analyses by TRACE code are presented. They are related to small and intermediate LOCA experiments executed in *ROSA/LSTF* integral test facility. The paper underlines the relevance of the validation activity in relation to the modeling of an NPP for safety analysis purposes.

A. Bousbia Salah and J. Vlassenbroeck present the analysis of three experimental tests performed in *PKL-III* integral test facility, executed in the framework of the OECD/NEA PKL-2 project. The tests are devoted to the study of the cool-down procedures operated after the reactor trip in order to bring the primary side temperature and pressure to the residual heat removal system (RHRS) operating conditions. The objective is to assess the impact of a chosen cool-down strategy upon the occurrence of natural circulation interruption (NCI) and the capabilities of CATHARE2 code in predicting such process. Relevance is given to the interaction between the key parameters governing the transient and the phenomena involved.

F. Reventós et al. analyze the results of three posttest calculations of the *LOBI* integral test facility experiments. The selected experiments are LOCA scenarios of different break sizes and with different availability of safety injection components. The objective of the analysis is to improve the knowledge of the phenomena reproduced in the facility in order to use them for nodalization qualification purposes of nuclear power plants or for establishing accuracy databases for uncertainty methodologies.

The last paper of the Western PWR technology group by A. Prošek discusses the assessment of how the accuracy of a simulation depends on the code version used. The code selected is RELAP5, widely used all over the world for safety analysis of nuclear power plants. The study is based on an experimental test executed in the *BETHSY* integral test facility, identified as 9.1b, which is the OECD International Standard Problem no. 27.

A. Del Nevo et al. discuss a benchmark activity among different thermal-hydraulic system codes (i.e., ATHLET, RELAP5-3D, KORSAR, and TECH-M) and institutions performed on the basis of the *PSB-VVER* integral test facility data. The activity is preformed in the framework of the OECD/NEA PSB-VVER project. The objective is to collect, analyze, and document the numerical activity (pre- and posttest) performed by the participants, describing the performances of the code simulations and their capabilities to reproduce the relevant thermal-hydraulic phenomena observed in the experiment.

G. Ézsöl et al. illustrate the *PMK-2* facility, which was the first integral-type facility for VVERs. The paper gives comprehensive information on the design features of PMK-2 facility with a special respect to the representativeness of phenomena, the experiments performed, and the results of the validation of ATHLET, CATHARE2, and RELAP5 codes. It discusses also the safety significance of the PMK-2 projects.

The paper by V. Kouhia et al. describes the construction and the experimental research activities of two integral test facilities: the former, *PACTEL*, devoted to the simulation of VVER-440 NPP and the latter, *PWR-PACTEL*, for research activities associated with the EPR™ reactor. The OECD International Standard Problem no. 33 and the PWR-PACTEL benchmark launched in 2010 are presented as sample activities.

V. Blinkov et al. present three LB LOCA tests, two MSLB tests, and one SB LOCA test carried out in the integral test facility *BC V-213*, which represents the bubble condenser system of Kola NPP (Unit 3). The paper provides information about the application of ATHLET code for supporting the design of the experiments and, then, describes in detail the validation activity related to the COCOSYS code.

The paper of D. Paladino and J. Dreier is focused on the multipurpose facility *PANDA*. The applications cover integral containment response tests, component tests, primary system tests, and separate effect tests. The paper provides an overview of the research programs performed in relation to BWR containment systems and those planned for PWR containment systems.

S. Leyer and M. Wich describe the *INKA* (integral test facility Karlstein) test facility, which was designed and constructed to test and demonstrate the performance of the passive safety systems of KERENA, the new AREVA boiling water reactor (BWR) design. The authors discuss the facility features and capabilities, the instrumentation systems, and the experimental program. INKA is within the KERENA development program devoted to single component/system tests of the emergency condenser, the containment cooling condenser, and the passive core flooding system. The paper outlines the integral system tests, which will be performed to simulate transients and LOCA (loss of coolant accident) scenarios. These experiments will involve the testing of the KERENA Passive Pressure Pulse Transmitter System.

S. Racca and T. Kozlowski present a validation activity carried out with TRACE code related to the simulation of spray cooling injection in a BWR reactor. The data, acquired

by experiments of the Swedish *GÖTA* test facility, are compared with the results derived from the code modeling. Focus is given to the countercurrent flow limiting (CCFL) phenomenon. The activity includes the application of the propagation of input errors (PIEs) method, which is used to perform the uncertainty analysis and to identify the input parameters having more influence on the figure of merit selected (in this case the peak cladding temperature).

The first paper of the innovative (integral-type) water reactor concepts group by F. Mascari et al. describes the integral test facility *MASLWR*. The multiapplication small light-water reactor (MASLWR) is the scaled-down model of a small modular PWR, relying on natural circulation during both normal and accident conditions. The paper includes a review of the main characteristics of the facility and summarizes the tests already executed and the related code validation activity. Finally, the reader can find information on the IAEA International Coordinated Research Program, currently ongoing, based on the MASLWR experimental tests.

The paper of A. Achilli et al. presents the *SPES-3* integral test facility. It is designed by SIET to simulate the W-IRIS reactor concept under normal and accident conditions. The authors give an overview of the design of the test facility underlining the uses of RELAP5 and RELAP5/GOTHIC coupled codes for the achievement of the final scaling concepts and layout of the facility.

In conclusion, the scientific and technical contributions from the authors provide the readers with useful information related to 14 experimental facilities and cover a broad spectrum of the recent past and current activities dedicated to this special issue.

Acknowledgments

The guest editors acknowledge all authors who have submitted papers to this special issue. Special thanks are due to our colleagues for the kind collaboration in reviewing these papers.

Klaus Umminger
Alessandro Del Nevo

Hindawi Publishing Corporation
Science and Technology of Nuclear Installations
Volume 2012, Article ID 891056, 16 pages
doi:10.1155/2012/891056

Review Article

Integral Test Facility PKL: Experimental PWR Accident Investigation

Klaus Umminger, Lars Dennhardt, Simon Schollenberger, and Bernhard Schoen

Technical Center, AREVA NP GmbH, Erlangen, Germany

Correspondence should be addressed to Klaus Umminger, klaus.umminger@areva.com

Received 15 August 2011; Accepted 16 November 2011

Academic Editor: Alessandro Del Nevo

Investigations of the thermal-hydraulic behavior of pressurized water reactors under accident conditions have been carried out in the PKL test facility at AREVA NP in Erlangen, Germany for many years. The PKL facility models the entire primary side and significant parts of the secondary side of a pressurized water reactor (PWR) at a height scale of 1 : 1. Volumes, power ratings and mass flows are scaled with a ratio of 1 : 145. The experimental facility consists of 4 primary loops with circulation pumps and steam generators (SGs) arranged symmetrically around the reactor pressure vessel (RPV). The investigations carried out encompass a very broad spectrum from accident scenario simulations with large, medium, and small breaks, over the investigation of shutdown procedures after a wide variety of accidents, to the systematic investigation of complex thermal-hydraulic phenomena. This paper presents a survey of test objectives and programs carried out to date. It also describes the test facility in its present state. Some important results obtained over the years with focus on investigations carried out since the beginning of the international cooperation are exemplarily discussed.

1. Introduction

Complex thermal-hydraulic system codes are used for the analysis of accident sequences in pressurized water reactors. The necessity to verify the knowledge gained using such codes by experiments in suitable test facilities resulted in the construction of the large-scale test facility PKL (from the German abbreviation for Primärkreislauf) modeling a 1300 MW class PWR.

The PKL test facility has been in operation since 1977; however, in the meantime, the objectives of the experiments performed at the PKL test facility have changed considerably with the result that the test rig has been refitted many times to suit the additional and ongoing tasks and also to match latest developments, for example, in the fields of measuring instrumentation and data processing. Since the commencement of experiments at the PKL test facility, the various phases of the experiments have always reflected and given priority to current safety issues.

The primary objective of all PKL experiments has been and remains the experimental investigation of thermal-hydraulic processes in PWRs with respect to the response of the overall system. To some extent the investigations also include the behavior of individual components and subsystems during the simulation of operational transients and accidents. The tests performed to date (in total more than 150 integral experiments) have altogether contributed to a better understanding of the sometimes highly complex thermal-hydraulic processes involved in various accident scenarios and to a better assessment of the countermeasures implemented for accident control. In addition, they have supplied valuable information regarding safety margins available in the plants. The test results have also found concrete application in the validation and further development of thermal hydraulic computer codes, the so-called system codes.

2. PKL Test Programs

Reactor safety research in the seventies centered above all on the theoretical and experimental analysis of large-break loss-of-coolant accidents (LOCAs), focusing on verifying the effectiveness of the emergency core cooling system

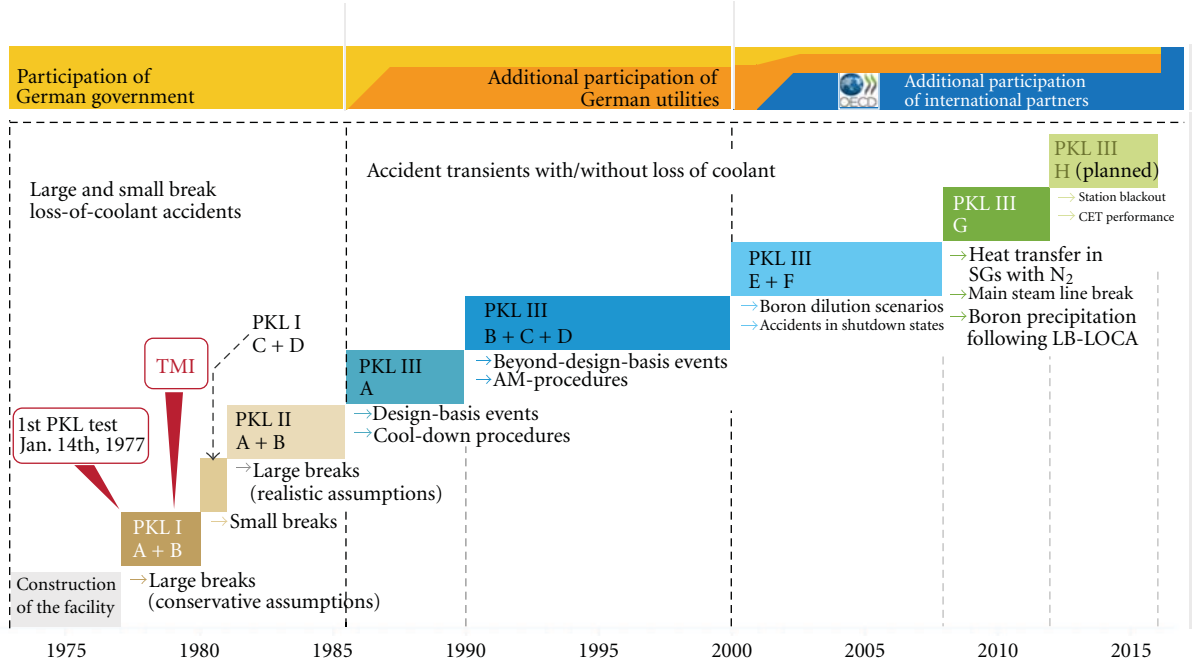

Figure 1: PKL tests programs.

(ECCS) required for controlling such events. Based on this original objective, the PKL test facility was constructed at Siemens/KWU (now AREVA NP) with the support of the German Ministry for Research and Technology and placed in service in 1977 (Figure 1).

The large-break LOCA experiments were interrupted in 1979 in the wake of the accident at three-mile island unit 2 (TMI-2) for the performance of experiments at the PKL test facility designed to contribute to gaining information as quickly as possible on issues raised by this event. Consequently, only a short time after the accident, it was possible to simulate small-break (SB) LOCA event sequences, which also included the TMI-2 scenario, at the PKL test facility. The investigations focused on demonstrating the safety margins of the operating units through the experimental verification of the effectiveness of the engineered safety features in the event of large- and small-break LOCAs were covered within the test programs PKL I and II [1, 2].

The subject of the subsequent PKL III program, started in 1986, has been the investigation of the so-called accident transients with and without LOCAs. While the first test series within PKL III covered design-basis accidents and cool-down procedures detailed in the operating manual, the main interest was then focused on beyond-design-basis accidents and the experimental verification of accident-management procedures [3]. Typical topics of investigation studied within the test series PKL III A to PKL III D were

(i) cool-down procedures with and without reactor coolant pumps under symmetric and asymmetric boundary conditions (e.g., one or more SGs isolated on the secondary);

(ii) cool-down procedures following small-break LOCAs or steam generator (SG) tube ruptures, partly in combination with additional system failures;

(iii) accident management procedures (e.g., secondary or primary side bleed-and-feed) following total loss of feed water or multiple failure situations;

(iv) systematic investigations within parametric studies such as

(1) single- and two-phase flow, reflux condensation, counter current flow limitation,

(2) influence of noncondensable gas on heat removal from the primary to the secondary.

Since 2001, the PKL project has been continued in the course of an international project initiated by the OECD. The major topics covered by the experiments between 2001 and 2007 were

(i) boron dilution events following SB-LOCA,

(ii) loss of residual heat removal under shut-down conditions.

The current test program PKL III G which will last until end of 2011, additionally addresses the following main topics.

(i) Subcooling transients after a break in the main steam line (with supplementary tests in the ROCOM test facility for mixing in the RPV downcomer and in the lower plenum).

(ii) Cool-down procedures with SGs isolated and emptied on the secondary side.

(iii) Boron enrichment and precipitation in the core after primary-side large-break accidents.

(iv) Systematic investigations of the heat transfer in the SGs in the presence of noncondensable gas (with complementary tests in the Hungarian PMK test facility for horizontal SGs).

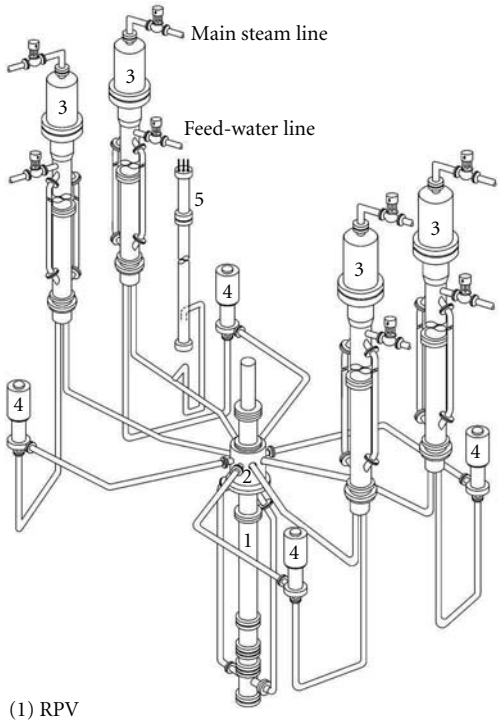

Figure 2: PKL test facility.

(v) Systematic study on heat transfer in the SG under reflux condenser conditions (influence of secondary side parameters).

(vi) Small break LOCA with failure of safety injection pumps and secondary-side depressurization as accident management measure (counterpart test with ROSA/LSTF).

(vii) Formation of RPV upper head void during cooldown under natural circulation (NC) conditions in emergency power mode.

3. Description of the Test Facility

The layout of the PKL-III facility (Figure 2, Table 1) is based on the "Vorkonvoi" type (4-Loop, 1300 MWe) of KWU pressurized water reactor, with the Philippsburg 2 nuclear power plant serving as the reference plant. The entire primary side and the most significant components of the secondary side (excluding turbines and condenser), including the appropriate system technology, are represented. Because the essential construction principles of the western types of PWRs are similar, it is possible to make statements concerning the behavior of other companies' plants. In any case, the analysis of plant-specific reactor transients must then be made with the help of computer codes.

Following the scaling concept, all geodetic heights are represented in a 1 : 1 ratio. The entire volume of the primary side and, as far as possible, the partition of the individual

Table 1: Scaling and operating parameters.

Elevations	1 : 1
Volumes	1 : 145
Max. core power	2.5 MW → 10%
Max. pressures	
Primary	45 bar
Secondary	60 bar
Flow rates	35 kg/s (RCPs operating)
Temperatures	
Primary fluid	300°C
Sec. fluid	300°C
Max. rod cladding	750°C

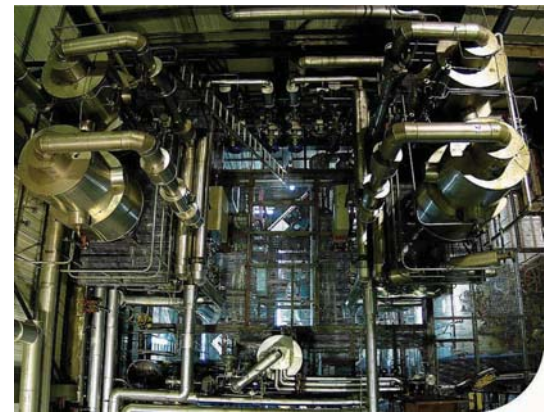

Figure 3: PKL steam generators (top view).

volumes corresponds to a scaling factor of 1 : 145, which corresponds to a hydraulic diameter reduction of 1 : 12. For some components, the exact volume scaling was not applied in order to simulate certain thermal-hydraulic phenomena, for example, countercurrent flow limitation in the hot legs. This allowed dimensionless numbers (e.g., the Froud number) to be maintained in the correct parameter range. The single-phase pressure losses, correspond to a large extent to the values in a PWR. Together with the thermal losses they have been determined in detail for every component and section for the entire load and temperature ranges (reactor coolant pump (RCP) operation and NC conditions under cold and hot conditions).

The core is modeled by a bundle of 314 electrically heated rods with a total power of 2.5 MW corresponding to 10% of the scaled nominal power. The core geometry is, like the SG geometry, constructed as an "actual section"; that is, the individual heated rods and U-tubes have the actual geometry, but the number of heated rods in the core and the number of U-tubes in the SG are reduced by the scaling factor 1 : 145, (volume and power scaling) as compared to the original plant. The PKL heater rod bundle has a uniform axial power profile, and the heater rods are arranged in three concentric zones (heated independently of one other) which enables radial power profiles across the test bundle to be simulated. The four fully scaled SGs (see top view in Figure 3) are

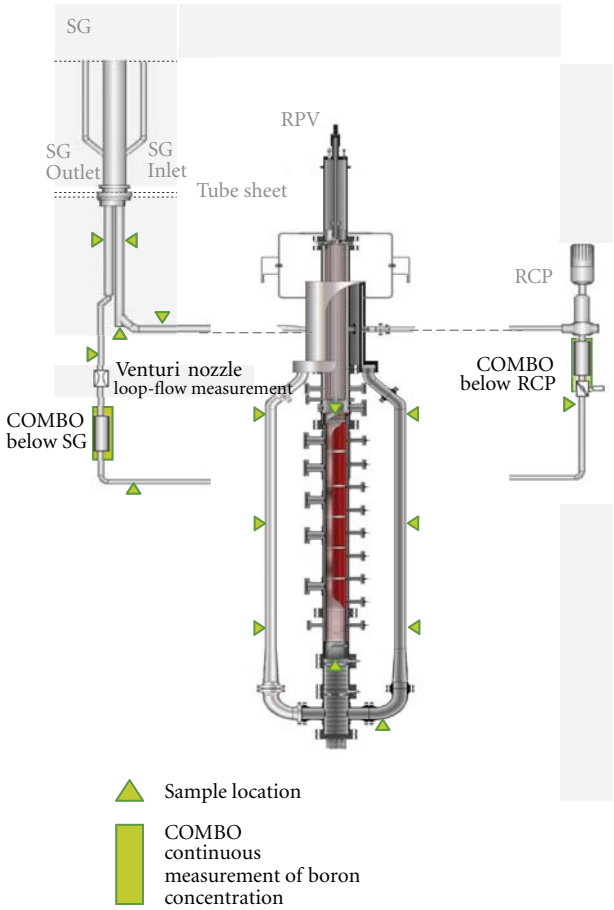

Figure 4: Boron concentration and loop-flow measurements.

equipped with prototypical tubing (diameter, wall thickness, differing lengths) and tube sheet. The RPV downcomer is modeled as an annulus in the upper region and continues as two stand pipes connected to the lower plenum. This configuration permits a symmetrical connection of the 4 cold legs to the RPV, reliable determination of flow rates, preserves the frictional pressure losses, and does not unacceptably distort the volume/surface ratio. This is of importance with respect of the removal of stored heat from the walls during cool down. In general, the structure masses resulting from the limitation of pressure to 45 bar return the relation between heat capacities of structures and coolant masses to be in good accordance with the reference plant.

The symmetrical arrangement of the 4 loops around the RPV also allows investigating the individual effects of multiple system failures.

Experiments on the behavior of a 3-loop (2-loop) plant can also be conducted by simply isolating one (two) loop(s). Each of the primary side loops contains active RCPs, which are equipped with speed controllers to enable any pump characteristics to be simulated. Preserving the frictional pressure losses in the SGs and in the core region, the integral pressure loss for the entire primary system is also very similar to that of the actual plant.

PKL is also equipped with all relevant engineered safety and operational systems on the primary and secondary side. On the primary side, four independent high- and low-pressure safety injection systems connected to both, the hot and cold legs, the residual heat removal system, 8 accumulators, the pressurizer pressure control system, and the chemical and volume control system are simulated. On the secondary side the feed, water system, the emergency feed water system and the main steam lines with all control features of the original systems are modeled. For the realistic representation of the events in secondary-side bleed-and-feed operations, the complex geometry of the feed water system (all heights 1 : 1, volumes 1 : 145, pressure losses 1 : 1) was modeled with the possibility of setting the corresponding temperature distributions. All these features allow the simulation of a wide spectrum of accident scenarios, the interaction between the primary and secondary side in combination with various safety and operational systems.

The maximum operating pressure of the PKL facility is 45 bar on the primary side and 60 bar on the secondary side. This allows the simulation over a wide temperature range. However, certain constraints are placed on the application of insights gained from the test results to a PWR plant because of the primary pressure limit and because of the geometric scaling of the test facility. With respect to limitation of primary pressure, the scaling of the experiments is subject to three categories.

The first category of experiments provides results on special physical phenomena such as countercurrent flow limitation or the influence of nitrogen on accidents from cold shut-down conditions that are expected to occur at pressures below 50 bar.

Other experiments "enter" a PWR transient at a pressure level of 45 bar. The conditions at the start of testing are set up by the use of code calculation for the PWR, an example being SB-LOCAs where the important phenomena occur at pressures below 50 bar.

The third category covers scenarios where phenomena occurring at high pressures can be simulated at pressures below 50 bar with the results being extrapolated to the original pressures with the help of codes or by comparison with results from full-pressure test facilities. A typical example for the latter is the initial phase of bleed-and-feed experiments.

A scaling study [4] showed that the thermohydraulic properties and certain phenomena (density, single- and two-phase heat transfer) do not change significantly between 40 and 80 bar. So most of the phenomena observed for pressures under 50 bar are in the first step qualitatively applicable to full scale PWR. In a second step, a quantitative application of experimental results to full-scale PWRs is always achieved by the use of further analyses with thermohydraulic codes. To what extent the test results from other test facilities (e.g., LSTF and BETHSY, pressure 1 : 1, or UPTF, geometry 1 : 1) [5, 6] or results from computer programs (e.g., ATHLET, CATHARE or RELAP) must be included is considered for individual cases.

With approximately 1500 measurement points (see Table 2), the PKL facility is comprehensively instrumented.

Figure 5: PKL-control room.

Table 2: Measurement installation in PKL III (selection).

	RPV	SG	Loops	Interfacing systems	PRZ	Total
Mass flow	1		14	64		79
Differential pressure	9	18	20	8	3	58
Fill level	12	48	40	47	5	152
Mass				3		3
Density	10	2		2	9	23
Absolute pressure	7	7	8	44	2	68
Temperature	286	345	182	158	29	1000
Boron concentration	16	4	32		1	53
Power measurement	5	4	6	5	2	22
Valve position [%]				68		68
Σ						**1526**

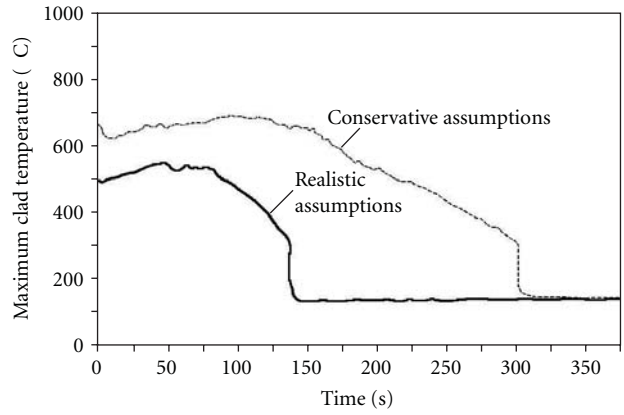

Figure 6: PKL test results for large-break LOCA.

This allows detailed analysis and interpretation of the phenomena that develop in the course of the tests. Besides conventional measurements (temperature, pressure, etc.), two-phase flow measurements are also used. In addition, special measurement devices for the detection of boron concentration have been installed. Figure 4 exemplarily depicts the loop mass flows and boron concentration measurement locations.

All measurement data are recorded by a data acquisition system with a maximum sampling rate of 25 Hz. In addition, all measurement signals can also be displayed and observed online during the test in the PKL control room. This includes the use of process visualization systems (Figure 5).

With regard to system technology and system design layout, the test facility is constantly being modified and expanded according to new project definitions and investigational emphases, and the applied measurement techniques are continually being updated to the state-of-the-art technology.

4. PKL Test Results

The number of integral experiments performed at the PKL test facility now totals more than 150. Consequently, only a representative sample of the test results and knowledge derived from them can be presented in summary for the various main areas of focus.

4.1. Large-Break LOCA. The hypothetical accident involving a large break in the reactor coolant system (RCS) piping (up to and including a complete guillotine break of a coolant line) is characterized by a large mass flow at the break and therefore by a rapid depressurization and loss of fluid from the RCS. The loss of cooling subsequently causes the clad temperatures to rise at first. In the so-called reflood and refill experiments which started from initial conditions with the system depressurized and the core heated up and with initiation of low-pressure safety injection, it was possible to obtain empirical verification of the ECCS concepts. In so doing, it was demonstrated that the restoration of core cooling is assured even with degraded operability of the ECCS (conservative assumptions). Further experiments which included the end of blowdown phase and which were performed under more realistic conditions, in particular as regards the operability of the ECCS and consideration of injection of the accumulator inventory, yielded even better results in relation to possible core degradation (lower clad temperatures and shorter time at elevated temperatures [1]). Figure 6 contrasts the results of two experiments performed under such conservative and realistic conditions.

4.2. Small-Break LOCA. Accidents involving small breaks in the RCS piping are characterized by the fact that a second energy sink such as the SG secondary side is needed for decay heat removal in addition to that provided by leakage makeup by the safety injection systems. First fundamental studies relating to small-break LOCAs performed shortly after the TMI-2 accident demonstrated that decay heat removal in PWRs with U-tube steam generators is assured even with a greatly reduced coolant inventory as long as the coolant level

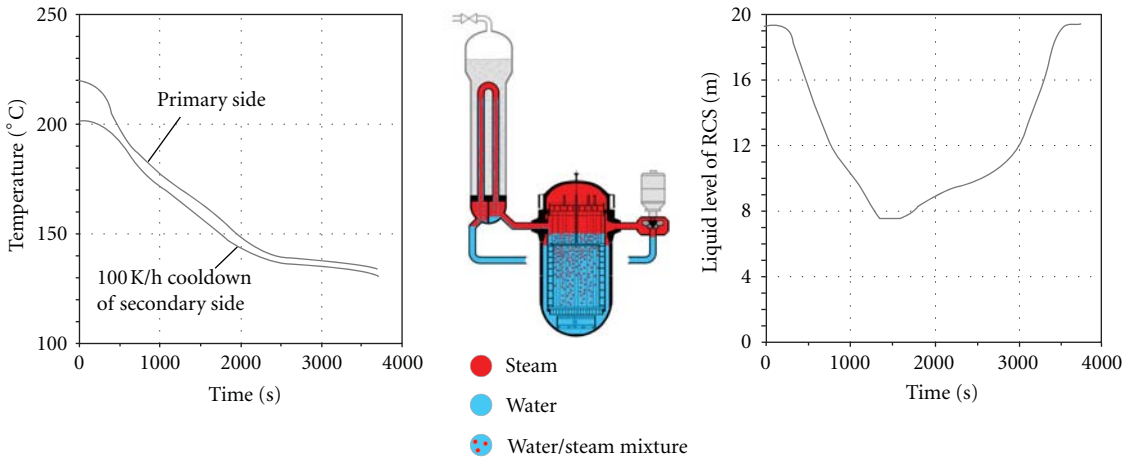

Small break in cold leg (0,02A), 2 safety injection pumps in cold leg

Figure 7: PKL test results for small-break LOCA.

in the reactor pressure vessel is at least as high as the top of the core. In this case, natural circulation breaks down and heat transport is provided by steam flow from the core to the SGs where the steam condenses and flows back to the core (reflux condenser mode). Furthermore, empirical verification was obtained that automatic plant cooldown is an effective means of quickly bringing the unit to a safe condition [2]. A typical result of a small-break LOCA experiment (2 of 4 high pressure safety injection pumps assumed operable) is shown in Figure 7 by the time histories for RCS and secondary-side pressure with the plant in the reflux condenser mode. In this case, the core is always filled with water or a water/steam mixture so that decay heat removal is assured at all times.

More extensive studies on small-break LOCA were performed in the course of the PKL III program considering additional failures and system malfunctions (e.g., loss of SGs as an energy sink, degraded heat transfer in the SGs due to the accumulation of inert gas in the SG tubes, reduced operability of the ECCS as far as the highly improbable situation of loss of all safety injection pumps, and simultaneous loss of automatic cool down). These showed that, even under these extreme conditions, it is possible to bring the plant safely to residual heat removal entry conditions by cooldown implementing the procedures prescribed in the operating manual or through beyond-design-basis accident management measures initiated by the operator. They, therefore, demonstrated the enormous safety reserves of PWR units. Investigation addressing boron dilution events during SB-LOCAs has been performed within the test program PKL III E and F (see below).

4.3. Cool-Down Procedures after Non-LOCA Events. In particular, cool-down procedures (50 K/h) were conducted with and without RCPs, in each case not combined with LOCA events, in order to confirm the operating manual procedures. Proceeding from a baseline test which modeled operational cooldown with 2 RCPs and 4 SGs, further tests were performed in which restricted operability of the circulation pumps (e.g., only one RCP) and emergency power conditions (no RCPs operable) and only partial operability of the SGs (e.g., only 3 or 1 SG operable for 50 K/h cool down) were assumed. Across the board, the test results confirmed the feasibility of the procedures prescribed in the operating manual to achieve a safe, depressurized condition with decay heat removal by the residual heat removal system [7]. The formation of steam bubbles in the RCS (e.g., in the RPV closure head) does not degrade the prescribed cool-down procedures.

Contrary to the original assumption that the closure head bubble could extend into the reactor coolant piping and give rise to violent condensation mechanisms due to contact with subcooled water, the maximum extent of the closure head bubble always remains restricted to an area significantly above the reactor coolant piping, even under natural circulation conditions.

On restarting of the RCPs after auxiliary power recovery (offsite power supply operable), condensation and mixing processes in the presence of a steam bubble in the RPV closure head are so slow that abrupt and undesired level changes do not occur in the pressurizer, and continued controlled cool down remains assured.

The formation of a closure head bubble during cool down under emergency power conditions and condensation on restarting of the RCPs are shown by way of example in Figure 8. A further test recently performed (within the current test program PKL III G) on the formation and expansion of the upper head steam bubble under natural circulation conditions—applying however a different cool down procedure—confirmed these results and the dominating phenomena.

4.4. Beyond-Design-Basis Accident Management Measures. Emergency procedures have been devised to avert core melt processes in the event of beyond-design-basis events such

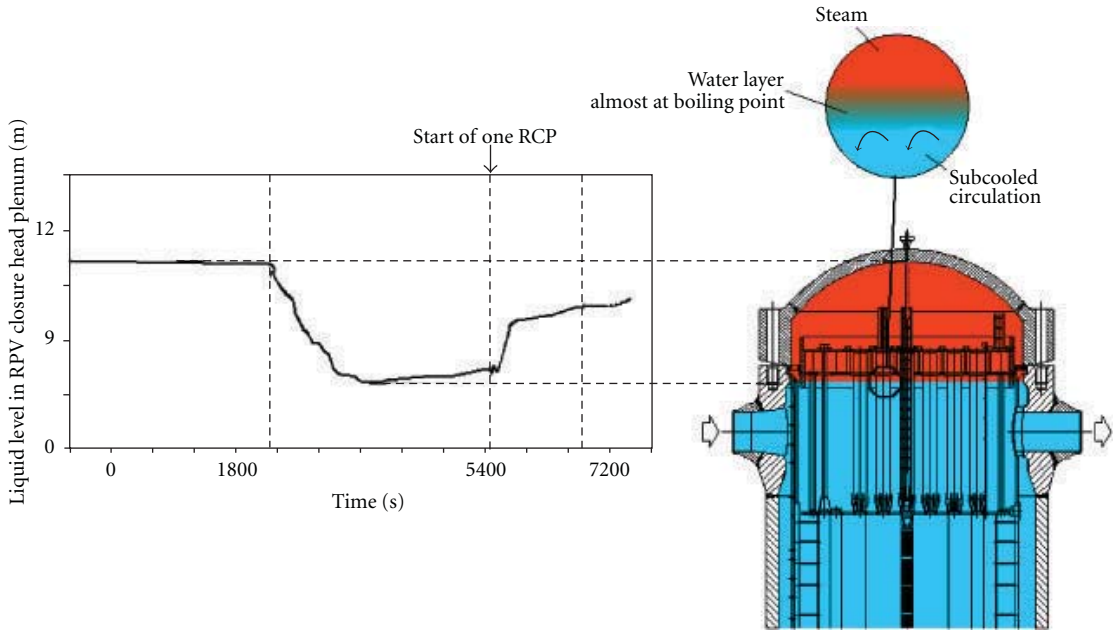

Figure 8: PKL III—Cooldown in emergency power mode with restarting of one RCP.

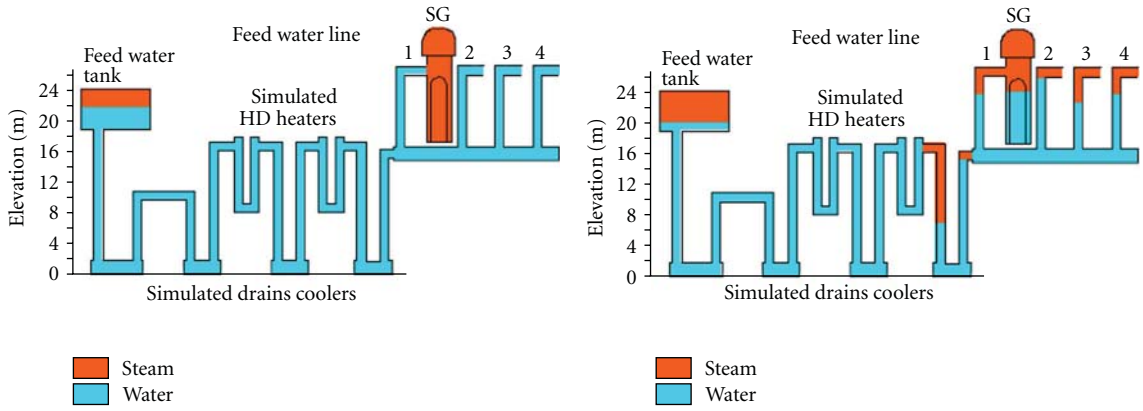

(a) Before secondary-side bleed

(b) After "passive" steam generator feed

Figure 9: Test results for secondary-side bleed and feed.

as complete loss of feed water supply (loss of secondary-side heat sink), station blackout (additional loss of all ECCS on the primary side), or even multiple failure situations (e.g., small-break LOCA or steam generator tube rupture combined with additional system failures). The investigation of emergency procedures such as primary-side or secondary-side bleed and feed was one of the focal points of the PKL III (A-D) program of experiments. For example, a series of experiments was conducted for the systematic investigation of the effectiveness of secondary-side bleed and feed on loss of feed water supply (loss of all feed water pumps incl. emergency feed water pumps) and on station blackout by variation of system conditions and the time of initiation of bleed [8].

All the experiments on secondary-side bleed and feed clearly confirmed the effectiveness of this emergency procedure. The pressure reduction on the secondary side induces a passive injection of water from the feed water piping as a result of steam flashing and hence a rapid, temporary restoration of primary-to-secondary heat removal. Passive injection from the feed water piping and subsequent injection from the charged feed water tank can provide secondary-side heat removal for several hours with the result that sufficient time is available to secure heat removal from external water sources (e.g., mobile pumps), should the loss of normal and emergency feed water pumps persist so long as to require such measures to be taken. The inventory present in the feed water piping system and in the SGs prior to the initiation of secondary-side bleed and after emptying the feed water tank is schematically shown by way of example in Figure 9.

4.5. Boron Dilution Following SB-LOCA. In the course of a SB-LOCA in a PWR, the flow regime in the RCS passes through a number of different phases and the filling level may decrease down to the point where the decay heat is

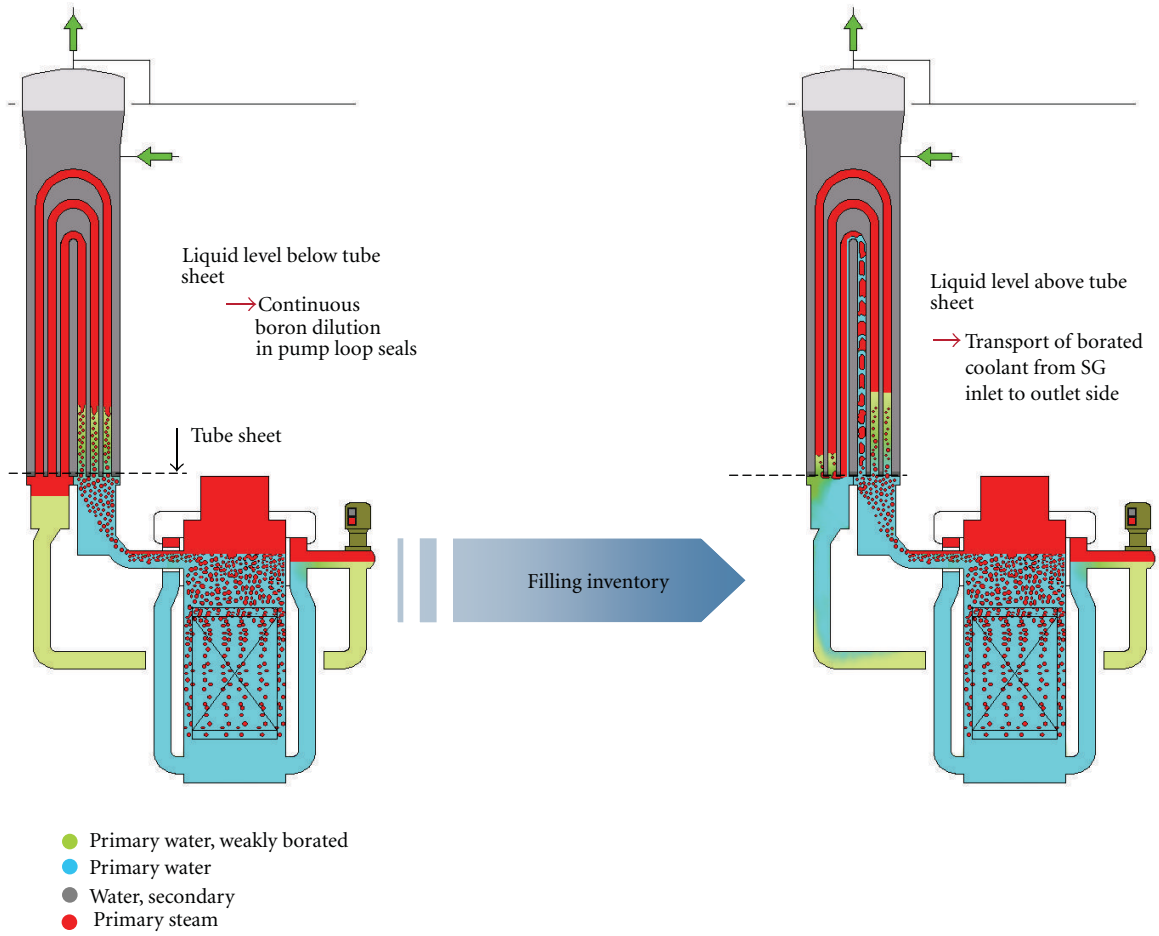

Figure 10: Initiation of RC operation and coolant transport dependent upon liquid level in SG outlet chamber.

transferred to the secondary side under reflux-condenser (RC) conditions (see Section 4.2). During RC, the steam formed in the core condensates in the SG U-tubes. For a limited range of break size and configuration, a continuous accumulation of condensate may cause the formation of boron-depleted slugs. If natural circulation reestablishes, as the RCS is refilled, boron-depleted slugs might be transported to the RPV and to the core raising the question if this could results in a local recriticality in the reactor core.

To draw conclusions on the risk of boron dilution processes in SB-LOCA transients in connection with recriticality, two important issues, the limitation of slug size and the onset of NC, have to be assessed on the basis of experimental data, as system thermal-hydraulic codes are limited in their capability to replicate the complex physical phenomena involved.

With regards to boron dilution, several integral and separate effect tests were conducted in the PKL test facility addressing the following issues:

(i) size of the "condensate slugs" that develop;

(ii) mixing in the SGs and during slug transport through loops with more highly borated water;

(iii) flow rate of the natural circulation onset transient;

(iv) difference in time between the start of natural circulation in the different loops.

All the PKL boron dilution tests were performed with actual boric acid and with adequate measurement technology (continuous online measurement and probe samples) for determining boron concentration.

Main objective of the separate effect tests was to investigate systematically the inherent boron dilution processes due to RC conditions as a function of the primary coolant inventory at a constant primary pressure (Figure 10). Within parametric studies under quasisteady state conditions, the primary side inventory was stepwise reduced and increased notably in order to investigate the behavior of the boron concentration at the SG outlet in the transition regime between 2-phase NC and RC conditions, which is passed through when the system is voided and, as well, when it is refilled. In that way, the onset of a boron dilution process during the voiding phase and the stopping of the boron dilution process during the refilling phase as function of the primary side inventory could be determined. The individual tests vary by different primary pressures (12 to 40 bar).

Major objective of the integral tests was to investigate the transient behavior, that is, the time history of SB-LOCA with inherent boron dilution under certain boundary

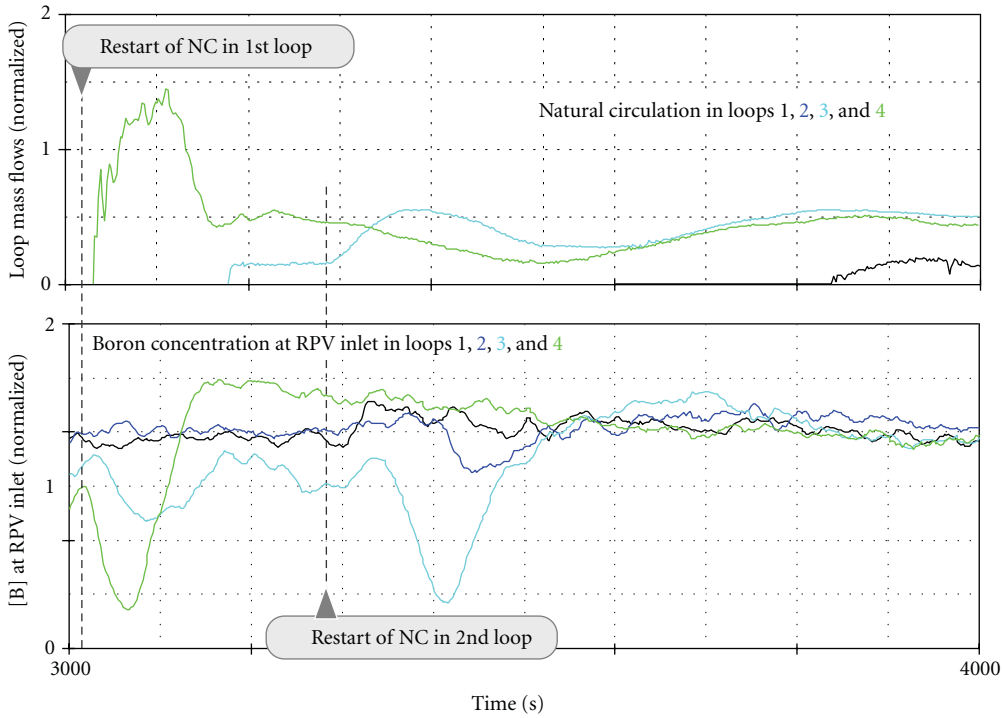

Figure 11: Loop mass flow rate and boron concentration.

conditions (e.g., different ECC injection configurations and cool-down rates). The results for natural circulation in the individual loops and for the conditions in the weakly borated slugs obtained from PKL tests serve as boundary conditions for complementary investigations on mixing in the RPV downcomer annulus and in the lower plenum (e.g., CFD analysis or mixing experiments in the ROCOM and JULIETTE test facilities).

Due to the pressure limitation, it is not possible to simulate the high-pressure portion of accident sequences (such as small-break LOCAs) starting from a PWR's actual operating pressure (155–160 bar) under original conditions. Hence, the OECD PKL tests "start" at a primary system pressure of 45 bar and with initial conditions corresponding to those that would prevail in a real plant at this time (i.e., when the primary system pressure is at this level). These initial conditions are obtained from analyses conducted using system codes (such as RELAP 5 or CATHARE) for a real PWR geometry and corresponding boundary conditions and are realized within the so-called conditioning phase.

The remainder of the accident sequence, where the most relevant phenomena are expected to occur (e.g., for the small break LOCA tests described here: refilling, onset of natural circulation, and transport of low-boron water in the direction of the RPV) is then simulated in the tests using real PWR pressures.

The findings for small-break accidents may be summarized as follows.

(i) For a large and long-lasting loss of coolant, weakly borated condensate slugs can build-up in the crossover leg. However, the buildup of weakly borated condensate in the crossover leg can only occur when the primary side liquid level in the outlet side of the SGs lies below the tube sheet (Figure 10). At higher water levels, transport processes of highly borated water from the inlet to the outlet side in some U-tubes prevent the further accumulation of condensate. As a consequence, the maximum slug size is limited to the volume of the crossover leg plus the volume of the SG outlet plenum.

(ii) The NC does neither start simultaneously in all loops nor isochronously in the U-tubes of a single SG. As circulation starts in one loop, the impetus is reduced for circulation to start in other loops. As a consequence weakly borated condensate from individual loops does not reach the RPV at the same time (Figure 11), a fact that reduces the risk of re-criticality.

(iii) In the refill process, effective mixing processes are present in the SGs and the loops before onset of natural circulation due to overspilling of borated water from the inlet to the outlet side of the SGs (partial disintegration of the boron-depleted slugs).

The OECD PKL tests on boron dilution greatly improved the knowledge of the transient and of the complex physical phenomena involved. With these PKL tests and the derived findings as a substantial element, the final assessment against boron dilution for specific plant designs is finally to be done in conjunction with thermohydraulic system codes (system behavior), investigations on mixing in the RPV downcomer

and lower plenum (CFD or mixing experiments) and neutronics analysis (consequences on core) [9].

4.6. Loss of Residual Heat Removal during Mid-Loop Operation. When a PWR is shut down for refueling, the main coolant inventory is reduced so that the level is at mid-loop elevation. For spatial replacement of water, nitrogen is injected into the primary. At the so-called mid-loop operation, removal of the decay heat from the core is maintained by the residual heat removal system (RHRS), which under these conditions represents the heat sink. Loss of RHRS under shut down conditions has occurred several times worldwide and still plays an important role in risk studies for PWRs. As long as the primary circuit is closed, a failure of the residual heat removal system can be compensated by one or more SGs, which remain filled with water on the secondary side and stay ready for use during refueling and other outages.

With regards to loss of RHRS with closed RCS, several integral and separate effect tests were conducted in the PKL test facility [10]. These tests also performed with actual boric acid and adequate measurement techniques for boron concentration were focusing on the following issues:

(i) heat transfer in the SG(s) in presence of nitrogen,

(ii) stabilization of primary pressure,

(iii) possible boron dilution processes.

If a long-term failure of the residual heat removal system occurs while the primary side is still closed, the reactor water heats up to boiling temperature resulting in steam production in the core. The steam flows towards the SG (mainly to the SG filled with water on the secondary side) where it condenses. A special kind of reflux condensation with nitrogen present in the region above the condensation zone is established. The steam production in the core also causes the coolant inventory in the core to froth up and the swell levels rise variously in the SGs depending on how many SGs are operable at the time. Secondary sides filled with water act as main heat-sinks; hence, the frothed primary inventory is predominantly displaced to heat-removing SGs, thereby manifesting in rising swell levels in their U-tubes. This represents reflux-condenser conditions superposed by a swell level present on the U-tube inlet sides. In absence of forward coolant transport (blocked by N_2), heat transfer may deteriorate (i.e., reactor coolant system temperature and pressure are higher) as more inventory is displaced into the heat-removing SG. In either case, pressure and temperature (i.e., ΔT to secondary) in the RCS rise up to the level, where a steady-state heat flux to secondary becomes established, sufficient to transfer the whole core power to secondary side. Even in the absence of active operator interventions, a quasisteady-state condition with assured heat removal to secondary side always becomes established even if only one SG is operable. The primary equilibrium pressure required for the removal of the entire decay power depends on the heat transfer area in the U-tubes and is thus directly connected to the swell levels in the U-tubes (i.e., the equilibrium pressure depends on the distribution of the primary inventory among the number of water filled SGs). The primary inventory again is determined by the prevailing boundary conditions (e.g., number of SG in operation, additional coolant injection by active or passive systems).

In systematic parametric studies within the current test program on heat transfer in the SG U-tubes (as function of the water inventory), a range of heat transfer mechanisms and basic coherences involving the inlet-to-outlet-side transport of coolant with different effects has been identified (Figure 12), for example, as follows.

(i) State 3: intermittent spillover of boron-depleted coolant through individual short SG tubes. Following the onset of intermittent spillover, slugs of boron-depleted coolant are transported over the apex of individual tubes because the condensation rate exceeds the coolant mass flow spillover. Equilibrium pressure on the RCS side is moderate and constant at 4-5 bar. This status provides potential for a continuous boron dilution process below the SG outlet tubes.

(ii) State 4: stationary slugs of subcooled water present in all SG tubes with nitrogen enclosed in the tube bends above. Tall columns of subcooled condensate reduce the heat transfer zone to the bottom part of all tubes. Degraded heat transfer capacity in the SGs leads to relatively high RCS pressure.

(iii) Sate 5: continuous circulation in some short tubes. If coolant inventory is sufficient to initiate continuous overflow in the short SG tubes, regardless of 1Φ or 2Φ flow, boron dilution resulting from the heat transfer process can be ruled out under these boundary conditions.

In order to investigate the transient behavior of events related to loss of RHRS, several integral tests applying different boundary condition were also conducted in the PKL test facility. These tests confirm the above-mentioned heat transfer mechanisms in the SG(s). However, they also demonstrate that the frame for the occurrence of the specific flow phenomena (discontinuous flow phenomenon with high steam loads) leading to boron dilution processes is very small.

In fact, in the PKL tests of series F and G, boron dilution (continuous accumulation of condensate below SG outlet(s)) as a result of coolant transport in the SGs was only observed for the scenarios with only one SG in operation (and with some additional other specific conditions). As an example Figure 13 shows in comparison the evolution of the primary pressure and the boron concentration below the SG outlet for two test runs with one and two SG in operation. Through the availability of 2 SGs and the smaller increase of primary-side inventory in the SG that results, a transfer of weakly borated water to the outlet side is avoided, and the system stabilizes at a lower pressure level.

In the international group of OECD participants in the PKL project, the so-called benchmark study with various computer programs (RELAP, CATHARE, ATHLET, TRACE, etc.) was performed for a similar scenario. The results

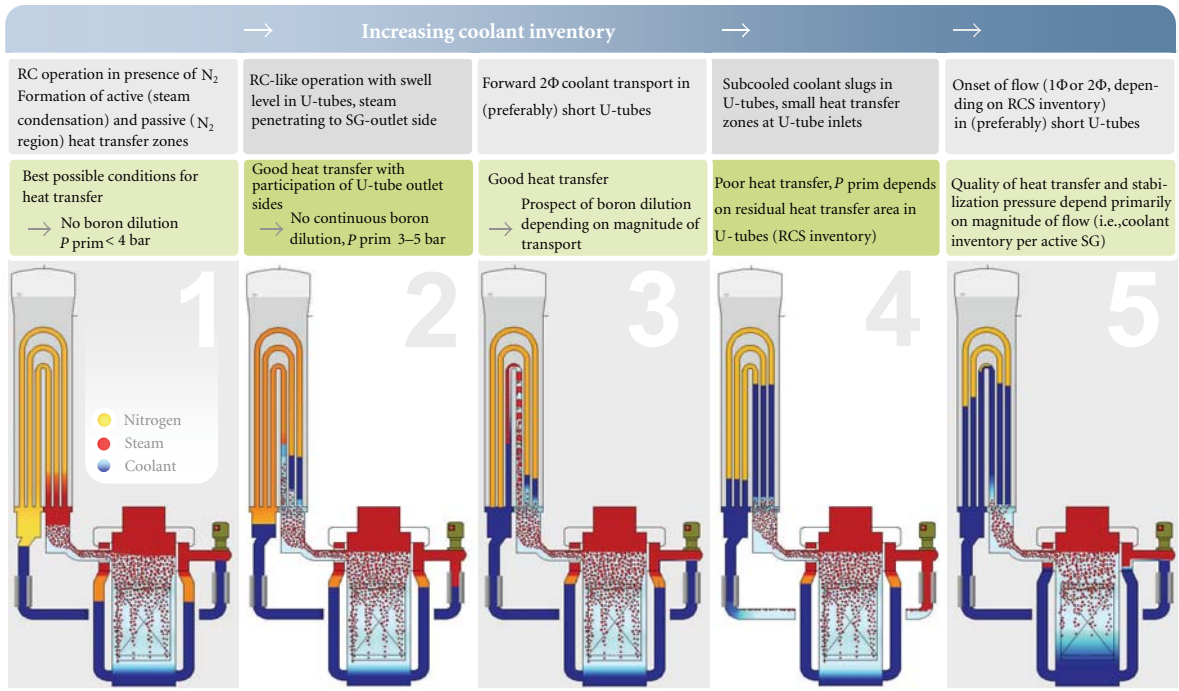

Figure 12: Heat transfer in the SG as function of the coolant inventory.

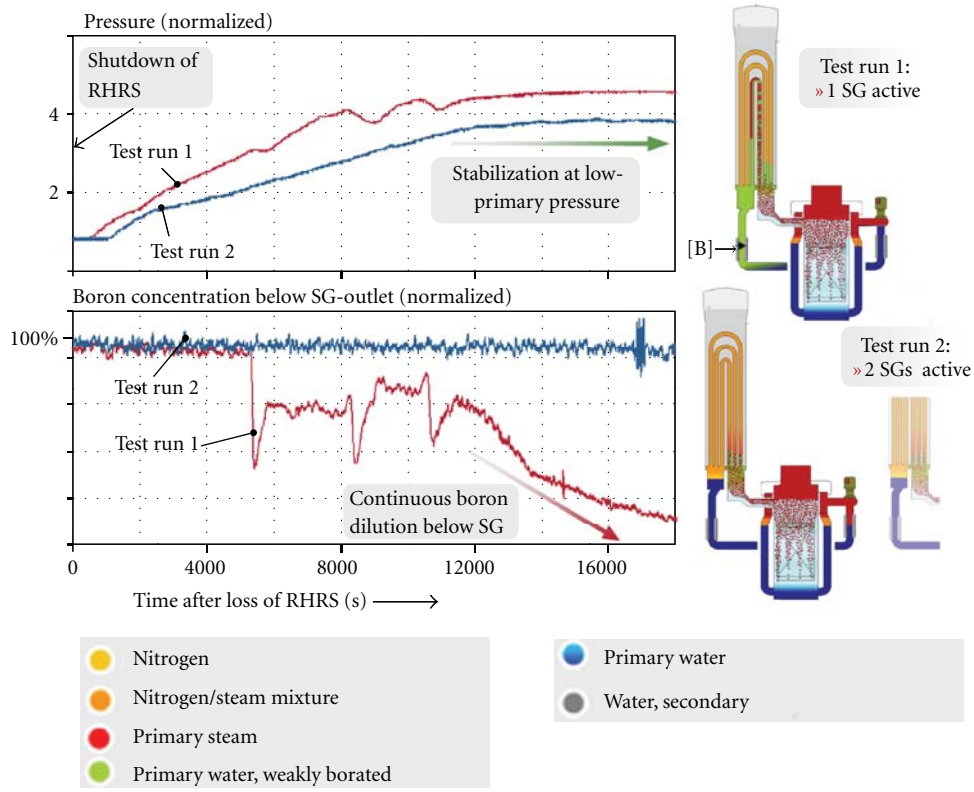

Figure 13: Primary pressure and boron concentrations for one and two SGs in operation.

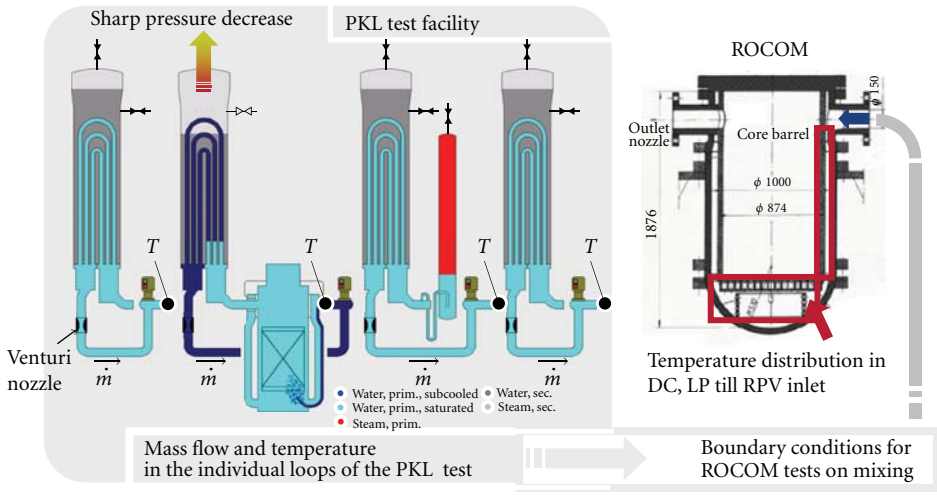

Figure 14: Main steam line break in the PKL test facility.

display a large variation and make clear that to describe such complex processes, on one hand, a very detailed nodalization is required (e.g., representing the SG tubes by 3 lengths appears insufficient) and, on the other hand, it appears that the models of boron dilution are in need of improvement. Therefore, the PKL tests deliver important, detailed information for the further improvement of system codes and for the development of CFD programs that describe localized processes.

4.7. PKL Test on Main Steam Line Break. Nonisolable main steam line breaks (MSLB) cause a rapid decrease in secondary-side pressure in the affected SG. This leads to increased heat transfer from the primary to the secondary side, and therefore to pronounced cooling of the primary coolant in the affected loop (subcooling transient). An important question during this process is whether a localized recriticality of the core and the resulting power excursion can occur due to the entry of cold water into the reactor core area.

The PKL test was started from hot-standby conditions; this is because low reactor power leads to a larger decrease in coolant temperature, which represents a disadvantageous boundary condition for subcooling and recriticality. With a completely filled primary circuit, the transient was started by completely opening a valve (representing a break) in the main steam line of SG 1 and the coastdown of the reactor coolant pumps (due to the MSLB). The cross-section of the opening was chosen to represent the transient conditions of a 10% break (corresponding to the most disadvantageous break size as determined by preparatory RELAP 5 analyses of the subcooling). It is assumed that the main steam line break is located inside containment and therefore cannot be isolated. The other SGs are isolated from the break (there is no connection through the turbine bypass, MS isolation valves are closed). Due to the limiting maximum pressure of the PKL test facility, the processes that normally occur at higher pressures were represented at a reduced pressure of 45 bar. For the extrapolation to real plant conditions, additional calculations with thermal hydraulic system codes (after validation by the experiment) are necessary.

An additional, important aspect of this accident scenario concerns RPV integrity under consideration of pressurized thermal shock (PTS) due to the discharge of cold water in the RPV downcomer. This is important above all when the cooling of the primary coolant is intensified by injection of emergency cooling water into the cold leg at high primary-side pressure (up to the actuation pressure of the pressurizer safety valve (PRZ-SV)). This case is relevant for some PWR plants and was investigated in the second phase of the PKL test described here, that is, after the affected SG was completely emptied. In this process, the primary-side pressure was increased by injection from the safety-injection pumps (cold-side injection in 2 of 4 loops, Loop 1 and 4) until the PRZ-SV responded. Steam flow out of the PRZ-SV was followed later by water flow. Earlier computer calculations of this scenario indicate that, under certain boundary conditions, a reduction and partial stagnation, or even a reversal, of the natural circulation flow can occur in the primary side loops with the intact SGs.

A general goal of the test was to create a reliable database for validating computer programs. In view of the test goals (concerning PTS and recriticality), the following parameters are of decided importance:

(i) the heat transfer in the affected SG and the determination of the minimum coolant temperature at the SG outlet and at the RPV inlet,

(ii) the circulation flow in the loops with the affected and the intact SGs.

Furthermore, the results of this PKL test, which is oriented to PWR system behavior, also provide the boundary conditions for complementary tests in the ROCOM facility (Rossendorf Coolant Mixing Test Facility, operated in the research center at Dresden-Rossendorf) ([11], Figure 14) on mixing cold

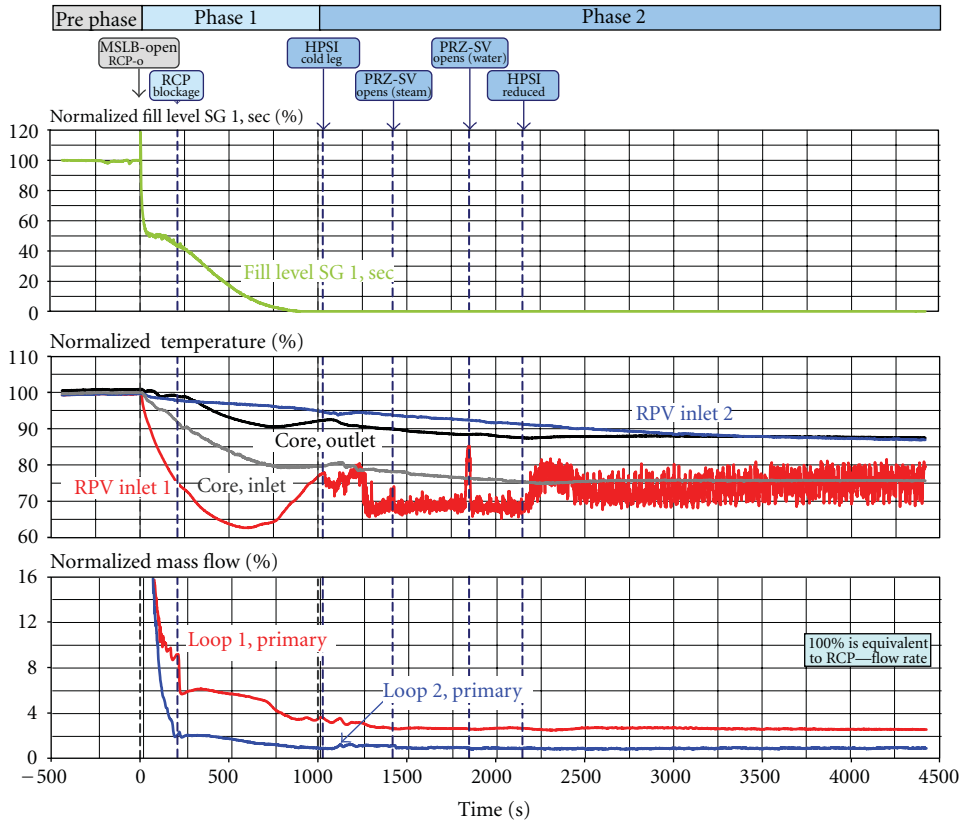

Figure 15: PKL test results—main steam line break.

and hot water in the RPV downcomer as well as in the lower plenum and for determining the fluid state at the core inlet.

The evolution of the main parameters of the PKL test for both phases is illustrated in Figure 15. The test results can be summarized as follows:

(i) evaporation of affected SG-inventory within approximately 1000 s;

(ii) temperature decrease at RPV inlet in the affected loop down to approximately 60% (in relation to the initial conditions);

(iii) intense natural circulation in the affected loop, also stable natural circulation (at lower intensity) in the unaffected loops;

(iv) pronounced temperature stratification in the cold leg as a consequence of high pressure safety injection, thereby no backflow of cold water to RCPs.

The combination of the PKL and of the ROCOM experiment covers all thermal hydraulic phenomena relevant for the MSLB scenario. The test results have been intensively used for validation and optimization of analytical tools, that is, for system codes in connection with PKL and for CFD in connection with ROCOM. The discussion of pre- and posttest calculations on PKL and ROCOM performed by the project partners was one major part of an analytical workshop hosted by University of Pisa in April 2010. In addition a benchmark activity among the participating project partners on the PKL experiment including pre- and posttest calculations with all relevant system codes currently used have been also coordinated by University of Pisa [12].

The final goal now is to be able to make accurate predictions for PWRs with regard to recriticality and PTS for relevant scenarios by using the computer programs that have been validated in this way for plant calculations with PWR geometry and PWR boundary conditions.

5. Benefits and Uses of PKL Results

The benefits and concrete uses of the test results can be summarized under the following headings.

5.1. Validation of Computer Codes. One major benefit of the PKL experiments has been the provision of a comprehensive data base for the further development and validation of thermal-hydraulic system codes such as RELAP, CATHARE, ATHLET, MARS, and TRACE. Computer codes have to be validated before they are used for the design and licensing of reactors. One effective method of quantifying the accuracy of full-scope thermal-hydraulic codes is the predictive and confirmatory analysis of dedicated experiments in sufficiently instrumented test facilities and comparing the results with those obtained with other codes. The objective of code validation is to check the physical models and the numeric solution methods. This must be based on the existing results

of experiments on individual phenomena and also, more particularly, on the results of integral tests. On the other hand side, the computer codes validated in this way are then used to extrapolate the experimental results to the PWR and to analyze scaling effects (geometry, pressure). Code calculations also support the performance of the tests by defining test initial and boundary conditions.

PKL test results have been widely used for validation of computer codes by the PKL project partners (e.g., [11–14]). Besides the regular PKL working group meetings where results from pre- and posttest calculations are discussed, four dedicated workshops on analytical activities related to the different international PKL Projects have been held up to now (Barcelona, September 2003; Pisa, October 2005; Budapest, November 2006; Pisa, April 2010). A further joint PKL-ROSA/LSTF workshop mainly focusing on analysis related to the recently performed counterpart tests in the PKL LSTF facilities is planned for October 2012.

Based on the presentation of simulation results performed by different organizations/countries using various codes, general and common goal for all workshops is to discuss modeling issues and practices. In so far, the workshops provide an efficient way to evaluate the current code capabilities for the transients under investigation and a good opportunity to share experiences and practices among the project participants. The workshops also include plant application analysis related to equivalent scenarios.

In addition, two analytical benchmark activities among the project participants were performed up to now. The first one was related to a PKL test on loss of RHRS during mid-loop operation (see Section 4.6). Seven participants of six different nations using four different codes have contributed to this exercise. For the second benchmark exercise a test of the current test program dealing with cool down after a main steam line break was selected (see Section 4.7). The activity was decided into two phases, a "blind" pretest phase on the basis of initial and boundary conditions by the test design and a posttest phase after the experimental data were available. Six institutions with five thermal-hydraulic system codes were involved in the comparative exercise [12].

5.2. Application of Test Results to Topical Safety Issues. The use of knowledge gained from PKL experiments in answering issues raised by authorized experts and licensing authorities has played an important role since the initiation of the PKL project. This is by no means restricted to the previously mentioned insights gained from the experiments performed in the wake of the TMI-2 accident. Since then there have been many examples of how such insights have contributed to clarifying concerns raised by the supervisory authorities in relation to cool down or emergency procedures or on the basis of operational occurrences. For example, the sound knowledge gained from PKL experiments performed in response to queries raised by the authorized inspection agency concerning the effect of nitrogen in the event of a LOCA demonstrated that heat transport to the SGs is assured even in the event of entrainment of large quantities of nitrogen into the RCS (e.g., due to inadvertent failure to isolate accumulators). It was thus possible to assuage the safety concerns of the authorized inspection agency. Further examples of the application of test results to topical issues covered within PKL III A to D are discussed in [5].

The investigations on system behavior for small breaks with boron dilution and on shut-down plant behavior for loss of RHRS are examples for topics covered in recent years within an international cooperation. These investigations deliver the only experimental data base worldwide on PWR system behavior for boron dilution scenarios, because actual boric acid is used and detailed measurements of the local boron concentrations are made. The results contribute to the answers to current safety questions, for example, with regard to the flow velocities, size, and remaining boron concentration of condensate slugs, which must be considered under specific conditions at the RPV inlet, where the evaluation of the minimal boron concentration entering the core of a PWR is important.

5.3. Verification/Extension of Operating Manuals and Emergency Procedure Manuals. Additions to and extension of the operating manual are an ongoing process for all operators of nuclear installations which involves all insights available for improving the procedures specified in the manuals. The relevant results of PKL experiments are used in this context as are operating experiences, detailed analyses, and advances in instrumentation technology.

The generation of emergency procedures, for example, for loss of feed water supply and station blackout (secondary- and primary-side bleed and feed), is largely based on knowledge gained from relevant PKL experiments.

5.4. Operator Training. PKL test results and knowledge derived from them for PWR units are used for the training of nuclear power plant operating personnel (complementary to simulator training courses). They provide graphic illustration of thermal-hydraulic processes during accidents and operational transients. Furthermore, the test results can be used to demonstrate the effectiveness of operator actions in a practically oriented fashion. Recently, practical training courses have been held at the PKL test facility itself.

5.5. Interaction with Other Test Facilities. The PKL test results are also used to provide initial and boundary conditions for further detailed investigations in special experimental facilities, as, for example, in the ROCOM facility [11], which is operated at the Helmholtz-Zentrum Dresden-Rossendorf in Germany or the JULIETTE facility at AREVA NP in Le Creusot, France. Mention should also be made at this point of the upper plenum test facility (UPTF [5]) which was also operated by Siemens/KWU (now AREVA NP) in Germany and has now been dismantled. The results of the tests performed at the UPTF have proven to be an excellent complement for the PKL experiments. Whereas the UPTF provided a full-scale model of large parts of the reactor coolant system (RCS) for investigating the response of plant subsystems and in particular for studying individual phenomena which are highly dependent on the geometry,

the PKL project concentrated on studying overall system response.

In order to investigate scaling effects, a number of PKL tests were also defined and carried out as counterpart to corresponding tests in other integral test facilities such as LSTF, BETHSY, and LOBI. Just recently, the test conditions for counterpart tests in the LSTF and PKL test facilities, both included in OECD Programs (ROSA 2 and PKL 2, resp.) have been intensively discussed and agreed with the international participants of both projects. The experiments dealing with SB-LOCA connected with complete failure of the high pressure safety injection pumps have been meanwhile completed in both test facilities. The results will be subject to intense scaling analyses and posttest calculations to be discussed also at the planned common analytical workshop in October 2012.

6. Conclusions and Outlook

For many years, extensive experimental investigations into the system response of PWRs under accident conditions have been being conducted at the PKL large-scale test facility which constitutes a full-height model of the entire RCS and major parts of the secondary side of a pressurized water reactor in the 1300 MW class (with diameters a factor of 12 smaller). With the original studies on large- and small-break LOCAs and the modeling of transients in the following years, in particular considering beyond-design-basis conditions, the PKL experiments have covered a very broad spectrum of topics. These investigations have played a key role in German reactor safety research and certainly also contributed to the safety assessment of PWR units worldwide

Since 2001, the PKL project has been continued in the course of an international project initiated by the OECD. The major topics covered by the experiments between 2001 and 2007 were

(i) boron dilution events following SB-LOCA,

(ii) loss of residual heat removal under shut-down conditions.

The tests were conducted utilizing boric acid and boron measuring instrumentation. They provide an important contribution for the evaluation of boron dilution events and represent a unique data source for the validation of computer codes.

Additional topical safety issues, such as main steam line break or boron precipitation processes in the core following large-break LOCA, are subject to investigation in the current OECD-PKL 2 project which is scheduled to run until the end of 2011.

The tests performed to date (in total more than 150 integral experiments) have altogether contributed to a better understanding of the sometimes highly complex thermal-hydraulic processes involved in various accident scenarios and to a better assessment of the countermeasures implemented for accident control. In addition, they have supplied valuable information regarding safety margins available in the plants. In particular, the test results have found concrete application in the validation and further development of thermal hydraulic computer codes, the so-called system codes.

In the light of the overriding objective of continuing to provide quick answers to topical safety concerns in the future, relevant topics of investigation for a new PKL program starting in 2012 have already been discussed with the national and international parties, such as

(i) accident situations under cold shut-down conditions with open RCS,

(ii) station blackout transients with very late initiated procedures to prevent a core melt scenario,

(iii) initiating events for severe accidents in connection with the performance of the core exit temperature.

The final program proposal will be agreed with the project partners and will consider the needs of the different countries and organizations.

References

[1] R. Mandl, B. Brand, and H. Watzinger, "PKL reflood tests including end-of-blowdown," in *Proceedings of the 13th Water Reactor Safety Research Information Meeting*, Gaithersburg, Md, USA, October 1985.

[2] R. M. Mandl and P. A. Weiss, "PKL tests on energy transfer mechanisms during small-break LOCAs," *Nuclear Safety*, vol. 23, no. 2, pp. 146–158, 1982.

[3] K. J. Umminger, W. Kastner, R. Mandl, and P. Weber, "Thermal hydraulic behavior of a PWR under beyond-design-basis accident conditions: conclusions from an experimental program in a 4-loop test facility (PKL)," in *Proceedings of the 2nd ASME-JSME Nuclear Engineering Joint Conference (ICONE '93)*, vol. 1, pp. 409–416, San Francisco, Calif, USA, March 1993.

[4] R. Mandl and B. Brand, "PKL III small breaks and transients experimental programme," in *Proceedings of the 14th Water Reactor Safety Research Information Meeting*, Gaithersburg, Md, USA, October 1986.

[5] J. Liebert, B. Brand, W. Schwarz, G. Sgarz, and K. Umminger, "Results of UPTF and PKL research projects for PWR plant operation," *VGB PowerTech*, vol. 79, no. 8, pp. 20–27, 1999.

[6] Y. Anoda, J. Katayama, Y. Kukita, and R. Mandl, "Secondary bleed and passive feed during PWR station blackout (TMLB') transient: experimental simulation at full pressure and temperature," in *Proceedings of the 113th ASME Annual Winter Meeting*, pp. 89–96, Anaheim, Calif, USA, November 1993.

[7] B. Brand, R. Mandl, and H. Watzinger, "Investigation of PWR transients in the PKL test facility," in *Proceedings of the 3rd International Topical Meeting on Nuclear Power Plant Thermohydraulics and Operations (NUPTHO '88)*, Seoul, Korea, November 1988.

[8] K. J. Umminger, W. Kastner, R. Mandl, and P. Weber, "Thermal hydraulic behavior of a PWR under beyond-design-basis accident conditions: conclusions from an experimental program in a 4-loop test facility (PKL)," in *Proceedings of the 2nd ASME/JSME International Conference on Nuclear Engineering (ICONE '93)*, pp. 409–416, San Francisco, Calif, USA, March 1993.

[9] K. Umminger, S. P. Schollenberger, S. Cornille, C. Agnoux, D. Quintin, and P. Freydier, "PKL tests on heterogeneous inherent boron dilution following Sb-Loca—applicability to reactor scale," in *Proceedings of the 18th International Conference on Nuclear Engineering, Proceedings (ICONE '10)*, vol. 4, pp. 433–439, Xi'an, China, May 2010.

[10] K. Umminger, B. Schoen, and T. Mull, "PKL experiments on loss of residual heat removal under shutdown conditions in PWRs," in *Proceedings of the International Congress on Advances in Nuclear Power Plants (ICAPP '06)*, pp. 1776–1784, Reno, Nev, USA, June 2006.

[11] K. Umminger, L. Dennhardt, and S. Kliem, "Experiments on main steam lineBreak in the test facilities PKL and ROCOM," in *Proceedings of the 14th International Topical Meeting on Nuclear Thermalhydraulics (NURETH '11)*, Toronto, Canada, September 2011.

[12] A. Del Nevo, E. Coscarelli, A. Kovtonyuk, and F. D'Auria, *Analytical Exercise on OECD/NEA/CSNI PKL-2 Project Test G3.1: Main Steam Line Break Transient in PKL-III Facility*, Pisa, Italy, 2010.

[13] F. Reventós, J. Freixa, L. Batet et al., "An analytical comparative exercise on the OECD-SETH PKL E2.2 experiment," *Nuclear Engineering and Design*, vol. 238, no. 4, pp. 1146–1154, 2008.

[14] A. Bucalossi, *Validation of Thermal-Hydraulic Codes for Boron Dilution Transients in the Context of the OECD/SETH Project*, EUROSAFE, Brussels, Belgium, 2005.

Hindawi Publishing Corporation
Science and Technology of Nuclear Installations
Volume 2012, Article ID 528241, 19 pages
doi:10.1155/2012/528241

Review Article

Analyses of the OSU-MASLWR Experimental Test Facility

F. Mascari,[1] G. Vella,[1] B. G. Woods,[2] and F. D'Auria[3]

[1] *Dipartimento dell'Energia, Università degli Studi di Palermo, Viale delle Scienze, Edificio 6, 90128 Palermo, Italy*
[2] *Department of Nuclear Engineering & Radiation Health Physics, Oregon State University, 116 Radiation Center, Corvallis, OR 97331-5902, USA*
[3] *San Piero a Grado Nuclear Research Group (SPGNRG), Università di Pisa, Italy*

Correspondence should be addressed to F. Mascari, mfulvio78@yahoo.it

Received 30 July 2011; Accepted 25 October 2011

Academic Editor: Alessandro Del Nevo

Today, considering the sustainability of the nuclear technology in the energy mix policy of developing and developed countries, the international community starts the development of new advanced reactor designs. In this framework, Oregon State University (OSU) has constructed, a system level test facility to examine natural circulation phenomena of importance to multi-application small light water reactor (MASLWR) design, a small modular pressurized water reactor (PWR), relying on natural circulation during both steady-state and transient operation. The target of this paper is to give a review of the main characteristics of the experimental facility, to analyse the main phenomena characterizing the tests already performed, the potential transients that could be investigated in the facility, and to describe the current IAEA International Collaborative Standard Problem that is being hosted at OSU and the experimental data will be collected at the OSU-MASLWR test facility. A summary of the best estimate thermal hydraulic system code analyses, already performed, to analyze the codes capability in predicting the phenomena typical of the MASLWR prototype, thermal hydraulically characterized in the OSU-MASLWR facility, is presented as well.

1. Introduction

Today, considering the sustainability of the nuclear technology in the energy mix policy of developing and developed countries, the international community, taking into account the operational experience of the nuclear reactors, starts the development of new advanced reactor designs. Some of the new nuclear reactor designs use passive safety systems based on the use of the natural circulation for the cooling of the core during the designed operational condition and for the removing of the residual heat during transient conditions [1–5]. Emergency systems based on natural circulation are considered, for example, in the AP600/1000 design, WWER-1000/V-392 and WWER-640/V-407 designs, AC-600 design, SMART design, IRIS design, SWR 1000 MWe design, and in the ESBWR design [4–7]. Examples of reactors that rely on natural circulation for the removing of the core power during normal operation are the MASLWR, the ESBWR, the SMART, and the CAREM design [5–7].

The MASLWR integral reactor concept [1, 2, 8–13], developed by Idaho National Engineering and Environmental Laboratory, OSU, and NEXANT—Bechtel, Figure 1, is a small modular PWR relying on natural circulation during both steady-state and transient operation, which includes an integrated steam generator (SG) consisting of banks of vertical helical tubes contained within the reactor pressure vessel (RPV). The primary coolant flows outside the SG tubes and the feed-water (FW) is fully vaporized resulting in superheated steam at the SG exit. The MASLWR module has a net output of 35 MWe, and a number of modules could be built in increments, in a *"field"* concept, to generate electricity in larger electricity grids [8, 11].

OSU has constructed, under a US Department of Energy grant, a system-level test facility, OSU-MASLWR [1, 2, 8–13], to examine natural circulation phenomena of importance to the MASLWR design. Four tests have been conducted in support of the MASLWR concept design verification.

Considering the thermal hydraulic phenomena simulating capability of this facility, the planned work will be not only to specifically investigate the MASLWR concept design further but also to advance the broad understanding of integral natural reactor plants and accompanying passive safety features as well.

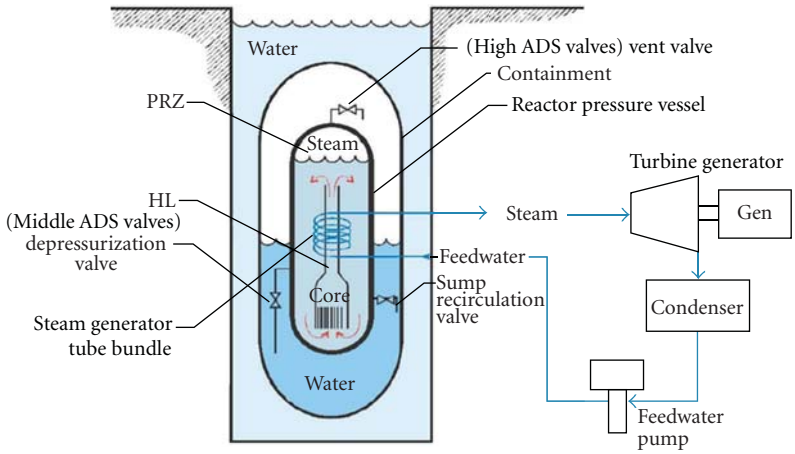

Figure 1: MASLWR conceptual design layout [1, 2, 8, 11, 13].

After the completion of the first test series, through a grant from the International Atomic Energy Agency (IAEA), the OSU-MASLWR test facility core was reconfigured to eliminate a recurring grounding problem and improve facility reliability [12] in anticipation of conducting an IAEA ICSP on "Integral PWR Design Natural Circulation Flow Stability and Thermo-hydraulic Coupling of Primary System and Containment During Accidents" [14–16]. This ICSP is being hosted at OSU and the experimental data will be collected at the OSU-MASLWR facility, to provide experimental data on single-/two-phase flow instability phenomena under natural circulation conditions and coupled containment/reactor vessel behavior in integral type light water reactors.

The target of this paper is to give a review of the main characteristics of the experimental facility, to analyse the main phenomena characterizing the tests already performed, the potential transients, of interest for integral reactor types, that could be investigated in the facility, and to describe the current IAEA ICSP. A summary of the best estimate thermal hydraulic system code analyses, already performed, to investigate the codes capability in predicting the phenomena typical of the MASLWR prototype, thermal hydraulically characterized in the OSU-MASLWR facility, is presented as well.

2. MASLWR Design

2.1. MASLWR Overview. The MASLWR [1, 2, 8–13], Figure 1, is a small modular integral PWR relying on natural circulation during both steady-state and transient operations. The use of natural circulation reduces the number of active components simplifying the configuration of nuclear steam supply system.

The RPV contains the core, the pressurizer (PRZ), and an integrated SG consisting of banks of vertical helical tubes located in the upper region of the vessel outside of the hot leg (HL) chimney. The MASLWR steady-state operating conditions are reported in Table 1.

The RPV is surrounded by a cylindrical containment, partially filled with water. This containment provides pressure suppression and liquid makeup capabilities and is submerged in a pool of water that acts as the ultimate heat sink.

Table 1: MASLWR steady-state operating conditions [8–10].

Primary side	
Reactor thermal power	150 MW
Primary pressure	7.60 MPa
Primary mass flow rate	597 kg/s
Reactor inlet temperature	491.80 K
Reactor outlet temperature	544.30 K
Saturation temperature	565 K
Reactor outlet void fraction	0.00%
Secondary side	
Steam pressure	1.50 MPa
Steam outlet quality	1
Steam temperature	481.40 K
Saturation temperature	471.60 K
Feedwater temperature	310 K
Feedwater flow rate	56.10 kg/s

The RPV can be depressurized using the automatic depressurization system (ADS), consisting of six valves discharging into various locations within the containment. In particular two independent vent valves (high ADS valve), two independent depressurization valves (middle ADS valve) and two independent sump recirculation valves are considered in the MASLWR design.

2.2. MASLWR SBLOCA Phenomenology Description. Considering the MASLWR integral arrangement, there are not pressurized primary components outside the RPV; therefore the possibility of large-break loss of coolant accident (LOCA) is eliminated and the small-break LOCA (SBLOCA) initiating events are reduced. Of particular interest is the SBLOCA passive mitigation strategy typical of the MASLWR design.

Following, for example, an inadvertent opening of an ADS valve, a primary side blowdown into the pressure suppression containment takes place. The RPV blowdown causes a primary pressure decrease and a consequent containment pressure increase causing a safety injection signal. It

Figure 2: OSU-MASLWR experimental facility photo [1, 2, 13].

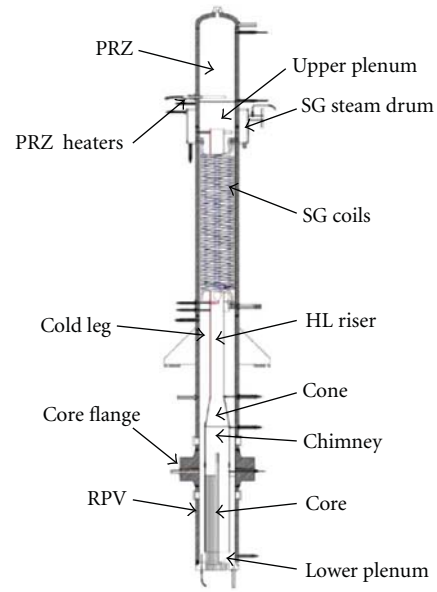

Figure 3: RPV internal components [1, 2, 11, 13].

automatically opens, Figure 1, the high ADS valves, the middle ADS valves, and the sump recirculation valves. As the primary and the containment pressures become equalized, the blowdown is terminated and a natural circulation flow path is established. In fact when the sump recirculation valves are opened, the vapour produced in the core goes in RPV upper part and, through the high ADS valve, goes to the containment where it is condensed. At this point through the sump recirculation lines and the downcomer, the fluid goes to the core again. The pressure suppression containment is submerged in a pool that acts as the ultimate heat sink. This mechanism permits the cooling of the core during the transient [8–11].

3. Description of the OSU-MASLWR Facility

3.1. OSU-MASLWR Test Facility. In the development process of advanced nuclear reactors, the analysis of single- and two-phase fluid natural circulation in complex systems [5, 10, 17–19], under steady-state and transient conditions, is crucial for the understanding of the physical and operational phenomena typical of these advanced designs characterized by the interaction between different parts of the system. The use of experimental facilities is fundamental in order to characterize the thermal hydraulics of these phenomena and to develop an experimental database useful for the validation of the computational tools necessary for the operation, design, and safety analysis of nuclear reactors.

In general it is expensive to design a test facility to develop experimental data useful for the analyses of complex system; therefore reduced scaled test facilities are in general used to characterize them. Since the experimental data produced have to be applicable to the full-scale prototype, the geometrical characteristics of the facility and the initial and boundary condition of the selected tests have to be correctly scaled. Since possible scaling distortions are present in the experimental facility design, the similitude of the main thermal hydraulic phenomena of interest has to be assured permitting their accurate experimental simulation [10, 11, 18, 19].

OSU has constructed, under a US Department of Energy grant, a system-level test facility to examine natural circulation phenomena of importance to MASLWR design. The scaling analyses of the OSU-MASLWR experimental facility was performed in order to have an adequate simulation of the single- and two-phase natural circulation, reactor system depressurization during a blowdown and the containment pressure response typical of the MASLWR prototype. The model used for the scaling analyses performed in [9, 10] is partly drawn from the USNRC's Severe Accident Scaling Methodology (SASM) presented in NUREG/CR-5809 [19]. The detailed OSU-MASLWR scaling analyses is reported in [9, 10].

As a result of the scaling analyses, the OSU-MASLWR test facility [8–13, 18, 19], shown in Figure 2, is scaled at 1 : 3 length scale, 1 : 254.7 volume scale, and 1 : 1 time scale, is constructed entirely of stainless steel, and is designed for full pressure and full temperature prototype operation. It includes the primary circuit, consisting of the RPV and ADS lines, the secondary circuit, and the containment structures. In addition to the physical structures that comprise the test facility, there are data acquisition, instrumentation, and control systems. Auxiliary lines and systems are present in the facility.

3.2. OSU-MASLWR RPV Overview. The internal components of the RPV [1, 2, 8–13], Figure 3, are the core, the HL

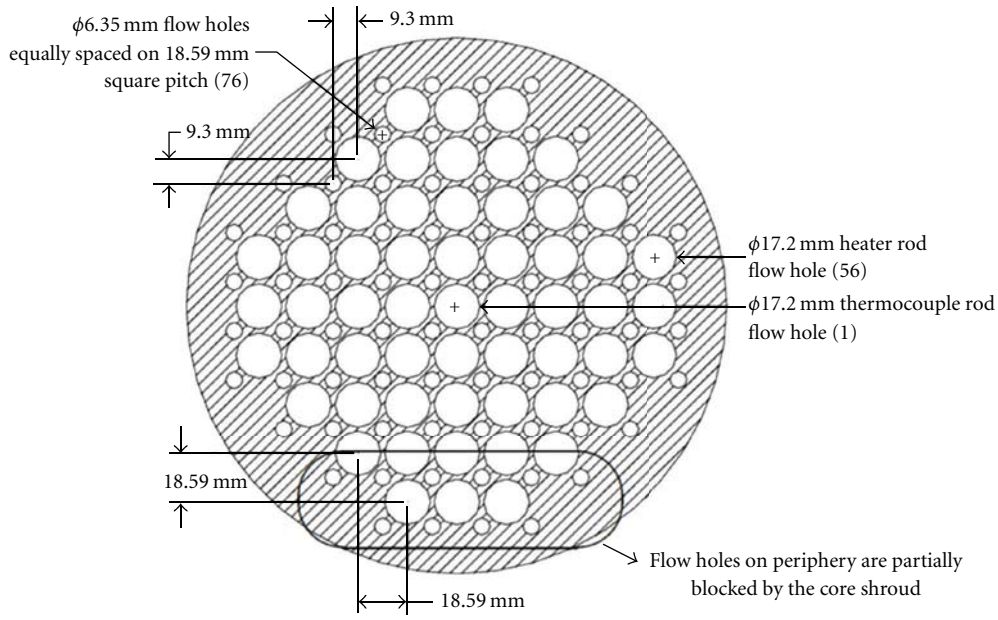

Figure 4: Lower core flow plate layout [12]. See Figure 5 for flow blockage detail.

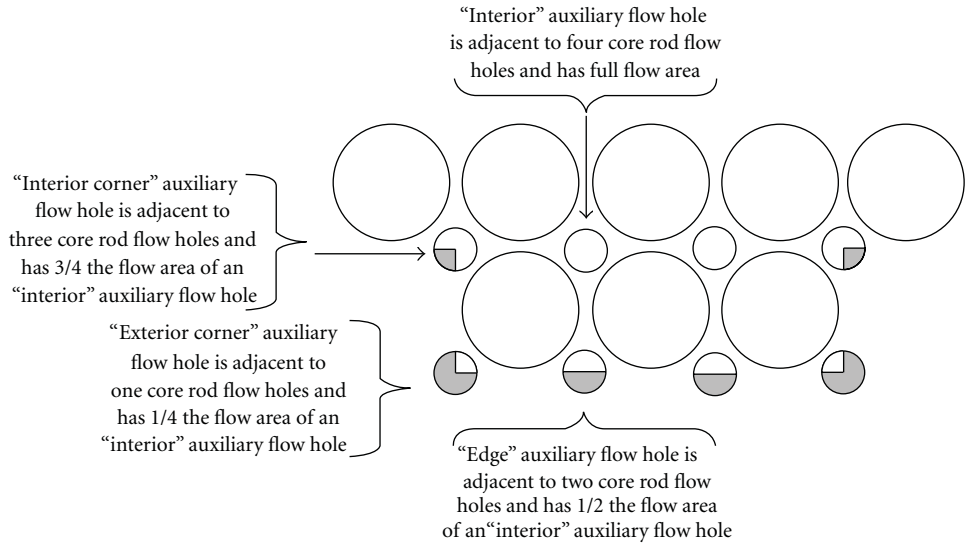

Figure 5: Auxiliary flow hole blockage by core shroud [12].

riser, the upper plenum (UP), the PRZ, the SG primary side, the cold leg (CL) downcomer, and the lower plenum (LP).

The core is modelled with 56 cylindrical heater rods. A lower core flow plate is located at the core entrance and is shown in Figure 4. The core is shrouded to ensure all flow enters the core via the bottom and travels the entire heated length and to separate the downcomer region from the core region. The core shroud is shaped to partially block the primary coolant flow through the outermost auxiliary flow holes in order to ensure that each heated rod receives approximately equal axial coolant flow, as shown in Figure 5. The amount of blockage is dependent on the number and location of heated rods adjacent to each auxiliary flow hole. The shaded area, Figure 5, indicates where core shroud blocks flow through auxiliary flow holes. A core grid wire, located at core midelevation, is considered in order to maintain the radial alignment of the core rods, Figure 6.

The HL riser, Figure 3, consists of a lower region, an upper region, and a cone transition region. The UP is separated from the heated upper PRZ section by a thick baffle plate having eight holes, spaced uniformly around the baffle plate periphery, which allow free communication of the PRZ to the remainder of the RPV during normal operation and for volume surges into and/or out of the PRZ due to transients. The PRZ is integrated in the RPV and is located in its upper part. In the PRZ are located heater elements, which are modulated

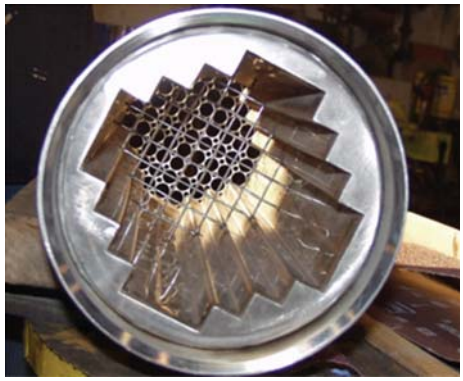

Figure 6: Photo of core shroud showing lower core flow plate behind the core grid wires [12].

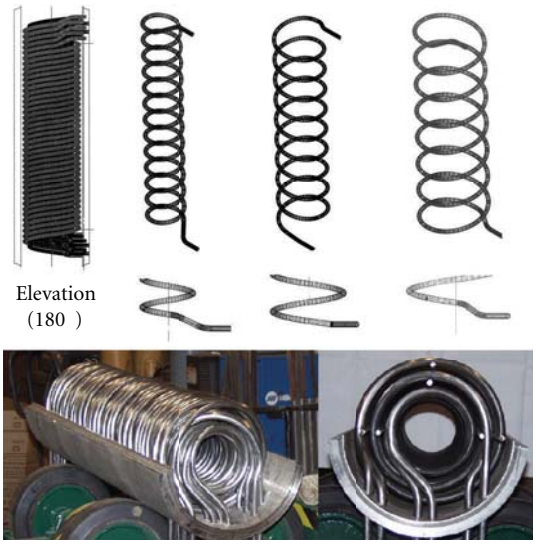

Figure 7: Helical coil SG bundle [13, 20].

by the test facility control system to maintain nominal primary system pressure at the desired value. The CL downcomer region is an annular region bounded by the RPV wall on the outside and the HL riser on the inside, and the flow area reduces at the HL riser cone. In the SG primary side section is inserted the SG helical coil bundle, Figure 7. The entire RPV is covered by Thermo-12 hydrous calcium silicate insulation.

3.3. OSU-MASLWR Secondary Side Overview. The secondary circuit [1, 2, 8–13] includes the FW treatment and storage system, the main FW pump (MFP), the main FW (MFW) system supply lines, the SG secondary side internal to the vessel, the main steam (MS) system, and associated FW and steam valves.

Potable water, coming from the city water supply, passes through a mechanical filter and a resin bed to remove impurities and flows to the FW storage tank. The MFW system supplies deionized and demineralized water to the SG. The MFP is a positive displacement pump and can be isolated from the downstream main FW system supply lines by pneumatic motor operated globe valve MF-508 (FW supply valve). The MFP controller is interlocked with the MFP discharge isolation valve MF-508 position, to ensure that the MFP is not energized unless MF-508 is fully open. The single MFW line splits into three supply lines, one for each coil bank of SG tubes.

The SG of the facility is a once through heat exchanger and is located within the RPV in the annular space between the HL riser and the inside surface of the RPV. The tube bundle, Figure 7, is a helical coil consisting of fourteen tubes. There are three separate parallel coils of stainless steel tubes. The outer and middle coils consist of five tubes each while the inner coil consists of four tubes. Each coil is joined at a common inlet header and each of them exhausts the superheated steam into a common steam drum from where it is subsequently exhausted to atmosphere via the MS system. The FW enters at the bottom of the SG and boils off after travelling a certain length in the SG. This boil-off length is a function of both core power and MFW flow rate. Nominally, the boil-off length is approximately 40% shorter than the actual length of the SG tubes so the steam will leave the SG superheated. The value of the degree of the steam superheat is changed in order to control the facility.

The steam received in the SG steam drum goes to the MS line, Figure 8, and that exhausts the SG superheated steam to atmosphere. A pneumatic motor operated globe valve MS-502 (MS header drain line isolation valve) is immediately downstream of the SG steam drum. Another motor operated globe valve, MS-503 (MS header isolation valve), isolates the MS header from the steam header drain line. In order to have always an open discharge for the SG, the MS-502 and MS-503 are interlocked to prevent them both from being simultaneously commanded shut.

3.4. OSU-MASLWR Containment Structures Overview. The OSU-MASLWR containment structures [1, 2, 8–13], Figure 9, consist of two vessels, a high-pressure containment vessel (HPC) and a cooling pool vessel (CPV), with a heat transfer surface between them to establish the proper heat transfer area. The HPC simulates the containment structure in which the MASLWR RPV sit and the CPV simulates the cavity within which the MASLWR containment structure is located.

The HPC consists of a lower cylindrical section, an eccentric cone section, an upper cylindrical section, and a hemispherical upper-end head. The entire HPC is covered by Thermo-12 hydrous calcium silicate insulation.

The CPV consists of a right cylindrical tank covered by Thermo-12 hydrous calcium silicate insulation. One disk rupture connects the HPC and the CPV.

The heat transfer plate, having the same height of the HPC without the hemispherical head, provides the heat conduction between the HPC and CPV. The heat transfer plate is scaled in order to model the heat transfer area between the MASLWR design high-pressure containment vessel and the cooling pool in which it sits.

For scaling reasons, in order to have an adiabatic boundary condition in all the wall of the HPC except through the heat transfer plate wall, where the condensation has to take place, containment heaters have been installed permitting the

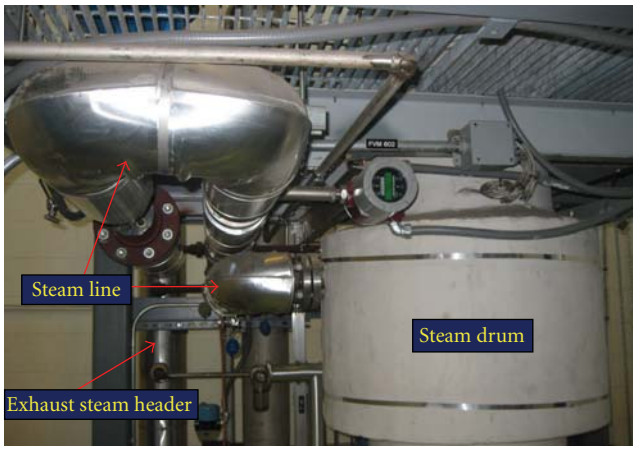

Figure 8: Main steam line photo.

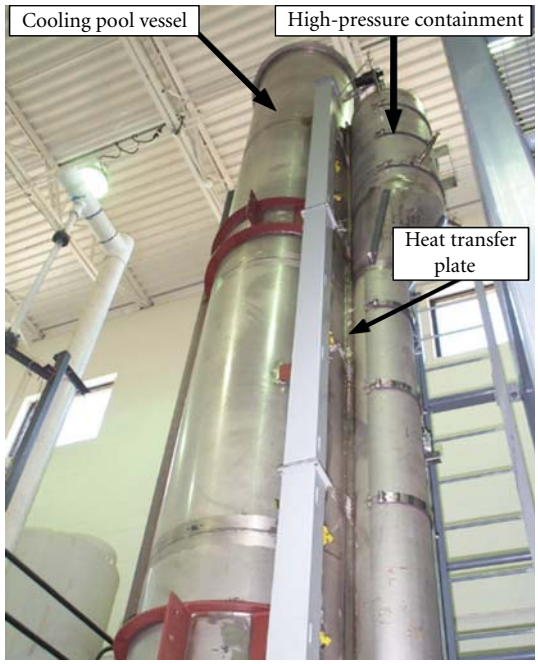

Figure 9: OSU-MASLWR containment structures photo [1, 2, 11].

heat transfer takes place only between the CPV and HPC containment. These heaters are located in the exterior surface of the HPC, under the insulation, and above the containment water level.

3.5. OSU-MASLWR ADS Lines Overview. The two middle ADS lines, two high ADS lines, and the two ADS sump recirculation lines are modelled separately [1, 2, 8–13]. Figure 10 shows the schematic diagram of the OSU-MASLWR RPV, ADS lines, and containment structures.

The ADS sump recirculation lines are horizontally oriented and connect the RPV lower CL to the HPC. A pneumatic motor operated globe valve is located in each line. Downstream from each isolation valve is a transition piece with an internal square-edge orifice. These two lines enter the HPC, penetrate it, and then turn downward before terminating below the HPC waterline. No sparger is considered for these lines.

The middle ADS lines are horizontally oriented and connect the RPV CL to the HPC. A pneumatic motor-operated globe valve is located in each line. Downstream from each isolation valve is a transition piece with an internal square-edge orifice. These two lines enter the HPC, penetrate it, and then turn downward before terminating below the HPC waterline. A sparger is considered at the end of this line.

The high ADS lines are horizontally oriented and connect the RPV PRZ steam space with the HPC. A pneumatic motor operated globe valve is located in each line. Downstream from each isolation valve is a transition piece with an internal square-edge orifice. The two ADS vent lines enter the HPC above the waterline, penetrate it, and then terminate with a sparger.

3.6. OSU-MASLWR Data Acquisition and Control Subsystem Overview. The data acquisition and control system [1, 2, 8–13] consist of various field input/output modules, a programmable logic controller module, and a desktop computer. The data acquisition and control subsystem process input signals from system components, generate control signals as determined by the control logic, and apply those control signals to applicable system components. The operator can monitor parameters and alarms in the main control screen, via a graphical user interface as it is shown in Figure 11.

Individual system component operation algorithms are considered in the facility. The PRZ heaters, for examples, can be operated manually or in automatic mode. In automatic mode, in order to control the primary pressure, the operator fixes the primary pressure set point and the control system, by using a proportional integral differential methods, and adjusts the heater controller electrical output. The core heaters, for example, can be operated in manual mode, constant power mode, or decay mode. In decay mode the core power follows a user specify curve.

4. OSU-MASLWR Testing Program

The first tests conducted in the OSU-MASLWR facility [8–13] were in support of the MASLWR concept design verification. Table 2 shows, in chronological order, the type of test already conducted in the facility. During this test program, the MASLWR normal startup, the operation, and its shutdown are thermal hydraulically demonstrated.

4.1. OSU-MASLWR-001 Description. The purpose of the test OSU-MASLWR-001 [1, 8–13], a design basis accident for MASLWR concept design, is to determine the behavior of the RPV and containment pressure following an "*inadvertent actuation of one middle ADS valve*" located below the HPC and RPV water level. The test successfully demonstrated the thermal hydraulic behavior of the MASLWR design during the transient sequence following this design basis event.

Following the inadvertent middle ADS actuation, the blowdown of the primary system takes place. A subcooled blowdown characterized by a fast RPV depressurization takes place after the start of the transient (SOT). A two-phase blowdown occurs when the differential pressure, at the break

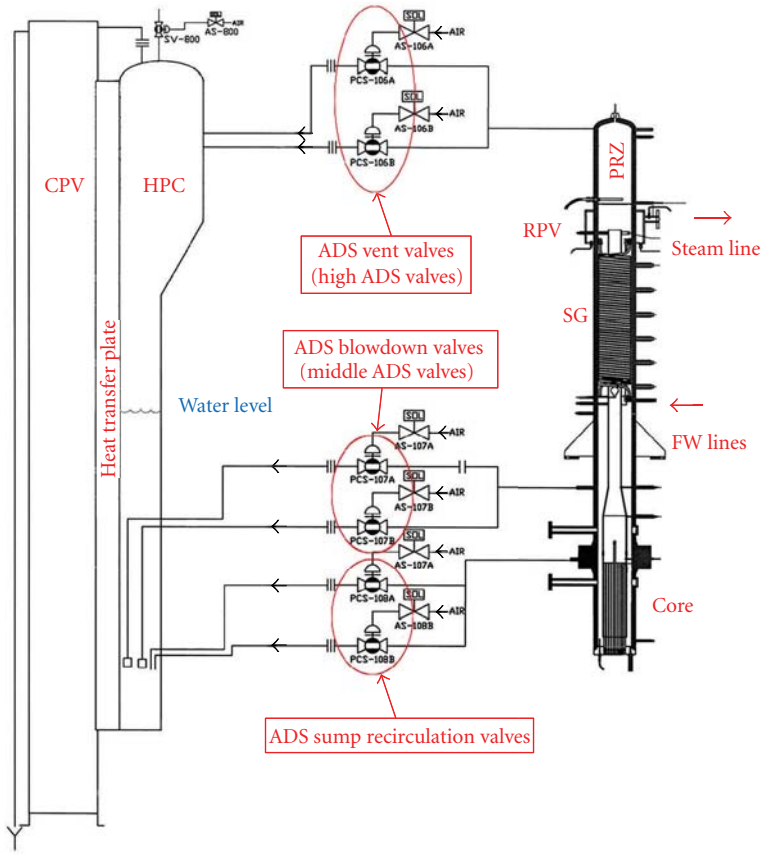

Figure 10: Schematic diagram of the OSU-MASLWR RPV, ADS lines, and containment structures [2, 20].

Table 2: Summary of the previous OSU-MASLWR testing program [8, 11, 13].

Name of the test	Type of test	ADS line configuration					
		Middle ADS 1 (%)	Middle ADS2 (%)	High ADS 1 (%)	High ADS2 (%)	Sump Recirc 1 (%)	Sump Recirc 2 (%)
OSU-MASLWR-00l	Inadvertent actuation of 1 submerged ADS valve.	Failed Shut	100	100	100	100	100
OSU-MASLWR-002	Natural circulation at core power up to 210 kW.	N/A	N/A	N/A	N/A	N/A	N/A
OSU-MASLWR-003A	Natural circulation at core power of 210 kW. (Continuation of test 002, establishing the initial conditions for the 003B test.)	Failed Shut	N/A	N/A	N/A	N/A	N/A
OSU-MASLWR-003B	Inadvertent actuation of 1 high-containment ADS valve	Failed Shut	100	Failed Shut	100	100	100

location, results in fluid flashing. A choked two-phase flow condition prevails, and a decrease in depressurization rate of the primary system is experimentally observed. When the PRZ pressure reaches saturation, single-phase blowdown occurs, and the depressurization rate increases. The primary and HPC pressure are shown in Figure 12.

At 539 s after the SOT, the pressure difference between the RPV and the HPC reaches a value less than 0.517 MPa, one of the high ADS valve is opened and, with approximately 10 s of delay, the other high ADS valve is opened equalizing the pressure of the primary and HPC system.

At 561 s after the SOT, the pressure difference between the RPV and the HPC reaches a value less than 0.034 MPa, one sump recirculation valve is opened, and, with approximately 10 s of delay, the other sump recirculation valve is opened terminating the blow-down period and starting the refill

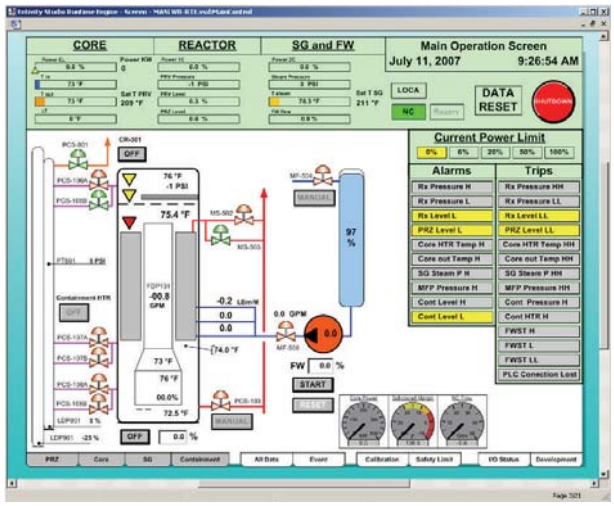

Figure 11: Data acquisition and control system main control screen [12].

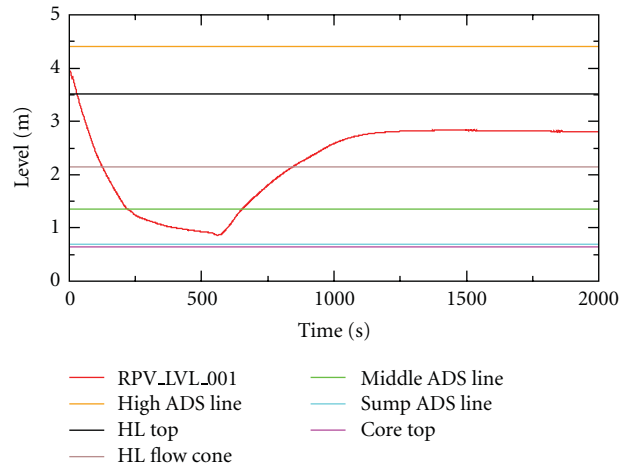

Figure 13: RPV water level inventory behaviour during the OSU-MASLWR-001 test [8, 11].

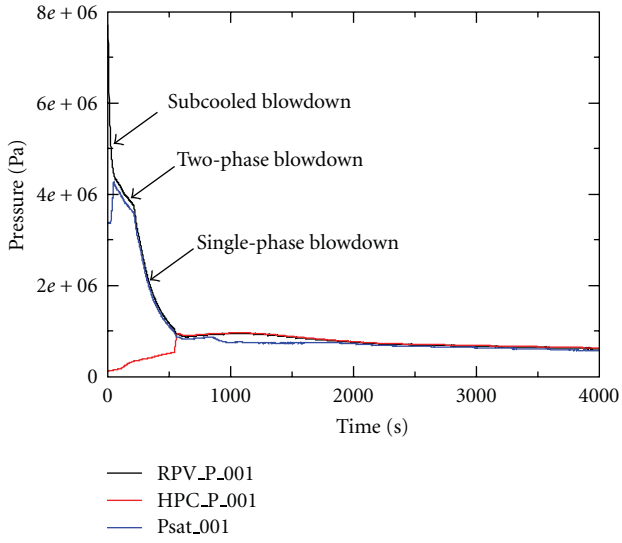

Figure 12: RPV and HPC pressure behaviour during the OSU-MASLWR-001 test (the Psat, saturation pressure, is based on the temperature at the core outlet) [8, 11].

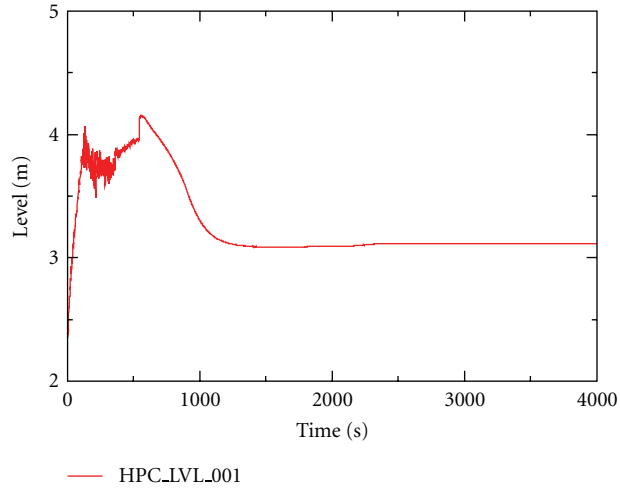

Figure 14: HPC level behaviour during the OSU-MASLWR-001 test [21, 22].

period. The refill period takes place for the higher relative coolant height in the HPC compared to the RPV. Figure 13 shows the RPV level evolution experimentally detected during the test. The RPV level water never fell below the top of the core during the execution of the test 1. Figure 14 shows the HPC level during the test.

During the saturated blowdown period, the inlet and the outlet temperature of the core are equal to each other assuming the saturation temperature value. A core reverse flow and a core coolant boiling off at saturation are present in the facility during this period. When the refill takes place, the core flow normal flow direction is restarted and a delta T core is observed depending on the refill rate and core power, Figure 15.

When the refill of the reactor takes place, the level of the coolant reaches the location of the flow rate HL measurement point; therefore an increase of the RPV flow rate is detected for this phenomenon, Figure 16.

4.2. OSU-MASLWR-002 and 003A Description. The test OSU-MASLWR-002 and OSU-MASLWR-003A [1, 8–13] investigated the primary system flow rates and secondary side steam superheat for a variety of core power levels and FW flow rate. Table 3 shows the OSU-MASLWR-002 and OSU-MASLWR-003A test conditions.

The OSU-MASLWR-002 stepped power level incrementally up to 165 kW, varying FW flow rate at each power level. Since the 210 kW data in OSU-MASLWR-002 was not used, because of liquid carryover in the SG, the OSU-MASLWR-003A was an extended 210 kW steady test establishing initial conditions for the following test OSU-MASLWR-003B.

Table 3: OSU-MASLWR-002 and OSU-MASLWR-003A test conditions [8, 11, 12].

Test	Primary							Secondary			
	Start time (s)	End time (s)	Core power (kW)	T_in (K)	T_out (K)	Flow (L/min)	Vel (m/s)	T_in (K)	T_out (K)	P (MPa)	Feedwater (kg/min)
002	0	127	80.0	489	506	65.6	0.13	292	482	1.41	1.13
	250	550	100.0	491	509	77.9	0.16	292	488	1.40	1.81
	750	1200	100.0	490	508	80.0	0.16	292	494	1.38	2.14
	1380	1570	100.0	486	505	81.9	0.17	292	494	1.37	2.50
	1670	1920	110.0	483	503	84.9	0.17	292	493	1.36	2.49
	2060	2250	125.0	482	503	88.5	0.18	292	493	1.35	2.50
	2450	2600	160.0	481	505	104.1	0.21	292	488	1.36	3.85
	2700	2930	165.0	478	503	105.0	0.21	293	482	1.35	3.83
003A	0	450	210.0	501	528	118	0.24	293	507	1.581	4.14
	550	1000	210.0	499	526	120	0.24	293	509	1.567	4.56

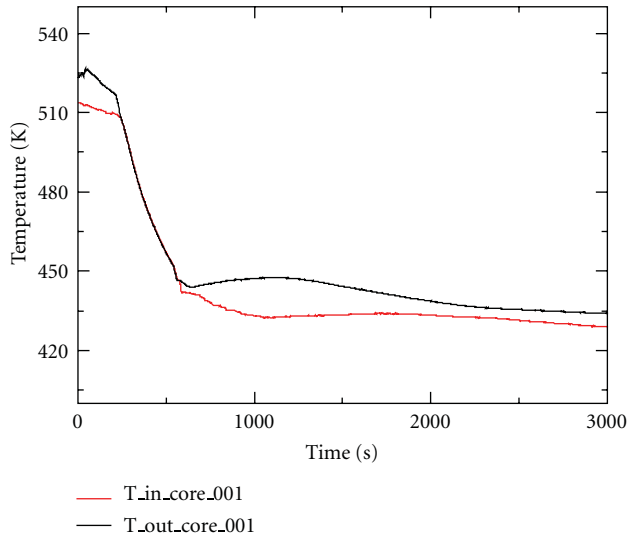

Figure 15: Inlet/outlet core temperature behavior during the OSU-MASLWR-001 test [8].

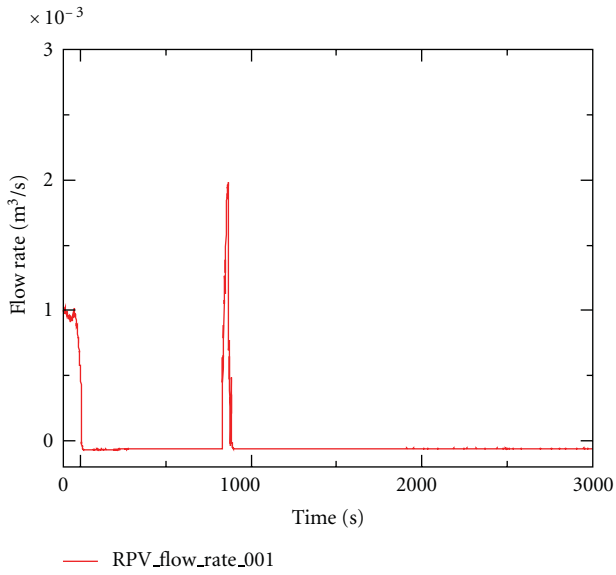

Figure 16: RPV flow rate behavior during the OSU-MASLWR-001 test [8].

During these two tests, seven different core powers were used as well as nine different FW flow rates. Figures 17 and 18 show the inlet, outlet core, and top of the HL temperature behaviour for the OSU-MASLWR-002 and OSU-MASLWR-003A test, respectively.

In general the value of the degree of the steam superheat is changed in order to control the facility. Since the slope of the MS superheat curve increases if the value of the core power increases and decreases if the value of the FW flow rate increases, the target of these tests was to acquire primary system flow rate and secondary side steam superheat for different core power and FW flow rate. The difference between the MS saturation temperature and the measured MS temperature is used to estimate the value of the MS superheat. Figures 19 and 20 show the steam superheat data for the test OSU-MASLWR-002 and 003A test, respectively. Figure 21 shows the difference of fluid temperature at the inlet of the core and at the exit of the SG primary side for the OSU-MASLWR-002 test. By analyzing the experimental data, related to the flow temperature after the SG coils primary side section and the core inlet temperature, it is evident that the direct heat exchange, through the internal shell, between the fluid ascending the HL and the fluid descending the CL, is a crucial parameter for the evaluation of the core inlet temperature and, therefore, the core outlet temperature. In fact, the experimental data show that, along the downcomer region, the fluid increases its temperature between the end of the SG primary side section and the core inlet [13].

4.3. OSU-MASLWR-003B Description. The normal opening sequence used in the MASLWR for the ADS valves is the middle lines first, then the high lines, and finally the sump recirculation lines [8–13]. This sequence minimizes the rise in containment pressure since a large fraction of the energy transferred to the containment is direct into the subcooled containment coolant. However, if the high lines are actuated first, the rise in containment pressure will be larger than

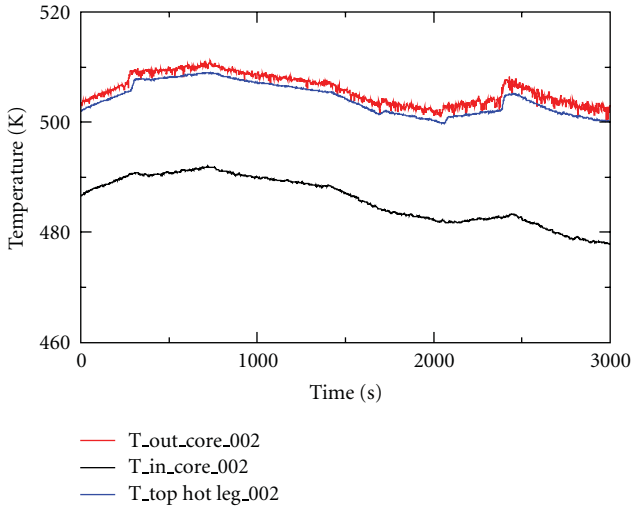

Figure 17: Inlet, outlet core, and top of the hot leg temperature behavior during the OSU-MASLWR-002 test [8].

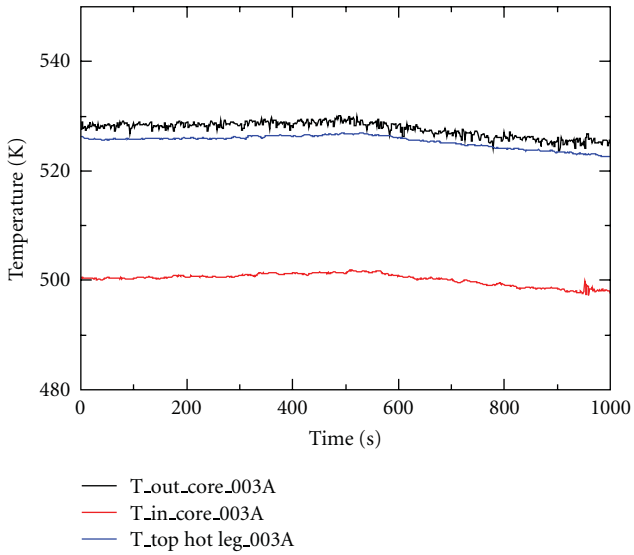

Figure 18: Inlet, outlet core, and top of the hot leg temperature behavior during the OSU-MASLWR-003A test [8].

the previous one, and, anyway, the chocked flow in the high containment line will limit the rate at which the containment and RPV pressure equalize.

Therefore the purpose of the test OSU-MASLWR-003B is to acquire the pressure transient in the containment and the primary system during the "*inadvertent actuation of one high containment ADS valve.*" This test represents a beyond design basis accident scenario for the MASLWR and thermal hydraulically characterizes the RPV/containment coupling and containment vessel condensation behavior during this kind of transient. During the test, core power is zero and there is not preheating of the containment noncondensation surface areas.

When the high ADS valves open, the pressure equalization of the primary side and containment starts, but it is limited by the chocked flow condition at the ADS nozzles.

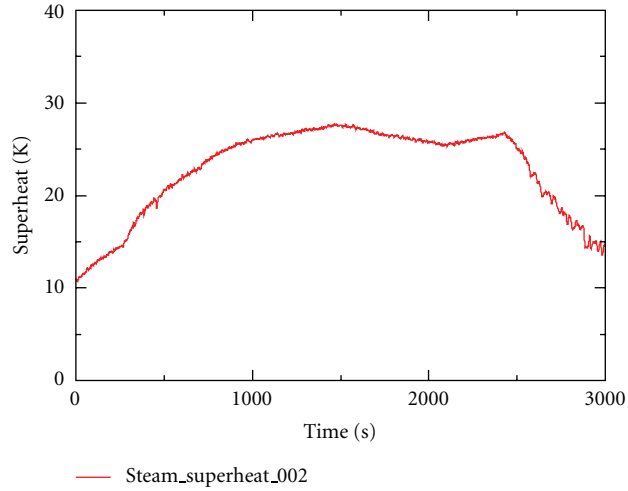

Figure 19: Steam superheat behavior during the OSU-MASLWR-002 test [11].

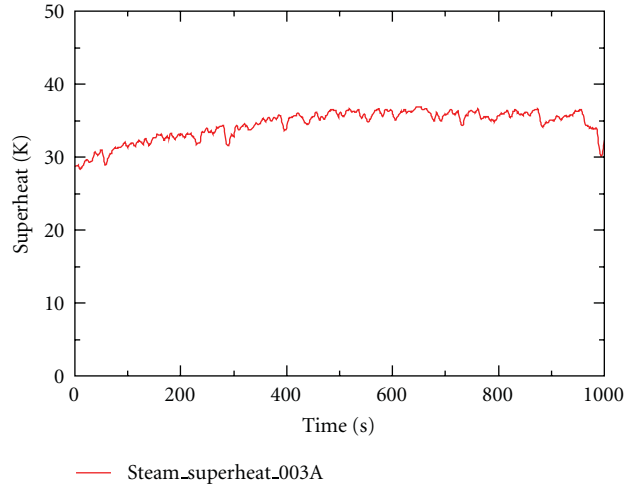

Figure 20: Steam superheat behavior during the OSU-MASLWR-003A test [11].

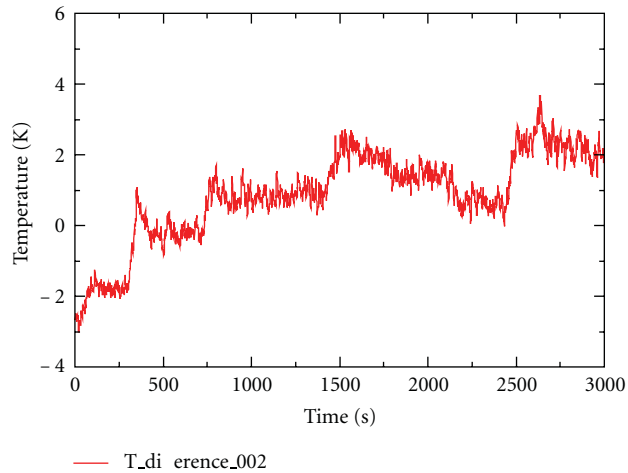

Figure 21: Difference of fluid temperature at the inlet of the core and at the exit of the SG primary side during the OSU-MASLWR-002 test [13, 22].

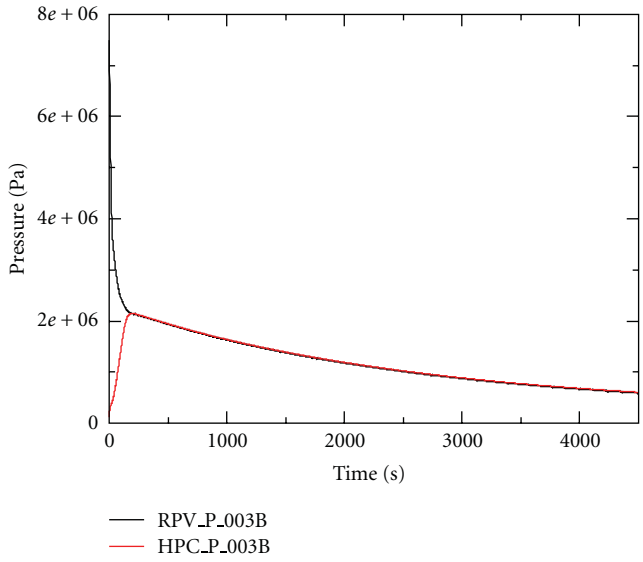

Figure 22: RPV and HPC pressure behaviour during the OSU-MASLWR test 003B [8, 11].

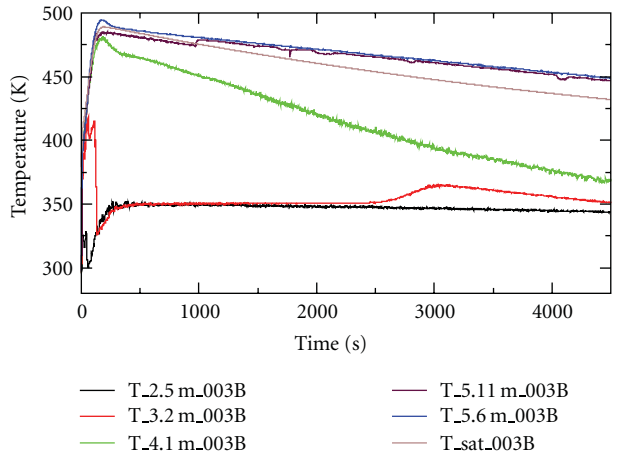

Figure 23: Containment condensation plate wall temperatures behavior during the OSU-MASLWR-003B [8, 11].

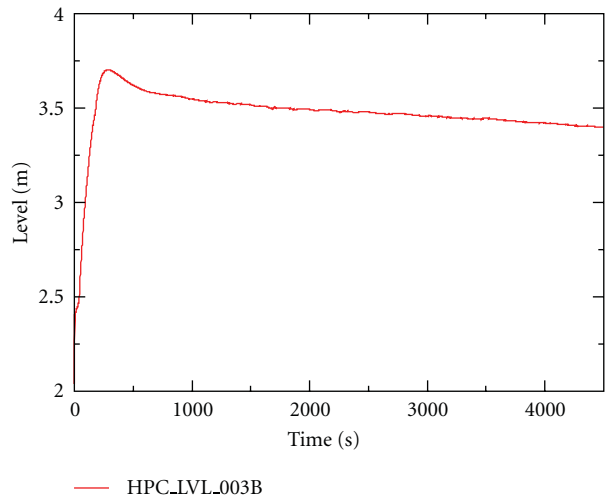

Figure 24: HPC liquid level behaviour during the OSU-MASLWR-003B test [8].

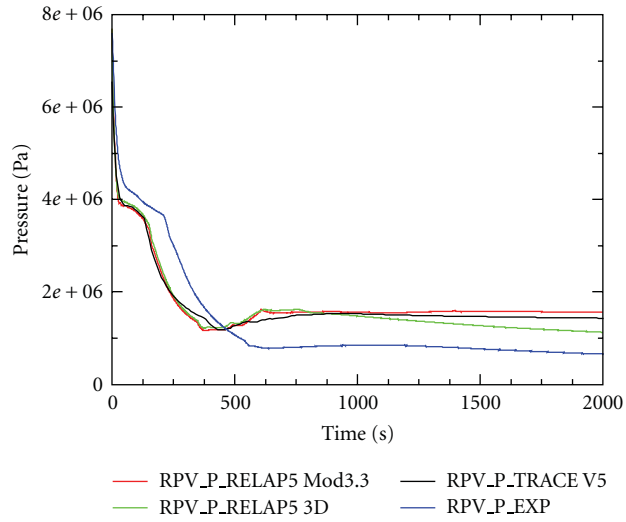

Figure 25: Experimental data versus RELAP5/MOD3.3, RELAP5-3D, and TRACE code calculations for primary system pressure behaviour of the OSU-MASLWR-001 test [23].

The upper part of the HPC is filled with the steam, coming from the primary side, where condensing transfers energy to the CPV. The analyses of the experimental data show that the HPC pressure reaches a maximum at 21.15 bar at 185 s after the SOT. Figure 22 shows the RPV and HPC pressure behaviour.

Since the preheating of the containment noncondensation surface is not considered during the transient, an adiabatic boundary condition in all the wall of the HPC except through the heat transfer plate wall is not maintained; therefore a small distortion at the beginning of the transient is present during the test.

The thermocouples measuring the water temperature located inside the HPC near the heat transfer plate reach quickly the saturation temperature, Figure 23. Since the HPC liquid level reaches about 3.7 m, when the lower thermocouples are submerged, they drop at the liquid temperature, Figure 24. The RPV level water never fell down the upper part of the core during the execution of the test 003B.

5. Code Analyses Performed

Different computer codes have been developed to characterize two-phase flow systems, from a system and a local point of view [1]. Accurate simulation of transient system behavior of a nuclear power plant or of an experimental test facility is the goal of the best estimate thermal hydraulic system codes. The evaluation of a code's calculation accuracy is accomplished by assessment and validation against appropriate system data developed either from a running system prototype or from a scaled model test facility and characterizes the thermal hydraulic phenomena during both steady-state and transient conditions [1, 2, 13, 21–23, 27, 28].

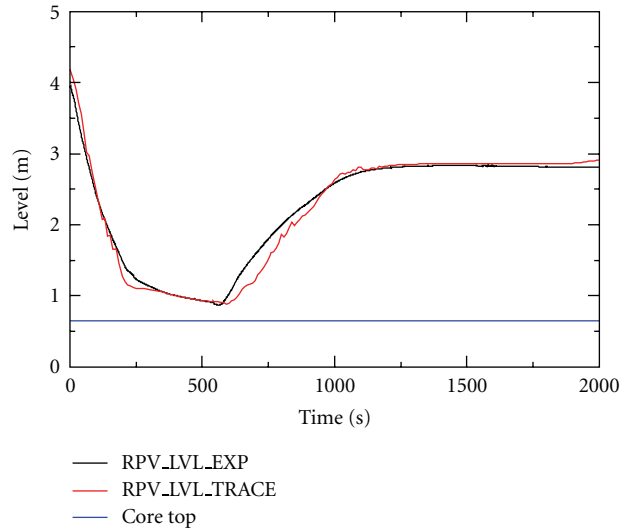

Figure 26: Experimental data versus TRACE V5 patch 02 code calculations for primary system level of the OSU-MASLWR-001 test [1].

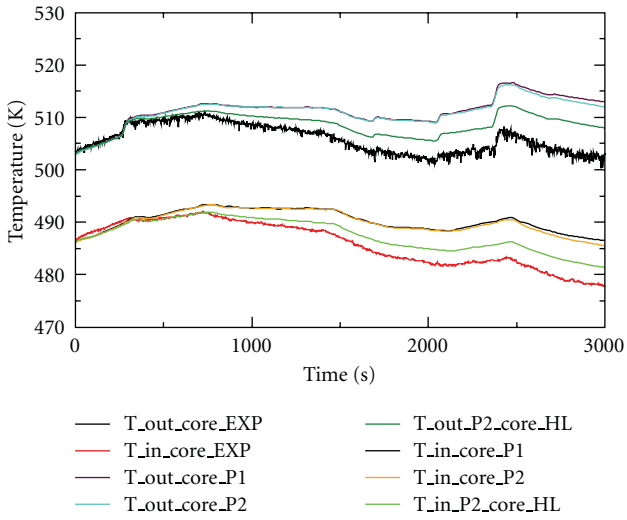

Figure 27: Experimental data versus TRACE V5 code calculations for fluid temperature at the core outlet/inlet of the OSU-MASLWR-002 test [1] (P1 = calculation performed with the TRACE V5 patch 01; P2 = calculation performed with the TRACE V5 patch 02; P2_HL calculation performed with the TRACE V5 patch 02 increasing the heat losses of the TRACE model).

In this framework, different analyses have been performed [1, 2, 13, 21–24, 27, 28], in order to analyze the capability of the best estimate thermal hydraulic system codes to predict the phenomena typical of the MASLWR prototype and their implication to its operation, thermal hydraulically characterized in the OSU-MASLWR test facility. All the previous tests have been analyzed by using different best estimate thermal hydraulic system code. In general the OSU-MASLWR test facility nodalizations qualification process is still in progress, considering the facility experimental characterization distributed in the framework of the previously mentioned IAEA ICSP [14–16, 20].

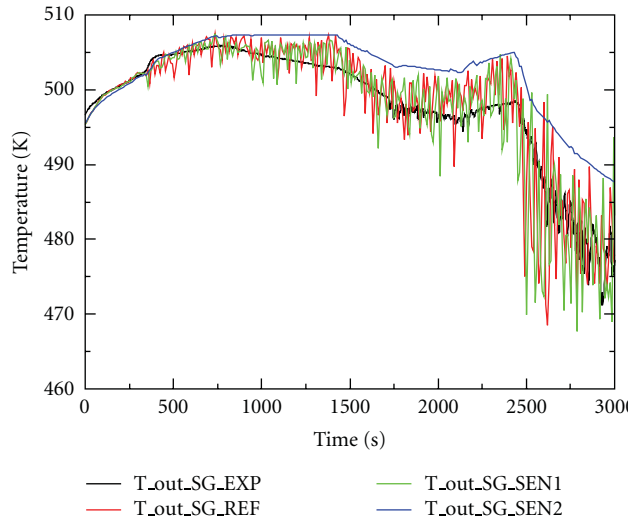

Figure 28: Experimental data versus TRACE V5 patch 01 code calculations for the fluid temperature at the SG coil outlet of the OSU-MASLWR-002 test [13]. (REF = SG coils modelled with three different "equivalent" oblique group of pipes in order to simulate the three separate parallel coils of tubes; SEN1 = SG coils modelled with three different "equivalent" vertical group of pipes; SEN2 = SG coils modelled with only one "equivalent" vertical group of pipes).

5.1. Code Analyses of the OSU-MASLWR-001 Test. The analysis of the OSU-MASLWR-001 test, performed by using RELAP5/MOD3.3, RELAP5-3D, and TRACE [23], shows that the codes are able to qualitative predict primary/containment coupling phenomena characterizing the test. The subcooled, saturated, and single-phase blowdown is predicted by the codes. The refill of the core, permitting its cooling, is predicted as well. The results of the calculated data show a general overprediction compared with the experimental data. It is thought that this could be due to a combination of selection of vent valve discharge coefficients and condensation models applied to the inside surface of the containment [23]. The pressure behaviour of the RPV predicted by these codes is reported in Figure 25. Different update analyses have been developed by using the TRACE code and reported in [1, 21, 22]. Figure 26 shows the experimental data versus code calculations for primary system level for the OSU-MASLWR-001 test predicted by the TRACE code [1].

5.2. Code Analyses of the OSU-MASLWR-002 Test. The analyses of the OSU-MASLWR-002 test, developed by using TRACE [1, 13, 21, 22, 27, 28], show that the TRACE code is able to qualitatively predict natural circulation phenomena and heat exchange from primary to secondary side by helical SG in superheated condition. An overestimation of the inlet/outlet core temperature, Figure 27, is predicted by the code. One of the reasons could be an underestimation of the helical coil heat transfer coefficient during the different phases of the transient.

The subcooled, saturated, and superheated regions of the SG secondary side are predicted by the code resulting in steam superheat at the SG exit, Figure 28. Figure 29, developed by using the symbolic nuclear analysis package

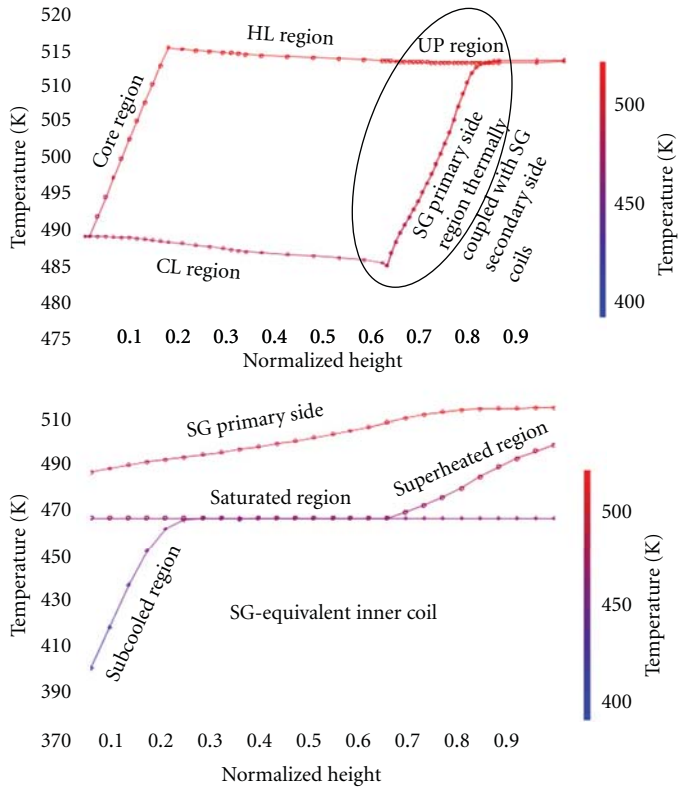

Figure 29: TRACE RPV temperature profile and SG primary side and equivalent inner coil temperature diagram for the OSU-MASLWR-002 test (2605 s after SOT), developed by using SNAP [1].

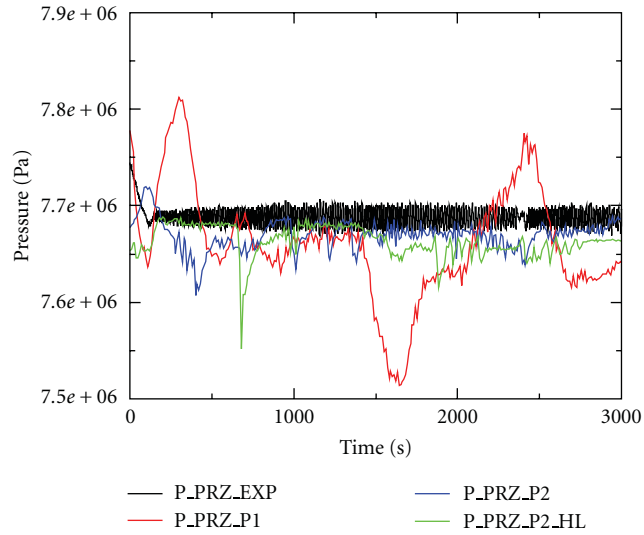

Figure 30: Experimental data versus TRACE V5 code calculations for the PRZ pressure of the OSU-MASLWR-002 test [1]. (P1 = calculation performed with the TRACE V5 patch 01; P2 = calculation performed with the TRACE V5 patch 02; P2_HL calculation performed with the TRACE V5 patch 02 increasing the heat losses of the TRACE model).

(SNAP), shows the fluid temperature profile, calculated by TRACE code, along the entire natural circulation loop. A detail of the fluid temperature profile along the inner helical coil cells and the fluid temperature profile along the SG primary side section are shown as well. From this figure, it is possible to identify the subcooled, saturated, and superheat region, of the inner equivalent helical coil. In agreement with the experimental data, the steam will leave the SG superheated.

The analyses of the TRACE calculated data show that one of the reasons of the instability of the superheat condition of the fluid at the outlet of the SG, already observed in [27], is the equivalent SG model used to simulate the different group of helical coils. In particular, if the helical coils are modelled

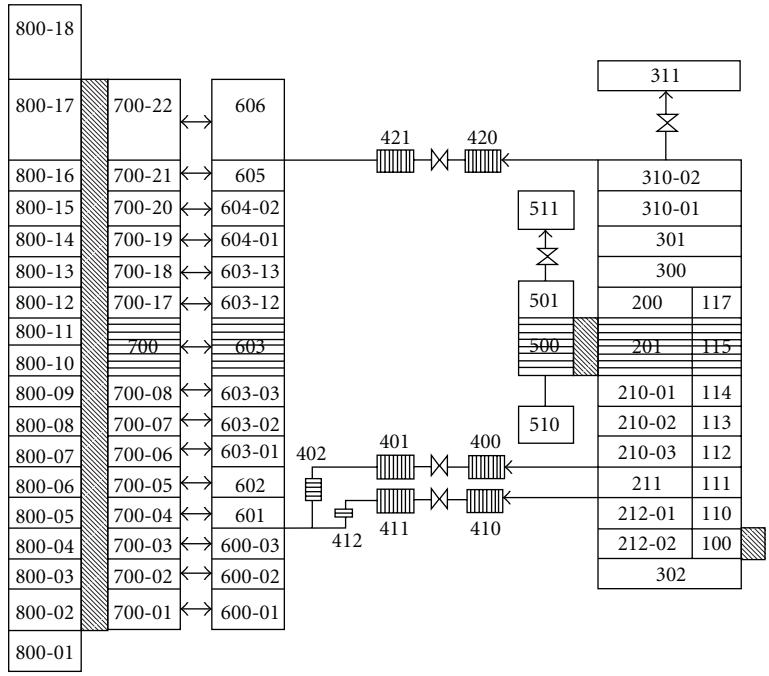

Figure 31: RELAP5-3D nodalization [24].

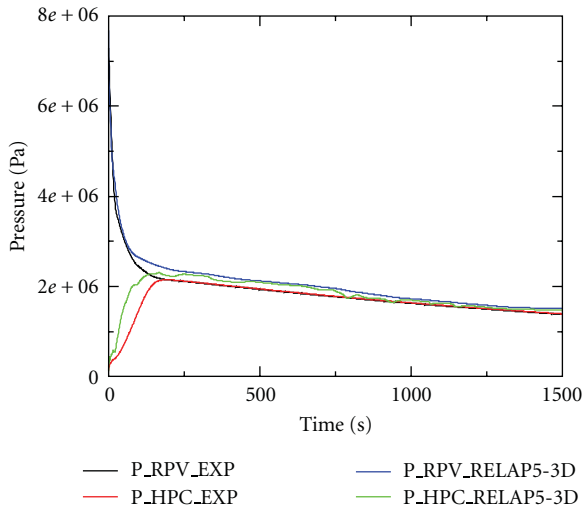

Figure 32: Experimental data versus RELAP5-3D code calculations for the RPV and HPC pressure behaviour of the OSU-MASLWR-003B [24].

by only one "equivalent" vertical tube, a more stable fluid temperature at the outlet of the helical tubes is predicted by the code. The model with three different oblique or vertical tubes needs more investigations, in order to study the possible instability conditions predicted by the code [13].

Previous PRZ pressure discrepancies, Figure 30, predicted by the TRACE V5 patch 01, are now not predicted by the patch 02 that shows, in general, a more stable prediction of PRZ pressure and level [1].

TRACE model heat losses and pressure drop calibration against an experimental characterization is necessary, as it is reported in [1, 13], in order to quantitatively evaluate the capability of these codes to simulate the OSU-MASLWR phenomena and therefore use the calculated data for the code assessment. Figure 27 shows the behavior of inlet/outlet core temperature by increasing the heat losses of the TRACE model.

5.3. Code Analyses of the OSU-MASLWR-003 Test. Analyses of the OSU-MASLWR-003 test [24] performed by using the RELAP5-3D code show a general qualitative agreement of the RPV and HPC pressure during the transient. Figure 31 shows the RELAP5-3D nodalization, and Figure 32 shows the RPV and HPC pressure behaviour predicted by the code during its simulations [24].

6. Activity Related to the OSU-MASLWR Facility

6.1. Phenomena Simulating Capability of the Facility. The purpose of the OSU-MASLWR test facility is to assess the prototypical MASLWR under normal operation conditions and to assess the passive safety systems under transient conditions. To this end, as said before, four tests were conducted [8–13].

The planned work of OSU, related to the OSU-MASLWR test facility, will be of value not only to specifically investigate the MASLWR concept design further but advance the broad understanding of integral natural circulation reactor plants and accompanying passive safety features as well. Topics of interest for integral reactor plants, which could be investigated in the OSU-MASLWR test facility, are flow stability under normal and transient conditions, the coupled containment-reactor vessel depressurization, and the emergency cooldown.

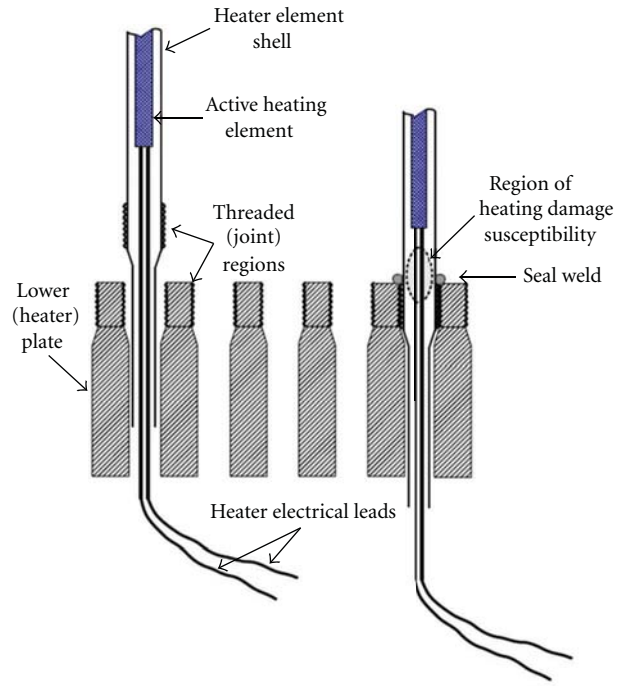

Figure 33: Sketch of original core design heater installation [12].

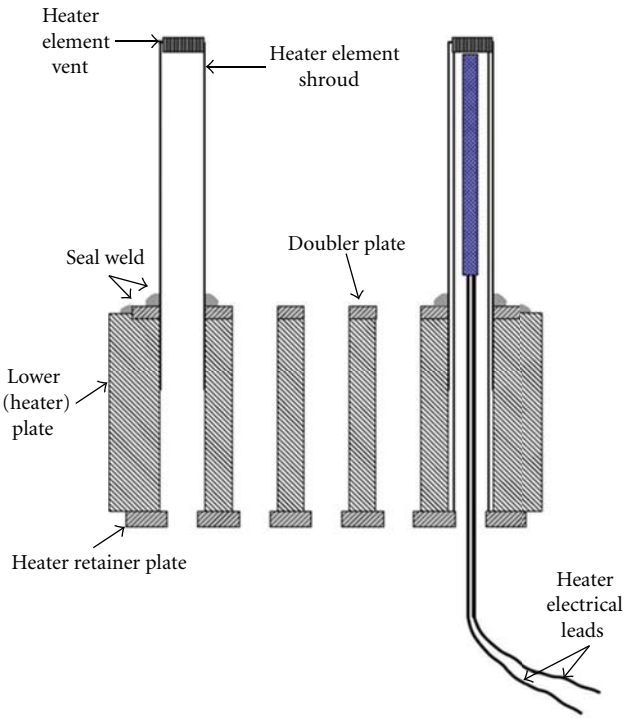

Figure 34: Sketch of modified core design heater installation [12].

In relation to the flow stability analyses, issues of interest are, for example, the investigation of primary flow rate versus heater power as a function of inlet subcooling, primary system pressure, and rate of heat removal by the SG; an investigation of primary loop fluid flow rate and its stability during long-term postaccident cooling conditions; an investigation of primary fluid flow stability during start up, maneuvering and shutdown transients.

In relation to the coupled containment-reactor vessel depressurization and emergency cooldown, issues of interest are, for example, a parametric investigation of the containment pressure behaviour and containment condensation during an automatic depressurization of the RPV; the analyses of the cooldown capability of the containment-reactor vessel coupling system by the helical coil SG; a parametric investigation of containment-reactor vessel pressure behaviour and containment condensation during a SBLOCA with or without the SG cooldown of the containment-reactor vessel coupled system.

Different parametric studies could be executed in the facility if its modifications are taken into account. An investigation of primary loop fluid flow rate and its stability as a function of heater power for various loop resistance condition, if through facility modification the loop resistance changes, could be of interest. By including in the facility a gravity FW tank, it is possible to study a parametric investigation of containment condensation and pressure behavior during a SBLOCA with a cooldown of the coupled containment-primary system using gravity-driven FW flow to the helical coil SG.

Considering the potential phenomena that could be investigated in this facility, an IAEA ICSP on "Integral PWR Design Natural Circulation Flow Stability and Thermo-hydraulic Coupling of Primary System and Containment During Accidents" is being hosted at OSU, and the experimental data will be collected at the OSU-MASLWR facility. The purpose of this IAEA ICSP is to provide experimental data on single-/two-phase flow instability phenomena under natural circulation conditions and coupled containment/reactor vessel behavior in integral-type light water reactors.

6.2. OSU-MASLWR Test Facility Core Modification Description. After the completion of the first test series, through a grant from the IAEA, the OSU-MASLWR test facility core was reconfigured [12] to eliminate a recurring grounding problem and improve facility reliability in anticipation of conducting the previous mentioned IAEA ICSP.

Figure 33 shows a sketch of original core design heater installation. The heater on the left is shown prior to seating into the lower heater plate. On right is view of an installed heater, indicating region of susceptibility of the electrical leads due to heat from the seal welding process.

Figure 34 shows a sketch of modified core design heater installation. The heater rod shroud on the left is inserted into the lower heater plate and seal welded prior to heater insertion from the bottom. On right is view of installed heater, held in heater shroud cavity by heater retainer plate.

Although a relatively minor modification to a complex and highly capable facility, both the availability for high power and rapid transient natural circulation phenomenology testing as well as the spectrum of operating transients that can be investigated using the test facility have been greatly improved [12, 15].

6.3. IAEA International Collaborative Standard Problem on OSU-MASLWR. In September 2006, a MASLWR Natural

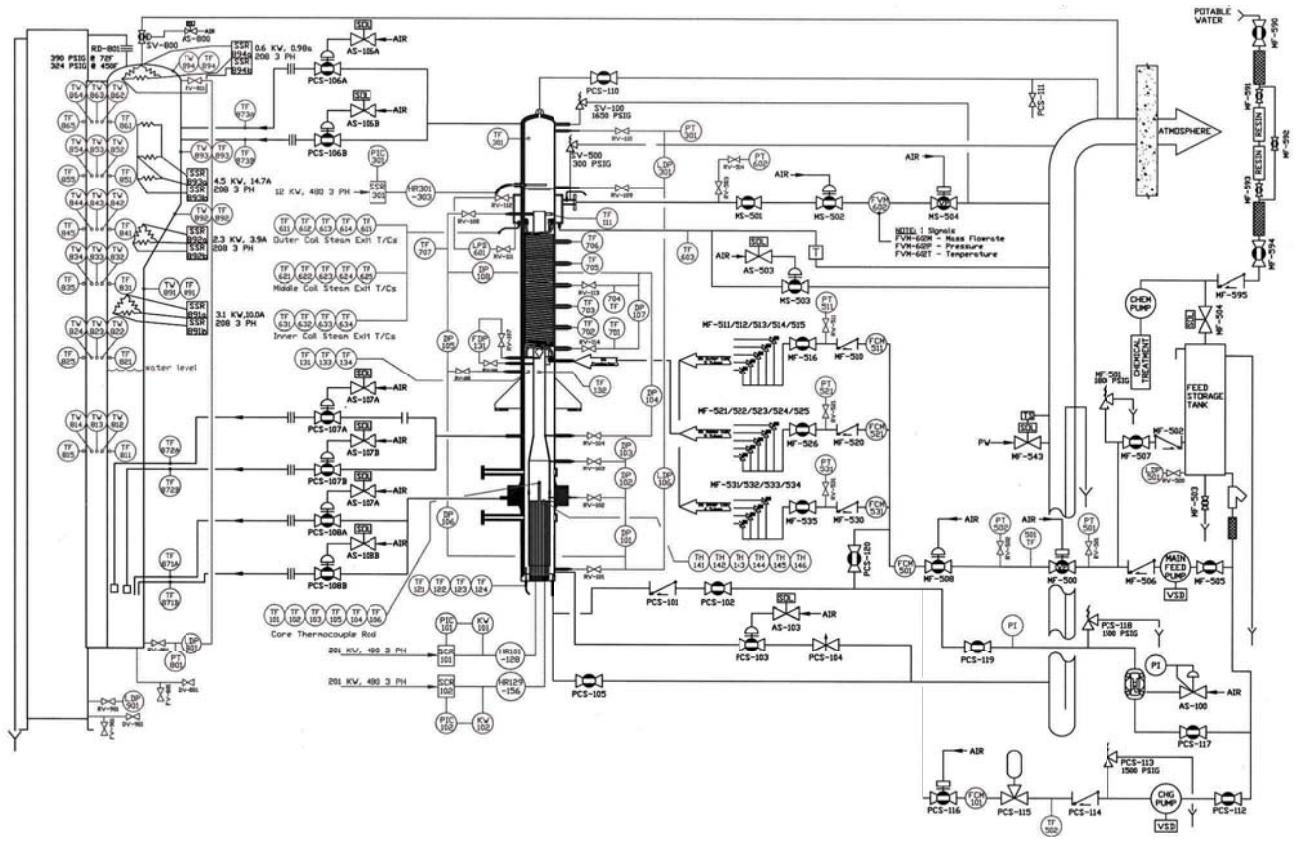

Figure 35: OSU-MASLWR test facility process and instrumentation diagram [20].

Figure 36: Photo of variable-position throttle valve located at the entrance of each helical coil.

Circulation Standard Problem Working Group was formed within the IAEA Coordinated Research Project (CRP) on Natural Circulation Phenomena, Modelling, and Reliability that Utilize Natural Circulation. Its purpose is to provide experimental data on flow instability phenomena under natural circulation conditions and coupled containment/reactor vessel behavior in integral-type reactors. A thermal hydraulic design test, ICSP test 1, involving a stepwise reduction in primary mass inventory of the facility while operating at reduced power (decay power), and an integral system safety test, ICSP test 2, involving a loss of FW transient with subsequent ADS blowdown and long-term cooling will be executed. These data can be used to assess computer codes for reactor system design and analysis. The ICSP is being hosted at OSU, and the experimental data will be collected at the OSU-MASLWR [1, 2, 14–16].

During the ICSP test 1, twelve different primary side water levels will be investigated. A valve located in the draining line of the facility is opened in order to drain the facility to fixed primary level set points. Following the ICSP specification each step is maintained for approximately 45 minutes in order to reach steady-state conditions. The inventory will not be reduced more than the 35% in order to prevent the core from becoming uncovered. The main target of this test is to examine the effect of mass inventory reduction on natural circulation flow rate in the small integral PWRs providing data on single-/two-phase flow instability phenomena.

The main target of the ICSP test 2 is to provide data on containment/reactor vessel behavior in integral-type light water reactor by examining the blow-down transient into the containment in a small integral PWR as a results of normal ADS opening and the subsequent long-term cooling phase using the sump natural circulation. Considering the maximum HPC operating pressure, different actions for the ADS valves are taken into account.

The ICSP will be conduct in three different phases: a "double blind phase," a "blind phase," and a "open phase."

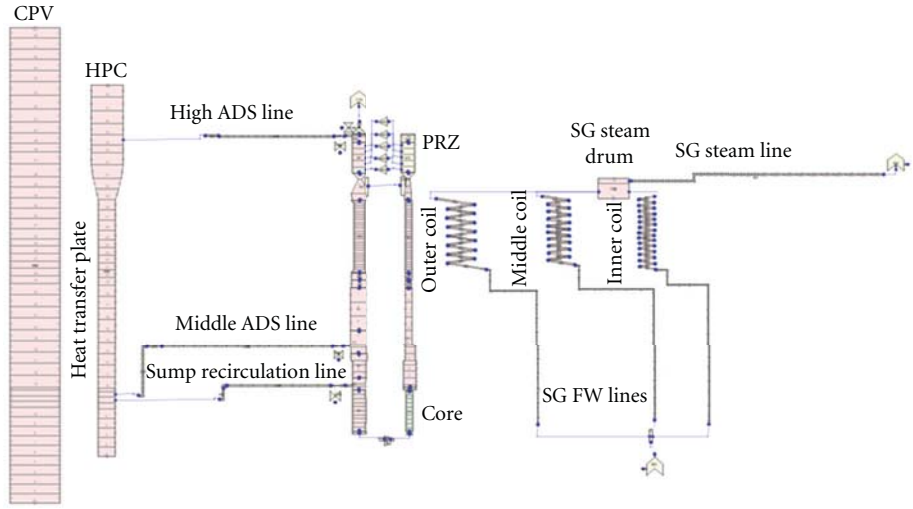

Figure 37: TRACE model developed for the participation at the IAEA ICSP [2, 25, 26].

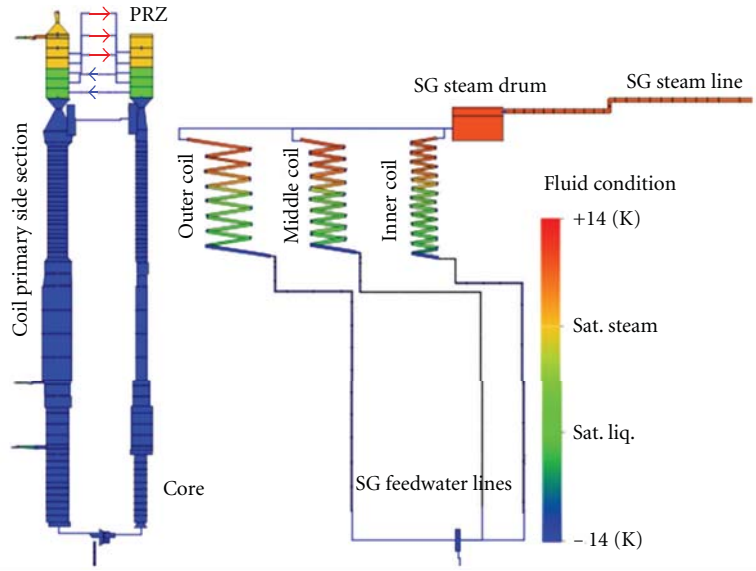

Figure 38: Facility fluid configuration, during the steady state analyses before the SOT of the ICSP test 1 [2, 25, 26].

During the "double blind phase," the ICSP tests have not been performed yet, and only test procedures with the specification boundary and initial condition are available at the ICSP participation. Then the ICSP participant will submit the so-called "double blind calculations." During the "blind phase," the test will be already conducted and only some selected real initial and boundary conditions will be available at the ICSP participants. Then the ICSP participants will submit the "blind calculations." At the end, the experimental data will be disclosed to the ICSP participant that will submit the "open calculation."

A detailed updated OSU-MASLWR test facility process and instrumentation diagram, distributed in the ICSP framework, is reported in the Figure 35. Figure 36 shows a photo of the variable-position throttle valve located at the entrance of each helical to allow to increase the pressure drop of the different helical coil in order to increase the stability of the circuit and to close some coils.

A TRACE model developed to participate at the IAEA ICSP is shown in Figure 37 [26]. An animation model, developed by using SNAP, is shown in Figure 38 and represents the fluid condition configuration of the facility before the SOT of the ICSP test 1 [2, 25, 26].

7. Conclusions

Oregon State University has constructed a system-level test facility to examine natural circulation phenomena of importance to MASLWR, a small modular integral PWR relying on natural circulation during both steady-state and transient operation.

Four tests have been conducted, in support of the MASLWR concept design verification, in the experimental facility. The MASLWR normal startup, the operation, and its shutdown are thermal hydraulically demonstrated. The behavior of the RPV and containment and their coupling is

thermal hydraulically demonstrated during a design basis accident test, "*inadvertent actuation of one middle ADS valve*" (OSU-MASLWR-001), and during a beyond design basis accident test, "*inadvertent actuation of one high containment ADS valve*" (OSU-MASLWR-003B). During these two tests, the RPV level never fell below the top of the core.

Since the degree of the steam superheat is changed in order to control the facility, the primary system flow rates and secondary side steam superheat for a variety of core power levels and FW flow rate were collected in the OSU-MASLWR-002 and 003A test.

Currently, considering the phenomena simulating capability of this facility, an IAEA ICSP on "Integral PWR Design Natural Circulation Flow Stability and Thermo-hydraulic Coupling of Primary System and Containment During Accidents" is being hosted at OSU and the experimental data will be collected at the OSU-MASLWR facility, to provide experimental data on single-/two-phase flow instability phenomena under natural circulation conditions and coupled containment/reactor vessel behavior in integral-type light water reactors.

Different analyses have been performed in order to analyze the capability of the best estimate thermal hydraulic system codes to predict the phenomena typical of the MASLWR prototype and their implication to its operation, thermal hydraulically characterized in the OSU-MASLWR facility. All the previous tests have been analyzed by using different best estimate thermal hydraulic system code. The results of the calculated data show that the selected best estimate thermal hydraulic system codes are in general able to qualitatively predict the phenomena typical of the MASLWR prototype design as the single- and two-phase natural circulation, the heat exchange from primary to secondary side by helical SG in superheated condition and primary/containment coupling. Considering the potential phenomena that can be investigated in the facility, the experimental data developed during the IAEA ICSP tests will be useful for the assessment of the thermal hydraulic codes for reactor system design and analysis of integral-type light water reactor.

In order to quantitatively evaluate the capability of these codes to simulate the OSU-MASLWR phenomena, and therefore use the calculated data for the code assessment, is necessary a code nodalization qualification against several facility operational characteristic like pressure drop at different primary mass flow rates and heat losses at different primary side temperatures. These experimental characterizations are currently under development in the ICSP framework.

Since the MASLWR prototype is the basis for the NuScale, Inc. reactor, the OSU-MASLWR experimental facility will be useful for the NuScale testing for safety and operation [29].

Abbreviations

ADS: Automatic depressurization system
AP600/1000: Advanced plant 600/1000 MWe
CAREM: Natural circulation-based PWR being developed in Argentina
CL: Cold leg
CRP: Coordinate research project
ESBWR: Economic simplified boiling water reactor
FW: Feedwater
HL: Hot leg
HPC: High-pressure containment
IAEA: International Atomic Energy Agency
ICSP: International Collaborative Standard Problem
IRIS: International Reactor Innovative and Secure
LOCA: Loss of coolant accident
LP: Lower plenum
MFW: Main feed water
MASLWR: Multi-application small light water reactor
MS: Main steam
OSU: Oregon State University
PRZ: Pressurizer
PWR: Pressurized water reactor
RPV: Reactor pressure vessel
SASM: Severe accident scaling methodology
SBLOCA: Small-break LOCA
SG: Steam generator
SOT: Start of transient
SMART: System integrated modular advanced reactor
SNAP: Symbolic nuclear analysis package
SWR-1000: Siedewasser reaktor, 1000 MWe
TRAC: Transient reactor analysis code
TRACE: TRAC/RELAP advanced computational engine
UP: Upper plenum
USNRC: US Nuclear Regulatory Commission
WWER: Water moderate, water-cooled energy reactor.

References

[1] F. Mascari, G. Vella, B. G. Woods, and F. D'Auria, "Analysis of the Multi-Application Small Light-Water Reactor (MASLWR) design natural circulation phenomena," in *Proceedings of the International Congress on Advances in Nuclear Power Plants (ICAPP '11)*, Nice, France, May 2011.

[2] F. Mascari, G. Vella, and B. G. Woods, "TRACE code analyses for the IAEA ICSP on integral PWR design natural circulation flow stability and thermo-hydraulic coupling of containment and primary system during accidents," in *Proceedings of the ASME Small Modular Reactors Symposium (SMR '11)*, Washington, DC, USA, September 2011.

[3] J. Cleveland, "Overview of Global Developments of Advanced Nuclear Power Plants," Annex 1, Natural Circulation In Water Cooled Nuclear Power Plants Phenomena, Models, And Methodology For System Reliability Assessments, IAEA TECDOC 1474, November 2005.

[4] IAEA-TECDOC-1281, "Natural Circulation Data and Methods for Advanced Water Cooled Nuclear Power Plant Design," April 2000.

[5] IAEA TECDOD-1474, "Natural Circulation in Water Cooled Nuclear Power Plants," November 2005.

[6] IAEA-TECDOC-1391, "Status of Advanced Light Water Reactor Designs 2004," May 2004.

[7] F. Mascari, G. Vella, P. Buffa, A. Compagno, and E. Tomarchio, "Passive safety systems in view of sustainable development," Final Report on the Round Tables, Erasmus Intensive Programme Project (IP) ICARO Intensive Course on Accelerator and Reactor Operation, Sicilia, Italia.

[8] S. M. Modro, J. E. Fisher, K. D. Weaver et al., "Multi-Application Small Light Water Reactor Final Report. DOE Nuclear Energy Research Initiative Final Report," Idaho National Engineering and Environmental Laboratory, December 2003.

[9] J. N. Reyes Jr. and J. King, "Scaling Analysis for the OSU Integral System Test Facility," Department of Nuclear Engineering Oregon State University 116 Radiation Center Corvallis, OR 97331-5902 NERI Project 99-0129, Prepared For U.S. Department of Energy.

[10] J. N. Reyes Jr., "Integral System Experiment Scaling Methodology," Annex 11, Natural Circulation In Water Cooled Nuclear Power Plants Phenomena, Models, And Methodology For System Reliability Assessments, IAEA TECDOC 1474, November 2005.

[11] J. N. Reyes Jr., J. Groome, B. G. Woods et al., "Testing of the multi-application small light water reactor (MASLWR) passive safety systems," *Nuclear Engineering and Design*, vol. 237, no. 18, pp. 1999–2005, 2007.

[12] M. R. Galvin, "OSU MASLWR Test Facility Modification Description Report," IAEA Contract Number USA-13386, Oregon State University, November, 2007.

[13] F. Mascari, G. Vella, B. G. Woods et al., "Sensitivity analysis of the MASLWR helical coil steam generator using TRACE," *Nuclear Engineering and Design*, vol. 241, no. 4, pp. 1137–1144, 2011.

[14] B. G. Woods and F. Mascari, "Plan for an IAEA International Collaborative Standard Problem on Integral PWR Design Natural Circulation Flow Stability and Thermo-Hydraulic Coupling of Containment and Primary System During Accidents," Department of Nuclear Engineering and Radiation Health Physics, Oregon State University, prepared for IAEA.

[15] B. G. Woods, M. R. Galvin, and B. C. Jordan, "Problem Specification for the IAEA International Collaborative Standard Problem on Integral PWR Design Natural Circulation Flow Stability and Thermo-Hydraulic Coupling Of Containment and Primary System During Accident," DRAFT.

[16] J. H. Choi, *Second Workshop of IAEA ICSP on Integral PWR Design Natural Circulation Flow Stability and Thermo-hydraulic Coupling of Containment and Primary System during Accidents*, Presentation, Vienna, Austria, March 2011.

[17] S. Levy, *Two-Phase Flow in Complex Systems*, Wiley-Interscience, New York, NY, USA, 1999.

[18] "An Integrated Structure and Scaling Methodology for Severe Accident Technical Issue Resolution," NUREG/CR-5809.

[19] N. Zuber, "Appendix D: Hierarchical, Two-Tiered Scaling Analysis," An Integrated Structure and Scaling Methodology for Severe Accident Technical Issue Resolution, U.S Nuclear Regulatory Commission, Washington, DC, USA, 20555, NUREG/CR-5809, November 1991.

[20] A. Weiss, J. Bowser, M. Galvin, and B. Woods, OSU MASLWR drawings. 2010.

[21] F. Mascari, G. Vella, B. G. Woods, M. Adorni, and F. D'Auria, "Analysis of the OSU-MASLWR natural circulation phenomena using TRACE code," in *Proceedings of the Technical Meeting on Application of Deterministic Best Estimate Safety Analysis*, University of Pisa, Pisa, Italy, September 2009, IAEA, organized in cooperation with the OECD Nuclear Energy Agency and the European Commission.

[22] F. Mascari, *Natural circulation and phenomenology of boron dilution in the pressurzied water reactors (circolazione naturale e fenomenologie di boron dilution in reattori ad acqua in pressione)*, Ph.D. thesis, University of Palermo, 2010.

[23] J. Pottorf, F. Mascari, B. G. Woods et al., "TRACE, RELAP5 Mod 3.3 and RELAP5-3D code comparison of OSU-MASLWR-001 test," in *Proceedings of the American Nuclear Society Winter Meeting and Nuclear Technology Expo*, vol. 101, Transactions of the American Nuclear Society, 2009.

[24] B. G. Woods, "Analysis of RELAP5-3D Modeling Techniques for Natural Circulation Small Integral Light Water Reactors," Department of Nuclear Engineering and Radiation Health Physics Oregon State University Prepared for NuScale, Inc., 2008.

[25] F. Mascari and G. Vella, "IAEA International Collaborative Standard Problem on Integral PWR Design Natural Circulation Flow Stability and Thermo-hydraulic Coupling of Containment and Primary System during Accidents Double Blind Calculation Results," Presentation, II Technical Meeting IAEA ICSP, March 2011.

[26] F. Mascari and G. Vella, "IAEA international collaborative standard problem on integral PWR design natural circulation flow stability and thermo-hydraulic coupling of containment and primary system during accidents double blind calculation results," Tech. Rep., Dipartimento dell'Energia, Università degli Studi di Palermo, Palermo, Italy, February 2011, Prepared for International Atomic Energy Agency.

[27] F. Mascari, B. G. Woods, and M. Adorni, "Analysis, by TRACE Code, of natural circulation phenomena in the MASLWR-OSU-002 test," in *Proceedings of the International Conference Nuclear Energy for New Europe*, Portoroz, Slovenia, September 2008.

[28] F. Mascari, G. Vella, B. G. Woods et al., "Sensitivity analysis of the MASLWR helical coil steam generator using TRACE," in *Proceedings of the International Conference Nuclear Energy for New Europe*, Bled, Slovenia, September 2009.

[29] NuScale's Passive Safety Approach, Presentation, NuScale Power, Inc. April 2011, http://www.nuscalepower.com/ot-Nuclear-Power-Presentations.php.

Hindawi Publishing Corporation
Science and Technology of Nuclear Installations
Volume 2012, Article ID 375070, 18 pages
doi:10.1155/2012/375070

Research Article

Major Achievements and Prospect of the ATLAS Integral Effect Tests

Ki-Yong Choi, Yeon-Sik Kim, Chul-Hwa Song, and Won-Pil Baek

Korea Atomic Energy Research Institute, Daedeok-daero 989-111, Yuseong-Gu, Daejeon 305-353, Republic of Korea

Correspondence should be addressed to Ki-Yong Choi, kychoi@kaeri.re.kr

Received 15 August 2011; Accepted 12 November 2011

Academic Editor: Klaus Umminger

A large-scale thermal-hydraulic integral effect test facility, ATLAS (Advanced Thermal-hydraulic Test Loop for Accident Simulation), has been operated by KAERI. The reference plant of ATLAS is the APR1400 (Advanced Power Reactor, 1400 MWe). Since 2007, an extensive series of experimental works were successfully carried out, including large break loss of coolant accident tests, small break loss of coolant accident tests at various break locations, steam generator tube rupture tests, feed line break tests, and steam line break tests. These tests contributed toward an understanding of the unique thermal-hydraulic behavior, resolving the safety-related concerns and providing validation data for evaluation of the safety analysis codes and methodology for the advanced pressurized water reactor, APR1400. Major discoveries and lessons found in the past integral effect tests are summarized in this paper. As the demand for integral effect tests is on the rise due to the active national nuclear R&D program in Korea, the future prospects of the application of the ATLAS facility are also discussed.

1. Introduction

ATLAS (Advanced Thermal-Hydraulic Test Loop for Accident Simulation) is a large-scale integral effect test facility with a reference plant of APR1400 (Advanced Power Reactor, 1400 MWe), which is under construction in Korea [1]. It was designed to have the capability of simulating various transients and accident conditions at full pressure and temperature conditions, including loss of coolant accident (LOCA) series as well as non-LOCA series. The ATLAS program started in 1997 under a nuclear R&D program funded by the Korean government. The complete installation of ATLAS was finished in 2005. In 2006, extensive commissioning operations were carried out, including startup tests and preliminary tests [2].

In 2007, ATLAS was used for a wide range of integral effect tests on the reflood phase of a large break LOCA to resolve the safety issues of the APR1400 raised by a regulatory body [3]. Afterwards, at the beginning of 2008, ATLAS was modified to have a configuration for simulating the direct vessel injection (DVI) line break accidents of the APR1400. One of the unique design features of ATLAS is its ability to simulate the DVI of the emergency core cooling water. Sensitivity tests for different DVI line break sizes were performed and an integral effect database was established for various break sizes of 5%, 25%, 50%, and 100% [4].

After a series of DVI line break tests were completed, small break LOCA (SBLOCA) tests commenced at the end of 2008. In order to provide an integral effect database for SBLOCA of the APR1400, sensitivity tests for different break sizes of the cold leg have been conducted. In addition, parameter survey tests were also taken into account in a test matrix in order to investigate the effects of break location. In addition, a counterpart test to the 6-inch SBLOCA data of the Large-Scale Test Facility (LSTF) in Japan was performed in order to evaluate the scaling of the ATLAS facility.

Among the DVI line break scenarios, 50% of the cross-section of a DVI nozzle was of interest because this break size is on the edge of the criterion provided by the EPRI requirement, where a core uncovery should be prevented by a best-estimate methodology [5]. In particular, the thermal-hydraulic phenomena occurring in the upper annulus downcomer region between the DVI nozzle and the cold leg nozzles are expected to be complicated due to the countercurrent flow of the upward break flow and the downward safety injection flow. Thus, the 50% DVI line break database was

selected as the 50th International Standard Problem (ISP-50) sponsored by the OECD/NEA Committee on the Safety on Nuclear Installation (CSNI) Working Group on Analysis and Management of Accidents (WGAMA) in 2009. The ISP-50 was started with a blind calculation, followed by an open calculation. It was successfully finished by approval of CSNI in 2011 [6].

The steam generator tube rupture (SGTR) events were investigated from the year 2010. A single-tube rupture and five-tube rupture events were successfully simulated in the ATLAS facility. The effects of leakage from either the hot side or cold side were examined for sensitivity work.

When the major integral effect tests on LOCA series accidents were completed, typical non-LOCA events were conducted from the second half of the year 2010, including the feed line break (FLB) and steam line break (SLB). Tests were performed either in conservative or in best-estimated initial and boundary conditions to support the nuclear industry and validate the safety analysis codes, respectively.

2. Scaling Methodology of the ATLAS

The three-level scaling methodology which consists of integral scaling, boundary flow scaling, and local phenomena scaling proposed by Ishii et al. [7] was applied to the design of ATLAS. There have been plenty of discussions concerning the height scaling, and finally the 1/2 height scaling was chosen based on the following key rationales [1]. (a) There is no absolute superiority between full- and half-height designs, and a decision should be made by considering the test objectives, prototype design characteristics, budget, and so on. (b) The integrated annular downcomer, which can be realized more easily in the half-height design, is superior to an externally separated downcomer in simulating multi-dimensional phenomena in a reactor vessel downcomer and in revealing new phenomena. (c) In the case of a direct vessel injection, the thermal-hydraulic phenomena expected to occur in the upper downcomer of the reactor vessel need further physical understanding. (d) There is no Integral Effect Test (IET) data for an Reactor Coolant System (RCS) with a DVI as in the APR1400; test data for the LBLOCA reflood and DVI line break will be valuable for a phenomena understanding and code assessment. (e) Air-water visualization tests reveal that there is no significant difference in the flow patterns for downcomer gaps of over around 2.5 cm [8]. (f) A lower height than 1/2 would induce too high a surface heat flux and many difficulties during the installation stage. Finally, the 1/2-height, 1/144-area scaling was selected by considering the available downcomer gap size, flow velocity, and nozzle distance [8].

After the integral scaling ratio was determined, in the second scaling level a boundary flow scaling methodology was applied, especially to the design of the break nozzle, containment, and relief valves. Mass inventory and energy balance was carefully taken into account to minimize scaling distortion during integral effect tests. For instance, several sets of spool pieces were fabricated depending on the test scenarios.

Table 1: Scaling table of the ATLAS facility.

Parameters	Scaling law	ATLAS design
Length	l_{OR}	1/2
Diameter	d_{OR}	1/12
Area	${d^2}_{OR}$	1/144
Volume	$l_{OR}{d^2}_{OR}$	1/288
Velocity	${l^{1/2}}_{OR}$	$1/\sqrt{2}$
Time	${l^{1/2}}_{OR}$	$1/\sqrt{2}$
Flow rate	$l^{1/2}_{OR}{d^2}_{OR}$	1/203.6
Core ΔT	ΔT_{OR}	1
Core power	${l^{1/2}}_{OR}{d^2}_{OR}$	1/203.6
Heat flux	$1/{l^{1/2}}_{OR}$	$\sqrt{2}$
Power/volume	$1/{l^{1/2}}_{OR}$	$\sqrt{2}$
Pressure drop	l_{OR}	1/2
Pump head	l_{OR}	1/2
Core rod diameter	1	1
SG U-tube diameter	${l^{1/2}}_{OR}$	$1/\sqrt{2}$
No. of core rods	${d^2}_{OR}$	1/144
No. of SG U-tubes	N_{OR}	1/72
SG U-tube heat transfer area	$l_{OR}{l^{1/2}}_{OR}N_{OR}$	1/203.6

In the third scaling level, local important phenomena which should be preserved in a scaled facility were examined, and the design was optimized to preserve those phenomena. In the primary piping, a flow pattern and a flow regime transition are the key phenomena, and the Froude number governs such phenomena. Thus, the horizontal sections of the primary piping were optimized to preserve the Froude number in ATLAS. Important local phenomena to be considered in a pressurizer are the critical flow of the surge line for LBLOCA, the critical flow of the safety valves, the CCFL in the surge line, and the offtake at the hot leg-to-surge line. Specially designed sleeves that can be easily installed and removed were manufactured and can be used depending on the test of interest. Void fraction and flow regime transition are the key local phenomena to be preserved in a reactor pressure vessel (RPV) downcomer gap, especially when boiling occurs. Finally, the downcomer gap size was slightly increased from 21 mm to 26.2 mm to preserve the effects of flow regime. The increased downcomer volume was counterbalanced by decreasing the same amount of volume in the lower plenum of the reactor pressure vessel. The major phenomena of concern in the steam generator are CCFL in the U-tubes and forward/reverse heat transfer. The internal tube diameter can be determined either by preserving the Wallis number, or heat transfer area. Here, the Wallis number of each phase j_k^* is defined as the follows:

$$j_k^* = \frac{j_k}{\sqrt{gD\left(\rho_f - \rho_g\right)/\rho_k}}, \tag{1}$$

where j_k^* and ρ_k are the superficial velocities and densities of phase k ($k = g$ for gas phase and $k = f$ for liquid phase), D is the tube diameter, and g the gravitational acceleration. In ATLAS, the U-tube diameter was determined by preserving the heat transfer area. A summarized scaling table of the ATLAS facility is shown in Table 1.

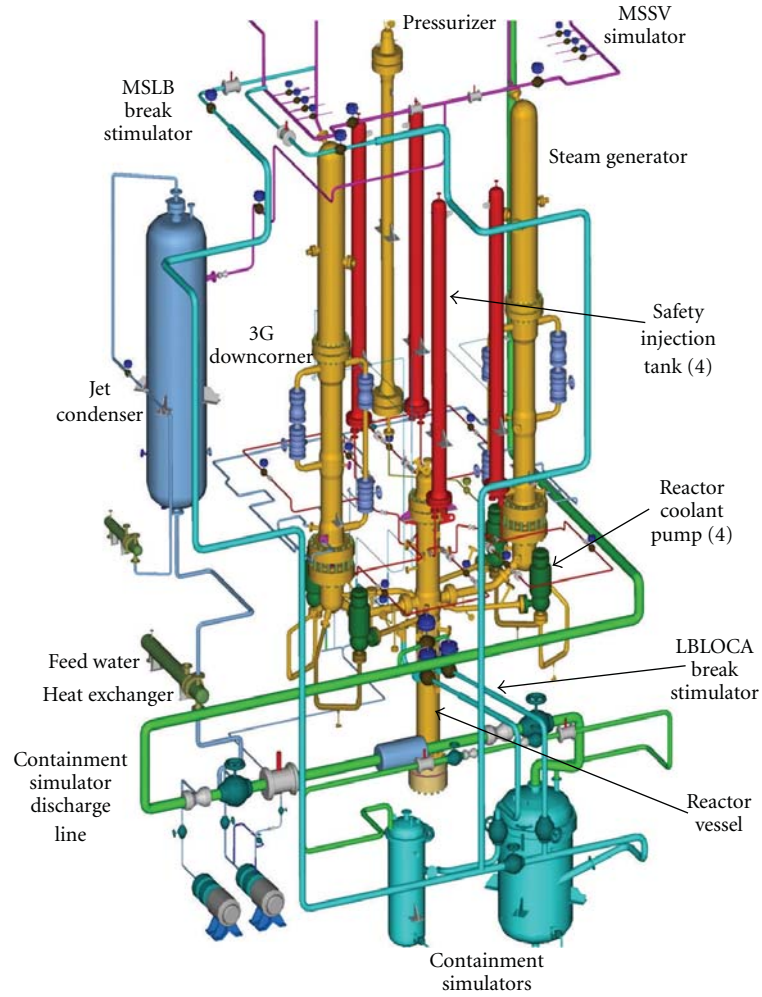

Figure 1: Schematic arrangement of the major components of ATLAS.

3. Major Design Features

ATLAS was designed to operate under prototypic pressure and temperature conditions. Its design pressure and temperature is 18.7 MPa and 370°C, respectively. Water is used as the working fluid, and thus property similarity between APR1400 and ATLAS is achieved. All equipment was made in stainless steel to avoid corrosion. It consists of a primary system, secondary system, safety system, auxiliary system, power supply system, instrumentation and control system, and data acquisition system (DAS). The same geometrical loop configuration as the APR1400 was maintained from a scaling viewpoint. All crucial components were designed and fabricated according to the ASME B&PV, Section-VIII, and Division 1 or 2 code. The core consists of 396 electrically heated rod, and the maximum power is 2.0 MW, which is around 10% of the scaled core power. It was heavily instrumented and the total number of measurement channels is over 1250. A schematic arrangement of the major components is shown in Figure 1. Further detailed information on the design features of ATLAS can be found in the literature [1, 2].

Compared with other major large-scale facilities that were built and operated in the past, ATLAS is a half-height facility. ATLAS was added to the existing sketch by Aksan [9] and compared with other facilities as shown in Figure 2. It can be seen from the sketch that ATLAS is a unique facility with 2 hot legs and 4 cold legs. Though ATLAS is a half-height facility, the inner diameter of the reactor pressure vessel is comparable to those of other facilities. In particular, the aspect ratio (l/d) of ATLAS has a similar value to that of the LSTF. Above all, ATLAS is equipped with four DVI nozzles for Emergency Core Cooling (ECC) injections, which is one of the special design features.

4. Major Outcomes of the Previous IETs

Since the complete installation of the ATLAS facility in 2005, a series of integral effect tests have been performed, with priority given to major design basis accidents. Major outcomes from the previous ATLAS tests relevant to nuclear safety are summarized in the following subsections.

4.1. LBLOCA Reflood Tests. The test for the LBLOCA reflood phase was selected as the first test item of the ATLAS facility,

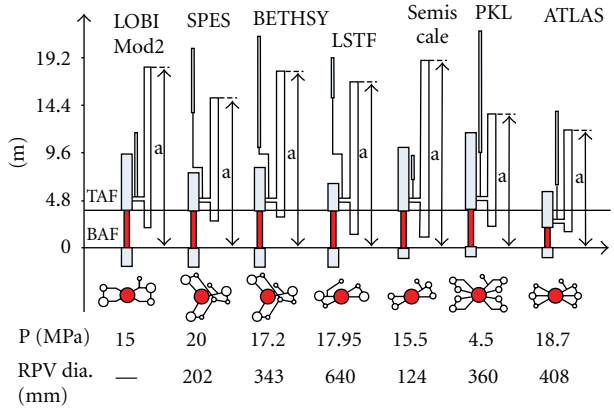

Figure 2: Comparison of ATLAS with the other facilities.

as a few safety concerns were raised regarding the thermal-hydraulic safety performance of the emergency core cooling system during LBLOCAs in the licensing review for the APR1400's Standard Design Approval: (a) the overall validity of the safety analysis code and analysis methodology for the reflood phase of LBLOCAs, regarding the direct ECC bypass, and (b) the adverse effect of downcomer boiling during the late reflood phase of large-break LOCAs.

These two phenomena are expected to occur in the annular downcomer region during a LBLOCA. These issues were raised due to a new safety feature of a DVI system that supplies the ECC directly into the reactor vessel downcomer. Unlike the conventional cold leg injection system, it has become important to quantify the ECC bypass at the upper downcomer along the lateral direction to the break during the reflood phase. Figure 3 schematically depicts the ECC bypass mechanism in the DVI system during the reflood phase. It is generally known that there are two ECC bypass mechanisms, a sweepout and a direct ECC bypass. A sweepout is caused by the steam injected from the intact cold legs, which interacts with the coolant in the downcomer and causes the coolant to be discharged to the broken cold leg. From the UPTF test results [10], it was found that a direct ECC bypass is the major bypass mechanism of the DVI system. The ECC bypass has been identified as playing an important role in the depletion of the coolant inventory in the reflood phase of an LBLOCA.

Therefore, an extensive series of tests were conducted to provide reliable integral and separate effect test data for resolution of the above issues. The ATLAS reflood test program progressed into two serial phases (Phase 1 and Phase 2) according to the target period to be simulated. The main objective of the Phase 1 tests was to identify the major thermal-hydraulic characteristics during the late reflood phase of a LBLOCA, and its main concern was the parametric effects on downcomer boiling [11]. The Phase 2 test was subsequently continued. The main objective of the Phase 2 tests was to investigate the thermal-hydraulic characteristics during an entire reflood period to provide reliable data to help validate the LBLOCA analysis methodology for the APR1400. Among the whole test matrix of the LBLOCA reflood tests, LB-CL-09, LB-CL-11, LB-CL-14, and LB-CL-15 were seriously analyzed to support the licensing process of the APR1400 in Korea, and their results dealing with the experimental results and analysis were already published [12–15]; only the major outcomes are summarized in this paper. Key test matrix for the LBLOCA tests is shown in Table 2.

In phase 1, LB-CL-05 was analyzed to investigate the effects of the downcomer boiling and safety injection flow rate. Figure 4 compares the measured collapsed water levels in the core and downcomer with those by the MARS code [16], which indicates deeper depressions in the water levels than the data. The maximum surface temperature variation of the core heater rods is shown in Figure 5. The MARS code predicted a much higher rod temperature than the data. In the MARS simulation, the peak rod temperature reached up to 792°C, possibly by an insufficient ECC injection due to the downcomer boiling in the downcomer region. In the test, however, the downcomer boiling was identified but the peak rod temperature was as low as 284°C. Based on these comparison results, it can be concluded that the downcomer boiling is a real phenomenon occurring in the lower downcomer regions, as expected in the safety analysis code, but its effects were not as significant as the code prediction. It was found that the interfacial drag model in the MARS code is responsible for the collapsed water level so the model needs to be carefully investigated by the code developers.

In phase 2, both the conservative initial and boundary condition (LB-CL-09) and best-estimate conditions (LB-CL-11, LB-CL-14) were simulated. A separate effect test at a much lower reflooding velocity condition (LB-CL-15) was supplemented in the test matrix to validate the RELAP5 reflood models for a core quenching phenomenon under a low flow rate ECC injection condition.

The maximum heater rod surface temperature during the LB-CL-09 test is shown in Figure 6. In this test, the reflooding was controlled to start at 1912 s [13]. The heater surface temperatures were measured at 12 axial locations, and the maximum surface temperature of the heater rod was 722°C. A temperature increase by 257°C from the reflood start time was obtained. A top quenching phenomenon was also observed in every heater group, but the quenching did not show radial homogeneity. The core heaters were quenched

Table 2: Key test matrix for the LBLOCA reflood tests.

Test ID	Test conditions
LB-CL-05	Separate effect test (Phase-1) (i) Late reflood condition focusing on downcomer boiling effect
LB-CL-09	Integral effect test at conservative condition (i) Decay power: ANS73x120% (ii) Containment pressure: 0.1 MPa (iii) Power distribution: radially uniform
LB-CL-11	Integral effect test at BE condition (i) Decay power: ANS79x102% (ii) Containment pressure: 0.2 MPa (iii) Power distribution: radially uniform
LB-CL-14	Integral effect test at BE condition (i) Decay power: ANS79x102% (ii) Containment pressure: varying (iii) Power distribution: radially non-uniform
LB-CL-15	Separate effect test (i) Complementary test at low reflooding rate

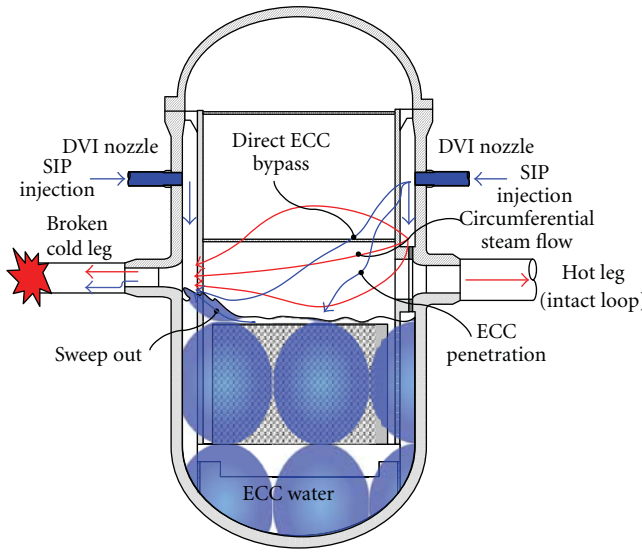

Figure 3: A schematic diagram of the direct ECC bypass and sweepout phenomena.

in the order of the middle region, center region, and outer region.

Figure 7 shows a typical ECC bypass ratio obtained from the LB-CL-11 test [14]. The ECC bypass ratio is defined as follows:

$$R_{\mathrm{ECC,bypass}} = \frac{W_{\mathrm{ECC,bypass}}}{W_{\mathrm{ECC}}} = \frac{W_{\mathrm{break,water}}}{W_{\mathrm{ECC}}}, \quad (2)$$

where $W_{\mathrm{ECC,bypass}}$, $W_{\mathrm{break,water}}$, and W_{ECC} are the bypassed ECC flow rate, the water component of a break flow, and the injected ECC flow rate. The obtained ECC bypass fraction shows a great fluctuation ranging from 0.2 to 2.1, especially during the initial period. Such great fluctuation turned out to be due to the sweepout occurring significantly during the earlier period. The ECC bypass rate was between 0.2 and 0.6 during the later period except for some irregular peaks. A similar trend in the ECC bypass ratio was found in the other tests.

A comprehensive integral effect database regarding the LBLOCA reflood phase of the APR1400 was successfully established through the above-mentioned LBLOCA program. Details of the test conditions were chosen based on in-depth discussions held occasionally with a regulatory organization and nuclear industries for a straightforward application of the test results toward the urgent licensing process of the APR1400. Korean industries used the LB-CL-15 data to obtain licensing approval from a regulatory organization and have been performing further detailed calculations by utilizing LB-CL-09, LB-CL-11, and LB-CL-14 in order to develop or improve their own safety analysis methodology of an LBLOCA.

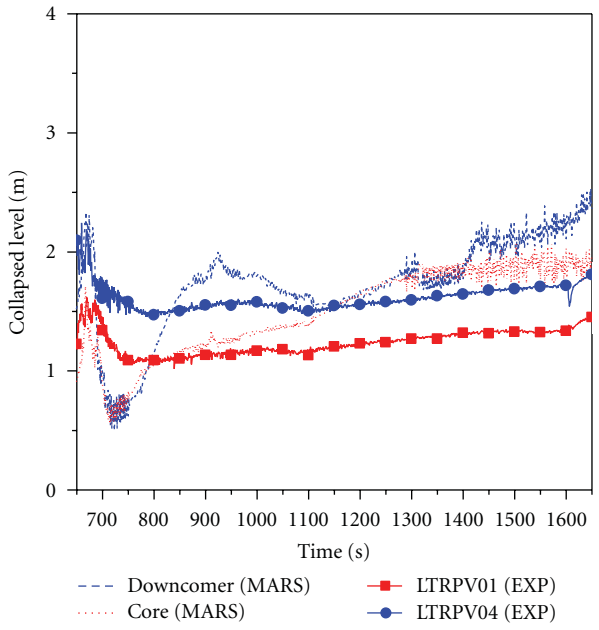

Figure 4: Comparison of measured water levels in the core and the downcomer with code calculations during LB-CL-05.

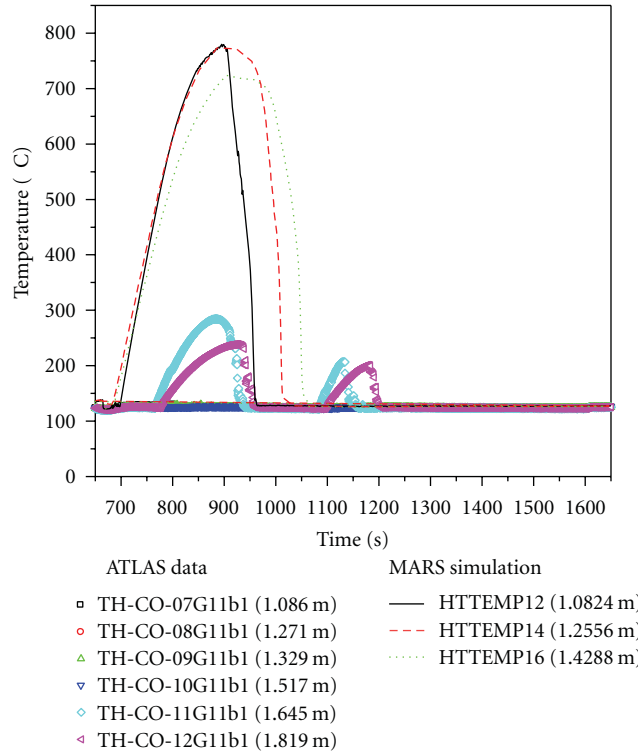

Figure 5: Comparison of measured PCTs with code predictions during LB-CL-05.

4.2. DVI Line SBLOCA Tests. A direct vessel injection (DVI) concept was first proposed in the Utility Requirement Document (URD) by the Electric Power Research Institute (EPRI) in the early 1990s. The AP600 (or the AP1000) was the first reactor to adopt a DVI method for an emergency core cooling system instead of a conventional cold leg injection method. The double-ended severance of a DVI line is taken as a limiting break case for a SB-LOCA analysis of the AP1000. The US-APWR also selected the DVI method for delivering borated ECC water from safety injection pumps into the core. The VVER-1000 passively injects borated water by four pressurized accumulation tanks into the reactor core through separate inlet nozzles attached to the reactor pressure vessel. In Korea, the APR1400 adopted the DVI method as one of the improved safety features compared with the OPR1000.

Those DVI-adopted plants treat a DVI line break as another spectrum among the SBLOCAs in their safety analysis because a DVI nozzle directly attached to a reactor vessel is vulnerable to a postulated break from a safety viewpoint. The thermal hydraulic phenomena in the RPV downcomer are expected to be different from those in the cold leg injection mode during postulated design basis accidents. In the event of a DVI line break, the vapor generated in the core is introduced to the RPV downcomer through the hot legs, steam generators, and cold legs. The vapor should then pass through the upper part of the RPV downcomer to be discharged through the broken DVI nozzle. Thus, a complex flow pattern and multi-dimensional aspects are anticipated, especially in the upper downcomer region. Thus, DVI relevant data and a reliable prediction tool for a DVI line break scenario are required by both regulators and industry.

Thus far, sensitivity tests on the break size were performed to establish an integral effect database for various break sizes: 5%, 25%, 50%, and 100% [3, 4, 17]. A test matrix for the DVI line SBLOCA tests is shown in Table 3.

Table 3: Test matrix for the DVI line SBLOCA tests.

Test ID	Break size		Remarks
	APR1400 (%/inch)	Break nozzle dia. (mm)	
SB-DVI-03	100%/8.5	15.13	Double-ended break
SB-DVI-04	25%/4.25	7.63	
SB-DVI-05	25%/4.25	7.63	Repeat of SB-DVI-04
SB-DVI-06	5%/1.9	3.41	
SB-DVI-07	50%/6.0	10.8	
SB-DVI-08	100%/8.5	15.13	Repeat of SB-DVI-03
SB-DVI-09	50%/6.0	10.8	ISP-50 test

All tests were performed with an assumption of loss of off-site power simultaneously with the break, and the worst single failure as a loss of a diesel generator, resulting in a minimum safety injection flow to the core. Furthermore, the safety injection flow to the broken DVI-4 nozzle was not credited. Eventually, ECC water was injected from one safety injection pump located opposite the broken DVI nozzle and three safety injection tanks, as shown in Figure 8.

Figure 9 shows the effects of the break size on the primary pressure; code prediction results by the MARS code are also plotted for comparison. In each break case, a clear pressure plateau was observed just before the loop seal clearing.

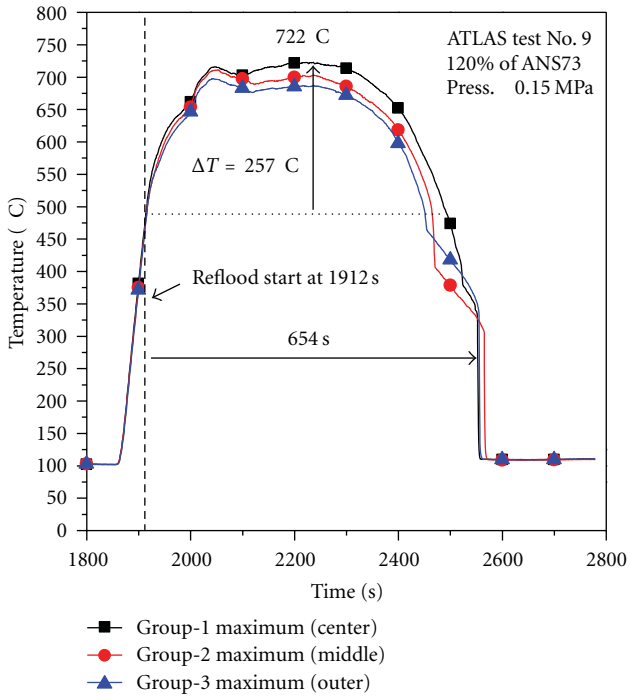

Figure 6: Maximum heater rod surface temperature variation of the core during LB-CL-09.

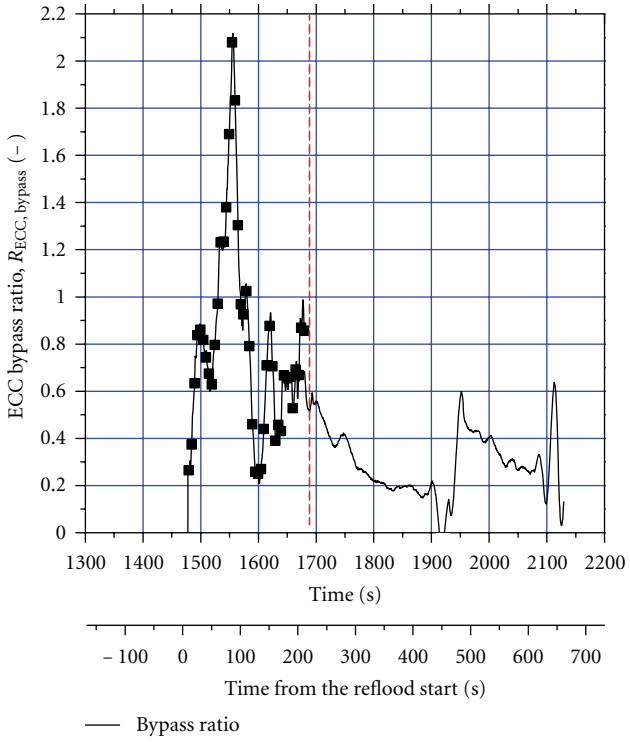

Figure 7: Comparison of estimated ECC bypass ratio with code calculations during LB-CL-11.

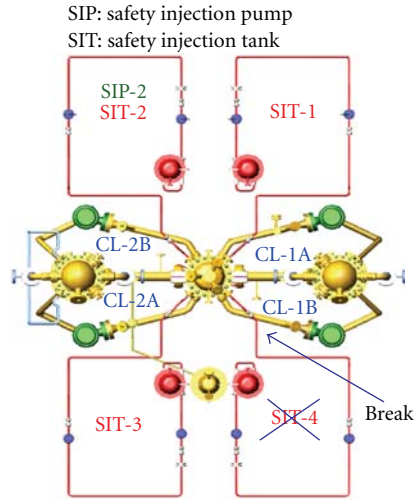

Figure 8: A loop arrangement for a DVI line break with a single failure assumption.

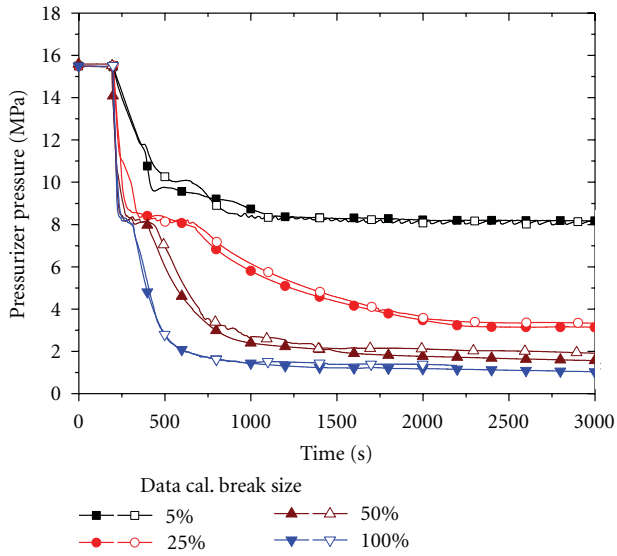

Figure 9: Effects of the break size of the DVI nozzle on the primary pressure.

As the break size became larger, the plateau became milder and lasted shorter.

Comparisons of the collapsed water levels of the core and downcomer with the calculated levels for a typical 100% break case are shown in Figure 10. In cases of breaks larger than 50%, the core was observed to be partly uncovered, leading to increases in the PCT. Such initial core level decreases were recovered when the loop seals in the intermediate legs were cleared. Thus, it was experimentally confirmed that the loop seal clearing plays a critical role in determining the minimum water level in the core, and consequently the PCT.

Among the test series, the 50% break case was selected for the 50th international standard problem (ISP-50) of the OECD/NEA in 2009. The ISP-50 consisted of two serial phases: blind and open phases. Sixteen calculations were

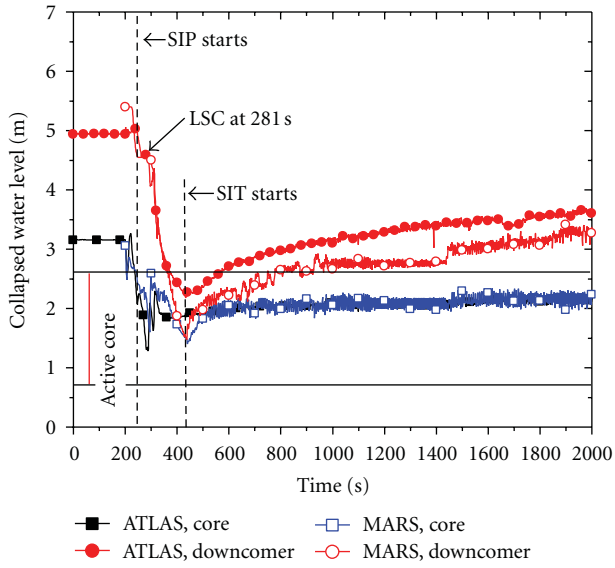

Figure 10: Comparison of collapsed core and downcomer water levels for a 100% DVI line break.

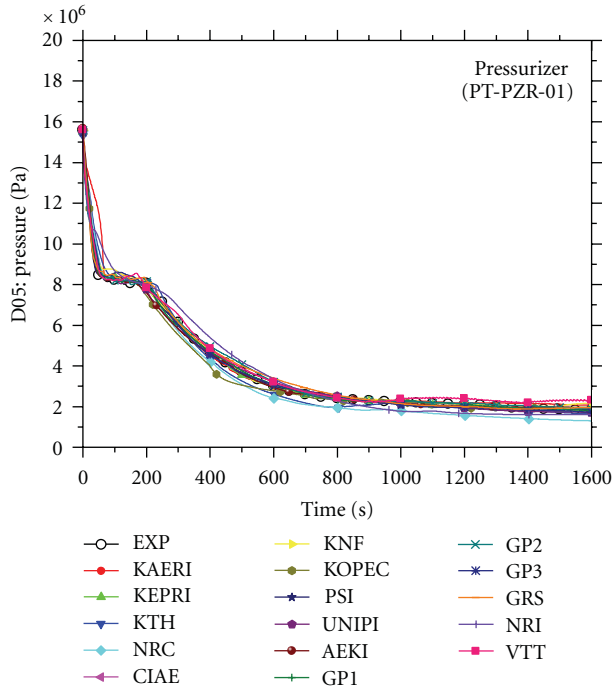

Figure 11: Comparison of the calculated primary pressures with the measurement (SB-DVI-09).

collected from 11 OECD countries, and seven leading safety analysis codes were utilized: RELAP5 series, MARS, TRACE 5.0, CATHARE, ATHLET, APROS, and KORSAR/GP. Detailed information on ISP-50 can be found in the final integration report [6]. Typical comparison results of the primary pressure and break flow rate are shown in Figures 11 and 12, respectively.

In this ISP-50 exercise, multidimensional phenomena such as ECC mixing in the upper downcomer observed in the

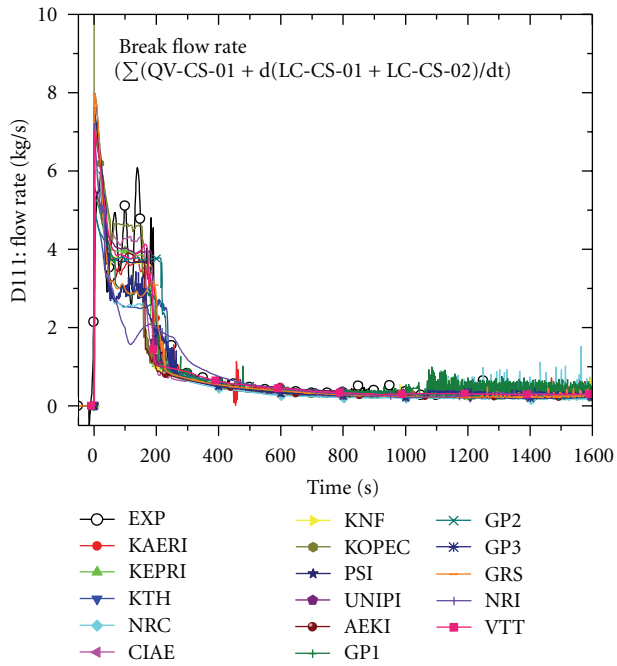

Figure 12: Comparison of the calculated break flow rates with the measurement (SB-DVI-09).

test were highlighted in terms of code prediction capability. In particular, detailed calculation results on the downcomer fluid temperatures were requested and compared. In the test, the cold ECC water introduced through the DVI nozzles was well mixed with the hot water in the upper downcomer region. However, such vigorous and instant mixing was not predicted appropriately by most codes. The fluid temperature of the intact loop side annulus was much lower than that of the broken side annulus. Temperature stratification in an azimuthal direction was predicted even in a lower downcomer region. A typical comparison of the downcomer fluid temperature in the upper downcomer region with the measurement is shown in Figure 13. The detailed downcomer fluid temperature measurement locations are shown in Figure 14. Six thermocouples were installed at six different elevations.

Another multidimensional aspect observed in the DVI line break test was a nonuniform distribution of the PCT; the PCT increased earlier in the side core region than in the center core region. In order to investigate this nonuniformity, a 3D calculation was performed with the MARS-3D and the TRACE code during the ISP-50 exercise. Figure 15 shows a typical mass flux distribution in the core region. The center region where the mass flux is high was effectively cooled, whereas the side region where the mass flux is either relatively low or negative was not adequately cooled, resulting in an increase in the PCT.

4.3. Cold Leg SBLOCA Tests. Many integral effect tests on cold leg SBLOCAs have been performed since the Three Mile Island Unit 2 accident. Either the existing facilities were modified or new facilities were built to perform SBLOCA

Table 4: Test matrix for the cold leg SBLOCA tests.

Test ID	Break size APR1400 (%/inch)	SI injection	Remark
SB-CL-01	1.78%/4	SIP-1, 3 and 4 SITs	
SB-CL-02	4.0%/6	SIP-1, 3 and 4 SITs	Closed core bypass path
SB-CL-03	7.11%/8	SIP-1, 3 and 4 SITs	
SB-CL-04	8.03%/8.5	SIP-1, 3 and 4 SITs	
SB-CL-05	1.78%/4	SIP-1, 3 and 4 SITs	Repeat of SB-CL-01
SB-CL-06	4.0%/6	SIP-2 and SIT-1, 2, 3	CPT for SB-DVI-09
SB-CL-07	0.44%/2	SIP-1, 3 and 4 SITs	No loop seal
SB-POSRV-01	2 POSRV/3.5	SIP-1, 3	IOPOSRV
SB-POSRV-02	1 POSRV/2.3	SIP-1, 3	IOPOSRV
SB-CL-08	4.0%/6	SIP-1, 3 and 4 SITs	Cold leg injection
SB-CL-09	4.0%/6	SIP-1, 3 and 4 SITs	
SB-CL-10	5.0% (LSTF)	4 SITs (CLI)	CPT for LSTF SB-CL-18 test

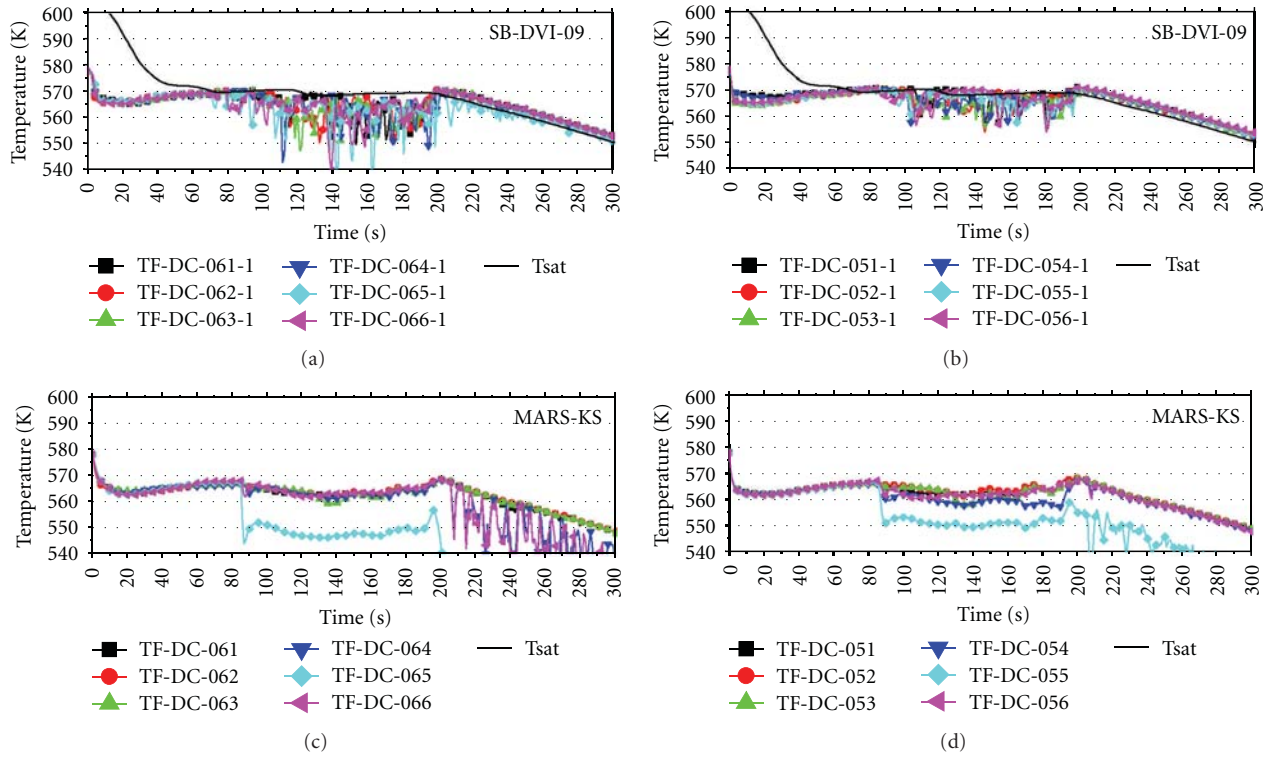

Figure 13: Comparison of upper downcomer fluid temperature with the measurement (SB-DVI-09).

tests. As the APR1400 has a unique loop configuration compared with the conventional nuclear power plants, two loops with two hot legs and four cold legs, there is a practical limit to apply the existing IET database to validate the safety analysis codes for the APR1400. Furthermore, the APR1400 was designed to inject ECC water not through the cold leg nozzle but through the DVI nozzles in the case of SBLOCAs. Thus, the DVI performance needs to be reevaluated and compared with the cold leg injection method. No integral effect database for DVI injection during SBLOCAs has yet been reported.

In order to establish a wide database for a cold leg SBLOCA, a test matrix was determined as shown in Table 4. First, the effects of break size from equivalent diameters of 2 to 8 inches of the APR1400 were investigated. All breaks were directed downward from the bottom side of the cold leg. Similar to the DVI break case, the assumption of loss of offsite power simultaneously with the break, resulting in the minimum safety injection flow to the core, was used. Then, two safety injection pumps and four safety injection tanks are available to provide ECC water into the core. In addition, several parametric effects were experimentally investigated:

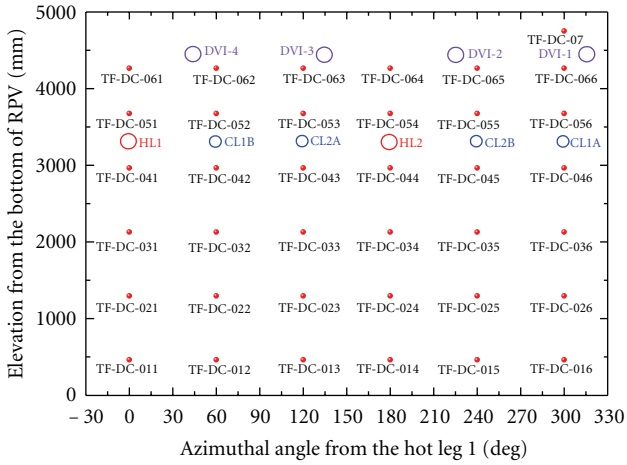

FIGURE 14: Measurement locations for downcomer fluid temperatures.

the effects of RPV bypass flow (SB-CL-02 versus SB-CL-09), effects of ECC injection (SB-CL-08 versus SB-CL-09), and counterpart test to the DVI line break (SB-CL-06 versus SB-DVI-09). Inadvertent opening of the pilot operated safety valve (IOPOSRV) with two different break sizes were also simulated in ATLAS. Finally, a counterpart to the SB-CL-18 test, which was performed using a large-scale test facility (LSTF) by JAEA, was accomplished. The scalability of ATLAS to real nuclear power plants was investigated using this counterpart test.

Five typical phases characterizing a SBLOCA scenario were identified in the test, as shown in Figure 16: (1) blow-down, (2) natural circulation, (3) loop seal clearance, (4) boil-off, and (5) core recovery [18, 19]. The duration of each phase depends on the break size and performance of the ECCS. Characteristic parameters such as the primary pressure (PT-PZR-01), secondary pressure (PT-SGSD1-01), and collapsed water level of the downcomer (LT-RPV-04A) were also plotted for comparison.

The blow-down phase is characterized by a rapid depressurization of the primary system until a flashing of the reactor coolant starts, and by an increase in the secondary pressure up to the opening of the main steam-safety valves (MSSVs). The break flow is maintained in a single-phase liquid during the blow-down period. The next phase is characterized by a two-phase natural circulation before the loop seal formation. A loop seal clearance and boil-off phase then follow. Finally, the core recovery phase starts when the ECC water is injected by the safety injection tank.

Effects of the break location were experimentally investigated by performing two counterpart tests: SB-CL-06 versus SB-DVI-09. The same initial and boundary conditions were used except for different locations of the cold leg and DVI nozzle, respectively. A comparison of the maximum PCT behavior is shown in Figure 17. It was found that the maximum heater surface temperature increased more in the SB-DVI-09 test than in the SB-CL-06 test, indicating that the DVI line break is more limiting than the corresponding cold leg break. As the DVI nozzle is located at a higher elevation than the cold leg, a higher core pressure is required to overcome the hydraulic static head in the downcomer region between the cold leg and DVI nozzle. This results in a lower and delayed core water level than the cold leg break case as shown in Figure 18 [20].

An inadvertent opening of the POSRV test was carried out as one of the SBLOCA spectra to construct a validation database for the Safety and Performance Analysis Computer Code (SPACE), which is under development. A break at a POSRV installed at the top head of the pressurizer was taken into account. Due to its small break size, the other phases except for the blow-down phase were not observed in the test. The loop seal was not cleared during the test period and the SITs were not activated. Measured primary and the secondary pressure trends are shown in Figure 19.

The coolant in the RCS remained in the liquid phase throughout most of the blow-down period, but steam began to form in the upper head, upper plenum, and hot legs as the blow-down period came to an end. The rapid depressurization ended when the pressure decreased to just above the saturation pressure of the SG secondary side. The break flow was in a single-phase liquid condition throughout the blow-down period [21].

A counterpart test to the SB-CL-18 of the LSTF was carried out to evaluate the scale-up capability of ATLAS. SB-CL-18 was a 5% cold break test and was utilized as ISP-26 under OECD/NEA WGAMA activity [22]. The integral (or global) scaling ratios of ATLAS with respect to the LSTF were calculated to be 1/1.84 in height, 1/1.59 in diameter, 1/4.65 in volume, and 1/3.45 in flow rate. The length scaling ratio can be different depending on which reference length is used in this global scaling. Here, the active core length was used as a reference height scaling. In order to determine the appropriate boundary conditions for simulating SB-CL-18 with ATLAS, the boundary flow scaling methodology was used to preserve the mass and energy as follows [23]:

$$\left(\frac{\tau m_{\text{out}}}{M_o}\right)_R = 1, \qquad \left(\frac{\tau m_{\text{in}}}{M_o}\right)_R = 1, \qquad \left(\frac{\tau Q}{M_o h_c}\right)_R = 1. \tag{3}$$

From (3), the break flow can be scaled

$$m_{\text{out,R}} = \frac{M_{o,R}}{\tau_R} = \frac{m_{\text{out,ATLAS}}}{m_{\text{out,LSTF}}} = \frac{{D_{\text{out,ATLAS}}}^2}{{D_{\text{out,LSTF}}}^2}, \tag{4}$$

where

$$M_{o,R} = \frac{M_{\text{ATLAS}}}{M_{\text{LSTF}}} = \frac{1.63}{7.23} = 0.22545,$$
$$\tau_R = \frac{\tau_{\text{ATLAS}}}{\tau_{\text{LSTF}}} = \frac{1}{\sqrt{2}}. \tag{5}$$

Thus, the break diameter can be calculated from (4) as follows:

$$D_{\text{out,ATLAS}} = D_{\text{out,LSTF}}\sqrt{\frac{M_{o,R}}{\tau_R}} = 22.5\sqrt{0.3188} = 12.7\,\text{mm}. \tag{6}$$

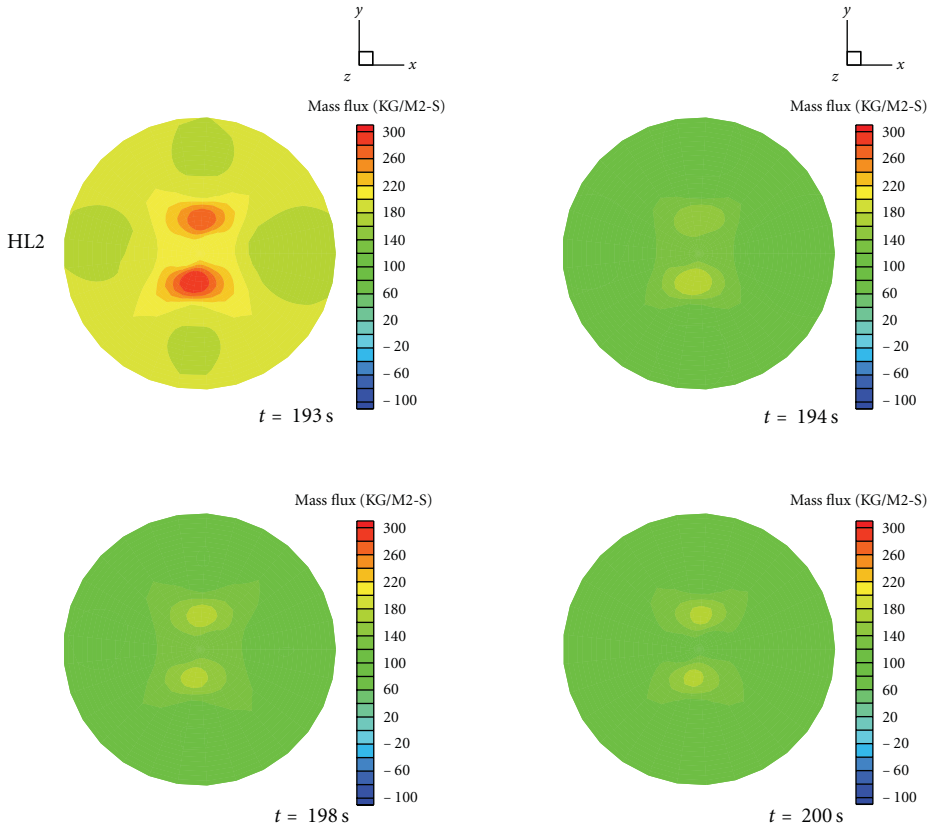

Figure 15: MARS-3D prediction of total mass flux at 11th elevation in the core, $z = 1645$ mm (SB-DVI-09).

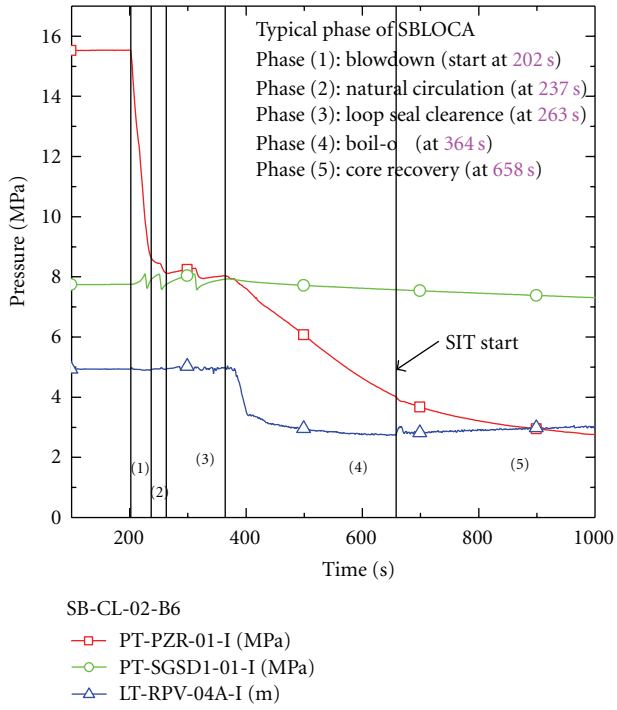

Figure 16: Identification of characteristic phases during the present SBLOCA test period.

Similar to the break nozzle, the safety injection flow rate and core power were scaled as follows:

$$m_{\text{in,ATLAS}} = \frac{M_{o,R}}{\tau_R} \cdot m_{\text{in,LSTF}} = 0.3188 \cdot m_{\text{in,LSTF}}, \quad (7)$$

$$Q_{\text{ATLAS}} = \frac{M_{o,R}}{\tau_R} \cdot Q_{\text{LSTF}} = 0.3188 \cdot Q_{\text{LSTF}}. \quad (8)$$

However, a smaller core power than an LSTF was applied to ATLAS because of its electrical power limit, as shown in Figure 20.

A comparison of the measured primary pressure with the LSTF measurement is shown in Figure 21. A delayed loop seal clearing occurred in the ATLAS test, and a steeper decrease in the primary pressure occurred after the loop seal clearing was obtained. Measured differential pressure and water levels are shown in Figure 22. In the LSTF test, a significant and rapid water level depression was observed, whereas in the ATLAS test, a relatively smooth water level depression was obtained. These differences seem to be caused by differences in loop configurations, elevation distributions of the major components, and core power between two facilities. Nonetheless, this counterpart test showed a promising prospect of the scale-up capability of ATLAS, and a more rigorous analysis is underway.

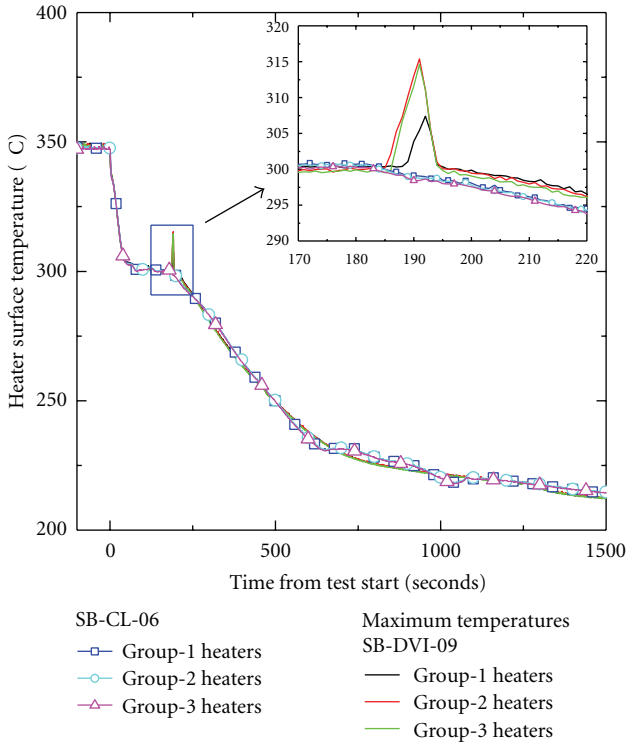

Figure 17: Comparison of cladding temperatures between SB-DVI-09 and SB-CL-06.

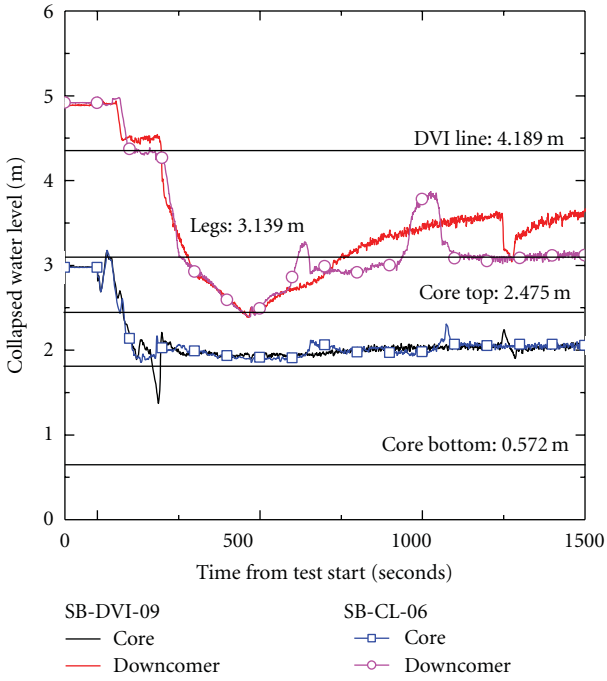

Figure 18: Comparison of the water levels between SB-DVI-09 and SB-CL-06.

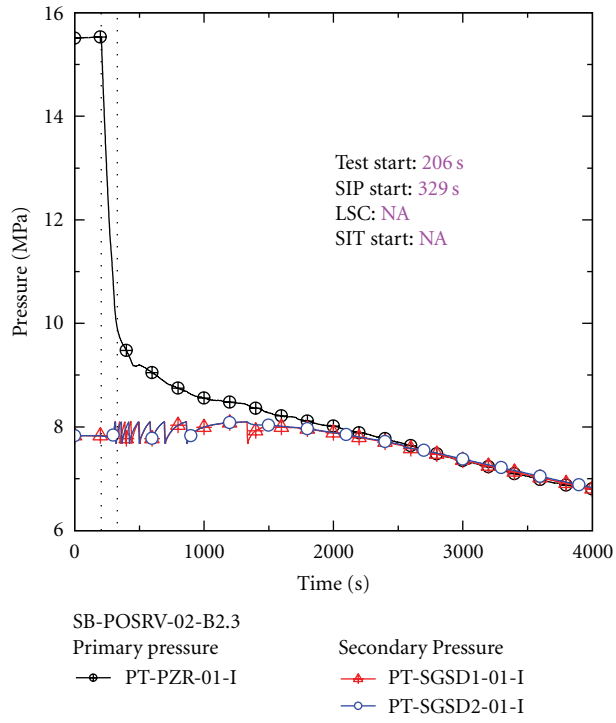

Figure 19: Primary and secondary pressure behavior during SB-POSRV-02-B2.3.

4.4. Steam Generator Tube Rupture (SGTR) Tests. An SGTR accident is a penetration of the barrier between the RCS and secondary system and is one of the design basis accidents having a significant impact on safety from the viewpoint of radiological release. This accident has a relatively higher occurring frequency, and the estimated frequency of a single SGTR is 1.5×10^{-2} per reactor year (RY) [24].

In order to simulate the SGTR accident of the APR1400, several tests, defined in Table 5, were performed by simulating a double-ended rupture of either a single or five U-tubes at either the hot or cold side of the ATLAS steam generator. Regarding a multiple steam generator tube rupture (MSGTR), there is demand for a design mitigating the MSGTR consequences for up to five U-tube ruptures, and on lowering the containment bypass to improve the design and operational procedures. The NRC estimated frequency for a multiple SGTR event is approximately 8.4×10^{-4}/RY [24].

A break was simulated using an external break simulating pipe, and its diameter was increased by a factor of $\sqrt{2}$ in order to simulate the double-ended guillotine break as shown in Figure 23. Different break locations—SG inlet plenum and outlet plenum—were simulated to see the effects of the break locations. A boundary flow scaling approach was taken to simulate a scaled break flow rate in the test. During the SGTR, the break flow can be choked or not depending on the differential pressure between the primary and secondary systems. A break spool piece, which consisted of an orifice and a tube, was designed to simulate both the choking or nonchoking break flow. Five U-tube ruptures were simulated in five tubes connected in parallel, as shown in Figure 24.

Table 5: Test matrix for SGTR tests.

Test ID	APR1400 Number of broken U-tubes/break area (inch)	Break location	Type of Rx. trip
SGTR-HL-04	1 ea/0.67	2 m hot side	HSGL*
SGTR-HL-05	5 ea/3.35	2 m hot side	HSGL
SGTR-HL-06	1 ea/0.67	2 m hot side	LPP**
SGTR-HL-07	5 ea/3.35	2 m hot side	LPP
SGTR-CL-01	1 ea/0.67	2 m cold side	HSGL
SGTR-CL-02	5 ea/3.35	2 m cold side	HSGL

*HSGL: High Steam Generator Level.
**LPP: Low Pressurizer Pressure.

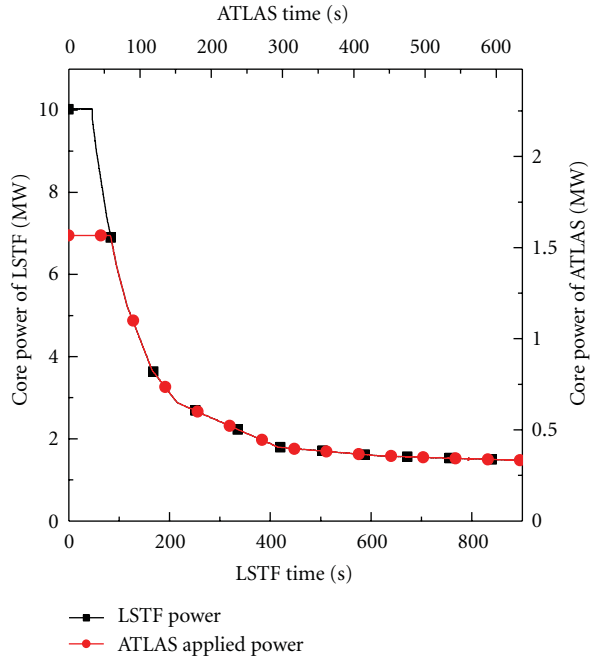

Figure 20: Comparison of the applied power in the LSTF counterpart test.

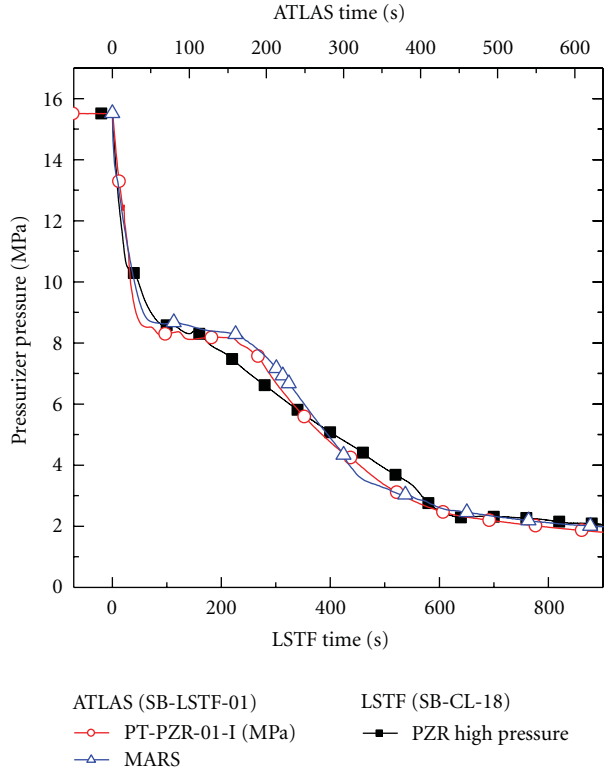

Figure 21: Comparison of the primary pressure in the LSTF counterpart test.

Two types of reactor trip conditions were used: HSGL and LPP.

A typical measured primary pressure for a single U-tube rupture is shown in Figure 25. In this figure, AFAS stands for Auxiliary Feedwater Actuation Signal and it implies that auxiliary feedwater was provided into the intact steam generator between 3153 s and 3911 s. More information can be found in the literature [25]. The typical sequence of events was experimentally identified. It was found that the break location affected the leak flow rate. The break at the cold side, where the external break simulating pipe was connected to the outlet plenum of the SG, resulted in a higher leak flow rate than the break at the hot side. However, the effect was not as significant as at the break area. In the case of the five U-tube ruptures, the safety injection pump was actuated earlier than in the single U-tube rupture due to higher depressurization. Earlier injection of cold ECC water reduced the average fluid temperature of the RCS, resulting in less heat transfer to the secondary side. Thus, the secondary pressure increased more slowly than in the single U-tube rupture case, eventually causing a retardation of the MSSV opening.

4.5. Feed Line Break (FLB) Tests. After the major tests on LOCA were completed, feed water line breaks were investigated as one a typical non-LOCA design basis accident. The effects of the break locations and break sizes were experimentally examined. The APR1400 has two nozzles for a feedwater supply: an economizer and a downcomer nozzle. Under normal operating conditions, 90% feedwater is supplied through the economizer, and the remaining 10% is provided through the downcomer nozzle for high thermal efficiency. Thus, two different nozzles were assumed to be broken in the

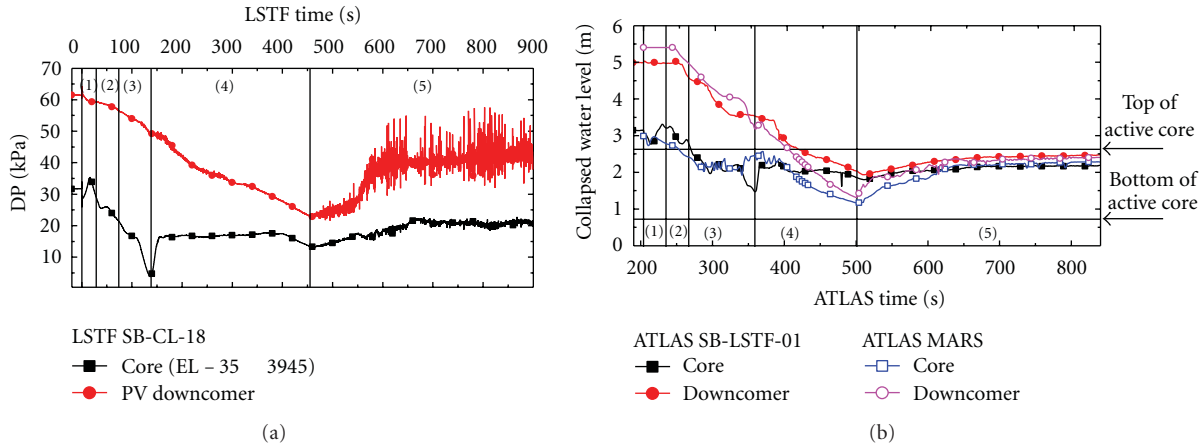

Figure 22: Comparison of collapsed water levels in the LSTF counterpart test.

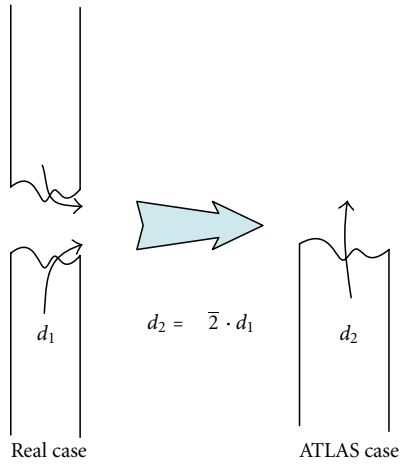

Figure 23: Simulation concept of the guillotine break of a SG U-tube.

Table 6: Test matrix for FLB tests.

Test ID	Break size APR1400 (area: ft^2)	Break size ATLAS (mm)	Break location	Type of Rx. trip
FLB-EC-01	0.4	15.24	Economizer	HPP*
FLB-EC-02	0.1	7.62	Economizer	HPP
FLB-EC-03	0.86	22.29	Economizer	HPP
FLB-EC-04	0.4	15.24	Economizer	LSGP**
FLB-DC-01	0.18	10.23	Downcomer	HPP

* HPP: High Pressurizer Pressure.
** LSGP: Low Steam Generator Pressure.

ATLAS test. According to the safety analysis results, the break of the economizer nozzle is found to be more limiting from the viewpoint of the pressurization of the primary system. However, the break of the downcomer nozzle is more or less close to a steam line break accident. Several different break sizes from 0.1 ft^2 (0.0093 m^2) to 0.86 ft^2 (0.0799 m^2) were taken into account. A test matrix is shown in Table 6.

Typical pressure trends at the pressurizer and steam generator dome are shown in Figure 26. Upon the break, the affected steam generator was rapidly depressurized. As ATLAS has a maximum power of 10%, pressurization of the primary system after the FLB could not be simulated realistically. Thus, the high pressurizer pressure trip (HPP) was intentionally triggered 10.6 seconds after the break. Contrary to the affected steam generator, the intact steam generator was pressurized until opening the MSSVs. This integral effect test data is being used to evaluate the prediction capability of the safety analysis codes, such as the MARS, RELAP5, and SPACE codes.

4.6. Steam Line Break (SLB) Tests. Compared with the feed line breaks, the main steam-line break in a pressurized water reactor is a core overcooling event characterized by a strong positive moderator reactivity feedback that can ultimately overcome the core shutdown margin. One of the most important safety concerns of SLB accidents is the return to power. The key thermal-hydraulic phenomena for the SLB transient include a fluid flashing in the reactor upper head and hot legs, a forced and natural circulation flow in the primary system, a steam generator heat transfer, and an asymmetric temperature distribution in the lower plenum of the core.

A similarity analysis of the ATLAS facility with an SLB event was analyzed, and it was confirmed that ATLAS has a reasonable similarity with respect to the prototype plant [26, 27].

A series of integral effect tests simulating various transient conditions were performed. The loss of offsite power (LOOP) was considered as one of the parameters to determine a test matrix for SLBs. The effects of the break area were also considered, based on the flow restrictor geometry at the exit nozzle of the steam generator. A test matrix for the SLB tests is shown in Table 7.

Measured pressure trends are shown in Figure 27. Upon a break, the primary pressure was rapidly depressurized and was recovered by actuation of the safety injection pump at around 500 seconds. The affected steam generator was rapidly depressurized, and the water inventory was also depleted within a short period of time. Though auxiliary feed

Table 7: Test matrix for SLB tests.

Test ID	Break size	Test conditions
SLB-GB-01	Guillotine break	100% rated condition with LOOP
SLB-GB-02	Guillotine break	8% power condition without LOOP
SLB-GB-03	Guillotine break	8% power condition with LOOP
SLB-PB-01	20% partial beak	100% rated condition with LOOP
SLB-PB-02	20% partial beak	8% power condition without LOOP
SLB-PB-03	20% partial beak	8% power condition with LOOP

* LOOP: Loss of Offsite Power.

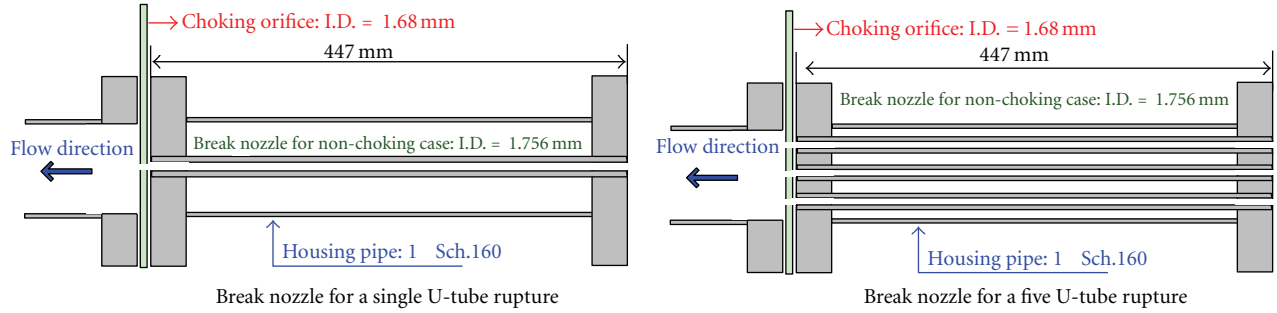

Figure 24: Designed break nozzles for a SGTR and MSGTR.

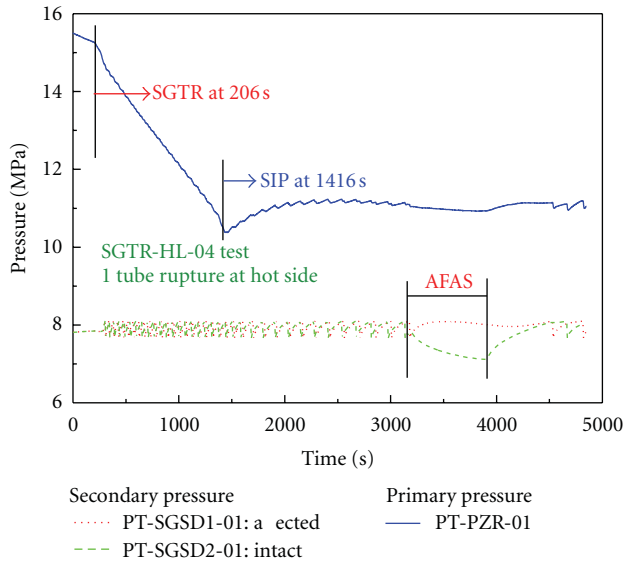

Figure 25: Typical trend of the primary pressure during the SGTR-HL-04 test.

water was provided to the broken steam generator, the water level was not recovered due to a large break size. The intact steam generator was also depressurized initially, but it was isolated when the low steam generator pressure (LSGP) trip signal was activated. Strong loop asymmetric behavior was observed and major thermal-hydraulic information was obtained.

5. Future Prospect

Nuclear power plants featuring more advanced safety and economic competitiveness than the current commercial nuclear plants in operation are essential in the world nuclear market. In particular, safety was a prime importance before the Fukushima accident, too. The Fukushima accident attracted national attention to high-risk multiple failures. In particular, an event that has an extremely low occurring frequency but results in high core damage frequency if it occurs needs to be reconsidered from the viewpoint of the "defense in depth" concept. Accidents not seriously considered from a design basis such as a station blackout (SBO), an anticipated transient without scram (ATWS), reactor vessel rupture (RVR), total loss of feed water (TLOFW), and medium break LOCA are considered as high-risk multiple failure accidents as safety concerns regarding severe accidents have magnified after the Fukushima accident.

Many people have become recently concerned about the safety of operating nuclear power plants in connection with the SBO accident. Therefore, SBO-related integral effect tests have the first priority in the coming ATLAS program. The SBO accident itself and multiple SBO-induced accidents, for instance, an SBO combined with LOCA, will be investigated in the near future. Primary inventory loss due to either opening the POSRV or leakage of the RCP seal can be one of the promising candidates. In addition, new safety features to mitigate the SBO accident efficiently are being proposed, and such concepts can be validated by performing a simulation with the ATLAS facility.

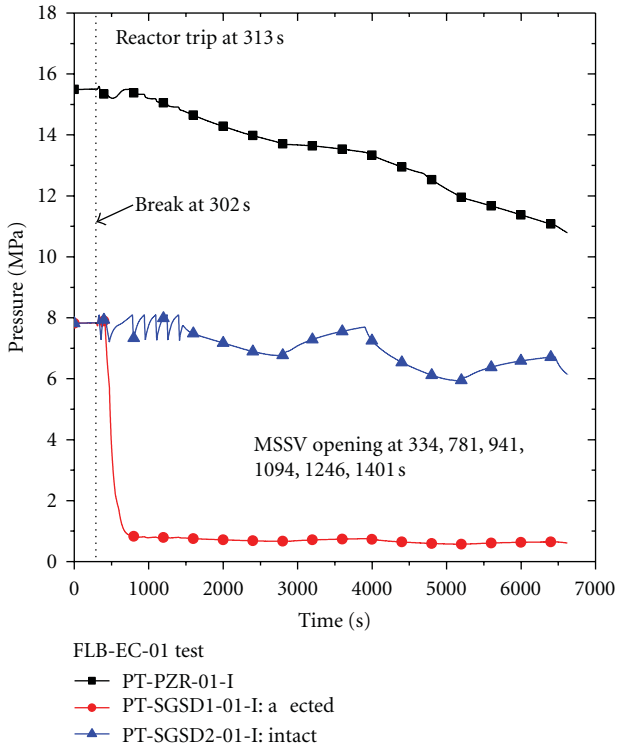

Figure 26: Pressure trends at the pressurizer and steam generator dome.

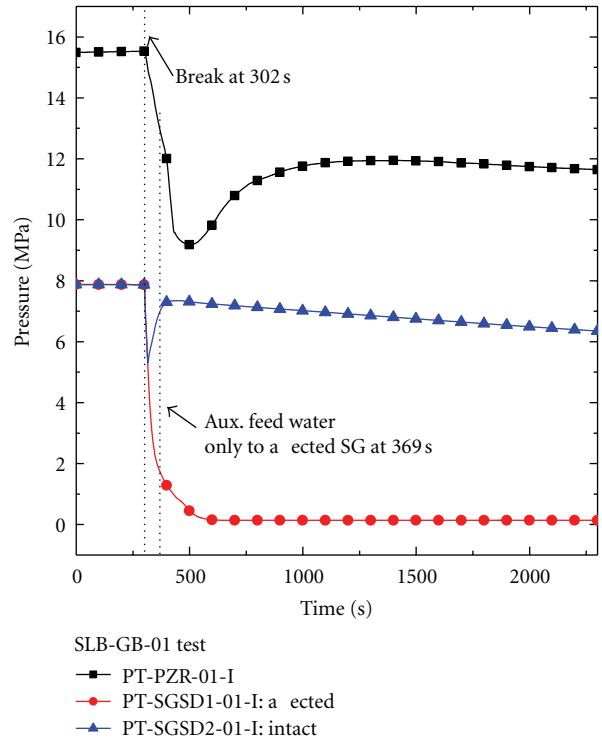

Figure 27: Pressure trends of the guillotine break of the steam line.

The NRC is planning to make risk-informed changes to 10CFR50.46 (ECCS acceptance criteria). As Korean regulations are primarily based on the NRC's regulations, the NRC's changes in regulatory position will significantly affect the domestic regulatory environment. In particular, a redefinition of a design-basis LOCA accident is a safety issue from the viewpoint of safety enhancement. The present domestic regulatory R&D is focusing on the safety analysis methodology of a LOCA larger than the transition break size (TBS) LOCA. Thus, the TBS LOCA of domestic plants needs to be analyzed, and the safety against a TBS LOCA should be validated. An integral effect test program focusing on a TBS LOCA is being planned. The Korean industry is developing a specific advanced nuclear power plant, called an advanced power reactor plus (APR+) to enhance safety and reliability by adopting advanced technology such as a passive feature [28, 29]. Among the newly introduced safety features, the passive auxiliary feedwater system (PAFS) completely replacing the existing active auxiliary feedwater system highlights the advanced technology. An integral effect test program to validate the heat removal performance of the PAFS has already been launched. In the first phase, one steam generator of ATLAS will be connected to the PAFS, and integral effect tests including a performance test will be performed in early 2012. Natural circulation characteristics along the PAFS loop, condensation performance inside the heat exchanger tube, pool boiling, and mixing phenomena in the large passive condensate cooling tank (PCCT) will be investigated in order to support its licensing process within its due schedule.

Even though the LBLOCA reflood tests were already completed in 2007, further expanded tests are on demand by domestic industry according to change in number of electrical trains of the ECCS in the APR1400. When the number of electrical trains is increased from 2 to 4, the safety injection water is introduced through three DVI nozzles rather than two nozzles. At the moment, the APR1400 is under a preapplication review process of the US NRC to get a design approval. Therefore, further supporting activities are waiting for the ATLAS.

Nowadays, only a few integral effect test facilities are available and a few are under refurbishment in the world. As the facilities available now or soon are based on their specific prototype plants, they cannot be a universal provider of the integral effect data. That is the main reason why many counterpart tests were performed in the past. Therefore, the ATLAS can be utilized together with other facilities to effectively solve the safety issues and interests as a future prospective.

6. Summary and Conclusions

ATLAS is a large integral effect test facility scaled down from the APR1400 at 1/2 in height and 1/288 in volume. This is considered by the international community as one of critical facilities to be monitored in the long term in the field of thermal hydraulics of an ALWR [30]. Since its first operation at the end of 2006, an integral effect database was established for major design-basis accidents of the APR1400, including LBLOCA reflood, SBLOCA, SGTR, FLB, and SLB tests.

The LBLOCA reflood test data were of critical importance to support a domestic licensing process of the APR1400. Technically, the ECC bypass and downcomer boiling issues were considered seriously to understand their physical phenomena and to assess the predictability of the safety analysis codes. In the SBLOCA tests, both a DVI line and cold leg break were simulated, and the phenomenological difference was investigated. It was experimentally confirmed that the DVI line break is a more limiting accident than the equivalent size break at the cold leg. Several sensitivity tests were accomplished in the SGTR tests. In addition to a single SGTR, a multiple SGTR of five U-tube ruptures was simulated. The effects of break location were also experimentally investigated.

Two major non-LOCA design-basis accidents such as the FLB and SLB were continued after completion of the abovementioned LOCA series tests. These databases are being used to reduce the design uncertainties and validate the models and correlation of the safety analysis codes under improvement or development.

During past short operating experiences, the operational technique and managing system of the ATLAS facility were set up well. In particular, successful coordination of the ISP-50 and domestic cooperation programs enabled the ATLAS data to be trusted within the relevant thermal-hydraulic communities.

Demands on the integral effect tests with ATLAS are increasing mainly due to the active nuclear R&D program in Korea. Either design modifications or new design concepts introduced to new plants in order to improve their safety and economic efficiency will be validated through the ATLAS test in the near future. In particular, after the Fukushima accident, much attention was placed on the safety of the existing plants. Thus, further experimental needs are expected to increase.

Finally, as public interest is being focused on beyond design basis accidents (BDBAs) due to the Fukushima accident, integral effect test facilities should be utilized to produce clearer knowledge of the actual phenomena and to provide the best guideline for accident management.

Acknowledgments

This work was carried out under the support of Ministry of Education, Science, and Technology (MEST) of the Korean government, under the national nuclear mid- and long-term R&D program.

References

[1] W. P. Baek, C. H. Song, B. J. Yun, T. S. Kwon, S. K. Moon, and S. J. Lee, "KAERI integral effect test program and the ATLAS design," *Nuclear Technology*, vol. 152, no. 2, pp. 183–195, 2005.

[2] Y. S. Kim, K. Y. Choi, H. S. Park et al., "Commissioning of the ATLAS thermal-hydraulic integral test facility," *Annals of Nuclear Energy*, vol. 35, no. 10, pp. 1791–1799, 2008.

[3] W. P. Baek, Y. S. Kim, and K. Y. Choi, "LBLOCA and DVI line break tests with the ATLAS integral facility," *Nuclear Engineering and Technology*, vol. 41, no. 6, pp. 775–784, 2009.

[4] K. Y. Choi et al., "Effects of break size on DVI Line break accidents of the ATLAS," *Nuclear Technology*, vol. 175, pp. 604–618, 2011.

[5] EPRI, "EPRI Utility Requirement Documents for the Advanced Light Water Reactor (Chapter 5)," 1995.

[6] K. Y. Choi et al., "OECD/NEA/CSNI International Standard Problem No. 50: Final Integration Report Volume I, II, III, Analysis of Blind/Open Calculations," NEA/CSNI/R(2012)6.

[7] M. Ishii, S. T. Revankar, T. Leonardi et al., "The three-level scaling approach with application to the Purdue University Multi-Dimensional Integral Test Assembly (PUMA)," *Nuclear Engineering and Design*, vol. 186, no. 1-2, pp. 177–211, 1998.

[8] W. P. Baek et al., "Thermal hydraulic integral effect tests for advanced reactors (in Korean)," KAERI/RR-2240/2001, 2002.

[9] N. Aksan, "International standard problems and small break loss-of-coolant accidents (SBLOCA)," *Science and Technology of Nuclear Installations*, vol. 2008, Article ID 814572, 22 pages, 2008.

[10] MPR-1324, "Summary of results from the UPTF downcomer injection/vent valve separate effects tests: Comparison to previous scaled tests, and application to Babcock&Wilcox pressurized water reactors," 1992.

[11] H. S. Park, K. Y. Choi, S. Cho et al., "Major findings from LBLOCA reflood tests using the ATLAS facility," *Nuclear Engineering and Design*, vol. 240, no. 12, pp. 3920–3929, 2010.

[12] H. S. Park, K. Y. Choi, S. Cho, K. H. Kang, Y. S. Kim, and W. P. Baek, "An integral effect test on the LBLOCA reflood phenomena for the APR1400 using ATLAS under a best-estimate condition," *Journal of Nuclear Science and Technology*, vol. 46, no. 11, pp. 1059–1069, 2009.

[13] H. S. Park, K. Y. Choi, S. Cho et al., "An integral effect test on the reflood period of a large-break LOCA for the APR1400 using ATLAS," *Nuclear Technology*, vol. 170, no. 1, pp. 100–113, 2010.

[14] H. S. Park, K. Y. Choi, S. Cho, K. H. Kang, and Y. S. Kim, "Major thermal-hydraulic phenomena found during ATLAS LBLOCA reflood tests for an advanced pressurized water reactor APR1400," *Nuclear Engineering and Technology*, vol. 43, no. 3, pp. 257–270, 2011.

[15] H. S. Park, J. H. Jeong, K. Y. Choi et al., "A separate effect test on the cooling behavior in a pressurized water reactor core under a low reflooding rate condition by using ATLAS and RELAP5/MOD3.3 code assessment," *Annals of Nuclear Energy*, vol. 38, no. 5, pp. 1053–1064, 2011.

[16] J. J. Jeong, K. S. Ha, B. D. Chung, and W. J. Lee, "Development of a multi-dimensional thermal-hydraulic system code, MARS 1.3.1," *Annals of Nuclear Energy*, vol. 26, no. 18, pp. 1611–1642, 1999.

[17] K. Y. Choi, H. S. Park, S. Cho et al., "Experimental Simulation of a Direct Vessel Injection line break of the APR1400 with the ATLAS," *Nuclear Engineering and Technology*, vol. 41, no. 5, pp. 655–676, 2009.

[18] Mitsubishi heavy industries, Ltd, "Small break LOCA sensitivity analyses for US-APWR," MUAP-07025-NP(R0), 2007.

[19] S. Cho, K. Y. Choi, H. S. Park et al., "Integral effect experiments on 6 inch cold-leg SBLOCA using the ATLAS facility," in *International Congress on Advances in Nuclear Power Plants (ICAPP '10)*, pp. 1375–1384, June 2010.

[20] H. S. Park, K. Y. Choi, S. Cho, K. H. Kang, and Y. S. Kim, "Counterpart tests of SBLOCA on the effect of break location with the ATLAS: DVI nozzle versus cold-leg breaks," *Journal of Nuclear Science and Technology*, vol. 48, no. 10, pp. 1319–1326, 2011.

[21] S. Cho et al., "Integral effect test for an inadvertent opening of POSRV using the ATLAS facility," in *18th International Conference on Nuclear Engineering (ICONE '10)*, Xian, China, May 2010.
[22] Y. Kukita et al., "ISP-26, OECD/NEA/CSNI International Standard Problem No.26, ROSA-IV LSTF cold-leg small-break LOCA experiment, Comparison report," OECD/NEA/ CSNI/ R(91)13, 1992.
[23] S. Cho et al., "Counter-part test results of the LSTF SB-CL-18 using the ATLAS," in *Korean Nuclear Society Autumn Meeting*, Jeju, Korea, October 2010.
[24] J. Taylor, "Policy, technical, and licensing issues pertaining to evolutionary and advanced light-water reactor (ALWR) design," SECY-93-087, NRC, 1993.
[25] K. H. Kang et al., "Integral effect test on the transient thermal-hydraulic behavior during the steam generator tube rupture accident in the APR1400," to appear in *Nuclear Technology*.
[26] K. Y. Choi, H. S. Park, D. J. Euh, T. S. Kwon, and W. P. Baek, "Simulation capability of the ATLAS facility for major design-basis accidents," *Nuclear Technology*, vol. 156, no. 3, pp. 256–269, 2006.
[27] K. Y. Choi et al., "Thermal hydraulic similarity analysis of the integral effect test facility for main steam line break events," in *the 11th International Topical Meeting on Nuclear Reactor Thermal-Hydraulics (NURETH '05)*, Avignon, France, October 2005.
[28] C. H. Song et al., "Thermal-hydraulic R&Ds for the APR+ developments in Korea," in *Proceedings of the 18th International Conference on Nuclear Engineering (ICONE '10)*, Xian, China, May 2010.
[29] C. H. Song et al., "Advanced design features and the thermal-hydraulic tests for the APR+ reactor," in *Proceedings of the 2011 International Congress on Advances in Nuclear Power Plants (ICAPP '11)*, Nice, France, May 2011.
[30] "Nuclear safety research in OECD countries, support facilities for existing and advanced reactors (SFEAR)," NEA/CSNI/ R(2007)6, 2007.

Hindawi Publishing Corporation
Science and Technology of Nuclear Installations
Volume 2012, Article ID 957285, 15 pages
doi:10.1155/2012/957285

Research Article

RELAP5 Analysis of OECD/NEA ROSA Project Experiment Simulating a PWR Loss-of-Feedwater Transient with High-Power Natural Circulation

Takeshi Takeda,[1] Hideaki Asaka,[2] and Hideo Nakamura[1]

[1] *Nuclear Safety Research Center, Japan Atomic Energy Agency (JAEA), Tokai-mura, Ibaraki-ken 319-1195, Japan*
[2] *Nuclear Energy System Safety Division, Japan Nuclear Energy Safety Organization (JNES), Minato-ku, Tokyo 105-0001, Japan*

Correspondence should be addressed to Takeshi Takeda, takeda.takeshi@jaea.go.jp

Received 6 August 2011; Accepted 12 November 2011

Academic Editor: Klaus Umminger

A ROSA/LSTF experiment was conducted for OECD/NEA ROSA Project simulating a PWR loss-of-feedwater (LOFW) transient with specific assumptions of failure of scram that may cause natural circulation with high core power and total failure of high pressure injection system. Auxiliary feedwater (AFW) was provided to well observe the long-term high-power natural circulation. The core power curve was obtained from a RELAP5 code analysis of PWR LOFW transient without scram. The primary and steam generator (SG) secondary-side pressures were maintained, respectively, at around 16 and 8 MPa by cycle opening of pressurizer (PZR) power-operated relief valve and SG relief valves for a long time. Large-amplitude level oscillation occurred in SG U-tubes for a long time in a form of slow fill and dump while the two-phase natural circulation flow rate gradually decreased with some oscillation. RELAP5 post-test analyses were performed to well understand the observed phenomena by employing a fine-mesh multiple parallel flow channel representation of SG U-tubes with a Wallis counter-current flow limiting correlation at the inlet of U-tubes. The code, however, has remaining problems in proper predictions of the oscillative primary loop flow rate and SG U-tube liquid level as well as PZR liquid level.

1. Introduction

High reliability of control rods results in relatively low risk for anticipated transient without scram (ATWS) of pressurized water reactor (PWR). Failure of scram during loss-of-feedwater (LOFW) transient, however, should lead to relatively high core power for a long time and significant thermal-hydraulic responses which may cause degradation in core cooling with gradual loss of primary coolant inventory. Such phenomena include high-power natural circulation with liquid entrainment in hot leg at the inlet of pressurizer (PZR) surge-line, and counter-current flow limiting (CCFL) at the PZR bottom that may hold a large amount of coolant in the PZR, as shown in Figure 1. In the transient following LOFW, power-operated relief valve (PORV) of PZR may continue cycle opening, resulting in loss of primary coolant inventory. The core cooling conditions would then be degraded especially after the natural circulation mode turns into reflux cooling.

A LOFW-induced ATWS experiment was conducted in the LOFT (Loss of Fluid Test) program in the USA and revealed that the primary pressure is kept below about 17.2 MPa by cycle opening of the PZR PORV and safety valve while the primary fluid temperature gradually increases [1]. A LOFW-ATWS experiment in the LOBI (loop-blowdown investigations) facility in Italy showed that cycle opening of the PORV causes depletion of primary coolant inventory resulting in no plant recovery while auxiliary feedwater (AFW) is actuated just after the initiation of core dryout [2]. Experimental data, however, have been scarcely obtained for such a LOFW transient without scram where the thermal-hydraulic phenomena change as the primary coolant inventory gradually decreases with time. An experiment on LOFW transient with scram simulating PWR TMLB' scenario [3] was performed with the Large Scale Test Facility (LSTF) [4] at JAEA in 1988. The TMLB' scenario involves prolonged complete loss of AC power, including the off-site power and the on-site emergency diesel generator power, and

unavailability of turbine-driven AFW. The test on LOFW with scram revealed that two-phase natural circulation continues for a long time until significant drop starts in liquid levels in upflow side of steam generator (SG) U-tubes [5].

OECD/NEA ROSA Project experiment using the LSTF was conducted simulating a PWR LOFW transient with assumptions of high-power natural circulation due to failure of scram and total failure of high pressure injection (HPI) system. The main test objectives are to clarify thermal-hydraulic phenomena specific to natural circulation under high core power condition due to failure of scram during the LOFW transient and to obtain the detailed data on the complicated coolant behaviors during natural circulation which are suitable for the validation of best-estimate computer codes (e.g., RELAP5 code). A test condition was similar to TMLB' scenario but with AFW actuation to well observe two-phase natural circulation under high core power for relatively long time. The core power curve for the LSTF experiment was obtained by analysis for PWR LOFW transient without scram using RELAP5/MOD3.2.1.2 code [6] with one-point neutron kinetics model. It was confirmed through SKETCH-INS/TRAC-PF1 code analysis [7] that influences of three-dimensional neutron flux distribution onto core power should be small due to entire core covery by two-phase mixture. Posttest analyses for the LSTF experiment were performed by the RELAP5 code to clarify the details of major phenomena and to validate the code predictability. This paper describes major observations in the LSTF experiment and the RELAP5 post-test analysis results to understand thermal-hydraulic responses during LOFW with high-power natural circulation.

2. OECD/NEA ROSA Project

The JAEA started OECD/NEA ROSA Project in 2005 to resolve issues in thermal-hydraulic analyses relevant to light water reactor (LWR) safety by using the LSTF of JAEA [8]. Eighteen organizations from 14 NEA member countries have joined the ROSA Project to date. The OECD/NEA ROSA Project intends to focus on the validation of simulation models and methods for complex phenomena such as multidimensional mixing, stratification, parallel flows, and oscillatory flows with or without influences of noncondensable gas, which may occur during design basis events (DBEs) and beyond-DBE transients.

The experimental program is defined to provide valuable and broadly usable database to achieve the objectives agreed among participants. The ROSA Project consists of twelve LSTF experiments that include the following six types:

(1) temperature stratification and coolant mixing during emergency core cooling system (ECCS) coolant injection,

(2) unstable and destructive phenomena such as water hammer,

(3) natural circulation under high core power conditions,

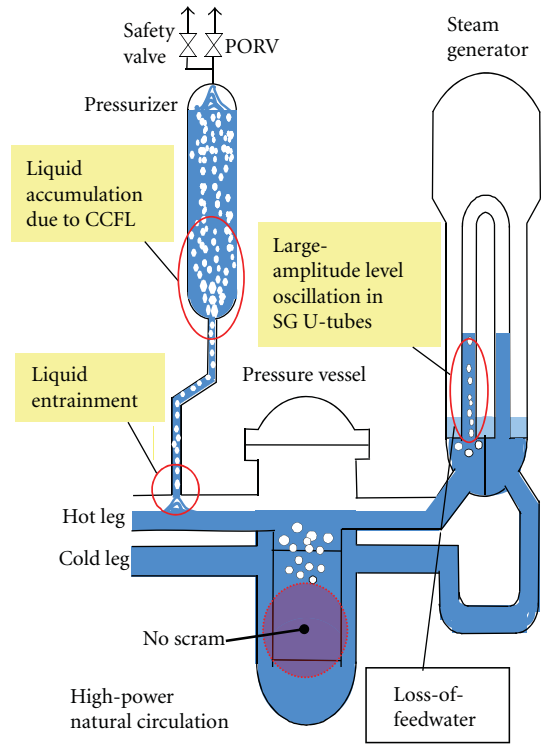

Figure 1: Thermal-hydraulic phenomena during LOFW transient without scram.

(4) natural circulation with superheated steam,

(5) primary cooling through SG secondary depressurization,

(6) request-based experiments such as small-break loss-of-coolant accident (LOCA) with break at the top or bottom of pressure vessel both being coupled with accident management measures with symptom-oriented operator actions and steam condensation on ECCS coolant during large-break LOCA.

This paper concerns the test and analysis results of LOFW transient without scram regarding the third item listed above.

3. ROSA/LSTF

The ROSA/LSTF is the world largest integral test facility designed to investigate multi-dimensional thermal-hydraulic responses during PWR transients and accidents. The LSTF simulates a Westinghouse-type four-loop 3423 MWt PWR by a two-loop system model with full-height and 1/48 in volume. The reference PWR is Tsuruga Unit-2 of Japan Atomic Power Company (JAPC). Experiments can be performed under wide range of primary and secondary pressures from reactor nominal operating pressures of 16 MPa and 8 MPa, respectively, to atmospheric pressure.

Figure 2 shows the schematic view of the LSTF that is composed of pressure vessel, PZR, and primary loops. An active SG, primary coolant pump, hot and cold legs are included in each loop. Each SG is furnished with 141 full-size

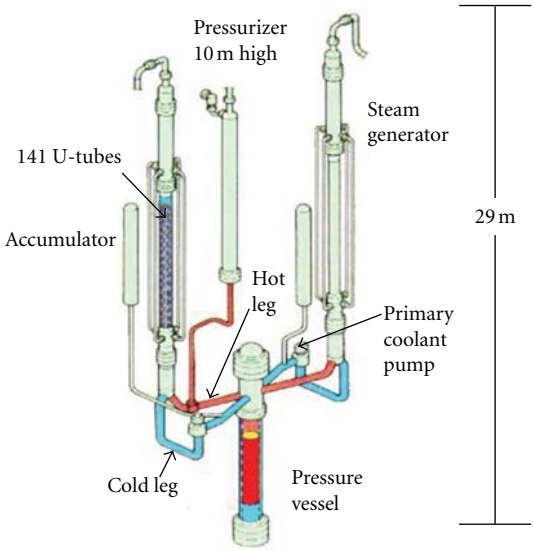

Figure 2: Schematic view of ROSA/LSTF.

Table 1: Details of LSTF U-tubes in each SG.

Type	Straight length (m)	Number of tubes	Instrumented tubes
1	9.44	21	Two short tubes
2	9.59	19	
3	9.74	19	
4	9.89	19	
5	10.04	17	Two medium tubes
6	10.19	15	
7	10.34	13	
8	10.49	11	
9	10.64	7	Two long tubes

U-tubes (inner diameter of 19.6 mm, nine different heights as shown in Table 1), inlet and outlet plena, boiler section, steam separator, steam dome, steam dryer, main steam line, four downcomer pipes, and other internals. Six U-tubes are instrumented for each SG. Instrumented tubes designated as Tubes 1 and 6 are short tubes (Type 1 in Table 1), Tubes 2 and 5 are medium tubes (Type 5), and Tubes 3 and 4 are long tubes (Type 9). The hot and cold legs, 207 mm in inner diameter, are sized to conserve the volumetric scaling (2/48) and the ratio of the length to the square root of the diameter to simulate the flow regime transitions in the horizontal legs [9]. All types of ECCS are equipped with additional features such as ECCS coolant temperature control especially for accumulators.

The LSTF core, 3.66 m in active height, consists of 1008 electrically heated rods in 24 rod bundles to simulate the fuel rod assembly in the reference PWR. Axial core power profile is a 9-step chopped cosine with a peaking factor of 1.495. The radial power profile is achieved by providing three different power bundles (high, mean, and low) with a maximum peaking factor of 1.51 for high-power bundle. The LSTF initial core power of 10 MW corresponds to 14% of the volumetric-scaled (1/48) PWR nominal core power because of a limitation in the capacity of power supply. The core power after the test initiation is then kept constant at 10 MW for a little while before the core power starts to follow predetermined decay curve.

Instrumentations around 1900 channels provide detailed information on thermal-hydraulic conditions and responses for such parameters as temperature, liquid level, pressure, flow rate, and fluid density. The break flow rate including discharge flow rate through PORV of PZR is estimated from the level increase rate in the catch tank called ST. Visual

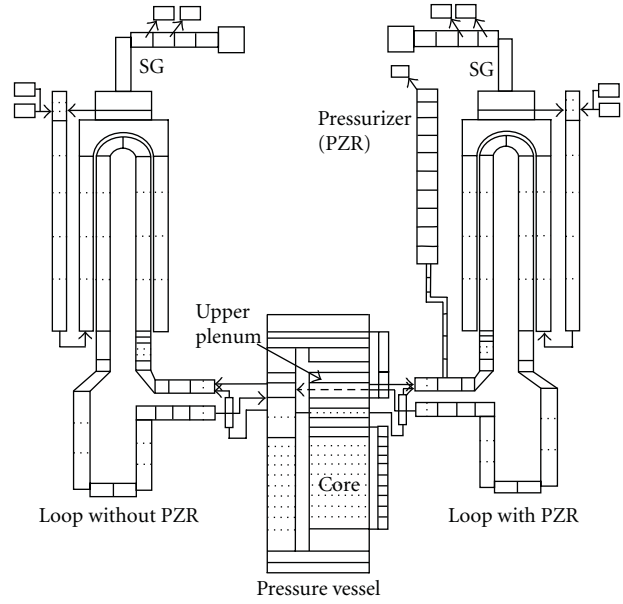

Figure 3: Noding schematic of PWR for RELAP5 analysis.

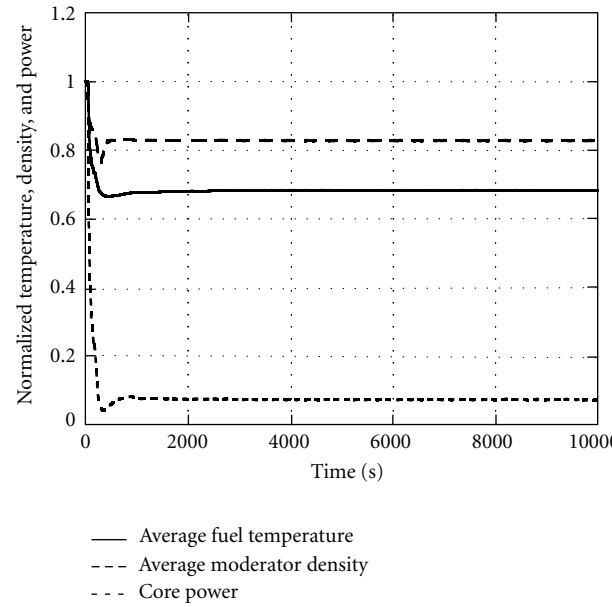

Figure 4: PWR average fuel temperature, average moderator density, and core power calculated by RELAP5 code.

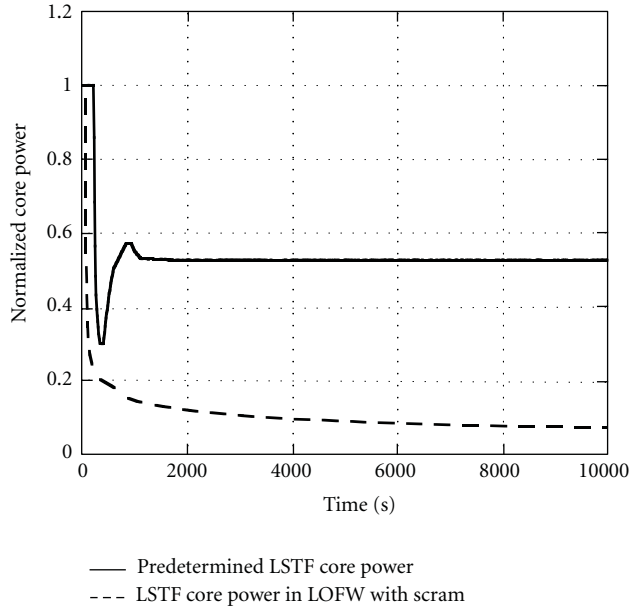

Figure 5: LSTF core power curve pre-determined through PWR analysis, being compared with LSTF core power decay curve in case of LOFW with scram.

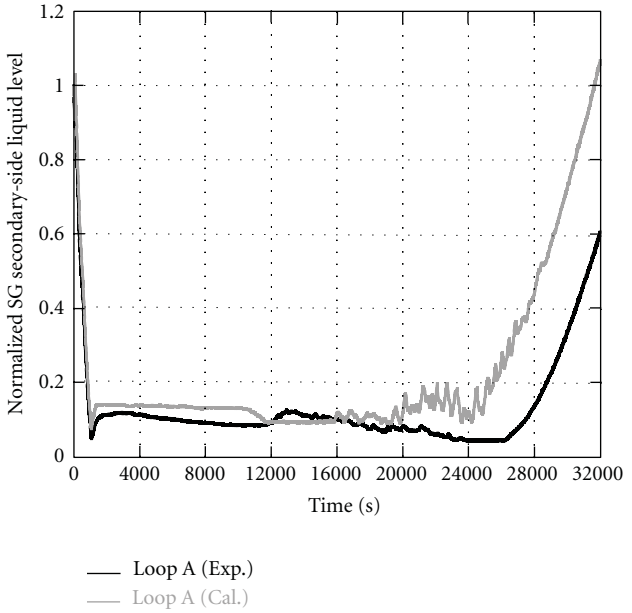

Figure 7: LSTF and RELAP5 results for SG secondary-side collapsed liquid level in loop with PZR.

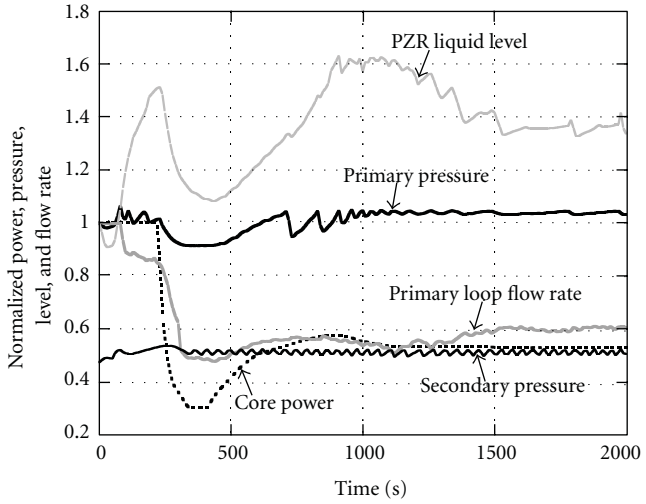

Figure 6: LSTF results for core power, primary and secondary pressures, PZR liquid level, and primary mass flow rate in loop with PZR (0 to 2000 s).

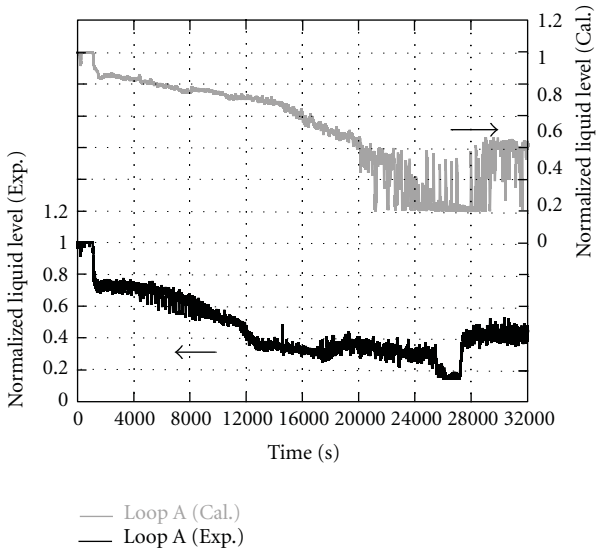

Figure 8: LSTF and RELAP5 results for hot leg liquid level in loop with PZR.

observation of flow is conducted in horizontal legs by using "video probe," a periscope that withstands high-temperature steam/water conditions employing cooling-free glass-fiber cables or air-cooled bore scopes.

Since the shakedown test in 1985, the LSTF has provided experimental data including the 5% cold leg break LOCA simulation for OECD/NEA ISP-26 and the Mihama Unit-2 SG tube rupture accident for the Nuclear Safety Commission of Japan. Throughout its operational history, the facility has demonstrated excellent experimental capabilities and has provided unique data for nonequilibrium, nonhomogeneous, and multidimensional phenomena that may arise during reactor accidents and abnormal transients.

4. PWR Analysis to Define LSTF Core Power

Analysis for PWR LOFW transient without scram was performed by the RELAP5/MOD3.2.1.2 code to define the LSTF core power to correctly simulate the power transient under influences of coolant conditions such as density and

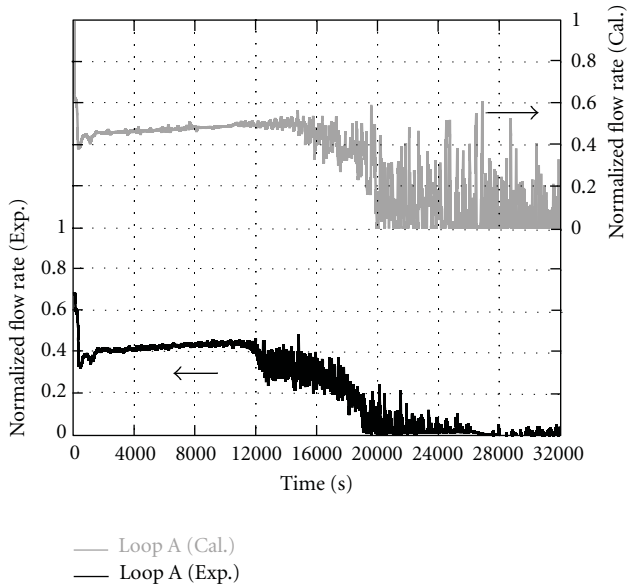

Figure 9: LSTF and RELAP5 results for primary mass flow rate in loop with PZR.

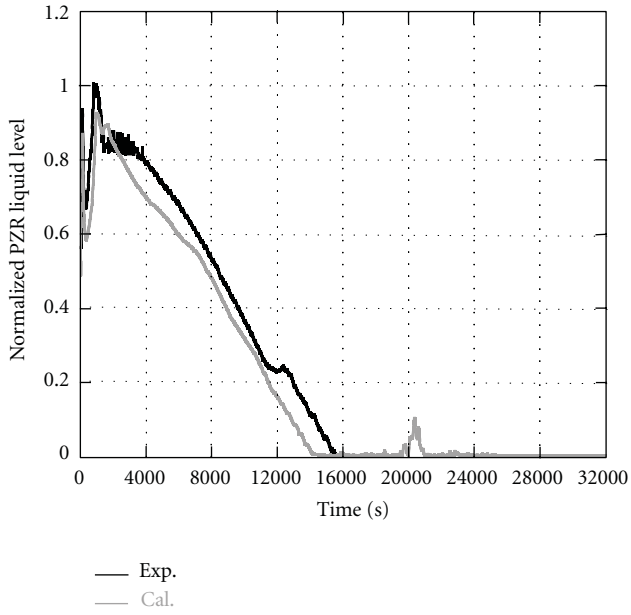

Figure 10: LSTF and RELAP5 results for PZR liquid level.

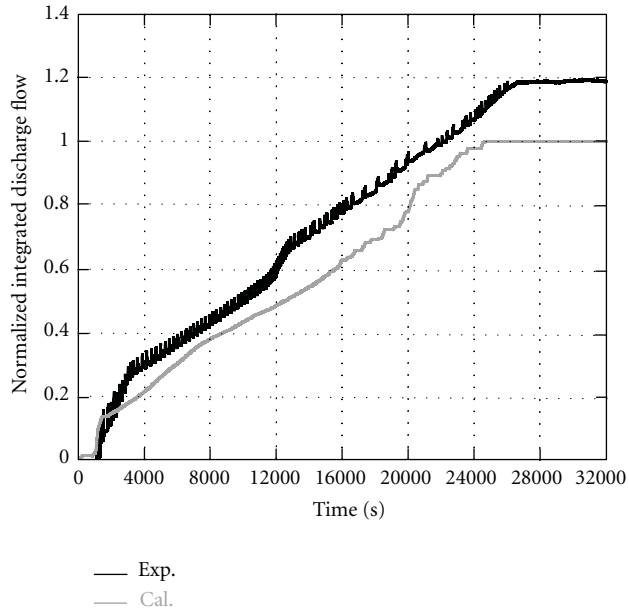

Figure 11: LSTF and RELAP5 results for integrated discharge flow through PORV.

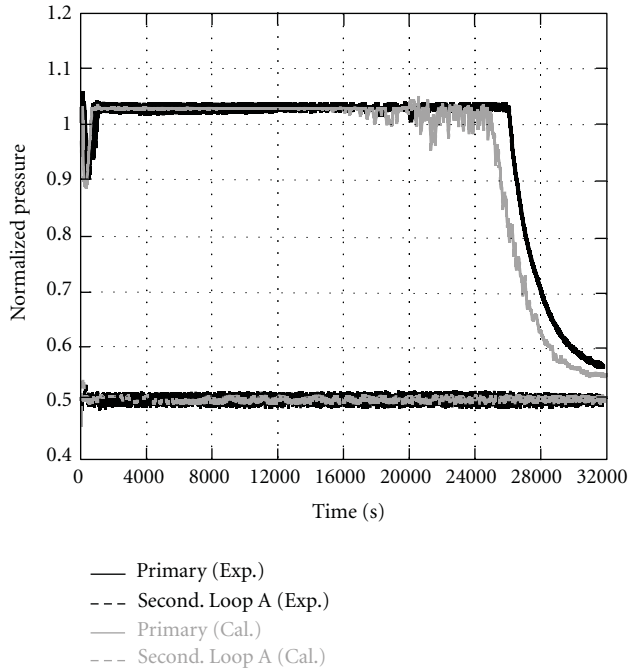

Figure 12: LSTF and RELAP5 results for primary and secondary pressures in loop with PZR.

void fraction in the core. Figure 3 shows a noding schematic of PWR for the RELAP5 analysis. PWR system is modeled in one-dimensional manner including pressure vessel, primary loops, PZR, SGs, and SG secondary-side system. Four-loop PWR is then modeled by a two-loop noding, similar to that for LSTF noding (to be shown in Figure 23), which is composed of one loop with PZR and the other loop corresponding to three loops without PZR. The Doppler and moderator density reactivity coefficients are based on four-loop PWR reference data at the beginning of cycle under the hot nominal core power condition [7]. The PWR analysis employed RELAP5 critical flow model for the PORV with a discharge coefficient of 1.0. Major assumptions include total failure of HPI system and loss of off-site power at scram signal.

"SG secondary-side narrow-range liquid level low" signal is generated to trigger scram signal. The set point of this signal is 10% of the SG secondary-side narrow-range liquid

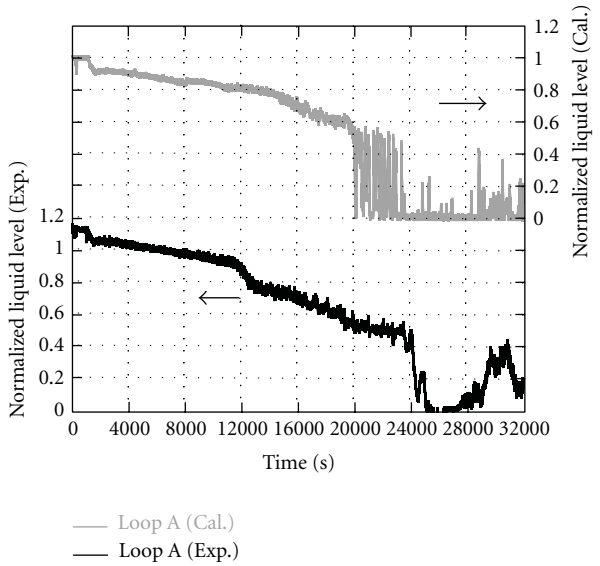

Figure 13: LSTF and RELAP5 results for SG inlet plenum collapsed liquid level in loop with PZR.

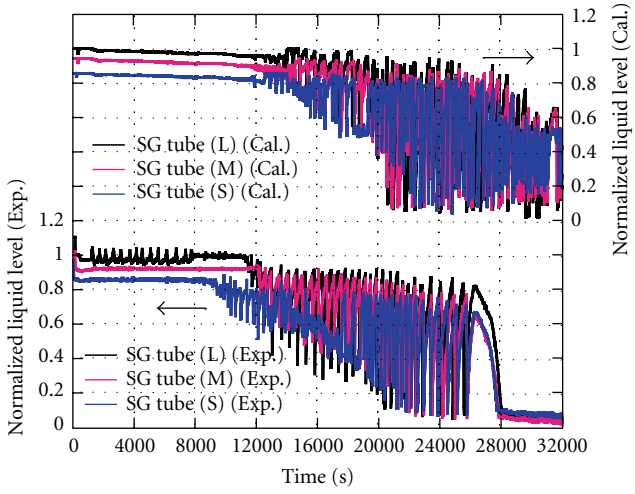

Figure 14: LSTF and RELAP5 results for collapsed liquid levels in upflow side of SG U-tubes in loop with PZR.

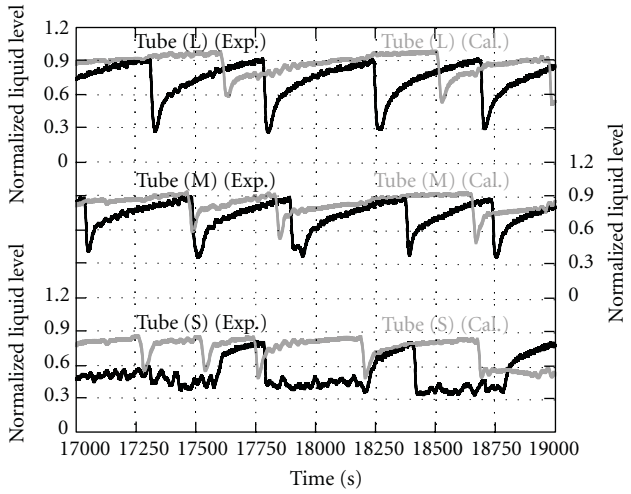

Figure 15: LSTF and RELAP5 results for collapsed liquid levels in upflow side of SG U-tubes in loop with PZR during large-amplitude level oscillation period.

level. The scram signal was generated at 50 s, causing the closure of SG main steam isolation valves (MSIVs) and the coastdown of primary coolant pumps. This condition was employed in the LSTF experiment. AFW in both loops was assumed to start when the SG secondary-side becomes empty of liquid.

Figure 4 compares the calculated average fuel temperature, average moderator density, and core power. The core power decreased due to negative feedback induced mainly by an increase in the average fluid temperature, thus a decrease in the average coolant density. The core power was kept at around 250 MW (7.4%) after about 1100 s due to the balance of Doppler and moderator density reactivity, reaching almost nearly equilibrium conditions. The core power curve obtained by the RELAP5 code analysis was referred in the LSTF experiment. Figure 5 shows the predetermined core power curve obtained from the PWR analysis and consideration of volumetric scaling of LSTF, being compared with LSTF core power decay curve in case of LOFW with scram [10]. The portion higher than 10 MW (14%) is cut off due to the limitation in the power supply.

5. LSTF Experiment and Code Analysis Results

5.1. LSTF Test Conditions. The PZR pressure, fluid temperatures in hot and cold legs during initial steady-state conditions were 15.5 MPa, 597 K, and 563 K, respectively, according to the reference PWR conditions. Initial secondary pressure was raised to 7.3 MPa from nominal value of 6.1 MPa to limit the primary-to-secondary heat transfer rate to 10 MW. Set point pressures for opening and closure of the PZR PORV are 16.20 and 16.07 MPa, respectively, and are 8.03 and 7.82 MPa for the SG relief valves (RVs), referring to the corresponding values in the reference PWR. Initial SG secondary-side collapsed liquid level was set to about 7.3 m based on the PWR analysis result, for better simulation of the liquid level transient in the reference PWR. To avoid deformation of SG structures including U-tubes (bottom) due to thermal shock from injection of cool AFW coolant onto high-temperature structures, AFW was initiated in both loops when the SG secondary-side collapsed liquid level still remained by at least about 0.5 m. AFW flow rate in each loop was fixed to about 0.85 kg/s, which corresponded to about 120% of the volumetrically scaled rate, to maintain a continuous primary-to-secondary heat removal under high core power through the LSTF pre-test analysis [11].

5.2. Major Phenomena Observed in the Experiment. The LSTF test results are shown in Figures 7–21 as a comparison with RELAP5 posttest analysis results, except for Figure 16. The major phenomena observed in the experiment are

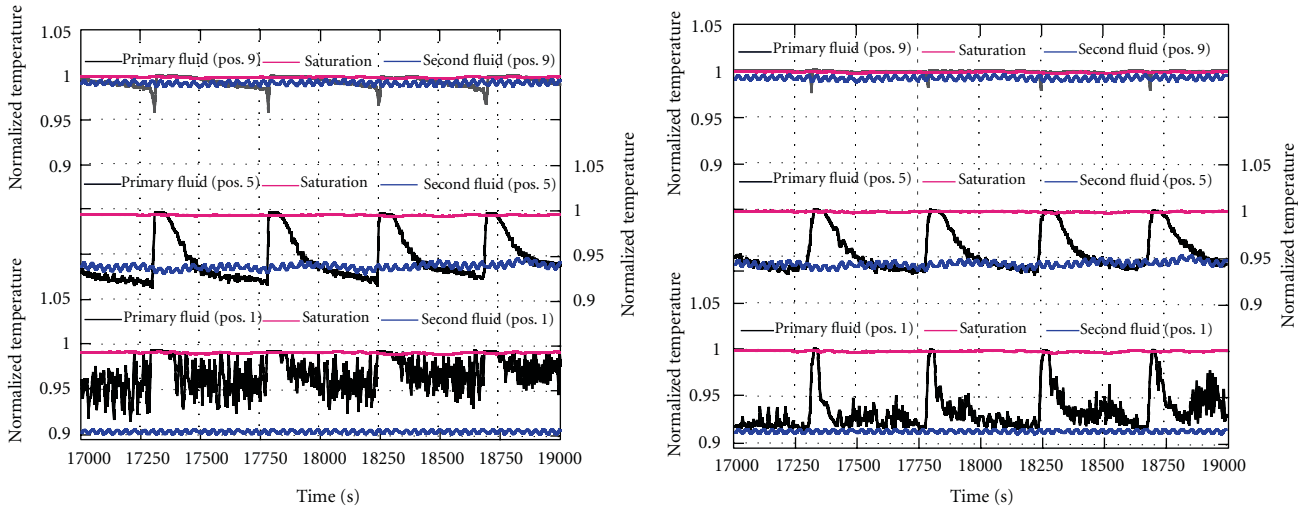

(a) Tube upflow side

(b) Tube downflow side

Figure 16: LSTF results for fluid temperatures in primary and secondary side of SG Tube 3 in loop with PZR at Positions 1, 5 and 9 during large-amplitude level oscillation period.

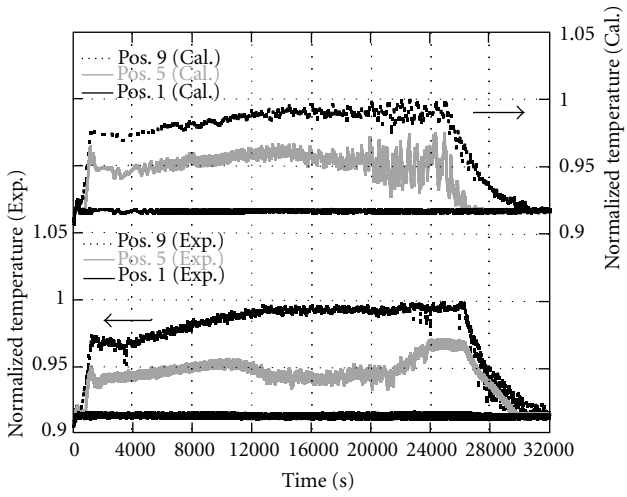

Figure 17: LSTF and RELAP5 results for fluid temperatures in secondary-side of SG Tube 3 in loop with PZR at Positions 1, 5, and 9.

explained by classifying them into the following three stages of transient.

(1) Before Initiation of AFW (0 to about 1030 s). The experiment was initiated by the termination of main feedwater at time zero. The core power was maintained at 10 MW for 170 s after the scram signal, while it was kept at around 5.3 MW (7.4%) after about 1100 s as shown in Figure 5 until automatic power reduction due to high core temperature.

Figure 6 compares major parameters in the initial transient. After the MSIV closure at about 55 s, the SG secondary-side pressure increased rapidly up to about 8.4 MPa, causing the SG RV to be kept opened for a while due to high core power. The primary pressure also increased rapidly after the MSIV closure up to around 16 MPa due to high core power and oscillated thereafter by cycle opening of the PORV. The PZR liquid level continuously increased after the MSIV closure irrespective of cycle opening of the PORV, except some while after about 230 s in response to the core power decrease thus the primary pressure decrease. The PZR became full of liquid temporarily after about 900 s by volumetric expansion of coolant. Single-phase liquid natural circulation started at about 300 s when the primary coolant pumps stopped. The SG secondary-side collapsed liquid level rapidly decreased to about 0.5 m at about 1030 s as shown in Figure 7, and the AFW was started the coolant injection in both SGs.

(2) After Initiation of AFW (about 1030 to 24000 s). The primary loop flow turned into two-phase natural circulation after about 1150 s when liquid level appeared in the hot leg as shown in Figure 8. The primary loop flow rate gradually increased thereafter as shown in Figure 6 and started to decrease with some oscillation after about 11500 s as shown in Figure 9 when the liquid level in the hot leg became lower than the half height. The PZR liquid level shown in Figure 10 decreased very slowly after the actuation of AFW. The PZR liquid level stayed at certain constant levels of about 83% at around 1500–3500 s and of about 23% at around 11500–12500 s probably due to flooding at the PZR bottom because of temporary high discharge rate through the PORV as shown in Figure 11. The PZR became empty of liquid at about 15800 s.

AFW initiated at about 1030 s provided a continuous primary-to-secondary heat removal. The SG secondary-side pressure was kept at around 8 MPa by frequent cycle opening of the RVs as shown in Figure 12. There was no apparent relationship between the cycle open timings of the PORV and the SG RVs.

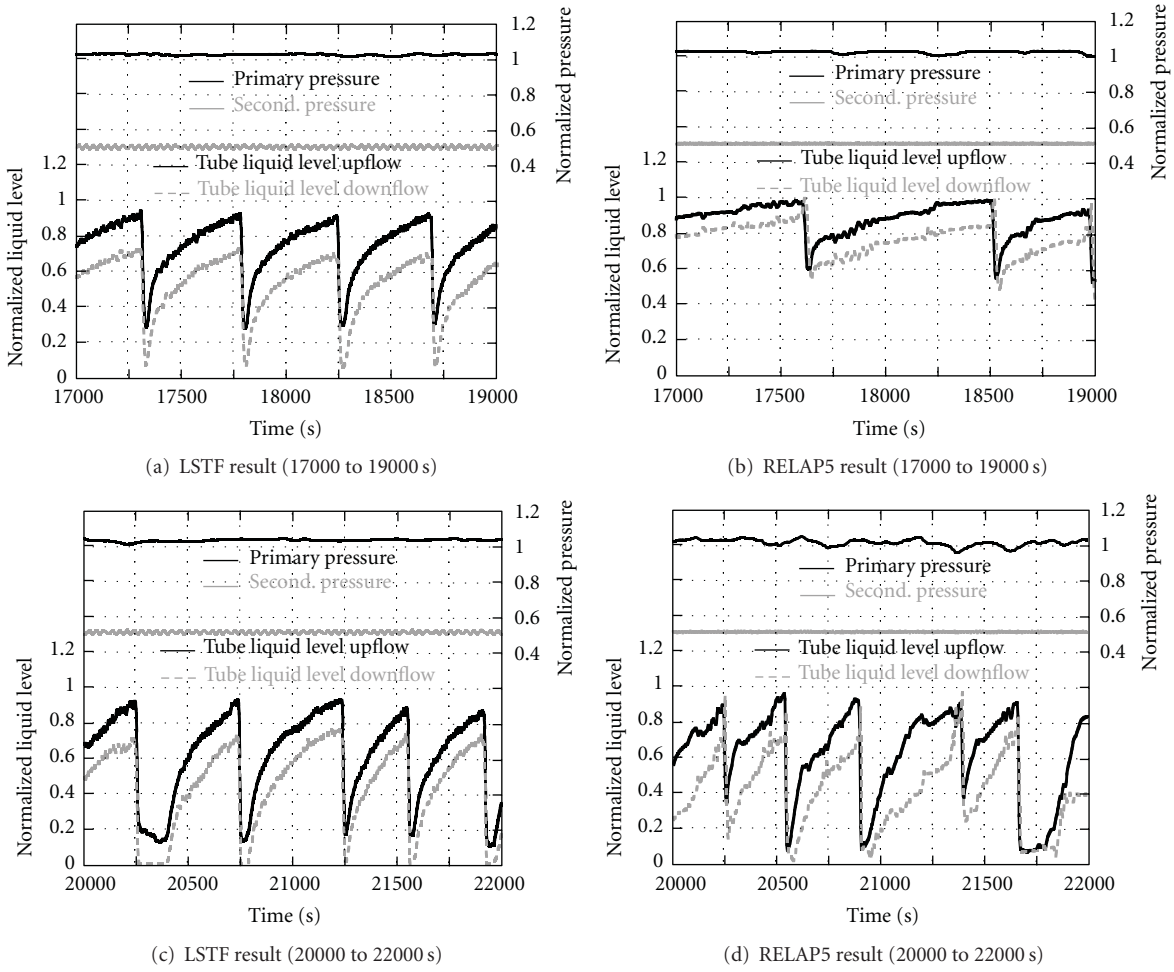

Figure 18: LSTF and RELAP5 results for collapsed liquid levels in SG Tube 3 in loop with PZR compared with primary and secondary pressures during large-amplitude level oscillation period.

Figures 13 and 14, respectively, show the collapsed liquid levels in SG inlet plenum and upflow side of SG U-tubes, typically Tube 1 designated as S, Tube 2 designated as M, and Tube 3 designated as L of SG in the loop with PZR (loop A). The void fraction in the SG inlet plenum gradually increased, but SG U-tubes were filled almost with single-phase liquid until around 11500 s. After the voiding started in the SG U-tubes, the primary loop flow rate shown in Figure 9 gradually decreased as the void fraction increased in the U-tubes. A large-amplitude long-term oscillation developed in the void fraction in each of U-tubes rather randomly as shown in Figure 15. Large-amplitude level oscillation, in a form of slow fill and dump, started after around 10200, 12000, and 11400 s, respectively, in Tubes S, M, and L in the loop with PZR. The onset timings were different among U-tubes but similar in the two instrumented tubes with the same length. The time period of the fill and dump depended on the tube length such that the period is longer in the longer tubes. Integration of such a random fill and dump behavior in many SG U-tubes resulted in the continuous natural circulation through the loop with rather small flow fluctuation.

Figure 16 shows the fluid temperatures in both the primary and secondary side of SG Tube 3 in the loop with PZR at Positions 1, 5, and 9, respectively, at about 0.8, 3.4, and 8.5 m from the bottom of SG boiler section during the large-amplitude level oscillation period. The primary saturation temperature based on the upper plenum pressure is compared as a reference. There was fluid temperature gradient in the secondary side as the temperature increased with the elevation. The primary fluid temperature at Position 9 stayed almost at the saturation temperature except when the dump phenomena (drain of low-temperature condensate column to downflow side) happened, indicating small steam heat removal to the secondary side thus less steam condensation. At the lower elevations, the primary fluid temperature fluctuated between the primary saturation and secondary-side temperatures. During the long-term fill period when the low-temperature condensate column develops, the primary coolant temperature in the upflow side became even lower than the secondary-side fluid temperature typically at Position 5 because low-temperature coolant rose from the lower elevation with lower secondary-side fluid temperature. At the entrance of the tube, saturated

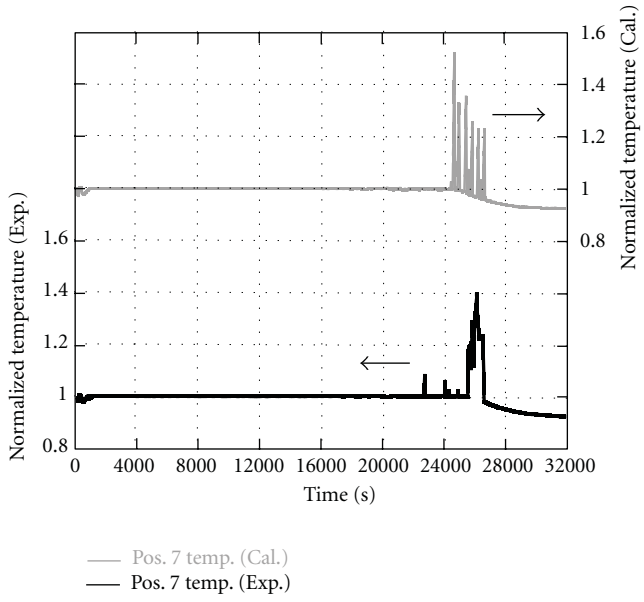

Figure 19: LSTF and RELAP5 results for cladding surface temperature.

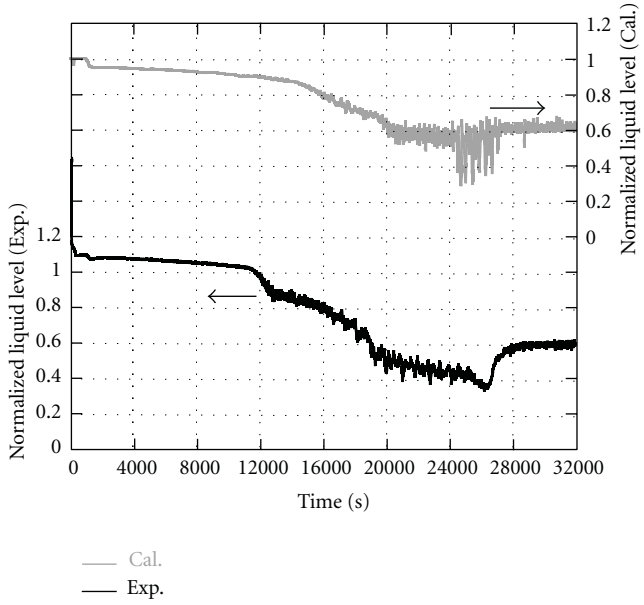

Figure 20: LSTF and RELAP5 results for core collapsed liquid level.

steam constantly entered probably as two-phase mixture, causing frequent temperature fluctuation. The primary fluid temperature in the downflow-side, on the other hand, stayed at the secondary-side fluid temperature and recovered to the primary saturation temperature only when the water column drains, because the SG outlet plenum was filled with subcooled coolant. Large temperature difference as much as 54 K between primary and secondary coolant at around the tube entrance enhanced the effective steam condensation. The SG secondary-side fluid temperature at Position 1 stayed almost at certain temperature as shown in Figure 17.

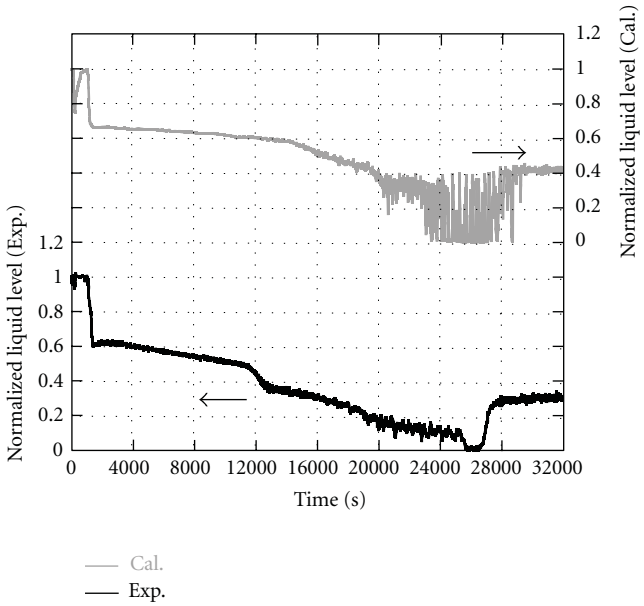

Figure 21: LSTF and RELAP5 results for upper plenum collapsed liquid level.

Figure 18 shows the collapsed liquid levels in SG Tube 3 in the loop with PZR during the large-amplitude level oscillation period, being compared with the primary and secondary pressures. Liquid levels slowly increased and suddenly dropped simultaneously in both the upflow side and downflow side of U-tube as the developed water column drained to the SG outlet plenum. This response appeared rather randomly at different timings among the U-tubes (Figure 15). The frequency of the water column development, thus the fill and dump frequency, was far lower than that of the cycle opening of the PORV and the SG RVs.

Such coolant behaviors in the SG U-tubes also appeared in LSTF experiment simulating two-phase natural circulation at high pressures under the constant secondary-side fluid temperature [12]. Intervals between the dumps in the tube with the same length in this experiment, however, were longer than in the natural circulation test due to influences of the vertical fluid temperature distribution along the SG boiler section shown in Figure 17.

(3) During Reflux Condensation Mode (about 24000 to 32000 s). Natural circulation mode may have changed into reflux condensation after around 24000 s when significant drop started in the SG inlet plenum liquid level (Figure 13). The liquid level in the SG U-tube did not decrease to zero (Figure 14) due to significant steam condensation at the tube entrance as well as CCFL till the end of the test.

The natural circulation contributed to maintain core cooling for rather long time as long as the core is covered by coolant even under high core power (Figures 19 and 20). Temporary large drop happened in the core liquid level when the water column developed in the SG U-tubes after about 22780 s though liquid level was still in the upper plenum (Figure 21), causing an intermittent increase that

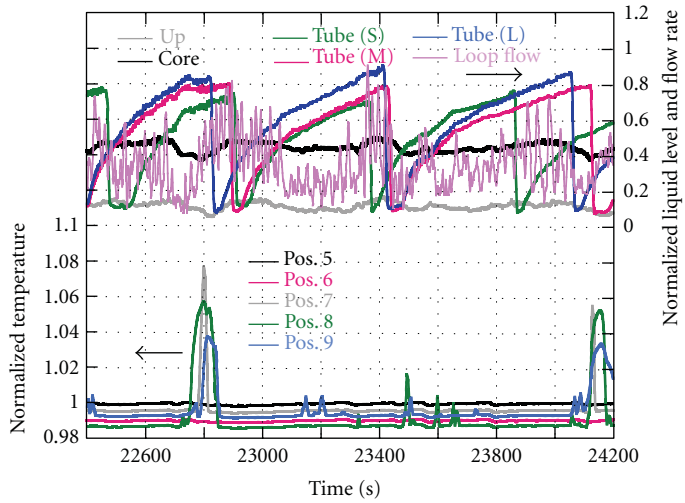

Figure 22: LSTF results for cladding surface temperature, collapsed liquid levels in upper plenum, core, and upflow side of SG U-tubes and primary mass flow rate in loop with PZR (22400 to 24200 s).

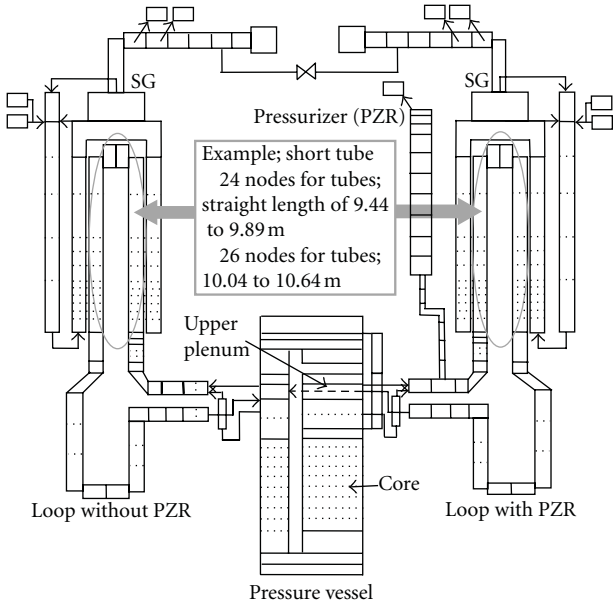

Figure 23: Noding schematic of LSTF for RELAP5 analysis.

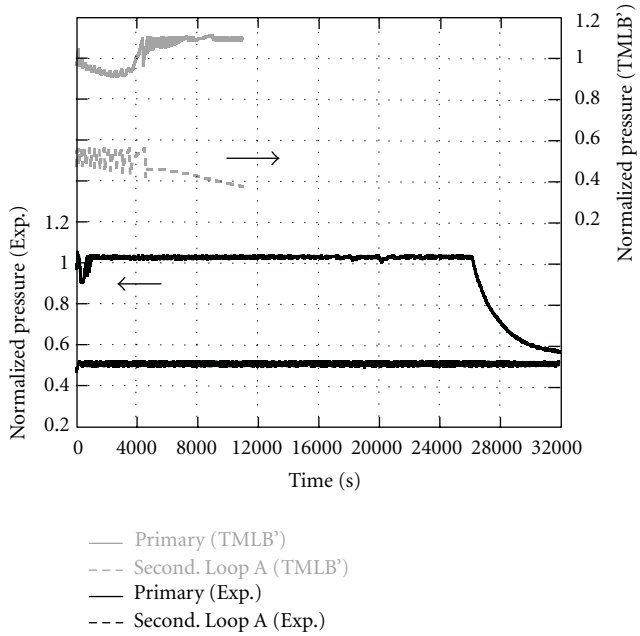

Figure 24: Comparison with TMLB' scenario test results for primary and secondary pressures in loop with PZR.

may occur in the cladding surface temperature of simulated fuel rods at higher than Position 7 (= about 0.8 m above the core center) as shown in Figure 22. A temperature excursion appeared in the core due to core boil-off after the upper plenum became empty of liquid. Therefore, core power was decreased to protect the LSTF core when the cladding surface temperature exceeded pre-determined criterion of 873 K. The peak cladding temperature (PCT) was observed at Position 7 when the core power control started. Then the core power was automatically decreased down to 75% of the pre-determined power level. Water column drained in the SG U-tubes rather slowly thereafter as the secondary-side fluid temperature became uniform (Figure 17) due to an increase in the secondary-side liquid level (Figure 7). Whole core was quenched, being followed by a decrease in the primary pressure (Figure 12) and an increase in the core liquid level.

5.3. RELAP5 Code Analysis

5.3.1. RELAP5 Analysis Conditions. Post-test analyses for the LSTF experiment were conducted with the RELAP5/MOD3.2.1.2 code by incorporating a two-phase critical flow model [13], which may correctly predict the discharge rate through a sharp-edge orifice to simulate the PORV. The

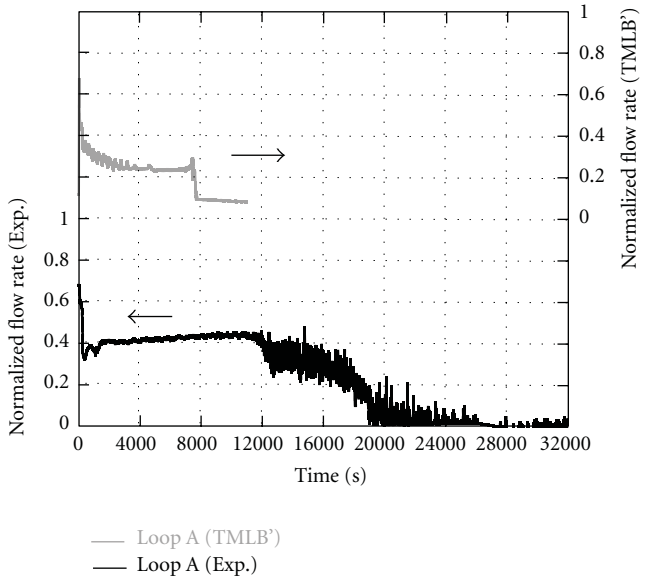

Figure 25: Comparison with TMLB' scenario test results for primary mass flow rate in loop with PZR.

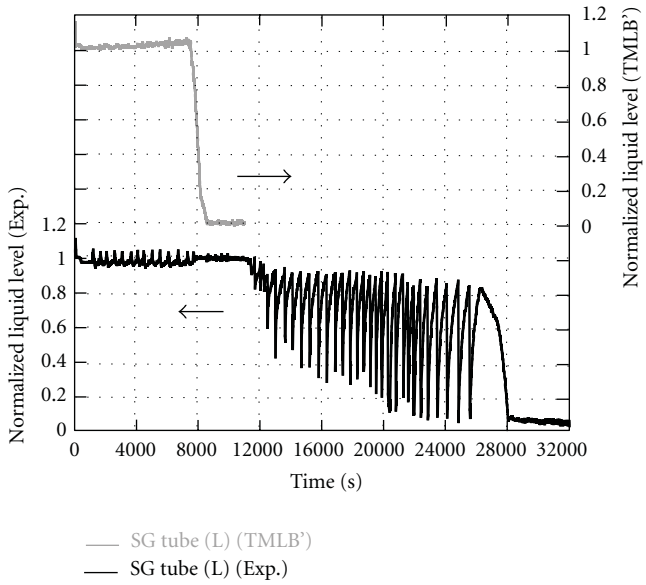

Figure 26: Comparison with TMLB' scenario test results for collapsed liquid level in upflow side of SG Tube 3 in loop with PZR.

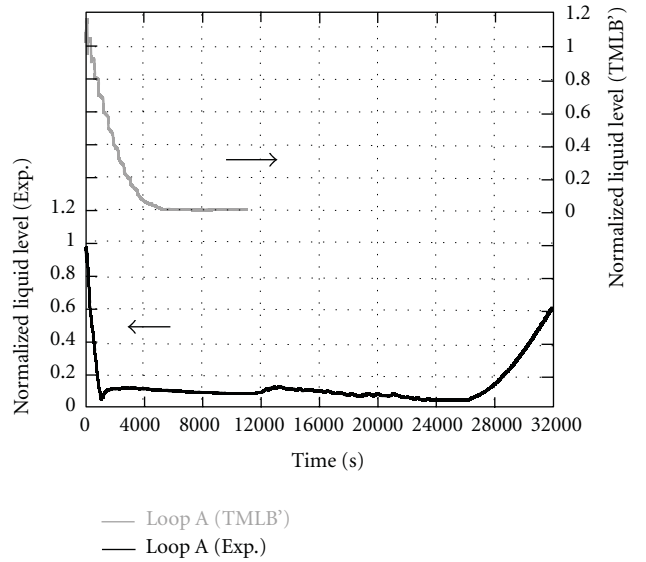

Figure 27: Comparison with TMLB' scenario test results for SG secondary-side collapsed liquid level in loop with PZR.

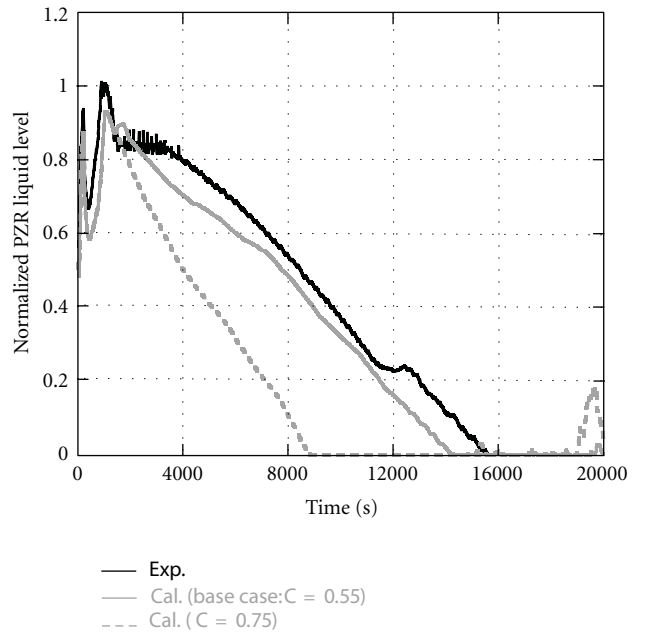

Figure 28: RELAP5 results for PZR liquid level in cases with different constants C of Wallis CCFL correlation at both all PZR and surge-line junctions.

model employs the maximum bounding flow theory with a discharge coefficient (Cd) of 0.61 for two-phase discharge flow [14]. Cd of 0.84 was used for single-phase discharge steam [15].

Figure 23 shows a noding schematic of LSTF for RELAP5 analysis. The LSTF system is modeled in one-dimensional manner including pressure vessel, primary loops, PZR, SGs, and SG secondary-side system. The SG U-tubes were modeled by nine parallel flow channels that correspond to 9 types of U-tubes with different height, namely, 24 nodes for short-to-medium tubes (straight length of 9.44 to 9.89 m, four cases in Table 1) and 26 nodes for medium-to-long tubes (straight length of 10.04 to 10.64 m, five cases), for better prediction of the complicated nonuniform coolant behaviors during natural circulation [16].

The core was represented by vertically stacked nine equal-height volumes according to 9-step chopped cosine power profile along the length of the core. The radial power distribution was then given considering the peaking factor and the number of high-, mean- and low-power rod bundles.

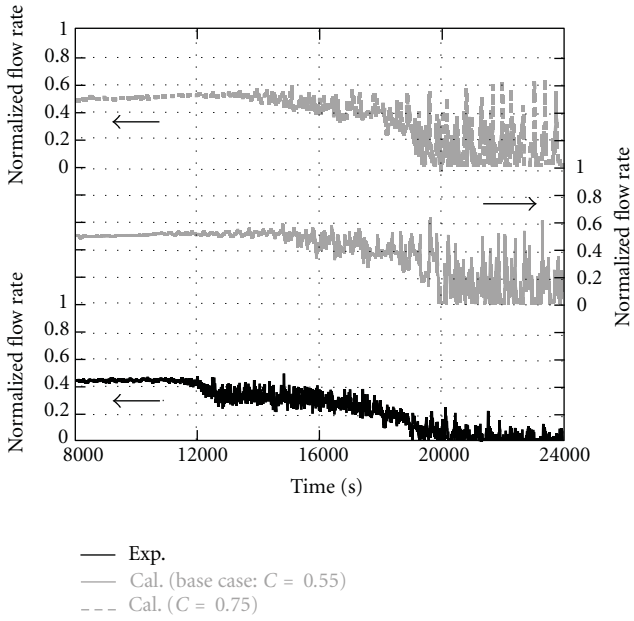

Figure 29: RELAP5 results for primary mass flow rate in loop with PZR in cases with different constants C of Wallis CCFL correlation at both all PZR and surge-line junctions.

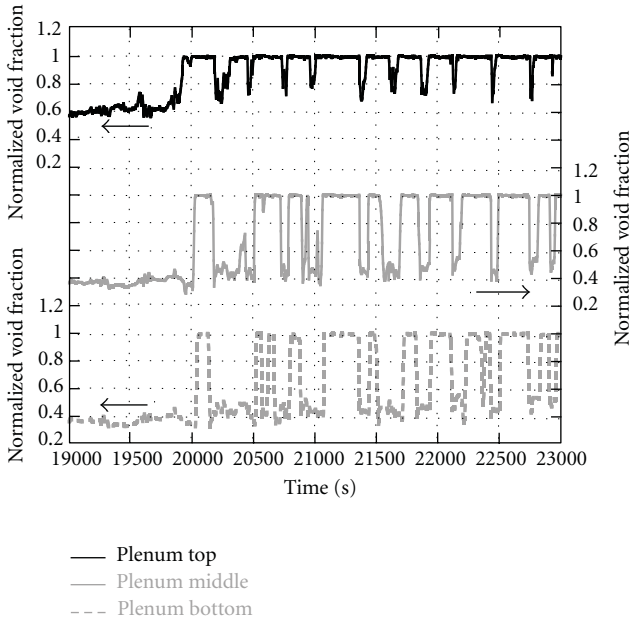

Figure 30: RELAP5 results for void fraction at top, middle, and bottom of SG inlet plenum in loop with PZR.

Following Wallis correlation [17] was applied to simulate CCFL at both the inlet of U-tubes and inlet plena of SGs:

$$j_G^{*1/2} + m j_L^{*1/2} = C, \quad (1)$$

where j^* is the nondimensional volumetric flux. Subscripts G and L denote gas and liquid phases, respectively. Constants of m and C for both the inlet of U-tubes and inlet plena of SGs were set to 1 and 0.75, respectively, obtained from LSTF experiment on CCFL at the SG U-tube inlet [18]. Influences of the CCFL correlation at the inlet of U-tubes are discussed in Section 6.2.

The PZR was represented by ten vertical nodes to simulate corresponding facility configuration. RELAP5 liquid entrainment model for a horizontal pipe was applied to the PZR surge-line inlet junction connected to the hot leg. Wallis correlation was also applied to simulate CCFL at both all the PZR and the surge-line junctions. Coefficients of m and C of the CCFL correlation were then given as 1 and 0.55 as trial values because of no empirical constants depending on flow channel structure, considering the LSTF test result for the timing when the liquid level was lost in the PZR (Figure 10). Influences of the constants of the CCFL correlation at both all the PZR and the surge-line junctions are discussed in Section 6.2. The core power was decreased down to 75% when the PCT reached 873 K as in the experiment. Other initial and boundary conditions were determined according to the LSTF test data.

5.3.2. Comparison of Analysis Results with Experimental Observations. The RELAP5 code predicted well the overall trend of the LSTF experiment for such parameters as primary and secondary pressures due to relatively well predictions of cycle opening of the PORV and the SG RVs as has been compared in Figures 7–21 except Figure 16. The code, however, underpredicted the integrated discharge flow through the PORV (Figure 11) due to earlier change from two-phase flow into single-phase steam discharge because of underprediction of the PZR liquid level (Figure 10) by influences of uncertainties in RELAP5 liquid entrainment model in the hot leg at the inlet of PZR surge-line under high-pressure conditions.

As shown in Figures 14 and 15, large-amplitude level oscillation with some randomness among the SG U-tubes during two-phase natural circulation was qualitatively reproduced by the employed noding with fine-mesh multiple parallel flow channels with a Wallis CCFL correlation at the inlet. Similar to the experiment, the longer tubes tended to have longer intervals between the dumps. However, there were still some differences in both frequency and amplitude of the SG U-tube level oscillation. The SG secondary-side collapsed liquid level and fluid temperature under influences of AFW agreed reasonably well with those in the experiment (Figures 7 and 17).

Two-phase natural circulation was well simulated, though with tendencies that the hot leg liquid level and the primary loop flow rate were overpredicted before about 11500 s probably due to underprediction of carryover of entrained liquid into the PZR surge-line (Figures 9 and 10). The decrease in the primary loop flow rate with some oscillation was well calculated too, though with a tendency that the oscillation amplitude of the loop flow rate was larger than in the experiment (Figure 9). Larger oscillation in the primary pressure resulted in large level oscillation in the hot

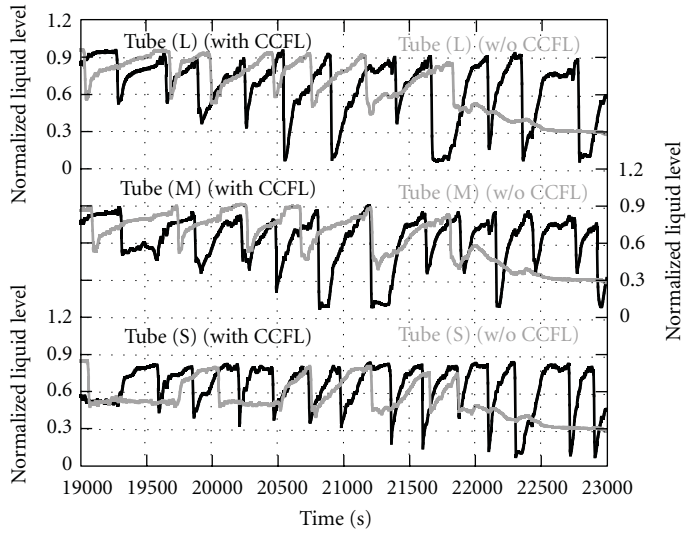

Figure 31: RELAP5 results for collapsed liquid levels in upflow side of SG U-tubes in loop with PZR in cases with or without application of Wallis CCFL correlation to inlet of U-tubes.

leg and the SG inlet plenum especially after about 21500 s (Figures 8, 13, and 18).

The code failed to reproduce the intermittent increase in the cladding surface temperature even before major core uncovery due to failure of large drop in the core liquid level probably because of some discrepancies in the SG U-tube level oscillation. Major core uncovery after the empty of liquid in the upper plenum started somewhat earlier than in the experiment probably due to influences of the differences in the SG U-tube level oscillation (Figures 20 and 21). Then the PCT was about 70 K higher than in the experiment (Figure 19).

6. Discussion

6.1. Comparison with TMLB' Scenario Test Results. The results of this experiment were compared with the TMLB' scenario test results [5] to clarify influences of the different conditions especially for core power and AFW actuation onto the major phenomena. In both experiments, the primary- and SG secondary-side pressures were kept high, respectively, by cycle opening of valves in the PZR and SG secondary-side system as shown in Figure 24. In this experiment, two-phase natural circulation started much earlier than in the TMLB' scenario test due to high core power as shown in Figure 25. Large-amplitude level oscillation also took place in the SG U-tubes for a long time while the two-phase natural circulation flow rate gradually decreased with some oscillation because of a continuous primary-to-secondary heat removal by the actuation of AFW. In the TMLB' scenario test, on the contrary, the primary loop flow rate became almost zero when significant drop happened in the SG U-tube liquid levels as shown in Figure 26 after the SG secondary-side became empty of liquid as shown in Figure 27 due to no AFW. In this experiment, therefore, a temperature excursion happened in the core much later than in the TMLB' scenario test. The influences of AFW were found so significant for the time to start major core uncovery.

6.2. RELAP5 Analysis Results. The CCFL at the PZR bottom may affect the PZR liquid level and the primary loop flow rate. Influences of the constants of the Wallis CCFL correlation at both all the PZR and the surge-line junctions onto the PZR liquid level and the primary loop flow rate were thus investigated as shown in Figures 28 and 29. The analysis with the constant C of the CCFL correlation in (1) to be 0.55 (trial value) was done as the base case, focusing on the timing of empty of liquid in the PZR, and was compared with the case with $C = 0.75$ obtained by LSTF experiment for CCFL at the SG U-tube inlet [18] under a common condition of constant $m = 1$. The PZR liquid level in the case with the constant $C = 0.75$ decreased after about 1400 s and was lost at about 8770 s which was much earlier than in the base case. The primary loop flow rate then became almost zero earlier than in the base case due to earlier depletion in the primary coolant inventory. Constants of the CCFL correlation at both all the PZR and the surge-line junctions for the LSTF were thus fixed to be $C = 0.55$ and $m = 1$.

The calculated results had some differences from the measured data especially in both frequency and amplitude of the SG U-tube level oscillation, though the SG U-tubes were finely modeled as described in Section 5.3.1 with a Wallis CCFL correlation at the inlet of U-tubes. The oscillation amplitude of the primary loop flow rate was also larger than in the experiment. The vertical secondary-side fluid temperature gradient was calculated reasonably well due to good prediction of steam upward flow towards the RVs under a condition that the void fraction in the secondary-side was kept high during the actuation of AFW.

The calculation revealed that liquid level appears in the SG inlet plenum due to very large void fraction as much as 50% and the top is filled almost with single-phase steam after around 20000 s, as shown in Figure 30. The calculated results for the SG U-tube liquid levels were compared in the cases with or without application of the Wallis CCFL correlation to the inlet of U-tubes to clarify influences of the CCFL at the tube inlet onto the level oscillation, as shown in Figure 31. Level oscillation amplitude in the tube with the same length in the case without the CCFL became smaller than in the case with the CCFL after around 20000 s. In the case without the CCFL, liquid levels gradually decreased with no oscillation in the tubes in uniform manner after around 22000 s. The CCFL at the inlet of U-tubes has thus affected large-amplitude level oscillation with some randomness among the SG U-tubes for a long time.

When the PWR transients are analyzed with best-estimate computer code, simplified input models are usually employed such that 3382 tubes in each SG are lumped into one equivalent tube to reduce the calculation time. However, a detailed modeling of the SG U-tubes with fine-mesh multiple parallel flow channels would be at least necessary when the complicated two-phase flow phenomena are involved similar to that encountered in the LSTF experiment on the PWR LOFW transient as well as the optimum constants for CCFL correlation to provide better predictions.

7. Summary

An LSTF experiment was performed for OECD/NEA ROSA Project, simulating a PWR LOFW transient with specific assumptions of failure of scram to observe high-power natural circulation, and total failure of high pressure injection system. The AFW was provided to well observe the long-term high-power natural circulation. The LSTF core power curve was pre-determined through the RELAP5 code analysis for PWR LOFW transient without scram. The results of the LSTF experiment were compared with the post-test analysis results by the RELAP5 code to clarify the details of major phenomena and remaining subjects in the code predictions. Obtained results are summarized as follows:

(1) Two-phase natural circulation started in very early stage of and continued through the transient where the primary and SG secondary-side pressures were kept almost constant at around the pressures for cycle opening of PORV of PZR and SG RVs. Major core uncovery happened due to core boil-off because of the primary coolant inventory loss through the PORV.

(2) Large-amplitude level oscillation occurred in SG U-tubes for a long time in a form of slow fill and dump while the two-phase natural circulation flow rate gradually decreased with some oscillation. The fill and dump behavior depended on the SG U-tube length under influences of vertical fluid temperature distribution along the SG boiler section caused by the AFW coolant injection. Temporary large drop happened in the core liquid level when the water column developed in the SG U-tubes, causing an intermittent increase in the cladding surface temperature at higher elevations even before the major core uncovery due to the core boil-off.

(3) The RELAP5 code predicted well the overall trend of the major phenomena observed in the LSTF experiment including the slow fill and dump behavior in the SG U-tubes. Some discrepancies from the measured data, however, appeared in the oscillative primary loop flow rate and SG U-tube liquid level as well as PZR liquid level. The coefficients of the CCFL correlation suitable for both all the PZR and the surge-line junctions were newly identified.

Acknowledgments

This paper contains findings gained through the OECD/NEA ROSA Project. It is noted that the value axis of all the data plot of LSTF test and RELAP5 analysis is normalized properly due to the agreement of the OECD/NEA ROSA Project. Authors are also grateful to the Management Board of the ROSA Project for their consent to this publication. Authors would like to thank to Messrs. M. Ogawa and A. Ohwada of Japan Atomic Energy Agency for performing the LSTF experiments under collaboration with members from Nuclear Engineering Co. (NECO) as well as Miss K. Toyoda of IX Knowledge Inc. for manipulating the experimental data.

References

[1] C. L. Nalezny, "Summary of nuclear regulatory commission's LOFT program experiment," Tech. Rep. NUREG/CR-3214, EGG-2248, 1983.

[2] W. Ambrosini, F. D'Auria, and G. M. Galassi, "Lesson learned from the application to LOBI tests of CATHARE and RELAP5 codes," in *Proceedings of the 1st Meeting of the Nuclear Society of Slovenia*, Bovec, Slovenia, 1992.

[3] United States Nuclear Regulatory Commission, "Reactor safety study—an assessment of risks in U. S. commercial nuclear power plants," Tech. Rep. WASH-1400 (NUREG-075/14), 1975.

[4] The ROSA-V Group, "ROSA-V large scale test facility (LSTF) system description for the third and fourth simulated fuel assemblies," JAERI-Tech 2003-037, Japan Atomic Energy Research Institute, Ibaraki, Japan, 2003.

[5] Y. Kukita, Y. Anoda, and K. Tasaka, "Summary of ROSA-IV LSTF first-phase test program—integral simulation of PWR small-break LOCAs and transients," *Nuclear Engineering and Design*, vol. 131, no. 1, pp. 101–111, 1991.

[6] K. E. Carlson, "RELAP5/MOD3 code manual (draft)," Tech. Rep. NUREG/CR-5535, EGG-2596, 1990.

[7] T. Takeda, H. Asaka, and H. Nakamura, "Analysis of the OECD/NEA ROSA project experiment simulating a PWR small break LOCA with high-power natural circulation," *Annals of Nuclear Energy*, vol. 36, no. 3, pp. 386–392, 2009.

[8] H. Nakamura, T. Watanabe, T. Takeda et al., "RELAP5/MOD3 code verification through PWR pressure vessel small break loca tests in OECD/NEA rosa project," in *Proceedings of the*

16th International Conference on Nuclear Engineering (ICONE-16 '08), pp. 659–668, Orlando, Fla, USA, May 2008.

[9] N. Zuber, "Problems in modeling small break LOCA," USNRC Report NUREG-0724, 1980.

[10] H. Kumamaru and K. Tasaka, "Recalculation of simulated post-scram core power decay curve for use in ROSA-IV/LSTF experiments on PWR small-break LOCAs and transients," Tech. Rep. JAERI-M 90-142, Japan Atomic Energy Research Institute, Ibaraki, Japan, 1990.

[11] ROSA Project Team, "Final integration report of OECD/NEA ROSA project," JAEA-Research 2010-9002, Japan Atomic Energy Agency, Ibaraki, Japan, 2010.

[12] Y. Kukita, H. Nakamura, K. Tasaka, and C. Chauliac, "Nonuniform steam generator U-tube flow distribution during natural circulation tests in ROSA-IV large scale test facility," *Nuclear Science and Engineering*, vol. 99, no. 4, pp. 289–298, 1988.

[13] H. Asaka, Y. Kukita, T. Yonomoto, Y. Koizumi, and K. Tasaka, "Results of 0.5% cold-leg small-break LOCA experiments at ROSA-IV/LSTF: effect of break orientation," *Experimental Thermal and Fluid Science*, vol. 3, no. 6, pp. 588–596, 1990.

[14] K. H. Ardron and R. A. Furness, "A study of the critical flow models used in reactor blowdown analysis," *Nuclear Engineering and Design*, vol. 39, no. 2-3, pp. 257–266, 1976.

[15] D. W. Sallet, "Thermal hydraulics of valves for nuclear applications," *Nuclear Science and Engineering*, vol. 88, no. 3, pp. 220–244, 1984.

[16] Susyadi and T. Yonomoto, "Analysis on non uniform flow in steam generator during steady state natural circulation cooling," JAERI-Research 2005-011, Japan Atomic Energy Research Institute, Ibaraki, Japan, 2005.

[17] G. B. Wallis, *One-Dimensional Two-Phase Flow*, McGraw-Hill Book, New York, NY, USA, 1969.

[18] T. Yonomoto, Y. Anoda, Y. Kukita, and Y. Peng, "CCFL characteristics of PWR steam generator U-tubes," in *Proceedings of the ANS International Topical Meeting on Safety of Thermal Reactors*, American Nuclear Society, Portland, Ore, USA, 1991.

Hindawi Publishing Corporation
Science and Technology of Nuclear Installations
Volume 2012, Article ID 474162, 16 pages
doi:10.1155/2012/474162

Research Article

Consistent Posttest Calculations for LOCA Scenarios in LOBI Integral Facility

F. Reventós,[1] P. Pla,[2] C. Matteoli,[1,3] G. Nacci,[1,3] M. Cherubini,[3] A. Del Nevo,[3] and F. D'Auria[3]

[1] *Department of Physics and Nuclear Engineering, Technical University of Catalonia (UPC), Diagonal 647, 08028 Barcelona, Spain*
[2] *European Commission, Joint Research Centre (JRC-IE), Institute for Energy 1755 ZG, Petten, The Netherlands*
[3] *San Piero a Grado Nuclear Research Group, University of Pisa (GRNSPG-UNIPI), 56126 Pisa, Italy*

Correspondence should be addressed to F. Reventós, francesc.reventos@upc.edu

Received 22 May 2011; Accepted 15 September 2011

Academic Editor: Klaus Umminger

Integral test facilities (ITFs) are one of the main tools for the validation of best estimate thermalhydraulic system codes. The experimental data are also of great value when compared to the experiment-scaled conditions in a full NPP. The LOBI was a single plus a triple-loop (simulated by one loop) test facility electrically heated to simulate a 1300 MWe PWR. The scaling factor was 712 for the core power, volume, and mass flow. Primary and secondary sides contained all main active elements. Tests were performed for the characterization of phenomenologies relevant to large and small break LOCAs and special transients in PWRs. The paper presents the results of three posttest calculations of LOBI experiments. The selected experiments are BL-30, BL-44, and A1-84. They are LOCA scenarios of different break sizes and with different availability of safety injection components. The goal of the analysis is to improve the knowledge of the phenomena occurred in the facility in order to use it in further studies related to qualifying nodalizations of actual plants or to establish accuracy data bases for uncertainty methodologies. An example of procedure of implementing changes in a common nodalization valid for simulating tests occurred in a specific ITF is presented along with its confirmation based on posttests results.

1. Introduction

Experimental data recorded in integral test facilities (ITFs) are traditionally used in order to validate best estimate (BE) system codes and to investigate the behaviour of Nuclear Power Plants (NPPs) under accidental scenarios. Posttest calculations are the normal practice carried out with this purpose. Further studies bring the analysts to go into deeper considerations like using posttest results either to establish comparisons in the frame of the so-called scaling calculations [1] or to evaluate accuracy [2]. The former is, by now, part of methodologies used by the authors in order to qualify nodalizations [3], while the latter is at the basis of the establishment of accuracy data bases used by CIAU uncertainty methodology.

The current practice intends, on the one hand to fulfil the usual goals of conventional posttests, and on the other hand to add some further value to the results by means of what the authors understand by mutual consistency among the calculations. The most important aspect of this mutual consistency is to simulate as many tests as possible by using the same nodalization of the involved ITF. Once a nodalization change carried out for one specific test results in a clear improvement of the predictions, it is useful to recalculate all the other tests and to check if the change is accepted and confirmed. Some explanation will be given on this point in several paragraphs below.

Three different LOBI tests have been selected in order to be simulated. They are all LOCA scenarios with break sizes between 5 and 10%. Relevant phenomena occurring in such scenarios are the main subject of investigation.

The test BL-30 was a 5% small break LOCA in the cold leg performed in the LOBI-MOD2 facility on April 15th 1989. The objectives of the test were to identify and/or verify major phenomenologies relevant to the response of a PWR to an SB LOCA, with particular reference to overall mass distribution, loop seal formation and clear-out and eventual core uncover. Other objective was the assessment of ECCs

effectiveness in the SB LOCA scenarios having the potential to cause temperature excursions in the core.

The test BL-44 was a 6% small break LOCA in the cold leg performed in the LOBI-MOD2 facility on April 26th 1990. The objective of the test was to enrich the experimental database with a Counter Part Test having high value for code assessment and scalability, in particular with reference to the problem of initial power scaling in SB LOCAs. Phenomenological objectives were the identification of the mass distribution in the primary system (PS), loop seal behaviour, core heatup, and rewet and accumulator performance.

The test A1-84 was a 10% break LOCA in the hot leg performed in the LOBI-MOD2 facility on October 14th 1985. The test belongs to the A-Matrix of the LOBI-MOD2 defined by the German contract partner. The objective of the test was to investigate the general system thermalhydraulic response during the course of the LOCA.

The three tests were LOCA scenarios performed with the same LOBI configuration, and an important part of hardware considerations was the same for the three tests as will be explained below.

Other similarities and differences in boundary conditions were identified. The size of the break was similar in two of them (BL-30 and BL-44) and different in the other. Two of them (in this case BL-30 and A1-84) had a secondary side cooldown, while, in the other, the secondary side was isolated.

The existing slight difference between break sizes of BL-30 and BL-44 could result in a slight quicker depressurization and as a consequence an advance of accumulator injection. The total failure of HPIS in BL-44 (while in BL-30 only 50% failed) could have a direct influence on core dryout. Each relevant thermalhydraulic aspect appearing in more than one test has been identified and considered consistent when the expected behavior on the given test was in accordance with the explanation produced from the apparent differences in boundary conditions.

The calculations have been carried out using the same code version and the same basic nodalization. Similarities and differences such as those depicted above have been carefully checked and unjustified distinctions strictly avoided.

2. The LOBI-MOD2 Facility and Hardware Considerations

The LOBI (LWR off-normal behaviour investigation) was a reactor thermalhydraulic safety research programme carried out by the EC JRC Ispra site [4]. The main objective was the investigation of basic phenomenologies governing the thermalhydraulic response of an ITF for a range of PWR operational and accident conditions; the programme was also aimed to the provision of an experimental data base for the development and improvement of analytical models and assessment of system codes used in LWR safety analysis.

The LOBI test facility (Figure 1) was a single plus a triple-loop (simulated by one loop) full-power high-pressure integral system test facility representing an 1 : 712 scale (core power, volume, and mass flow) model of a 4-loop, 1300 MWe PWR (KWU type). It incorporates the essential features of a typical PWR primary and secondary cooling system. The test facility was commissioned in December 1979 and was operated until June 1982 in the MOD1 configuration for the investigation of large break LOCAs; it was then extensively modified into the MOD2 configuration which was operated from April 1984 to June 1991 for the characterization of phenomenologies relevant to small break LOCAs and special transients in PWRs. The measurement system comprised a total of about 470 measurement channels which allowed the measurement of all relevant thermal-hydraulic quantities at the boundaries (inlet and outlet) of each major primary and secondary system loop component and within the reactor pressure vessel model and steam generators. A process control system allowed the simulation of time- or pressure-dependent parameters such as core decay heat release, main coolant pump hydraulic behaviour, and safety injection flow rates. A fast running data acquisition system complemented the experimental installation.

Experimental data and documentation of tests performed at the facility are available online for code validation purposes through the JRC STRESA (storage of thermal reactor safety analysis data) web database platform [5], which was developed with the objective of the preservation of these amounts of thermalhydraulic experimental data produced in ITFs programmes and the associated supporting information/documentation.

The following paragraphs include an explanation on hardware considerations for LOBI-MOD2 experiments BL-30 [6, 7], BL-44 [8, 9], and A1-84 [10, 11].

Each paragraph covers one related item and stresses on hardware similarities and differences among the three considered tests. In case no reference to any specific test is given, the piece of hardware is identical in three experiments.

For tests BL-30 (single-ended 5% break, orifice diameter 6.7 mm) and BL-44 (single-ended 6% break, orifice diameter 7.36 mm) the *break assembly* consisted of a T-shaped spool piece located in the cold leg, between the main coolant pump and the pressure vessel inlet. For test A1-84 the break assembly consisted also of a T-shaped spool piece but inserted within the hot leg pipe work (single ended 10% break orifice, diameter 9.5 mm). In all tests, break includes a side-oriented break orifice, a quick opening on/off valve for initiation of the rupture and a measurement insert for density, velocity as well as pressure, and temperature of the outflow. The break outflow is diverted to a condensing tank system where it is collected and measured.

The externally mounted *upper head* is connected to the upper plenum and to the upper downcomer, in all tests. An additional connection exists between the downcomer and the top of the upper head and this is used for conditioning the fluid in the upper head to about the temperature of the downcomer. This line is normally isolated sufficient time before transient initiation.

In all tests, the *by-pass flow* between upper downcomer and upper plenum includes three main flow paths: (1) upper head connection lines (about 1% nominal flow in the three tests); (2) two holes of diameter 5 mm in the core barrel tube, each connecting downcomer and upper plenum at

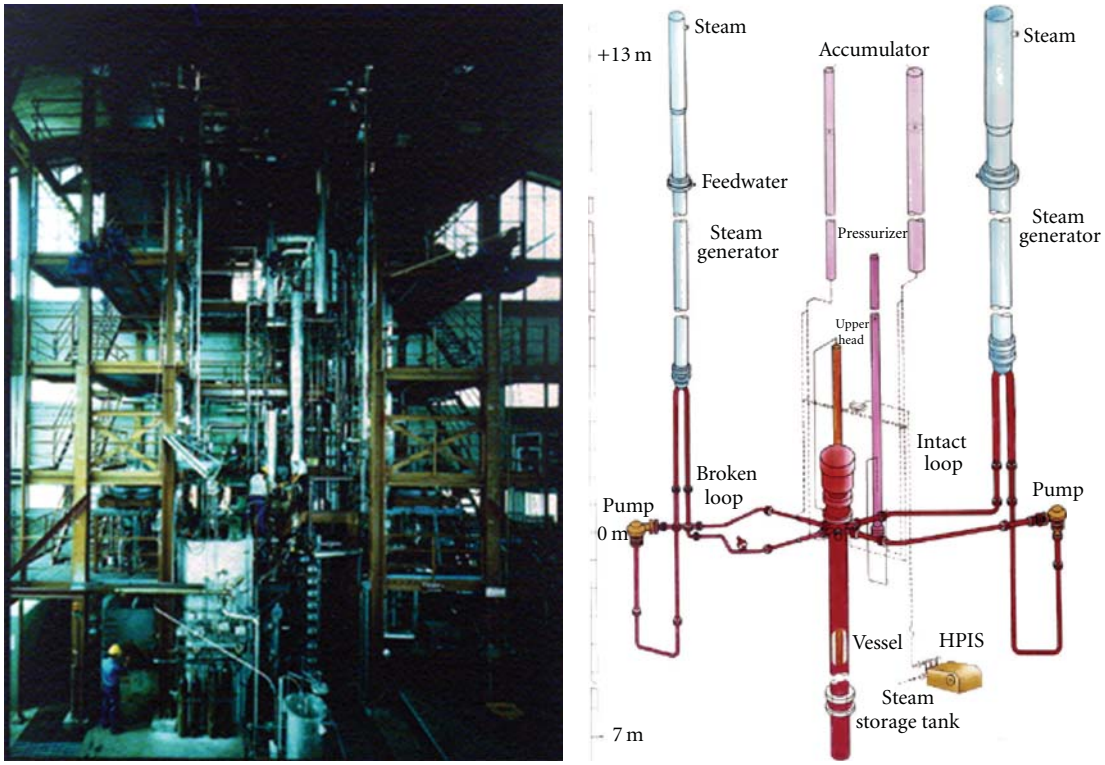

(a) (b)

Figure 1: LOBI-MOD2 test facility and schematic representation of the cooling system (STRESA JRC database).

the uppermost elevation; (3) possible hot leg to core barrel clearance fit. The sum of (2) and (3) by-pass flows mentioned has been estimated at 2.4 to 3.7% of nominal core flow.

Main Coolant Pumps Seal Water Drainage. Before the initiation of the experiments, the fraction of cooling water which enters the primary system is normally drained from the upper plenum using the pressurizer water level control system. During the transient, the draining system is isolated and the injected seal water is added to the inventory of the primary system in test A1-84. The LOBI-MOD2 test facility has also a closed loop pump seal water compensation system with drainage from the lower plenum, generally activated in SB LOCAs, which is activated in the two other tests.

The locked rotor hydraulic resistance of the LOBI main coolant pumps is used to obtain the same resistance as in the reference reactor. To ensure a more symmetrical mass flow behavior in both pumps during period of natural circulation following pump coast down, the *pump-locked rotors* are installed at the pump discharge, each consisting in a valve that can be properly orificed to provide the required additional resistance. In the intact loop, this resistance is negligible, but in the broken loop it is significant and a perforated plate type orifice is installed. In the tests, the orifice provides an area reduction of about 18% of the normal flow area, and it is normally inserted 4 s after pump coast down to zero speed.

In tests BL-30 and A1-84 additional transient assumptions were typical of the LOBI reference reactor, the German Biblis B plant; as such a symmetric *cooldown* of the two Steam Generators (SG) at 100 K/hour was imposed after SCRAM. Cooldown is achieved via steam venting from the SG relief valves. Cooldown procedure is not considered in test BL-44.

ECCS water is injected into the primary loops through the accumulators and the low- and high-pressure injection system (LPIS, HPIS).

In BL-30 and BL-44 tests, *the accumulator* was connected to the intact loop cold leg only. In order to avoid unrealistic frequent opening and closing of the valve, due to the LOBI accumulators pressure control system, an orifice with a diameter of 8 mm (in BL-30) and of 7.2 mm (in BL-44) was inserted in the injection line. In A1-84 test, *the accumulators* are connected to both legs of the intact loop and to the cold leg of the broken loop.

In BL-30 test, the *HPIS* was connected to the intact loop cold leg only, simulating 2 of 4 pumps. In test A1-84, the *HPIS* is connected to the hot leg of the intact loop, simulating 2 of 4 pumps. The remaining two pumps (that exist in the reference plant) are assumed to be one in maintenance and the other connected to the broken loop. In BL-44 only the *LPIS* was available for both loops cold leg at a rate of 0.4 kg/s and activated on high heater rod temperature.

The *pressurizer surge line* was connected to the intact loop hot leg in BL-30 and A1-84 tests and to the broken loop hot leg in BL-44 test.

Main feedwater (FW) was not available in all tests. In test BL-30, *auxiliary feedwater* (AFW) was available for both

Table 1: LOBI-MOD2 tests BL-30, BL-44, and A1-84 experimental and calculated steady-state values.

LOBI Parameter (Units)	BL-30		BL-44		A1-84	
	Experiment	Calculation	Experiment	Calculation	Experiment	Calculation
Core thermal power (MWth)	5.17	5.17	5.24	5.25	5.15	5.15
PRZ pressure (top of the PRZ) (MPa)	15.80	15.80	15.46	15.46	15.80	15.80
SG-IL pressure (top of the SG) (MPa)	6.530	6.531	5.11	5.11	6.548	6.550
SG-BL pressure (top of the SG) (MPa)	6.510	6.504	5.120	5.119	6.527	6.526
Accumulator IL pressure (MPa)	2.77	2.77	3.91	3.91	2.8	2.8
Primary mass inventory (kg)	430.95	440.62	448.0	465.05	432.86	440.33
Core inlet temperature (C)	295.97	295.31	280.50	280.15	295.22	295.33
Core outlet temperature (C)	327.31	325.81	313.0	312.23	326.76	326.91
Hot leg IL temperature (C)	326.00	325.68	311.39	312.10	328.94	326.91
Hot leg BL temperature (C)	327.00	325.63	314.84	312.05	329.4	326.9
Cold leg IL temperature (C)	295.00	293.59	281.24	278.32	294.23	293.87
Cold leg BL temperature (C)	294.00	293.34	280.07	278.27	292.29	292.21
Hot leg IL mass flow (kg/s)	20.76	20.42	21.30	21.15	20.2	20.02
Hot leg BL mass flow (kg/s)	6.92	6.98	7.40	7.23	6.2	6.175
SG-IL feedwater mass flow (kg/s)	1.99	1.99	1.95	2.11	2.07	2.038
SG-BL feedwater mass flow (kg/s)	0.69	0.69	0.75	0.71	0.61	0.643
Pressurizer level, collapsed (m)	5.10	5.10	5.03	5.03	5.346	5.346
Core pressure drop (kPa)	117.16	121.54	125.0	125.86	112.59	118.4
IL Pump velocity (rpm)	4896.86	4896.65	4834.99	4831.95	4832.93	4927.43
BL Pump velocity (rpm)	3812.61	3812.54	3822.72	3829.26	3912.36	3911.94

loops, but used for the broken loop SG only. AFW was not used in tests BL-44 and A1-84.

3. Nodalization and Steady-State Calculations

The RELAP5 Mod 3.3 nodalization input deck was based on the same approach of original previous works performed for LOBI test BL-44 either in cooperation between the two universities [12] or at the University of Pisa, [13, 14]. All these previous calculations were performed with RELAP5 Mod 3.3. Older results, like those obtained at the Technical University of Catalonia for LOBI test BL-30 [15] or at JRC Ispra [16] with previous version of the code (RELAP5 Mod 2.5), were also taken into account only as preceding information.

The input deck reflects as far as possible hardware configuration described in Section 2. Boundary and initial conditions are set up according with the tests specifications. The prediction of the break flow rate is important when LOCAs are simulated. Ransom and Trapp [17] chocked flow model is activated at break in these three tests. Since discharge structure was the same, discharge coefficients used had the same value for all tests; in this sense unjustified distinctions were avoided as usual.

A schematic representation of the original nodalization is shown in Figure 2. The purpose of showing such diagram is only to illustrate the degree of detail used for the analyses performed.

The initial conditions of the experimental tests (BL-30, BL-44, and A1-84) are compared with the achieved steady state results of the code simulations; see Table 1 that shows for every test the agreement between each experiment and its corresponding calculation.

Usual steady-state controllers have been set in order to stabilize the nodalization. Pressures are imposed by means of Relap5 time-dependent volumes removed later on. Main feedwater is controlled trying to match SG levels and a fictitious charging system is set to establish the right pressurizer level.

Once each steady state is achieved properly, one additional comment can be made related to what has been announced as consistency checks between the three different calculations performed. It is a comment related to temperature ranges in primary and secondary sides.

BL-44 secondary pressure is established at about 5.1 MPa, while in the other two tests it takes a value of about 6.5 MPa. This brings to saturation temperatures of 265°C for BL-44 secondary side and 281°C for the other two tests. Under these conditions, BL-44 steady-state values for primary temperatures stabilize at about 296°C (CL) and 327°C (HL) with temperature differences between primary and secondary sides, respectively, of 15°C and 46°C. For the other tests these values are 280°C (CL) and 313°C (HL) with temperature differences, respectively, of 15°C and 48°C. This similarity in temperature differences between primary and secondary side shows the consistency with the fact that heat transfer from primary to secondary side occurs at similar mass flows, identical heat transfer correlations (same code version), and SG nodalization (reflecting an identical SG geometry).

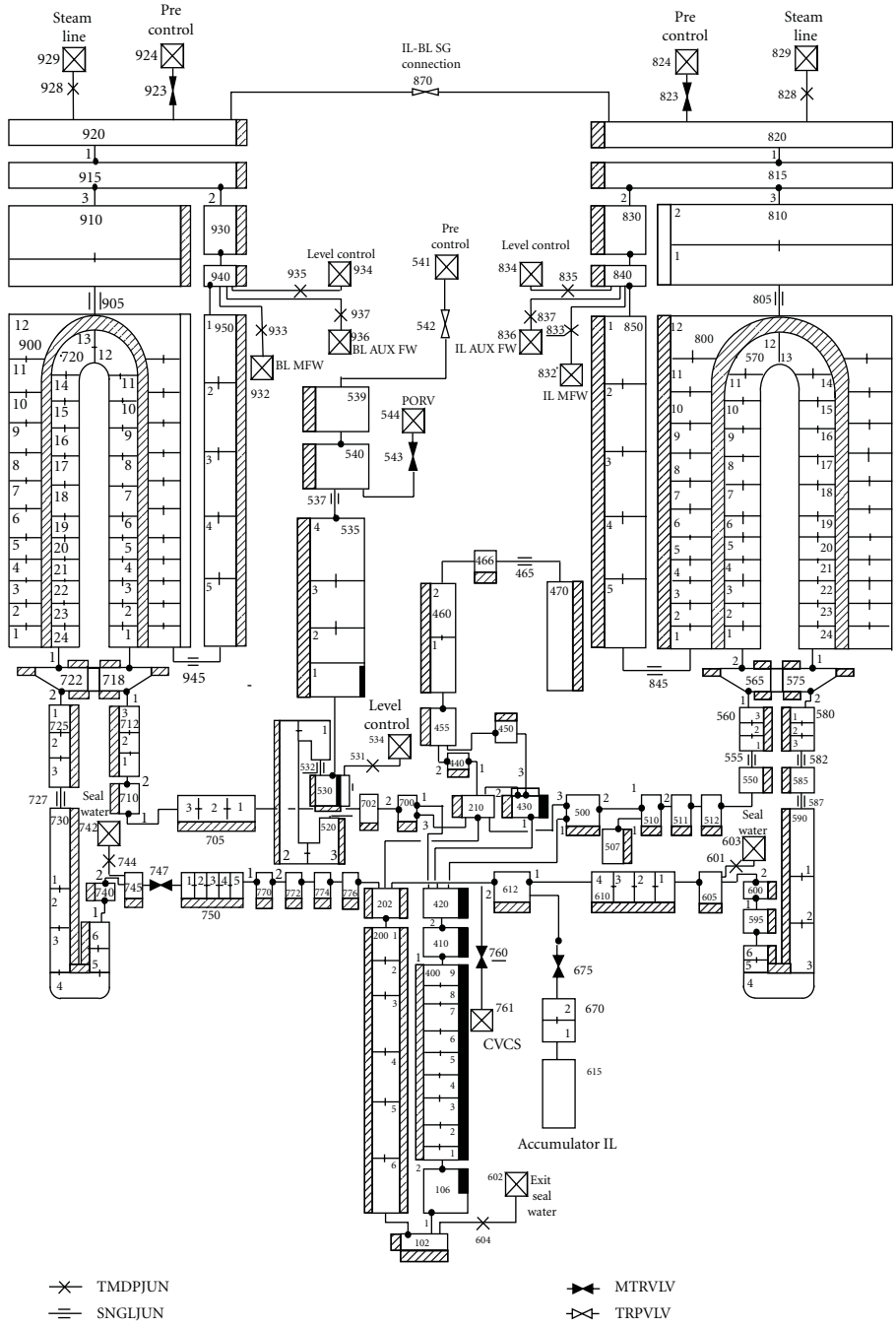

Figure 2: LOBI-MOD2 nodalization for relap code.

4. BL-30 Scenario

4.1. Experiment Description

The test BL-30 was a 5% small break LOCA in the cold leg performed in the LOBI-MOD2 facility. The test included the hardware configuration presented in Section 2. The general objective of the test was to reproduce major phenomena relevant to the response of a PWR to SB LOCA and to provide data for: mass distribution, loop seal formation and clearance, eventually core uncover, and assessment of ECCS effectiveness in SB LOCA scenarios. Some main set points of test BL-30 are shown in Table 2 (all pressures values, if not specified, correspond to UP) together with the sequence of experimental events and calculated simulation.

Initial and boundary conditions were applied as specified.

After rupture of break device, PS started to depressurize reaching pressure signal SCRAM at 13.2 MPa and 2.8 s and leading to saturation in hot legs, upper plenum and surge line. Power-time curve was applied to the electrically heated

Table 2: Sequence of main events for test BL-30 experimental and posttest calculation.

Events/set points	Time after experiment initiation (s)	Calculated time after transient initiation (s)
Break opening	0.0	0.0
Secondary side cooldown 100 K/h actuation (at 13.2 MPa)	2.3	1.62
SCRAM signal (at 13.2 MPa + delay 0.5 s)	2.8	2.12
Saturation in hot legs	4.9	3.0
Saturation in upper plenum	5.0	3.0
Pressure in PS 11.7 MPa	7.0	8.01
MCPs start coastdown (at 10.8 MPa)	9.0	10.8
Pressurizer surge line uncovers	19.2	20.0
HPIS actuation (at 11.7 MPa + delay 35 s)	42.0	43.01
Saturation in lower plenum	42.0	34.0
MCPs stop	79.0	80.0
PS pressure falls below SS pressure	188.0	211.0
Broken loop seal clearance	200.0	275.0
Break uncovers	200.0	277.0
Intact loop seal clearance	230.0	273.0
Occurrence of minimum primary side mass	623.0	580.0
Accumulator actuation (at 2.8 MPa, disabled when accumulator water volume is 22 l (5% of total volume))	625.0	579.9
Auxiliary feedwater in broken loop (SG level < 5 m), at 7% of the nominal initial flow and 150°C	1023.0	1070.0
Accumulator injection stops	1683.0	2130.0
End of the test	1683.0	2790.0

rod bundle; the heated power remained at 100% till SCRAM, afterwards it simulated decay power and release of stored energy.

At the same time, trip signals for secondary-side isolation and MCP coastdown were generated. MCPs coasted down in accordance with the specified curves at 9 s till 79 s. The main FW in both SGs remained nominal till 2.8 s, afterwards SGs were isolated (main FW lines and main steam lines closed). The secondary sides of both SGs remained, however, connected during the entire test. Cooldown was applied at 100 K/h after 13.2 MPa PS trip signal. Cooldown was controlled and achieved through SRV venting.

HPIS was directed into the intact loop cold leg when PS pressure was 8.5 MPa. The programmed flow-versus-pressure curve was matching the capacity of 2 out of 4 HPIS trains.

At 42 s PS reached the saturation pressure of the fluid in the lower plenum. Primary to secondary heat transfer degraded. When the forced circulation (driven by MCPs) stopped, the onset of two phase natural circulation and of the reflux condenser heat transfer modes, is essentially shattered by the early voiding of the upper parts of the primary system and by the loss of the heat sink (steam generators), as the secondary pressure overtakes the primary one. At 188 s the PS pressure fell below the SS pressure and reverse heat transfer in the SGs was established. The break uncovered at about 200 s causing reduction of break flow which was compensated by HPIS flow. Broken and intact loops seals started to clear at about 200 s and 230 s, respectively.

Accumulator injection was activated at 625 s when PS pressure was 2.7 MPa and accumulator was disabled when the water volume had decreased to 5% of its total volume. Primary system mass inventory decreased and started to recover after accumulator intervention.

AFW was activated in the SG of the broken loop due to achievement of SG downcomer level to 5 m, while in the SG of the intact loop the level was always higher than the specified set point.

The vessel liquid level was never low enough to cause the uncover of the heater rod bundle. Adequate core cooling was ensured by sufficient PS mass inventory replenish by ECCS. Rod surface temperature decreased following saturation temperature. Test was terminated when PS pressure arrived to 0.9 MPa.

Figure 3 shows a snapshot of a video of the experimental real-time collapsed levels and plots of primary and secondary pressures.

4.2. Posttest Calculation. The input deck used reflects as far as possible hardware configuration described in Section 2 and imposes initial, boundary conditions and set points shown in Table 2; one HPIS pump was used for the intact loop representing 2 of 4 pumps, one accumulator in the intact loop was simulated and cooldown of 100 K/h was adjusted to both SGs experimental values.

The sequence of the main events is summarized in Table 2 for the calculation compared to the BL-30 experiment. The agreement is quite close.

The results of the BL-30 experiment calculation (descriptor BL30POST) are shown plotted in the following figures compared with the experimental data (descriptor EL30) and described below.

Figure 4 shows PS (pressurizer) pressure, the depressurization, and the change of depressurization rate after the break uncover (at about 250 s) is correctly simulated. On the long term, both pressures decrease with same rate.

Figure 5 shows SS pressure, in the broken loop (vols. 87, 915) and intact loop (vols. 97, 815) for the experiment and BL-30 calculation. Pressure increases till SRV opens at 8.3 MPa and few seconds' later secondary side cooldown (100 K/h) starts: cooldown behaviour was correctly simulated in the calculation.

Figure 6 shows the ECCS (HPIS mass flow and accumulators mass injected) together with the integral mass flow flowing out of the break. HPIS mass flow is injecting from the beginning of the transient in the PS depending on PS

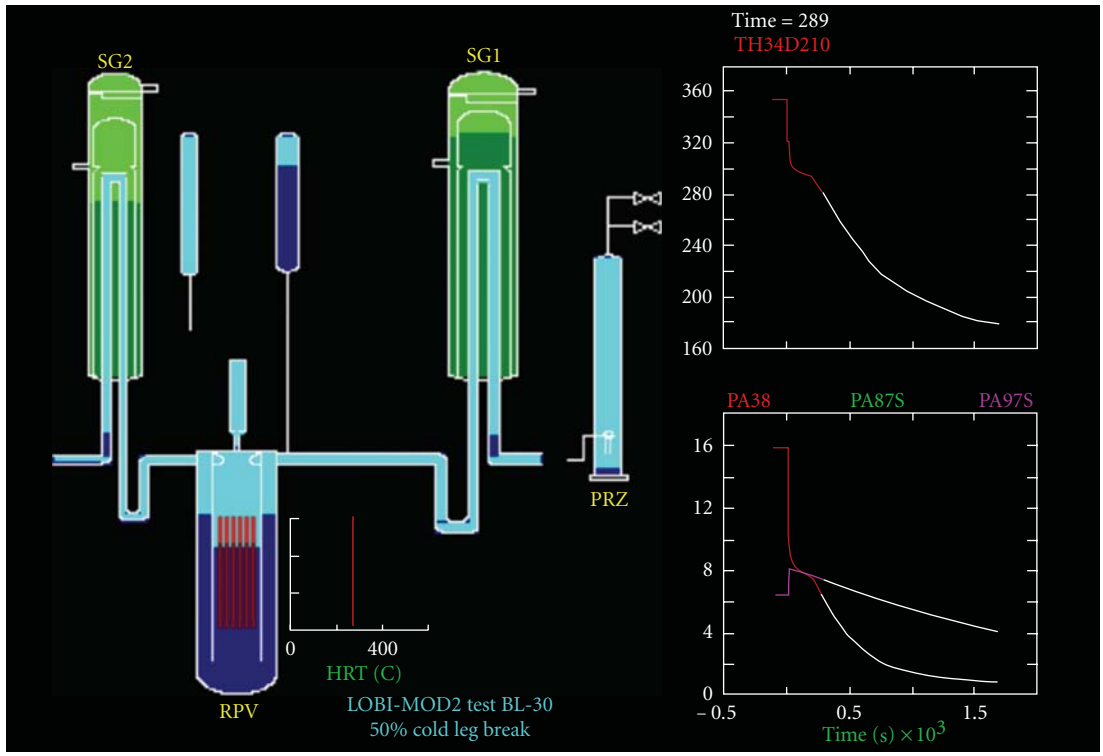

Figure 3: BL-30 experiment collapsed levels display and primary and secondary pressures (STRESA JRC database).

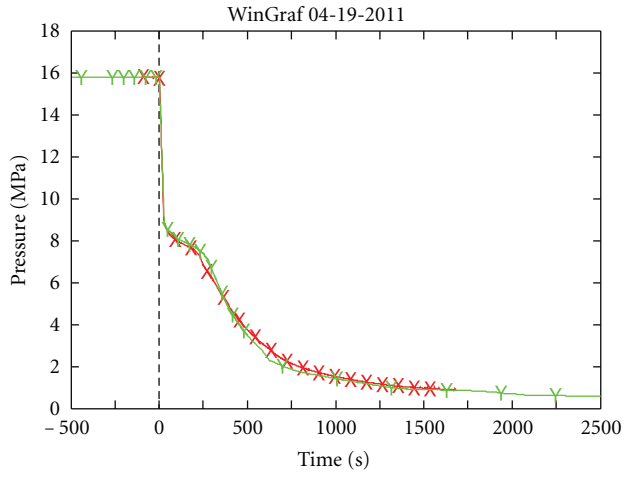

Figure 4: Primary system pressure.

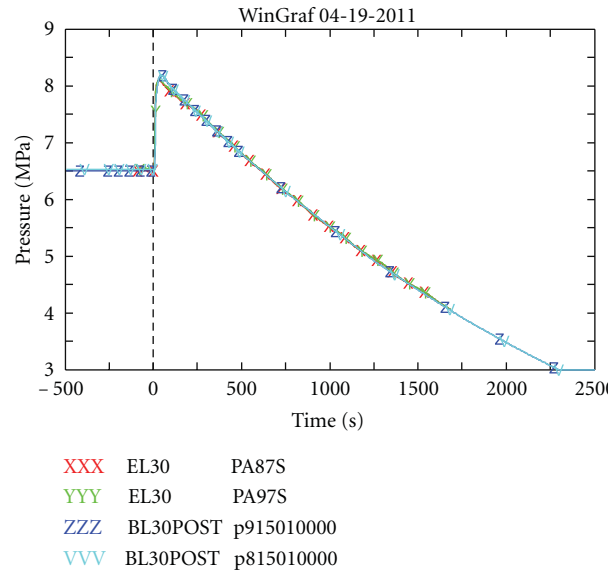

Figure 5: Secondary system pressure.

pressure (lower pressure means more injection power). At about 580 s the accumulator starts to inject dependent also on PS pressure trend. In general, good agreement is obtained for the ECCS mass flow in the calculation compared to the BL-30 experiment.

Figure 7 shows PS total mass. It decreases after the break and starts to recover due to HPIS and accumulators injection.

Figure 8 shows fuel cladding temperatures at different heights in the core region, no dryout is observed and temperatures decrease due to the combined effect of HPIS, loop seal clearing, and accumulator's injection. Since HPIS-injected mass is quite similar in experiment and calculation the difference lays in the accumulators injected mass. For the calculation after about 600 s cladding temperatures are slightly lower than the experiment.

Finally, Figures 9 and 10 show density at the pump inlet zone in the intact and broken loops showing good agreement

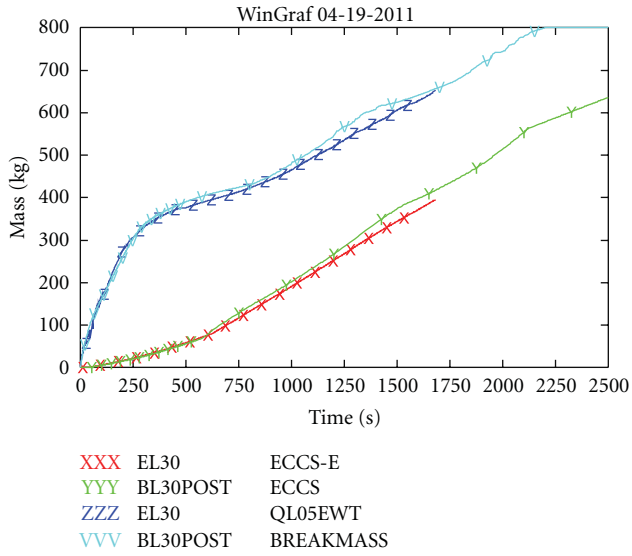

Figure 6: ECCS integral mass flow and integral break flow.

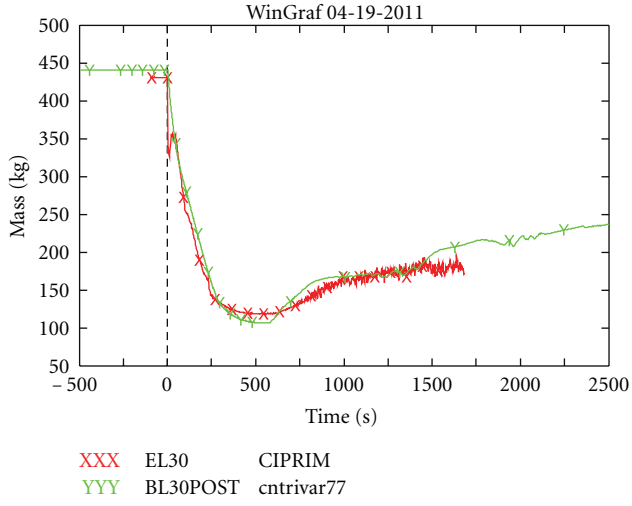

Figure 7: Primary system mass.

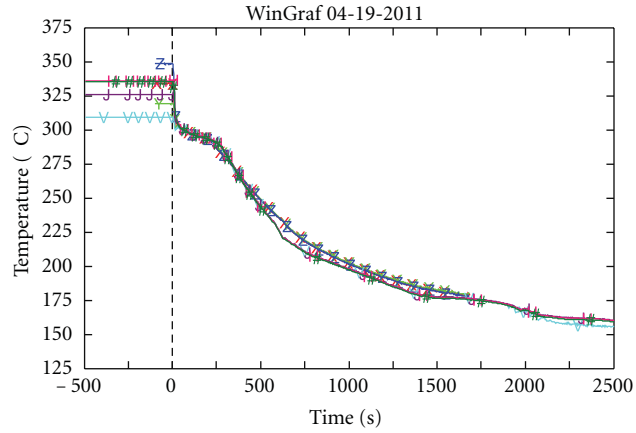

Figure 8: Cladding temperature at different core heights.

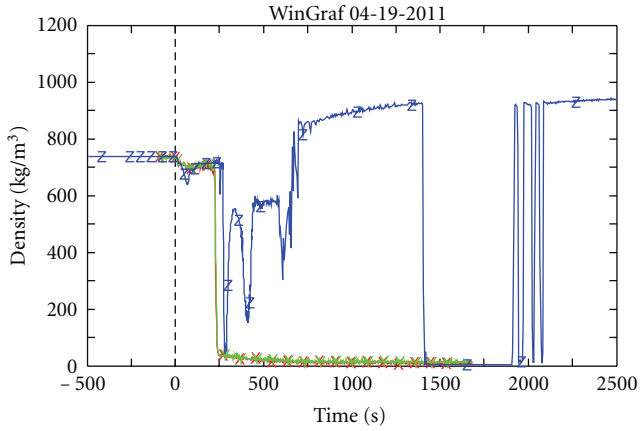

Figure 9: Intact loop seal (pump inlet) density.

of the calculations with the experimental occurrence of the loop seals clearance.

5. BL-44 Scenario

5.1. Experiment Description. The test BL-44 is 6% a Small Break LOCA originated by a rupture in the cold leg.

For the test BL-44, the LOBI-MOD2 test facility was predisposed in the basic configuration for the cold leg break LOCA experimental.

The sequence of interventions of the various systems is typical of this kind of transient in a plant: after the break occurrence, scram and pumps trips are provided, together with a signal for the isolating steam generators (feed water and steam line closure). Accumulator's intervention is foreseen when primary pressure is below 3.91 MPa. After the accumulator emptying, the flow rate from the break causes mass depletion from the primary side, leading to core dryout. Low-pressure injection system actuation is expected after the occurrence of core dry out and is effective in rewetting the rods.

Main set points of the test BL-44 are shown in Table 3.

Following the break, the primary system started to depressurize up to the achievement of the saturation conditions upstream the break, this occurs at about 80 s into the transient. The sharp initial pressure decrease lead to scram (at 0.6 s), main coolant pump speed reduction (at 0.9 s) and isolation of steam generators (at 1.3 s). At 5.1 s, the upper plenum and the hot legs reach the saturation condition, and the depressurization rate is largely reduced. The pressurizer

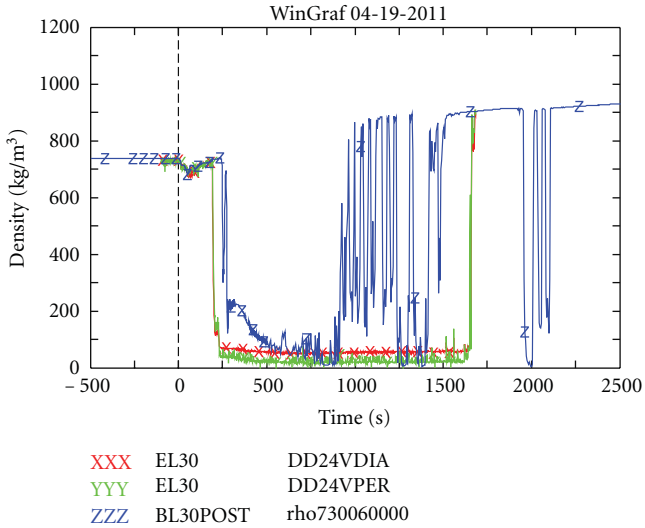

Figure 10: Broken loop seal (pump inlet) density.

surge line uncover at about 20 s determines an increase of the depressurization rate. Pressurizer emptying occurs in about 25 s. During this phase, U-tubes draining occurs in primary side (at about 90 s) for the loss of the natural circulation between core and downcomer through the steam generators: at this time, the saturation temperature in the primary loop is still few degrees higher than saturation temperature in the secondary side. The stop in natural circulation, essentially due to voiding and mass depletion in the upper zones of the loop, causes manometers type situation, in the primary loop piping: the steam produced in the core partly flows directly in the break through the bypass and partly pushes over the vessel level and over the IL and BL loop seals. In this situation, core dryout occurs at about 170 s.

At 197 s loop seal clearing is present in the intact loop.

The core boil off (produced steam flows almost entirely to the break) causes a second dry out at about 351 s at a pressure near, but higher than the accumulators pressure (3.91 MPa). Probably the reverse speed of the pump (at −28 rpm during the transient) contributes to the formation of liquid holdup in the broken loop seal, pump side. In this period, the heat transfer from secondary side is quite small compared with core power, because of the high void fraction in the U-tubes.

At 429 s, the primary pressure reached the accumulator setpoint and therefore the accumulator started to inject (in the intact loop, cold leg) a mass flow rate greater than the break flow. The accumulator's intervention causes the recovery of the liquid level in the core and a second rewet that is completed at about 595 s. The accumulator mass flow is stopped at about 971 s: in the period, from 429 s to 966 s, the primary system mass increases and the total mass discharged by the accumulator is 135 kg of water.

The stop of the accumulator's injection, at 970 s, causes another mass depletion period, leading to the third dry out at about 1644 s, when the primary pressure is about 1 MPa. In this period, the mixture level in the core drops below the top of heated length. When, at 2073 s, the rod's surface temperature reaches 772 K the low-pressure injection system is actuated (2073 s) in the intact loop cold leg; at this time, the pressure is about 0.73 MPa.

The LPIS flow rate (0.4 kg/s) is effective in causing the third core quench and in recovering the facility. The quench front velocity is larger than 0.02 m/s and, at 2173 s the core is completely recovered. Core refill occurs in this period. The test was terminated at 2400 s with a pressure of 0.55 MPa.

Figure 11 shows a snapshot of a video of the experimental real-time collapsed levels and plots of primary and secondary pressures.

Table 3: Resulting sequence of events, comparison between experimental test and calculated results of BL-44.

Events/set-points	Time after experiment initiation (s)	Calculated time after transient initiation (s)
Break opening	0.0	0.0
Scram power curve enabled	1.4	2.6
Start of the main coolant pumps coast down	0.9	0.0
Main steam line valve closure	—	3.6
Feedwater valve closure	1.3	2.6
Upper plenum in saturation condition	10.0	13.0
Pressurizer emptied	25.0	25.0
Break two-phase flow	117.0	115.0
First dry out	189.0	—
Loop seal clearing—intact loop	197.0	2250.0
Loop seal clearing—broken loop	—	250.0
Occurrence of minimum primary side mass		
First	427.0	445.0
Second	2071.0	2070.0
Primary-secondary pressure reversal	208.0	212.0
Second dry out	372.0	420.0
Accumulator injection starts	429.0	439.0
Accumulator injection stops	970.0	1065.0
Rewetting due to accumulator	547.0	525.0
Final dry out	1711.0	1795.0
LPIS start	2065.0	2073.0
Final rewetting	2203.0	2207.0
End of the test	2400.0	3000.0

5.2. Posttest Calculation. The input deck [18] is chosen on the basis of the agreement between the trends of the calculation and experimental parameters and also taking into account that in the simulation the initial and boundary conditions of the experiment are preserved. In Table 3 are shown the sequence of the main events and the set points for the calculation compared to the BL-44 experiment. The agreement is quite close. A comment loop seal clearing follows below.

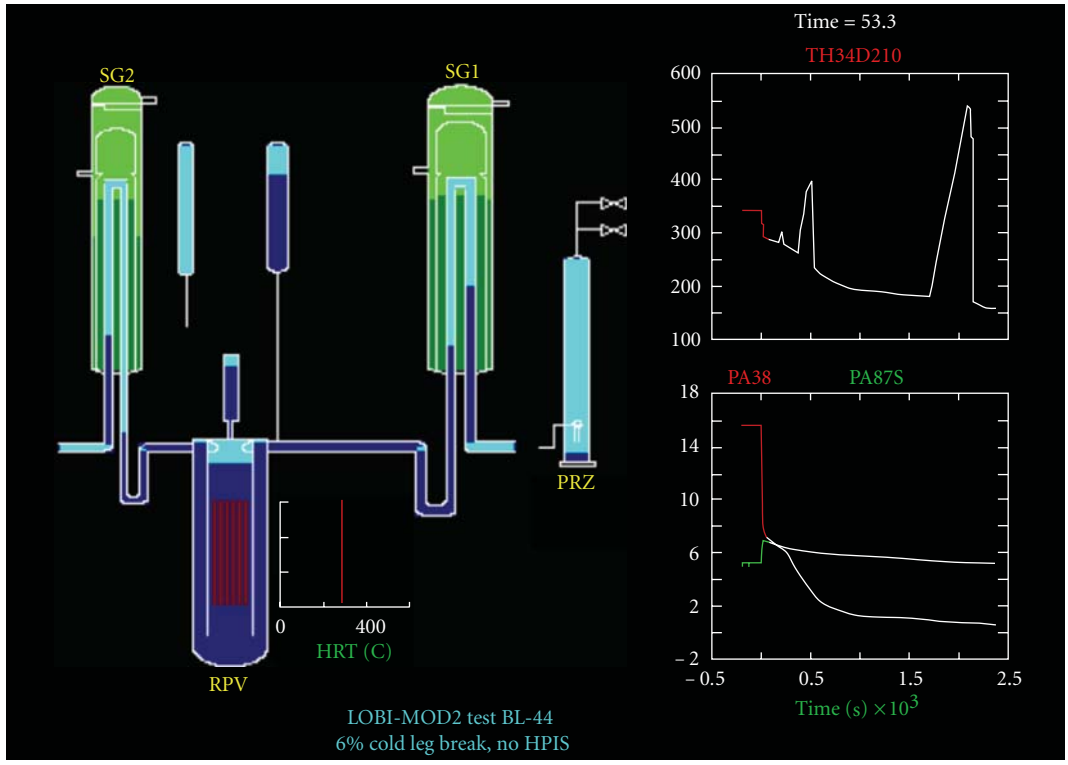

Figure 11: BL-44 experiment collapsed levels display and primary and secondary pressures (STRESA JRC database).

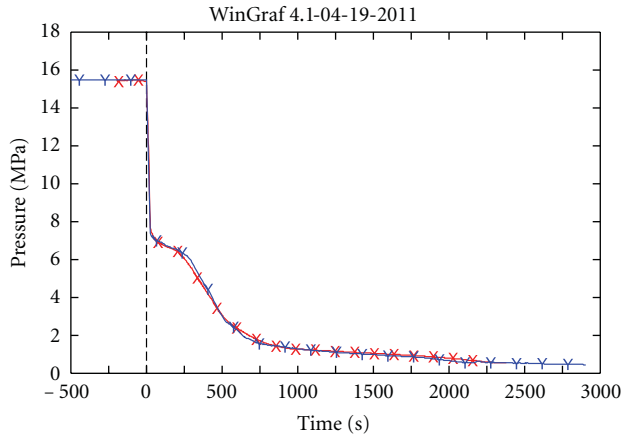

Figure 12: Primary system pressure.

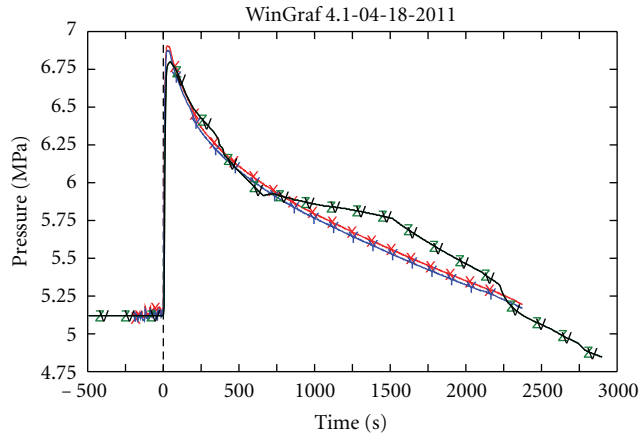

Figure 13: Secondary system pressure.

In the following figures are shown the results of BL-44 experiment calculation (descriptor BL44_G), compared with the experimental data (descriptor EXP44).

The primary system pressure is well predicted by the code and the phenomenological phases (e.g., subcooled blowdown, saturated blowdown, and steam flow from the break) can be easily recognized from the calculated time trend, as shown in Figure 12.

Loop seal clearing is a very sensitive phenomenon. In BL-44 test, both loop seals were about to be cleared by the end of two-phase flow discharge. Once one loop seal is effectively cleared, differential pressures change completely and the other loop seal remains uncleared for quite a long time. While in the test, intact loop seal is effectively cleared, in the simulation this happens with broken loop.

Figure 13 shows that the secondary system pressure, in the intact loop (vols. 97, 815) and in the broken loop (vols. 87, 915), is in quite good agreement with the experimental

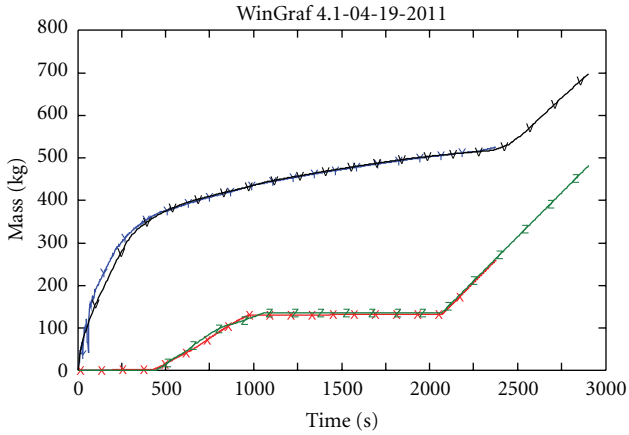

XXX EXP44 "INTECCSFR"
YYY EXP44 QL05EWT
ZZZ BL44_G ECCSintegralFlow
VVV BL44_G IntegralBreakFlow

Figure 14: ECCS integral mass flow and integral break flow.

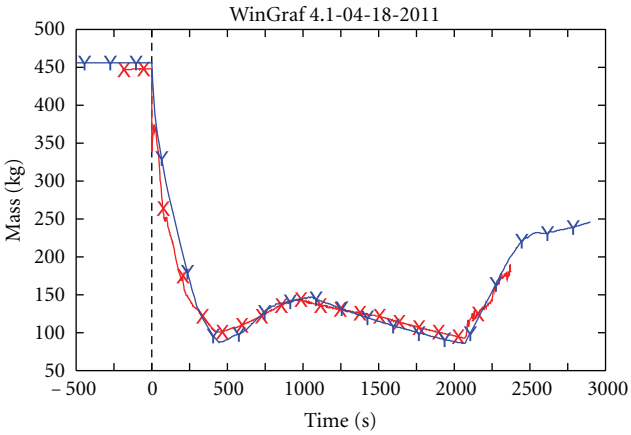

XXX EXP44 CIPRIM
YYY BL44_G cntrlvar77

Figure 15: Primary system mass.

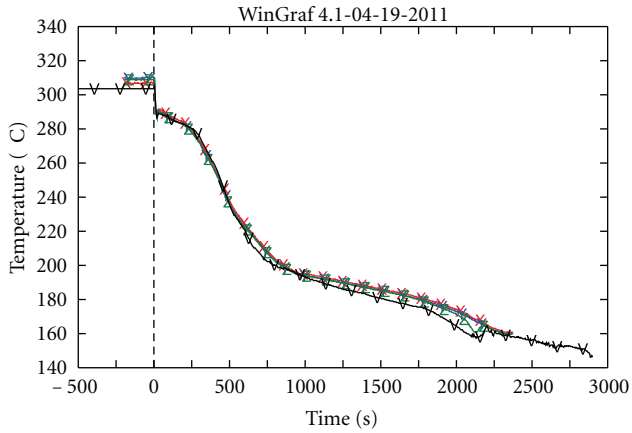

XXX EXP44 TH35F402
YYY EXP44 TH34D402
ZZZ EXP44 TH34E103
VVV BL44_G httemp995000115

Figure 16: Cladding temperature at bottom level.

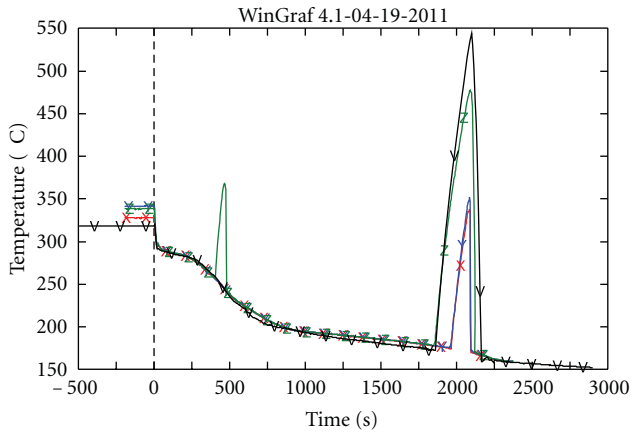

XXX EXP44 TH37A407
YYY EXP44 TH34A407
ZZZ EXP44 TH34G208
VVV BL44_G httemp997000115

Figure 17: Cladding temperature at middle level.

trend. The calculated pressure is slightly underestimated in the first part of the transient (before 700 s) and overestimated in the final part of the transient (after 700 s). Since in this test, the secondary side is isolated and no cooldown is carried out, its behavior is very sensitive. Secondary pressure depends in this case on two quite small heat extractions: heat transfer from secondary to primary side and heat losses to environment. Both aspects were studied performing sensitivity calculations. Setting the right time of closure of the feedwater helped the simulation but that of the steam lines was not available and a standard value was used. Heat losses were also studied in relation the other two tests. This will be commented in the last section.

ECCS (accumulator mass injected and LPIS mass flow) and integral break mass are shown in Figure 14. Accumulator starts to inject when primary pressure below 3.91 MPa (at about 439 s), the LPIS starts to inject when the rods surface temperature reaches 772 K, at 2073 s. The trends of ECCS and integral break mass flow are well predicted.

The primary system mass is shown in Figure 15, after the break PS mass decrease, then, with the accumulator and LPIS injection, the PS mass start to increase.

Representative experimental data at three core levels (bottom, middle, high region), in the axial direction, have been selected for the comparison with the calculated data (Figures 16, 17, and 18). Calculated rod surface temperature trends follow well the measured values. The first dryout is not predicted by the code. The second and the third dry out situation are well predicted.

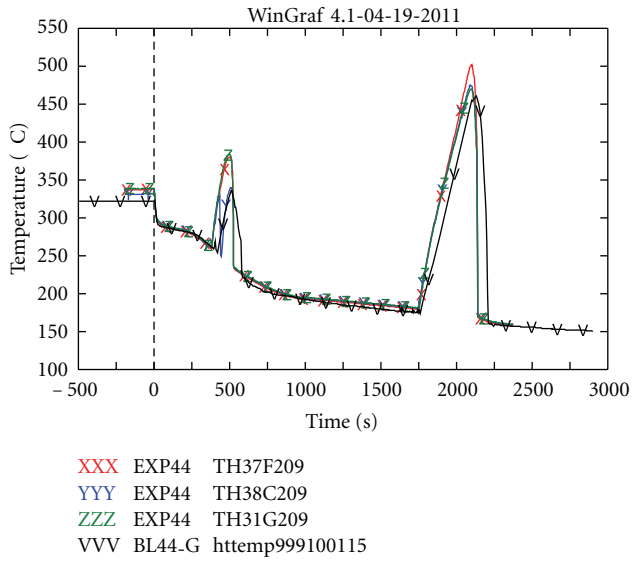

Figure 18: Cladding temperature at high level.

6. A1-84 Scenario

6.1. Experiment Description. Test A1-84 simulates a 10% hot leg break (break orifice diameter = 9.5 mm, side oriented) in the main coolant pipe of a PWR. Cooldown is applied to the secondary side at a rate of 100 K/h. Emergency core cooling water is injected into the primary loops by the Accumulators and the HPIS. The Accumulators are connected to both legs of the intact loop and to the cold leg of the broken loop. The high pressure injection system is connected to the hot leg of the intact loop. The injection rate is representative of two injection pumps (out of four). The remaining two pumps (that exist in the reference plant) are assumed to be one in maintenance and the other connected to the broken loop.

Boundary conditions during the test follow the behavior of the reference plant after leak detection.

Within 1 s after rupture, the primary system depressurizes to 132 bar, and this enables the core heating power and the secondary system cooldown signals. The isolation procedure (closure of feedwater valves and main steam valve at condenser inlet) together with the automatic cooldown (100 K/h) of the secondary system are actually initiated at 1.3 s after the rupture, and this causes a delay in the primary and secondary pressures responses.

Saturation pressure in hot leg is reached at about 2 s; the attainment of this pressure brings to a moderate change in primary system depressurization, which continues at a reduced rate as the fluid, in the upper vessel internals, started to flash.

At 5 s into the transient, the HPIS pressure set point (117 bar) is reached, but the high pressure emergency core cooling system initiates with a delay of 35 s, at about 40.6 s.

At 7 s, coastdown of the main coolant pump starts, upon actuation, at 6 s, at the 110 bar low primary system pressure set point.

As the primary mass inventory lowers because of the outflow from the break, the pressurizer surge line eventually uncovers at about 17.5 s.

At 23 s the saturation front reaches the cold leg elevation and at 42 s the whole primary system achieves saturation condition as the system depressurizes to the saturation pressure of the fluid in the lower plenum.

At about 84 s into the transient the primary pressure falls below the secondary one, giving rise to potential reverse heat transfer in the steam generator.

After the uncovering of the break, at about 150 s, the primary cooling system depressurizes faster and soon reaches the pressure setpoint for the accumulators' actuation (2.8 MPa).

Within 850 s the system has a pressure of 1 MPa, which is the pressure set-point for test termination.

Figure 19 shows a snapshot of a video of the experimental real-time collapsed levels and plots of primary and secondary pressures.

6.2. Posttest Calculation. The input deck [19] is chosen on the basis of the agreement between the trends of the calculation and experimental parameters and also taking into account that in the simulation the initial and boundary conditions of the experiment are preserved.

The sequence of main events which characterize the course of the transient is shown in Table 4. The agreement is quite close.

The results obtained from A1-84 test simulation (descriptor A1-84-11.0) are plotted and described below, in comparison with the experimental data available (descriptor EX84).

In Figure 20, the PS pressure is shown; the prediction is in close agreement with the experiment, the depressurization rate is well reproduced, and it is clearly highlighted that the moment in which saturation in the primary side is reached because there is an important decrease in the curve slope.

Figure 21 shows SS steam dome pressure in the broken loop (vols. 87, 915) and in the intact loop (vols. 97, 815) for A1-84 experiment and RELAP5 Mod 3.3 simulation. The secondary pressure behavior is very well simulated, and the cooldown (100 K/h) is correctly implemented.

Figures 22, 23, and 24 show the ECCS mass flow rate (HPIS mass flow and integral flow, accumulators' levels) together with the integral mass flow flowing out of the break. HPIS is actuated after 40 s in the code calculation and in the experiment. The mass flow rate injected depends on the primary system pressure. The code simulation perfectly matches the experiment. The accumulators start to inject at about 350 s, but the BL injection is stopped at about 560 s, and the IL accumulator injection is never stopped. The accumulator levels shows an acceptable trend if compared to the experimental (Figure 23).

Moreover the simulated integral mass flow through the break (Figure 24) is in agreement with the corresponding time trend derived from experimental data.

Figure 25 shows PS total mass inventory: it decreases after the break, reaching a minimum at 350.0 s and starts to recover due to HPIS and accumulators injections.

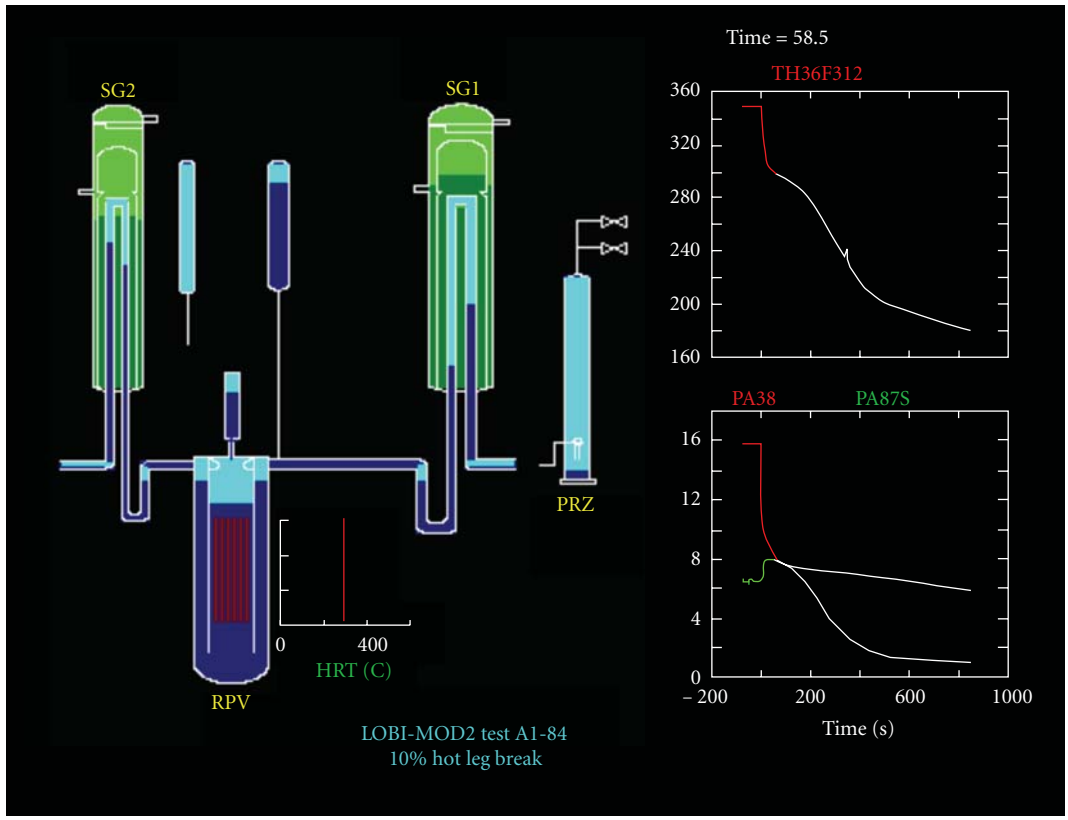

Figure 19: A1-84 experiment collapsed levels display and primary and secondary pressures (STRESA JRC database).

Table 4: Resulting sequence of events, comparison between experimental test and calculated results of A1-84.

Events/set points	Time after experiment initiation (s)	Calculated time after transient initiation (s)
Break opening	0.0	0.0
SCRAM signal (at 13.2 MPa + delay 0.5 s)	1.0	1.0
Secondary side cooldown 100 K/h actuation (at 13.2 MPa + 1.5 s valve closure time)	1.3	13.0 (imposed by time)
Pressure in PS 11.7 MPa	5.0	4.76
MCPs start coastdown (at 11.0 MPa + delay 1.0 s)	7.0	7.0
Upper plenum in saturation conditions	15.8	19.3
HPIS actuation (at 11.7 MPa + delay 35 s)	40.0	39.76
PS pressure falls below SS pressure IL/BL	90.8/97.8	101.3/101.83
Occurrence of minimum primary side mass	347.4	350.0
Accumulator actuation IL/BL (at 2.8 MPa, disabled at 11 Mpa + delay 500 s in cold leg, not disabled in hot leg)	347.0/349.9	335.1/335.0
Auxiliary feedwater in broken loop	—	—
Accumulator injection stops Cold leg IL/BL	509.0/520.0	487.4/558.7
Accumulator injection stops Hot leg IL	849.0	849.0
End of the test (0.1 Mpa)	850.0	850.0

Figure 26 shows fuel cladding temperatures at middle-heated length height, in the core region: no dry-out is observed and temperatures decrease because of the combined injection of HPIS and accumulators. No loop seal clearing is observed, according to what happens in the experiment.

The temperature trend is well matched, with the exception of the second half of transient, when the calculated results slightly underestimate the experimental data.

Figure 27 shows the pressure drop along the vessel, from the inlet of the downcomer, to the outlet of the vessel (hot leg inlet). The trend is well reproduced by the code during

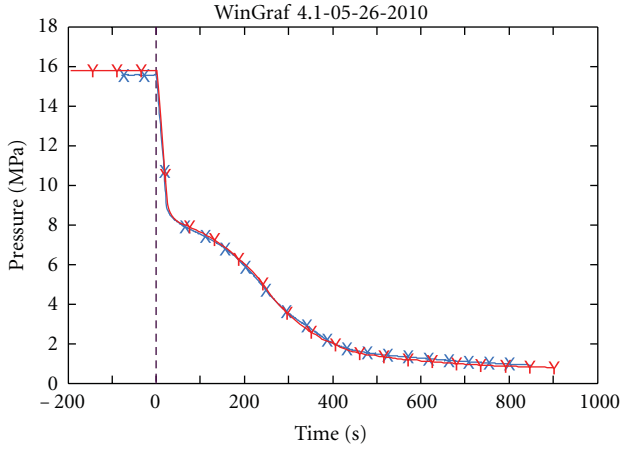

XXX EX84 PA40
YYY A1-84-11 p539010000

Figure 20: Primary system pressure.

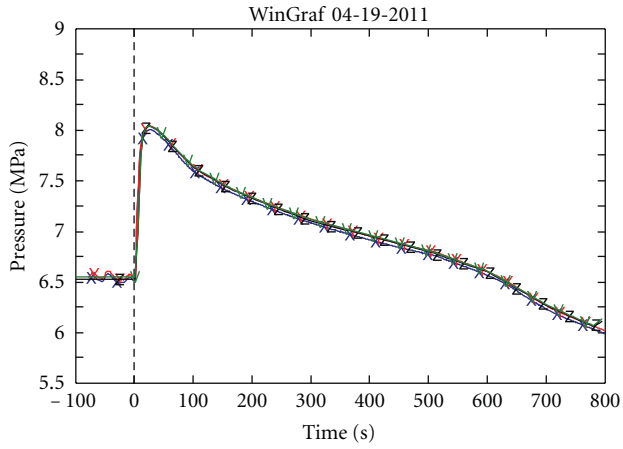

XXX ex84 PA87S
YYY ex84 PA97S
ZZZ A1-84-11 p915010000
VVV A1-84-11 p815010000

Figure 21: Secondary system pressure.

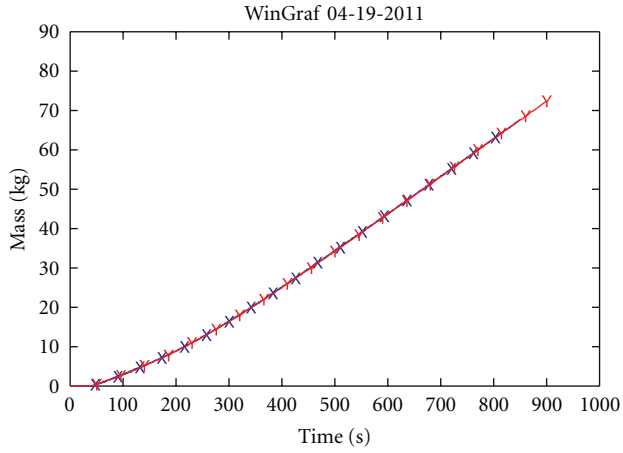

XXX EX84 IntegralFLHPISex84
YYY EX84 IntegralFlowrateHPIS

Figure 22: HPIS integral mass flow.

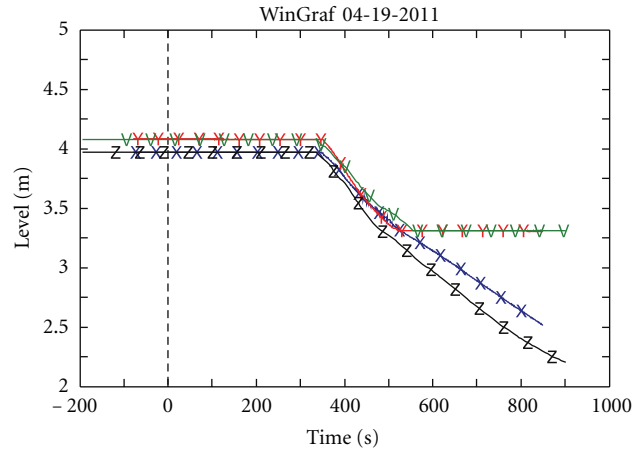

XXX ex84 CL51
YYY ex84 CL52
ZZZ A1-84-11 cntrlvar201
VVV A1-84-11 cntrlvar202

Figure 23: Accumulators levels.

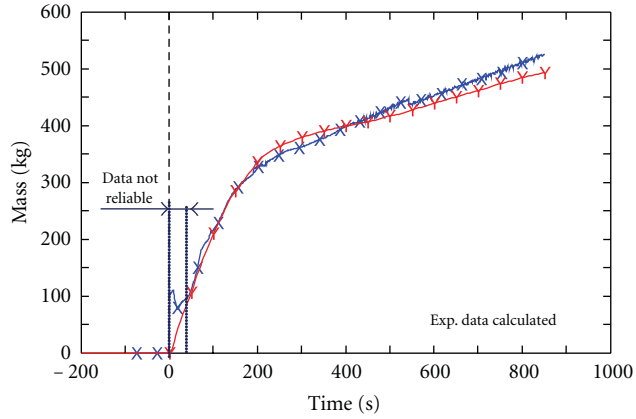

XXX EX84 INTBRK
YYY A1-84 INTEGRALBRK

Figure 24: Integral break flow rate.

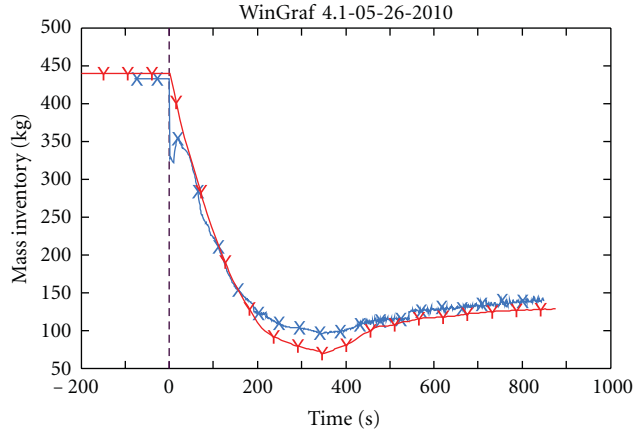

XXX EX84 CIPRIM
YYY A1-84-11 cntrlvar77

Figure 25: Primary system mass.

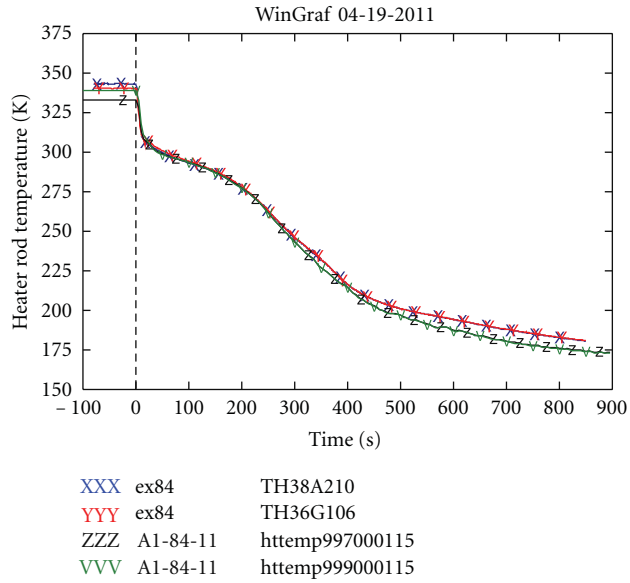

Figure 26: Cladding temperature, middle- and top-heated length level.

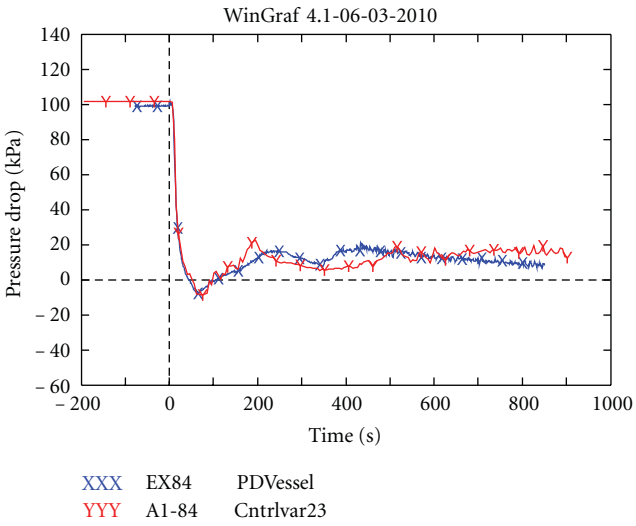

Figure 27: Vessel pressure drop.

steady state and the beginning of the transient demonstrating that the RELAP5 model was correctly setup. Once the MCP are stopped reasonable prediction implies that reasonable mass distribution in the vessel is achieved (considering the primary pressure and coolant temperature are correctly predicted).

7. Discussion and Conclusions

Posttest calculations of LOBI tests BL-30, BL-44, and A1-84 have been carried out successfully. The results are in close agreement with experimental data and will become an interesting starting point for both future scaling calculations and accuracy evaluations.

The three tests have been simulated using the same LOBI facility nodalization. The procedure to come up with the final version of the common nodalization involved some iteration. Once a clear improvement of the predictions was obtained for one test by means of a nodalization change, the other tests were recalculated and following the quality the new results the suggested change was accepted and confirmed.

All posttests show good predictions for primary system mass time trends. The final set of values corresponding to hydrodynamic loss coefficients on primary side are exactly the same for the three tests. These final values were carefully chosen taking into account the results of preliminary calculations (mainly delta-p and mass inventory), and they have been confirmed after recalculating all tests.

By-pass paths through vessel upper head and also the general lay-out it, are quite complex, but general geometry is about the same for all the involved tests. Hydrodynamic loss coefficients, as well as interconnecting areas between upper-head volumes follow a similar consolidating practice.

Heat losses to environment are only sensitive in tests or phases of tests in which they become comparable to other heat extractions. In this case, heat loss coefficients were reasonable adjusted for BL-44 (in the time window where heat losses were comparable to other heat extractions) and the adjusted value was used for the other two tests, where the secondary side cooldown was the dominant effect which completely shadows environment impact.

This mutual consistency among the presented calculations is a relevant point that adds value to the results and confirms the procedure of implementing changes in a common nodalization valid for simulating tests occurred in a specific ITF.

The outcome of the presented analysis will be helpful to support the involved steps of integral plant model qualification procedures and uncertainty evaluation methodologies.

Acronyms

AFW:	Auxiliary feedwater of SGs
BE:	Best estimate
CIAU:	Code with the capability of internal assessment of uncertainty
EC:	European commission
ECCS:	Emergency core cooling
FW:	Main feedwater of SGs
HPIS:	High-pressure injection system
ITF:	Integral test facility
JRC:	Joint research centre
KWU:	Kraftwerk Union
LB LOCA:	Large break loss of coolant accident
LOBI:	LWR off-normal behaviour investigations
LPIS:	Low pressure injection system
LWR:	Light water reactor
MCP:	Main coolant pump
NPP:	Nuclear power plant
PCT:	Peak cladding temperature
PS:	Primary system
PWR:	Pressurized water reactor
SB LOCA:	Small break loss of coolant accident
SG:	Steam generators
SRV:	Steam relief valve

SS: Secondary system
STRESA: Storage of thermal reactor safety analysis data
UNIPI: University of Pisa
UPC: Universitat Politècnica de Catalunya, Technical University of Catalonia
UP: Upper plenum.

Acknowledgments

The authors would like to thank Giorgio Galassi, from the GRNSPG-UNIPI, and Alessandro Annunziato, and Carmelo Addabbo, from the JRC Ispra, for their constructive discussions, explanations, and help during all the posttest analysis period regarding the modeling and the LOBI facility hardware details. From JRC of Petten, authors are grateful also to Manuel Martin Ramos for his constructive discussions during the BL-30 posttest activity and to Marcello Barboni for the informatics support related to the STRESA Database.

References

[1] V. M. Martínez, F. Reventós, C. Pretel, and I. Sol, *Code Validation and Scaling of the ROSA/LSTF Test 3-1 Experiment*, European Nuclear Society, Dubrovnik, Croatia, 2008.

[2] F. D'Auria, N. Debrecin, and G. M. Galassi, "Outline of the uncertainty methodology based on accuracy extrapolation," *Nuclear Technology*, vol. 109, no. 1, pp. 21–38, 1994, OECD-CSNI Special Workshop on Uncertainty Analysis Methods, London (UK).

[3] F. Reventós, L. Batet, C. Llopis, C. Pretel, M. Salvat, and I. Sol, "Advanced qualification process of ANAV NPP integral dynamic models for supporting plant operation and control," *Nuclear Engineering and Design*, vol. 237, no. 1, pp. 54–63, 2007.

[4] C. Addabbo and A. Annunziato, "The LOBI test matrix—LOBI project, "STRESA database web platform.

[5] "JRC STRESA database web platform, "http://stresa.jrc.ec.europa.eu/stresa/.

[6] A. Annunziato, "Quick look report on LOBI-MOD2 test BL-30 (5% Cold Leg Break LOCA)," Tech. Rep., Joint Research Centre, Ispra, Italy, 1990.

[7] J. Sanders and E. Ohlmer, "Experimental data report on LOBI-MOD2 test BL-30 (5% Cold Leg Break LOCA)," Tech. Rep., Joint Research Centre, Ispra, Italy, 1990.

[8] A. Annunziato, "Quick look report on LOBI-MOD2 test BL-44 (6% Cold Leg Break LOCA)," Tech. Rep., Joint Research Centre, Ispra, Italy, 1992.

[9] C. Addabbo, G. Leva, and A. Annunziato, "Experimental data report on LOBI-MOD2 test BL-44 (6% Cold Leg Break LOCA)," Tech. Rep., Joint Research Centre, Ispra, Italy, 1992.

[10] C. Addabbo, R. Wampach, and G. Leva, "Quick look report on LOBI-MOD2 test A1-84 (10% Hot Leg Break LOCA)," Tech. Rep., Joint Research Centre, Ispra, Italy, 1986.

[11] J. Sanders and E. Ohlmer, "Experimental data report on LOBI-MOD2 test A1-84 (10% Hot Leg Break LOCA)," Tech. Rep., Joint Research Centre, Ispra, Italy, 1986.

[12] A. Berthon, *Caracterización de la evaluación de seguridad del reactor WWER-1000 mediante metodología "Best Estimate" con análisis de incertidumbres*, M.S. thesis, University of Pisa, Italy, 2005.

[13] F. D'Auria, M. Frogheri, and W. Giannotti, *RELAP5/MOD3.2 Post Test Analysis and Accuracy Quantification of LOBI Test BL-44;NUREG/IA-0153*, University of Pisa, Italy, 1999.

[14] F. D'Auria and W. Giannotti, "Development of a code with the capability of internal assessment of uncertainty," *Nuclear Technology*, vol. 131, no. 2, pp. 159–196, 2000, CAMP Meeting, Bariloche, Argentina, 1999 (invited paper), Relap5 International Users Seminar, Park City (Utah, USA), 1999.

[15] C. Pretel and F. Reventós, "Post-test analysis of LOBI test BL-30 using RELAP5/MOD2.5," Tech. Rep. I.93.64, Technical University of Catalonia, Asociación Nuclear Ascó, Spain, 1993.

[16] B. Worth and H. Staedtke, "Relap5 base input data for LOBI-MOD2," Tech. Rep., Joint Research Centre, Ispra, Italy, 1985.

[17] U. S. Nuclear Regulatory Commission, *RELAP5/MOD3.3 Code Manual*, vol. 4, U. S. Nuclear Regulatory Commission, Idaho Falls, Idaho, USA, 2001.

[18] G. Nacci, *Post-test analysis of BL-44*, M.S. thesis, University of Pisa, Italy, 2011.

[19] C. Matteoli, *Post-test analysis of A1-84*, M.S. thesis, University of Pisa, Italy, 2011.

Hindawi Publishing Corporation
Science and Technology of Nuclear Installations
Volume 2012, Article ID 158617, 17 pages
doi:10.1155/2012/158617

Research Article

Remarks on Consistent Development of Plant Nodalizations: An Example of Application to the ROSA Integral Test Facility

J. Freixa and A. Manera

Laboratory for Reactor Physics and Systems Behaviour (LRS), Paul Scherrer Institut (PSI), 5232 Villigen, Switzerland

Correspondence should be addressed to J. Freixa, jordi.freixa@psi.ch

Received 4 May 2011; Accepted 3 September 2011

Academic Editor: Klaus Umminger

Experimental results obtained at integral test facilities (ITFs) are used in the validation process of system codes for the transient analyses of light water reactors (LWRs). The expertise and guidelines derived from this work are later applied to transient analyses of nuclear power plants (NPPs). However, the boundary conditions at the NPPs will always differ from those at the ITF, and hence, the soundness of the ITF model needs to be maximized. An unaltered ITF nodalization should prove to be able to simulate as many tests as possible, before any conclusion is derived to NPP analyses. The STARS group at the Paul Scherrer Institut (PSI) actively participates in several international programs, where ITFs are being used (e.g., ROSA, PKL). Several tests carried out at the ROSA large-scale test facility operated by the Japan Atomic Energy Agency (JAEA) have been simulated in recent years by using the United States Nuclear Regulatory Commission (US-NRC) system code TRACE. In this paper, 5 different posttest analyses are presented, along with the evolution of the employed TRACE nodalization and the process followed to track the consistency of the nodalization modifications. The ROSA TRACE nodalization provided results in a reasonable agreement with all 5 experiments.

1. Introduction

In the last decades, integral test facilities (ITFs) have been used to validate thermal-hydraulic codes with the final objective of performing safety analyses for nuclear power plants (NPPs). The experiments carried out at facilities like PKL, LOFT, LOBI, BETHSY, or LSTF have been employed to build up expertise in the usage of system codes. User guidelines have been derived, models and correlations have been corrected or further developed, and limitations on the use of system codes have been identified. Such expertise is later on applied to the modelling of NPPs. One of the lessons learned with the use of ITFs for system codes validation is that even though a given code with a given nodalization is able to capture correctly the phenomena occurring in one test, it might not be the case in a successive test with different boundary conditions. This can be true even for single phenomena such as the critical flow at a break location, so that one should not assume that the phenomenon will be well simulated in an NPP model. As a matter of fact, it has to be considered that the conditions to be simulated in the NPPs differ from those simulated with the ITF models, so that confidence in the system code and the associated nodalization can be built only after successful simulations of a wide range of tests.

The large number of available experiments in test facilities like the ROSA large-scale test facility (LSTF) operated by the Japanese Atomic Energy Agency (JAEA) offers the possibility to validate various physical models under different conditions, at the same time developing guidelines and strategies for building up the system nodalization. When developing an ITF nodalization, it is essential to simulate as many tests as possible by using exactly the same nodalization. The extend of expertise and guidelines obtained by a model that is able to reproduce several tests at the same time is far larger than what one can obtain with few tests, because the performance of the models and correlations is tested in different conditions. Users must not resort to simulate the different tests independently, because if done so, the robustness and the soundness of the model will be lost. Generally speaking, each time a new test is simulated and modifications are introduced to the main model other than

initial or boundary conditions, all previous tests should be recalculated to assure the consistency of the modifications. In principle, any improvement undertaken in the nodalization must be valid for all previous tests. Obviously, this supposes a considerable effort, especially when various full models of facilities or power plants are to be maintained. Hence, it is recommendable to establish a clear and easy methodology, aimed at reducing the efforts of the analyst. Examples of this consistent quality assurance can be found in [1, 2].

The STARS group [3] of the Paul Scherrer Institut (PSI) actively participates in several international programs where ITFs are employed (e.g., ROSA, PKL). Several tests of the ROSA/LSTF have been simulated at PSI in the recent years, within the OECD/NEA ROSA 1 and 2 projects. These projects aim at addressing thermal-hydraulic safety issues relevant for light water reactors through experiments making use of the ROSA/LSTF facility. The experiments are used for the development and validation of simulation methodologies of the complex phenomena occurring during design basis accidents (DBAs) and beyond DBAs. ROSA/LSTF, operated by the Japan Atomic Energy Agency (JAEA), is a full-height and 1/48 volumetrically scaled test facility of a 1100 MWe-class pressurized water reactor (PWR). The facility allows to perform system integral experiments simulating the thermal-hydraulic responses at full-pressure conditions during small break loss-of-coolant accidents (LOCAs) and other transients. The reference plant is Unit-2 of Turuga NPP of the Japan Atomic Power Company.

A nodalization of the ROSA facility has been built in the PSI STARS group using the United States Nuclear Regulatory Commission (US-NRC) thermal-hydraulic code TRACE. The nodalization has been employed to calculate 5 different ROSA experiments, focusing mainly on small and intermediate break LOCAs. From test to test, sensitivity studies have been performed which have led to nodalization modifications and corrections. This paper focuses on the evolution of the nodalization, and the work carried out in order to maintain a sole nodalization able to satisfactorily simulate all the transients.

2. Model Description

The ROSA/LSTF nodalization has been produced by using the US-NRC thermal-hydraulic code TRACE (version 5.0). The nodalization had been derived combining the information of existing TRAC-p and RELAP input decks provided by JAEA together with the original technical drawings of the facility.

The TRACE model of the LSTF, shown in Figure 1, consists of a 3D vessel, two separate loops with two steam generators, and a pressurizer. The primary system is completed with pressurizer control systems (spray system, relief and safety valves, and base and proportional heaters) and safety injection systems (accumulators and low- and high-pressure injections). The secondary system is provided with main and auxiliary feedwater systems, a set of relief and safety valves, a main steam line, and a common steam header.

The 3D vessel component is composed by 20 axial levels, 4 radial rings, and 10 azimuthal sectors. The three first rings cover the core region, and the fourth ring represents the downcomer (DC). The heater rods are simulated by means of 30 heat structures, one for each section in the radial plane. The rods are grouped in three categories according to the power regions of the LSTF.

All bypasses are nodalized according to the geometrical specifications, and the friction k-factors were adjusted such that the mass flow at the bypasses during the steady-state calculation matched the experimental values. An additional leakage between the DC and the UP was added, as it was seen to be the only way to represent the evolution of the void fraction in the downcomer. The considerations that lead to the nodalization of this additional leakage will be discussed in Section 4.1.1.

The 8 control rod guide tubes (CRGTs) are simulated by 12 pipes connecting the core outlet with the upper head. The two inner CRGTs are linked geometrically with three different core volumes as shown in Figure 1. In order to keep the same connections from the core exit to the upper head (UH), the two inner CRGTs were split into three pipes. Volumes and sections were divided by three, while the hydraulic diameter was kept. Hence, each of the two inner tubes is simulated by means of three parallel pipes connected with three out of ten azimuthal cells of the inner ring. The other guide tubes are simulated by using a single pipe component for each tube.

The correct simulation of metal structures and heater rods is of main importance to capture the system behavior during small break LOCA (SBLOCA) and intermediate break LOCA (IBLOCA) scenarios. The ROSA nodalization developed at PSI includes all heat structures corresponding to walls, heated rods, unheated rods, internal metal structures, and support plates. All these components are simulated by a total of 53 heat structures.

The ROSA/LSTF has a core protection logic aimed at avoiding damage to the heater rods in the core, by limiting the maximum allowed core temperatures. Basically, the core power is decreased when the rods temperature rises above $\approx$960 K. The logic of this protection is included in the control system simulated within the TRACE input data set.

The two loops are simulated separately, and a single pipe component is used in the nodalization to represent the U-tube bundle. The pressurizer is nodalized with a 7-cell pipe. The steam generators are represented by separator components, and the heat losses through the outer walls are taken into account as well.

The countercurrent flow limitation (CCFL) model was activated in correspondence of two locations:

(i) the top plate at the top of the core region. The Wallis correlation [4] was used with the same coefficients specified in the OECD BEMUSE project ($m = 1.0$ and $c = 0.8625$) [5];

(ii) the steam generator (SG) inlet plenums and U-tube section. Again the Wallis correlation was used although in this case the coefficients suggested by Yonomoto [6] were used ($m = 1.0$, $c = 0.75$).

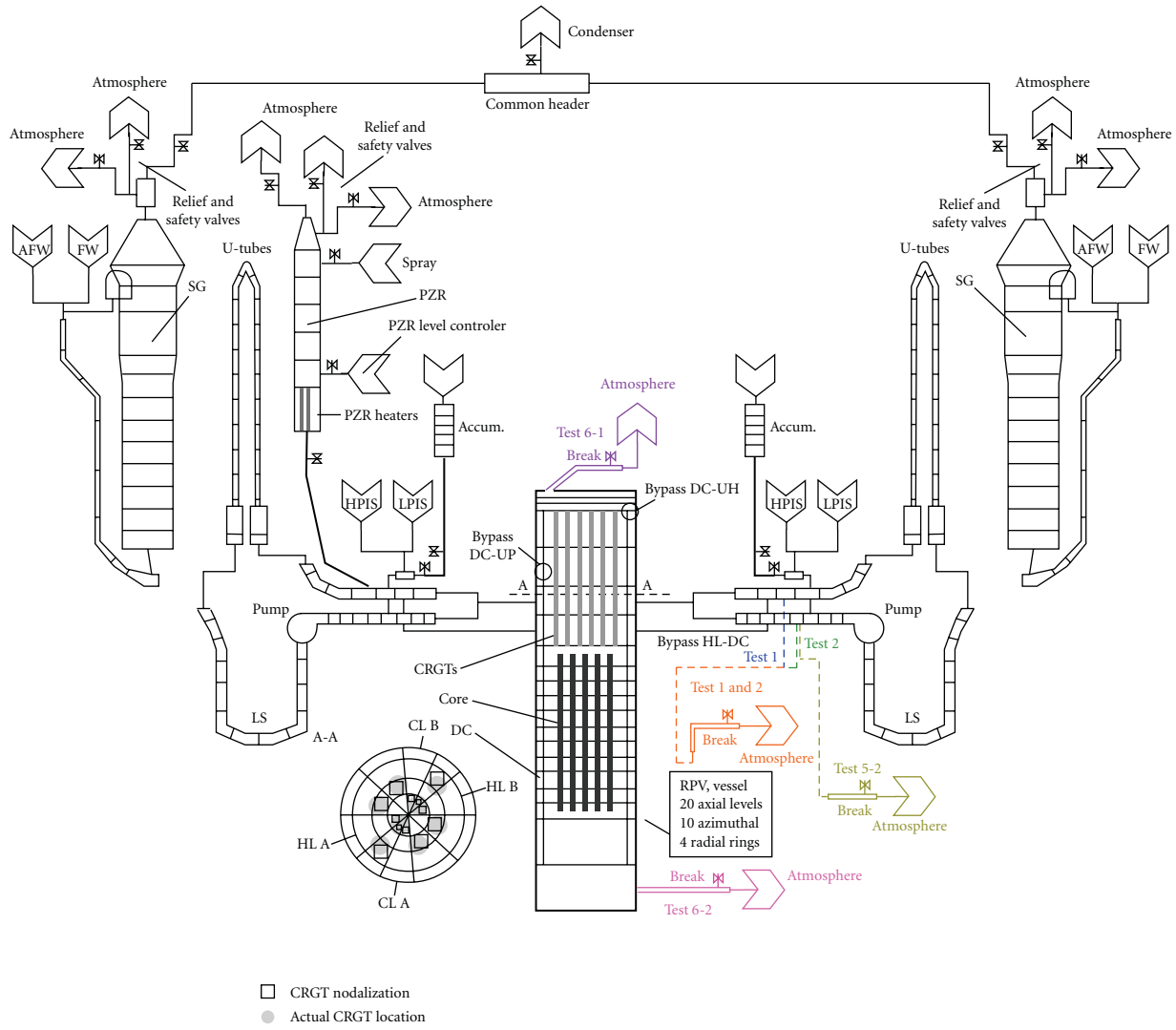

Figure 1: TRACE nodalization of the ROSA/LSTF.

2.1. Steady-State and Initial Conditions. A steady-state calculation was carried out in order to reach the experimental initial conditions. The initial conditions obtained by the TRACE model (Table 1) after the steady-state calculation are in quite close agreement with the experimental values. All steady-state parameters are within the error bands of the measurements. The most significant discrepancy is a 3% error in the steam flow rate. The high percentual errors in the bypasses flows are within the error bands of the measurements which are quite large.

The use of a three-dimensional vessel was seen to be crucial. Different flows were detected in the CRGTs depending on the position of the pipe relative to the vessel cross-section, that is, depending on the radial and azimuthal cell where the CRGTs were connected. While some CRGTs showed upward flow, others experienced downward flow, allowing natural convection in the upper head. Capturing this phenomenon was found to be crucial in order to correctly reproduce the UH temperature, which would have been otherwise too high.

Table 1: Percentual error between the calculated steady state and the experimental values.

	Percentual error (%)
Core power	0.0
DC to UH bypass flow	17.0
Hot leg to DC bypass flow	17.0
Primary pressure	0.3
Hot leg fluid temperature	0.3
Cold leg fluid temperature	0.2
Mass flow rate	0.0
Pressurizer level	2.0
Main steam pressure	0.0
Secondary side liquid level	0.5
Steam flow rate	1.9
Main feedwater flow rate	1.5

Table 2: Control logic of Test 6-1 [7].

Event	Condition
Break	Time zero
Generation of scram signal	Primary pressure 84% of initial value
PZR heater off	Generation of scram signal or PZR liquid level below 2.3 m
Initiation of core power decay curve simulation	
Initiation of primary coolant pump coastdown	
Turbine trip (closure of stop valve)	Generation of scram signal
Closure of main steam isolation valve	
Termination of main feedwater	
Opening and closing of the SG relief valves	SG pressures 110%/103%
Generation of SI signal	Primary pressure below 79% of initial value
Initiation of auxiliary feedwater	Generation of SI signal
Initiation of SG secondary-side depressurization as accident management (AM) action by fully opening relief valves	Core exit temperature reaches 623 K
Initiation of accumulator system	Primary pressure below 29% of initial value
Initiation of LPSI system	LP pressure below 8% of initial value

3. Tests

This section describes the final results of 5 different ROSA/LSTF tests that were simulated with the ROSA TRACE nodalization. The results shown in this section were obtained by the last integrated version of the model after simulating test 5-2 of the ROSA-1 project. All the relevant modifications undertaken during the process are described in Section 4. All tests start with the same initial conditions.

3.1. Test 6-1. Test 6-1 is an SBLOCA case with the break located in the UH of the reactor pressure vessel (RPV). The break was realized in the facility by using a sharp-edge orifice mounted downstream of a horizontal pipe that was connected to the upper head (the orifice flow area corresponded to 1.9% of the volumetrically scaled cross-sectional area of the reference PWR cold leg). The test started by opening the break valve, and by increasing at the same time the rotation speed of the primary coolant pumps up to 1500 rpm, for a better simulation of the expected pressure and flow values that would prevail in a similar transient in the reference PWR. Proportional heaters were used in the pressurizer (PZR) to control the primary pressure, while backup heaters compensated for system heat losses. The proportional heater power was turned off simultaneously with the activation of the scram signal, while the backup power was reduced and only completely shut down immediately after the PZR liquid level became lower than 2.3 m. This particular operation of the reactor coolant pumps and the PZR heaters was performed in all the tests analyzed in the work presented here. The description of the control logic of Test 6-1 is detailed in Table 2.

The scram signal was set to be dependent on the primary pressure by a set point of 84% of the initial pressure and initiated the core power decay, the primary coolant pumps coastdown, the termination of the feedwater system, and the closure of the main steam isolation valve. The safety injection (SI) signal was generated when the primary pressure fell below 79%. When the core exit temperature reached 623 K, depressurization of the steam generator secondary side as accident management action by fully opening the relief valves was initiated. The auxiliary feedwater was also triggered by the SI signal. The ECC system was directed towards the two cold legs and consisted of two accumulators (Accs) injecting at a primary pressure of 29% of the initial primary pressure and two low-pressure safety injection (LPSI) pumps that were started at a lower plenum (LP) pressure of 8%. The high-pressure safety injection (HPSI) system was not actuated in this test. Further details on the experimental procedures and results can be found in [7].

3.1.1. Results. Table 3 shows the chronology of the main events that occurred in Test 6-1, comparing the experimental values with the calculated ones. All the events in the TRACE simulation occur similarly as in the experiment. Discrepancies are found to be within a reasonable range of less than 80 seconds. The calculation was ended at 3000 seconds as all main events had occurred by that time.

The most important parameters for Test 6-1 are shown in Figure 2. Since the break was located at the top of the RPV, the transient can be easily divided into three different phases according to the break flow conditions: blowdown phase, break discharge in two-phase choked regime, and break discharge in single-phase vapor.

The first two phases, blowdown and two-phase flow phases, were simulated very well by the TRACE model. The distribution of coolant was correctly reproduced, as shown in the bottom graph of Figure 2. The early drop of the DC level and cold leg level (see [8]) (at about 250 s and 200 s, resp.,) could only be simulated assuming a hypothetical bypass between the UP and the DC (this assumption which will be explained and justified in Section 4.1.1). During this phase, the primary and secondary pressures were steady around the SG relief valves set points (middle graph of Figure 2). After

Table 3: Chronology of the main events in Test 6-1 [7].

Event	Exp.	TRACE
Break valve opened	0	0
Scram signal	26	20
SI signal	27	21
Break flow from subcooled to two-phase flow	50	46
Primary coolant pumps stopped	277	270
Break flow to single-phase vapor	700	741
Primary pressure lower than SG pressure, core level decreases	784	761
Full opening of SG relief valves	1090	1071
Core protection activated	1205	1271
Initiation of Acc system	1305	1225
Initiation of LPSI	2893	—
End of test	3266	3000

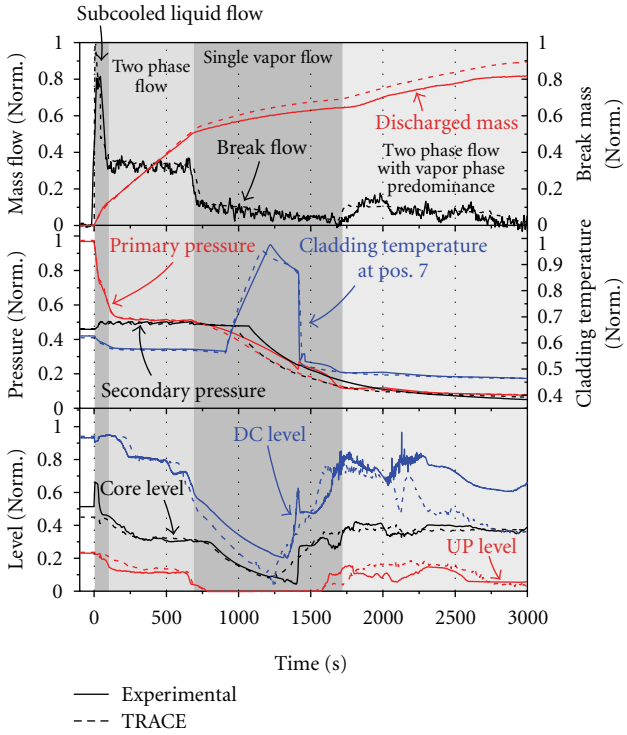

Figure 2: TRACE results for Test 6-1. From top to bottom: (1) break flow and integrated discharged mass, (2) primary and secondary pressure along with the maximum cladding temperature, and (3) RPV water levels.

this first reduction of mass inventory, the UP level dropped and the penetration holes at the bottom of the CRGTs started to void, and thus steam flew to the upper head and was expelled through the break. The transition from two-phase flow to single-vapor flow at the break was well matched by the TRACE nodalization although a delay in the transition of 50 seconds was detected. Due to this delay, the integrated discharged mass at the end of the two-phase flow part was higher in the simulation. Afterwards, the single-phase vapor choked flow at the break reported slightly higher values (see top graph in Figure 2). As a consequence, the primary pressure fell at a higher rate and the UH mass experienced a larger reduction. The drop of core level occurring during this phase was satisfactorily simulated (Figure 2). The maximum PCT, one of the most interesting signals of this test, was also correctly simulated by the model as shown in the middle graph of Figure 2. The PCT reached the core protection set points similarly in both the test and the calculation, and the power was reduced to 10% after the PCT reached 970 K. Afterwards, the PCT started to decrease. The core level started to rise again right after the opening of the accumulator valves (at $t = 1225$ s). Since the primary pressure decreased faster in the calculation, the valves opened earlier than in the experiment, so the core level rose earlier as well.

Further details on the simulation of Test 6-1 can be found in [8].

3.2. Test 6-2. Test 6-2 was started by opening a 0.1% break in the LP. The break was realized by using an inner-diameter sharp-edge orifice mounted downstream a horizontal pipe connected to the LP. The scram signal was triggered when the primary pressure was lower than 84% of the initial value [9]. The PZR heaters were operated as explained in Section 3.1 (page 4). The control logic of Test 6-2 is detailed in Table 4.

The SI signal was generated when the primary pressure decreased below 79%, and it was ensued by initiation of the auxiliary feedwater (AFW). Thirty minutes after the generation of the SI signal, asymmetrical steam generator secondary-side depressurization as accident management action was activated in order to achieve a depressurization rate of 55 K/h in the primary system. A loss of offsite power was considered, so that the HPSI pumps were not available. The LPSI and accumulator systems were fully operable and were actuated as shown in Table 4. Further details on the experimental procedures and results can be found in [9].

3.2.1. Results. Table 5 shows the chronology of the main events that occurred in Test 6-2, comparing the experimental values with the calculated ones.

The most relevant results of Test 6-2 are shown in Figure 3, which displays the cladding temperature, RPV collapsed water levels, primary and secondary pressures, and the loop mass flow rates. Overall good agreement between simulation and experimental results was obtained for the whole transient.

The primary and secondary pressures are shown in the third graph of Figure 3. During the first part of the transient, the primary pressure decreases slightly faster in the calculation, and therefore, some of the associated events occurred earlier (see the chronology, Table 5). Once the depressurization is started in loop B, the primary pressure remains close to the loop A secondary pressure until the reflux-condenser mode in this loop is interrupted (around 4000 s). Afterwards, the primary pressure follows the loop B depressurization. As shown in Figure 3, the primary pressure stabilizes around 15 bars during the latter period

Table 4: Control logic of Test 6-2 [9].

Event	Condition
Break	Time zero
Generation of scram signal	Primary pressure 84% of initial value
PZR heater off	Generation of scram signal or PZR liquid level below 2.3 m
Initiation of core power decay curve simulation	
Initiation of primary coolant pump coastdown	
Turbine trip (closure of stop valve)	Generation of scram signal
Closure of main steam isolation valve	
Termination of main feedwater	
Generation of SI signal	Primary pressure below 79% of initial value
Opening and closing of the SG relief valves	SG pressures 110%/103%
Initiation of auxiliary feedwater	Generation of SI signal
Initiation of asymmetrical SG secondary-side depressurization as AM action to achieve a depressurization rate of 55 K/h in the primary system	30 minutes after generation of SI signal
Initiation of accumulator system	Primary pressure below 29% of initial value
Initiation of LPSI	LP pressure below 8% of initial value

Table 5: Chronology of the main events in Test 6-2 [7].

Event	Exp.	TRACE
Break valve opened	0	0
Scram signal	569	453
SI signal	736	545
Primary coolant pumps stopped	819	708
Asymmetrical SG secondary-side depressurization	2548	2345
Closure of SG RV in loop with PZR	2679	2345
Initiation of accumulator system	≈5150	5450
Inflow of nitrogen gas from Acc, loop with PZR	≈10030	10995
Inflow of nitrogen gas from Acc, loop w/o PZR	≈11070	11013
Core uncovery	≈20400	22370
Initiation of LPSI	≈21940	—
Core protection activated	≈23270	23510
Second actuation of LPSI system	≈23320	—
End of transient	24034	24000

of the test (12000–25000 seconds), which overestimates the experimental results. On the one hand, the secondary-side depressurization stops at a slightly higher pressure. This depressurization depends on the capacity of the relief valve, and thus on its area and friction losses along the line. The k-factors along this line were adjusted according to the correct flows expected at high pressures. On the other hand, the higher pressure can also be caused by an overestimation of the injected nitrogen, or by an inaccurate treatment of the heat transfer in the U-tubes under the presence of nitrogen. The nitrogen concentrates in the U-tubes and induces a degradation of the heat transfer from the primary to the secondary system. As a consequence of having a slightly higher primary pressure, the set point for the LPSI intervention was never reached in the calculation, and hence, the core was not quenched as in the experimental test. In any case, it is important to notice that the set point in the facility was reached very late and with a very small margin (see small window in the third graph of Figure 3).

The evolution of the natural circulation in both loops is well predicted (bottom graph of Figure 3). After the primary pumps are completely stopped, the computed mass flows drop to the correct value. The end of natural circulation in loop A occurs slightly earlier in the simulation, and afterwards, the loop B mass flow was slightly overpredicted.

The maximum cladding temperature was measured in position 7 on rod (4,4) of element B17 (top graph of Figure 3). Two peaks were observed in the experiment, the first one was quenched by a temporary injection of the LPSI system, while the second peak reached the core protection set point, triggering a reduction of the core power. Afterwards, the LPSI system started again and quenched the core rapidly. In the calculation, the first peak did not appear, and the second one reached the first protection set point, and as the core power was reduced, the cladding temperature started to decrease slowly. However, quenching did not occur since the LPSI did not intervene in view of the too high primary pressure. Further calculations showed that the temperature would have kept rising when disabling the LSTF core protection system, leading eventually to core damage.

The DC, core, and upper plenum levels are displayed in the second graph of Figure 3. The overall behavior as simulated by means of the PSI TRACE nodalization is in accordance with the experiment. Reasonably, large discrepancies are observed when the LPSI system starts in the experiment and the primary system is refilled. There is also a time delay on the plunging of the core level at 2000 seconds.

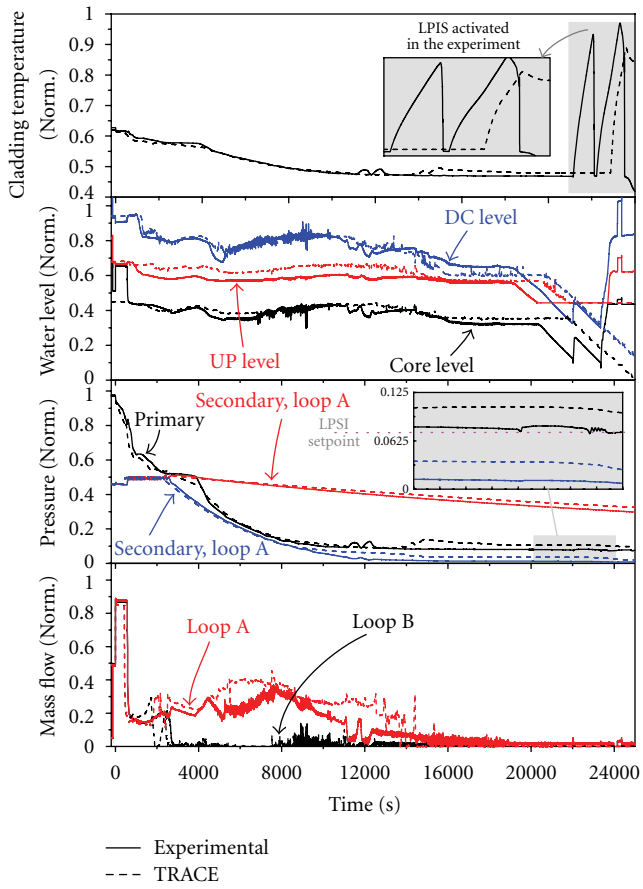

FIGURE 3: TRACE results for Test 6-2. From top to bottom: (1) cladding temperature in position 7 of rod (4,4), (2) RPV water levels, (3) primary and secondary pressures, and (4) loop mass flows.

3.3. Test 1. Test 1 is an intermediate break LOCA transient, in which a complete rupture of the surge line and the concurrent unavailability of the HPSI system are assumed. The control logic of the test is displayed in Table 6. The test is started by isolating the pressurizer and by opening the break valve located in the hot leg. Since a large amount of coolant is released through the break short after its opening, the primary pressure and the RPV level plunge. At the time when the hot leg of the broken loop becomes empty and the break flow switches from two-phase flow to single-phase vapor flow, the coolant that remains in the core starts to flash, and the core level is further reduced. An increase in the cladding temperature occurs as the heater rods become uncovered. Almost at the same time, the accumulator's valves open due to the drop of the primary pressure below the accumulators (Accs) set point. When the core level starts to drop, a large amount of steam is produced in the core, so that the pressure difference between the UP and the DC increases. The pressure drop is further enhanced by steam condensation in the cold legs due to the Acc's injection. When this pressure drop is large enough to drag the mass of water in the loop seal (LS), an LS clearance occurs. The core is refilled by means of the Acc's injection and the LS clearance. The timing between these three phenomena (Acc's injection, LS clearance, and break flow conditions) will confine the maximum peak cladding temperature.

The pressure set points for the opening and closure of the SG relief valves are 110% and 103%, respectively. Due to the assumed loss of offsite power, the HPSI is disabled for this test. The LPSI and Acc systems are available for this test and are actuated as shown in Table 6. Further details on this test and its simulation can be found in [10, 11].

3.3.1. Results. The chronology of the main events of Test 1 is shown in Table 7. All the events as simulated by TRACE occurred at very similar times as for the experiment (within 5 seconds difference), except for the initiation of the LPSI which was delayed in the experiment due to an increase of the primary pressure after the core was quenched. This increase in the primary pressure could not be explained by the experimentalists at the moment of writing.

The most important results of Test 1 are shown in Figure 4 where three different graphs display (from top to bottom): the break mass flow and integrated discharged mass, the primary and secondary pressures along with the PCT and the core, and UP and DC collapsed water levels.

The break flow in Test 1 was overpredicted by TRACE even though a two-phase discharge coefficient of 0.85 was used. The primary and secondary pressures were very well predicted once the discharge coefficient was reduced. The calculated maximum PCT was also found to be in accordance with the experimental results; however, the maximum PCT took place at a different elevation (around 1 meter difference). The maximum temperature in the TRACE calculation was detected at position 7 (see [12] for details), which is the place where the maximum PCT is usually detected. In the experiment, the maximum temperature was measured at position 5 instead (see [12] for details), which is about 1 meter below. This might be due to a slightly different core level evolution in the experiment. The water levels in the vessel are shown in the bottom graph of Figure 4 presenting a good agreement with the experiment.

3.4. Test 2. Test 2 is an intermediate break LOCA transient for which a complete rupture of the ECC line connected to the cold leg is assumed. The 17% break, corresponding to the volumetrically scaled cross-sectional area of the reference PWR cold leg, was realized by using a nozzle mounted on the top of the cold leg (upward direction). Due to the ECC line rupture, the ECC is only available in the intact loop. The failure of a diesel generator was assumed as well. Considering that the test intends to simulate a 4-loop Westinghouse design transient, the HPSI and LPSI flows injected into the intact loop correspond to 3/8 of the total nominal flow because, from the nominal 8 available pumps (2 per each cold leg), four are lost due to the failure of the diesel generator, and an extra one is lost because of the ECC line rupture. The Acc's volume to be injected in the intact loop corresponds to the volumetrically scaled volume of three Accs of the reference plant.

The control logic of the test is reported in Table 8. The test was started by opening the break; after the scram signal

Table 6: Control logic of Test 1 [10].

Event	Condition
Close of PZR spray line valves and PZR heaters	30 minutes before break
Isolation of PZR by closing surge line valve	1 minute before break
Break opening	Time zero
Generation of scram signal	4 seconds
Initiation of primary coolant pump coastdown	
Initiation of core power decay simulation	
Turbine trip (closure of stop valve)	Generation of scram signal
Closure of main steam isolation valve	
Termination of main feedwater	
Opening and closing of the SG relief valves	SG pressures 110% and 103%
Initiation of accumulator system	Primary pressure below 29% of initial value
Initiation of low-pressure injection system	LP pressure below 8% of initial value

Table 7: Chronology of the main events in Test 1 [10].

Event	Exp.	TRACE
PZR isolation	−60 s	−60 s
Onset of break	0 s	0 s
Scram signal	1 s	4 s
Turbine trip	1 s	4 s
Primary coolant pumps stopped	4 s	4 s
Main FW isolated	8 s	4 s
Start of decay heat	20 s	22 s
Actuation of ACC	154 s	155 s
PCT increases	164 s	163 s
Maximum PCT	182 s	185 s
Start of LPSI	504 s	349 s
End of test	1533 s	500 s

was reached, the typical sequence of action is realized: initiation of core power decay, initiation of primary coolant pumps coastdown, turbine trip, closure of main steam isolation valve, and termination of main feedwater flow.

Further details on this test can be found in [13].

3.4.1. Results. The chronology of the events taking place during Test 2 is shown in Table 9. Most of the events took place similarly in the simulation and in the experiment. The main difference is that in the simulation the core protection limit was not reached, and therefore the power was not reduced. As a consequence, the primary pressure remained slightly higher, and the LPSI setpoint was also not reached before the first 500 s of the transient. Some of the other discrepancies in the chronology are due to inconsistencies between the actuated experimental procedures and the ones described in the protocols since some experimental timings differ from the control logic shown in Table 8. For example, the initiation of the HPSI system was defined to be 12 seconds after the SI signal, but in the experiment, the HPSI started 25 seconds after the SI signal.

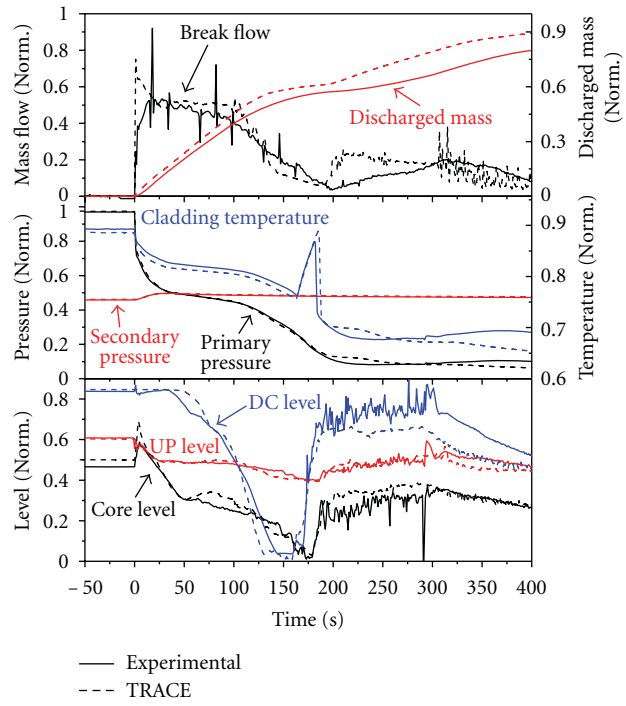

Figure 4: TRACE results for Test 1. From top to bottom: (1) break flow and integrated discharged mass, (2) primary and secondary pressure along with the maximum cladding temperature, and (3) RPV water levels.

The most relevant results of Test 2 are displayed in Figure 5: primary and secondary pressures, maximum PCT, break flow and integrated discharged mass, and the RPV collapsed water levels.

The top graph is showing the primary and secondary pressures along with the PCT at position 7. The primary and secondary pressures were found to be in good agreement with the experiment; however, the PCT was underestimated by about 20 degrees although the experimental temperature reached the LSTF protection system, and thus, the hypothetical maximum value that the PCT would have reached cannot

Table 8: Control logic of Test 2 [13].

Event	Condition
Break	Time zero
Generation of scram signal	Primary pressure 84% of initial value
PZR heater off	Generation of scram signal or PZR liquid level below 2.3 m
Initiation of core power decay curve simulation	
Initiation of primary coolant pump coastdown	
Turbine trip (closure of stop valve)	Generation of scram signal
Closure of main steam isolation valve	
Termination of main feedwater	
Generation of SI signal	Primary pressure below 79% of initial value
Initiation of HPIS in the loop with PZR only	12 s after SI signal
Initiation of accumulator system	Primary pressure below 29% of initial value
Initiation of low-pressure injection system	LP pressure below 8% of initial value
Opening and closing of the SG relief valves	SG pressures 110%/103%

Table 9: Chronology of the main events in Test 2 [13].

Event	Exp.	TRACE
Onset of break	0	0
Scram signal	5	6
SI signal	7	9
Turbine trip and MSIVs closed	10	9
Primary pumps trip	11	6
Termination of SG FW	13	6
SG relief valves open	≈27–57	≈25–55
Initiation of core power decay	29	24
Initiation of HPSI	≈35	21
Loop seal clearing	≈40	≈60
Primary pressure lower than SG pressure	≈55	74
Initiation of Acc system	≈110	126
Core protection activated	≈140	—
Max. PCT	≈150	141
Whole core was quenched	≈180	212
Primary coolant pumps stopped	260	256
Termination of Acc injection	≈280	≈285
Initiation of LPSI	≈290	—
End of test	1212	500

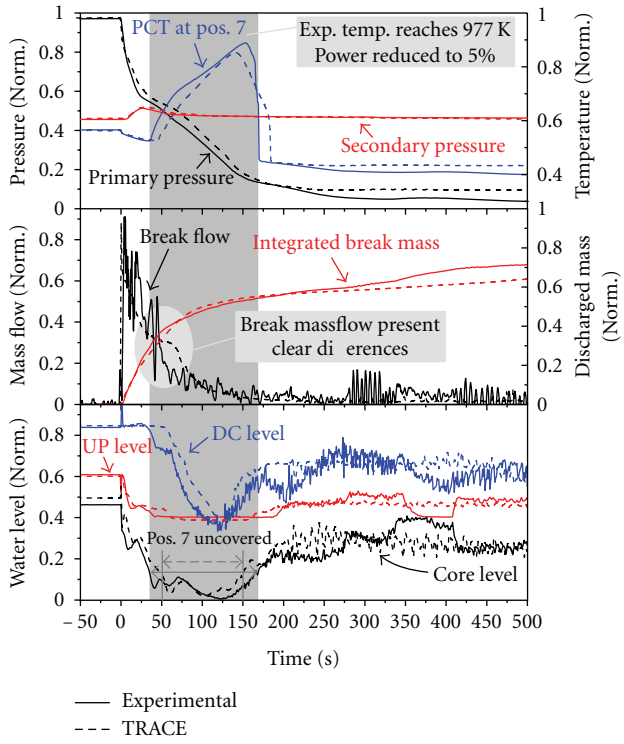

Figure 5: TRACE results for Test 2. From top to bottom: (1) primary and secondary pressure along with the cladding temperature at pos. 7 rod (4,4), (2) break flow and integrated discharged mass, and (3) RPV water levels.

be known. In this sense, it is better to examine the core water level shown in the bottom graph of Figure 5. Overall, the water levels in the RPV were well predicted by TRACE. However, as indicated in Figure 5 the window of time where the heated rods were uncovered was slightly longer in the experiment, and therefore, the PCT was underpredicted. The graph in the middle focus on the break mass flow and the integrated discharged mass. The time evolution of the break flow was not correctly simulated by TRACE. Even though the break device was identical to the one used in Test 1, in this case, the break mass flow under subcooled conditions was underpredicted (first 30 seconds, see Figure 16 for details). Figure 5 shows results with a two-phase choked coefficient of 1.1. It was found that the variations on the subcooled choked coefficients had no effect on the results, probably due to a limitation of the flow within the TRACE code (which could be derived from an internal bug), and the two-phase choked coefficient was increased to compensate the total discharged mass rather than to better predict the flow during this phase. Even though small modifications of the discharge coefficients are in general accepted by the international community, these changes must be consistent, and the user must not use

Table 10: Control logic of Test 5-2 [14].

Event	Condition
Break	Time zero
Generation of scram signal	Primary pressure 84% of initial value
PZR heater off	Generation of scram signal or PZR liquid level below 2.3 m
Initiation of core power decay curve simulation	
Initiation of primary coolant pump coastdown	
Turbine trip (closure of stop valve)	Generation of scram signal
Closure of main steam isolation valve	
Termination of main feedwater	
Generation of SI signal	Primary pressure below 79% of initial value
Opening and closing of the SG relief valves	SG pressures 110%/103%
Initiation of SG secondary-side depressurization by fully opening of the relief valves with auxiliary feedwater	10 minutes after generation of SI signal
Initiation of enhanced SG secondary-side depressurization by fully opening of safety valves	Primary pressure below 13% of initial value
Initiation of accumulator system	Primary pressure below 29% of initial value

different values depending on the case (unless the break conditions and geometry are very different). The differences observed between Tests 1 and 2 indicate that a revision of the choked flow of the TRACE code is needed. As a matter of fact, the choked flow in the latest version of TRACE (TRACE 5.0 patch 2) has been improved, and the problems experienced in Test 2 might have been solved, nonetheless additional problems may arise with the new code version (see Section 5 on page 15 for further details on this issue).

3.5. Test 5-2. Test 5-2 is a small break LOCA located in the cold leg of the loop without PZR. The test was started by opening a 0.5% break which was realized in the facility by using an inner-diameter sharp-edge orifice. The boundary conditions and control logic of this test is shown in Table 10. As for previous tests, the scram signal was actuated when the primary pressure fell below 84% of the nominal value and triggered the typical events for an SBLOCA case, as described in Table 10.

The SI signal was generated when the primary pressure decreased below 79%. Ten minutes after the generation of the SI signal, full symmetrical SG secondary-side depressurization as accident management action was activated by fully opening the relief valves. Auxiliary feedwater was also activated concurrently. When the primary pressure fell below 13%, enhanced SG secondary-system depressurization was started by fully opening the safety valves.

A total failure of the HPSI system was assumed in the test. The accumulators started to discharge when the primary pressure was reduced below 29%. The LPSI was disabled for this test, in order to observe the phenomena occurring in the SG under the influences of gas inflow when the primary pressure is below the LPSI actuation pressure. The logic of the ROSA/LSTF core protection system for Test 5-2 was the same as the one used for Test 6-1. Further details on this test can be found in [14].

Table 11: Chronology of the main events in Test 5-2 [14].

Event	Exp. (s)	TRACE (s)
Break valve opened	0	0
Scram signal	95	65
SI signal	145	112
Primary coolant pumps stopped	349	319
full opening of SG relief valves	756	696
AFW starts	756	696
Initiation of Acc system	≈1320	1293
Full opening of SG safety valves	≈2420	2586
End of test	13376	12000

3.5.1. Results. The chronology of the main events of Test 5-2 are shown in Table 11, where the experimental results are compared with the calculation. Due to a slightly overprediction of the depressurization rate of the primary side at the beginning of the transient, all the events in the simulation occurred about 30 seconds earlier than in the experiment.

The most relevant results obtained for Test 5-2 are displayed in Figure 6 (break flow and discharged mass, primary and secondary pressures, and RPV collapsed water levels).

The simulation of Test 5-2 is in fair agreement with the experiment. The primary and secondary pressure trends were correctly simulated by the ROSA TRACE nodalization. In Figure 6, the first 1000 seconds are zoomed in for a better view on the comparison between experiment and calculation. In a similar manner as in Test 6-2, the depressurization rate at the beginning of the transient was slightly overpredicted by TRACE. The full depressurization of the system by opening the relief valves and later on the safety valves was steeper at the beginning and slower at the end although the overall evolution in the simulation is acceptable. The initial break flow (first 1000 s of transient) was correctly

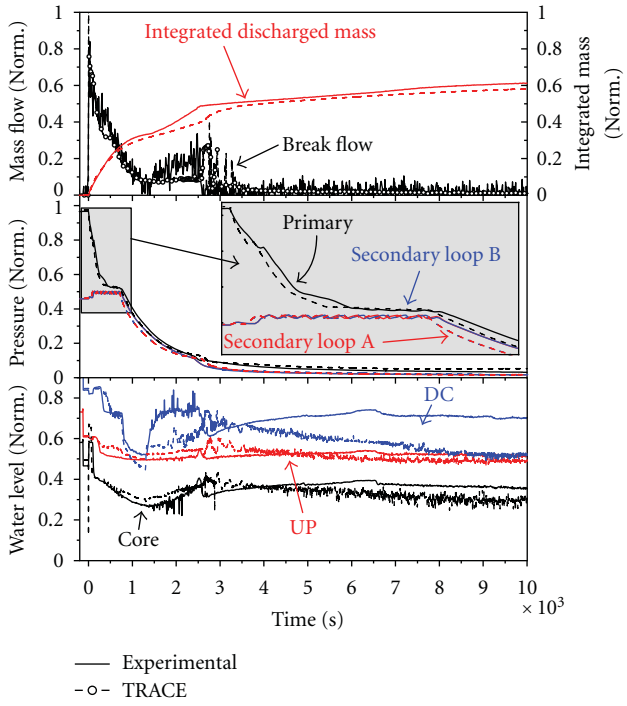

FIGURE 6: TRACE results for Test 5-2. From top to bottom: (1) break flow and integrated discharged mass, (2) primary and secondary pressures, and (3) RPV collapsed water levels.

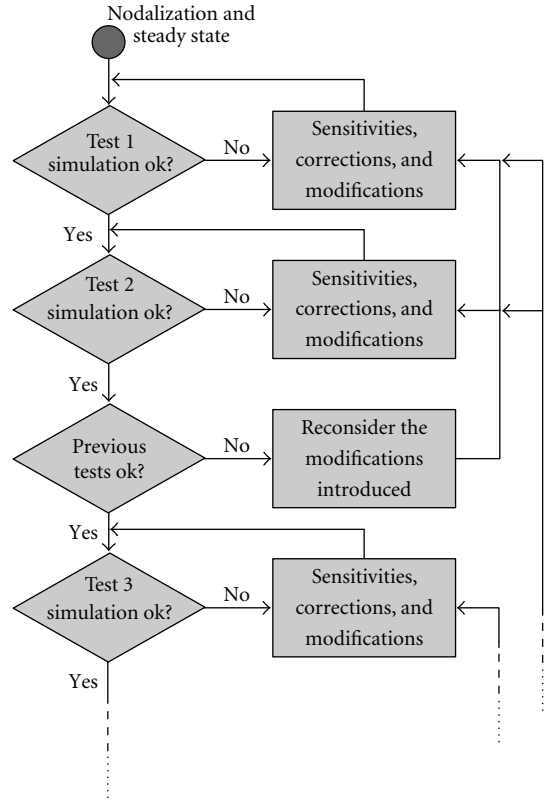

FIGURE 7: Flowchart for the model maintenance.

reproduced. Afterwards, discrepancies on the DC level were observed, as well as for the break flow (from 1000 to 3000 seconds).

All in all, a good agreement with the experimental results was obtained.

4. Model Evolution

The results presented in Section 3 were all obtained with the same TRACE nodalization, and only the boundary conditions specific for each test were modified from case to case. However, when the tests were first simulated, modifications and corrections of the nodalization accompanied by sensitivity studies were needed. The control systems were finally modified with the aim of allowing the user to run all previous cases with a minimum number of changes. In order to ensure the consistency of the modifications introduced, all previous tests were recomputed with the updated model after each posttest. To perform this action, it is important to maintain the model as compact as possible and to keep track of the included modifications. A basic methodology has been drawn for this purpose, which allows the user to recalculate any previous transient at any time in order to assure any important modification. The flowchart followed for the maintenance of the TRACE input deck is shown in Figure 7.

Basically, once the nodalization is developed and a satisfactory steady state is achieved, the nodalization is applied to the simulation of a first experimental test. At this stage, the original nodalization might be modified on the basis of sensitivity tests, in the case that the comparison with the experimental data is not satisfactory and the deficiencies are identified to be in the nodalization approach and not in the constitutive correlations hardwired in the system code. Then, the same nodalization is used to simulate a second test. Again, changes to the nodalization might be necessary to correctly reproduce the significant phenomena of the given experimental test. This time, however, before proceeding to the simulation of a third test, the nodalization would be applied "as it is" to the simulation of the previous test, in order to ensure that the modifications to the nodalization do not lead to unsatisfactory behaviors (i.e., the results obtained with the new nodalization should remain in close agreement with the previous validation results or result in an even better agreement with the experimental data). Once this step is concluded satisfactorily, the analyst can proceed to a third test, and so on. A compromise might be required between two different nodalizations when the results of previous tests are worsened. In this case, one nodalization must be picked up as the most appropriate.

This very procedure was employed at PSI for the TRACE ROSA nodalization presented in this work.

The ROSA/LSTF TRACE nodalization developed at PSI has been used for more than 5 years and has therefore undergone several modifications. The most relevant of those are described in the following chapters. Since the modifications and corrections to the nodalization were triggered by the discrepancies found when comparing to a given experimental test, they are classified accordingly.

4.1. Corrections Introduced during the Simulation of Test 6-1

4.1.1. Leakage from the Upper Plenum to the Downcomer. The cold leg and DC level evolution during the first part of Test 6-1 (until 700 s) pointed out interesting differences between the TRACE model and the experiment. While the level evolution in the core, upper plenum, upper head, and hot legs were reasonably predicted, the cold leg and DC level could not be correctly simulated. What the TRACE nodalization was not able to simulate was exactly the DC pressure drop, which was reduced in the experiment after the interruption of the natural circulation. The root of the discrepancy was the earlier presence of steam in the upper part of the DC, which modified the pressure drop inducing an earlier drop of the DC and the cold leg water levels. A series of sensitivity calculations was performed to analyse the possible reasons. After investigating all plausible causes and following the recommendations given in [15], it was concluded that the discrepancy could derive from a hypothetical leak from the DC to the upper plenum through the seal of the core support barrel. This seal ring was broken in August 1995, when the UH-UP bypass was plugged and then repaired in November 2001. It was found out that both the cold leg and the DC level evolutions were correctly simulated if a small leakage (1% of steady-state core flow) was assumed to exist in this region. The results of the DC and cold leg levels with and without the leakage are shown in Figure 8. Further details on this analysis can be found in [16]. This modification was then kept for the simulation of all successive tests producing a closer or equal agreement for all tests.

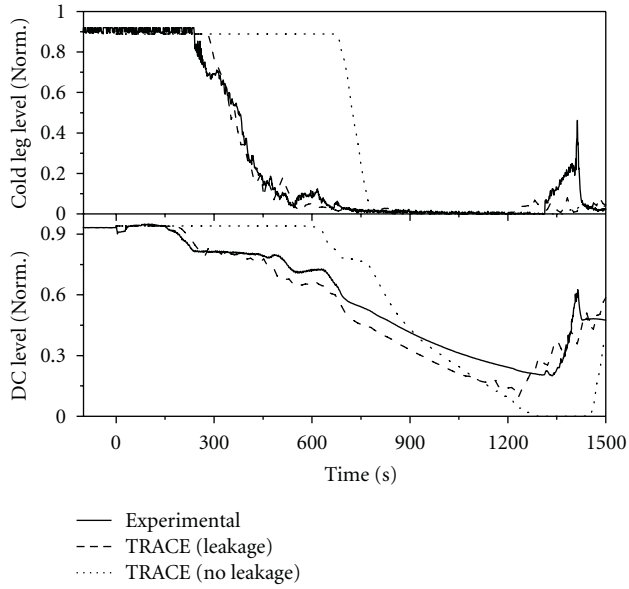

Figure 8: Collapsed water levels of the DC and the cold leg for Test 6-1 with and without a leakage between the UP and the DC.

4.1.2. UH Nodalization. Test 6-1 constituted a perfect experiment to study the performance of the choked flow model, since the location at the top of the RPV allowed a clear differentiation between the phases that a choked flow may experience, namely, subcooled-liquid phase, two-phase, and single-phase vapor flows (Figure 2 on page 5). The TRACE nodalization performed very well for the first two phases; however, when the flow at the break turned into single-phase vapor, the break flow rate was overestimated by TRACE. Sensitivities on the break nodalization and possible modifications on the TRACE model were carried out and constituted the bulk of a previous publication [8]. One of the main modifications to the model consisted in a refinement of the nodalization of the RPV upper head. As a matter of fact, it was found that a finer nodalization of the upper head was essential to correctly predict the void fraction and the saturation temperature at the break location. Initially, only one axial level between the CRGTs exits and the top of the RPV (0.504 m of height) was used. In order to enhance mixing and allow convection in this region, the number of axial levels was finally increased. With this modification, the steam temperature at the break inlet was more accurately predicted (around 2 degrees lower). It is important to notice that the gas velocity under single-phase vapor conditions and choked flow is basically a function of the stagnant temperature and the specific heat ratio; hence, an accurate prediction of the temperature close to the break is crucial. In this simulation, with an increased number of cells, the saturation temperature at the break was reduced and so was the break mass flow (see Figure 9 for details). The initial nodalization with only one axial level was split in three and 6 smaller nodes of 0.168 m and 0.084 m of height, respectively. There was almost no difference between the results obtained with 3 and 6 additional levels, but the computational time was very high for the 6-level calculation. Therefore, 3 levels for the upper part of the UH were used in the final nodalization (i.e., 20 axial levels for the entire RPV). The improvement obtained in the simulation of the break mass flow can be seen with the integrated break flow plotted in Figure 9. Further details can be found in [8].

4.2. Corrections Introduced during the Simulation of Test 6-2. After a satisfactory simulation of Test 6-1, the same TRACE nodalization was employed for the simulation of Test 6-2. As a first approach, an early interruption of natural circulation was predicted leading to an increase of the primary pressure, as shown in Figure 10. Afterwards, the transient evolution could not be correctly captured by the simulation. The early stop of natural circulation (NC) indicated a wrong estimation of the U-tube levels and heat transfer to the secondary side. The reason could be related to the use of a single U-tube in representation of the whole bundle. However, it was found eventually that the U-tube nodalization (1 pipe) was too coarse and the discrepancies could be fixed by simply refining the axial nodalization of the corresponding pipe component. Figures 10 and 11 show the pressure and the mass flow in loop B, respectively, obtained with the two nodalizations. The old and new nodalization of the SG are shown in Figure 12.

The new nodalization was then used to simulate again Test 6-1. The results were improved with the new nodalization.

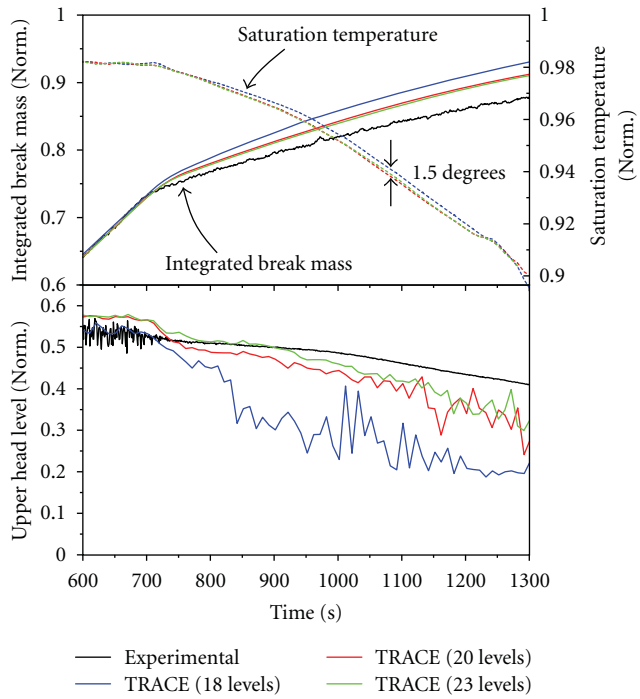

FIGURE 9: Sensitivity on the UH nodalization for Test 6-1 with finer and coarser meshing of the UH. Top: integrated break mass and saturation temperature at the top of the UH dome. Bottom: UH collapsed water level.

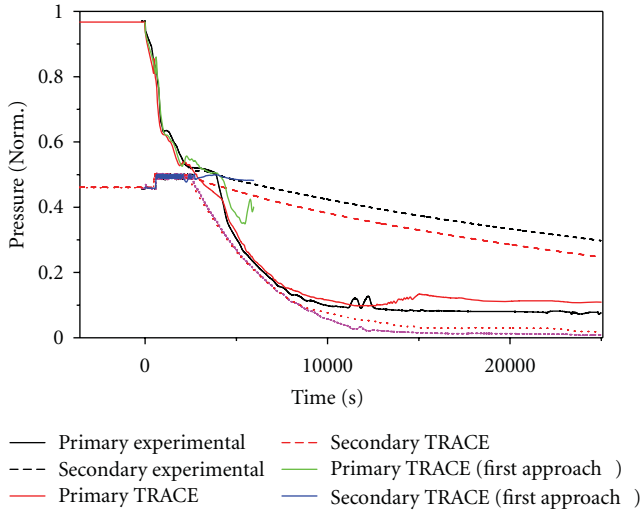

FIGURE 10: Primary and secondary pressures for Test 6-2 using both nodalizations of the SG's primary and secondary sides.

4.3. Corrections Introduced during the Simulation of Test 1. Test 1 was first carried out as a blind calculation along with the evaluation of its uncertainties [11], performed by applying the GRS SUSA methodology [17, 18]. Even though the maximum PCT temperature in the blind calculation showed lower values than in the experiment, the accompanying uncertainty evaluation helped confining the possible problems. Three modifications were included in the nodalization

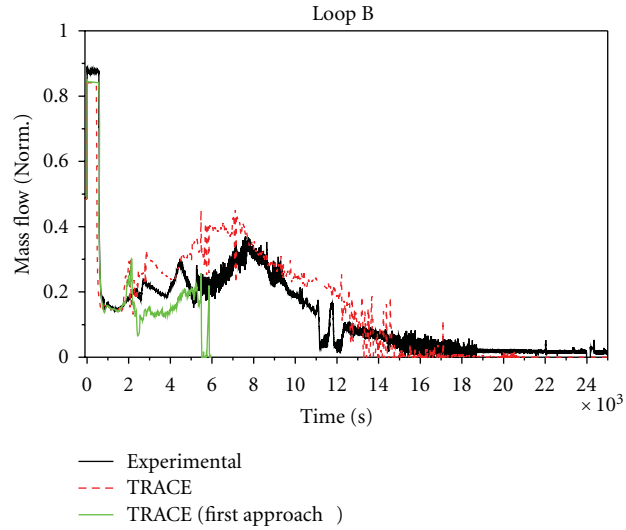

FIGURE 11: Mass flow in loop B using both nodalizations of the SG's primary and secondary sides.

used for the posttest calculation: a correction of the Acc's lines, the reduction of the two-phase choked coefficient, and the inclusion of the CCFL model at the top of the core.

The blind calculation of Test 1 displayed considerably larger accumulator flows than the experiment; hence, this line was revised and finally renodalized from scratch, in order to achieve a better representation of the pressure drops along the line. Figure 13 shows the results of the blind calculation and the modification on the Acc's line. It must be noticed that the rest of modifications included during the posttest process further increased the quality of the Acc's mass flow results (line labeled as "final TRACE result" in Figure 13).

Since the break flow was clearly overestimated during the two-phase flow regime, a parametric study on the two-phase choked flow coefficient was performed. A coefficient of 0.8 provided results in a closer agreement with the experiment, as shown in Figure 14. The final coefficient used for this test was 0.85. This modification was introduced after recalculating the test by following the methodology for a consistent nodalization.

The height of the PCT was confined by two factors. On the one hand, the time difference between the start of the core uncovery and the LS clearance was crucial for this transient. Both the LS clearance and the Acc's injection helped quenching the core. However, it was the LS clearance the phenomenon that triggered the reflood of the core. LS clearance occurs when the pressure difference between the UP and the DC is large enough to drive the LS water column into the DC. This occurred thanks to steam condensation in the cold leg with the injection of cold water from the Accs. The second phenomena that will define the height of the maximum PCT is the speed at which the core level drops during this window of time. The first phenomenon here described was well simulated even in the blind calculation; however, the level decreased at a slower rate, and therefore, the PCT was lower.

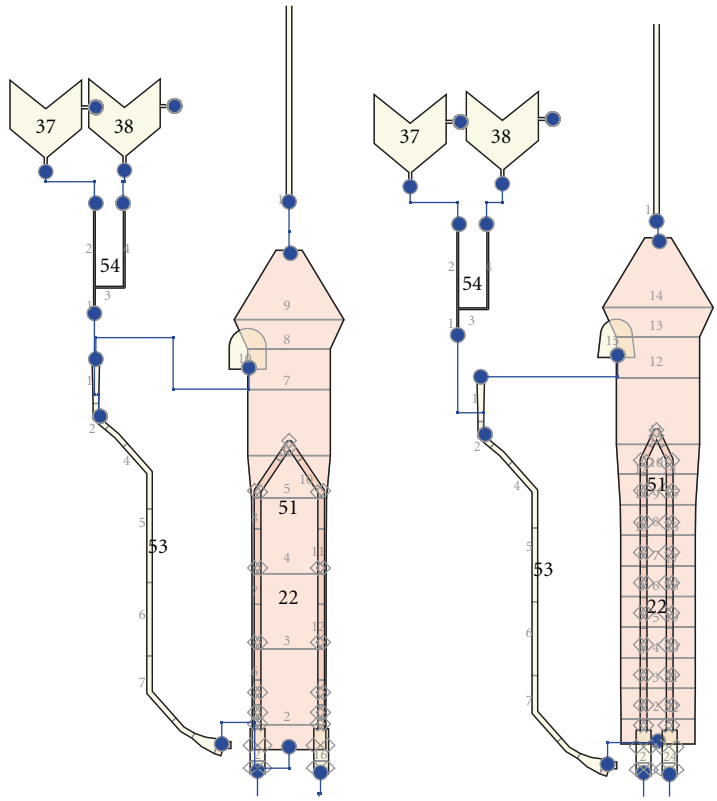

Figure 12: Old and new nodalization of the SG and U-tubes. Modification introduced during the analysis of Test 6-2.

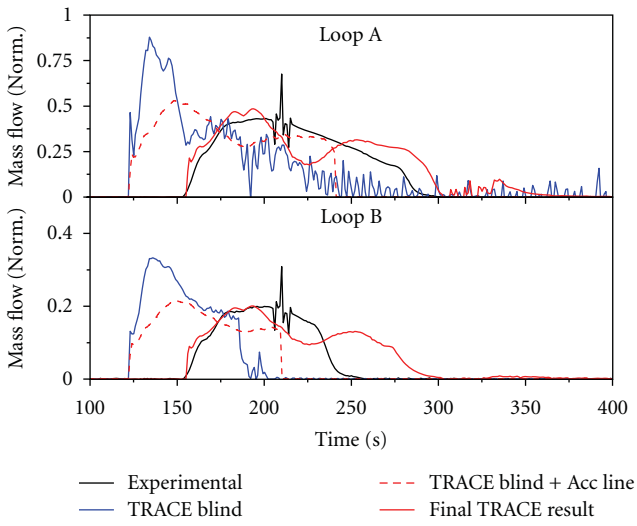

Figure 13: Accumulator injection during Test 1 with the new nodalization of the Acc's lines.

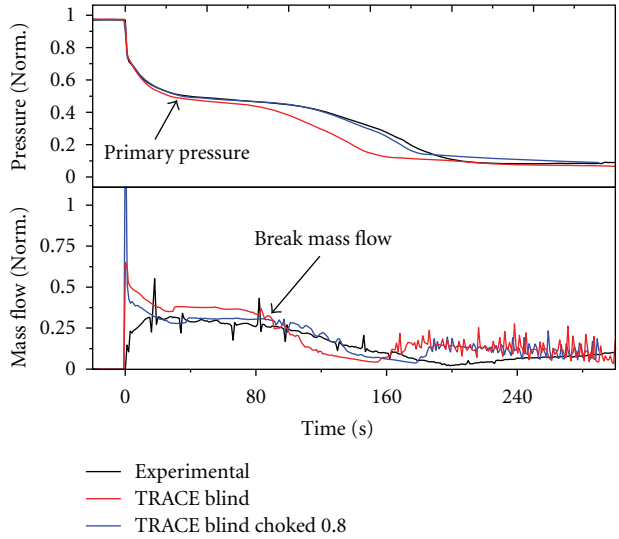

Figure 14: Primary pressure and break mass flow for Test 1, pretest results with different two-phase break discharge coefficients.

At this point of the analysis, it became obvious that an additional phenomenon significant for the evolution of this transient was the occurrence of CCFL conditions at the top of the core. Due to the fact that the CCFL was (mistakenly) not activated for the blind calculation, the core level remained higher than in the experiment due to the amount of water falling from the UP. In the experiment, the drop of water falling from the UP was prevented by the steam flowing out of the core. Once the CCFL model at the location of the upper core plate was activated, the core level dropped faster, in better agreement with the experimental data. The effect of using the CCFL model is shown in Figure 15, where the results of the cladding temperature are shown for

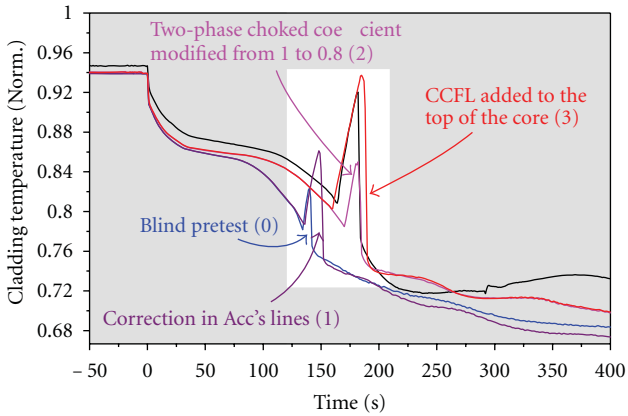

Figure 15: Maximum PCT for Test 1, evolution of the results with different modifications.

the different posttest steps. Summarizing, starting from the blind calculation, firstly the accumulator's lines were corrected, then the two-phase choked coefficient was decreased, and finally the CCFL model was used at the top of the core. Further details on these modifications can be found in [11].

After this nodalization modifications, all previous tests were recalculated, and there was no significant difference.

4.4. Corrections Introduced during the Simulation of Test 2. Since the IBLOCA of Test 2 occurs in the cold leg, CCFL phenomena may take place at the entrance of the U-tubes or at the connection between the pipes and the SG plenums. Therefore, the CCFL was activated in this region during the simulation of Test 2, and the simulation results were consequently improved. All cases were recalculated satisfactorily. For Test 1, the choked two-phase flow coefficient was slightly shifted from 0.8 to 0.85.

4.5. Corrections Introduced during the Simulation of Test 5-2. For this test, only corrections on the control systems in order to accommodate the test particularities were introduced. No further modification to the nodalization was necessary. However, all previous tests were recalculated to avoid any inconsistency or possible error introduced during the configuration process.

5. Choked Flow Response

The modeling of choked flows is one of the most important issues in nuclear thermal hydraulics, since it affects the prediction of the flow-rate at break locations, and therefore plays a key role in the evolution of all LOCA transients. The tests performed in LSTF within the ROSA-1 and 2 projects dealt with breaks of different sizes and location and thus provided a good database to evaluate the performance of the TRACE chocked flow models.

The v5.0 version of the TRACE code has been used for all simulations presented in this paper and has provided a good agreement with the experiments. The discharge coefficients used for each test are described in Table 12.

Table 12: Choked flow discharge coefficients used for all break locations, subcooled discharge (C_{sub}) and two-phase flow discharge (C_{2p}) coefficients.

Test	Type	C_{sub}	C_{2p}
Test 6-1	Orifice	1.0	1.0
Test 6-2	Orifice	1.0	1.0
Test 1	Nozzle	1.0	0.85
Test 2	Nozzle	1.0	1.1
Test 5-2	Orifice	1.0	1.0

A coefficient of 1.0 was used in all the orifice breaks providing reasonable enough results. However, for the two nozzle cases, the use of different two-phase flow discharge coefficients (C_{2p}) was needed even though they presented exactly the same geometry.

The disagreement of the choked flow patterns obtained for Test 2 and especially the need to use different discharge coefficients than those used for Test 1 motivated us to test newer versions of the code. Even though small modifications on discharge coefficients are in general accepted by the international community, these must be consistent, and the user must not use different values depending on the case (unless the break conditions and geometry are very different). The differences observed between Tests 1 and 2 indicated that a revision of the choked flow of TRACE was required. Once we tested the same model with the latest official release of the code (TRACE 5.0 patch 2), it was found out that the choked model was providing indeed a much better agreement with the experiment. Further studies indicated that, in Test 2 by using v5.0, the subcooled choked flow (first 33 seconds) was limited within the code subroutines, so that variations of the subcooled discharge coefficient (C_{sub}) would not have an impact on the results. As a matter of fact, a sensitivity on the C_{sub} showed that the results were influenced only when values of C_{sub} under 0.85 were being employed, so all calculations with a higher coefficient were equivalent with those obtained with a coefficient of 0.85 (see Figure 16). This behaviour was not observed by using the latest TRACE release. Since the flow was much lower at the beginning of the transient (with the v5.0 RC3 version), a higher value for the C_{2p} was needed to compensate the total discharged mass (see Table 12). This explains the differences between the C_{2p} used in Tests 1 and 2. It is important to point out that the subcooled break flow in the rest of the tests does not play an important role, and this might be the reason why this problem did not become evident until the simulation of Test 2.

The problems with the subcooled part of the choked flow model have been solved in patch 2; however, other issues have arisen with this version which hinders its usage. The methodology presented in this paper can also be used to quickly test new code versions, and in this case, patch 2 presented several deficiencies indicating that the new version cannot be used consistently.

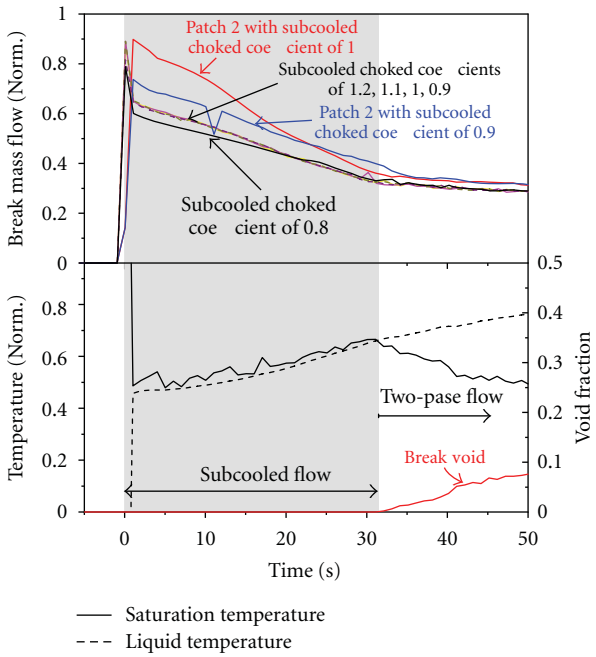

FIGURE 16: Break mass flow during the subcooled phase for Test 2; different subcooled choked coefficients are used for the TRACE v5.0 RC3 and patch 2 versions.

6. Conclusions

A nodalization of the ROSA/LSTF facility has been developed by using the US-NRC system code TRACE v5.0. The nodalization has been used to simulate 5 different tests focused on small and intermediate break LOCA cases. The simulations have been performed during the last 4 years; however, the model evolution has been tracked, and a methodology has been drawn to maintain a single consistent nodalization for all tests. Every time that a new posttest analysis was completed, the previous posttests simulations were carried out again, in order to guarantee that any new modification to the nodalization would only improve the overall performance of the nodalization. Finally, a reasonable agreement with all of the five tests was obtained. However, the calculated subcooled choked flow in Test 2 underestimated the experimental results. It was found out that the subcooled choked flow in the TRACE v5.0 version presented deficiencies, which have been solved in the latest TRACE release (5.0 patch 2). It is important to point out that the subcooled break flow in the previous tests does not play an important role, and thus this problem was not identified earlier. Even though the problems with the subcooled choked flow were solved with patch 2, the methodology presented in this paper allowed a quick assessment of the new version, and different issues were detected; therefore, TRACE5.0 was used in this paper.

Acknowledgments

This work was partly funded by the Swiss Federal Nuclear Safety Inspectorate ENSI (Eidgenössisches Nuklearsicherheitsinspektorat), within the framework of the STARS project (http://stars.web.psi.ch/). The authors are as well grateful to the OECD/NEA ROSA-2 project participants: JAEA for experimental data and the Management Board of the OECD/NEA ROSA-2 project for providing the opportunity to publish the results.

References

[1] F. Reventós, L. Batet, C. Llopis, C. Pretel, M. Salvat, and I. Sol, "Advanced qualification process of ANAV NPP integral dynamic models for supporting plant operation and control," *Nuclear Engineering and Design*, vol. 237, no. 1, pp. 54–63, 2007.

[2] C. Llopis, F. Reventós, L. Batet, C. Pretel, and I. Sol, "Analysis of low load transients for the Vandellòs-II NPP. Application to operation and control support," *Nuclear Engineering and Design*, vol. 237, no. 18, pp. 2014–2023, 2007.

[3] Paul Scherrer Institut, "Steady-state and transient analysis research of the swiss reactors (STARS project)," 2011, http://stars.web.psi.ch/.

[4] G. B. Treybal, *One-Dimensional Two-Phase Flow*, McGraw-Hill, New York, NY, USA, 1969.

[5] NEA-CSNI. Bemuse Phase V Report, "Uncertainty and sensitivity analysis of a LB-LOCA in ZION nuclear power plant," Tech. Rep., Committee on the Safety of Nuclear Installations, OECD, Nuclear Energy Agency, 2011.

[6] T. Yonomoto, "CCFL characteristics of PWR steam generator U-tubes," in *Proceedings of the ANS International Topic Meeting on Safety of Thermal Reactors*, Portland, Ore, USA, 2001.

[7] T. Takeda, M. Suzuki, H. Asaka, and H. Nakamura, "Quick-look data report of OECD/NEA ROSA project test 6-1 (1.9% pressure vessel upper-head small break LOCA experiment)," Tech. Rep. JAEA-Research 2006–9001, Japan Atomic Energy Agency, 2006.

[8] J. Freixa and A. Manera, "Analysis of an RPV upper head SBLOCA at the ROSA facility using TRACE," *Nuclear Engineering and Design*, vol. 240, no. 7, pp. 1779–1788, 2010.

[9] T. Takeda, M. Suzuki, H. Asaka, and H. Nakamura, "Quick-look data report of OECD/NEA ROSA project test 6-2 (0.1% pressure vessel bottom small break LOCA experiment)," Tech. Rep. JAEA-Research 2006–9002, Japan Atomic Energy Agency, 2006.

[10] T. Takeda, M. Suzuki, H. Asaka, and H. Nakamura, "Quick-look data report of test 1, test for hot leg intermediate break loss of coolant accident with break size equivalent to 17Flow area," Tech. Rep. JAEA-Research 2010-, Japan Atomic Energy Agency, 2010.

[11] J. Freixa, T.-W. Kim, and A. Manera, "Thermal-hydraulic analysis of an intermediate LOCA test at the ROSA facility including uncertainty evaluation," in *Proceedings of the 8th International Topical Meeting on Nuclear Thermal-Hydraulics, Operation and Safety (NUTHOS '10)*, Shanghai, China, October 2010.

[12] The ROSA-V Group, "ROSA-V large scale test facility (LSTF) system description for the third and fourth simulated fuel assemblies," Tech. Rep. JAERI-Tech 2003-037, Japan Atomic Energy Agency, 2003.

[13] T. Takeda, M. Suzuki, H. Asaka, and H. Nakamura, "Quick-look data report of ROSA-2/LSTF Test 2 (cold leg intermediate break LOCA IB-CL-03 in JAEA," Tech. Rep. JAEA-Research 2010-, Japan Atomic Energy Agency, 2010.

[14] T. Takeda, M. Suzuki, H. Asaka, and H. Nakamura, "Final data report of ROSA/LSTF Test 5-2 (primary cooling through

steam generator secondary-side depressurization experiment SB-CL-40 in JAEA)," Tech. Rep. JAEA-Research 2009-, Japan Atomic Energy Agency, 2009.

[15] H. Austregesilo and H. Glaeser, "Results of post-test calculation of LSTF Test 6-1 (SB-PV-09) with the code ATHLET," in *OECD/NEA ROSA Project, 4th PRG Meeting*, Tokai-mura, Japan, 2006.

[16] J. Freixa, "Post-test thermal-hydraulic analysis of ROSA Test 6.1," Tech. Rep. TM-41-08-10, Paul Scherrer Institut, 2008.

[17] H. Glaeser, "GRS analysis for CSNI uncertainty methods study (UMS)," Tech. Rep., Committee on the Safety of Nuclear Installations, OECD, Nuclear Energy Agency, 2011.

[18] E. Hofer and M. Kloos, *Relap5/Mod3.3 Code Manual. Volume I: Code Structure, System Models, and Solution Methods*, 2003.

Hindawi Publishing Corporation
Science and Technology of Nuclear Installations
Volume 2012, Article ID 548513, 8 pages
doi:10.1155/2012/548513

Research Article

PACTEL and PWR PACTEL Test Facilities for Versatile LWR Applications

Virpi Kouhia, Heikki Purhonen, Vesa Riikonen, Markku Puustinen, Riitta Kyrki-Rajamäki, and Juhani Vihavainen

LUT Energy, Lappeenranta University of Technology, P.O. BOX 20, 53851 Lappeenranta, Finland

Correspondence should be addressed to Heikki Purhonen, heikki.purhonen@lut.fi

Received 19 May 2011; Accepted 14 September 2011

Academic Editor: Klaus Umminger

This paper describes construction and experimental research activities with two test facilities, PACTEL and PWR PACTEL. The PACTEL facility, comprising of reactor pressure vessel parts, three loops with horizontal steam generators, a pressurizer, and emergency core cooling systems, was designed to model the thermal-hydraulic behaviour of VVER-440-type reactors. The facility has been utilized in miscellaneous applications and experiments, for example, in the OECD International Standard Problem ISP-33. PACTEL has been upgraded and modified on a case-by-case basis. The latest facility configuration, the PWR PACTEL facility, was constructed for research activities associated with the EPR-type reactor. A significant design basis is to utilize certain parts of PACTEL, and at the same time, to focus on a proper construction of two new loops and vertical steam generators with an extensive instrumentation. The PWR PACTEL benchmark exercise was launched in 2010 with a small break loss-of-coolant accident test as the chosen transient. Both facilities, PACTEL and PWR PACTEL, are maintained fully operational side by side.

1. Introduction

Since 1976, thermal-hydraulics of nuclear power plants has been studied experimentally at Lappeenranta University of Technology (LUT). During the years, several experiment facilities have been built to study the behaviour of light water reactors. Experimental work with the separate effect test facilities and the large integral test facility has generated a wide data base containing about 900 experiments. Along the years the cooperation with Technical Research Centre of Finland (VTT) induced the decisions to build many of the test facilities utilized at LUT, including the largest one, that is, the parallel channel test facility (PACTEL), described in [1–4].

In Finland, in addition to international cooperation, own research and continuous development of know-how has always been part of the national nuclear safety concept, especially when connected with the specific nuclear power plant types operated in Finland. Hence, the PACTEL facility was constructed in 1990 to have a large-scale test facility available for studies of thermal-hydraulics of a VVER-440 type nuclear power plant. The two units of the Loviisa power plant in Finland are of this type. PACTEL has been utilized in several versatile experimental applications along the years as presented, for example, in [1].

As a new EPR-type pressurized water reactor (PWR) is under construction in Olkiluoto in Finland, national research activities on PWR behaviour are being intensified. The new PWR PACTEL facility, a modified version of the original PACTEL facility, has been introduced in order to stimulate research activities on PWR and EPR specifics. PWR PACTEL shares some parts with PACTEL but includes several completely new parts to fulfil the specific facility research purposes. As the original PACTEL facility is also maintained, both PACTEL and PWR PACTEL are fully operational at the moment, as discussed in [5, 6].

This paper includes a description of the PACTEL facility setup and a presentation of specific facility characteristics. The experimental work with PACTEL is introduced through a short review of some chosen research cases. In particular, the OECD International Standard Problem ISP-33, based on one of the PACTEL natural circulation experiments, is presented. The latter part of this paper introduces the PWR PACTEL facility setup and specific characteristics connected

to it. The ongoing PWR PACTEL benchmark exercise case is presented concisely, as through the exercise the first experiment results with this new facility concept are published.

2. PACTEL

2.1. PACTEL Facility Description. The PACTEL facility is a 1 : 305 volumetrically scaled, out-of-pile, full height model of a six loop Russian design VVER-440 type PWR. The reference reactor for PACTEL is the Loviisa VVER-440 reactor in Finland. PACTEL includes pressure vessel parts, three primary loops with horizontal steam generators, a pressurizer, and an emergency core cooling system (ECCS). The pressure vessel model is of U-tube shape modelling the downcomer, lower plenum, active core, and upper plenum. The system component heights and elevations have been preserved to simulate gravity dominated natural circulation flow processes correctly. The original facility description is made available by Tuunanen et al. in [4] and presented also by Purhonen et al. in [1–3]. Some of the PACTEL facility characteristics compared with the reference reactor are shown in Table 1. PACTEL in the laboratory site is shown in the photograph in Figure 1, and a schematic view of the facility can be seen in Figure 2.

The core rod bundle of PACTEL consists of 144 electrically heated fuel rod simulators. The outer diameter of the simulators is 9.1 mm and the thickness of the stainless steel cladding is 0.9 mm. The rods are fixed in a triangular grid, with a lattice pitch of 12.2 mm. The fuel rod simulators are organized in three parallel channels that each includes 48 rods. All the rods have a nine-step chopped cosine axial power distribution. The axial peaking factor is 1.4, and the total heated length is 2420 mm. The number and construction of the rod spacers are identical to the reference reactor. The core is powered by a 1 MW electric power supply. This is ~22% of the scaled thermal power (originally 1375 MW) of the reference reactor. Different power levels can be used in the three separate core channels. Diffusers are installed in the hot and cold leg connections to prevent direct ECC water flow to the loops. There is no bypass from the upper plenum to the downcomer in the facility.

PACTEL has three almost symmetric equal volume primary loops and each of these models two loops of the reference reactor. Froude scaling, together with volumetric scaling, was the main design principle in selecting the pipe dimensions of the facility hot and cold legs. Together these two scaling methods result in larger diameter and in about 50% shorter hot and cold legs than in the reference reactor. Larger diameter pipes lead to better simulation of flow regime transitions in the horizontal parts of the loops. The use of volumetric scaling has an effect on the pressure loss distribution around the loops. Also, the relative volume of loop seals is larger than in the reference plant.

Each loop has a horizontal steam generator with heat exchange U-tubes, a primary cooling pump, and a loop seal both in the hot and cold legs. The horizontal steam generators as well as the hot leg loop seals are a unique feature of the VVER-440 design. In the current steam generators of PACTEL, the average length of the heat exchange tubes is about 3 m and the diameter of the steam generator shell is 1.0 m. The diameter of the tubes (16 × 1.5 mm) is the same as in the reference plant, but the vertical distance between the tube rows is doubled to get the height of the PACTEL steam generator closer to that of the reference steam generator. The earlier first-generation horizontal steam generators of PACTEL were of a different design. The average length of the heat exchange tubes was about 8.5 m, and the diameter of the steam generator shell was smaller (0.4 m) than in the current

Figure 1: PACTEL facility in laboratory.

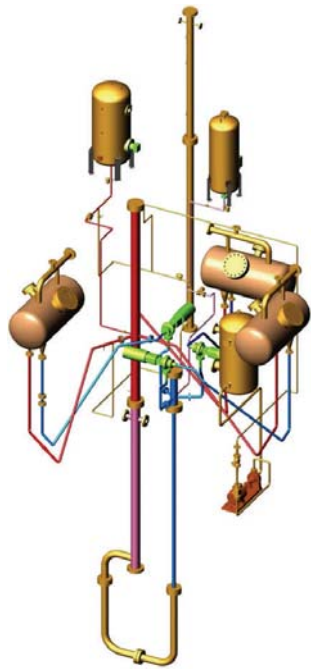

Figure 2: Schematic view of PACTEL.

Table 1: PACTEL facility characteristics and comparative reference reactor values.

Characteristic	PACTEL	VVER-440 (Loviisa)
Reference power plant	VVER-440	—
Volumetric scaling ratio	1 : 305	—
Scaling factor for component heights and elevations	1 : 1	—
Number of primary loops	3	6
Steam generator type	Horizontal	Horizontal
Maximum heating power/thermal power [MW]	1	1500 (1375)
Number of rod simulators—fuel rods	144	39438
Outer diameter of rod simulators—fuel rods [mm]	9.1	9.1
Rod simulator—fuel rod pitch [mm]	12.2	12.2
Heated length of rod simulators—fuel rods [m]	2.42	2.42
Axial power distribution	Chopped cosine	—
Maximum cladding temperature [°C]	800	—
Maximum operating pressure [MPa]	8.0	12.3
Maximum operating temperature [°C]	300	300
Maximum secondary pressure [MPa]	5.0	5.0
Maximum secondary temperature [°C]	260	260
Feedwater tank pressure [MPa]	2.5	2.5
Feedwater tank temperature [°C]	225	225
Accumulator pressure [MPa]	5.5	5.5
Low-pressure ECC-water pressure [MPa]	0.7	0.7
High-pressure ECC-water pressure [MPa]	8.0	8.0
ECC-water temperature [°C]	30–50	30–50
Main material of components	Stainless steel	—
Insulation material	Mineral wool (Aluminium cover)	—

design. Yet, the heat exchange U-tube diameter was the same as with the present steam generator U-tubes.

The full-length pressurizer is connected to the hot leg of loop one. The pressurizer is made of two equal diameter parts one above the other, joined with flanges. Heating and spray systems have been attached to the pressurizer. The total height of the pressurizer is 8.8 m.

The system component heights and elevations have been preserved to simulate gravity-dominated natural circulation flow processes correctly. In scaled down facilities, not all thermal-hydraulic phenomena necessarily occur in the same way and order as in the reference systems. Despite of preserving component heights and elevations in PACTEL, other factors lead to scaling distortions. Heat losses and the amount of energy stored in the structures are in scaled test facilities different from those of the systems that they are simulating.

The basic instrumentation of PACTEL consists of thermocouples, pressure and differential pressure transducers, and flow meters. The temperature measurements include rod cladding, structure wall and coolant as well as reference temperature measurements. There are two pressure measurements in the primary side, the first one in the upper plenum and the second one at the top of the pressurizer. Secondary pressures are measured in discharge steam line in each steam generator. There are 43 differential pressure transducers in PACTEL, mainly used to determine liquid levels in different parts of the primary circuit and in the secondary sides of the steam generators. Loop flows are measured in the vertical part of each cold leg below the steam generator. The total primary flow is measured in the downcomer. Accumulator and high-pressure injection system flows as well as feedwater flows to each steam generator are also measured. The break flow rate in loss of coolant accident (LOCA) experiments can be measured both directly and indirectly.

2.2. Design Upgrades. During the years, the PACTEL facility has gone through several structural changes due to the different objectives and scaling requirements of the individual test programs. Equipment upgrades dictated by maintenance needs as well as instrumentation and software upgrades to take advantage of the developments in the field of measurements and data acquisition have also been made as presented in [2, 3].

As described in Chapter 2.1, PACTEL has introduced already two sets of different steam generators, the original long and narrow ones and the present short and thick ones described by Purhonen et al. in [1–4]. Recently, the core channel construction has also been refurbished and renovated, yet the geometry and core configuration principles

Table 2: PACTEL experiments, examples on performed experiment types.

Experiment type	Specific focuses	Related NPP
Small break loss of coolant accident (SBLOCA)	Natural circulation, steam generator behaviour, feed and bleed procedures	VVER-440
Stepwise coolant inventory reduction (SIR)	Natural circulation, ISP-33 case	VVER-440
Primary to secondary leakage (PRISE)	Multiple-tube rupture	VVER-440
Anticipated transient without scram (ATWS)	Natural circulation with reduced primary inventory, maximum pressure while inadvertent control rod withdrawal	VVER-440
Pressure and heat loss experiments	Facility characterization	VVER-440
Loss of secondary feedwater (LOF)	Deterioration of heat transfer	VVER-440
Improved accident management (IMPAM)	Starting of depressurization during SBLOCA	VVER-440
Passive safety injection, core make up tank (CMT) behaviour	Break size and location effect, CMT position effect	APWR
Passive heat removal system behaviour	Start up of natural circulation and long term cooling	VVER-640
Thermal stratification	Hot and cold water stratification effect on thermal loads	—
Dissolved noncondensable gases	Effect of noncondensable gases on system thermal-hydraulics and heat transfer in steam generators	—

have been maintained. Reconstructions and modifications to the facility setup have been introduced also during various versatile applications, for example, VVER-640-related experiments discussed in references [1–3]. However, the fundamental and original PACTEL construction has been restored each time.

2.3. PACTEL Experiments. As described earlier, PACTEL was originally designed to model the thermal-hydraulic behaviour of VVER-440-type PWRs. Still, the facility has served also in many other purposes. The facility has been modified on a case-by-case basis according to the needs of each configuration and positioning of auxiliary equipment, leading to a versatile use of PACTEL for a large spectrum of thermal-hydraulic research, as presented by Purhonen et al. in [1–3]. The PACTEL facility is ideal for investigating planned recovery procedures during accidents and operational transients. For this purpose, experimental series among others on small break loss-of-coolant accidents, primary-to-secondary leakages, and on anticipated transients without scram have been carried out. The PACTEL natural circulation experiment with stepwise coolant inventory reductions formed the basis for the OECD International Standard Problem (ISP-33) as presented in [7, 8]. In addition, many other one-phase and two-phase natural circulation tests have been executed as discussed in more detail by Purhonen et al. in [1–3]. Table 2 introduces very shortly some of the main research topics that dealt with the PACTEL experiments, whose total number is more than 200. PACTEL is included also in the OECD NEA's validation matrixes available in references [9, 10]. The PACTEL experiments have provided valuable data for the validation processes of several codes, such as APROS, RELAP, CATHARE, and TRACE, for example, presented in reference [11].

2.4. Standard Problem ISP-33. The ISP-33 studied natural circulation in the PACTEL facility with stepwise reduced coolant inventories as presented by Purhonen et al. in [1–3]. The ISP-33 is discussed in more detail in [7, 8]. The PACTEL natural circulation experiment with stepwise coolant inventory reductions formed the basis for the OECD International Standard Problem (ISP-33) dealing with problems found in the ability of the computer codes to model reduced inventory situations correctly. The main goal of the OECD International Standard Problem ISP-33 experiment was to study natural circulation in a VVER plant including several single- and two-phase natural circulation modes. A VVER-440-type reactor was addressed for the first time in the framework of the OECD international standard problems.

The general purpose of the ISP-33 test was to produce data for code assessment and development dealing with problems found in the ability of the computer codes to model reduced inventory situations correctly. The large number of participants produced a spectrum of calculation results with different thermal-hydraulic codes. The variation in calculation results showed the importance of comparison to experimental data, of which an example, regarding primary pressure, is presented in Figure 3. Despite of some inaccuracies in the original specifications, ISP-33 proved to be a successful and valuable exercise. The observed discrepancies in the calculation results were easier to investigate than in most ISPs, because the experiment was not excessively complicated, [1].

3. PWR PACTEL

3.1. PWR PACTEL Facility Design. The PWR PACTEL test facility has been designed and constructed in 2009 to be utilized in the safety studies related to thermal-hydraulics of pressurized water reactors with EPR-type vertical steam generators. A significant design and construction basis for the PWR PACTEL facility has been the utilization of some parts of the original PACTEL facility. PWR PACTEL consists of a reactor pressure vessel model, two loops with vertical steam generators, a pressurizer, and emergency core cooling

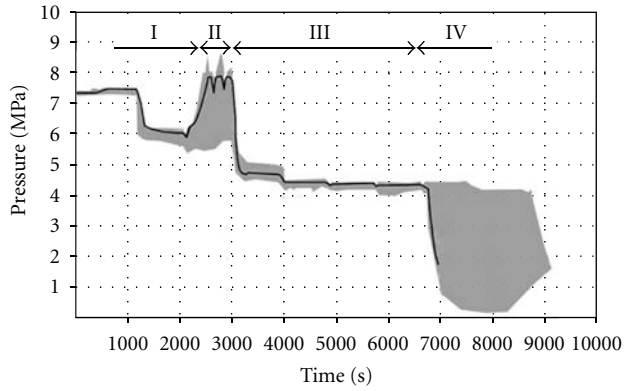

Figure 3: Example of ISP-33 results, primary pressure in experiment (solid line) and variation in ISP-33 posttest calculations (gray area). Flow conditions: (I) one-phase flow, (II) flow stagnations, (III) two-phase flow, and (IV) boiler condenser mode, [2].

systems (ECCSs). The pressure vessel model is comprised of a U-tube construction modelling the downcomer, lower plenum, core, and upper plenum. Figure 4 shows the PWR PACTEL facility. The possibility to use the original PACTEL facility for future needs is preserved. The PWR PACTEL facility is presented in detail by Riikonen et al. in [5] as well as by Rantakaulio et al. in [6].

The heated length of the core is about 2 m shorter than in the EPR core. However, the centre of the core is at the correct elevation. The maximum core power corresponds roughly to the scaled residual heating power of the EPR reactor. The total height of the PWR PACTEL pressure vessel model corresponds to the pressure vessel height of EPR. The volume ratio between the pressure vessels in PWR PACTEL and EPR is about 1/405. The pressurizer is shorter than in EPR. The volume ratio between pressurizers of PWR PACTEL and EPR is 1/562. The ECCS of PWR PACTEL is basically the same as with PACTEL including high and low pressure pumps and two separate accumulators for injection of water to the downcomer and to the upper plenum. The low-pressure safety injection system can inject water to the downcomer and to the upper plenum. The high-pressure system of PACTEL can be used also in PWR PACTEL, or a new injection point can be installed later for PWR PACTEL.

The main design principle of PWR PACTEL is to focus on the proper construction of the loops and vertical steam generators. The setup of the loops and steam generators is designed to allow simulation of PWR and EPR features and studying loop and steam generator behaviour in particular. The two primary loops with identical vertical steam generators are fully representative for PWR applications. PWR PACTEL has two primary loops, both simulating one reference EPR loop. As there are four primary loops in EPR, half of the rated EPR capacity is simulated with PWR PACTEL. Both of the PWR PACTEL loops have one vertical steam generator. The hot legs with an inner diameter of 52.5 mm are on the same elevation as the cold legs. The cold legs have loop seals. At present, there are no circulation pumps in PWR PACTEL. However, there are places reserved

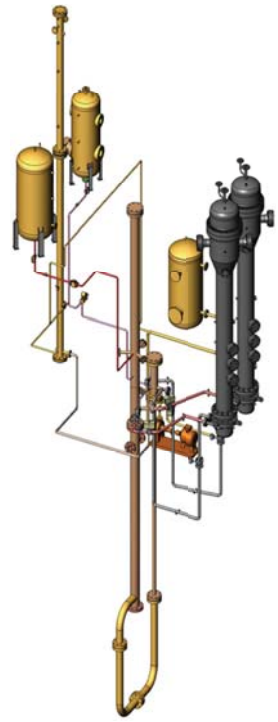

Figure 4: PWR PACTEL facility.

in both of the loops for the main circulation pumps for future plans.

Both of the steam generators in PWR PACTEL contain 51 heat exchange U-tubes. The average length of the tubes is 6.5 m. The U-tubes are in a triangular grid with a lattice pitch of 27.4 mm. The U-tubes are arranged in five groups according to the lengths, each group containing two rows of tubes. The heat transfer area of the tube bundles and the primary-side volume of each steam generator are scaled down with a ratio of 1/400 compared to the reference steam generator. The inner diameter of the steam generator U-tubes in PWR PACTEL is the same as in the EPR steam generator. The same dimension is important for the correct simulation of CCFL phenomena.

The secondary side of the steam generators includes a downcomer, riser, and steam dome volumes, whereas there are no steam separators. On the other hand, the secondary side is also divided into hot and cold parts. Due to the used manufacturing method, the compartments are not fully water tight. Hence, minor cross flows can occur between the hot and cold parts, and also pressure balancing between the downcomer and steam volume is possible. The water volume of the secondary side is about double compared to the volumetrically scaled volume of the secondary side of the EPR steam generator. The secondary side includes feedwater injection systems for the both steam generators. From the secondary side, the steam flows to the atmosphere.

The laboratory building sets some limitations on the precise scaling of the steam generators. Hence, the height of the PWR PACTEL steam generators is about 1/4 of the height of

Table 3: PWR PACTEL characteristics.

Characteristics	PWR PACTEL	PWR/EPR[2] (Olkiluoto 3)
Reference power plant (loops and steam generators)	PWR/EPR	—
Volumetric scale[1]: pressure vessel/steam generators/pressurizer	1 : 405/1 : 400/1 : 565	—
Height scale[1]: pressure vessel (core; relative elevation)/steam generators/pressurizer	1 : 1/1 : 4/1 : 1.6	—
Number of primary loops	2	4
Steam generator type	Vertical	Vertical
Maximum heating power[1]—thermal power [MW]	1	4300
Number of rod simulators[1]—fuel rods	144	63865
Heated length of rod simulators[1]—active core height [m]	2.42	4.2
Axial power distribution[1]	Chopped cosine	—
Maximum cladding temperature[1] [°C]	800	—
Maximum operating pressure[1]—operational/design pressure [MPa]	8.0	15.5/17.6
Maximum operating temperature[1]—inlet/outlet coolant temperature [°C]	300	296/329
Maximum secondary pressure—design secondary pressure [MPa]	5.0	10
Maximum secondary temperature—design secondary temperature [°C]	260	311
Main material of components	Stainless steel	—
Insulation material	Mineral wool (Aluminium cover)	—
Steam generator U-tube diameter/thickness [mm]	19.05/1.24	19.05/1.09
Average steam generator U-tube length [m]	6.5	—
Number of U-tubes in steam generator	51	5980
Number of instrumented U-tubes in steam generator 1/steam generator 2[3]	8/14 (51[3])	—

[1] PWR PACTEL and PACTEL utilize the same pressure vessel and pressurizer parts (see Table 1).
[2] Reference NPP characteristics are taken from "Nuclear Power Plant Unit, Olkiluoto 3" (12/2010) which is a publication of Teollisuuden Voima Oyj (TVO) company.
[3] Each of the 51 U-tubes in steam generator 2 has at least one temperature measurement.

the EPR steam generators. Therefore, the volumetric scaling approach is not fully attained.

The instrumentation of the loops and especially of the primary side U-tubes is considerably extensive. Altogether about 250 temperature, pressure, and differential pressure measurement transducers are attached to allow deeper analysis of steam generator behaviour. Table 3 presents PWR PACTEL characteristics in brief. A schematic view of a PWR PACTEL steam generator is shown in Figure 5. The facility description of PWR PACTEL can be found in [5], and the facility characteristics are also discussed in [6].

3.2. PWR PACTEL Experiments. The characterizing experiments including pressure and heat loss, natural circulation, and steam-generator feedwater system-related experiments have been carried out. From this series one SBLOCA experiment was chosen to be the basis for the PWR PACTEL benchmark exercise described in the next chapter. This first experiment series, was designed to determine the behaviour of the facility and the steam generators.

PWR PACTEL offers a possibility to carry out experiments with large flexibility. The new different scale compared to the other PWR test facilities offers yet another prospect for future research activities. PWR PACTEL, a new setup in the scenery of thermal-hydraulic test facilities, offers also another viewpoint to code validation processes.

3.3. PWR PACTEL Benchmark Exercise. The PWR PACTEL benchmark exercise is organized in Lappeenranta, Finland by Lappeenranta University of Technology (LUT). It is presented in more detail in reference [12]. This benchmark gives a unique opportunity for system code users to participate in an exercise where they can model a new facility configuration. The PWR PACTEL benchmark was launched in 2010 as part of the PWR PACTEL facility introduction.

The chosen transient for the PWR PACTEL benchmark is a small break loss-of-coolant accident (SBLOCA) case. This experiment (SBL-50) is discussed by Riikonen in [13]. The results of the first phase of the benchmark, that is, blind calculations, are available in [12]. As an example of the benchmark experiment, Figure 6 presents primary and secondary pressure progression in PWR PACTEL during the transient.

The first benchmark workshop, where the blind calculation case was introduced and discussed, was held 5th of October 2010. Seven organizations from Czech Republic, Germany, Italy, Sweden, and Finland participate to the benchmark exercise, and they utilize four different system codes

Figure 5: PWR PACTEL steam generator.

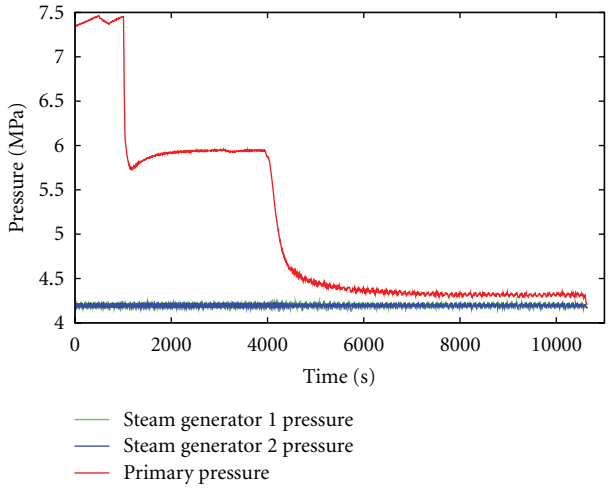

Figure 6: Primary- and secondary-side pressures in PWR PACTEL benchmark experiment.

within the exercise case. The blind calculation work was followed by an open calculation exercise. The second workshop was held in May 2011 in Lappeenranta, Finland.

4. Conclusions

In Finland, own research and continuous development of know-how has always been part of the national nuclear safety concept, especially when connected with the specific nuclear power plant types operated in Finland. Both PACTEL and PWR PACTEL have been constructed partly for this purpose for the field of experimental thermal-hydraulic research. PACTEL was designed particularly for VVER studies and PWR PACTEL especially for EPR specifics with focus on the vertical steam generator behaviour. Considering the future research activities, both facility setups are maintained and kept in a fully operational status.

The PACTEL facility was originally designed to model the thermal-hydraulic behaviour of VVER-440-type reactors. The facility consists of reactor pressure vessel parts, three loops with horizontal steam generators, a pressurizer, and emergency core cooling systems. The facility has been utilized in miscellaneous applications and experiments, for example, in the OECD International Standard Problem ISP-33. More than 200 experiments have been conducted with the PACTEL test facility. PACTEL has been upgraded and modified on a case-by-case basis.

The latest configuration of PACTEL is the PWR PACTEL facility that has been constructed for EPR studies. A significant design basis is the utilization of some parts of PACTEL. At the same time, the focus was set on a proper construction of two new loops and vertical steam generators with an extensive instrumentation. The PWR PACTEL benchmark exercise was launched in 2010 with a small break loss-of-coolant accident test as the chosen transient. PWR PACTEL is an excellent example of the PACTEL facility entity of being multifaceted and giving possibilities to carry out experiments with large flexibility. The new different scale of PWR PACTEL compared to the other PWR test facilities offers yet another prospect for future research activities. PWR PACTEL, a new configuration in the scenery of thermal-hydraulic test facilities, offers also another viewpoint to code validation processes.

Acknowledgments

The planning and construction of the PACTEL facility was organized in 1990 by Technical Research Centre of Finland (VTT) in cooperation with LUT. Financial support at the time was provided by the Ministry of Trade and Industry, VTT and LUT. Along the years, support for the PACTEL-related experimental activities at LUT has been provided by power companies and other organizations. The planning and construction work for PWR PACTEL was performed at Lappeenranta University of Technology by the Nuclear Safety Research Unit. Financial support for the construction and commission of the test facility has been provided by the Finnish Funding Agency for Technology and Innovation (Tekes) and the Finnish power companies Teollisuuden Voima Oyj (TVO) and Fortum Oyj. PWR PACTEL-related experimental activities at LUT are continuing in 2011 under the PAX project within the Finnish Research Programme on Nuclear Power Plant Safety 2011–2014 (SAFIR2014).

References

[1] H. Purhonen, *Experimental Thermal Hydraulic Studies on the Enhancement of Safety of LWRs*, vol. 293, Acta Universitatis Lappeenrantaensis, Lappeenranta, 2007.

[2] H. Purhonen, M. Puustinen, V. Riikonen, R. Kyrki-Rajamäki, and J. Vihavainen, "PACTEL integral test facility—description of versatile applications," *Annals of Nuclear Energy*, vol. 33, no. 11-12, pp. 994–1009, 2006.

[3] H. Purhonen, M. Puustinen, V. Riikonen, R. Kyrki-Rajamäki, and J. Vihavainen, "PACTEL—a versatile facility for research of thermal hydraulics," in *Proceedings of the 11th International Topical Meeting on Nuclear Reactor Thermal-Hydraulics (NURETH-11)*, Popes' Palace Conference Center, Avignon, France, October 2005.

[4] J. Tuunanen, J. Kouhia, H. Purhonen et al., General description of the PACTEL test facility, VTT Research Notes, 1929. 35 p. + app. 75 p. VTT Technical Research centre of Finland, Espoo, 1998.

[5] V. Riikonen, V. Kouhia, A. Räsänen, and H. Partanen, "General description of the PWR PACTEL test facility," Tech. Rep. number, Lappeenranta University of Technology, Nuclear Safety Research Unit, YTY 1, Lappeenranta, 2009.

[6] A. Rantakaulio, V. Kouhia, V. Riikonen et al., "A new integral facility PWR PACTEL for vertical steam generator simulation," in *Proceedings of the International Congress on Advances in Nuclear Power Plants (ICAPP '10)*, pp. 13.6–17.6, San Diego, California, USA, 2010.

[7] H. Purhonen, J. Kouhia, and H. Holmström, ISP-33 OECD/NEA/CSNI International Standard Problem No. 33 (ISP 33), PACTEL Natural Circulation Stepwise Coolant Inventory Reduction Experiment. Comparison Report, Volumes I and II (December 1994), VTT Energy, Nuclear Energy, 1994.

[8] H. Purhonen, J. Kouhia, and H. Kalli, "ISP-33 Standard problem on the PACTEL facility," in *Proceedings of the 7th International Topical Meeting on Nuclear Reactor Thermal Hydraulics, NURETH-7*, vol. 3, pp. 2146–2158, Saratoga Springs, New York, USA, September 1995.

[9] OECD, *CSNI Integral Test Facility Validation Matrix for the Assessment of Thermal-Hydraulic Codes for LWR LOCA and Transients*, OECD, Paris, France, 1996.

[10] OECD/NEA, "Validation matrix for the assessment of thermal-hydraulic code validation matrix," Tech. Rep. NEA/CSNI/R, OECS Support Group on the VVER Thermal-Hydraulic Code Validation Matrix, Paris, France, 2001.

[11] J. Vihavainen, V. Riikonen, and R. Kyrki-Rajamäki, "TRACE code modeling of the horizontal steam generator of the PACTEL facility and calculation of a loss-of-feedwater experiment," *Annals of Nuclear Energy*, vol. 37, no. 11, pp. 1494–1501, 2010.

[12] V. Riikonen and V. Kouhia, "Summary report of PWR PACTEL benchmark experiment blind calculations," Tech. Rep. PAX 1, Lappeenranta University of Technology, Nuclear Safety Research Unit, Lappeenranta, 2011.

[13] V. Riikonen, "Natural circulation experiments with PWR PACTEL facility," type YTY 3, Lappeenranta University of Technology, Nuclear Safety Research Unit, Lappeenranta, 2010.

Hindawi Publishing Corporation
Science and Technology of Nuclear Installations
Volume 2012, Article ID 480948, 15 pages
doi:10.1155/2012/480948

Research Article

Validation of Advanced Computer Codes for VVER Technology: LB-LOCA Transient in PSB-VVER Facility

A. Del Nevo,[1] M. Adorni,[1] F. D'Auria,[1] O. I. Melikhov,[2] I. V. Elkin,[2] V. I. Schekoldin,[3] M. O. Zakutaev,[3] S. I. Zaitsev,[3] and M. Benčík[4]

[1] *GRNSPG, University of Pisa, Livornese street 1291, San Piero a Grado, 56126 Pisa, Italy*
[2] *TH Division, Electrogorsk Research and Engineering Centre, Elektrogorsk, Russia*
[3] *FSUE EDO "GIDROPRESS", Podolsk, Russia*
[4] *TH Analyses Department, Nuclear Research Institute Řež, 250 68 Řež, Czech Republic*

Correspondence should be addressed to A. Del Nevo, alessandro.delnevo@enea.it

Received 9 May 2011; Accepted 15 September 2011

Academic Editor: Klaus Umminger

The OECD/NEA PSB-VVER project provided unique and useful experimental data for code validation from PSB-VVER test facility. This facility represents the scaled-down layout of the Russian-designed pressurized water reactor, namely, VVER-1000. Five experiments were executed, dealing with loss of coolant scenarios (small, intermediate, and large break loss of coolant accidents), a primary-to-secondary leak, and a parametric study (natural circulation test) aimed at characterizing the VVER system at reduced mass inventory conditions. The comparative analysis, presented in the paper, regards the large break loss of coolant accident experiment. Four participants from three different institutions were involved in the benchmark and applied their own models and set up for four different thermal-hydraulic system codes. The benchmark demonstrated the performances of such codes in predicting phenomena relevant for safety on the basis of fixed criteria.

1. Introductory Remarks

VVER reactors have some unique and specific features (e.g., large primary and secondary side fluid inventory, horizontal steam generators, and core design), which require dedicated experimental and numerical analyses in order to assess the performance of safety systems and the effectiveness of eventual accident management strategies. The predictive capabilities of computer codes used in reactor safety analysis needs be validated against relevant experimental data, prior to their application to simulate the behavior of a nuclear power plant. To this purpose a "VVER code validation matrix" [1] was developed in the framework of the OECD/NEA activities, based on the experience of the validation matrices for light water reactor already developed in the 80 and then extended in the 90 [2–5].

2. The PSB-VVER Project

The OECD/NEA PSB-VVER project (2003–2008) has been set with the objective to obtain the required experimental data not covered by the VVER validation matrix [1]. A test matrix was defined considering the inputs received by the Russian Safety Authority Gosatomnadzor [6]. Five tests were executed in PSB-VVER integral test facility, operated at Electrogorsk Research and Engineering Centre, Elektrogorsk (EREC) [7], which are briefly outlined below and summarized in Table 1. The main objectives of the experiments were as follows:

(i) to generate experimental data in order to validate computer codes for transient analysis of VVER reactors,

(ii) to address the scaling issue,

(iii) to contribute to the investigations of postulated accident scenario and actual phenomena occurring VVER-1000,

(iv) to support safety assessments for VVER-1000 reactors.

The first experiment is an intermediate break loss of coolant accident, that is, *11% upper plenum break*. It simulates

Table 1: OECD/NEA PSB-VVER project: test matrix.

Number	ID	Test	Main phenomena under investigation	Justification	Note
(1)	UP-11-08	11% upper plenum break"	Break flow Two-phase natural circulation Phase separation without mixture level formation Entrainment in the core ECCS mixing and condensation Heat transfer in steam generator Flow stratification in horizontal pipes Heat transfer in the covered core Heat transfer in uncovered core (dryout) Rewet Thermal-hydraulics in pressurizer	Identification of similarities and differences in processes/phenomena behaviour at ISB-VVER and PSB-VVER (i.e., manifestation of "scaling effect") and their quantitative characterization	Similar test of the ISB-VVER test
(2)	NC-1	Natural circulation	Single-phase natural circulation Two-phase natural circulation Mixture level and entrainment in the core Heat transfer in steam generator Heat transfer in covered core Heat transfer in partly uncovered core Loop seal clearance	Basic phenomena in transients, need of data in "clean" boundary conditions (outcome of VVER validation matrix). Recommended by Gosatomnadzor	—
(3)	CL-4.1-03	4.1% cold leg break test	Break flow Two-phase natural circulation Asymmetrical loop behaviour Mixture level and entrainment in the core ECCS mixing and condensation Pool formation in the upper plenum Heat transfer in the covered core Heat transfer in uncovered core (dryout) Rewet and quenching Thermal-hydraulics in pressurizer Loop seal clearance	Relevant bounding case phenomenon. Data lacking, as from recommendation of OECD support group on the VVER validation matrix. Relevant for VVER safety assessment. Recommended by Gosatomnadzor	Counter-part of LOBI, BETHSY, SPES, and LSTF
(4)	PSh-1.4-04	Primary to secondary leak	Break flow Two-phase natural circulation Mixture level and entrainment into SG Mixture level and entrainment into the core ECCS mixing and condensation Pool formation in the upper plenum Heat transfer in the covered core Heat transfer in uncovered core (dryout) Heat transfer in steam generator Thermal-hydraulics in pressurizer Loop seal clearance	Absence of test data for "primary to secondary leak" (VVER validation matrix). Recommended by Gosatomnadzor. Highly relevant for VVER safety assessment from point of view of radiological consequence	Analytical exercise among project participants (blind test)
(5)	CL-2x100-01	Large cold leg break	Break flow Asymmetrical loop behaviour Mixture level and entrainment in the core ECCS mixing and condensation CCFL Pool formation in the upper plenum Heat transfer in the covered core Heat transfer in uncovered core (dryout) Quenching Thermal-hydraulics in pressurizer Loop seal clearance	Important for safety assessment evaluations, strongly supported by Gosatomnadzor	Benchmark among project participants

a rupture on one upper plenum accumulator line and it is a "similar test" performed in another facility, ISB-VVER, which is scaled down 1 to 2000. It was also used as shake-down test for the PSB-VVER facility, namely, to check the instrumentation and the system behavior [8]. The comparison with the data of the integral ISB-VVER facility provided feedbacks about the scaling effects on the accident behavior. The transient is initiated by an intermediate break simulating the rupture of one hydroaccumulator line located in upper plenum. The high-pressure injection system (HPIS), connected to one hot leg, is available only in one loop. The onset of the injection of hydroaccumulator systems occurs shortly before the fuel rod simulator bundle heat up starts. Then, continuous heat up and rewet of fuel rod simulators is experienced during the transient, because the stepwise intervention of the hydroaccumulators.

The second experiment is a *natural circulation* test [9]. The design of the experiment is aimed to obtain a set of data in natural circulation. The test consists in step wise reduction of the primary side mass inventory. Between two consecutive drainage phases, "quasi" stationary conditions are achieved in the system. These conditions are suitable to investigate main modes of operation, which might occur during a small break LOCA. In particular, the phenomena connected with the single- and two-phase natural circulation, boiler condenser mode up to the dryout occurrence are studied at various primary coolant inventories in a VVER-1000 configuration.

A small break LOCA is the third experiment [10]. It is a "counterpart test" of the experiments carried out in LOBI, SPES, BETHSY, and LSTF facilities. The experiment is a *4.1% cold leg break test* aimed at providing data on the scaling criteria of the facility and its performance in comparison with the other integral test facilities simulating different pressurized water reactor designs. Starting from the past experiments, the design of the small break LOCA test has been a collaboration between EREC and University of Pisa. The boundary and initial conditions, and the imposed sequence of events have been defined on the basis of well-defined scaling laws in order to carry out a correct "counterpart test" [11]. Focus is also given on the identification and verification of the thermal hydraulic phenomena, according with the validation matrices for transients [1–3]. Similarities and differences of the processes/phenomena running in the PSB-VVER and LOBI test facilities have been also analyzed.

The fourth experiment of the test matrix is related to the *primary-to-secondary leak* issue [12]. The initiating event is the opening of the steam generator header lid with an equivalent break size of about 100 mm, that is, an intermediate break. This scenario is relevant for VVER safety analysis, because it occurred in Rovno nuclear power plant. In this scenario, the primary liquid can be released into the containment through the steam generator relief valves and, without actions of the operator, might be the cause of core degradation. The experiment is executed accounting also for the single failure. It consists in the occurrence of the relief valve stuck open in the affected steam generator. This test is selected by the OECD/NEA PSB-VVER project participants as one for analytical exercise (blind test). Five countries with six codes participated to the blind test, and four countries with five codes performed the posttest calculations [13].

The last test is a large cold leg break LOCA. The test is a double-ended guillotine break in cold leg, between pump and pressure vessel, downstream of the emergency core cooling injection to be performed at "full power" [14]. This corresponds to 10 MW in PSB-VVER integral test facility (ITF) that is scaled one to three hundred. Nevertheless, the fuel core is simulated with indirect electric heated cans, which are not able to withstand to such power. Therefore, the test is performed at "low" power (1.5 MW) and has been used for a benchmark activity, hereafter described [15].

3. The Experiment

3.1. PSB-VVER Facility Description. PSB-VVER is an integral test facility [7] simulating the Russian-designed pressurized light water reactor VVER-1000 v320 (see Figure 1). It is installed at the Electrogorsk Research and Engineering Centre, near Moscow (Russia). The role of such integral test facility in accident analysis, within the nuclear reactor safety technology framework, is primarily to confirm the predictive capabilities of thermal-hydraulic system codes and to trigger the process of code improvement, if needed. The PSB-VVER is characterized by the "time-preserving," "full-pressure," "full-height," "full-linear-heat-generation-rate," and "power-to-volume" scaling laws, such as other experimental facilities (i.e., PKL, LOBI, SPES, BETHSY, LSTF, PMK, SEMISCALE, and LOFT). It is designed and constructed with the following purposes:

(i) obtain experimental data for studying phenomena and processes specified in the validation matrices developed for VVER nuclear power plants,

(ii) assess the efficiency of the existing safety systems and verify engineering approaches proposed in new VVER nuclear power plants designs,

(iii) check and evaluate the existing accident management recommendations and procedures,

(iv) expand the experimental database used for thermal-hydraulic code validation for VVERs.

The PSB-VVER facility is scaled down 1 to 300. It models the entire primary system and most of the secondary system (except turbine and condenser). The facility allows the modeling and representation of phenomena and physical phases that are relevant to VVER-1000 reactor under transient and emergency conditions and to investigate the regimes in accordance with accident management. It is equipped with a data acquisition system that includes more than 1000 measuring channels with a sampling frequency up to 100 Hz. The complete description of the PSB-VVER facility can be found in [7, 16, 17]. The scaling concepts fulfill the requirements needed to simulate the overall

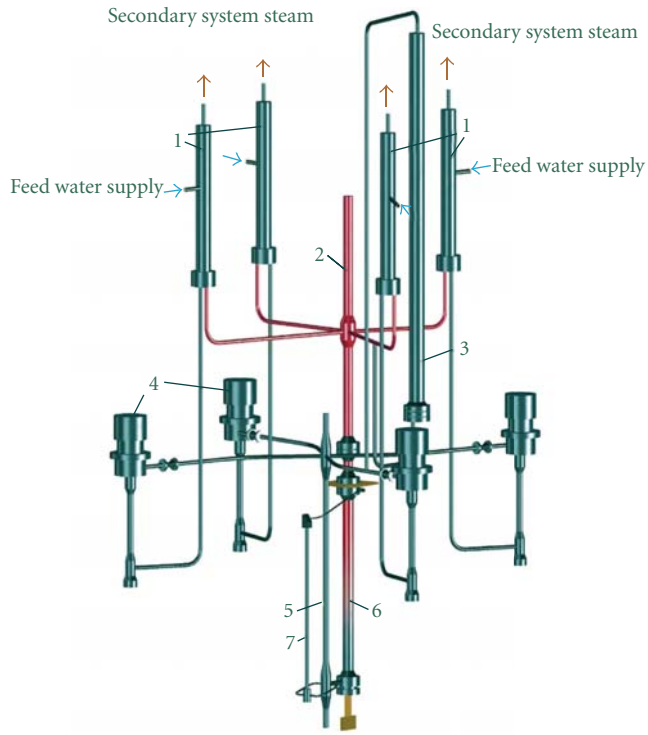

(a) General view of the facility

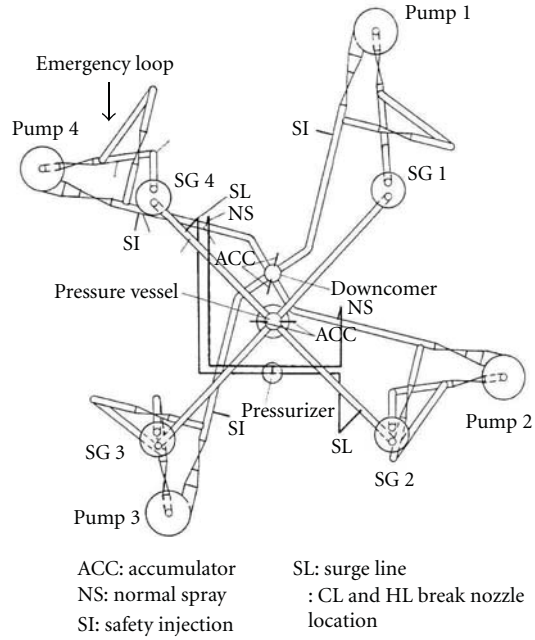

(b) Primary system top view

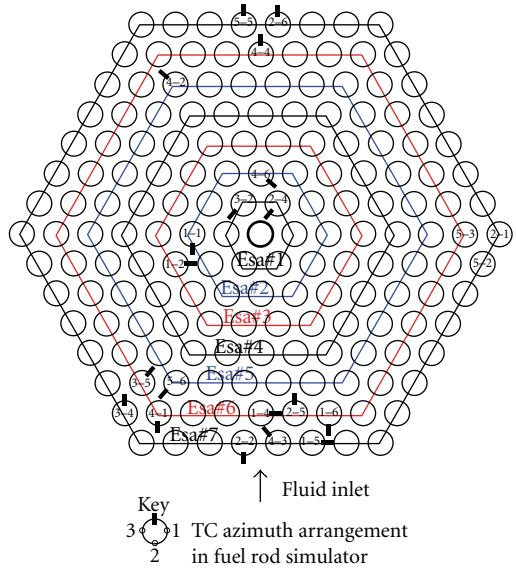

(c) Arrangement of the thermocouples in the FRSB

Figure 1: PSB-VVER facility installed at EREC (Russia).

thermal-hydraulics behavior of the full-scale power plant. Relevant features are hereafter listed:

(i) facility elements scaled in elevation 1 : 1;

(ii) power, volume, and cross-sectional area scaling factor of 1 : 300;

(iii) full pressure of the primary and secondary systems;

(iv) simulation of all four loops;

(v) fuel rod and horizontal SG tubes scaled in length 1 : 1.

3.2. Test 5a "CL-2x100-01" Description. The main objectives of the test 5a, identified as "CL-2x100-01", are as follows [14, 18]:

(i) to obtain experimental data not covered by the VVER validation matrix,

(ii) to investigate the thermal-hydraulic response of the VVER-1000 primary system during a double-ended guillotine break in cold leg;

(iii) to obtain experimental data for validation of thermal-hydraulic system codes applied to LB-LOCA analysis of VVER-1000;

(iv) to evaluate the capability of the PSB-VVER facility to simulate the LB-LOCA in VVER-1000.

The experiment starts with the ruptures of the membranes in cold leg number 3 and the closure of the valve located between the two break devices, simulating the occurrence of the double-ended guillotine break in the facility. Six phenomenological windows are distinguished in the experiment, which are hereafter outlined.

(1) *Blowdown Phase*: from the start of the transient (SoT) up to reactor pressure vessel level increase. Once the break (double ended) is opened, the loss of offsite alternating current (AC) power is assumed simultaneously. This implies the following events: SCRAM occurrence, the onset of the main coolant pumps coastdown, the turbine valve, and the main feed water pumps closures. The loss of offsite AC power causes the inhibition of the active emergency core cooling system, up to 40 s (availability of the diesel generators). The primary pressure decreases fast (Figure 2), therefore the primary side coolant evaporates. Condition for critical heat flux occurs in the core. However, no dryout is observed in the experimental data due to the SCRAM at time 0 s and the low energy stored in the fuel. The accumulators start to inject in upper plenum and downcomer at about 10 s. At the end of this phase, the measured reactor pressure vessel collapsed level reaches a minimum.

(2) *Refill Phase*: up to the accumulators effectiveness ends. The refilling of the lower plenum is driven by the accumulators' injections and later on, 40 s after the SoT, by the ECCS injection. During this phase a pool formation in upper plenum is observed and lasts until the end of this phase. The phase ends when the accumulators' injections are less effective, because they are almost empty.

(3) *Primary Side Mass Inventory Reduction Phase*: up to the onset of core heatup. During this phase the reactor pressure vessel level decreases again because the accumulators are empty. The loop seals in the intact loops are completely emptied. The downcomer level increases at the beginning of the phase and then, oscillates at the end of the phase before the dryout phase starts (Figure 3).

(4) *Dryout Phase*: up to core quenching. The phase is characterized by the temperatures excursions in the fuel rod simulator bundle. During this phase, the primary system mass inventory slightly increases, because the positive mismatch between the active ECCS and the mass released through the break.

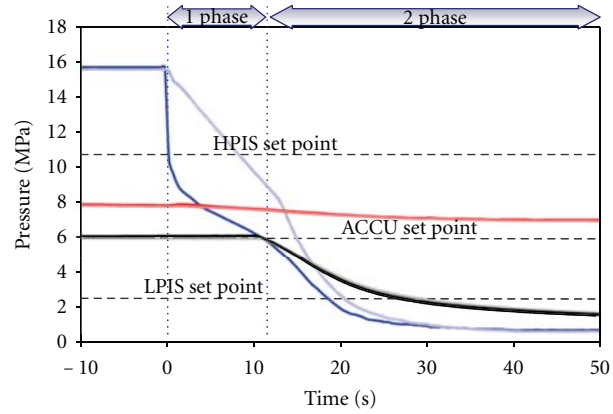

(a) Zoom from −10 s to 50 s

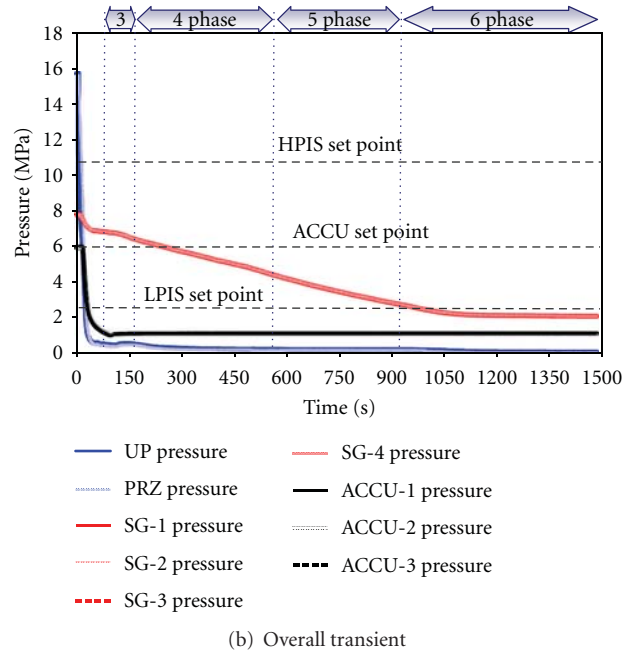

(b) Overall transient

Figure 2: OECD/NEA experiment PSB-VVER CL-2x100-01: measured trends of upper plenum (YC01P16), pressurizer (YP01P01) steam generators (YB01-04P01), and accumulators pressures (TH01-04P01).

(5) *Stable Safe Condition Phase*: up to the active ECCS tanks emptying. This is a transition phase, since the safe conditions are achieved. The primary mass inventory continuously increases as well as the collapsed level in the riser-side of the reactor pressure vessel. Once the active ECCS have injected 1.86 m^3 of water, according to the scenario specifications, the LPIS and HPIS pumps are switched off.

(6) *Primary Side Mass Inventory Depletion Phase and End of Transient* (*EoT*): the last phase is characterized by a slow empting of the primary system until the final dryout occurs. The test ends at 1477 s when the maximum core temperature measured reaches about 515 C.

The complete description of the test is available in the experimental data report, issued by EREC [18].

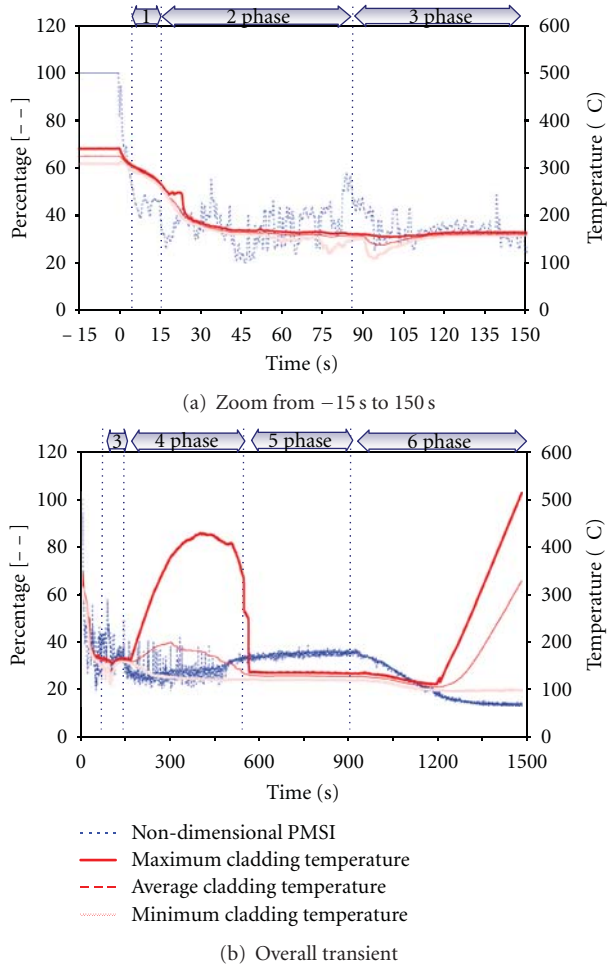

(a) Zoom from −15 s to 150 s

(b) Overall transient

Figure 3: OECD/NEA experiment PSB-VVER CL-2x100-01: non-dimensional trend of primary side mass inventory (PMSI); upper and lower envelops and average value of all cladding temperatures measurements.

4. Benchmark on LB-LOCA Transient in PSB-VVER Facility

4.1. Objectives of the Activity. The OECD/NEA PSB-VVER Test 5a benchmark [15] is focused on the assessment of Western and Eastern thermal-hydraulic system codes in predicting large break LOCA phenomena occurring in VVER-1000 prototype reactor. The main objectives of the benchmark are as follows:

(i) to assess the current capabilities of the thermal-hydraulic system codes on the domains of interest,

(ii) to develop a common understanding and to promote an exchange of knowledge,

(iii) to draw conclusions on the possible use of the codes for regulatory bodies and the industry.

4.2. Procedure for Code Assessment. The assessment of a thermal-hydraulic system code involves the availability of a qualified nodalization and of qualified experimental data from a qualified experimental facility. It also requires standard procedures and the fulfillment of specific criteria. In this context, references have been provided by University of Pisa to define the meaning of "qualified nodalization," to develop the procedure and the criteria necessary for preparing a "qualified nodalization," to perform the assessment activities, and, finally, to execute qualified computer code calculations.

The procedure for code assessment consists of three main steps, see also [19–21].

(1) The steady state results (i.e., "*steady state qualification*"), which may include the nodalization development phase (e.g., volume, heat transfer area, elevations, pressure drops distribution, etc.). This step is concluded with the simulation of the nominal steady state conditions against specific acceptability thresholds.

(2) The reference calculation results (i.e., "*on transient qualification*") that shall satisfy qualitative and quantitative accuracy-related criteria. According with this procedure, the reference calculation is not "the best" calculation achievable by the code.

(3) The results from sensitivity study (which is also part of the "*on transient qualification*") is carried out to demonstrate the robustness of the code calculations, to characterize the reasons for possible discrepancies between measured and calculated trends, to optimize code results and user options choices, and to improve the knowledge of the code by the user.

The comparative analysis, described in the following sections, is carried out on the basis of the steps 1 and 2 above.

4.3. Comparison among Participants Input Decks. The simulation of test 5a has been performed by four participants belonging to three different institutions with four different thermal-hydraulic system codes [15]. Gidropress (EDO-GP) submitted both pretest and posttest calculations. In details:

(1) *KORSAR-GP* V9.027.004, pretest, and V9.031.000, posttest (*Gidropress—Russia*),

(2) *TECH-M* (*Gidropress—Russia*),

(3) *ATHLET 2.1 Cycle A* (*Nuclear Research Institute Řež—Czech Republic*);

(4) *RELAP5-3DV2.4.2* (*University of Pisa—Italy*).

Table 2 provides information regarding the adopted code resources, the nodalization features, and the main code options.

4.4. Comparison and Evaluation of Steady State Results. The steady state results have been analyzed and compared. The procedure involves two main tasks, which are as follows:

(i) the verification and evaluation of the geometrical fidelity of the model developed, also called the "nodalization development phase,"

(ii) the capability of the analytical model to achieve stable steady state with the correct initial conditions.

Table 2: Information on nodalizations and the code options.

Number	Quantity	Unit	EDO-GP pretest KORSAR	EDO-GP posttest KORSAR	EDO-GP pretest TECH-M	EDO-GP posttest TECH-M	NRI posttest ATHLET	UNIPI posttest R5-3D
1	Adopted code resources							
1.1	Tot. no. of hydraulic components primary system	—	—	—	—	—	142	482
1.2	Tot. no. of hydraulic components	—	185	193	—	—	164	620
1.3	Tot. no. of hydraulic nodes (meshes) primary system	—	—	—	76 + 36	76 + 36	693	—
1.4	Tot. no. of hydraulic nodes (meshes)	—	858	825	81 + 36	81 + 36	820	2474
1.5	Tot. no. of heat structures	—	52	65	81 + 36	81 + 36	90	2171
1.6	Tot. no. of mesh points in the heat structures	—	509	629	4	4	2108	11263
1.7	Tot. no. of core active structures	—	10	10	30	30	20	20
1.8	Tot. no. of core radial meshes in the active structures	—	—	—	7	7	3	13
2	Nodalization features							
2.1	No. of modeled loops	—	4	4	4	4	4	4
2.2	No. of horizontal tubes per SG	—	4	4	1	1	5	17
2.3	Core model (3D or 1D)	—	1D	1D	1D	1D	1D	1D
2.4	No. of hydraulic channels in core region	—	1	1	3	3	2	2
2.5	Cross-flow junctions between parallel channels in the core	—	Yes	Yes	No	No	No	Yes
3	Code options							
3.1	Reflood model top-down	—	—	Yes	Yes	Yes	No	Yes
3.2	Reflood model bottom-up	—	—	Yes	Yes	Yes	No	Yes
3.3	CCFL model	—	—	No	Yes	Yes	Wallis	No

Although the *first task* is outside of the scope of the activity, the participants provided relevant geometrical data with the objective to allow a more comprehensive understanding of the differences among the results of the codes [15].

The achievement of the steady state conditions (*task two*) deals with the comparisons between the experimental measurements and the calculated results at the start of transient (SoT). The selection of the key parameters for steady state verification is done taking into account the availability of the experimental data. Anyway, some parameters are compared, even though they are not available in the experimental database (i.e., steam generators power exchanged, maximum fuel centerline temperature, accumulators mass inventory, steam generators mass inventory, core and, upper head-downcomer bypass flow rates). No error is considered if the calculated value is inside the bands of the measurement accuracy. If it is outside, the error is calculated as difference between the calculated value and upper or lower limit of the measured value.

Figure 4 shows the verification of the pressure drops in the reactor pressure vessel and in the reactor coolant system. The verification of the pressure drop across the vessel reports two different set of experimental data: one (reported with the blue dashed line label "YC01DP16b" in Figure 4(a)) is the direct measure from inlet to outlet of the pressure drop and the second (black line) is calculated through the chain of the pressure drops measurements available in the reactor pressure vessel. Almost all calculated values are inside or close the experimental value (19.80 kPa) considering the measurement uncertainty (± 1.5 kPa). On the other side the

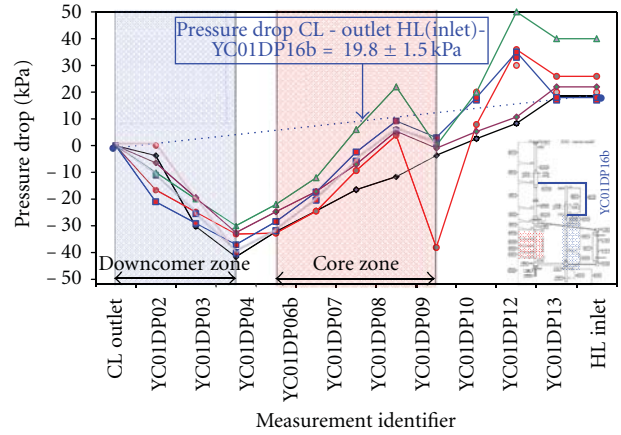

(a) RPV pressure drop versus length

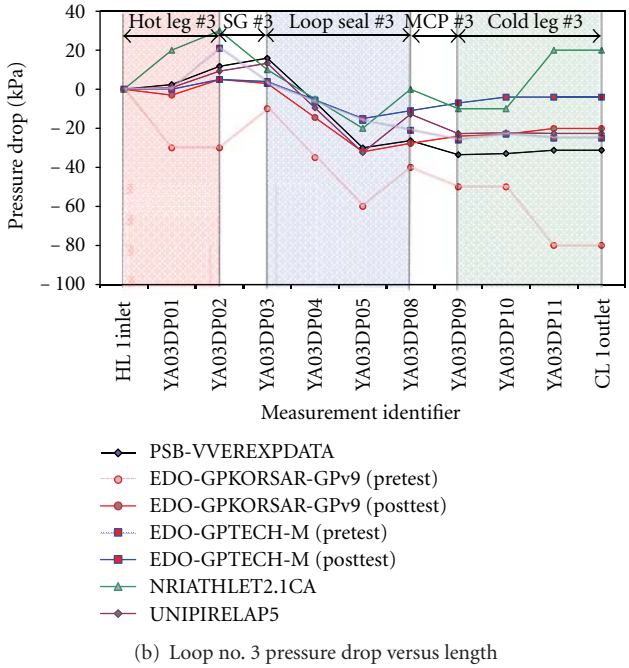

(b) Loop no. 3 pressure drop versus length

Figure 4: Primary system pressure drop versus length.

verification of the pressure drop in the loop seal number 3 shows larger discrepancy between the calculated values and the measurement trend. These differences can be attributed to the propagation of the errors connected with the chain of measured pressure drops used. Indeed, the final absolute value should be equal to the pressure drop across the reactor pressure vessel. The analysis [15], not detailed in the present paper, demonstrated that the codes results are in general acceptable, even though some errors exceed the acceptability thresholds [19].

4.5. Comparison and Evaluation of Reference Results. The analysis of the results is based on a comprehensive comparison between measured and calculated trends and values, aimed at demonstrating that the codes simulations are capable to reproduce the relevant thermal-hydraulic phenomena observed in the experiment. This is performed in four relevant checks.

The *first check* consists in comparing the values of quantities characterizing the sequence of events, and is part of the qualitative evaluation of the results (see Section 4.2 no. (2)). Table 3 reports the list of the relevant events and the timing of their occurrences.

The *second check* (qualitative evaluation) is the comparisons between experimental and calculated time trends on the basis of selected variables. The complete set of time trends used for the analysis is based on 55 parameters [15]. Among those parameters, 18 are selected for the quantification of the accuracy by the application of the FFTBM (check four, below). These represent the minimum number of quantities describing the experimental scenario and the code performances. The description of the parameter trends is provided by grouping the homogeneous quantities: that is, absolute pressures, coolant temperatures, mass flow rates, integral mass, pressure drops, levels, cladding temperatures, and powers. As sample, the time trends of the upper plenum pressures and of the maximum cladding temperatures provided by the participants are compared in Figure 5.

The primary pressure trend is well simulated by the codes, with the exception of a pretest calculation. The cladding temperatures reported in Figure 5(b) represent the code predictions at the height, where the experimental measure experiences the maximum cladding temperature (2.8–3.2 m from bottom of active fuel). The figure shows the first dryout occurrence and the maximum PCT well simulated by RELAP5 and the final core heat up by ATHLET. It should be noted that the maximum cladding temperature by ATHLET code is predicted at higher elevation and it is close to the experimental value (398 C instead of 428 C measured in the experiment), see [15].

The *third check* is the qualitative accuracy evaluation of the results on the basis of the relevant thermal-hydraulic aspects. These are derived from the analysis of the transient, its subdivision in phenomenological windows, and then the identification of the relevant phenomena following a rigorous approach [20].

The transient has been divided in 8 different RTA. They are break flow rate behavior, PRZ behaviour, first dryout occurrence, UP pressure behavior, accumulator behavior, ECCS (HPIS and LPIS) behavior, primary side mass behavior, and final dryout occurrence. Each RTA has been characterized by several quantities, which are used for evaluating the accuracy of the code simulations: that is, time sequence of event (TSE), integral parameter (IP), single value parameter (SVP), and nondimensional parameter (NDP). For each of these quantities an engineering judgment is provided according with the following criteria:

(a) "E" mark: the code predicts qualitatively and quantitatively the parameter (excellent—the calculation result is within experimental data uncertainty band);

(b) "R" mark: the code predicts qualitatively, but not quantitatively the parameter (reasonable—the calculation result shows only correct behavior and trends);

Table 3: Resulting sequence of main events.

Number	Event description	Exp (sec)	EDO-GP pretest KORSAR	EDO-GP posttest KORSAR	EDO-GP pretest TECH-M	EDO-GP posttest TECH-M	NRI posttest ATHLET	UNIPI posttest R5-3D	Note
(1)	DEGB occurrence	**0.0**	0.0	0.0	0.0	0.0	0.0	0.0	Imposed event
(2)	Reactor SCRAM	**0.0**	0.2	0.2	0.2	0.2	0.0	0.0	Imposed event
(3)	MCP trip and coastdown	**0.0**	0.0	0.0	0.4	0.4	0.0	0.0	Imposed event
(4)	Turbine valve closure begins	**0.0**	0.0	0.0	0.1	0.1	0.0	0.0	Imposed event
(5)	Flashing of coolant at the outlet of core model	**0.4**	0.4	1.0	1.0	0.2	0.4	0.2	
(6)	UP pressure < 10.8 MPa	**0.54**	0.4	0.8	0.8	0.9	0.35	0.2	
	Coolant reaching saturation in CLs SGs outlet								
(7)	(i) loop no. 1	**2.8**	—	—	—	—	—	5.0	
	(ii) loop no. 2	**2.3**	—	—	—	—	—	4.9	
	(iii) loop no. 3	**0.03**	—	—	—	—	—	2.0	
	(iv) loop no. 4	**3.1**	—	—	—	—	—	4.7	
(8)	Coolant reached saturation at core inlet	**1.0**	1.0	1.0	1.0	0.6	1.4	1.3	
(9)	Primary pres. below secondary pressure	**4.0–4.3**	7.7	6.5	9.0	6.0	6.5	5.2	
(10)	Stop of FW pumps	**4.1–8.7**	5.2	4.0	0.4.0	0.4	0.0	0.0	
(11)	ECC acc injection start	**10.2–10.7**	9.2	11	10.0	12.0	10.9	11.1	
(12)	PRZ emptied (level < 0.1 m)	**11**	6.3	7.0	9.7.0	12.4	8.6	11.9	
(13)	Turbine valve fully closed	**15.5**	16.0	15.0	—	—	—	15.7	Imposed event
(14)	Pressure in UP < 2.5 MPa	**18.6**	14.7	19	18.0	19.8	18.0	17.9	
(15)	UP and PRZ pressures equalization	**31**	8	8	28	30	21	36.8	
(16)	ECCS connected to an emergence power supply	**40**	40	40	40	40	40.3	40	Imposed event
(17)	ECCS HPIS injection	**40**	40	40	40	40	40	40	
(18)	ECCS LPIS injection	**40**	40	40	40	40	40	40	
(19)	ECC acc. injection stop				113	104	95		
	(i) acc no. 1	**89**	77	93				88	
	(ii) acc no. 3	**107**	77	100				91	
	(iii) acc no. 4	**92**	77	96				94	
(20)	First dry out occurrence	**159**	94*	150	177	134	43	153	
(21)	End of MCP coastdown	**231**	232	231	217	231	232	232	
(22)	Max. PCT in the core	**395**	109*	339	232	476**	296	385	
(23)	Overall quenching	**559**	117*	462	—	559	487	493	
(24)	All ECCS stop	**921**	862	872	898	884	903	923	
(25)	Second dry out occurrence	**1187**	106	1258	911	904	1148	1072	Top of the core
(26)	End of calc. (max Tcl = 516 C)	**1477**	1100	1566	1241	1230	1500***	1360	

(*) First out of 5 dryout experienced at different axial levels, especially in the lower part of the core.
(**) Second out of two dryout.
(***) Corresponding to a maximum cladding temperature equal to 500 C.

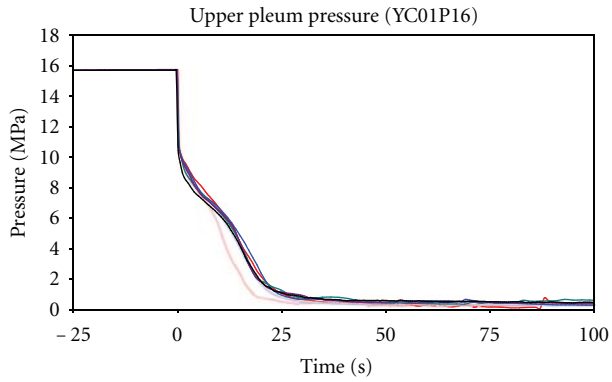

(a) UP pressure trends (zoom from −25 s to 100 s)

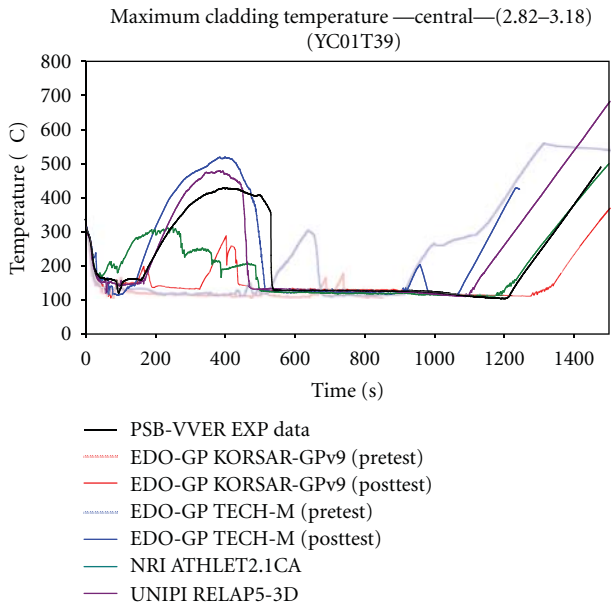

(b) Maximum cladding temperature trends in central zone between 2.82 and 3.18 m

Figure 5: Qualitative evaluation of the results: experimental versus calculated time trends.

(c) "M" mark: the code does not predict the parameter, but the reason is understood and predictable (minimal—the calculation result lies within experimental data uncertainty band and sometimes does not have correct trends);

(d) "U" mark: the code does not predict the parameter and the reason is not understood (unqualified—calculation result does not show correct trend and behavior, reasons are unknown and unpredictable).

A positive overall qualitative judgment is achieved if "U" mark is not present. The qualitative accuracy evaluation supports the conclusion that the posttest calculations are qualitatively correct. Details of the results are not reported for sake of brevity and are available in [15].

The *fourth check* is the quantitative accuracy evaluation by using the fast fourier transform-based method (more details in [21]). This tool, developed at University of Pisa, is applied once the other checks, previously discussed, are positively fulfilled and the code results are judged satisfactory from the qualitative point of view. This tool provides an error function, which satisfies the following requirements:

(i) at any time of the transient this function should remember the previous history,

(ii) engineering judgment should be avoided or reduced,

(iii) the mathematical formulation should be simple,

(iv) the function should be nondimensional,

(v) it should be independent from the transient duration,

(vi) compensating errors should be taken into account (or pointed out),

(vii) its values should be normalized.

The FFTBM is used for the quantification of the accuracy of the code results. This tool gives an accuracy coefficient (AA) and a weighted frequency (WF) for each variable and for the overall transient. The most significant information given by AA is the relative magnitude of the discrepancy coming from the comparison between the calculation and the corresponding experimental variable time history. When the calculated and the experimental data are equal, then the error function is zero (AA is also equal to zero), characterizing perfect agreement. The WF factor characterizes the kind of error, because its value emphasizes where the error has more relevance either at low or high frequencies. For instance, oscillations of the calculated values around an average trend can be readily identified by the method. Depending on the transient, high-frequency errors may be more acceptable than low (in thermal-hydraulic transient, better accuracy is generally represented by low AA values at high WF values), see also [22, 23].

The method was applied on the basis of 18 parameters (see Figure 6). They were selected as the minimum number relevant to describe the transient (see also step 2), considering the peculiarities of the transient, as well as the quality and availability of the experimental data. Then, those parameters are combined to give an overall picture of the accuracy of a given calculation (AA_{tot} in Figures 6 and 7). The total average amplitude of the transient (AA_{tot}) is the result of the sum of all the average amplitudes with their "weights." The "weight" of each contribution is dependent on the experimental accuracy, the relevance of the addressed parameter, and a component of normalization with reference to the average amplitude evaluated for the primary side pressure (more details in[20, 24]). The reference results of

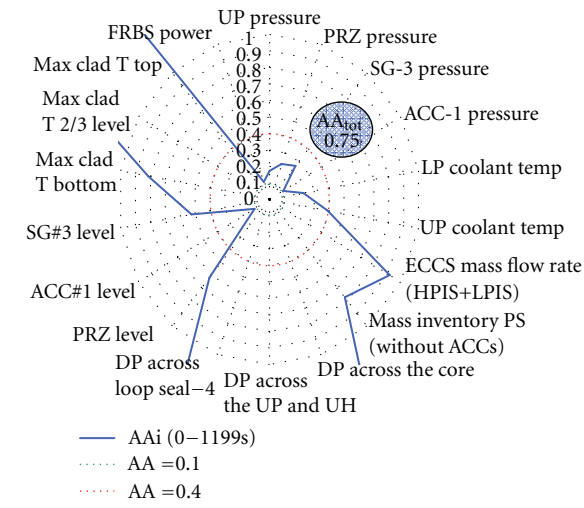

(a) KORSAR pretest (zoom from AAi = 0 and AAi = 1.0)

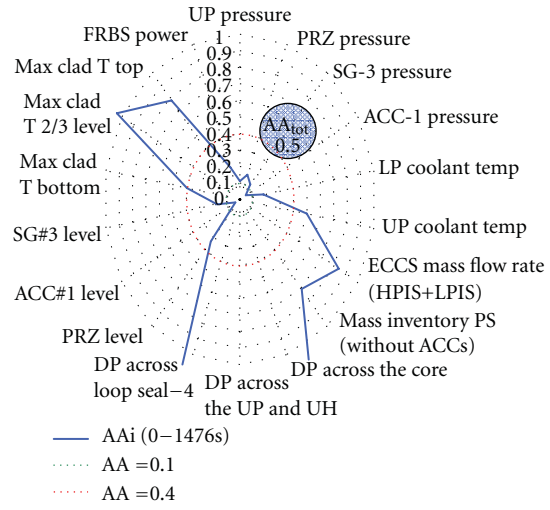

(b) KORSAR posttest (zoom from AAi = 0 and AAi = 1.0)

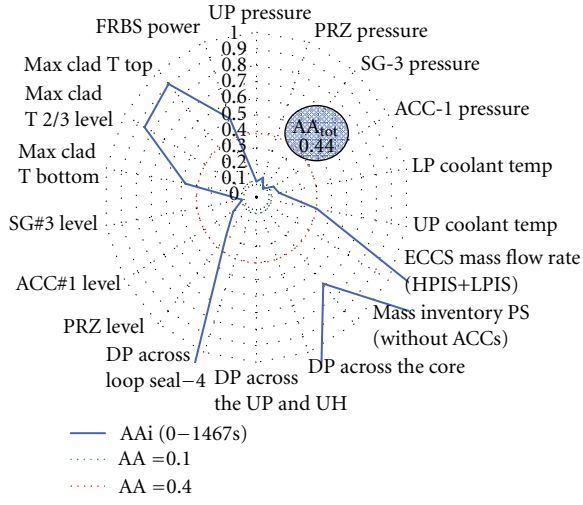

(c) TECH-M pretest (zoom from AAi = 0 and AAi = 1.0)

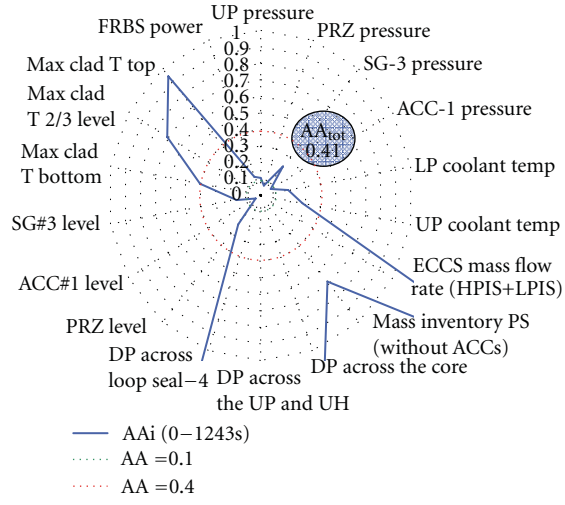

(d) TECH-M posttest (zoom from AAi = 0 and AAi = 1.0)

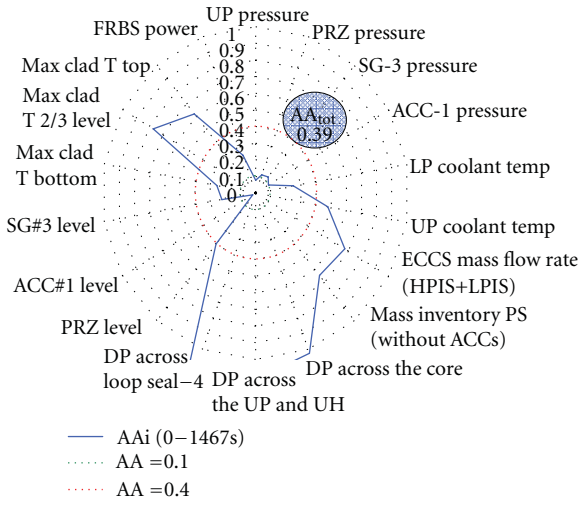

(e) ATHLET posttest (zoom from AAi = 0 and AAi = 1.0)

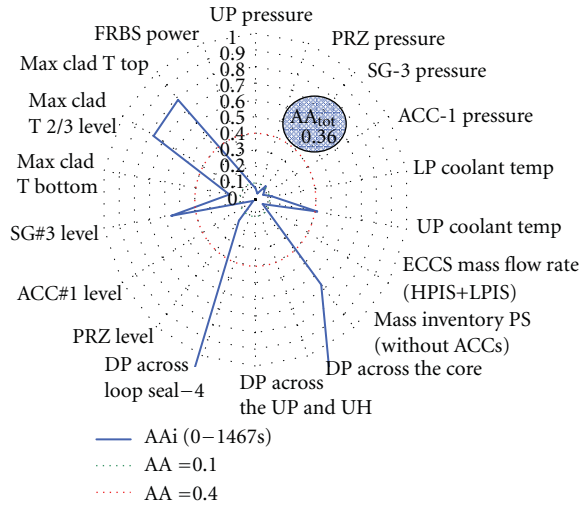

(f) RELAP5-3D posttest (zoom from AAi = 0 and AAi = 1.0)

Figure 6: FFTBM application: quantitative accuracy evaluation of the results (overall transient).

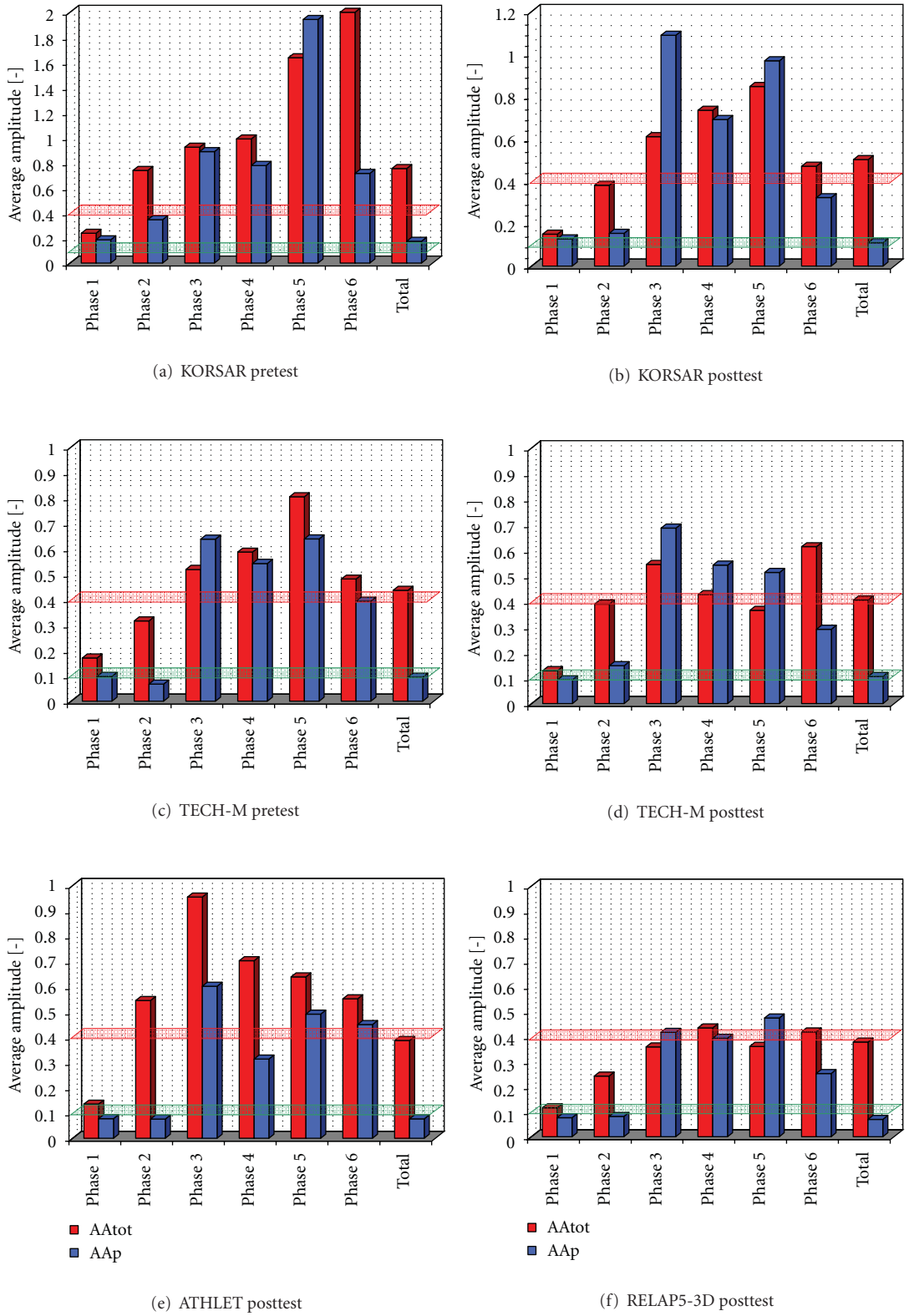

(a) KORSAR pretest

(b) KORSAR posttest

(c) TECH-M pretest

(d) TECH-M posttest

(e) ATHLET posttest

(f) RELAP5-3D posttest

Figure 7: FFTBM application: quantitative accuracy evaluation of primary pressure, and total for detail of each phenomenological window and overall transient.

the method are usually focused on two values: the average amplitudes of the primary pressure and of the global (or total) response.

Figure 6 summarizes the average amplitudes of the 18 selected parameters for each code calculation. Figure 7 provides the primary pressure amplitudes and total average amplitudes as function of each phenomenological windows, according to the description of the test.

The following main conclusions are derived by the quantitative evaluation of the results [15].

(i) Three out of six code applications (ATHLET, RELAP5-3D, and TECH-M) have an average amplitude of the primary pressure equal to or lower than 0.1, which indicate high accuracy of the results. Among these, it should be highlighted the TECH-M simulation is a pretest. The KORSAR and the TECH-M (posttest) primary pressure trends are very close to this threshold.

(ii) Poor accuracies are calculated for the pressure drops (the AA value is larger than 1), as showed in Figure 6. The parameters considered are the pressure drop trends across the core, the upper plenum (including the upper head), and the loop seal number 4. These parameters are qualitatively predicted by the ATHLET, REALP5, and TECH-M (posttest) simulations.

(iii) The primary pressure and the total average amplitudes are lower during the first 100 s (PhW 1 and 2, according to Section 3.2), see Figure 7.

(iv) Two out of six code applications (ATHLET, RELAP5-3D) showed a good prediction of the experiment, having a total average amplitude lower than 0.4. The TECH-M simulation evidenced a fair prediction of the experiment, having a total average amplitude between 0.4 and 0.5.

5. Conclusions

The OECD/NEA PSB-VVER project provided unique and useful experimental data for code validation by the scaled-down integral test facility PSB-VVER. In this framework, four participants and three different institutions simulated the test 5a (identification CL-2x100-01), which is the last experiment of the project test matrix. The Western (i.e., ATHLET and RELAP5-3D) and Eastern (KORSAR and TECH-M) advanced computer codes were applied in this context. The initiating event is the double-ended guillotine break in cold leg.

The objective of the activity is to collect, analyze, and document the numerical activity (posttest) performed by the participants, describing the performances of the codes simulations and their capability to reproduce the relevant thermal-hydraulic phenomenaobserved in the experiment. The objective is fulfilled through comprehensive comparisons based on the following steps:

(i) comparison of the features of the analytical models applied,

(ii) verification of the code performance "at steady state level,"

(iii) assessment of the code performance at "on transient level" based on a qualitative and quantitative (FFTBM) accuracy evaluation of the results.

The analysis of the results demonstrates the following:

(i) all code runs were able to predict the primary pressure trend with satisfactory accuracy;

(ii) the core cladding temperature was predicted by all posttest analyses. In particular, the maximum cladding temperature was generally overestimated (posttest) with the exception of the ATHLET simulation that highlighted an excellent accuracy;

(iii) the primary mass inventories predicted by the simulations resulted in general lower than the experimental (indirect) measurement.

The application of the FFTBM, related to the quantification of the accuracy, showed the following:

(i) almost all code simulations have an average amplitude of the primary pressure equal or lower 0.1 and the others are very close to this threshold,

(ii) all code simulations showed a good prediction of the experiment (total average accuracy lower than 0.4) or a fair prediction ($0.4 < AA_{tot} < 0.5$),

(iii) the parameter trends of the pressure drops during the transient and the timing of the final cladding temperature excursions affected the total average by increasing the final values.

In conclusion, the availability of the experimental data and the present benchmarking activity brought to the following achievements.

(i) The experiment PSB-VVER test 5a, executed in the largest ITF currently available for VVER-1000 type reactors, contributes to extend the experimental database for code validation.

(ii) The applications of the numerical models represent an enlargement of the validation activity for computer codes. In this connection, the comparison of Western and Eastern computer codes represent a further valuable achievement.

Nomenclature

AA_{pp}: Average amplitude primary pressure
AA_{tot}: Average amplitude total
ACC: Hydraulic accumulator
CCFL: Counter current flow limiting
CL: Cold leg
CSNI: Committee on the Safety of Nuclear Installations
DC: Downcomer
DP: Pressure drop
ECCS: Emergency core cooling system
EDO-GP: EDO-Gidropress (the VVERs designer)
EoT: End of transient
ESA: Hexagon
FFTBM: Fast Fourier transform-based method
GP: Gidropress (the VVERs designer)
GRS: Gesellschaft für Anlangen—und Reaktorsicherheit
HL: Hot leg
HPIS: High-pressure injection system
INL: Idaho National Labs
ITF: Integral test facility
LB-LOCA: Large break-loss of coolant accident
LOCA: Loss of coolant accident
LP: Lower plenum
LPIS: Low-pressure injection system
LS: Loop seal
MCP: Main coolant pump
NEA: Nuclear Energy Agency
NRI: Nuclear Research Institute Czech Republic
OECD: Organization for Economic Cooperation and Development
PCT: Peak cladding temperature
PhW: Phenomenological windows
PMI: Primary mass inventory
PRZ: Pressurizer
RCS: Reactor coolant system
RPV: Reactor pressure vessel
RTA: Relevant thermalhydraulic aspect
SBLOCA: Small break loss of coolant accident
SG: Steam generator
SoT: Start of transient

TH-SYS: Thermal-hyrdraulic system
UH: Upper head
UNIPI: Università di Pisa
UP: Upper plenum
VVER: Russian-designed pressurized water reactor
WF: Weight frequency.

Acknowledgments

The Authors would like to acknowledge the OECD Nuclear Energy Agency (NEA) that promoted the PSB-VVER project, Jean Gauvain who managed the project, and the Institutions involved, which contributed to develop a common understanding and to promote an exchange of knowledge.

References

[1] Group of Experts of the NEA/CSNI, "Validation matrix for the assessment of thermal-hydraulic codes for VVER LOCA and transients," NEA/CSNI/R(2001)4, 2001.

[2] N. Aksan, D. Bessette, I. Brittain et al., "CSNI code validation matrix of thermal-hydraulic codes for LWR LOCA and transients," OECD/NEA-CSNI Report 132, 1987.

[3] A. Annunziato, H. Glaeser, J. Lillington, P. Marsili, c. Renault, and A. Sjöberg, "CSNI integral test facility validation matrix for the assessment of thermal-hydraulic codes for LWR LOCA and transients," NEA/CSNI/R(96)17, 1996.

[4] N. Aksan, F. D'Auria, H. Glaeser, R. Pochard, C. Richards, and A. Sjöberg, "Separate effects test matrix for thermal-hydraulic code validation. Volume I: phenomena characterisation and selection of facilities and tests," NEA/CSNI/R(93)14/Part 1, Paris, 1994.

[5] N. Aksan, F. D'Auria, H. Glaeser, R. Pochard, C. Richards, and A. Sjöberg, "Separate effects test matrix for thermal-hydraulic code validation. Volume I: facility and experiment characteristics," NEA/CSNI/R(93)14/ Part 2, Paris, 1994.

[6] O. I. Melikhov, V. I. Melikhov, and I. V. Parfenov, "PSB-VVER test priority for the OECD PSB-VVER project," OECD PSB-VVER Project, PSB-VVER Report, PSB-01, EREC, Electrogorsk, Russia, 2003.

[7] O. Melikhov, I. Elkin, I. Lipatov et al., "Report about PSB-VVER description (including measurement system)," OECD PSB-VVER Project, PSB-VVER Report, PSB-03, EREC, Electrogorsk, Russia, 2003.

[8] O. I. Melikhov, I. V. Elkin, I. A. Lipatov et al., "Post-test full experimental data report (test 1)," OECD PSB-VVER Project Report PSB-08, EREC, Electrogorsk, Russia, 2003.

[9] O. I. Melikhov, I. V. Elkin, I. A. Lipatov et al., "Post-test full experimental data report (test 2)," OECD PSB-VVER Project Report PSB-15, EREC, Electrogorsk, Russia, 2003.

[10] O. I. Melikhov, I. V. Elkin, I. A. Lipatov et al., "Post-test full experimental data report (test 3)," OECD PSB-VVER Project Report PSB-18, EREC, Electrogorsk, Russia, 2004.

[11] F. D'Auria, M. Cherubini, G. M. Galassi, and N. Muellner, "Analysis of measured and calculated counterpart test data in PWR and VVER 1000 simulators," *Nuclear Technology and Radiation Protection*, vol. 20, no. 1, pp. 3–15, 2005.

[12] O. I. Melikhov, I. V. Elkin, I. A. Lipatov et al., "Post-test full experimental data report (test 4)," OECD PSB-VVER Project Report PSB-26, EREC, Electrogorsk, Russia, 2005.

[13] O. I. Melikhov, I. V. Elkin, I. A. Lipatov, M. P. Gashenko, and A. V. Kapustin, "Final AE comparison report," OECD PSB-VVER Project report PSB-29, EREC, Electrogorsk, Russia, 2008.

[14] I. V. Elkin, I. A. Lipatov, A. V. Kapustin et al., "Proposal teport test 5: large cold leg break," OECD PSB-VVER Project. PSB-VVER Report, PSB-28, EREC, Electrogorsk, Russia, 2008.

[15] A. Del Nevo, M. Adorni, F. D'Auria et al., "Benchmark on OECD/NEA PSB-VVER project test 5A: LB-LOCA transient in PSB-VVER facility," DIMNP NT 638(08) Rev. 2, University of Pisa, Pisa, Italy, 2009.

[16] I. V. Elkin, G. I. Dremin, I. A. Lipatov, and S. A. Galchanskaya, "Report about PSB-VVER heat losses, OECD PSB-VVER project," PSB-VVER REPORT, PSB-04, EREC, Electrogorsk, Russia, 2003.

[17] I. V. Elkin, M. A. Berezutskaya, G. I. Dremin, I. A. Lipatov, and I. A. Antonova, "Report about PSB-VVER hydraulic losses," OECD PSB-VVER Project, PSB-VVER Report, PSB-05, EREC, Electrogorsk, Russia, 2003.

[18] I. V. Elkin, A. I. Suslov, and O. I. Melikhov, "Experimental data deport test 5a (version 1)," OECD PSB-VVER Project, PSB-VVER REPORT, PSB-31, EREC, Electrogorsk, Russia, 2008.

[19] F. D'Auria, A. Bousbia-Salah, A. Petruzzi, and A. Del Nevo, "State of the art in using best estimate calculation tools in nuclear technology," *Nuclear Engineering and Technology*, vol. 38, no. 1, pp. 11–32, 2006.

[20] M. Bonuccelli, F. D'Auria, N. Debrecin, and G. M. Galassi, "A methodology for the qualification of thermalhydraulic code nodalizations," in *Proceedings of the 6th International Topical Meeting on Nuclear Reactor Thermalhydraulics (NURETH '93)*, Grenoble, France, October 1993.

[21] R. Bovalini, F. D'Auria, and M. Leonardi, "Qualification of the fast Fourier transform based methodology for the quantification of thermalhydraulic code accuracy," DCMN Report, NT 194 (92), Pisa, Italy, 1992.

[22] W. Ambrosini , , F. D'Auria, R. Bovalini, and F. D'Auria, "Evaluation of accuracy of thermal-hydraulic code calculations," *Energia Nucleare*, vol. 7, no. 2, pp. 5–16, 1990.

[23] A. Prosek, F. D'Auria, and B. Mavko, "Review of quantitative accuracy assessments with fast Fourier transform based method (FFTBM)," *Nuclear Engineering and Design*, vol. 217, no. 1-2, pp. 179–206, 2002.

[24] N. Muellner , E. , A. , F. D'Auria, E. Seidelberger, A. Del Nevo, and F. D'Auria, "Application of the fast Fourier transform based method (FFTBM) to assist in the qualification process of for the PSB-VVER1000 relap5," in *Proceedings of the International Conference Nuclear Energy for New Europe 2005*, vol. CD, Bled, Slovenia, September 2005.

Hindawi Publishing Corporation
Science and Technology of Nuclear Installations
Volume 2012, Article ID 238090, 11 pages
doi:10.1155/2012/238090

Research Article

RELAP5 Calculations of Bethsy 9.1b Test

Andrej Prošek

Reactor Engineering Division, Jožef Stefan Institute, Jamova Cesta 39, 1000 Ljubljana, Slovenia

Correspondence should be addressed to Andrej Prošek, andrej.prosek@ijs.si

Received 21 April 2011; Accepted 14 September 2011

Academic Editor: Klaus Umminger

Recently, several advanced computational tools for simulating reactor system behavior during real and hypothetical transient scenarios were developed. The TRAC/RELAP Advanced Computational Engine (TRACE) is the latest in a series of advanced, best-estimate reactor system codes developed by the United States Nuclear Regulatory Commission (US NRC). Nevertheless, the RELAP5/MOD3.3 computer code will be maintained in the next years. The purpose of the present study was to assess how the accuracy of Bethsy 9.1b test calculation depends on the US NRC RELAP5 code version used. Bethsy 9.1b test (International Standard Problem no. 27) was 5.08 cm equivalent diameter cold leg break without high-pressure safety injection and with delayed ultimate procedure. Seven different RELAP5 code versions were used and as much as possible the same input model. The obtained results indicate that the results obtained by the oldest and latest RELAP5 versions are in general comparable for Bethsy 9.1b test. This is very important for the validity of the results, obtained in the past with older RELAP5 versions. Due to the fact that observation was restricted to Bethsy 9.1b posttest, with its own physical phenomena, this conclusion could be generalized only for scenarios having similar range of the considered Bethsy transient conditions.

1. Introduction

Recently, several advanced computational tools for simulating reactor system behavior during real and hypothetical transient scenarios were developed. In the past, the United States Nuclear Regulatory Commission (US NRC) RELAP5 computer code was one of the most used in the international community. Since the release of RELAP5/MOD2 in 1985 the code was continuously improved and extended. Several new models, improvements to existing models, and user conveniences have been added to the latest RELAP5/MOD3.3 Patch 04 release in 2010 [1].

In the past, the Jožef Stefan Institute (JSI) activities in the area of RELAP5 analyses have been aimed also to extend the experiences in simulations of small break loss of coolant accidents (LOCAs) and two-phase natural circulation cooling. Therefore, its own RELAP5 input model of Bethsy facility [2] has been developed. The Bethsy-experiences-based improved modeling methods have been used in simulations of real plant transients and evaluation of plant accident management procedures [3–5]. In 1996 the BETHSY 9.1b test has been analyzed with three different versions of RELAP5 code (MOD2, MOD3.1, and MOD3.1.2 without any modification of the codes and with guidelines consideration) using experimental data [4]. The aim of this study was to perform calculations with to JSI available RELAP5 versions using as much as possible the same input model in order to see the differences between the code versions. Namely, in the past, typical comparisons were done between new and old versions, while this comparison covers the last 25 years of US NRC RELAP5 development.

2. Methodology Description

First the Bethsy experimental facility is described. Then the Bethsy 9.1b test is described. Then the RELAP5 code versions used are listed, followed by description of RELAP5 input model development. Finally, the calculations are described.

2.1. Description of Bethsy Integral Test Facility. Bethsy is an integral test facility, which was designed to simulate most pressurized water reactor accidents of interest, to study accident management procedures and to validate the computer codes. It is a scaled down model of three-loop Framatome (now AREVA NC) nuclear power plant with the thermal power 2775 MW (see Figure 1). Volume, mass flow, and power

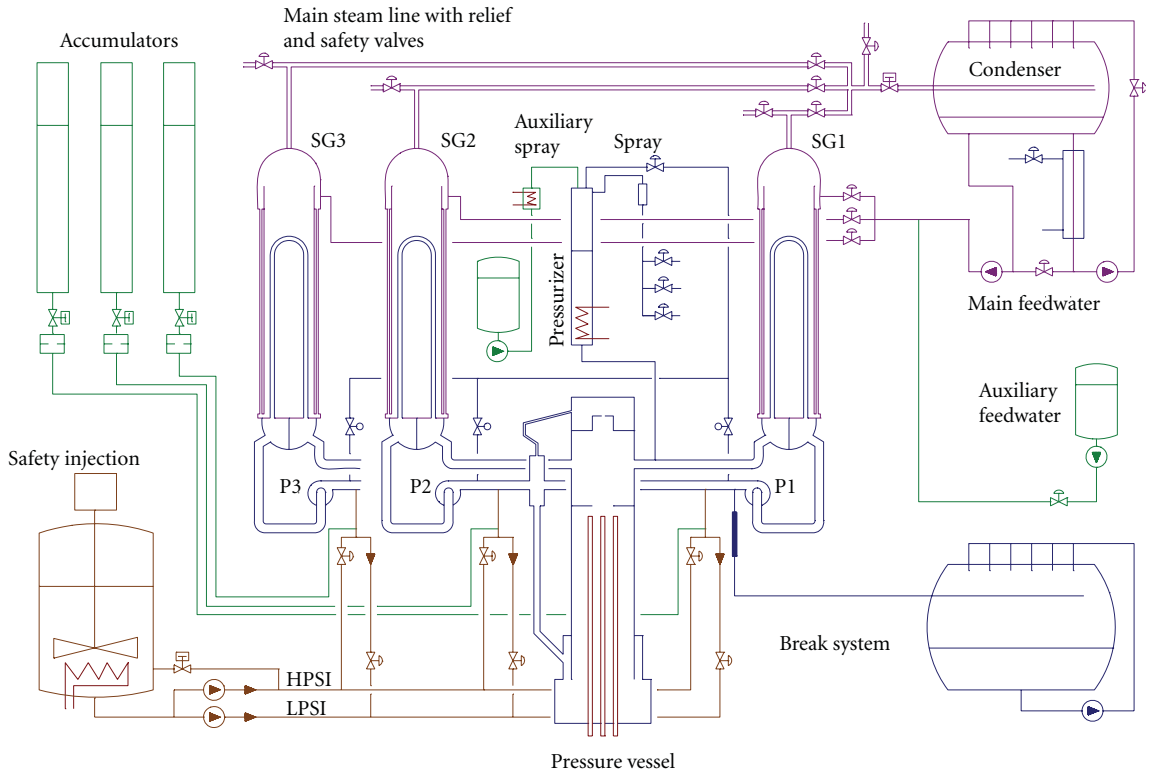

Figure 1: Bethsy facility.

are scaled to 1 : 96.9, while the elevations and the pressures of the primary and secondary systems are preserved [2]. The design pressure on the primary side is 17.2 MPa and on the secondary side 8 MPa. The power is limited to the decay heat level, therefore the transient without reactor trip cannot be simulated. The facility is equipped with all systems and measurement system needed for the performance and for observing the analyzed transients. The facility consists of pressure vessel, reactor coolant pumps and piping, heat tracing system, the system for break simulation, instrumentation, and the control systems. The core is cylindrical and is composed of 428 electrically heated rods and of 29 guide thimbles. The rods are arranged to the 17×17 core square lattice. The core power is 3 MW, which is 10% of the reference power considering scaling. The break system enables simulation of the break in different locations, that is, in cold leg, lower plenum, pressurizer, steam generator U tubes, and feedwater pipe. The instrumentation data system measures all data needed for the transient analysis. The control system can simulate the plant control systems and operator actions.

2.2. Description of 9.1b Test Performed in BETHSY Facility. The Bethsy 9.1.b test is a scaled 5.08 cm cold leg no. 1 break without high-pressure safety injection and with delayed operator action for secondary system depressurization. Due to core heatup the operator depressurized the secondary side by atmospheric relief steam dump valves. In the simulation this operator action was delayed. The test was analyzed in the frame of international standard problem 27 (ISP 27) performed to validate the thermal hydraulic computer codes. The test scenario was the following: break was opened in the cold leg no. 1 (initiation of the transient). When the maximum heater rod cladding temperature reache 723 K, the ultimate procedure is started by opening three steam line dumps to atmosphere. When pressurizer pressure dropped below 4.2 MPa, accumulators started to inject and they stopped to inject below 1.46 MPa. The low-pressure safety injection system was activated when the primary pressure was below 0.91 MPa. When stable residual heat removal system operating conditions prevailed, the transient was terminated.

2.3. Description of RELAP5 Computer Code. The US NRC RELAP5 computer code is one of the most widely spread system thermal hydraulic codes in the world. In spite of the fact that US NRC priority is TRACE [6], RELAP5 computer code is still maintained. In spite of its wide use, the RELAP5 is one-dimensional code and its importance will fall with time, especially when TRACE will be fully developed.

The basic RELAP5 thermal-hydraulic model uses six equations: two mass conservation equations, two momentum conservation equations, and two energy conservation equations. Closure of the field equations is provided through the use of constitutive relations and correlations. Since the release of RELAP5/MOD2 in 1985 the code was continuously improved and extended. Several new models, improvements to existing models, and user conveniences have been added to the latest RELAP5/MOD3.3 Patch 04 release in 2010. In Table 1 RELAP5 versions which were used in this study are listed.

Table 1: The RELAP5 code versions used.

Name	Version	Release date	Label
RELAP5/MOD2	36.05	March 1987	MOD2
RELAP5/MOD3	5M5	March 1990	MOD3
RELAP5/MOD3.1		March 1993	MOD3.1
RELAP5/MOD3.2.2 Beta	3.2jb	July 1998	MOD3.2
RELAP5/MOD3.3	3.3bf	February 2002	MOD3.3
RELAP5/MOD3.3 Patch03	3.3gl	March 2006	MOD3.3P3
RELAP5/MOD3.3 Patch04	3.3iy	October 2010	MOD3.3P4

2.4. RELAP5 Input Model Description. The RELAP5/MOD2 input model was developed, when participating to ISP-27. It was initialized according to the specified data for each test. Each of the three coolant loops was represented explicitly without taking into account the small asymmetry between the loops. The base RELAP5/MOD2 model of Bethsy facility for pretest calculations contained 196 volumes, 207 junctions, and 191 heat structures [7]. This base RELAP5/MOD2 input model was further upgraded to RELAP5/MOD3.1 and RELAP5/MOD3.1.2, which is shown in Figure 2 [7]. The base RELAP5/MOD2 input model was renodalized, increasing the number of nodes in reactor coolant system piping (from 9 to 45 nodes), reactor coolant pumps (2 nodes more not shown in Figure 2), core bypass sections (from 1 to 12 nodes), reactor vessels (two more in the head), and downcomers (from 5 to 14 nodes). The elevations of parallel volumes of the reactor downcomer, in bypass, reactor core, hot leg, and cold leg were preserved. Nodalization of the reactor core, pressurizer, reactor head, upper plenum, and lower plenum remained the same. This RELAP5 input model of Bethsy facility, called middle input model, is shown in Figure 2 and contains 332 volumes, 343 junctions, and 330 heat structures. This RELAP5 model was further refined, increasing the number of nodes in the steam generator. The U-tubes were modeled with 20 nodes instead of 10, and the downcomer and riser regions of steam generator were modeled with 11 nodes instead of five, which gives 22 more nodes per steam generator and 66 more nodes in total. The large RELAP5 input model of Bethsy facility thus contains 398 volumes, 408 junctions, and 396 heat structures. The nodalization study [4] showed that in general for most parameters and control variables there are no essential differences between the results of the more detailed and less detailed nodalizations. It was also found that a more detailed nodalization may lead to more accurate prediction of void fraction but it also may lead to less accurate prediction of other variables, for example, maximal cladding temperature. The developed RELAP5 input models [7] were extensively used to extend the experiences in simulations of small break loss of coolant accidents and two-phase natural circulation cooling. The Bethsy-experiencesbased improved modeling methods were used in the simulations of real plant transients and evaluation of plant accident management procedures.

Later, the middle input model was used for Bethsy 6.2TC [8] calculations by RELAP5/MOD3.2, with some slight nodalization changes. The junction from the guide tube to the upper plenum was removed based on previous experience and downcomer—upper head bypass volume has been subdivided into 3 volumes. Such model consisted of 335 volumes, 344 junctions, and 333 heat structures.

The detailed input model developed for Bethsy 9.1b test was used also for Bethsy 6.9c test calculations [9], with some minor modifications. There were some geometrical differences between both tests, and some elements from the detailed input model for Bethsy 9.1b test were excluded. Some new elements were introduced. A broad check on the consistency of the geometrical changes has been made by rerunning test 9.1, using the new modified model for test 6.9c. In the input model the following elements and systems are included: 377 volumes, 381 junctions, and 404 heat structures.

In 2000, a common RELAP5/MOD3.2 input model was developed based on the model developed for Bethsy 6.9c test, which evolved from the large input model. The common input model for all available Bethsy tests consisted of 398 volumes, 408 junctions, and 402 heat structures [10] (see Table 2). This input model is very similar to the large input model, with the exception that the vessel upper head was modeled with more nodes and only one auxiliary feedwater system was modeled in steady-state contributing to less nodes (in case of Bethsy 9.1b test two systems need to be defined, one before and one after ultimate procedure). The needed components were then added during restart calculation. This input model was adapted for the use of RELAP5/MOD3.3, with no changes in the geometry and the number of hydrodynamic components and heat structures. The hydrodynamic view was generated by SNAP from RELAP5 input model (in ASCII) and then arranged manually using Model Editor of SNAP (see Figure 3). The RELAP5/MOD3.3 input model in terms of SNAP consists of 141 hydrodynamic components and 72 heat structures. The difference is that pipes consist of several volumes; however they are considered as one component. Similar is the case with the heat structures.

2.5. Description of RELAP5 Calculations. Most of the calculations listed in Table 3 were performed in 2011. However, as middle input deck should be restored from the report [4] and RELAP5/MOD3 was not running on the SUN, for three calculations the archived results were used. The calculations presented in [4] were performed on SUN SPARCstation 20

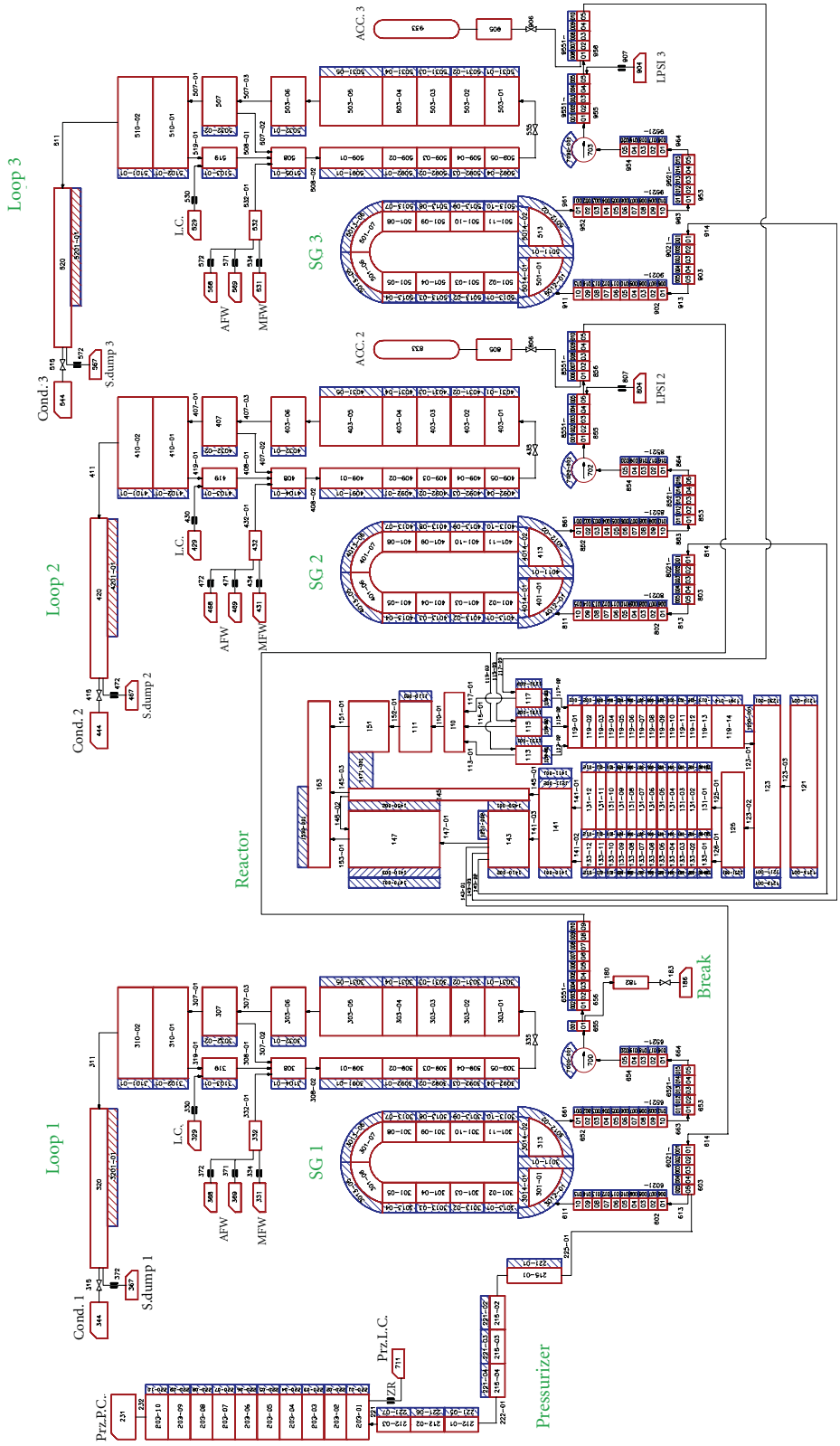

Figure 2: RELAP5/MOD3.1 input model of Bethsy facility.

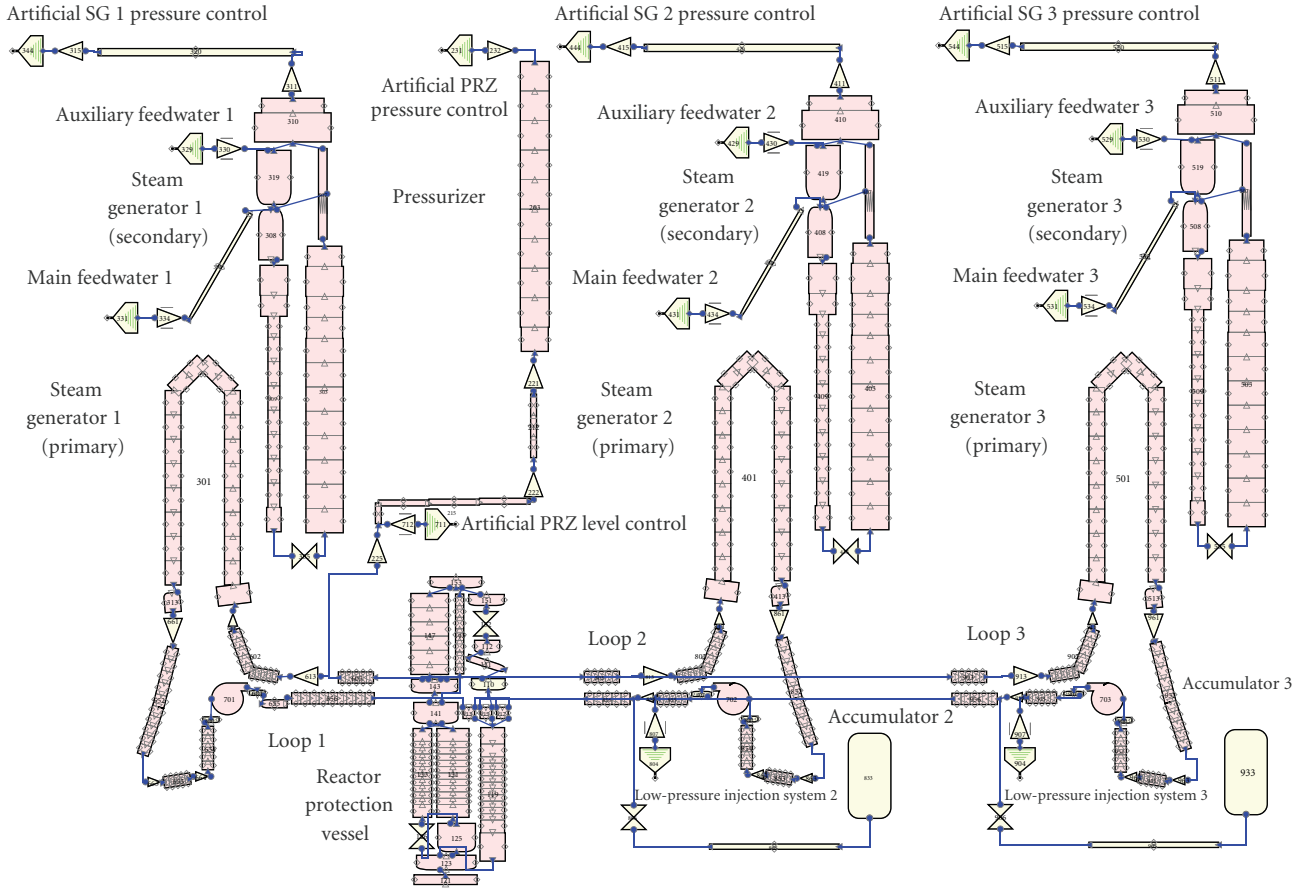

Figure 3: SNAP hydrodynamic component view of RELAP5/MOD3.3 input model of Bethsy facility.

Table 2: RELAP5 input models used.

Name	Label	Volumes	Junctions	Heat structures/mesh points
Small input model	(S)	198	207	191/754
Middle input model	(M)	332	343	330/1290
Large input model	(L)	398	408	396/1554
Common input model	(C)	398	408	401/1573

Table 3: RELAP5 calculations performed.

Analyzed Case	Code used	Input model used	Discharge coefficient	Machine	Operating system	Year
MOD2 (S)	RELAP5/MOD2	Small	0.85, 1.2	SUN	SOLARIS 9	2011
MOD3 (M)	RELAP5/MOD3	Middle	0.85, 1.2	SUN	SOLARIS 2.5	1998
MOD3.1 (M)	RELAP5/MOD3.1	Middle	0.8, 1.0, 1.1	SUN	SOLARIS 2.5	1998
MOD3.1 (C)	RELAP5/MOD3.1	Common	0.8, 1.0, 1.1	SUN	SOLARIS 9	2011
MOD3.2 (L)	RELAP5/MOD3.2	Large	N.A.	SUN	SOLARIS 8	2001
MOD3.2 (C)	RELAP5/MOD3.2	Common	0.8, 1.0, 1.1	SUN	SOLARIS 9	2011
MOD3.3 (C)	RELAP5/MOD3.3	Common	0.8, 1.0, 1.1	SUN	SOLARIS 9	2011
MOD3.3 P3 (C)	RELAP5/MOD3.3 Patch 03	Common	0.8, 1.0, 1.1	PC	Windows XP Sp3	2011
MOD3.3 P4 (C)	RELAP5/MOD3.3 Patch 04	Common	0.8, 1.0, 1.1	PC	Windows XP Sp3	2011

(4-processor workstation) which uses multiuser and multitasking operating system SOLARIS 2.5. The other calculations were performed on a SUN FIRE V880 server (with four UltraSPARC III 750-megahertz processors, with 16 gigabytes main RAM, running under the SOLARIS 9 operating system) except the RELAP5/MOD3.3 Patch 03 and Patch 04 running on PC. Finally, one calculation with large input model, very similar to common input model, was performed on a SUN Enterprise 450 workstation with a 4×400 megahertz central processing unit (CPU) and 4×2 gigabytes of random-access memory, running under a SOLARIS 8 operating system. The information on computers and operating systems is given as the code versions were created on the specific computers and the executables could not be moved to other computers. Without still running old SUN machines the calculations could not be performed without building the new executables (for PC versions this would be quite demanding). The objective of this study was not to study dependence on computers and operating systems. The platform dependency study has been done in [11] for RELAP5/MOD3.3 Patch 04, showing very small differences for the LOFT L2-5 test and no differences for the LOFT L3-7 test.

Also, it should be noted that RELAP5/MOD2 was not able to run large input model due to not enough virtual space furnished for unit = 54. Finally, as was previously mentioned, the study [7] concluded that more detailed nodalization can lead to more accurate prediction of void fraction which is very important for correct break discharge forecast. However, it also may lead to less accurate prediction of other variables as maximum cladding temperature in the case of MOD2 and MOD3.1.

3. Results

The results are shown in Figures 4, 5, 6, 7, 8, 9, 10, 11, 12, 13, and 14 for nine cases described in Table 3. For calculations not performed in 2011 some variables were missing in the archive. In such cases the calculation is labeled as N.A. Nevertheless, the majority of data was available. Also, as can be seen from Table 4, the cases with some missing variables have been performed at slightly different boundary conditions and nodalization details. According to [7] this influence is not so big; therefore the response could be assigned mostly to the code version. Also the discharge coefficients were as much as possible the same. In old RELAP5 versions two values of discharge coefficient were specified (subcooled and two phase), while in newer RELAP5 versions three values of discharge coefficient were specified (subcooled, two phase, and superheated).

3.1. Steady-State Calculation. The initial conditions for steady-state calculation are shown in Table 4. For the common input model the initial conditions are the same. Some very small differences are due to different code versions. Older the code version is, a bit larger they are. In the case of small, medium, and large input model the initial conditions were selected somewhat different compared to common model. However, they were within the measurement uncertainty. In general it can be said that the initial conditions were practically the same for all calculations.

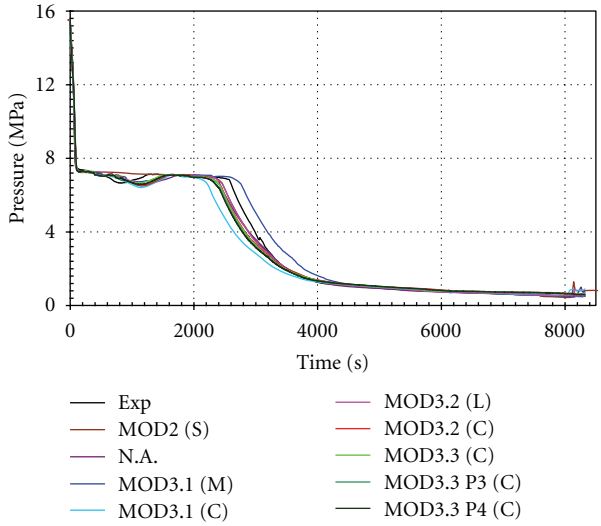

Figure 4: Pressurizer pressure.

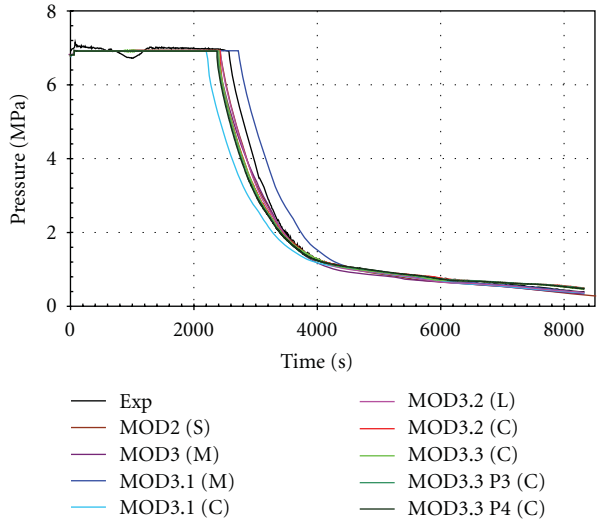

Figure 5: Secondary pressure.

3.2. Transient Calculation. Table 5 shows the sequence of the main events. The sequence of events is shown only for the calculations with the oldest and the latest RELAP5 version. The timing is similar for both code versions. After break opening the scram signal is generated, followed by safety injection (SI) signal. The main feedwater system is off and secondary pressure is kept constant until ultimate procedure initiation. The secondary inventory loss is recovered by auxiliary feedwater system operation. The primary pump is coasted down 300 s after SI signal. All these times are in quite close agreement with the experimental data. As high pressure injection is not available, the core starts to uncover and when maximum heater rod cladding temperature reaches 723 K, the ultimate procedure was started by opening three steam

Table 4: Initial conditions for Bethsy 9.1b test.

Parameter	Measured	MOD2 (S)	MOD3 (M)	MOD3.1 (M)	MOD3.1 (C)	MOD3.2 (L)	MOD3.2 (C), MOD3.3 (C), MOD3.3 P3 (C), MOD3.3 P4 (C)
Core thermal power (kW)	2864 ± 30	2864	2864	2864	2864	2864	2864
Cold leg temperature (per loop) (K)	559.9 ± 0.5	560.3	560.3	560.3	559.35	559.8	559.35
Downcomer mass flow rate (kg/s)	150.0 ± 5.0	151	152.7	154.3	154.1[a]	150.0	155.4
Reactor coolant pump speed (per loop) (rpm)	2940 ± 30	2970	2970	2940	2970	2970	2970
Pressurizer pressure (MPa)	15.51 ± 0.09	15.51	15.51	15.51	15.51	15.51	15.51
Pressurizer level (m)	4.08 ± 0.1	N.A.	N.A.	4.12	4.08	4.08	4.08
Reactor coolant system mass (kg)	1960	1948	1948	1948	1948	1949	1948
Secondary side pressure (per SG) (MPa)	6.91 ± 0.04	6.83	6.81	6.81	6.74	6.81	6.76
Steam generator level (per SG) (m)	13.45 ± 0.05	13.44	N.A.	13.45	13.20	13.14	13.25
Feedwater temperature (K)	491.1 ± 2.0	491.0	491.0	491.0	491.0	491.0	491.0
Secondary coolant mass (per SG) (kg)	820 ± 30	800	819	821	790	790	790
RCS trace heating (kW)	107.5	107.5[a]	107.5[a]	107.5[a]	107.5[a]	107.5[a]	107.5[a]

[a] No heat losses considering when the trace heating system is on; rather, heat losses are simulated after accumulator emptying.

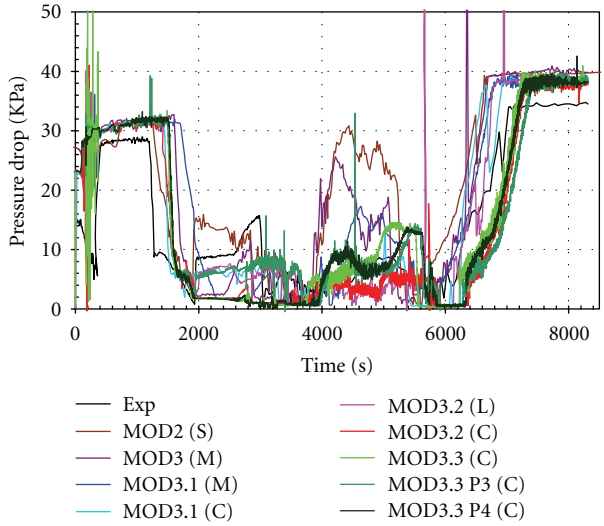

Figure 6: Cross-over leg 1 downflow side differential pressure.

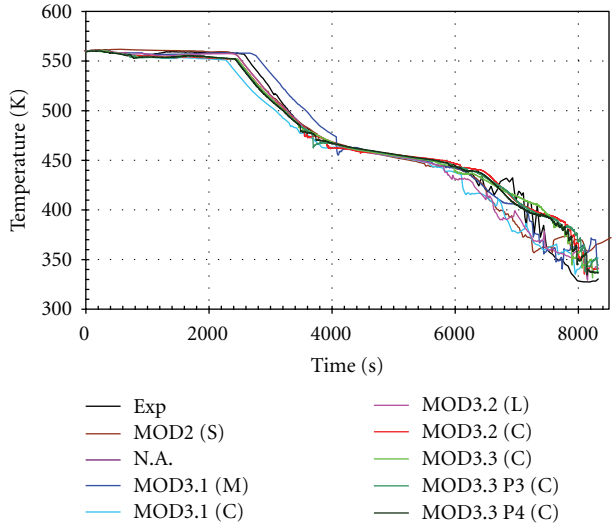

Figure 7: Core inlet temperature.

line dumps to atmosphere, in the calculations a bit earlier than in the experiment. This causes secondary pressure decrease, followed by primary system pressure decrease. When primary system dropped below the accumulator injection setpoint, the injection started and soon the cladding temperature started to decrease. Again the heatup in the calculation is earlier than in the experiment. Later the accumulators are emptied; however, cooling is established through the secondary side, and therefore the primary pressure decreases. Reaching the low-pressure injection system setpoint, the low-pressure injection started and the experiment lasted until the stable residual heat removal system conditions were reached.

In Figures 4–14 calculated results are shown for the main variables. As it is difficult to compare so many calculations, line colors are selected in such a way that MOD3.3 versions have green color palette, MOD3.2 are in red and pink, and MOD3.1 has blue palette. Pressurizer pressure is shown in Figure 4. It may be seen that all calculated lines are like a bunch except lines for RELAP5/MOD3.1 version. In addition, RELAP5/MOD2 calculation has no pressure drop around 1000 s as the other code versions. Similar is the situation for secondary pressure shown in Figure 5. Again RELAP5/MOD3.1 calculations are outside the bunch of lines. Figure 6 for crossover leg no. 1 downflow side differential pressure shows that the code versions behave much differently. The core inlet and outlet temperature lines shown in Figures 7 and 8 also look like a bunch. In addition, some differences appear also after low-pressure injection. For core outlet temperature shown in Figure 8 the calculated values are fluid temperatures only, which explains the mismatch with experimental data during the core heatup period, measuring mixture temperature. Break flow is shown in Figure 9 and mass discharged at the break in Figure 10. Up to 340 s the RELAP5/MOD2 deviates from the bunch, later the largest

Table 5: Sequence of main events for Bethsy 9.1b test.

Events	Time (s)		
	Exp	MOD3.3 P4 (C)	MOD2 (S)
Break opening	0	0	0
Scram signal (13.1 MPa)	41	32	39
Safety injection signal (11.9 MPa)	50	54	54
Main feedwater off, turbine bypass	54	58	58
Core power decay start (17 s after scram)	58	49	56
Auxiliary feedwater on (30 s after SI signal)	82	84	84
Pump coastdown start (300 s after SI signal)	356	354	354
End of pump coastdown	971	969	969
Start of the first core level depletion	1830	1841	1760
Start of second core uncover	2180	2102	2060
Ultimate procedure initiation	2562	2375	2410
Accumulator injection start (4.2 MPa)	2962	2750	2840
Primary mass inventory is minimum	2970	2750	2840
Maximum core cladding heatup	3053	2910	2900
Accumulator isolation (1.5 MPa)	3831	3809	3888
Low-pressure injection system start (0.91 MPa)	5177	5627	5139
End of test/calculation	8200 to 8330	8330	8900

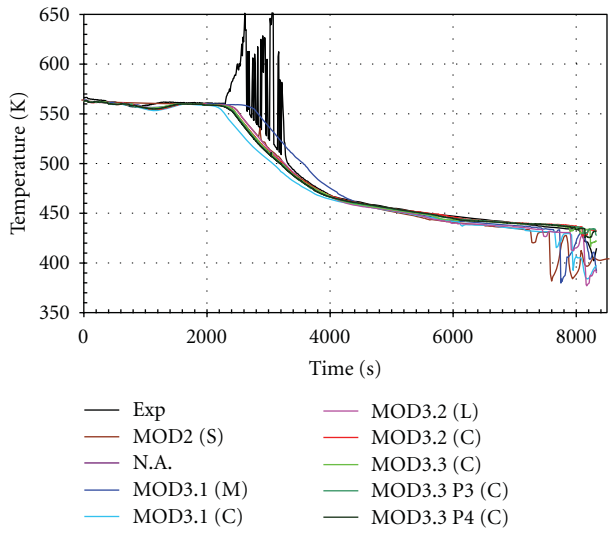

Figure 8: Core outlet temperature.

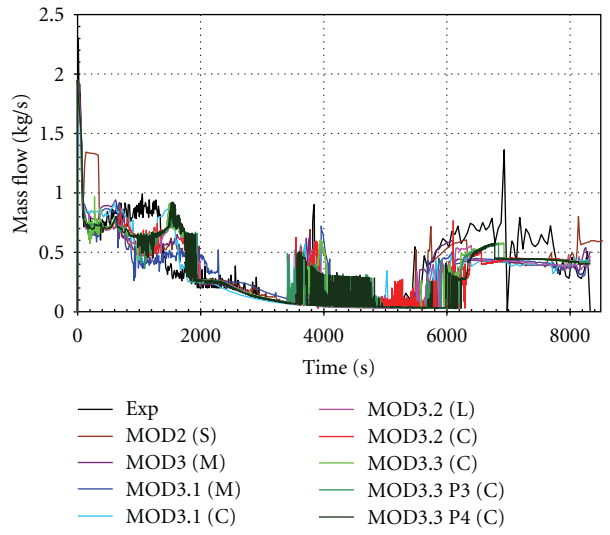

Figure 9: Break flow.

deviation is for RELAP5/MOD3.1, which causes earlier and later core heatup, as shown in Figure 11. The largest peak cladding temperature was obtained by RELAP5/MOD2 code, where the largest core uncovery was predicted as shown in Figure 12. Again only RELAP5/MOD3.1 calculations deviate from the bunch of lines. The time of low-pressure injection depends on the primary pressure prediction, showing a spectrum of delays, indicating that there are some differences between the code versions in spite of bunch behavior for most of the variables. Finally, Figure 14 shows the mass of the primary circuit. Mass is in the agreement with the mass discharged through the break and the mass injected with accumulators and low-pressure injection system. The differences are the largest at the end of transient, with the older RELAP5 version overpredicting and the newer versions underpredicting the mass.

3.3. Results Discussion. The results showed that qualitatively all RELAP5 versions in general produce similar results in spite of some differences in the boundary conditions and the nodalization details. Nevertheless, it may be very easily noted that RELAP5/MOD3.1 code is the only code version which more significantly deviates for some of the variables, mostly

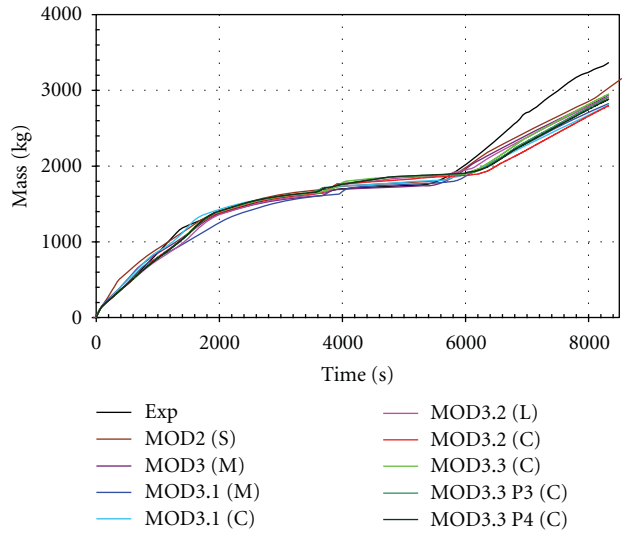

Figure 10: Mass discharged at the break.

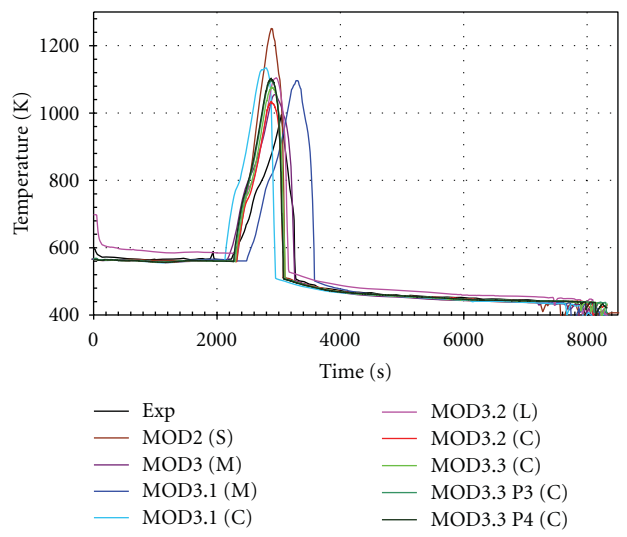

Figure 11: Maximum heater rod cladding temperature.

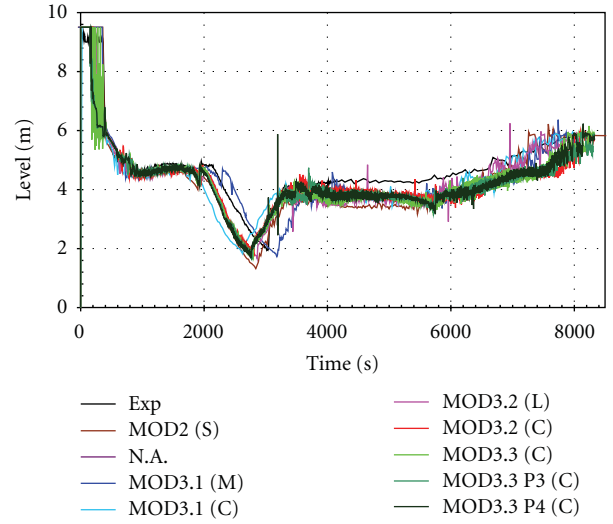

Figure 12: Core collapsed liquid level.

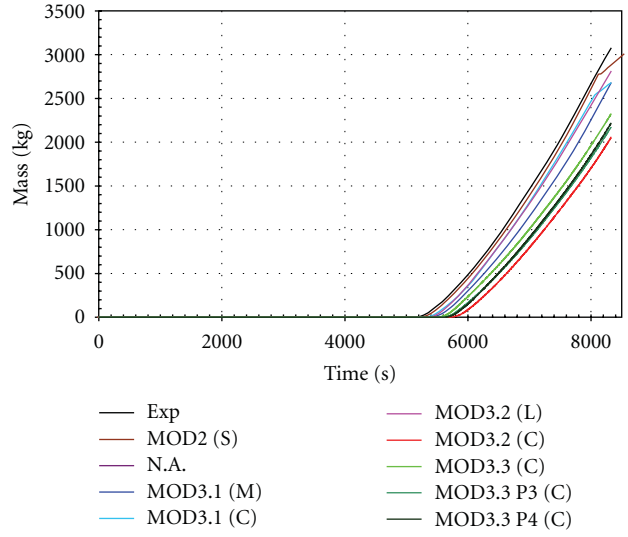

Figure 13: Injected mass by low-pressure system.

due to timing of heatup start, influencing the ultimate heat procedure initiation.

For peak cladding temperature the largest deviation from measured peak cladding temperature was obtained for RELAP5/MOD2 version. This may be due to small nodalization used. When referring to [7], it can be seen that large nodalization produces lower peak cladding temperatures. For RELAP5/MOD3.1 the difference is of the order 100 K, while the difference between small and middle versions is of the order 50 K. As RELAP5/MOD2 code version is limited by virtual memory for the code version we had, the calculation with common model was not possible. When looking the break flow one must be aware that RELAP5 old versions use only two discharge coefficients, while newer versions use three discharge coefficients. Nevertheless, based on Figures 9 and 10 significant differences were only for RELAP5/MOD2 calculation in the initial time interval from 100 s to 300 s (overprediction) and RELAP5/MOD3 calculation in the time interval 1000 s to 3000 s (underprediction).

An important aspect was also second loop seal clearing due to condensation in the cold legs following the accumulator injections, which plays an important role upon the conditions of core temperature turnaround. When looking cross-over leg 1 downflow side differential pressure shown in Figure 6 it may be seen that the RELAP5 code versions do not predict the second loop seal clearing exactly in the same manner as seen in the test data. In the time interval from 2000 s to 4000 s the code versions are qualitatively different (even RELAP5/MOD3.3 Patch 03 and RELAP5/MOD3.3 Patch 04). When the accumulator stopped to inject, the older RELAP5 versions (MOD2 and MOD3) overpredicted differential pressure in the time interval 4000 s to 6000 s.

In spite of the fact that significant development of the RELAP5 code was done, based on the obtained results one

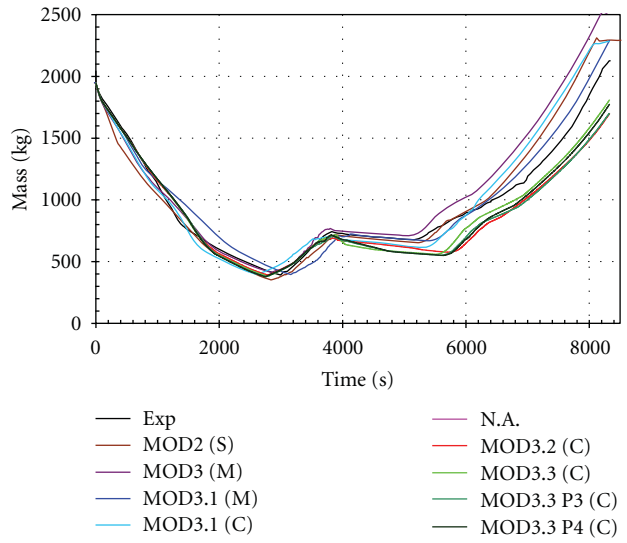

Figure 14: Primary system mass.

may conclude that the frozen RELAP5/MOD2 code can give comparable results to those of the latest RELAP5/MOD3.3 Patch 04 computer code. The agreement is good for the main variables describing the transient conditions such as pressures, temperatures, and system mass. On the other hand, for special phenomena of interest significant differences may appear, for example, break flow and condensation. It should be noted that the code accuracy was judged on the comparison of the trends. Due to the fact that the observation was restricted to the Bethsy 9.1b test, with its own physical phenomena, this conclusion could be generalized for scenarios having similar range of the considered Bethsy transient conditions. Nevertheless this does not mean that no development was made in the newer RELAP5 code versions or that development was not needed. Rather, the Bethsy 9.1b test was performed at the time when the RELAP5/MOD2 was developed and the code version had the capabilities to simulate most important phenomena, which occurred during Bethsy 9.1 test. On the other hand, the JSI calculation was among the top ranked as judged by fast Fourier transform method for code accuracy quantification [12, 13] and further improvements are more difficult. These are one of the reasons why calculations performed later with newer versions were comparable, besides the fact that several developments were done to other phenomena not occurring or not important during such transient conditions, for example, the 3D phenomena and neutronics. Therefore it is not surprising that the RELAP5 results for the selected Bethsy 9.1b test are almost as good as the results obtained by TRACE computer code using RELAP5 converted input model [14]. This is in agreement with the conclusion in [15] that maturity of thermal hydraulic codes was recognized also in the US NRC code consolidation program and further development was considered necessary only in specific areas, for example, multidimensional and multiphysics treatment of phenomena and transport of interfacial area. The development of thermal hydraulic codes was needed also because of special models for advanced reactors, for example, passive systems.

4. Conclusions

The Bethsy 9.1b test, which is 5.08 cm equivalent diameter cold leg break without high-pressure safety injection and with delayed ultimate procedure, was simulated by different RELAP5 code versions using input models, originating from the same RELAP/MOD2 posttest input model developed at Jožef Stefan Institute. The results showed that the calculations obtained by different RELAP5 versions are in general comparable, with the exception that RELAP5/MOD3.1 shows some deviations in timing of the heatup initiation. The agreement is good for the main variables describing the transient conditions such as pressures, temperatures, and system mass. On the other hand, for special phenomena of interest significant differences may appear, for example, break flow and condensation. This is very important for the validity of the results, obtained in the past with older RELAP5 versions. Due to the fact that observation was restricted to Bethsy 9.1b posttest, with its own physical phenomena, this conclusion could be generalized for scenarios having similar range of the considered Bethsy transient conditions. Nevertheless, development of RELAP5 was needed in the past, for example, RELAP5/MOD2 has limitations on the number of hydrodynamic components (limited nodalization details), which may influence the results. Finally, this example confirmed that the RELAP5 code performs satisfactorily for what was intended, while development of new U.S. NRC TRACE code replacing U.S. NRC RELAP5 has been primarily needed to extend the code capabilities, for example, multidimensional and multiphysics treatment of phenomena and special models needed for advanced passive reactors. Of course, modernization of the codes to current computers and higher accuracy is also a constant goal of code developers.

Acknowledgments

The author acknowledges the financial support from the state budget by the Slovenian Research Agency Program no. P2-0026 and financial support from Slovenian Nuclear Safety Administration and Krško Nuclear Power Plant by Project no. POG-3473.

References

[1] USNRC, "RELAP5/MOD3.3 code manual," Patch 04, Vols. 1 to 8, Information Systems Laboratories, Inc., Rockville, Maryland, Idaho Falls, Idaho, prepared for USNRC, 2010.

[2] CEA, "BETHSY, General Description," Note SETh/LES/90-97, CEA (Commissariat à l'énergie atomique et aux énergies alternatives), Grenoble, France, April 1990.

[3] S. Petelin, B. Mavko, I. Ravnikar, and Y. A. Hassan, "Data transfer from BETHSY 9.1b experiment to real NPP," in *Proceedings of the ASME International Mechanical Engineering Congress and Exposition*, vol. 21, pp. 71–80, American Society of Mechanical Engineers, New York, NY, USA, November 1997.

[4] S. Petelin, B. Mavko, I. Ravnikar, P. Cebull, and Y. A. Hassan, "Nodalization study for BETHSY experiment," in *Proceedings of the 4th ASME/JSME International Conference on Nuclear*

Engineering, vol. 1, pp. 955–962, New Orleans, La, USA, March 1996.

[5] S. Petelin, B. Mavko, B. Končar, and Y. A. Hassan, "Scaling of the small-scale thermal-hydraulic transient to the real nuclear power plant," *Nuclear Technology*, vol. 158, no. 1, pp. 56–68, 2007.

[6] U. S. Nuclear Regulatory Commission, TRACE V5.0 User Manual, Division of Risk Assessment and Special Projects, Office of Nuclear Regulatory Research, Washington, DC, USA.

[7] S. Petelin, B. Mavko, O. Gortnar, I. Ravnikar, and G. Černe, "Result of BETHSY test 9.1.b using RELAP5/MOD3," (NUREG/IA, 0141), U.S. Nuclear Regulatory Commission, Washington, DC, USA.

[8] S. Petelin and B. Končar, "RELAP5/MOD3.2 assessment on the BETHSY 6.2TC SBLOCA test," in *Proceedings of the 4th Regional Meeting, Nuclear Energy in Central Europe*, Bled, Slovenia, September 1997.

[9] S. Petelin, B. Mavko, and M. Jurkovič, "BETHSY—loss of the residual heat removal system during mid-loop operation," in *Proceedings of the 5th International Conference on Nuclear Engineerin*, pp. 1–10, The American Society of Mechanical Engineers, New York, NY, USA, May 1997.

[10] S. Hrvatin, A. Prošek, and I. Kljenak, "Quantitative assessment of the BETHSY 6.2 TC test simulation," in *Proceedings of the 8th International Conference on Nuclear Engineering*, The American Society of Mechanical Engineers, New York, NY, USA, 2000.

[11] RELAP5/MOD3.3 Patch04 PLATFORM DEPENDENCY, Information Systems Laboratories, Inc. Rockville, Maryland and Idaho Falls, Idaho, USA, 2010.

[12] F. D'Auria, M. Leonardi, and R. Pochard, "Methodology for the evaluation of thermalhydraulic codes accuracy," in *Proceedings of the International Conference on New Trends in Nuclear System Thermohydraulics*, Pisa, Italy, May-June 1994.

[13] A. Prošek, "Code accuracy evaluation of BETHSY experiments using FFTBM and SARBM," in *Proceedings of the Annual Meeting on Nuclear Technology*, Stuttgart, Germany, May 2002.

[14] A. Prošek and O.-A. Berar, "Analysis of small-break loss-of-coolant accident test 9.1b at BETHSY facility with TRACE and RELAP5," in *Proceedings of the International Congress on Advances in Nuclear Power Plants (ICAPP '11)*, Nice, France, May 2011, Paper 11160.

[15] "OECD/NEA," in *Proceedings of the Workshop Advanced Thermal-Hydraulic and Neutronic Codes: Current and Future Applications*, Barcelona, Spain, April 2000, Report NEA/CSNI/R(2001)2/VOL1.

Hindawi Publishing Corporation
Science and Technology of Nuclear Installations
Volume 2012, Article ID 439374, 12 pages
doi:10.1155/2012/439374

Research Article

The Integral Test Facility Karlstein

Stephan Leyer and Michael Wich

Department PTBD-G, AREVA NP GmbH Germany, Kaiserleistr 29, 63067 Offenbach, Germany

Correspondence should be addressed to Stephan Leyer, stephan.leyer@areva.com

Received 23 March 2011; Accepted 3 September 2011

Academic Editor: Klaus Umminger

The Integral Test Facility Karlstein (INKA) test facility was designed and erected to test the performance of the passive safety systems of KERENA, the new AREVA Boiling Water Reactor design. The experimental program included single component/system tests of the Emergency Condenser, the Containment Cooling Condenser and the Passive Core Flooding System. Integral system tests, including also the Passive Pressure Pulse Transmitter, will be performed to simulate transients and Loss of Coolant Accident scenarios at the test facility. The INKA test facility represents the KERENA Containment with a volume scaling of 1 : 24. Component heights and levels are in full scale. The reactor pressure vessel is simulated by the accumulator vessel of the large valve test facility of Karlstein—a vessel with a design pressure of 11 MPa and a storage capacity of 125 m^3. The vessel is fed by a benson boiler with a maximum power supply of 22 MW. The INKA multi compartment pressure suppression Containment meets the requirements of modern and existing BWR designs. As a result of the large power supply at the facility, INKA is capable of simulating various accident scenarios, including a full train of passive systems, starting with the initiating event—for example pipe rupture.

1. Introduction

The KERENA is a medium-capacity boiling water reactor (BWR). It combines passive safety systems with active safety equipment of service-proven design. The passive systems utilize basic laws of physics, such as gravity and natural convection, enabling them to function without electric power or actuation by electric instrumentation and control (I&C) equipmentThey are designed to bring the plant to a safe and stable condition without the aid of active systems. Furthermore, the passive safety features reduce the number of active systems, significantly reducing costs, while providing a safe, reliable, and economically competitive plant design [1, 2].

The Integral Test Facility Karlstein (INKA) test facility was designed and erected to experimentally analyze the passive safety systems of KERENA. Therefore, all passive safety features necessary to simulated accident scenarios (loss of coolant accident [LOCA] and non-LOCA) are included in the design. The following section gives a brief description of these passive systems. The INKA setup simulates the KERENA Containment in a 1 : 24 scale. Component size and levels are full scale in order to match the driving forces for natural circulation in systems. The steam accumulator vessel of the large valve test facility in Karlstein represents the reactor pressure vessel.

At INKA, the systems can be tested individually analyzing their performance, and during integral tests analyzing the interaction between the systems and therefore the capability of the KERENA passive systems performing their design function. Even as KERENA is the reference for INKA, other tests dealing with generic tasks for BWR plants or even other Light Water Reactor design could be performed. The detailed instrumentation concept also allows investigation of several single effect problems. Within this paper, the design of the test facility and the potential of the test facility will be shown. The instrumentation concept will also be briefly explained.

For Generation III BWRs, like for example, the ESBWR (formerly SBWR), several test programs at the test facilities PANDA [3, 4], PUMA [5], and Giraffe [6] have been performed to validate the passive safety features. Recently, tests for the passive containment cooling system for the ABWR have been performed at the TIGER test facility [7, 8]. The qualification program for the AP 1000 passive safety system has been done at the APEX and SPES test facilities [9–14].

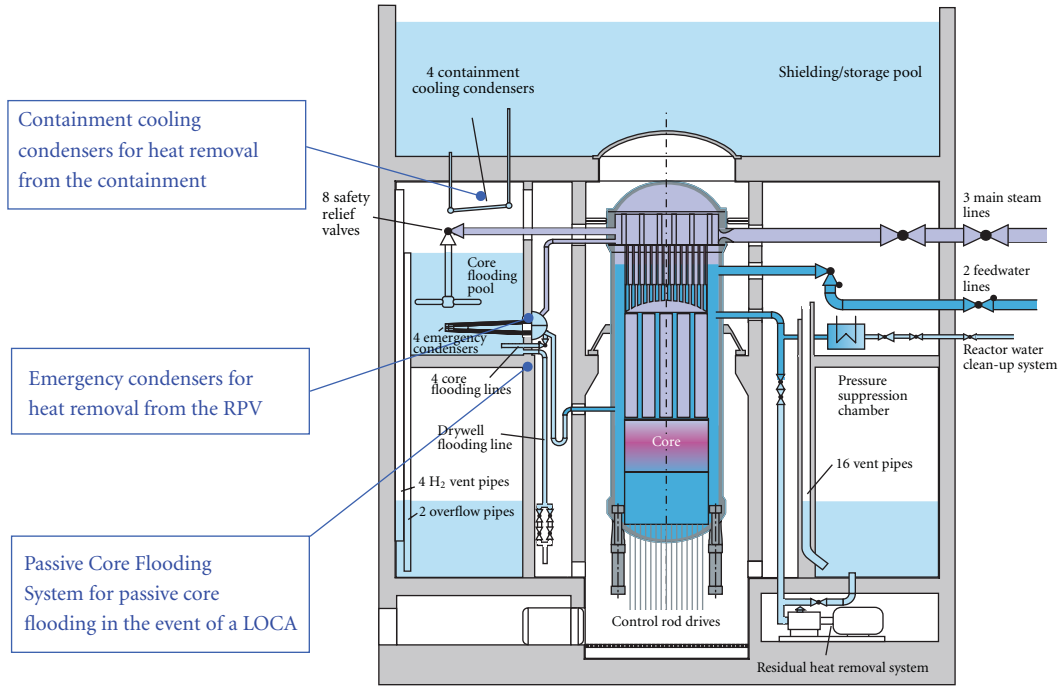

Figure 1: Section through KERENA containment with passive safety systems to be tested at INKA. (Passive Pressure Pulse Transmitter is shown in Figure 2.)

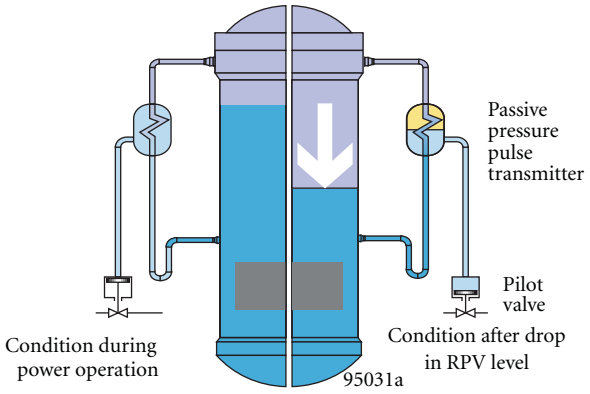

Figure 2: Operating Principle of the Passive Pressure Pulse Transmitter.

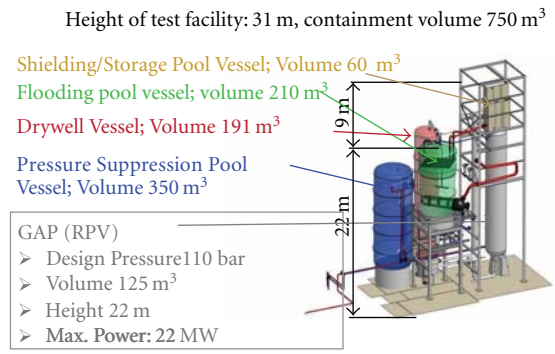

Figure 3: 3-D Image of INKA Test Facility at Karlstein.

2. Passive Safety Systems at INKA

Figure 1 shows a section through the KERENA containment with the passive safety systems that are included in the INKA design. The Passive Pressure Pulse Transmitter is illustrated in Figure 2. In the event of an accident, the Passive Pressure Pulse Transmitters actuate reactor scram, containment isolation, and an automatic depressurization of the reactor pressure vessel. They operate without any power supply or actuation by electronic I&C signals, activating their designated functions as a result of a drop of the reactor pressure vessel water level.

The Emergency Condenser (see Figure 1) system is provided to remove residual heat from the reactor after shutdown. It consists of four tubular heat exchangers with a nominal heat transfer capacity of about 60 MW each. During normal plant operation, the heat exchanger tubes are full of water and the Emergency Condenser is not in operation. If there is a drop in reactor pressure vessel water level after, for example, a reactor scram caused by an LOCA, steam fills the tubes and the Emergency Condenser operates. The efficiency of the Emergency Condenser increases with increasing reactor pressure and decreasing reactor water level. The temperature of the Core Flooding Pools and the Containment pressure (on the secondary side of the heat exchanger) have only a small effect on Emergency Condenser efficiency. The Containment Cooling Condenser

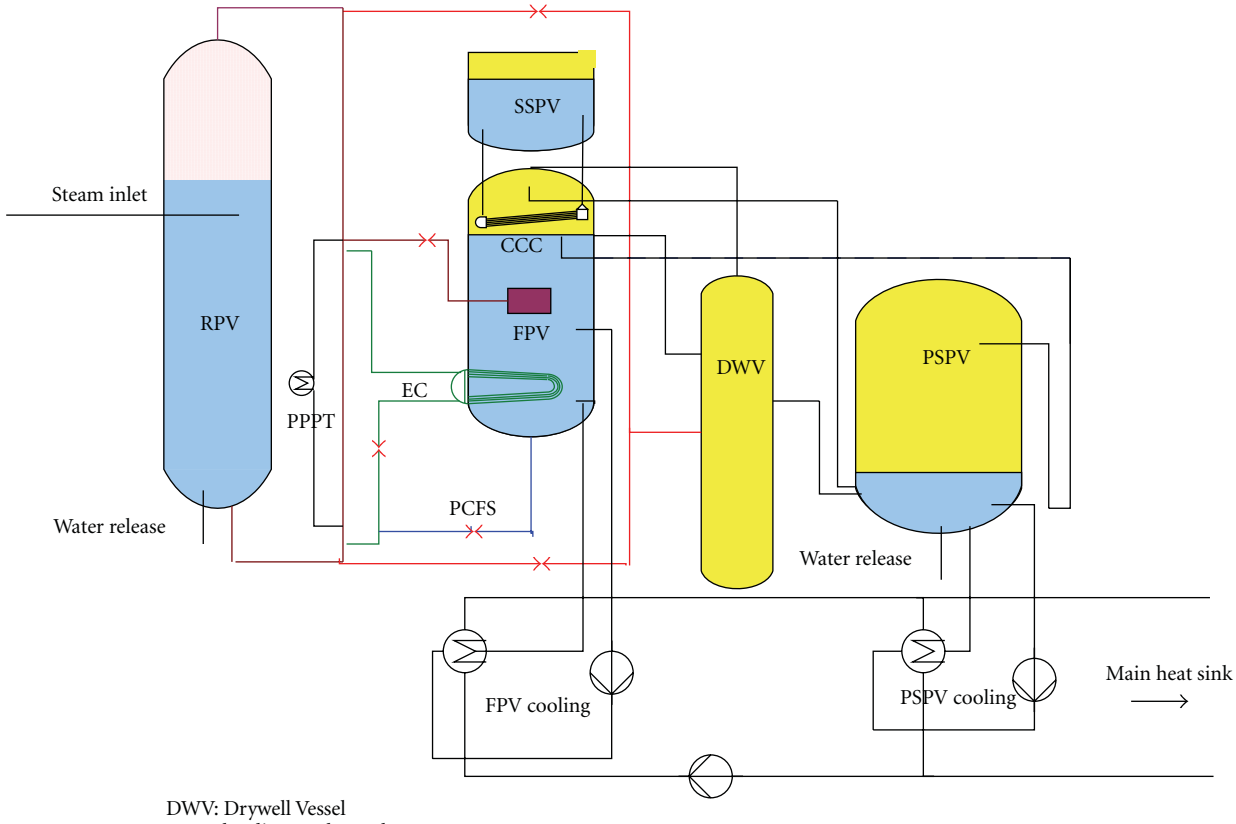

Figure 4: Simplified P&ID of the INKA Test Facility.

is designed to ensure long-term containment heat removal (for a grace period of approximately three day). The system also consists of four tubular heat exchangers. The tubes of each Containment Cooling Condensers are filled with water from the shielding/storage pool above the containment. Steam released into the drywell in the event of an accident condenses on the primary side of the Containment Cooling Condenser (inside the containment). The water inside the Containment Cooling Condenser tubes heats up, causing natural circulation to be established. The efficiency of the system increases with increasing containment pressure. The Emergency Condenser and Containment Cooling Condenser together represent the passive cooling chain connecting the heat source (reactor pressure vessel) with the heat sink—the shielding/storage pool located above the containment.

The Passive Core Flooding System is designed to ensure sufficient core cooling in the event of an LOCA. A check valve opens as soon as the pressure difference between the reactor pressure vessel and the Core Flooding Pools reaches a defined value. Water then flows from the pools into the reactor pressure vessel. The components of the passive systems are installed in a full-scale configuration at INKA.

3. INKA Test Setup

The INKA test facility has been designed for performing steady-state full-scale Emergency Condenser, Containment Cooling Condenser, Passive Core Flooding System, and Passive Pressure Pulse Transmitter tests and for simulating transients/LOCA conditions in a smaller-scaled configuration [15]. The Passive Pressure Pulse Transmitter is used to actuate the safety-relief valve during the tests. The Containment volumes are modeled to a scale of 1 : 24. The interconnecting piping is designed such that the pressure drops match those of a real KERENA plant. Instrumentation is provided to determine the heat transfer capacity of the components as well as the thermodynamic conditions in the vessels simulating the various KERENA containment compartments.

The vertical distances between components, water levels, floors, and ceiling of the KERENA containment that are important for the performance of the tested components are simulated in full scale at INKA. Figure 3 is a 3D computer image of the test facility. The vessel water and gas volumes result from downscaling of the KERENA volumes by a factor

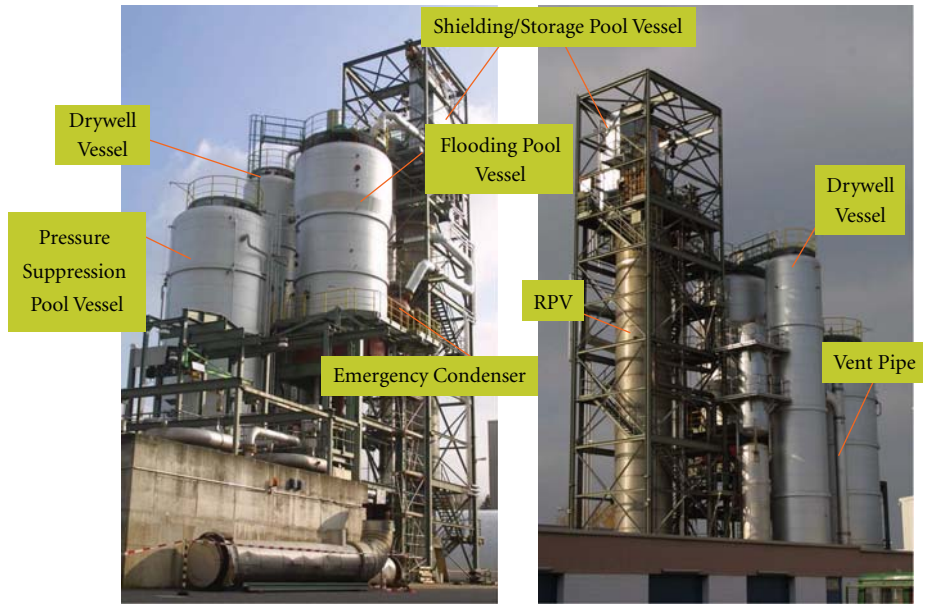

Figure 5: Picture of the INKA Test Facility from two different views.

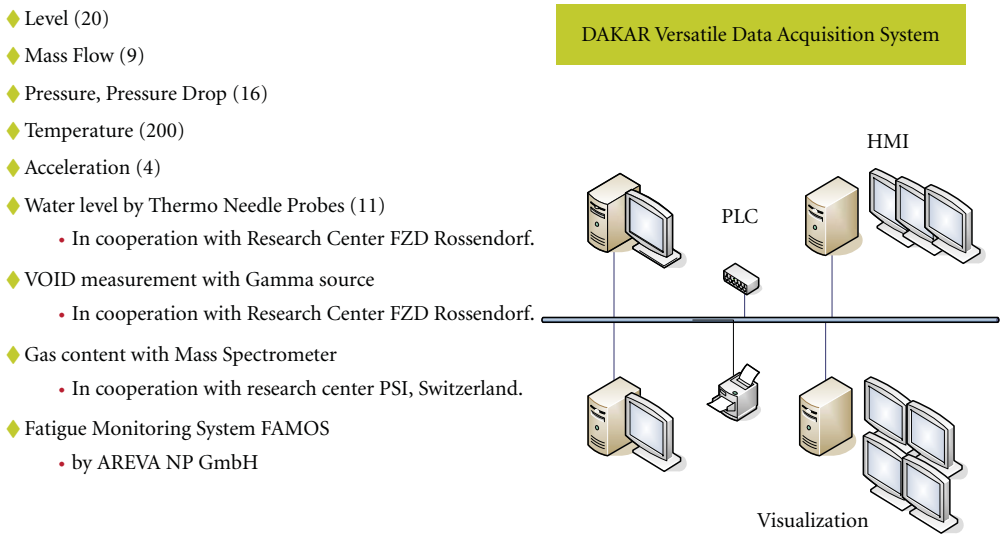

Figure 6: Instrumentation and Data Acquisition System.

of 1 : 24. The volume of the vessels and the test facility height are given in Figure 3.

INKA is integrated into the Large-Valve Test Facility Grossarmaturen-Prüfstand (GAP) that has been in operation in Karlstein for many years. The GAP test facility consists of a steam accumulator (height: 21.7 m, volume: 125 m^3) fed by a 22-MW boiler. This accumulator (GAP Vessel—in the following called pressure vessel) will supply the steam needed for the experiments and will replicate the reactor pressure vessel in the integral tests. An additional vessel with a water volume of about 50 m^3 is placed inside the GAP support frame at the top. This vessel simulates the shielding/storage pool and will therefore supply water for the secondary side of the Containment Cooling Condenser. The containment will be simulated by three vessels.

The Flooding Pool Vessel represents the core flooding pools that contains the Emergency Condenser and the Containment Cooling Condenser. The Passive Core Flooding System connects the Flooding Pool Vessel with the return line of the Emergency Condenser. The Passive Pressure Pulse Transmitter is connected to the down comer line. The Drywell Vessel simulates the residual gas volume of the drywell. The Pressure Suppression Pool is simulated by a third vessel.

During tests of the individual passive components, only the Flooding Pool Vessel is needed.

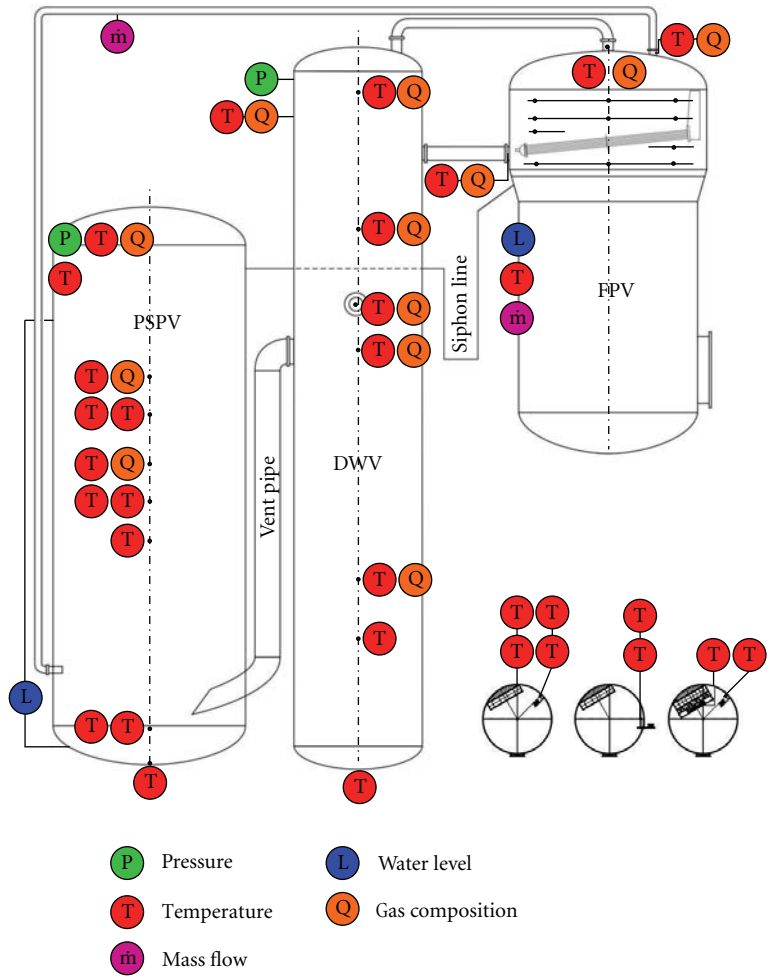

Figure 7: Drawing of the INKA vessel instrumentation.

For the integral transient and LOCA experiments, all vessels and components are in use.

Figure 4 shows a simplified P&ID of the INKA test facility with the containment vessels Flooding Pool Vessel, Drywell Vessel, and Pressure Suppression Pool Vessel. Two pipes connect the Flooding Pool Vessel with the Drywell Vessel and represent the connections between the gas spaces of these compartments. The Flooding Pool Vessel is connected to the Pressure Suppression Pool Vessel via the overflow pipe limiting the Flooding Pool Vessel water level. A second connection is the hydrogen overflow pipe used for pressure limitation during severe accident mitigation at KERENA. The Drywell Vessel and the Pressure Suppression Pool Vessel are connected via a full-scale vent pipe. Additionally, the function of the Safety and Relief valve is included in the design. The system is connected to the down comer line and goes into the Flooding Pool Vessel. For LOCA test scenarios, two different lines enter the Drywell Vessel, one for the simulation of breaks of a water line and the other for breaks of a steam line.

The water of the Flooding Pool Vessel and the Pressure Suppression Pool Vessel can be cooled down via two pool cooling systems. These systems are used for the preconditioning of the test facility and can be used for the experimental simulation of active system accident management. At KERENA, the active heat removal from the containment is done via the cooling of the Core Flooding Pools and the Pressure Suppression Pool. Active core cooling and flooding of the KERENA reactor pressure vessel is done via low pressure injection systems injecting water taken from the wetwell into the reactor pressure vessel. Currently no such active low pressure injection is installed at INKA. The impact of this active system can be simulated be removing water from the Pressure Suppression Pool Vessel and water introduction into the pressure vessel.

Figure 5 shows two pictures of the test facility taken from two different views.

4. Instrumentation Concept

Figure 6 gives an overview of the sensors installed at the INKA test facility. Overall, there are more than 300 sensors available at INKA. Most of them are conventional instrumentation like temperatures, mass flow measurements, pressures,

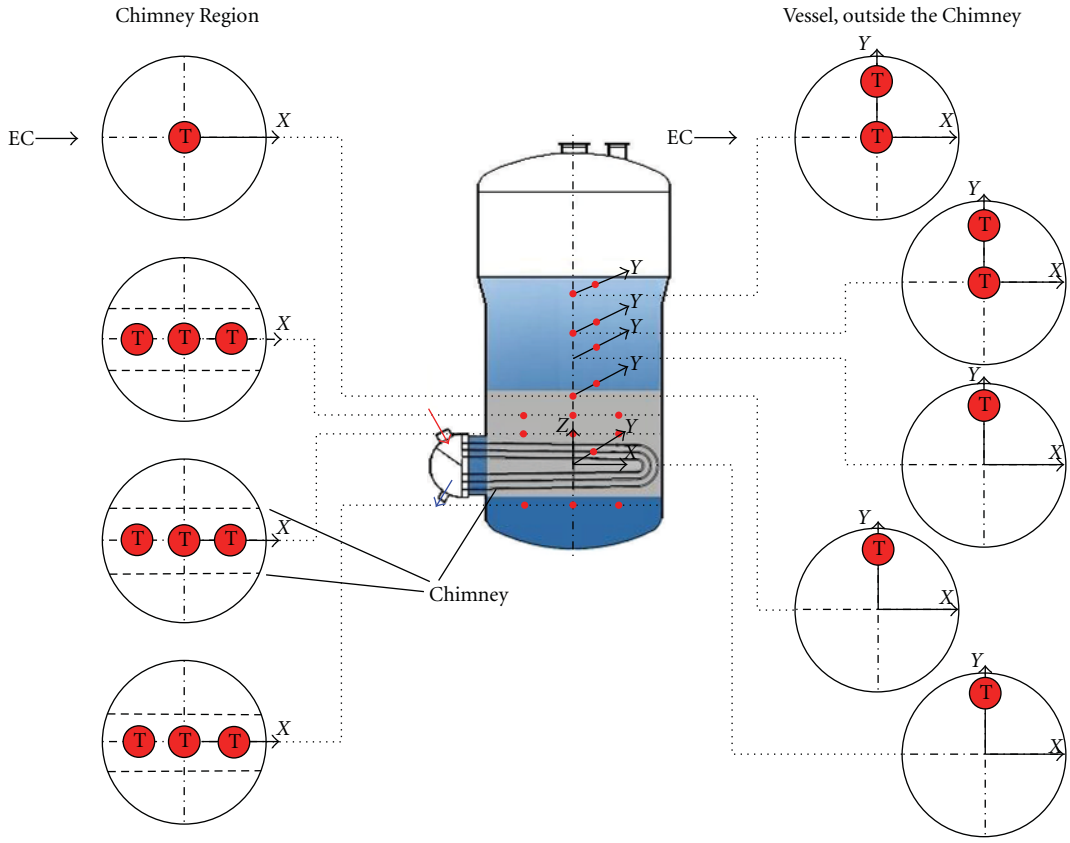

Figure 8: Instrumentation of the water volume of the Flooding Pool Vessel.

and differential pressure sensors. Additionally, two-phase flow instrumentation (Thermo Needle Probes and Gammadensitometer) in cooperation with Forschungszentrum Dresden/Rossendorf (FZD) is installed. The gas mixture in the vessels is measured via a probe sampling system analyzed by a mass spectrometer (cooperation with Paul Scherrer Institut in Switzerland). In the Emergency Condenser condensate line, the AREVA Fatigue Monitoring System (FAMOS) is tested under plant relevant conditions.

The data acquisition system Data Acquisition System Karlstein (DAKAR), which was developed by AREVA in Karlstein, is used. The system allows the time synchronized combination of fast and slow data recording.

4.1. Instrumentation of the Test Vessels. Figure 7 gives an overview of the instrumentation of the INKA vessels. The Flooding Pool Vessel has the highest sensor density due to the fact that this vessel contains the passive systems Emergency Condenser and Containment Cooling Condenser. The Pressure Suppression Pool Vessel has thermocouples in the water volume at four different levels, located in three different chains (parallel to the vessel axis). In the gas space of the vessel, the temperature field is measured at five levels in the same three chains. At all levels in the gas space, the thermocouples at the chain in the center line of the vessel are connected to a gas probe sampling sensor. Like in all other vessels, the pressure and the water level is measured.

In the Drywell Vessel, the gas temperature is measured at six levels. The upper five levels are equipped with a probe sampling sensor.

The instrumentation of the water space in the Flooding Pool Vessel is shown in Figure 8. The temperature of the water space is measured at nine levels along the vessel axis and on a parallel chain outside the chimney of the Emergency Condenser bundle. Like in the other two vessels, the pressure and the water level is measured. In the Flooding Pool Vessel, the water level cannot exceed the level of the inflow of the overflow pipe connecting the Flooding Pool Vessel with the Pressure Suppression Pool Vessel. The gas space of the Flooding Pool Vessel is extensively instrumented with thermocouples and probe sampling sensors in order to determine the impact on gas compositions to the heat transfer capacity of the Containment Cooling Condenser and the influence of the Containment Cooling Condenser operation to gas and temperature stratification (see Figure 9).

The Emergency Condenser system instrumentation is shown in Figures 10 and 11. The system is connected to the stand pipe of the large valve test facility which represents the down comer of the KERENA reactor pressure vessel. In the test facility, pressure vessel itself and the water and steam temperature, pressure, and water level are measured. In the down comer, the differential pressure and the temperature are measured at different elevations to be able to determine the water level with sufficient accuracy. Above the water

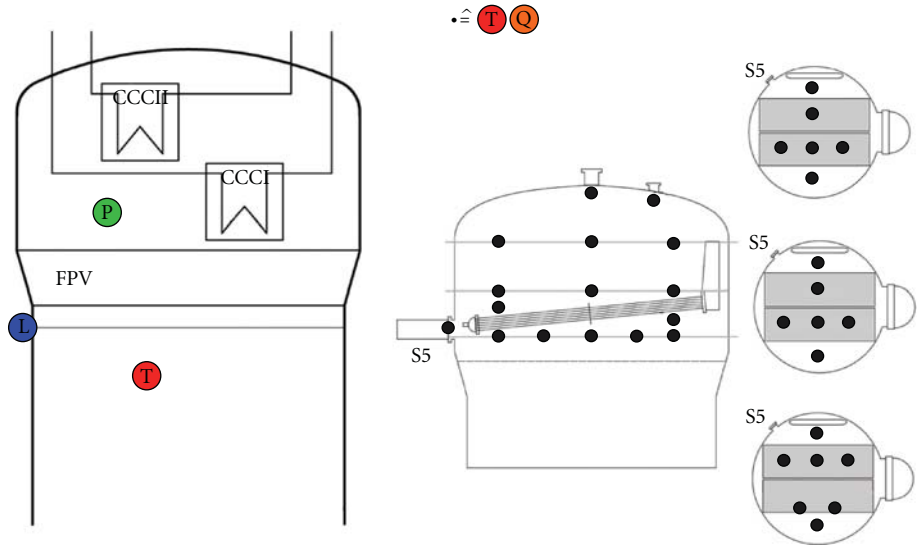

Figure 9: Instrumentation of the water space of the Flooding Pool Vessel.

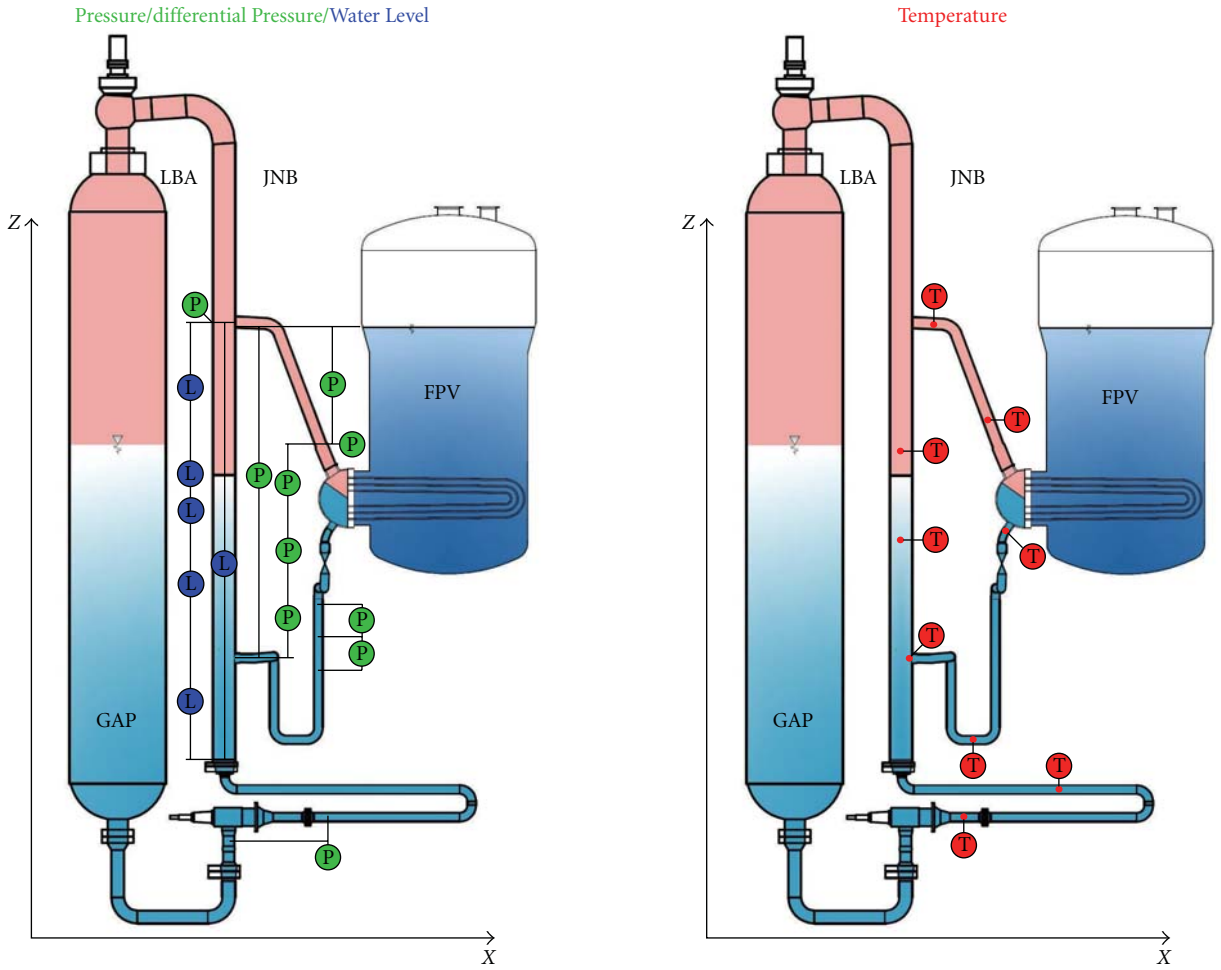

Figure 10: Instrumentation of the Emergency Condenser System (I).

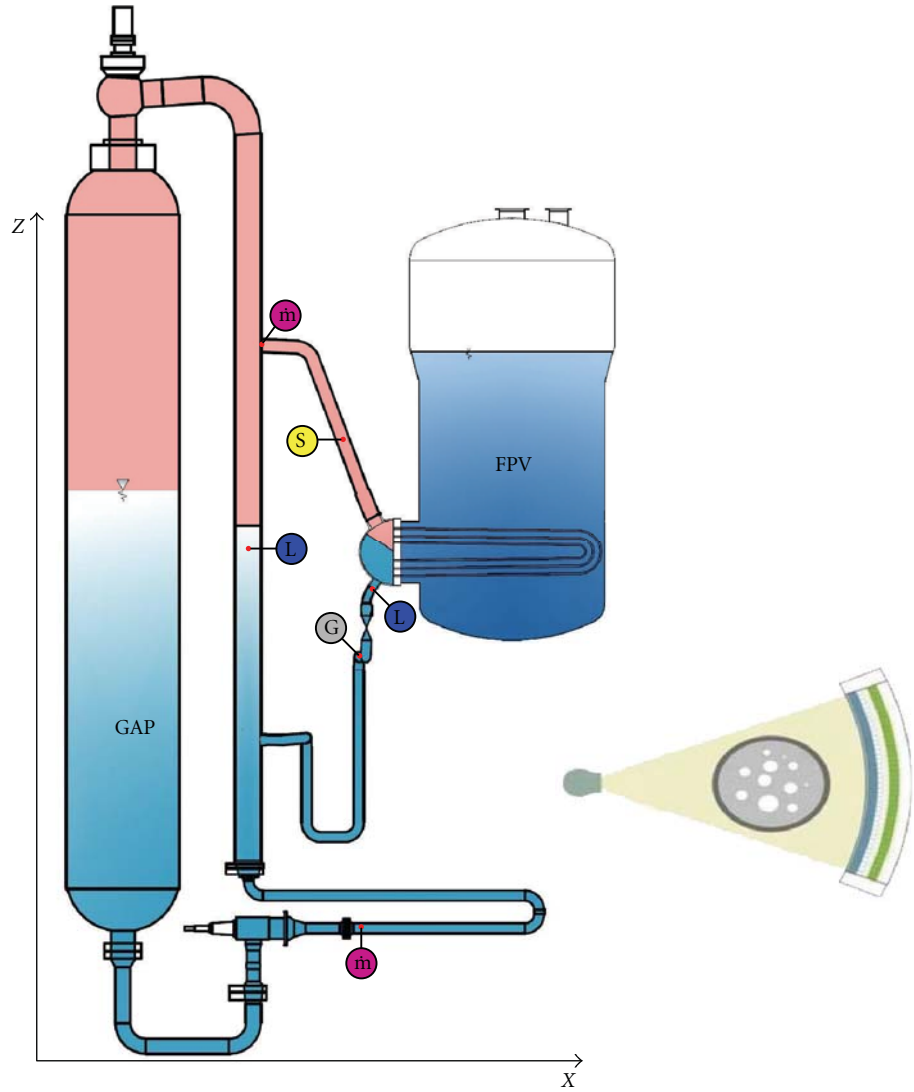

Figure 11: Instrumentation of the Emergency Condenser System (II).

level, the absolute pressure is measured. The inlet line, return line, and the Emergency Condenser component itself are equipped with several differential pressure measurements. In the piping system the temperature is determined at different positions. Figure 12 highlights the mass flow measurements, the local void fraction measurement outside the Emergency Condenser component (Thermo Needle Probes in the Emergency Condenser outlet line and the down comer line), the acceleration measurements for the determination of vibrations in the system during operation, and the integral void measurement in the outlet line. The operation principle of the latter measurement is described in Figure 11. It consists of a radiation source and a detector array. The pipe in which the void fraction should be determined is located in between. Based on the attenuation of the emitted radiation, the void fraction in the pipe can be determined.

4.2. Instrumentation of the Systems. Two of the outer heat exchanger tubes in the Emergency Condenser heat exchanger bundle are equipped with instrumentation. One with thermocouples and the other with nine thermo needle probes. At most of the locations indicated in Figure 12, the thermocouples are located in the tube axis. At three different positions, there are four additional thermocouples at the inner side and the outer side of the heat exchanger tube wall. With the combination of the local void fraction measurements, and the five thermocouples per location, the heat transfer and the type of two-phase flow in the tube can be determined.

Figure 13 shows the instrumentation of the Containment Cooling Condenser system and component. The differential pressure of the inlet line, return line, and the component itself is measured. In the return line also the absolute pressure is measured. Thermocouples are installed at different locations in the piping system. In the return line, several thermocouples are located at different position over the pipe cross-section to identify stratification of the flow. In the case of two-phase flow operation, the integral void fraction can be determined via a gammdensitometer located

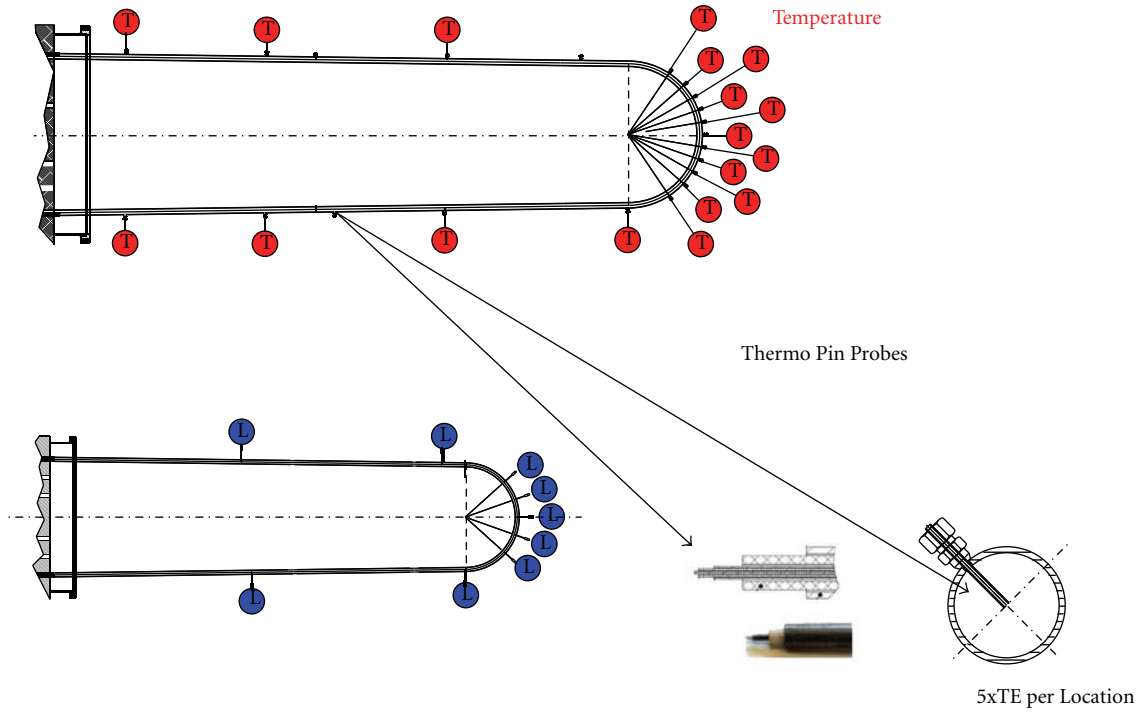

Figure 12: Instrumentation of the Emergency Condenser component.

on the return line. The heat exchanger tubes are equipped with thermocouples along the tube axis to determine the heatup of the coolant.

Figure 14 shows the instrumentation of the Passive Core Flooding System. The differential pressure over the valve and the line connecting the valve to the Flooding Pool Vessel is measured. At the lowest location of the system also the absolute pressure is measured. At different locations in the system, thermocouples are installed. The mass flow measurement can determine flow in both directions.

5. Preconditioning of the Test Facility

All vessels and systems of INKA can be operated individually. The connections between the vessels are realized by pipes that can be opened and closed as needed. Each of the vessels can be heated independently via direct steam injection. The water volume of the Flooding Pool Vessel and the Pressure Suppression Pool Vessel can be cooled via the two pool cooling systems. The containment vessels of INKA (Flooding Pool Vessel, Drywell Vessel, Pressure Suppression Pool Vessel) are designed for pressures between 0.5 and 4 bar. The water level of these vessels can be set individually (the water level of the Flooding Pool Vessel is limited via the overflow pipe). The test facility pressure vessel is designed for a maximum pressure of 110 bar. The water level can be set and controlled during test execution with the help of water release. Energy can be introduced via steam introduction with a maximum power of 22 MW.

6. Test Programs Performed at the INKA Test Facility

Several test programs have already been performed at the INKA test facility. All of them were done in the cause of the KERENA development program. The first test program in 2009 dealt with the KERENA Fuel Pool Cooler. The goal was to qualify the component and to validate the CFD model [16].

Since 2009, the key features of the KERENA passive safety concept are tested in full-scale single component tests at INKA. The goal of the tests was again to qualify the components/systems and validate the numerical tools used for the KERENA accident analysis. Among these features are the Emergency Condenser (2009-2010, [17, 18]) and the Containment Cooling Condenser (2009, [17]). In 2010 the passive core flooding system has been tested as single component and together with the Emergency Condenser in order to determine the interaction between the passive residual heat removal and the passive replenishing of the reactor pressure vessel [19]. The passive pressure pulse transmitter has already been tested in 2003 at Karlstein in a single component qualification program. All four systems will be used in the integral test, experimentally simulating accident scenarios and demonstrating the interaction between the systems.

7. Test to Be Run at INKA

INKA is a test facility that simulates a multicompartment containment of a BWR. The reference plant is KERENA.

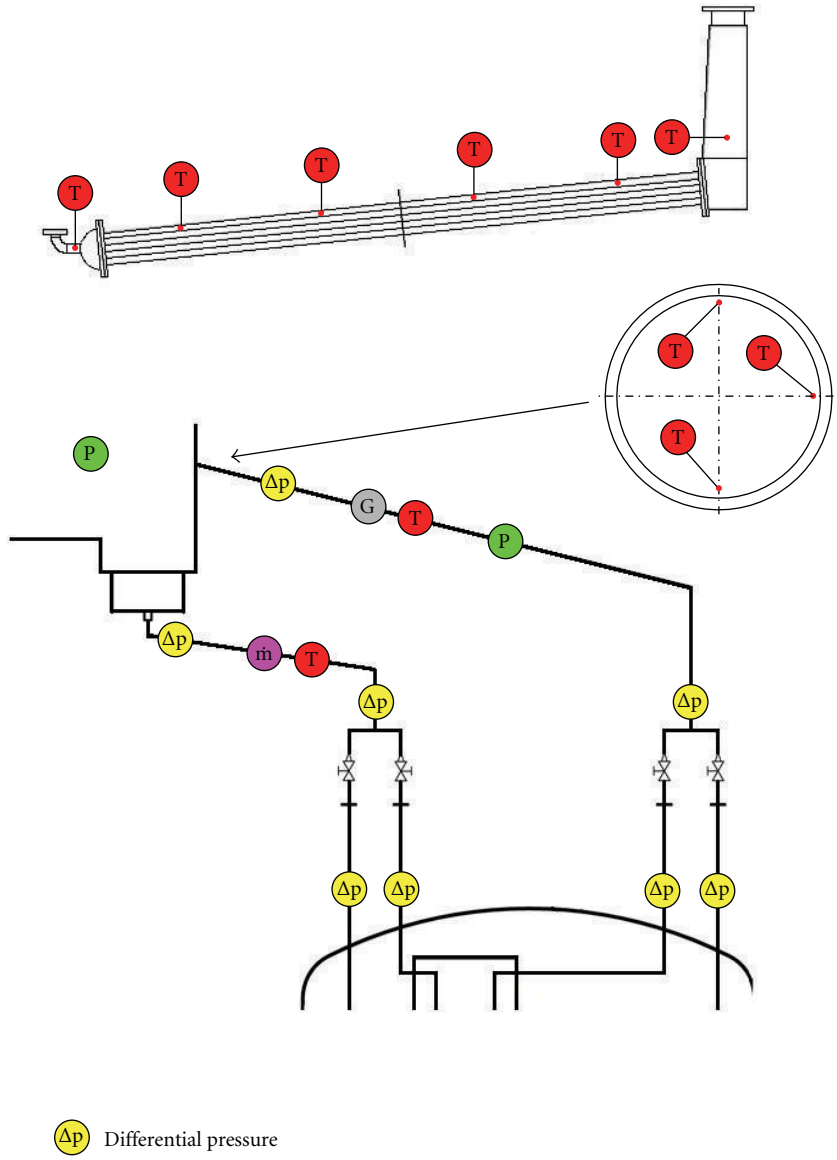

Figure 13: Instrumentation of the Containment Cooling Condenser System and Component.

The test facility containment is divided in drywell and wetwell and has therefore a pressure suppression function. The primary system is simulated by the GAP vessel and the down comer line, which simulates a simplified model of a BWR reactor pressure vessel. The primary system is coupled to the containment via the Emergency Condenser the Safety and Relief Valve system and the two lines simulating leak mass flows. A complete set of passive safety features for the performance of passively controlled accident scenarios is available. The function active safety systems can at least qualitatively be simulated. Therefore, integral tests especially the simulation of accident scenarios for BWRs with passive and active accident management can be performed. These tests can be started with the initiating event, for example, the rupture of a pipe, and can be executed until very late phase of the accident. The required decay heat can be realized via steam introduction into the GAP vessel. The participating safety features can be chosen individually and even the scaling of the systems can be adjusted if necessary.

Because of the preconditioning capability of INKA and the option to operate all vessels and systems individually, many single-effect phenomena can be addressed.

The following list gives an overview about effects to be analyzed:

(i) heat transfer on surfaces—water surface containment walls, for example, in the Pressure Suppression Pool Vessel of INKA;

(ii) heat transfer on the inside and outside of heat exchanger tubes and the impact on natural circulation systems—for example, impact of subcooling to the Emergency Condenser system;

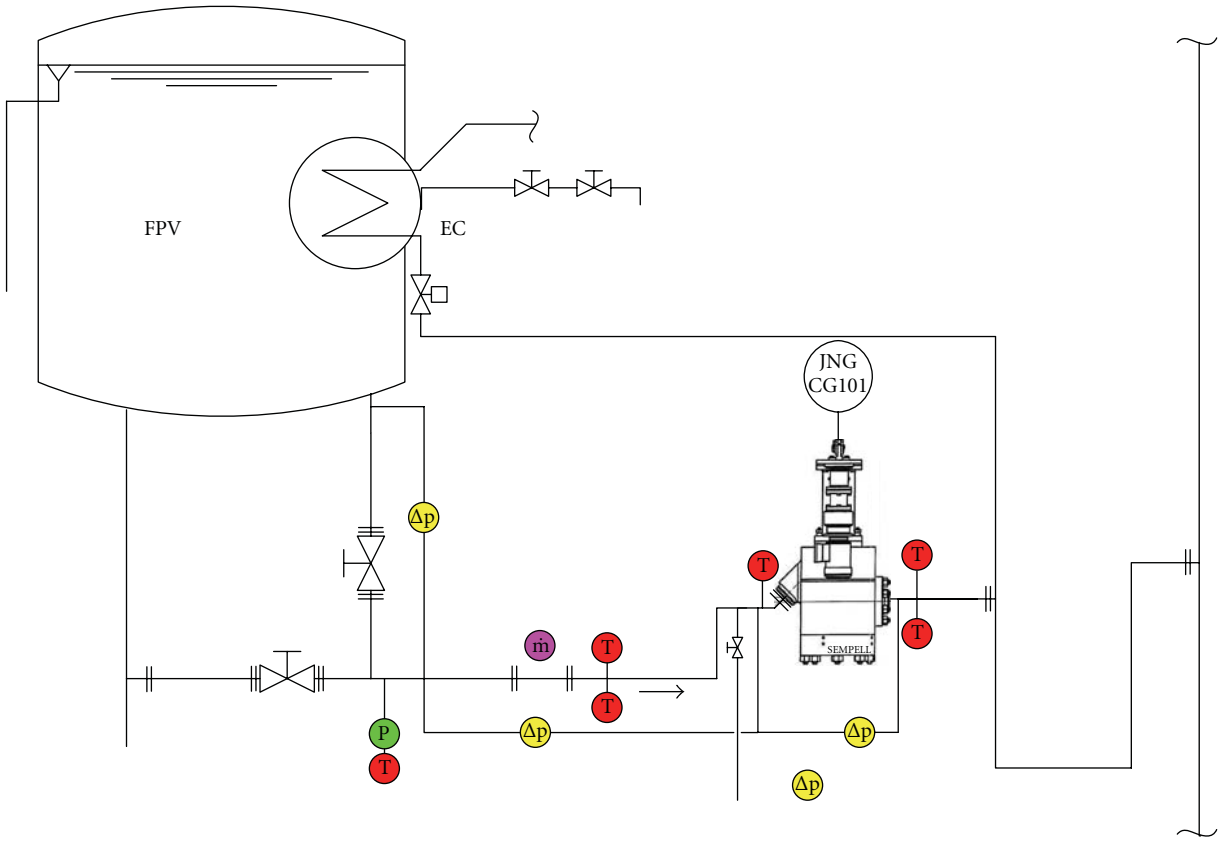

Figure 14: Instrumentation of the Passive Core Flooding System.

(iii) influence of noncondensable gases to the heat transfer—for example, for the Emergency Condenser and Containment Cooling Condenser;

(iv) temperature stratification in the water and gas space of compartments/vessels—for example, INKA, Flooding Pool Vessel, and Pressure Suppression Pool Vessel;

(v) gas compositions in the gas space of compartments/vessels—for example, INKA, Flooding Pool Vessel, and Pressure Suppression Pool Vessel;

(vi) impact of natural convection on temperature stratifications and gas compositions in compartments or vessels—for example, the influence of Containment Cooling Condenser operation on the FPV;

(vii) gas concentrations in drywell and wet well after blowdown depending on the leak size;

(viii) temperature stratification in the wet well after blowdown depending on the leak size.

The integral test as well as the single effect tests can be simulated in a scaling close to real plant conditions. The instrumentation concept and the sensor density are sufficient for the validation of thermohydraulic codes like RELAP or TRACE, for example, or containment codes like COCOSYS or GOTHIC. Nevertheless, for special tasks, the instrumentation concept can be easily upgraded. Also, the installation of additional systems matching tasks of other reference plants can be realized.

8. Summary

The INKA test facility was built to test the passive safety systems of KERENA. INKA simulates the KERENA containment in scaling of 1 : 24. The primary system is represented by the GAP vessel and the GAP main steam line representing the reactor pressure vessel down comer. The systems to be tested at INKA are constructed in full scale. Because of the possibility of INKA to precondition and operate all vessels and systems individually, integral testing such as the experimental simulation of BWR accident scenarios, as well as the analysis of single effects, can be performed. The large energy storage capacity and power supply of INKA allow the performance of tests in a scaling that is relevant for full-scale commercial nuclear power plants.

References

[1] Brosche and J. Mattern, "The BWR 1000—an advanced boiling water reactor with medium power," VGB Power Tech 11/99.

[2] Z. Stosic, W. Brettschuh, and U. Stoll, "Boiling water reactor with innovative safety concept: the Generation III+ SWR 1000," *Nuclear Engineering and Design*, vol. 238, no. 8, pp. 1863–1901, 2008.

[3] M. Huggenberger, C. Aubert, T. Bandurski, J. Dreier, H. J. Strassberger, and G. Yadigaroglu, "ESBWR related passive decay heat removal test in PANDA," in *Proceedings of the 7th International Conference on Nuclear Engineering (ICONE-7)*, Tokyo, Japan, April 1999.

[4] M. Huggenberger, C. Aubert, J. Dreier, O. Fischer, H. J. Strassberger, and G. Yadigaroglu, "New passive decay heat removal test in PANDA," in *Proceedings of the 6th International Conference on Nuclear Engineering (ICONE-7)*, San Diego, Calif, USA, May 1998.

[5] M. Ishii, H. J. Yoon, Y. Xu, and S. T. Revankar, "Modular simplified boiling water reactor design with passive safety systems," in *Proceedings of the International Atomic Energy Agency Meeting (IAEA '05)*, 2005.

[6] G. Yadigaroglu, "Scaling of SBWR related tests," GE, NEDC-32288, 1994.

[7] R. Hamazaki et al., "The enhanced severe accident mitigation systems for a BWR," in *Proceedings of the 13th International Topical Meeting on Nuclear Reactor Thermal Hydraulics (NURETH-13)*, Kanazawa City, Japan, September 2009.

[8] Y. Kojima, K. Arai, T. Kurita et al., "Performance of horizontal U-tube type passive containment cooling system in a BWR," in *International Congress on Advances in Nuclear Power Plants (ICAPP '10)*, pp. 1135–1142, San Diego, Calif, USA, June 2010.

[9] K. B Welter, S. M. Bajorek, and J. Reyes, "APEX-AP1000 confirmatory testing to support AP1000 design certification," United States Nuclear Regulatory Commission number NUREG-1826, 2005.

[10] J. N. Reyes, J. T. Groome, A. Y. Lafi, D. Wachs, and C. Ellis, "PTS thermal hydraulic testing in the OSU APEX facility," *International Journal of Pressure Vessels and Piping*, vol. 78, no. 2-3, pp. 185–196, 2001.

[11] A.Y. Lafi and J. N. Reyes, "Two-inch cold leg break tests in APEX and ROSA/AP600 comparative study," in *Proceedings of the 9th International Topical Meeting on Nuclear Reactor Thermal Hydraulics (NURETH-9)*, San Francisco, Calif, USA, October 1999.

[12] D. E. Bessette and M. Di Marzo, "Transition from depressurization to long term cooling in AP600 scaled integral test facilities," *Nuclear Engineering and Design*, vol. 188, no. 3, pp. 331–344, 1999.

[13] R. F. Wright, "Simulated AP1000 response to design basis small-break LOCA events in the APEX-1000 test facility," *Nuclear Engineering and Technology*, vol. 39, no. 4, pp. 287–299, 2007.

[14] G. Bianconi and M. Rigamonti, "Scaling, design,and verification of SPES-2," Westinghouse Corporation, Piacenza, Italy, WCAP-13277 Rev.1., 1992.

[15] S. Leyer, M. Wich, and H. Schafer, "SWR 1000 integral and full scale tests of the passive safety systems," in *Proceedings of the International Conference on Advances in Nuclear Power Plants (ICAPP '08)*, pp. 87–92, Anaheim, Calif, USA, June 2008.

[16] S. Leyer, F. Maisberger, B. Schaub et al., "Full scale steady state component tests of the SWR 1000 fuel pool cooler at the INKA test facility," in *Proceedings of the Annual Meeting of Nuclear Technology*, Dresden, Germany, May 2009.

[17] S. Leyer, F. Maisberger, V. Herbst, M. Doll, M. Wich, and T. Wagner, "Status of the full scale component testing of the KERENA emergency condenser and containment cooling condenser," in *Proceedings of the International Conference on Advances in Nuclear Power Plants (ICAPP '10)*, p. 5, San Diego, Calif, USA, June 2010.

[18] T. Wagner, M. Wich, M. Doll, V. Herbst, and S. Uhrig, "Tests with the emergency condenser at the integral test stand Karlstein for KERENA," in *Proceedings of the Annual Meeting of Nucluar Technology*, Berlin, Germany, May 2010.

[19] T. Wagner, M. Wich, M. Doll, and S. Leyer, "Full scale tests with the passive core flooding system and the emergency condenser at the integral test stand Karlstein for KERENATM," in *Proceedings of the International Conference on Advances in Nuclear Power Plants (ICAPP '10)*, Nice, France, May 2011.

Hindawi Publishing Corporation
Science and Technology of Nuclear Installations
Volume 2012, Article ID 239319, 9 pages
doi:10.1155/2012/239319

Research Article

PANDA: A Multipurpose Integral Test Facility for LWR Safety Investigations

Domenico Paladino and Jörg Dreier

Nuclear Energy and Safety Research Department, Paul Scherrer Institut (PSI), 5232 Villigen, Switzerland

Correspondence should be addressed to Domenico Paladino, domenico.paladino@psi.ch

Received 18 April 2011; Accepted 25 August 2011

Academic Editor: Klaus Umminger

The PANDA facility is a large scale, multicompartmental thermal hydraulic facility suited for investigations related to the safety of current and advanced LWRs. The facility is multipurpose, and the applications cover integral containment response tests, component tests, primary system tests, and separate effect tests. Experimental investigations carried on in the PANDA facility have been embedded in international projects, most of which under the auspices of the EU and OECD and with the support of a large number of organizations (regulatory bodies, technical dupport organizations, national laboratories, electric utilities, industries) worldwide. The paper provides an overview of the research programs performed in the PANDA facility in relation to BWR containment systems and those planned for PWR containment systems.

1. Introduction

The research programs performed in the PANDA facility are devoted to improving safety and economics of current (Generation II) as well as more advanced (Generation III) LWR types.

Past and ongoing programs performed in PANDA are listed in Table 1, while photos of the PANDA facility are shown in Figure 1. In Table 1, the project investigating LWR containment is marked in grey, whereas projects devoted to produce data on separate effects with high safety relevance are marked in white. The facility has been initially built and used in a consortium between PSI and (Electric Power Research Institute) EPRI/(General Electric) GE to study the passive decay heat removal systems and containment response for the Simplified boiling water reactor (SBWR). Later the PANDA facility was used for investigations related to the (passive containment cooling system) PCCS of the ESBWR (Economic/European SBWR) (Figure 2, Section 3.2) in the framework of the European Union (EU) 4th Framework Program (FWP) TEPSS Project [1]. The SBWR/ESBWR containments are represented in the PANDA facility by six cylindrical vessels and four condensers immersed in four water pools. In the EU 4th FWP IPSS project, in the PANDA facility have been performed investigations related to the Building Condenser of the SWR1000 (AREVA design) [2]. With the OECD/ISP42 program, a specific test consisting of six phases has been performed and analyzed in the PANDA facility to study the PCCS performance in very challenging situations. In the EU 5th FWP TEMPEST project, experimental investigations in the PANDA facility focused on the effects of noncondensable light gas (as hydrogen) on the PCCS performance [3], and, in the EU 5th FWP NACUSP project, the investigations in the PANDA facility focused on the natural circulation and stability of BWRs [4]. The part of investigations of the OECD/SETH project which were performed in the PANDA facility has dealt with separate effect tests addressing phenomena such as gas mixing, transport, stratification, and condensation relevant to LWR containment integrity [5–9]. The investigations performed in the PANDA facility within the OECD/SETH-2 project dealt with phenomena leading to the breakup of gas stratification in a LWR containment [10] by different means (basic phenomena, such as plumes and jets, or activation of component systems, e.g., spray, cooler, recombiner).

Table 1: PANDA programs.

Program	Investigations
1991–1995 EPRI/GE	Investigation of passive decay heat removal systems for SBWR
1996–1998 EU-4th FWP	Passive decay heat removal system tests for SWR1000 (IPPS project) and ESBWR (TEPSS Project)
1998–2002 OECD/ISP-42	Passive containment cooling system (PCCS) performance in very challenging situations represented in six different phases
1999–2004 EU-5th FWP	Effect of hydrogen distribution on passive systems (TEMPEST project) and Investigation of BWR-natural circulation stability (NACUSP Project)
2002–2006 OECD/NEA	Gas mixing and distribution in LWR containments (SETH project): separate effects
2007–2010 OECD/NEA	Resolving LWR containment key computational issues (SETH-II project): separate effects, components, and systems
2010–2013 EU-7th FWP	Containment thermal-hydraulics of current and future LWRs for severe accident management (ERCOSAM project)

(a) Construction phase (b) During a test (c) Internal view

Figure 1: PANDA facility.

The EU 7th FWP ERCOSAM is an ongoing project cooperating with ROSATOM project SAMARA and is designed to investigate containment thermal-hydraulics of current and future LWRs for severe accident management [11].

The project aims at elaborating the effect of scaling on the phenomena evolution (e.g., gas transport, stratification, stratification breakup, condensation, convection, etc.) investigated in various experimental facilities (PANDA, MISTRA, TOSQAN, and KMS-like) of different scales.

The present paper provides an overview of the PANDA facility program results and some planned activities for incoming projects. The focus is in the investigations related to BWR and PWR containment systems. The PANDA facility investigations related to separate effect tests are just mentioned in this paper (Section 3.7).

2. PANDA in Figures

In Table 2, PANDA facility specifications are shown. It should be pointed out that upgrading PANDA instrumentation is a continuous process. The main criterion behind the effort to improve the facility instrumentation is to meet the requirements specified in the various PANDA test campaigns.

3. PANDA Programs

3.1. Simplified Boiling Water Reactor (SBWR). In the SBWR, passive containment condensers (PCCs) are positioned in water pools on top of the containment building. After the depressurization of the reactor pressure vessel (RPV) to the drywell (DW), a steam/nitrogen mixture flows to the PCCs, which are permanently connected to the containment without any control devices. Steam condensing in the PCCs heats the pools, which are open to the atmosphere, and gradually evaporate the pool water inventory (3-day capacity). The primary side condensate returns via make-up water tanks, that is, the Gravity Driven Cooling System (GDCS) to the RPV, and the nitrogen is purged to the suppression chamber (SC) gas space. The volume, temperature, and gas

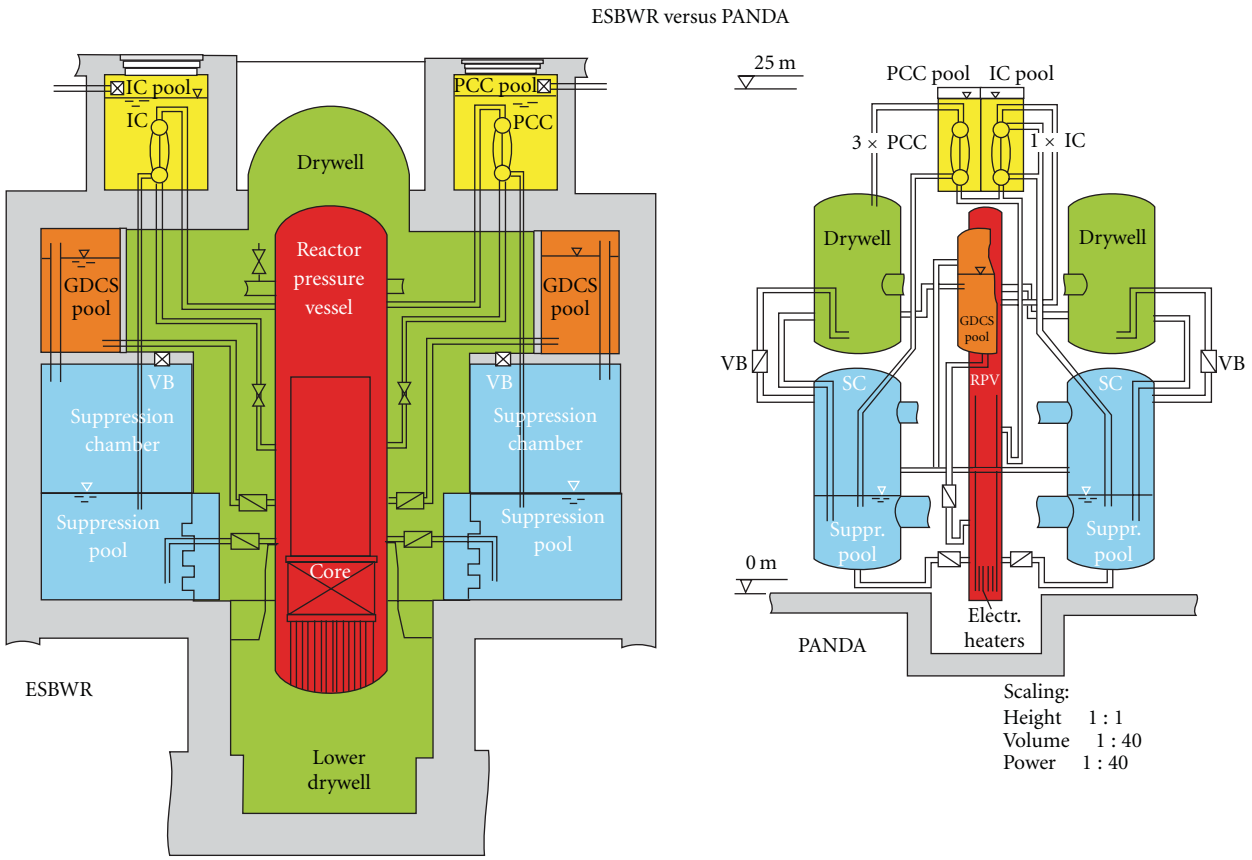

Figure 2: Schematic representation of ESBWR containment and PANDA.

Table 2: PANDA in figures.

Operating specification for the pressure vessels	Up to 10 bar/200 C fluid conditions
Power	1.5 MW electric heat power
Total volume	515 m^3 (modular structure based on 6 main vessels)
Total height	25 m
Instrumentation	1000 sensors (temperature, pressure, flow rate, levels, etc.) PIV (Particle Image Velocimetry (2D velocity fields) Mass spectrometer (air, steam, and helium gas concentration)
Control system	Hierarchical programmable logic control system Graphical-display man-machine interface with process visualization and online/offline trending

inventory of this gas space determine the pressure level for the containment system [12].

PANDA was configured as a thermal-hydraulic model of the SBWR containment and passive decay heat removal system; power, volumes, horizontal areas, and flow rates were scaled with the system scale of 1 : 25, while relevant elevations, pressures, and pressure drops were scaled 1 : 1 [13]. Yadigaroglu's (1996) scaling study included also the identification of any distortions in the representation of phenomena and the manner in which this distortion could be considered when the experimental data are used for computer code qualification.

The PANDA transient system tests performed for the SBWR concept demonstrated very favourable and robust overall containment behaviour, even under extreme boundary conditions [14].

Figure 3 shows the PCC behaviour in terms of active/inactive area for heat transfer. The term "active" is used to indicate the absence of air inside the PCC tubes and presence of water from the secondary side. The air is a noncondensable gas which deteriorates the heat transfer. At the beginning of a postulated LOCA, the PCC tubes are fully immersed in the water pool. The steam generated in the RPV is transferred into the DW and from there to the PCC where a part condenses and returns into the RPV and a part is vented to the WW pool where it condenses. During this initial phase, the air present in the DW and PCC tubes is vented into the wetwell (WW) [15], so all the active tube length (red in Figure 3) is available for heat transfer, leading to the steam condensation. As the transient continue, further and the decay heat decreases, the PCCs have an overcapacity and

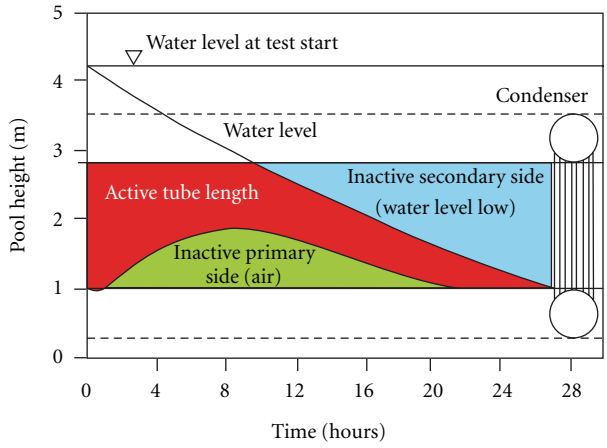

Figure 3: Schematic representation of PCC active area for heat transfer during a transient.

the pressure in the DW decreases below the WW pressure. In this situation, the vacuum breakers (between drywell and wetwell) open, and a steam-air gas mixture is transported back to the DW.

The air transported back to the DW will flow in the PCC tubes where it accumulates in the lower part of the tubes (green area in Figure 3). Because of the presence of air, the lower part of the PCC tubes becomes "inactive." The inactive area increases because the decreasing decay heat produces less steam than the nominal condensing capacity, and air is not any more vented to the WW but accumulates in the lower part of the tubes. The PCC "automatically adjusts" it power with noncondensable gas. After some time (9 hours in Figure 2) due to boiling of the PCC pools the water level decreases and consequently the "active area" of the tube (from the pool side) is decreased. To compensate the diminished active areas from pool side, the air inside the tube is gradually vented to the WW.

3.2. Economic Simplified Boiling Water Reactor (ESBWR). A schematic representation of ESBWR containment in PANDA is shown in Figure 2. (It should be pointed out that the ESBWR-PANDA containment arrangement in Figure 2 corresponds to an earlier design of the ESBWR (4000 MWt) where the GDCS gas space was connected to the WW gas space. In the present ESBWR (4500 MWt) design, the GDCS pool is open to the drywell as in the original SBWR, and the condensate return line of the PCC is connected to the GDCS pool.) The two green vessels are interconnected by a large diameter pipe (IP) (the IP is not shown in Figure 2) and represent the DW; the blue vessels represent the WW (in PANDA these two vessels are interconnected by two large diameter pipes: one in the water pool space, and one in the gas space). The red vessel represents the reactor pressure vessel (RPV), whereas the brown vessel represents the gravity driven cooling system (GDCS) tank. The yellow pool and condensers represent the pool of the passive cooling condensers (PCCs) and the isolation condenser (IC). The ESBWR utilizes basically the same passive containment cooling system as the SBWR. However, the make-up water tanks are completely separated from the DW and connected to the SC gas space. This provides, after draining of the makeup water tanks, more volume for the noncondensable gases which are purged from the DW via the PCCs to the SC. The SC pressure increase and ultimately the containment pressure are lower than in a SBWR configuration with identical dimensions. The condensate from the PCCs is directly routed to the RPV. The ESBWR containment is represented in PANDA at about 1 : 40 system scale [16]. The PANDA tests with the ESBWR configuration are similar to the SBWR tests but extend into areas not fully explored before. Some of the investigations were also devoted to the possible degradation of the PCCS performance in postulated severe accident scenarios with hydrogen release due to the fuel cladding metal-water reaction. Helium was used to simulate hydrogen. Other tests covered the deferred release of air which had supposedly been "trapped" in the DW, low water level in the PCC pools, startup, and system interaction. Generally speaking, the conclusions of the SBWR series test were confirmed. Figure 4 shows as example the containment pressure during a long transient (28 hours) and the decrease of water level in pools of the PCCs (during the transient the release of light gas hydrogen was not simulated). As can be noted, the pressure remains nearly constant until when the water level in the pool reaches nearly the elevation corresponding to the PCC lower drum.

Figure 5, related to PANDA Test T1.2, shows the system pressure during the evolution of PANDA test in which helium (used to simulate hydrogen) was also released.

The initial conditions for Test T1.2 (temperatures, pressures, partial pressures, and water levels) were based on the transient status predicted for the ESBWR at one hour after scram in the course of a MSLB LOCA. At this time, the RPV has been depressurized, and the actual containment pressure is about 2.5 bar. Test T1.2 addresses a core overheat and release of hydrogen. The Test T1.2 allowed for investigating gas stratification and retention in dead-end containment volumes (the "stand-by" volume) and the effect of light gas (helium) on the overall system behavior.

The Test T1.2 included three main phases: in Phase 1 (up to 10000 s) was simulated the release in the drywell of steam (i.e., the normal PCCS containment heat removal mode), in Phase 2 (10000 s to 17200 s), the release of hydrogen and steam (simulating the zircaloy oxidation), and then in Phase 3 (17200 s to 42000 s) again only the release of steam.

The quantity of helium injected in the test was scaled by assessing the amount of hydrogen that would be generated by assuming 100% cladding M-W reaction in an ESBWR core with 1132 fuel bundles and by considering a 1/40-volume scale of PANDA. It should be pointed out that the timing for steam or helium release does not correspond to any specific severe accident scenarios. Figure 5 shows the RPV pressure (sensor identified by MP.RP1), DW pressure (sensor identified by MP.D1), and WW pressure (sensor identified by MP.S1).

In the early stage of the accident, the noncondensable gases initially filling the DW are purged through the Main Vent (MV) lines and the PCC vent lines to the WW. The DW to WW pressure difference can vary only within a small range

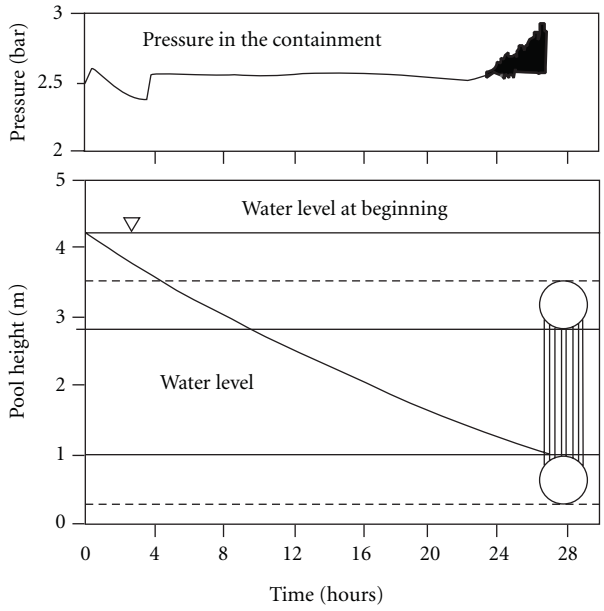

Figure 4: Pressure in the containment (above) as function of water level in the PCC pools.

given by the hydrostatic head of the vent line submergence in the pressure suppression pool. Venting of noncondensable gases from the DW to the WW causes a shift of both pressures to higher values due to a WW pressure increase.

For the first 1000 s into the tests, the PCCs were slightly overloaded; therefore, the pressure in the system slightly increased (by about 0.1 bar). In accordance with the decreasing decay heat power generated in the RPV, the steam rate released from the RPV to the DW vessels decreased with time. Therefore, about 1000 s after test started, the PCC units were able to condense all the steam and the pressure in the DW reached its maximum during Phase 1. For $t > 1000$ s the pressure started to slightly decrease until the start of helium injection.

The release of helium caused a sudden increase in DW pressure. The increase continued also when the injection of helium was stopped because after release of non condensable gas was completed, it took some additional time until the stratification process in the DW reached a steady state, and most of the helium was vented to the WW. The highest pressure in the DW was around 5.7 bar and was reached at about 20000 s. Then, until the end of the transient, the pressure remained nearly constant, that is, a new equilibrium was reached by the heat generated in the RPV (energy source) and the energy extracted by the PCCS [17].

3.3. SWR-1000 with Building Condenser. The SWR-1000 BWR design passively transfers decay heat from the RPV to core flooding pools, which are located in the upper part of the DW and gradually start heating the DW with steam. Containment cooling condensers installed above the core flooding pools condense steam from the gaseous mixture present within the DW. Schematically how the SWR-1000 building condenser is represented in PANDA is shown in

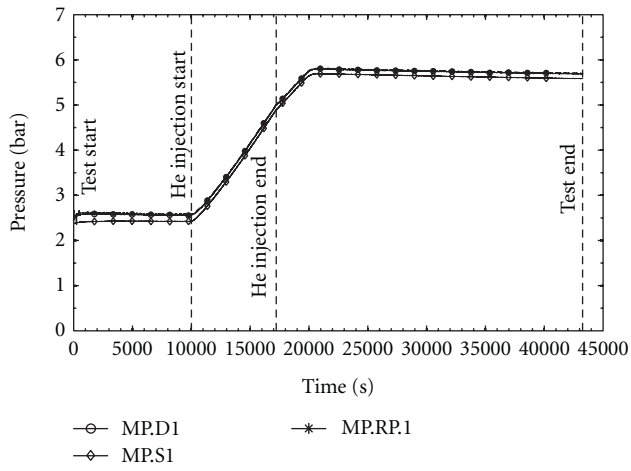

Figure 5: RPV, DW, and WW pressure curves.

Figure 6. These condensers consist of inclined finned tube. The low and high ends of their secondary sides are connected to the bottom and to the higher level of the dryer/separator storage pool, which is situated on top of the containment. The containment cooling condenser system of the SWR-1000 is represented in PANDA at about 1 : 26 scale, except for the dryer/separator storage pool, which is much smaller, leading to a time compression factor of about 8 for the transient system tests. Different types of tests were performed, based on different small, medium, and large-break LOCAs with and without core degradation, in the former case with helium injected to simulate the release of hydrogen. The test series as a whole identified important containment phenomena and successfully demonstrated the robustness of the SWR-1000 containment-cooling system [2].

3.4. Natural Circulation and Stability of BWRs. Figure 7 shows the facility configuration for natural circulation and stability of BWR investigations in PANDA. In this program only part of the facility was used (i.e., mainly the RPV and the IC). The investigations address the flashing-induced instability which could occur at low pressure and low power (e.g., during startup and shutdown). In the tests, the water flowed down from the downcomer then was heated up in the riser.

The water column in the riser during the test was in the order of 11 m, so the overhead pressure for the water was 1.1 bar. The coolant at the bottom of the riser was subcooled and becomes super-heated while flowing in the riser (i.e., due to the decrease of pressure and of the saturation temperature (red curve in Figure 8) caused by the lower water column head) and consequently vaporize (flash).

Additionally, Figure 8 shows the temperature profiles measured along the RPV vertical central axis (black). The water flashes at around 8 m.

Figure 9 shows, as an example, the velocity measured in the downcomer during a test. The flow oscillations were analyzed for all the different tests, and the detailed results and analysis were reported in [4].

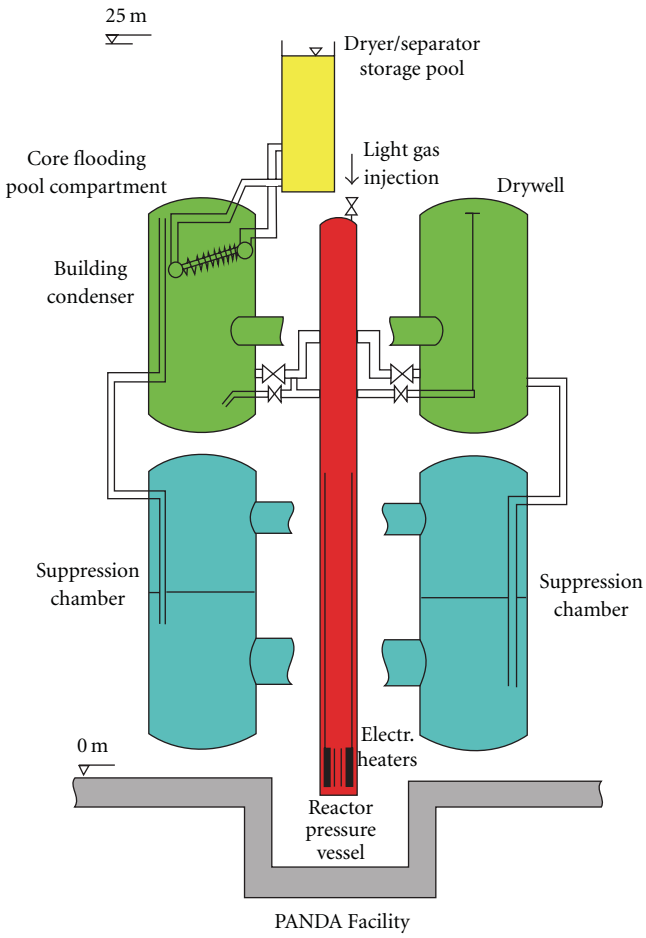

Figure 6: In the PANDA test facility is represented the SWR-1000 building condenser.

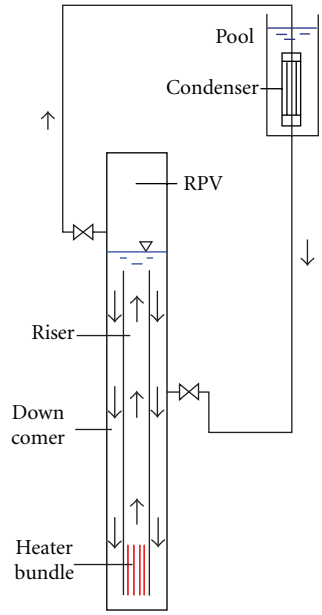

Figure 7: Configuration of PANDA RPV and pool condenser.

3.5. Investigations Related to PWR Systems. PANDA has been used for investigations related to PWR in the recent OECD/SETH-2 project and in the ongoing ERCOSAM project (Table 1).

In these two projects, in relation to PWR, the investigations dealt with safety component tests and with containment system tests. The component tests addressed the effect of activation of containment cooler [18, 19], sprays [19], or recombiners on the containment atmosphere, particularly on the hydrogen concentration.

PWR containment system investigations in PANDA were performed with respect to the opening hatched series. These tests addressed the issue of gas distribution in two large volumes (Figure 10, vessels 1-2 form the first volume, vessels 3-4 form the second volume), having different gas concentrations and at different pressures when they are suddenly interconnected. This situation occurs in the case of the sudden opening of a rupture disk and could be directly related to the EPR^{TM} design. Data on the mixing of fluids of different density in two adjacent vessels as the result of the sudden opening of an aperture are rather scarce and do not encompass data at large-scale facilities.

Gas transport, mixing, and distribution within the containment compartments is driven by the pressure difference between the two large volumes in the early phase of the test and by temperature gradient and gas mixture concentration differences after the pressure between the vessels has been equalized [20].

3.6. Other Foreseen PANDA Application to PWR. Advanced PWR containments are designed with a large number of compartments and safety systems. For example, the EPR^{TM} is designed with a containment which includes about 140 compartments or rooms and different types of active and passive safety systems (e.g., spray, recombiners, rupture disks, core catcher, etc.) [21]. From a conceptual point of view, such type of containment is constituted of two main volumes or "compartments": one "inner compartment", in which components of the primary circuit (reactor pressure vessel, steam generator, pressurizer, pumps, etc.) are located and one "external compartment" where other components and systems are located. Safety components, for example, recombiner are located in both volumes, while the spray system rings are located in the dome of the external volume. Rupture foils and convection foils are positioned in the upper regions above the steam generator mixing dampers are positioned in the lower region, that is, above the in-containment refuelling water storage tank (IRWST). Rupture foils and convection foils break when the pressure difference between the inner and external compartments exceeds around 50 mbar (convection foils will open if temperature is higher than 80–85 C), while the mixing dampers open for a pressure difference of around 35 mbar (for pressure above 1.2 bar).

Therefore, during postulated accident sequences with release of steam (and later also hydrogen), the inner compartment would be pressurized, rupture, and convection foils and mixing dampers would open, and steam air hydrogen would flow from the inner to the external compartment.

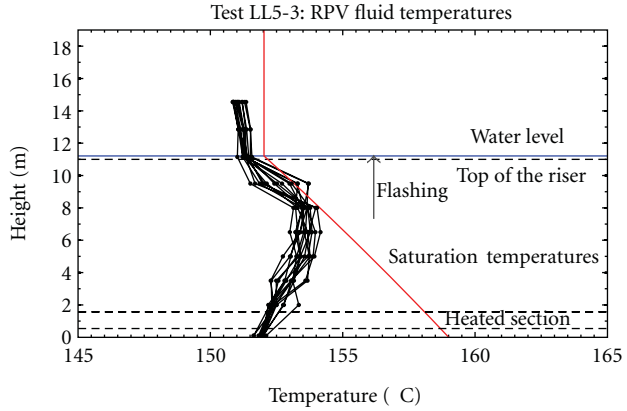

Figure 8: Fluid temperature profiles measured along RPV central axis indicate flashing in the upper riser region.

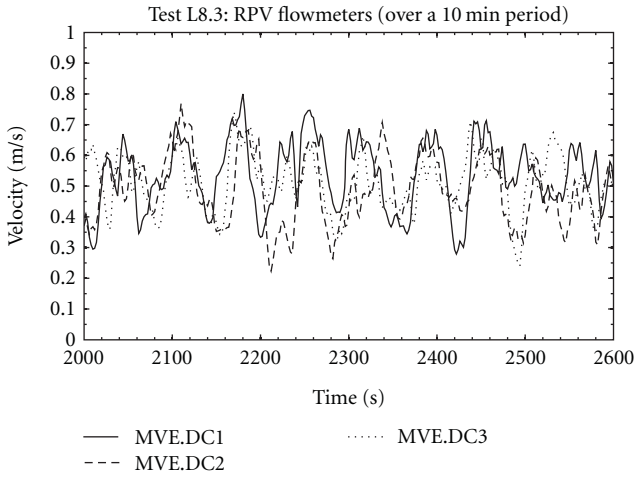

Figure 9: One-component velocity in the downcomer.

Spray activation would reduce the system pressure by inducing condensation and will also enhance atmospheric mixing. The condensed water would flow down and accumulate in the IRWST, while gas (steam air hydrogen) flow could establish a natural circulation loop. The mixture distribution in the containment will depend on the number of rupture and convection foil openings and by the mixing dampers (Figure 11, left). With respect to PWR system, the topic proposed to investigate is the interaction between the natural circulation flow within containment compartments (inner and external compartments) and the convection flow induced by safety systems activation. PANDA tests addressing the discussed scenarios are proposed.

Figure 11 shows, on the left, a schematic representation of the main EPR^{TM} containment compartments and, on the right, the respective compartments in PANDA. The inner compartment (margins made with brown-dotted lines) including the IRWST is represented mainly by the lower two vessels and the lines R31–R42 (the volume ratios in PANDA between external and internal regions are not in scale with EPR^{TM}). The external compartment is represented by the upper two vessels and by downcomers DC1, D13, and DC2 and D24. The spray nozzle is installed in the external volume

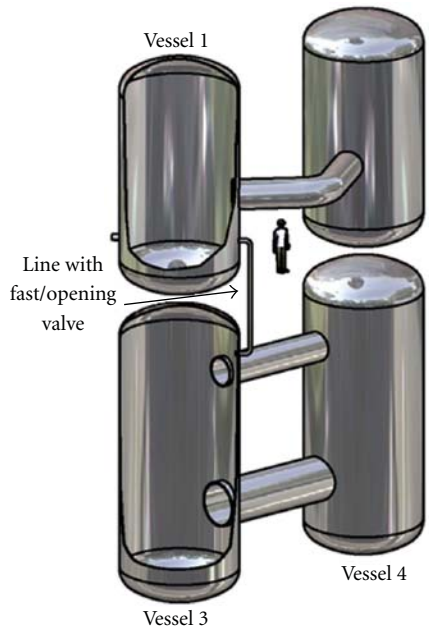

Figure 10: Schematic for the rupture disk tests.

and the heat source in the Drywell downcomers 1 and 2. In Figure 11 (left side), the rupture foils (green rectangles) and convection foils (magenta) are located in the upper regions. In PANDA (Figure 11 right), these are represented with the same color (magenta). The mixing dampers are located in the lower region above the IRWST (gold color). These PANDA investigations have been proposed in the frame of a new OECD/NEA project named HYMERES [22]. It should be pointed out that the main heights and volumes of EPR^{TM} and PANDA are not to scale; therefore the results for PANDA investigations cannot directly be extrapolated to the EPR^{TM}. The main aim with these investigations is the creation of a database at large scale, for code assessment and validation purposes.

3.7. Separate Effect Tests. In PANDA, separate tests were performed for a broad range of conditions in the frame of the OECD/SETH and SETH-2 projects. The main objective of these tests was to generate an experimental database of containment code validations.

The OECD/SETH PANDA investigations included three series of tests characterized by wall plumes, free plumes, and horizontal high-momentum jets. In addition to these series of tests, one specific three-gas test, identified in the SETH-1 project as Test 25, with air, steam, and helium has been carried out.

The OECD/SETH-2 PANDA separate effect investigations included vertical fluid release (jet or plume series [23, 24] and horizontal fluid release series [25].

The description of the PANDA SETH and SETH-2 experimental results goes beyond the scope of the present paper and therefore will be omitted.

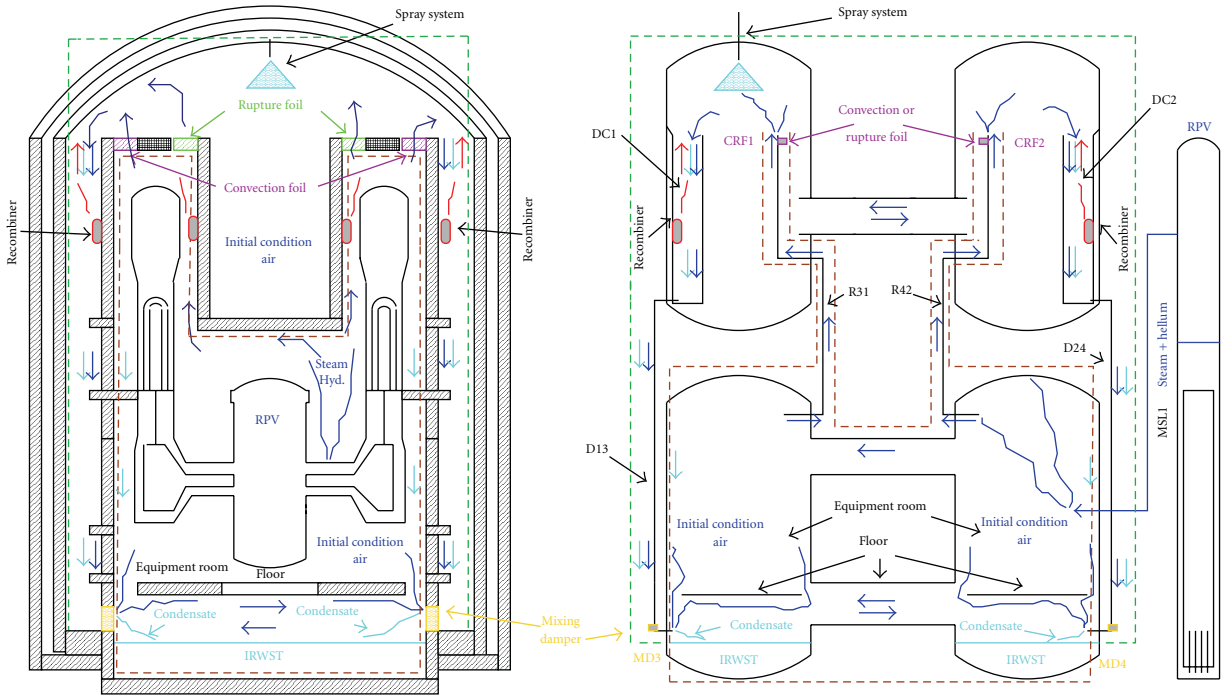

Figure 11: Schematic of PANDA facility versus EPR™ containment (height and main volumes are not in scale).

4. Conclusion

The paper provides an overview of the research programs performed and ongoing in the PANDA facility. The facility is well suited to investigate the safety system of several Generation III+ type reactors. The experimental results obtained are unique. Some of the tests related to the SBWR went through an audit from the NRC and are used as reference for the PCCS performance and for the certification of the ESBWR by the US NRC. Also, the tests related to the SWR1000 provided experimental data on the system behaviour under a variety of accident scenarios. PANDA was used in the framework of several European and OECD projects and has allowed the generation of large experimental database which were used to develop and validate CFD and safety analysis codes. The planned investigations of EPR™-type systems will further provide the experimental database at large scale on flow circulation between containment compartments and with the activation of safety systems. These results will not be directly extrapolated to EPR™ but will be used for assessing and validating computational tools to the PANDA scale, before their use for the real reactors.

References

[1] M. Huggenberger, C. Aubert, T. Bandurski et al., "ESBWR related passive decay heat removal tests in PANDA," in *Proceedings of the 7th International Conference on Nuclear Engineering (ICONE '99)*, Tokyo, Japan, 1999.

[2] J. Dreier, C. Aubert, M. Huggenberger, H. J. Strassberger, J. Meseth, and G. Yadigaroglu, "The PANDA Tests for the SWR1000 passive containment cooling system," in *Proceedings of the 7th International Conference on Nuclear Engineering (ICONE '99)*, Tokyo, Japan, 1999.

[3] D. Paladino, O. Auban, M. Huggenberger, and M. Andreani, "Investigation of light gas effects on passive containment cooling system in ALWR," in *Proceedings of the 10th International Topical Meeting on Nuclear Reactor Thermal Hydraulics (NURETH '03)*, Seoul, Korea, 2003.

[4] O. Auban, D. Paladino, and R. Zboray, "Experimental investigation of natural-circulation flow behavior under low-power/low-pressure conditions in the large-scale panda facility," *Nuclear Technology*, vol. 148, no. 3, pp. 294–312, 2004.

[5] O. Auban, R. Zboray, and D. Paladino, "Investigation of large-scale gas mixing and stratification phenomena related to LWR containment studies in the PANDA facility," *Nuclear Engineering and Design*, vol. 237, no. 4, pp. 409–419, 2007.

[6] D. Paladino, R. Zboray, P. Benz, and M. Andreani, "Three-gas mixture plume inducing mixing and stratification in a multi-compartment containment," *Nuclear Engineering and Design*, vol. 240, no. 2, pp. 210–220, 2010.

[7] D. Paladino, R. Zboray, and O. Auban, "The panda tests 9 and 9bis investigating gas mixing and stratification triggered by low momentum plumes," *Nuclear Engineering and Design*, vol. 240, no. 5, pp. 1262–1270, 2010.

[8] D. Paladino, R. Zboray, M. Andreani, and J. Dreier, "Flow transport and mixing induced by horizontal jets impinging on a vertical wall of the multi-compartment PANDA facility," *Nuclear Engineering and Design*, vol. 240, no. 8, pp. 2054–2065, 2010.

[9] R. Zboray and D. Paladino, "Experiments on basic thermal-hydraulic phenomena relevant for LWR containments: gas mixing and transport induced by buoyant jets in a multi-compartment geometry," *Nuclear Engineering and Design*, vol. 240, no. 10, pp. 3158–3169, 2010.

[10] D. Paladino, M. Huggenberger, M. Andreani et al., "LWR containment safety research in PANDA," in *Proceedings of the International Conference on Advances in Nuclear Power Plants (ICAPP '08)*, pp. 1853–1861, Anaheim, Calif, USA, June 2008.

[11] ERCOSAM: containment Thermal-hydraulics of current and future LWRs for severe accident management, SP5-Euratom, Collaborative Project, Small or medium-scale focused research project, FP7-Fission-2009, Grant Agreement No 249691, 2010.

[12] B. S. Shiralkar, M. D. Alamgir, and J. G. M. Andersen, "Thermal hydraulic aspects of the SBWR design," *Nuclear Engineering and Design*, vol. 144, no. 2, pp. 213–222, 1993.

[13] G. Yadigaroglu, "Derivation of general scaling criteria for BWR containment tests," in *Proceedings of the 4th International Conference on Nuclear Engineering (ICONE '96)*, pp. 547–558, New Orleans, La, USA, March 1996.

[14] G. Yadigaroglu, J. Dreier, and M. Huggenberger, "The PANDA tests for the SBWR," in *Proceedings of the 25th Water Reactor Safety Information Meeting*, Bethesda, Md, USA, October 1997.

[15] T. Bandurski, M. Huggenberger, J. Dreier et al., "Influence of the distribution of noncondensibles on passive containment condenser performance in PANDA," *Nuclear Engineering and Design*, vol. 204, no. 1–3, pp. 285–298, 2001.

[16] H. W. Schenck and A. M. Hoft van Huysduynen, "Scaling analysis of passive containment cooling tests," INNO-TEPSS (96)-DO04. ECN, Petten, Nederland, 1997.

[17] D. Paladino, O. Auban, M. Huggenberger, and J. Dreier, "A PANDA integral test on the effect of light gas on a Passive Containment Cooling System (PCCS)," *Nuclear Engineering and Design*, vol. 241, no. 11, pp. 4551–4561, 2011.

[18] G. Mignot, R. Kapulla, N. Erkan, R. Zboray, and D. Paladino, "Containment cooler performance in the presence of light non condensable gas with cooler location as a primary parameter," in *Proceedings of the 14th International Topical Meeting on Nuclear Reactor Thermalhydraulics*, Toronto, Canada, September 2011.

[19] N. Erkan, R. Kapulla, G. Mignot, R. Zboray, and D. Paladino, "Experimental investigation of spray induced gas stratification break-up and mixing in two interconnected vessels," *Nuclear Engineering and Design*, vol. 241, no. 9, pp. 3935–3944, 2011.

[20] D. Paladino, G. Mignot, N. Erkan, R. Zboray, R. Kapulla, and M. Andreani, "Sudden discharge of gas mixture in a confined multi-compartment," in *Proceedings of the 14th International Topical Meeting on Nuclear Reactor Thermalhydraulics (NURETH '10)*, Toronto, Canada, September 2011.

[21] R. P. Martin, C. A. Bonilla, and E. S. Williams, "Combustible gas control system evaluation for the U.S. EPR," in *Proceedings of the 13th International Topical Meeting on Nuclear Reactor Thermal Hydraulics (NURETH '09)*, Kanazawa city, Ishikawa Prefecture, Japan, September 2009.

[22] CSNI, Summary record of the Forty-ninth CSNI Meeting, NEA/SEN/SIN(2011)2, Paris, France, June 2011.

[23] R. Kapulla, D. Paladino, G. Mignot, R. Zboray, and S. Gupta, "Break-up of gas stratified in LWR containment induced by negatively buoyant jets and plumes," in *Proceedings of the International Conference in Nuclear Engineering (ICONE '09)*, Brussels, Belgium, July 2009.

[24] G. Mignot, D. Paladino, R. Kapulla, and R. Zboray, "Overview of vertical fluid release series," in *Proceedings of the 13th International Topical Meeting on Nuclear Reactor Thermal Hydraulics (NURETH '09)*, Kanazawa City, Ishikawa Prefecture, Japan, September 2009.

[25] R. Zboray, D. Paladino, G. Mignot, and R. Kapulla, "Mixing of density stratified containment atmosphere by horizontal jet release," in *Proceedings of the International Conference Nuclear Energy for New Europe*, Bled, Slovenia, September 2009.

Hindawi Publishing Corporation
Science and Technology of Nuclear Installations
Volume 2012, Article ID 275693, 20 pages
doi:10.1155/2012/275693

Research Article

Experimental Studies for the VVER-440/213 Bubble Condenser System for Kola NPP at the Integral Test Facility BC V-213

Vladimir N. Blinkov,[1] Oleg I. Melikhov,[1] Vladimir I. Melikhov,[1] Mikhail V. Davydov,[1] Holger Wolff,[2] and Siegfried Arndt[2]

[1] *Thermo-Hydraulics Division, Electrogorsk Research and Engineering Center for Safety of Nuclear Power Plants, Saint Constantine Street 6, Electrogorsk, Moscow 142530, Russia*
[2] *Gesellschaft für Anlagen- und Reaktorsicherheit (GRS) mbH, Kurfürstendamm 200, 10719 Berlin, Germany*

Correspondence should be addressed to Vladimir I. Melikhov, vladimir.melikhov@erec.ru

Received 3 May 2011; Accepted 19 August 2011

Academic Editor: Alessandro Del Nevo

In the frame of Tacis Project R2.01/99, which was running from 2003 to 2005, the bubble condenser system of Kola NPP (unit 3) was qualified at the integral test facility BC V-213. Three LB LOCA tests, two MSLB tests, and one SB LOCA test were performed. The appropriate test scenarios for BC V-213 test facility, modeling accidents in the Kola NPP unit 3, were determined with pretest calculations. Analysis of test results has shown that calculated initial conditions and test scenarios were properly reproduced in the tests. The detailed posttest analysis of the tests performed at BC V-213 test facility was aimed to validate the COCOSYS code for the calculation of thermohydraulic processes in the hermetic compartments and bubble condenser. After that the validated COCOSYS code was applied to NPP calculations for Kola NPP (unit 3). Results of Tacis R2.01/99 Project confirmed the bubble condenser functionality during large and small break LOCAs and MSLB accidents. Maximum loads were reached in the LB LOCA case. No condensation oscillations were observed.

1. Introduction

The VVER-440/213 Pressurized Water Reactors (Russian design) are equipped with a Bubble Condenser Containment (BCC) for the confinement of radioactive releases following design basis accidents [1]. The BCC structure consists of the hermetic compartment system which surrounds the complete primary system and a pressure retaining bubble condenser system comprising a complex pressure-suppression system and air traps, Figure 1. The main function of bubble condenser system is to reduce the pressure of the entire containment in case of a design basis accident, such as a loss of coolant accident (LOCA).

In the case of a postulated large break LOCA, up to a break of 500-mm diameter piping, the steam-air mixture generated within the hermetic compartment system is transferred into the bubble condenser system through the bubble condenser shaft. It penetrates the horizontal spaces between the water trays. The steam-air mixture passes through a large number of vertical openings, the gap/cap inlet openings, to the water trays. These gap/cap inlet openings are lengthy rectangular gaps covered by rectangular caps forcing the steam-air mixture to flow through the water pools, that is, the initial upward directed flow is turned 180 degrees by the caps into a downward oriented flow (see Figure 3). The increasing pressure of the steam-air mixture below the water tray forces the steam-air mixture to move down the water inside the cap around the gap until the lower edge of the cap is reached and the steam-air mixture flows into the water pool in the water tray, distributing the steam/air flow into the water by the zigzag-shaped lower edge of the cap. The steam is condensed by the cold water in the water trays; the residual air leaves the surface of the water pool and is collected within the space above.

The gas volumes above the water levels are connected to large volumes of the air traps by one way check valves, which allow the air to flow into the air trap volumes preventing its backflow. This results in a reduction of the maximum

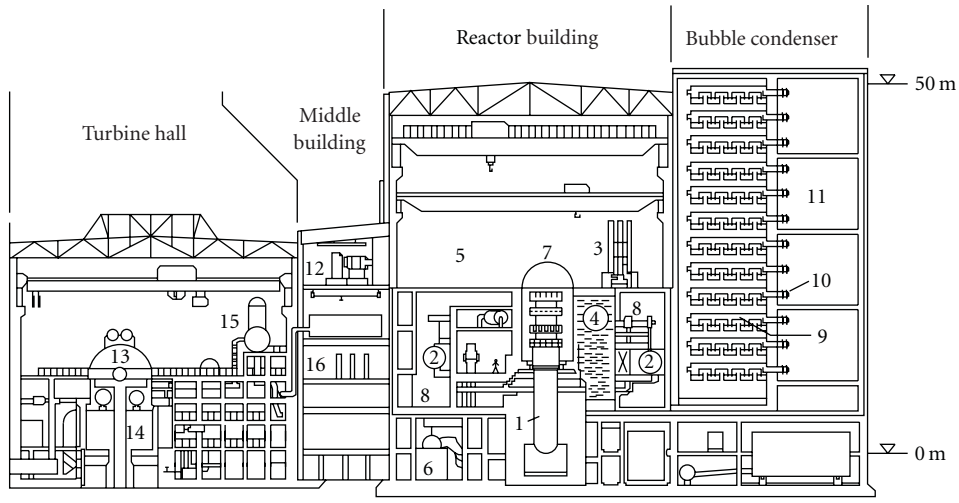

(1) Reactor pressure vessel
(2) Steam generator
(3) Refueling machine
(4) Spent fuel pit
(5) Reactor hall
(6) Make-up feedwater system
(7) Protectice cover
(8) Confinement system
(9) Bubble condenser trays
(10) Check valves
(11) Air traps
(12) Intake air unit
(13) Turbine
(14) Condenser
(15) Feedwater tank with degasifier
(16) Electrical instrumentation and control compartments

Figure 1: VVER-440/213 plant layout.

pressure in the upstream volumes and the hermetic compartment system below atmospheric as soon as the residual steam has been condensed at the corresponding surfaces, by the active spray system and the reverse flow of the bubble condenser (BC) water (so-called passive spray) expected during LB LOCA.

The bubble condenser system was designed to withstand design basis accident conditions and to maintain its integrity in order to fulfill its safety function. Nevertheless, particularly for design basis accidents, detailed analyses identified the need to improve the modeling of accidents and to extend the knowledge of integral and separated effects. There was also a need to produce qualified experimental data in order to strengthen the basis for computer code validation.

During the 1990s, a number of investigations, including analyses and experiments, have been performed in order to ascertain the capabilities of the VVER-440/213 bubble condenser. The large-scale test facility BC V-213 at the Electrogorsk Research and Engineering Center on NPPs Safety (EREC) was developed for experimental investigation of the bubble condenser system of VVER-440/213 in the frame of Tacis/Phare Project PH 2.13/95 [2]. The test facility is an integral model of the NPP's hermetic compartments with full-scale fragment of BC. The BC V-213 test facility is equipped with a system of high pressure vessels and pipelines that makes it possible to simulate both primary and secondary coolant blowdown under conditions analogous to those under NPPs design accidents.

According to the PH 2.13/95 Project there were performed tests simulating LB LOCA conditions as applied to Paks NPP, Hungary. However, the obtained results may not be used completely to justify the response of Bubble Condenser Containment System at unit 3 of the Kola NPP, since there are two distinctive features in design. They are as follows:

(i) twice the number of DN 500 check valves installed between the BC and the air traps at Kola NPP against Paks NPP;

(ii) there is only one corridor with an area of 15.7 m^2 between steam generator boxes and dead-end volume at Kola NPP.

The specific features mentioned above may exercise a significant influence on the BC behavior as well as on the variables characterizing its operation. So, specific thermohydraulic experimental qualification of the BC is required in this case. This was the main objective of the R2.01/99 Project, which was performed in 2003–2005.

Main results obtained in the frame of these tests are described in the paper.

2. Short Description of the BC V-213 Test Facility

The test facility is an integral model of the NPP's hermetic compartments built in scale 1 : 100 as regards the volumes

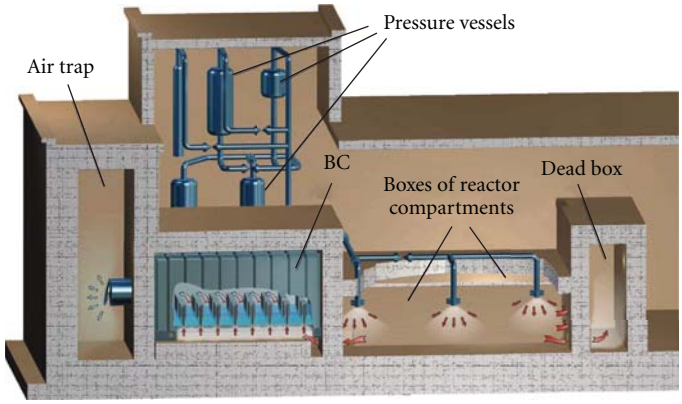

(a) General view of the facility

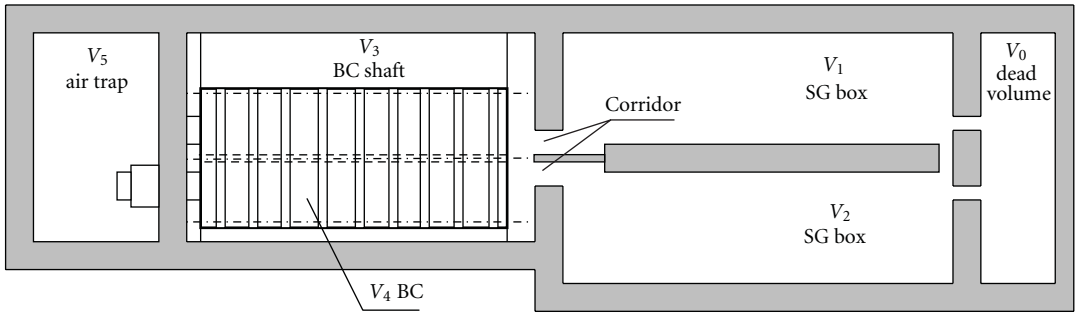

(b) Top view

Figure 2: BC V-213 test facility.

and flow areas with full-scale fragment of bubbler condenser, Figures 1 and 2.

Main elements of the BC V-213 test facility are as follows:

(i) five hermetic boxes composed of the dead-end volume V_0, two steam generators boxes V_1 and V_2, BC shaft V_3, and air trap V_5;

(ii) full-scale fragment of bubbler condenser volume V_4 located in V_3 with the relief valve DN250 and two check valves DN173; the BC fragment consists of two sections with nine gap/cap units each; the tray is filled with nonborated water (initial level 500 mm) (Figure 3);

(iii) five high-pressure vessels V_{v1}, V_{v2}, V_{v3}, V_{v4}, and V_{v5} for preparation of the coolant (water and steam) with predefined parameters (Figure 4);

(iv) additional steam supply pipeline connected to the V_{v1} pressure vessel;

(v) blowdown lines DN220 with three branches located in the V_1 box at different distances from corridor to BC inlet;

(vi) blowdown nozzles and rupture disks installed at the ends of the blowdown lines' branches;

(vii) sprinkler system with two nozzles located in the V_1 and V_2 boxes.

The specific features of the test facility with reference to Kola NPP unit 3 are two check valves DN173 and only one corridor between V_1 and V_0 boxes. The corridor between V_2 and V_0 boxes is closed.

Table 1: Geometrical parameters of the hermetic compartments of the test facility.

Hermetic box (designation)	Volume, (m^3)	Total area of walls, (m^2)	Heat insulated area, (m^2)
Dead volume (V_0)	46,5	98	0
Steam generator box (V_1)	71,8	121	40
Steam generator box (V_2)	72,5	124	41
BC shaft (V_3)	75	200	98
BC gasroom (V_4)	61,1	77	0
BC water in trays	12,8	73	0
Air trap (V_5)	176,5	206	93

Main geometrical parameters of the boxes and high-pressure vessels are presented in Tables 1 and 2, correspondingly.

The test facility instrumentation comprises standard and nonstandard instruments, quasistatic measurements with a sampling rate of 10 Hz, and dynamic measurements of sampling rate up to 1000 Hz. The total number of measuring channels, including the major and auxiliary ones is about 300.

Detailed descriptions of the test facility and its measuring system are presented in [3, 4].

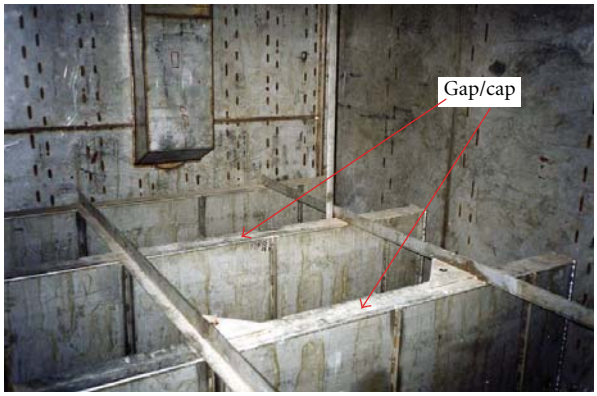

(a) General view of the BC (without water)

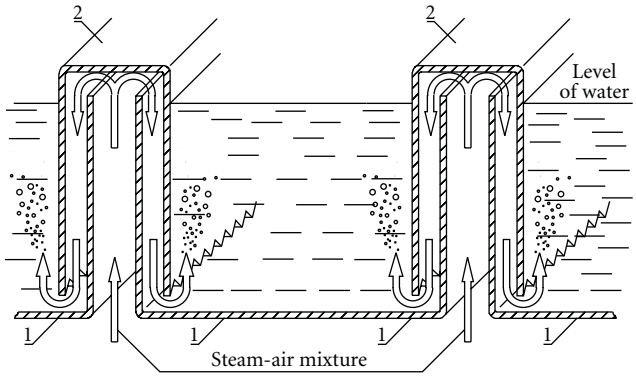

(b) Gap-cap unit: 1 –tray, 2 –cap

Figure 3: Gap/cap systems of the BC V-213 test facility.

3. Test Plan and Methodology of Investigations

Based on analysis of test matrix developed in the frame of Tacis/Phare PH2.13/95 [5] six tests were specified for investigation of BC system under accident conditions of Kola-3 NPP, Table 3.

General methodology of investigations and the main steps are the following.

(1) Modelling of an accident at Kola NPP with the ATHLET code [6], where the mass flow rate and specific enthalpy of discharged coolant through the break are calculated (so called MER—Mass and Energy release Rate).

(2) Variant calculations of coolant discharge from the high-pressure system of BC V-213 test facility are performed with the same code ATHLET in order to define facility operation conditions (water temperature in the high pressure vessels, nozzle diameter, etc.), allowing to simulate the NPP coolant blowdown parameters reduced by 100 times (in accordance with scale of the test facility). Test scenario is specified on the basis of these ATHLET calculations.

(3) The test is performed in accordance with the specified scenario.

Table 2: Geometrical parameters of the high-pressure vessels.

Vessel designation	Volume, (m^3)	Inner diameter, (m)	Height, (m)
V_{v1}	1.95	1,03	2,887
V_{v2}	1.2	1,03	1,83
V_{v3}	0.91	1,0	0,73
V_{v4}	2.25	1,0	2,435
V_{v5}	0.44	0,4	4,31

(4) Experimental MER is determined by posttest analysis of the coolant discharge from the high-pressure system of the test facility with the ATHLET code.

(5) Validation of the COCOSYS code [7] on experimental data concerning thermal-hydraulic processes in BC and hermetic compartments at BC V-213 test facility.

(6) Application of the validated COCOSYS code for analyzing of thermal-hydraulic processes in the hermetic compartments and BC loading during a corresponding accident at Kola NPP.

The detailed investigations of BC response under LB LOCA conditions are one of the important aims of the project. The double-ended break of main circulation line (MCL) close to the inlet reactor nozzle with simultaneous total loss of electricity is considered. Nodalization scheme of VVER-440/213 and corresponding ATHLET input deck are prepared. Two loops are used for modeling of one accidental loop and five intact ones, respectively. Pressurizer is connected with the intact loop. Nodalization scheme includes 80 thermofluid objects consisted of 294 control volumes and 219 junctions. Heat conduction objects are divided into 186 control volumes with 756 cells. For calculation of core power the point reactor kinetics model is used. Initial conditions for the LB LOCA accident are presented in Table 4.

Leak opening time is 0.01 s. Table 5 presents sequence of main events and timing during LB LOCA.

The scram signal due to decreasing of pressure in the primary circuit is switched on at 0.03 s and core power is decreased. Coolant is mainly discharged from pressure vessel side, because of coolant supply from cold legs of intact loops. The pressure in the primary circuit is sharply decreased down to saturation pressure (≈8 MPa), the pressure in the pressurizer is slower decreased due to saturation conditions in the pressurizer at the initial moment. The pressurizer is emptied at 15 s. The vapor in the core is raised very quickly due to reverse of direction of coolant flow. In the upper plenum vapor is appeared earlier than in the lower plenum. Hydroaccumulators start supplying the coolant to the reactor vessel at 5.4 s. Total mass of the coolant in the primary circuit is more or less stabilized after ≈20 s. The cooling of the core is secured due to supply of the coolant from hydroaccumulators. The maximum flow rate of discharged coolant through the break ~18000 kg/s is achieved at the initial moment, after that mass flow rate decreases down to ~6000 kg/s at 10 s and later on to about 2000 kg/s at 25 s

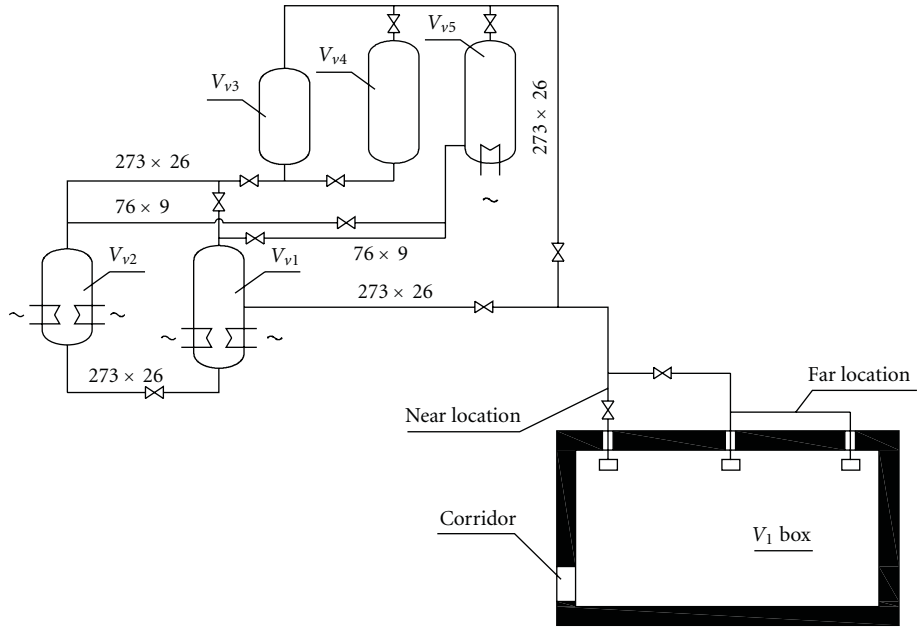

Figure 4: High-pressure system.

Table 3: Test plan.

Test designation (according to [5])	Accident	Test purpose
Test 1	LB LOCA	Integral behavior of the compartment and bubble condenser system
Test 4	LB LOCA	Response of bubble condenser system to maximum steam loading
Test 5	LB LOCA	Response of bubble condenser system to maximum air loading
Test 7	MSLB	Response of bubble condenser system to maximum air loading
Test 9	MSLB	Response of bubble condenser system to maximum steam loading
Test 12	SB LOCA	Observation of condensation oscillations

and to ~300 kg/s at 55 s. The subcooled water is discharged through the break during the whole transient.

An instantaneous double-ended guillotine break of the MCL DN500 is considered as a limiting design basis LOCA, that is, the design basis LOCA defining the necessary capacity of the accident localization system (hermetic compartments, BC, and spray system).

For design basis accidents, the following design criteria are considered (specific for the Kola NPP, unit 3, i.e., different from other units with BCC):

(i) maximum absolute pressure and temperature in hermetic compartments shall not exceed 0.20 MPa and 128°C, respectively;

(ii) an under pressure not exceeding 0.0196 MPa shall be created in hermetic compartments within 30 minutes (minimum absolute pressure shall not be below 0.078 MPa).

The test scenarios for LB LOCA are developed for different stages of the accident. The reason for that is as follows. We try to obtain coincidence with scaled 1 : 100 NPP leak functions (mass flow rate and enthalpy) by varying of the nozzle diameter. Satisfied coincidence during a relatively long time (~20–30 s) is not reached for any values of nozzle diameter due to some limitations inherent to the test facility. So two criteria for selection of necessary nozzle diameter are used. First criterion is connected with coincidence of maximum flow rates to reproduce maximal loads on BC system and second one is coincidence of total discharged mass and energy for first 10 s to reproduce integral loads. So, it is decided to model different stages of LB LOCA (initial stage and middle-term stage) during different tests with corresponded nozzle diameter.

Tests 4 and 5 in Table 3 are aimed to model only the initial stage of LB LOCA, which is characterized by large pressure differences (~15–20 kPa) across the gap/cap system and BC walls and the nonuniformities of the flow distribution inside the BC. For example, Figure 5 shows scaled Kola-3 NPP MER and test facility MER for Test 4 calculated with the ATHLET code. The test facility MER provides adequate reproduction of the NPP MER during the very initial stage (~5 s) and after that the test facility MER is more conservative than the NPP one.

The difference between Test 4 and Test 5 is related to the position of the discharge nozzle in SG box V1 (Test 4: near BC for providing large steam concentration in the air-steam flow directed to the BC (lower floors in BC tower), Test 5: far BC for providing large air concentration in the air-steam flow directed to the BC (upper floors in BC tower)).

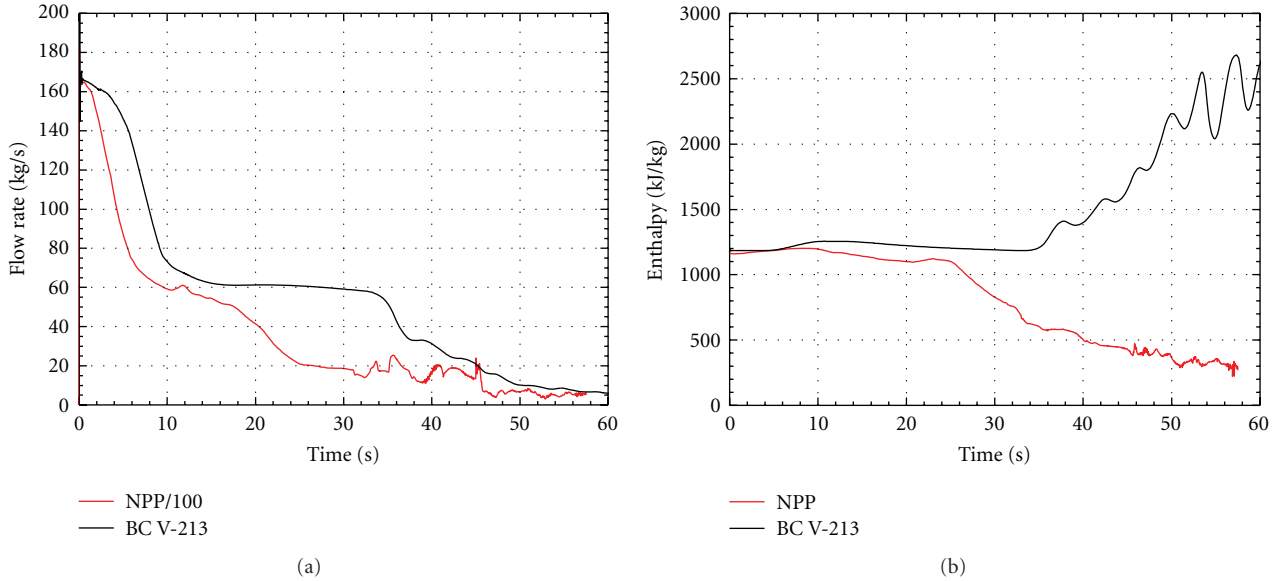

Figure 5: Calculated test facility and NPP MERs for Test 4. (a) Break flow rate, (b) break enthalpy.

Table 4: Initial conditions of LB LOCA.

Parameter	Value
Upper plenum pressure, (MPa)	12.24
Core outlet temperature of coolant, (°C)	297.2
Core inlet temperature of coolant, (°C)	267.1
Loop flow rate, (kg/s)	1463
Main coolant pump pressure difference, (MPa)	0.47
Pressurizer temperature, (°C)	325.7
Pressurizer level, (m)	5.97
Core power, (MW)	1375
Steam generator pressure, (MPa)	4.66
Live steam temperature, (°C)	259.5
Feed water temperature, (°C)	222.8
Live steam and feed water flow rate, (kg/s)	128
Water level in steam generator, (m)	1.831
Power of steam generators, (MW)	1375
Initial pressure in hydroaccumulators, (MPa)	5.9
Initial water level in hydroaccumulators, (m)	5.6
Water temperature in hydroaccumulators, (°C)	55
Pressure in low pressure system, (MPa)	0.695

Test 1 is aimed to model (in average) thermohydraulic processes under LB LOCA conditions for the time period ~100 s, when the bubble condenser and hermetic boxes are mostly impacted by the break. Special pretest calculation procedure, based on the methodology developed in the frame of the German-Russian Project INT 9142 [8], was performed to determine the scenario of Test 1. Main stages of this procedure are the following:

(i) defining with the COCOSYS code main parameters ranges, specifying thermohydraulic conditions for bubble-condenser inlet for the Kola NPP, based on the Kola NPP data base prepared in frame of the Tacis Project RF/TS [9];

Table 5: Chronology of events during LB LOCA.

Time, sec	Event
0.0	Double-ended guillotine break
0.0	Total loss of electricity
0.0	Turbine isolation begins
0.03	Scram signal
0.1	More then three main coolant pumps dropped out
4.76	Pressurizer pressure <10,8 MPa
5.41	Start of hydroaccumulator injection to downcomer
5.46	Start of hydroaccumulator injection to upper plenum
6.99	Pressurizer level <2.76 m
8.22	Pressurizer level <2.26 m
16.00	Start of high-pressure injection system
32.90	Start of low-pressure injection system

(ii) these parameters (criteria) are

criterion C1: mass flow density entering the BC gap/caps [kg/(s*m^2)]

$$C_1 = \frac{G}{A \cdot n} \quad (1)$$

with G: total mass flow entering all gap/caps, [kg/s], A: cross section area of one gap/caps system, [m^2], n: number of gap/caps systems, [-].

criterion C2: specific steam mass flow entering the BC water layer [kg/(s*t)]

$$C_2 = \frac{n \cdot G_{\text{steam}}^{\text{gap/cap}}}{m_{\text{water}}} \quad (2)$$

with n: number of gap/caps systems, [-], m_{water}: water mass, [t], $G_{\text{steam}}^{\text{gap/cap}}$: steam mass flow entering a gap/cap system, [kg/s].

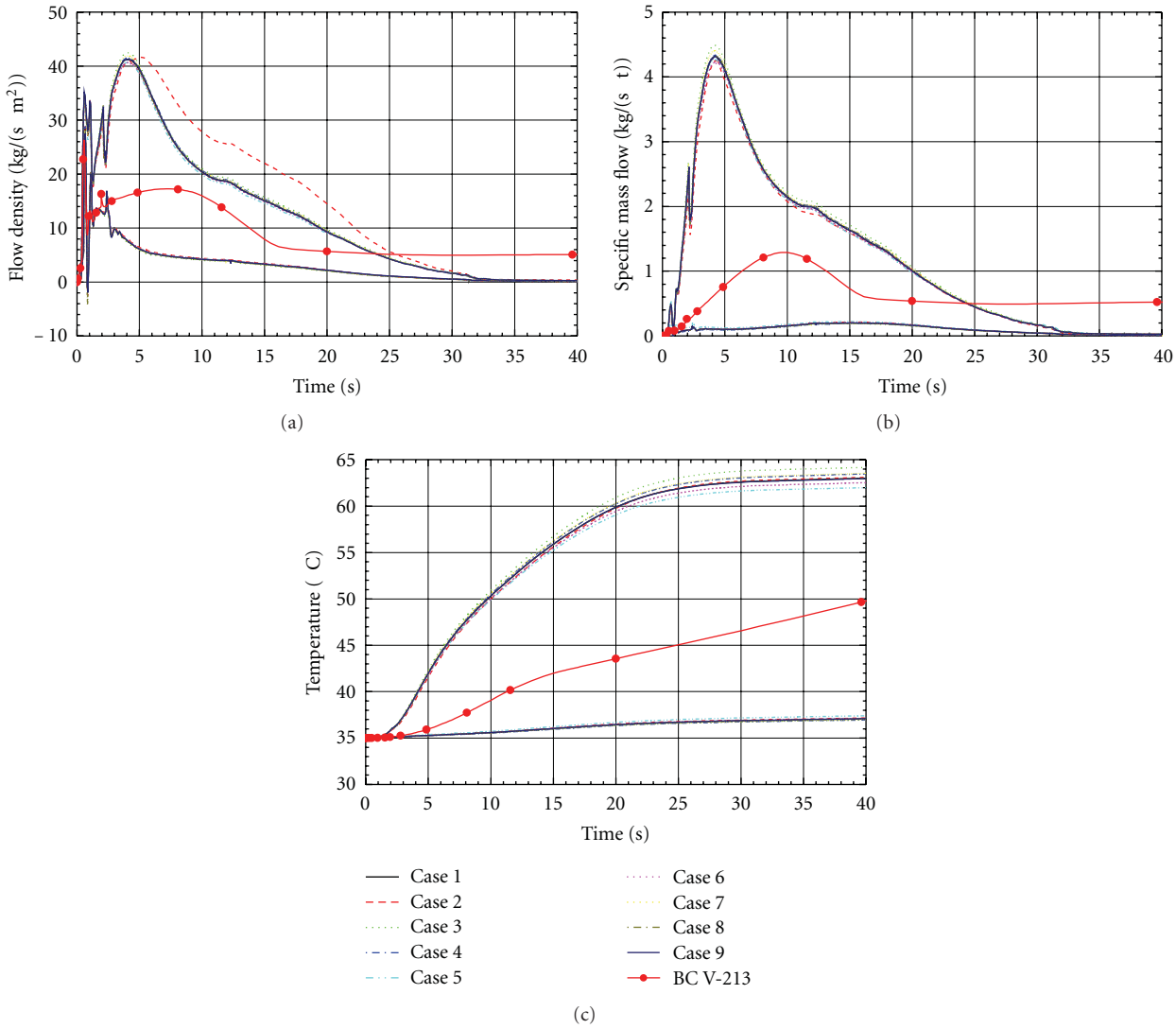

Figure 6: Criteria C1—C3. (a) C1: mass flow density entering BC gap/caps (and NPP bandwidth), (b) C2: specific steam mass flow entering BC water layer (and NPP bandwidth), (c) C3: BC water temperature (and NPP bandwidth).

criterion C3: BC water temperature [°C]. These criteria will be calculated for the NPP (beside the main parameters pressure, temperature and pressure differences) for the lowest and the uppermost condensing trays for different initial and boundary conditions of the defined LB LOCA scenario, which results in bandwidths;

(iii) performing iterative calculations of coolant blowdown from the high-pressure vessel system by means of ATHLET code and processes in the bubble-condenser system and BC V-213 compartments by means of the COCOSYS code in order to define the test scenario, allowing to reach BC loading conditions representative for the reference NPP, Figure 6.

Test scenarios for MSLB and SB LOCA tests are specified without any difficulties.

As a result of pretest calculations [10], initial and boundary conditions of the tests (Table 6) have been specified. Initial water level in the BC tray is 500 mm, and initial temperature of the tray water is about 35°C for all tests.

4. Main Test Results

In accordance with specified test scenarios six tests were performed for qualification of BC system under accident conditions at Kola-3 NPP [11–16]. Main experimental results are summarized in Table 7.

Analysis of the test results has shown that calculated initial conditions and test scenarios were properly adjusted in the tests.

5. Posttest Analysis of the Tests Performed at BC V-213 Test Facility

5.1. Modeling of High-Pressure System of BC V-213 Test Facility with the ATHLET Code. The ATHLET 1.2 Cycle D

Table 6: Initial and boundary conditions of the tests.

Test facility parameter	Test 1	Test 4	Test 5	Test 7	Test 9	Test 12
V_{v1}	Fully filled with water $T = 271.5°C$	Fully filled with water $T = 271.5°C$	Fully filled with water $T = 271.5°C$	Water level 2.325 m $T = 259°C$	Water level 2.325 m $T = 259°C$	Fully filled with water $T = 271.5°C$
V_{v2}	Fully filled with water $T = 298.5°C$	Fully filled with water $T = 298.5°C$	Fully filled with water $T = 298.5°C$	Water level 1.370 m $T = 259°C$	Water level 1.370 m $T = 259°C$	It is not used
V_{v3}	It is not used	It is not used	It is not used	Steam $T = 259°C$	Steam $T = 259°C$	It is not used
V_{v4}	It is not used	It is not used	It is not used	It is not used	It is not used	It is not used
V_{v5}	Water level 1.270 m $T = 327°C$	Water level 1.270 m $T = 327°C$	Water level 1.270 m $T = 327°C$	Steam $T = 259°C$	Steam $T = 259°C$	Water level 3.000 m $T = 327°C$
System pressure	12.5 MPa	12.5 MPa	12.5 MPa	4.7 MPa	4.7 MPa	12.5 MPa
Additional supply of steam ($P = 8$ MPa, $T = 300°C$) into V_{v1}	It is not used	It is not used	It is not used	0.4 kg/s (100–500 s) 0.2 kg/s (after)	0.4 kg/s (100–500 s) 0.2 kg/s (after)	It is not used
Position of discharge nozzle	Middle	Near	Far	Far	Fear	Middle
Nozzle diameter	45 mm	56 mm	56 mm	56 mm	56 mm	4 mm

Table 7: Summary of main experimental results.

No.	Parameter	Tests					
		Test 4 LB LOCA	Test 5 LB LOCA	Test 1 LB LOCA	Test 7 MSLB	Test 9 MSLB	Test 12 SB LOCA
(1)	Maximum absolute pressure in box V_1, (MPa)	0,202	0,214	0,197	0,1835	0,175	0,111
(2)	Time of achievement of maximum pressure in box V_1, (s)	8,07–9,77	8,89	70–90	90–100	90.5–96	353–388
(3)	Maximum pressure difference across BC, (kPa)	14,55	15,73	11,62	7,8	7,7	4,9
(4)	Maximum absolute pressure in air trap V_5, (MPa)	0,193	0,200	0,191	0,177	0,169	0,106
(5)	Maximum temperature in box V_1, (°C)	120	122	120	118	118	86
(6)	Maximum temperature of BC water, (°C)	78	78	60	56	63	38,5
(7)	Time of check valve closure, (s)	90	87	114	212	185	2240
(8)	Absolute pressure in box V_3 when relief valve opened, (MPa)	0,19	0,17	0,191	0,174	0,167	0,106
(9)	Time of relief valve opening, (s)	88,6	90,3	115	207,6	180	2300
(10)	Occurrence of reverse flow from BC	no	yes	no	no	no	no
(11)	Break location	near	far	middle	far	near	middle

version [6] was used for performing posttest analysis of coolant discharging.

The corresponding ATHLET nodalization scheme is presented in Figure 7. It consists of 41 thermofluid objects with 331 control volumes and 337 junctions. Also 46 heat structures with 326 heat conduction volumes (1326 layers) are used for description of tubes' and vessels' walls and thermoinsulation. The object AMBIENT (time-dependent volume) with constant pressure 0.1 MPa and temperature 25°C is used to model heat exchange with the environment. Heat transfer coefficient from the surface of thermoinsulation to the environment equals to $10\,W/(m^2\,K)$.

Since the discharge mass flow rate is one of the most important thermal-hydraulic boundaries dominating the course of a LOCA or a blowdown experiment, an accurate simulation of the critical flow is required. The one-dimensional thermodynamic nonequilibrium model CDR1D of ATHLET is used with consideration of geometric details of the discharge flow path for calculation of the critical discharge.

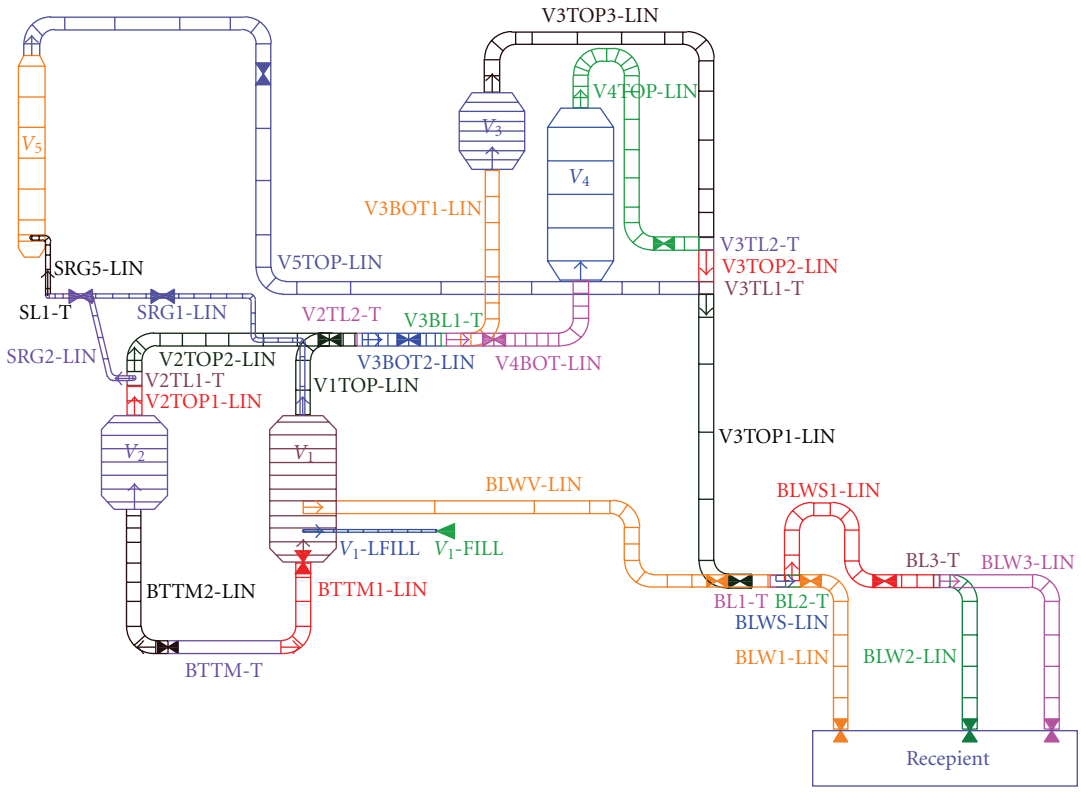

Figure 7: Nodalization scheme of the high-pressure system.

Form loss coefficients essentially influence the blowdown dynamics. Their values were based on [17].

The ATHLET input deck, prepared by EREC, for modeling of high-pressure system of BC V-213 test facility was carefully reviewed by GRS experts in the frame of the German-Russian Project INT 9142 [8]. Their comments permitted to improve the ATHLET input deck and the quality of modeling of thermohydraulic processes in the high-pressure system of the BC V-213 test facility.

5.2. Modeling of BC and Compartments of BC V-213 Test Facility with the COCOSYS Code. One of the main purposes of the posttest analysis was the development of the COCOSYS basic input deck, which allows to adequately simulate all tests performed in the frame of the Tacis Project R2.01/99. Only the final version of the input deck is described here.

The nodalization of the BC V-213 test facility consists of 24 zones, 34 atmospheric and 21 drain junctions, 4 pump systems, and 109 heat conducting structures. The input deck is based on a deck developed by GRS in frame of the German-Russian Project INT 9142 for analysis of the SLB experiments. This input deck was modified in accordance with modifications of the BC V-213 test facility [4].

The corresponding nodalization scheme is presented in Figure 8.

The subdivision of the SG box V_1 into three zones reflects the three possible break locations. In the lower parts of the facility compartments water can accumulate. Thus, they are modelled as separate sumps. At initial time a small amount of water is assumed in the sumps. Water carryover between the nodes is considered by values reducing downstream from the break location.

Zones are connected by atmospheric junctions to simulate the transport of accident-generated 2-phase 2-component mixture.

The gasroom of the BC is connected with the air trap V_5-AT via the dynamic flap F1 to model the two DN173 check valves including their inlet protection ducts. It should be noted that one DN173 check valve installed at BC V-213 test facility simulates twenty four DN500 check valves (2 in series) installed at Kola NPP in the scale 1 : 100 with regards to cross-section area. Opening pressure difference both check valve DN173 and check valve DN500 is the same (0.49 kPa), full opening of them is achieved under the pressure difference 9.8 kPa.

The full-scale DN250 relief valve connecting BC gasroom and BC shaft is simulated by the dynamic flap F2. Flap F2 will be locked in closed position, if the pressure in the BC shaft rises higher than locking pressure value. The value of unlocking pressure for F2 is changed from 163.7 kPa in pretest calculations to corresponding values observed in the tests (Table 7), for example, 190.0 kPa in Test 4.

The facility compartment system is assumed to be leak tight. The two special rupture disks and their structures in the SG compartment V_2, designed to protect the facility from overpressure failure, were considered as heat structures only.

Drain junctions in COCOSYS are foreseen to simulate flow processes of water, for instance the drainage of injected water or condensate (drain junctions D1…D15) or the flow

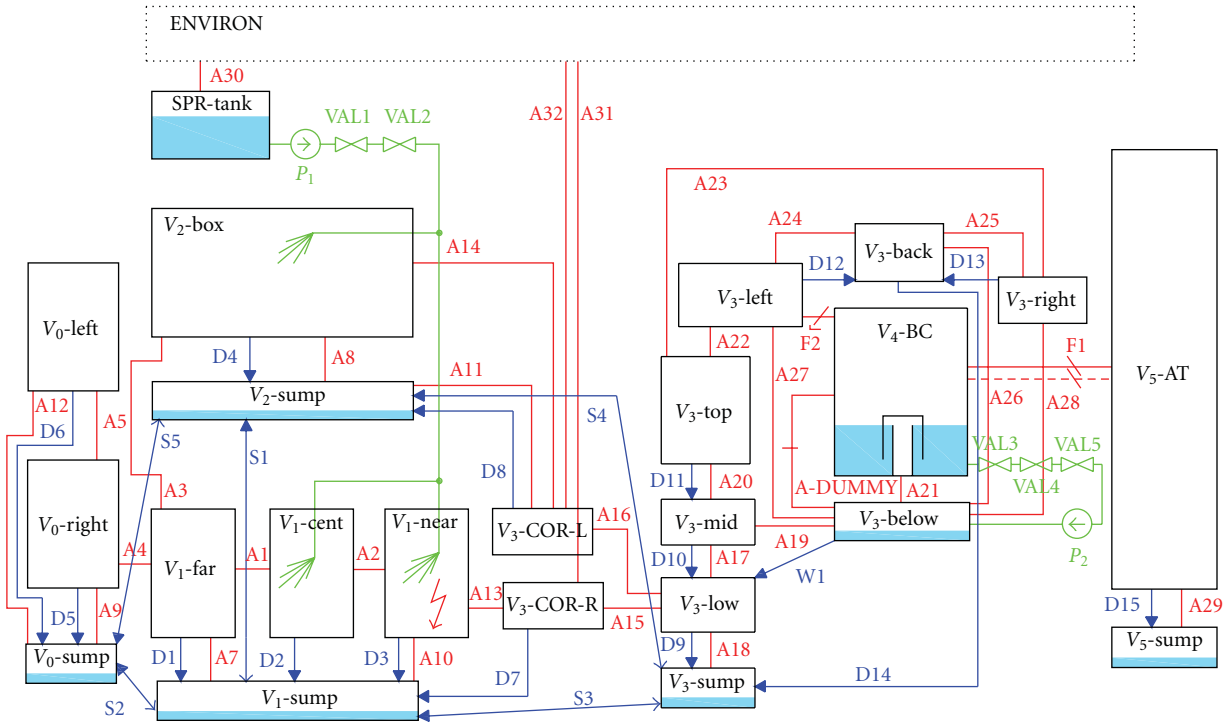

Figure 8: COCOSYS, 24 zone nodalization for the EREC BC V-213 test facility.

between different sumps to equalise the water surface levels (S1…S5). It is assumed that during any experiment all drain junctions to the facility outside are closed and, thus, not considered in the input deck.

The spray system, which injects water into both SG boxes V_1 and V_2, is simulated by a pump system. Activation of the spray system is to be set according the test performance.

Heat transfer and heat conduction processes are considered by so-called heat slabs. For each zone the relevant surfaces were defined as floor, side walls, and ceiling. The BC walls are subdivided into different heat slabs to consider that wall sides are linked with the pool (water), the gasroom, or the gap/cap system.

Some parts of the wall surfaces in the SG boxes V_1 and V_2 in the BC shaft volume V_3 and in the air trap V_5 are insulated with wooden plates. This is a known important uncertain boundary condition. This insulation is considered in the input deck with reasonable geometry and physical material properties. All surfaces except the stainless steel walls of the bubble condenser are treated to be coated with paint (epoxide layer). According to [8] modified material properties of reinforced concrete and wood are used.

In the 24 zone data set, all 18 gap/cap systems of the BC V-213 facility are modelled by one zone of the DRASYS type. Consequently, only an average BC behaviour is simulated (average pool temperature heat up).

To model the water carryover into the gasroom and the air trap special pumps are defined. The corresponding time-dependent water mass flow rates were defined as about 50% of the gas mass entering the gasroom and the air trap (via junction F1).

In the applied developer version COCOSYS 2.0AA (status 2005) the DRASYS zone model was improved on the basis of EREC BC V-213 experiments to permit the simulation of humid air flowing through the BC water pool to the gasroom. Up to the earlier code version V2.0v2 only dry air option is available. Corresponding additional parameter AWET = 1.0 in the input decks was incorporated to provide 100% humidity of the mentioned air flow. The COCOSYS model parameter AFAL (factor of gas cooling during carryover) was set to 0.75. Thus, a better coincidence of the calculated and measured atmospheric temperature in the BC gasroom was achieved.

The results of the ATHLET posttest calculations as mass and energy release rate were used as main boundary of the COCOSYS calculations.

Initial and boundary conditions for the particular tests were set in accordance with experimental data [11–16].

5.3. Tests 1, 4, and 5 (LB LOCA). Tests 4 and 5 are aimed to model thermohydraulic processes under LB LOCA conditions taking into account large steam (Test 4) or air (Test 5) concentration in the air-steam flow before BC tray in order to investigate mainly the maximum pressure difference across the gap/cap system and BC walls and the nonuniformities of the flow distribution inside the BC. The scenarios of these tests were determined by means of ATHLET calculations. The intention of these calculations was to adjust the coolant blowdown from the BC V-213 high-pressure vessel system in order to meet coolant blowdown parameters at the NPP reduced by 100 times.

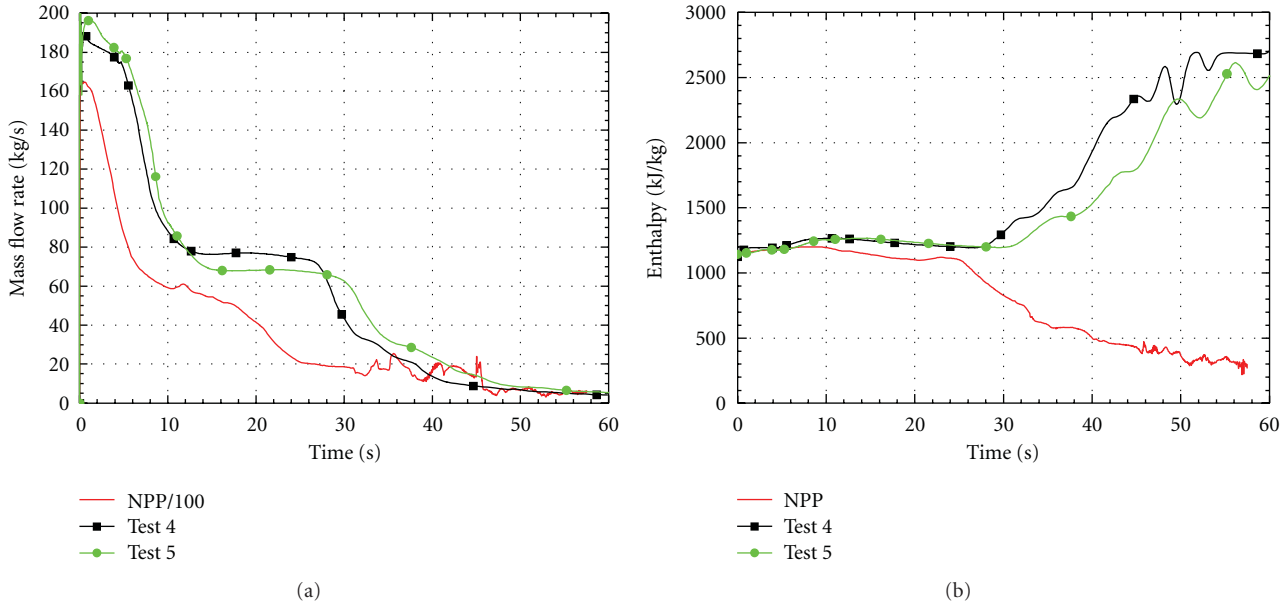

Figure 9: Comparison of experimental MERs with NPP scaled MER. Tests 4 and 5. (a) Break mass flow rate, (b) break enthalpy.

The comparison of the test results with pretest calculations has shown that initial conditions and test scenarios obtained in the pretest analysis were adjusted adequately at the BC V-213 test facility. However, some deviations between initial and boundary conditions assumed in the ATHLET pretest calculations and those realised in the test took place, for example, the initial water level in V_{v5}. So, the initial and boundary conditions realized in the test were finally used in the ATHLET posttest calculations.

The aim of the posttest analysis of thermo-hydraulic processes in the high-pressure system is to determine MER (coolant mass flow rate and specific enthalpy). The measurement of the mass flow rate of discharged coolant with VTI tube is valid only during first seconds, when discharge of subcooled water takes place. Mass flow rate of the two-phase mixture is not measured correctly by this kind of gauge. So, the MER should be determined by posttest analysis with the ATHLET code; if ATHLET results agree well with other significant experimental data (pressure, temperature, collapsed level, and mass flow rate of single-phase coolant), so it is possible to conclude that ATHLET provides reliable MER as for single-phase and two-phase regions.

Comparison of experimental MERs determined by posttest analysis with NPP scaled MER is shown in Figure 9. Experimental mass flow rates are greater than NPP ones; break enthalpies are essentially differed after 25 s, when steam discharge starts at the test facility. However, the main aim of Tests 4 and 5 is to model only the initial stage of LB LOCA (~2 s), which is adequately adjusted at the test facility.

Test 4 (LB LOCA) was analyzed with COCOSYS code in detail. Many variant calculations were performed to adequately reproduce behaviors of experimental parameters. Other tests were analyzed with model parameters adjusted for Test 4.

Posttest analysis of thermal-hydraulic processes in hermetic compartments and BC with the COCOSYS code has shown reasonable agreement between calculated and experimental data. Comparison of BC pressure differences is presented in Figure 10. Predicted maximum values of the pressure difference are higher and occur earlier than experimental values. Reasonable explanation of it is elastic deformation of the BC steel walls during the very initial phase, not considered in the code. A second reason might be the blocking of the left channel by the counter-current flow revealed in the test and not simulated in the calculation [18].

Test 1 was aimed to be the representative LB LOCA with regard to the maximum absolute pressure and temperature in the compartment system of the reference NPP Kola-3. The test scenario was determined with iterative ATHLET and COCOSYS pretest calculations based on the above-described methodology to realize adequate BC loading conditions at the test facility as in the Kola-3 NPP [8]. Figure 11 illustrates comparison of criteria C1–C3 obtained in the posttest analysis of Test 1 with the COCOSYS code and corresponding criteria for NPP case. A similar picture as for pretest calculations is obtained: during ~22 s criteria C1 (mass flow density entering the BC gap/caps) and C2 (specific steam mass flow entering the BC water layer) lie inside NPP bandwidth, after that the test is conservative in comparison with NPP case. These peculiarities are explained by exceeding of experimental MER, especially after 20 s. It is difficult to reproduce the complex behaviour of the NPP primary system at the late stage of LB LOCA (after 20 s) using simple three vessels configuration of the BC V-213 test facility high-pressure system. As to the third criterion C3 (temperature of BC water), both experimental and post calculated curves lie inside the NPP bandwidth. The curves Cases 1 to 9 are result

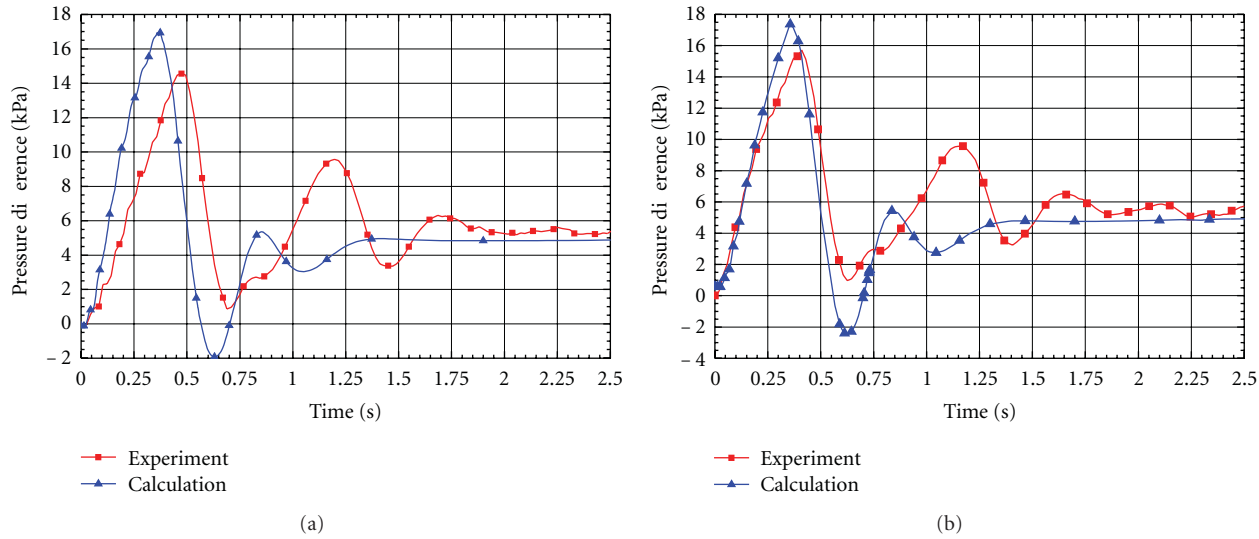

FIGURE 10: Experimental and calculated pressure difference across BC walls. (a) Test 4; (b) Test 5.

of the sensitivity study for bandwidth determination. They are described in [10].

So, adequate BC loads were obtained in the BC V-213 test facility in comparison with NPP in accordance with applied methodology.

In Figure 11(d) the calculated and measured pressures in the box V_1 and in the air trap V_5 are compared. Measurement uncertainties due to limited accuracy of gauges are illustrated with error bars on experimental curves. In the first phase the pressurisation is overestimated, whereas later on the calculation lays inside the measurement uncertainty range.

5.4. Tests 7 and 9 (MSLB). Tests 7 and 9 are aimed to model thermo-hydraulic processes under MSLB conditions taking into account large air (7) or steam (9) concentration in the air-steam flow before BC tray. The scenarios of these tests were determined by means of ATHLET calculations as explained above for Tests 1, 4, and 5. Finally, the NPP scaled MER is adequately reproduced in the tests, Figure 12.

Posttest analysis of thermal-hydraulic processes in the hermetic compartments and BC with the COCOSYS code has shown a good agreement between calculated and experimental data. A comparison of experimental and calculated absolute pressures in boxes V_1 and V_5 for Test 7 is shown on Figure 13. Measurement uncertainties due to limited accuracy of gauges are illustrated with error bars on experimental curves. For the box V_1 a rather good agreement is obtained on the whole time range except the period from 200 to 400 s. The calculated maximum value of the absolute pressure in the box V_1 is in good coincidence with experimental one (0.185 MPa and 0.184 MPa, correspondingly, but the difference is within uncertainty range of the gauge). In the box V_5 calculated absolute pressure is slightly higher than experimental one all the time. The maximum difference amounts to about 7 kPa at 1800 s; it is slightly larger than uncertainty range. Similar results were obtained in posttest analysis of Test 9.

5.5. Test 12 (SB LOCA). Test 12 was aimed to model thermo-hydraulic processes under SB LOCA conditions. The scenario of this test was determined by means of ATHLET calculations as explained above.

Posttest analysis of the thermal-hydraulic processes in the boxes and BC has shown that loads on BC and hermetic compartments are practically negligible under SB LOCA conditions. The deviations of calculated and measured parameters are in the order of the gauge uncertainty (pressure) or less (temperature). The main idea of the SB LOCA test performance was to investigate experimentally whether the gap/cap systems tend to condensation oscillations under SB LOCA conditions. Main outcome of this test is that no condensation oscillations of the BC pool water were observed.

5.6. Main Calculated Results. Evaluating the results of posttest analysis with regard to the safety relevance, it can be concluded that LB LOCA conditions have higher degree of the safety relevance compared with MSLB and especially SB LOCA. Main thermal-hydraulic parameters characterizing loads on BC and hermetic compartments are presented in Table 8. It should be taken into account that Test 4 and Test 5 (both LB LOCA) were aimed to investigate only the initial stage of the accident and determine the maximum pressure difference across BC. These tests were not representative for maximum pressure and temperature in the hermetic compartments. Test 1 was aimed to be the representative LB LOCA with regard to the maximum pressure and temperature in the compartment system of the reference NPP Kola-3.

So, the COCOSYS code was successfully validated on experimental data concerning thermal-hydraulic processes in the BC and hermetic compartments at the BC V-213 test facility, which was a scaled model (1 : 100) of unit 3 of the Kola NPP. The next step is the application of the validated COCOSYS code for analyzing thermal-hydraulic processes in the hermetic compartments and BC loading during a corresponding accident at the Kola NPP.

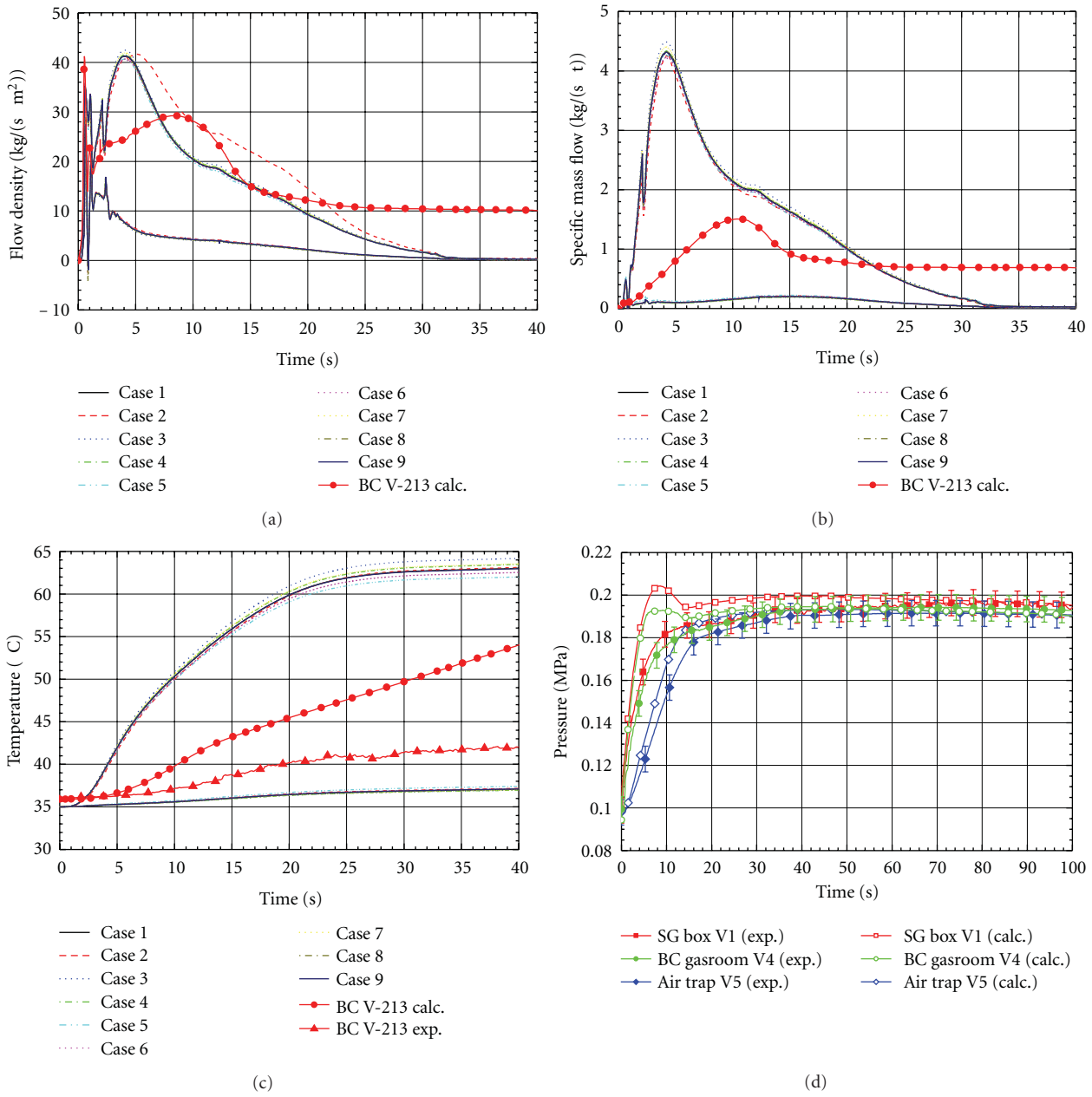

FIGURE 11: Comparison of posttest calculation of Test 1 and NPP bandwidth. (a) C1 criterion; (b) C2 criterion; (c) C3 criterion; (d) experimental and calculated absolute pressure in SG box V_1, BC gasroom V_4, and air trap V_5.

6. Analysis of BC Operation and Thermohydraulic Processes in Hermetic Compartments of Unit 3 of Kola NPP under LB LOCA with the COCOSYS Code

For the analyses of the LB LOCA accident for the Kola NPP BC the input deck developed in [10] is used with some modifications. 46 zones, 62 atmospheric and 35 drain junctions, 2 pump systems, and 162 heat conducting structures of the Kola NPP, unit 3 were considered. The corresponding nodalization scheme is presented in Figure 14.

Table 9 lists the COCOSYS model zones (nodes), gives an explanation of the allocation of the zones to the NPP compartments, and includes the main characteristics of the zones. The steam generator box (compartment A201/1) is divided into two equal parts SGBOXA and SGBOXB. The break is assumed to occur in zone SGBOXB.

In the lower parts of the BCC compartments water can accumulate. Thus, they are modelled as separate sumps.

Special attention was paid to the modelling of the BC shaft (compartment A263/1). Inside this compartment the bubble condenser system is located. The system consists of twelve bubble condenser trays situated on separate floors spaced on various elevations of the BC shaft. For the purpose of obtaining the bandwidths of the inlet parameters for the different BC trays the bubble condenser shaft and the BC

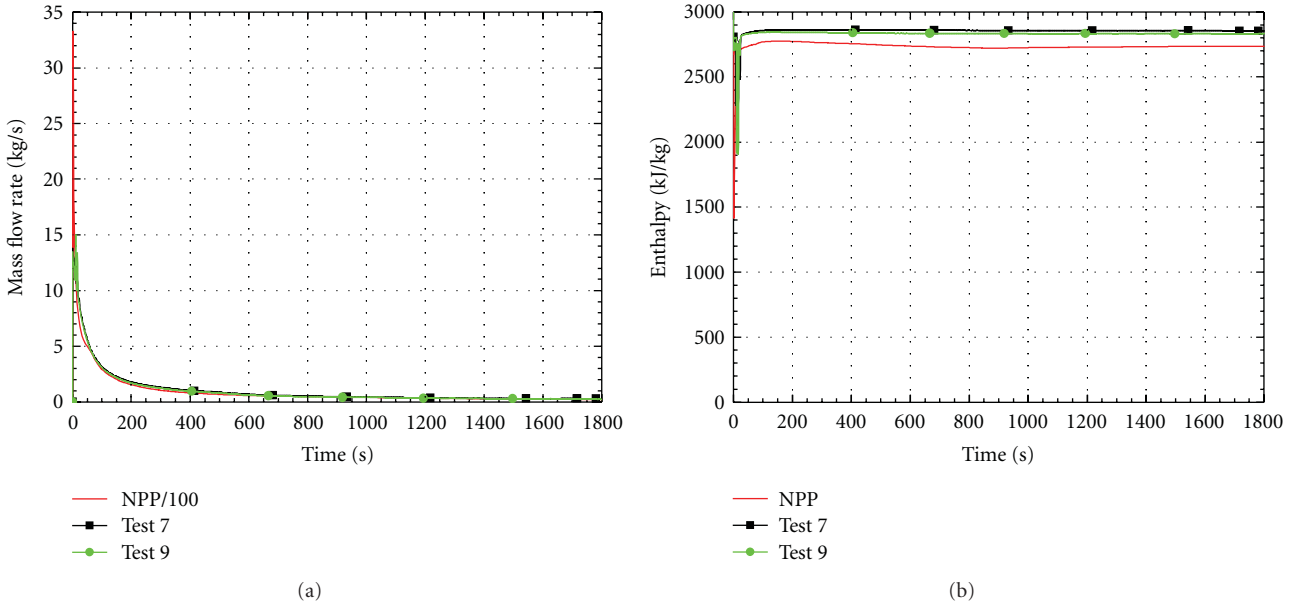

Figure 12: Comparison of experimental MERs with NPP scaled MER. Tests 7 and 9. (a) Break mass flow rate, (b) break enthalpy.

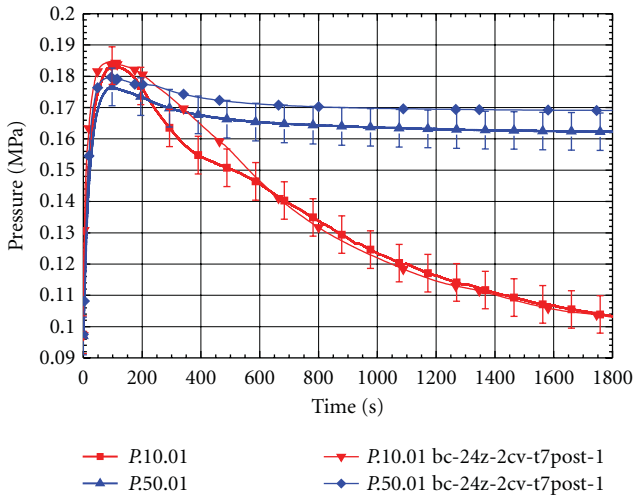

Figure 13: Measured and postcalculated absolute pressures in V_1 and V_5 boxes, Test 7.

itself are divided into 21 parts with various volumes and elevations. The lowest and uppermost BC trays are modelled by separate zones.

Water carryover between the nodes is considered by values reducing downstream from the break location.

Zones are connected by atmospheric junctions (J1...J62) to simulate the transport of accident-generated 2-phase 2-component mixture. The gas volumes of the BC trays TRYA...TRYF are connected with the air traps ATRAPA...ATRAPF via the dynamic flaps J52...J57 to model the DN500 check valves including the inlet protection ducts. The DN250 relief valves are simulated by the dynamic flaps J46...J51. The flaps will be locked in closed position, if the pressure in BC shaft rises higher than 163,7 kPa. This is controlled by the signals SIG250A...SIG250D. For calculations longer than investigated here, that is, longer than 40 s, the unlocking pressure is of importance. It influences the occurrence of the reverse flow. Based on the experimental results, it was set to 190 kPa.

The BCC is assumed to be leak tight. Thus, there are no connections between compartment zones and zone ENVIRON which presents the environment.

There are 35 drain junctions in the Kola-3 NPP model. Drain junctions are assigned to simulate flow processes of water, for instance the drainage of injected water or condensate or the flow between different sumps to equalise the water surface levels.

The spray system, which injects water into SG boxes SGBOXA and SGBOXB, is simulated by two pump systems and emergency water storage tank TANKA. The operation of the pump systems is controlled by time- and process-dependent valves.

Heat transfer and heat conduction processes are considered by so-called heat slabs. For each zone the relevant surfaces were defined as floor, side walls, and ceiling. The BC tray walls are subdivided into different heat slabs to consider that wall sides are linked with the pool (water), the gasroom or the gap/cap system.

In accordance with the results of COCOSYS posttest analysis of tests performed in BC V-213 test facility the developer version 2.0AA of the COCOSYS code was used for analysis of thermo-hydraulic processes in hermetic compartments of unit 3 of Kola NPP under LB LOCA, that is, the validated code was applied. In this version of COCOSYS the DRASYS zone model was improved to permit the simulation of humid air flowing from the BC water pool to the gasroom. Also for modelling of the water carryover into the gasroom and the air trap, special pumps were defined as for the analysis of the test facility.

Table 8: Main experimental/calculated parameters characterizing loads on BC and boxes.

No.	Parameter	Test[a]					
		Test 4 LB LOCA	Test 5 LB LOCA	Test 1 LB LOCA	Test 7 MSLB	Test 9 MSLB	Test 12 SB LOCA
(1)	Maximum absolute pressurein box V_1, (MPa)	0.202	0.214	0.197	0.1835	0.175	0.111
		0.224	0.232	0.204	0.185	0.179	0.118
(2)	Maximum absolute pressure in gasroom V_4, (MPa)	0.191	0.199	0.194	0.177	0.169	0.107
		0.206	0.210	0.195	0.180	0.173	0.110
(3)	Maximum absolute pressure in air trap V_5, (MPa)	0.193	0.200	0.191	0.177	0.168	0.106
		0.191	0.196	0.193	0.180	0.174	0.113
(4)	Maximum pressure difference across BC, (kPa)	14.55	15.73	11.62	7.8	7.7	4.9
		16.9	17.4	13.9	6.5 [b]	6.7 [b]	5.5
(5)	Maximum pressure difference across check valve, (kPa)	50.6	54.3	37.8	13.6	10.9	1.3
		64.8	67.2	55.9	18.1	15.7	1.6
(6)	Maximum temperature in box V_1, (°C)	120	122	120	118	118	86
		124	125	121	172	181	101
(7)	Maximum temperature of BC water[c], (°C)	78	78	60	56	63	38.5
		77	78	64	52	53	35
(8)	Average temperature of BC water[d], (°C)	61	59	45	48	52	36
		77	78	64	52	53	35

[a] Experimental results are presented in upper part, calculation ones—in the lower part of table's cells;
[b] calculated values are the first peaks; due to COCOSYS model specifics only first pressure difference peak is reproduced in calculations;
[c] calculated values of maximum temperature are obtained at the end of calculation: for Test 4, Test 5, and Test 1 values are given at 100 s, for Test 7, Test 9, and Test 12—at 1800 s. Experimental values of maximum temperature are observed for Test 4 during interval ~55–230 s, for Test 5 during interval ~45–85 s, for Test 1 during interval ~160–250 s, for Test 7 during interval ~800–1800 s, for Test 9 during interval ~1100–1800 s, and for Test 12 during interval ~2700–5000 s;
[d] for Test 4, Test 5, and Test 1 values are given at 100 s, for Test 7, Test 9, and Test 12—at 1800 s. Calculated maximum and average temperatures of BC water are equal to each other due to using of only one node for BC pool in calculation.

The full-scale NPP MER (coolant mass flow rate and specific enthalpy as calculated with ATHLET) is used for COCOSYS analysis as boundary condition.

The following initial conditions are used in the calculation.

Air temperatures in the hermetic compartments are

(i) 50°C—in all compartments before shaft;

(ii) 35°C—in the shaft;

(iii) 30°C—in the air traps.

Water temperature in BC trays is 35°C.
Humidity in the hermetic compartments is

(i) 60%—in all compartments before the BC shaft;

(ii) 90%—in the BC shaft;

(iii) 20%—in the air traps.

Water carryover factor (COCOSYS model parameter) is

(i) 0.4—in the break node;

(ii) 0.2—in the nodes adjacent to the break node;

(iii) 0.1—in the other nodes.

In Figure 15(a) the calculated pressure behavior in the break node is presented. For the NPP the maximum pressure ~184 kPa is achieved at 3.8 s, whereas the maxima in Test 1 were 204 kPa after 8,5 s (calculated) and 197 kPa after 78 s (measured) as shown in Figure 11(d). The reasons for the deviation from the NPP value is explained above in chapter 5 (Tests 1, 4, and 5).

The temperature history in the break node is shown on the Figure 15(b). The maximum value is about 118°C.

The pressure difference over gap/cap systems in the short time phase is illustrated on Figure 15(c). The highest pressure differences occur in the upper trays (~26 kPa), lower trays are effected by a maximum pressure difference of about 17 kPa. However, as it is shown in chapter 5 lumped-parameter containment codes like CONTAIN, TRACO, VSPLESK, or COCOSYS overpredict the values of the BC pressure difference [18]. One reason for that was identified to be the neglection of elastic compression of the BC walls. Another reason was the occurrence of counter-current flow in the channel connecting V_2 and V_3, which was not considered also.

The BC water temperature is shown on Figure 15(d). The maximum value (~59°C) is achieved in TRYA (1st tray). This value is still relatively far below the saturation temperature, knowing that BC-related posttest calculations with different codes showed a strong overestimation of the water heatup in LB LOCA cases.

Table 9: List and characteristics of the Kola-3 BCC zones.

Node	Kola NPP compartment	Node type	Volume, m^3	Centre elevat. m	Floor area m^2	Floor elevat. m
SGBOXA	SG box A201/1; left half	E(1)	2601.73	12.57	520.0	7.74
SUMPA	SG box A201/1; lower part	NE	750.0	7.02	520.0	6.30
SGBOXB	SG box A201/1; right half	E	2594.43	12.57	520.0	7.74
SUMPB	SG box A201/1; lower part	NE	750.0	7.02	520.0	6.30
MCPBOX	MCP electric motors compartment A301/1	E	2186.24	13.98	348.0	10.567
ISOLA	Corridor of penetrations with ECCS isolation valves A202/1	E	1578.35	11.86	327.76	6.32
ISOLB	Corridor of penetrations with ECCS isolation valves A203/1	E	1731.4	11.86	350.96	6.32
CAVTY	Reactor cavity (below the support ring) A004/1	E	290.73	8.10	36.32	−6.10
ACCUMA	HA compartment A525/1	E	372.96	21.95	29.70	18.90
ACCUMB	HA compartment A526/1	E	372.96	21.95	29.70	18.90
VALVC	Valves chamber A306/1	E	100.92	12.05	34.80	10.60
PRESR	Pressurizer box A527/1	E	357.02	21.95	52.45	18.90
VALVSG	Chamber of SG box valves A211/1	E	567.2	12.18	107.44	6.26
FILTRI	Compartment for filters of installation I A302/1	E	105.94	14.0	15.60	10.60
CORRDA	Transition room between SG box and BC shaft A265/1	E	602.18	9.85	93.23	6.60
CORRDB	Transition room between SG box and BC shaft A266/1	E	602.18	9.85	92.73	6.60
VENTC	HVAC systems machine hall A00032/1	E	4722.14	−0.75	655.84	−6.50
SHFRA	Bubble condenser shaft A263/1; front part	E	491.38	12.76	52.0	8.04
SHFRB	Bubble condenser shaft A263/1; front part	E	412.5	22.54	40.8	17.49
SHFRC	Bubble condenser shaft A263/1; front part	E	412.5	32.65	40.8	27.60
SHFRD	Bubble condenser shaft A263/1; front part	E	453.3	43.26	40.8	37.71
SHLTA	Bubble condenser shaft A263/1; lateral part	E	561.64	12.76	58.35	8.04
SHLTB	Bubble condenser shaft A263/1; lateral part	E	589.9	22.54	58.35	17.49
SHLTC	Bubble condenser shaft A263/1; lateral part	E	589.9	32.65	58.35	27.56
SHLTD	Bubble condenser shaft A263/1; lateral part	E	723.0	43.26	58.35	37.71
BTWTRA	Bubble condenser shaft A263/1, volume below BC trays	E	131.0	7.84	218.6	7.19
BTWTRB	Bubble condenser shaft A263/1, volume below BC trays	E	262.0	12.29	437.2	10.39
BTWTRC	Bubble condenser shaft A263/1, volume below BC trays	E	414.0	21.16	689.4	17.49
BTWTRD	Bubble condenser shaft A263/1, volume below BC trays	E	414.0	31.27	689.4	27.60
BTWTRE	Bubble condenser shaft A263/1, volume below BC trays	E	276.0	39.69	459.6	37.71
BTWTRF	Bubble condenser shaft A263/1, volume below BC trays	E	130.0	44.745	216.3	44.45

Table 9: Continued.

Node	Kola NPP compartment	Node type	Volume, m^3	Centre elevat. m	Floor area m^2	Floor elevat. m
SUMPC	Bubble condenser shaft A263/1; lower part	NE	303.2	7.36	110.35	6.68
TRYA[(2)]	Bubble condenser tray; 1st floor	D	565.386	9.34	208.78	7.79
TRYB	Bubble condenser trays; 2nd, 3rd floors	D	1130.772	13.89	417.56	10.99
TRYC	Bubble condenser trays; 4th, 5th, 6th floors	D	1898.869	22.85	656.37	18.09
TRYD	Bubble condenser trays; 7th, 8th, 9th floors	D	1898.869	32.96	656.37	28.20
TRYE	Bubble condenser trays; 10th, 11th floors	D	1265.946	41.38	437.58	38.31
TRYF	Bubble condenser tray; 12th floor	D	815.222	46.44	203.06	45.05
ATRAPA	Air trap compartment A264/1; lower part	E	1386.17	8.65	446.55	7.0975
ATRAPB	Air trap compartment A264/1; upper part	E	2772.33	13.31	446.55	10.20
ATRAPC	Air trap compartment A423/1	E	4014.48	22.03	446.55	17.53
ATRAPD	Air trap compartment A530/1	E	4014.48	32.14	446.55	27.64
ATRAPE	Air trap compartment A635/1; lower part	E	3230.05	41.37	446.55	37.75
ATRAPF	Air trap compartment A635/1; upper part	E	1615.02	46.79	446.55	44.98
TANKA	ECCS tanks[(3)]	E	1000.0	1.94	257.14	0.00
ENVIRON	Environment	E	1×10^6	2.50	1×10^4	0.00

[(1)] "E": equilibrium zone model, "NE": nonequilibrium zone model, "D": PSS zone model DRASYS according to COCOSYS concept [7].
[(2)] Total volume of D-type node includes both gas and water ones.
[(3)] Comprising several tanks (introduced for correct water mass balance).

7. Conclusion

In the framework of the Tacis Project R2.01/99 EREC has performed six tests according to the PH2.13./95 Project test matrix:

(i) three LB LOCA tests (Tests 1, 4, and 5 according to the test matrix);

(ii) two MSLB tests (Tests 7 and 9);

(iii) one SB LOCA test (Test 12).

The appropriate test scenarios for BC V-213 test facility, modeling accidents in the Kola NPP unit 3, were determined with pretest calculations performed with the ATHLET code. The analysis of the test results has shown that calculated initial conditions and test scenarios were properly reproduced in the tests. The tests were performed successfully and are of high importance with regard to the assessment of the functioning of the Bubble Condenser with specific Kola-3 NPP features under accident conditions. They are also very important for code validation purpose.

The main aim of the posttest analysis of the tests performed at BC V-213 test facility is to validate the COCOSYS code for calculating the thermo-hydraulic processes in the hermetic compartments and BC. BC loadings and pressure increase in the compartments are mainly determined by mass and energy release rate (MER) of the coolant discharged through the break. The measurement of the mass flow rate of discharged coolant with VTI tube is valid only during the first seconds, when discharge of subcooled water takes place. Mass flow rate of the two-phase mixture is not measured correctly by this gauge, because density of two-phase mixture (parameter required for determination of the mass flow rate) is not measured at the test facility. So, MER can be determined by posttest analysis with best estimate thermal-hydraulic code, for example, ATHLET code. If ATHLET results agree well with other important experimental data (pressure, temperature, collapsed level, and mass flow rate of single-phase coolant), it is possible to conclude that ATHLET provides reliable MER as for single-phase and two-phase regions.

Results of ATHLET Posttest Analysis. In general, results of ATHLET calculations agree well with experimental data (pressure, temperature, collapsed level, and mass flow rate of single-phase coolant) for all tests. Performed sensitivity study permitted to determine optimal model parameters and to reach good agreement with experimental data. So, it can be concluded that ATHLET has provided reliable MER both for single-phase and two-phase regions, which can be used as boundary condition for subsequent COCOSYS

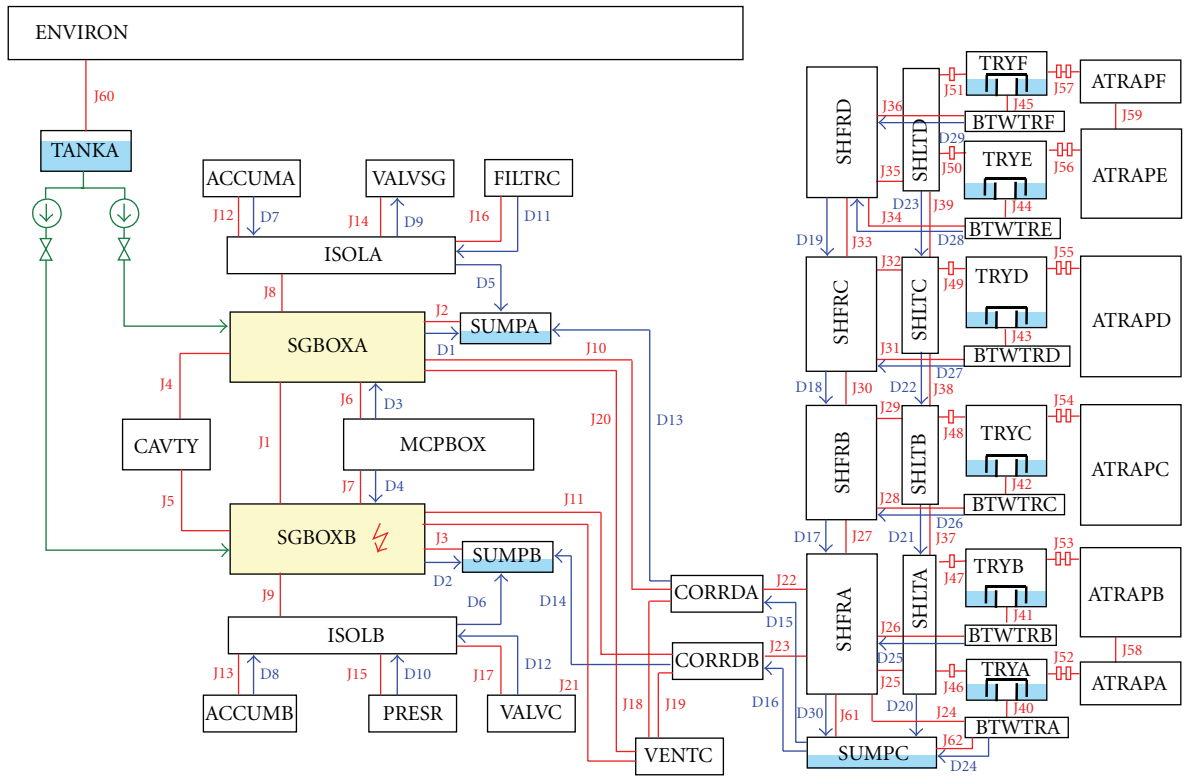

Figure 14: Nodalization scheme of Kola NPP unit 3 Bubble Condenser Containment.

(or other containment code) calculations of thermal-hydraulic processes in the hermetic compartments and BC.

LB LOCA Tests. Test 4 (LB LOCA) was analyzed with the COCOSYS code in detail. Many variant calculations were performed to adequately reproduce the behavior of measured parameters. Other tests were analyzed with model parameters determined for Test 4.

The results of the sensitivity study with the COCOSYS code using experimental data led to certain model changes, which is a further step of code validation. In general, satisfied agreement between calculated and experimental data is obtained.

Calculations revealed that the main problem for LB LOCA tests is an overestimation of BC pool water heatup with the COCOSYS code. Similar results were obtained with other containment codes as CONTAIN, TRACO, and VSPLESK [18]. The predicted heatup of BC pool water is approximately twice greater than the experimental one. Furthermore, it can be concluded that the overestimation of the pool water heatup is accident dependent and much larger for LB LOCA tests.

Possible reasons for such overestimation are the following:

(1) steam condensation before BC module is not adequately described by the code (nonrealistic value of heat transfer coefficient or occurrence of any peculiarities of heat structures which are not taken into account e.g., exact simulation of wooden insulation);

(2) strong nonuniform distribution of water temperature observed in the test (difficulties with correct definition of average BC water temperature, possible steam breakthrough in the most loaded parts);

(3) occurrence of counter-current flows between V_0 dead-end volume and break node and/or V_2 and break node, which cannot be reproduced by calculations with lumped-parameter codes.

Comparison of experimental and calculated pressure differences across BC walls shows that predicted maximum value of the pressure difference is higher than experimental value for all tests (exp./calc. pressure difference: Test 4—14.55 kPa/16.9 kPa, Test 5—15.73 kPa/17.4 kPa, Test 1—11.62 kPa/13.9 kPa). Reasonable explanation of it is an elastic deformation of the BC steel walls, not considered in the COCOSYS code. A second reason might be the blocking of the left channel by the counter-current flow revealed in the test and not simulated in the calculation.

Another important finding of posttest analysis is the influence of the opening of the DN250 relief valve on the occurrence of the reverse water flow. The reverse water flow from the BC trays into the BC shaft is caused by reverse pressure difference; when the pressure in the BC gasroom (above water seal) becomes higher than the pressure in the BC shaft, DN250 relief valve connecting BC gasroom and BC shaft should be locked for occurrence of the reverse

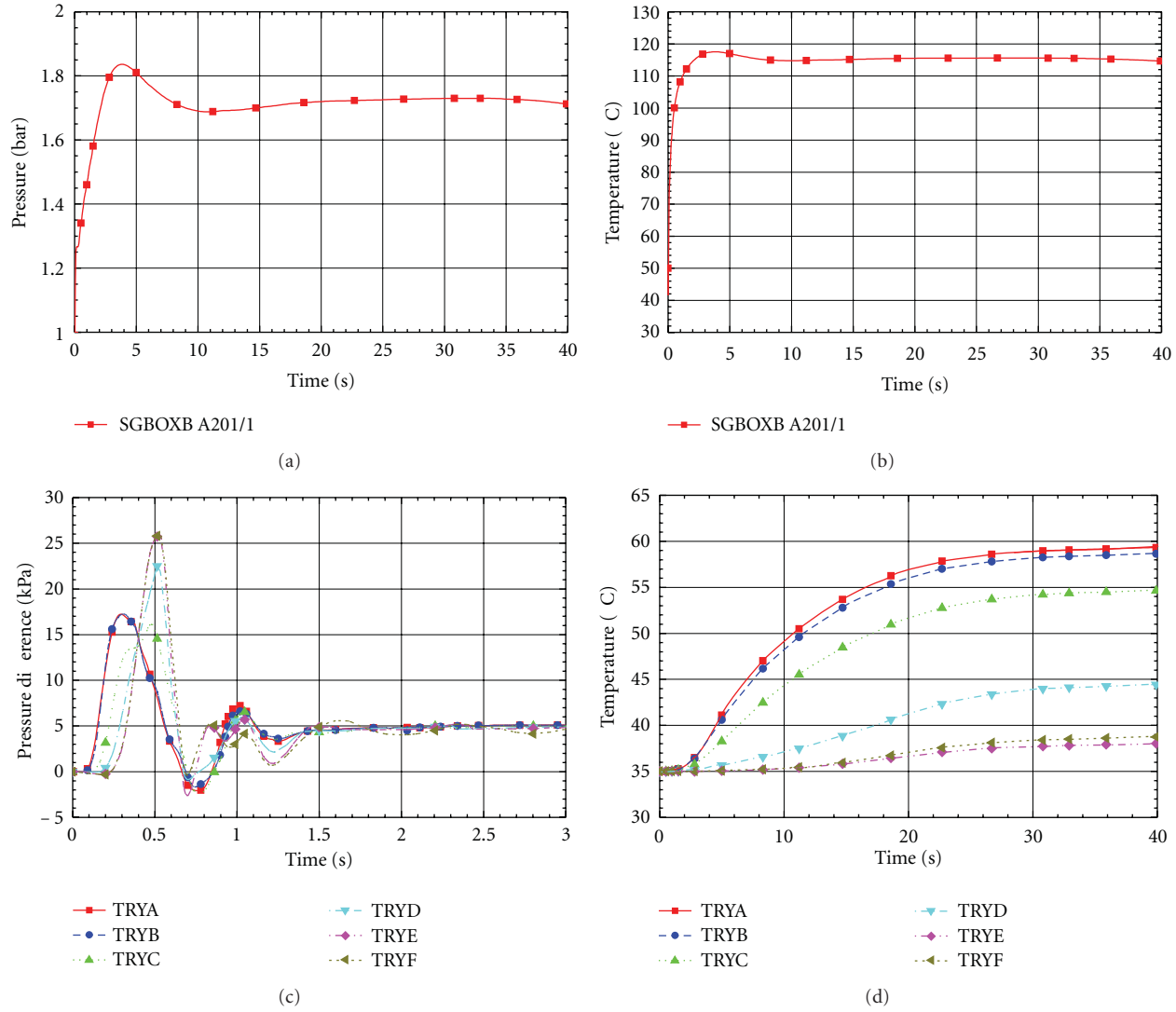

Figure 15: Calculation of LB LOCA at unit 3 of Kola NPP with the COCOSYS code. (a) Pressure history in the break node A201/1; (b) temperature in the break node A201/1; (c) pressure difference across the BC wall; (d) BC water temperature.

flow. So, locking/unlocking pressure value of DN250 relief valve influences the occurrence of the reverse flow. The special gauge for DN250 cover opening permits to determine moment of valve opening and corresponding value of the pressure in the shaft. In the tests it was revealed that the relief valve opened at a pressure in BC shaft exceeding the design unlocking value. This is caused by the heatup of the valves bellow (causing a pressure increase in the bellow), which is accident dependent also. Using a nonrealistic value for the unlocking pressure can prevent the reverse flow, so in the posttest calculations the experimental values of unlocking pressures were used. It permitted to calculate reverse flow in Test 5.

MSLB Tests. They are rather well simulated by the COCOSYS code. Calculated pressure and temperature in the boxes are in good coincidence with experimental values. The water heatup is overpredicted by the code, but not as strong as in the previous LB LOCA tests (the relative difference is reduced 10 times).

Predicted values of the first peak of pressure difference across BC walls for MSLB tests coincide with experimental values rather well. However, it is necessary to note that in the experiment maximum values of the pressure difference across BC walls were achieved during the second peak. Due to the model specifics used in COCOSYS, only first pressure difference peak is reproduced in the calculations.

SB LOCA Tests. Posttest analysis of thermal-hydraulic processes in the boxes and BC has shown that loads on BC and hermetic compartments are practically negligible under SB LOCA conditions. The deviations of calculated and measured parameters are in the order of the gauge uncertainty (pressure) or less (temperature).

The main idea of the SB LOCA test performance was to investigate experimentally whether the gap/cap systems tend

to condensation oscillations under SB LOCA conditions. Main outcome of this test is that no condensation oscillations of the BC pool water were observed.

Evaluation of the results of posttest analysis with regard to the safety relevance was implemented comparing main thermal-hydraulic parameters characterizing loads on BC and hermetic compartments. LB LOCA conditions have a higher degree of safety relevance compared with MSLB and especially SB LOCA.

COCOSYS Analysis of Kola-3. The COCOSYS code was exemplarily used in NPP calculations for Kola-3. The findings revealed during posttest analysis of the tests performed at the BC V-213 test facility were taken into account for the development of the COCOSYS model of unit 3 of Kola NPP. The main results of calculation are maximum pressure—184 kPa, maximum temperature—118°C, and BC pool water temperature—59°C. These values are below design limits. However, it should be noted that a consequence of the Kola NPP configuration (twice number of check valves,...) is a pressure level more close to the design value compared to the other NPPs with VVER 440/V-213.

Finally, results of the experimental campaign carried out under the Tacis R2.01/99 Project [19] confirmed the Bubble Condenser functionality during large and small break LOCAs and MSLB accidents in Kola-3 NPP. Maximum loads were reached in the LB LOCA case. No condensation oscillations were observed.

Nomenclature

ATHLET:	Bestestimate thermal-hydraulic code for the reactor circuit
BC:	Bubble condenser
BCC:	Bubble Condenser Containment
COCOSYS:	Containment thermohydraulic code
EREC:	Electrogorsk Research and Engineering Centre on NPPs safety
GRS:	Gesellschaft für Anlagen- und Reaktorsicherheit
HS:	Heat structures
LB LOCA:	Large break loss-of-coolant accident
LOCA:	Loss-of-coolant accident
MER:	Mass and energy release rate
MSLB:	Main steam line break
NPP:	Nuclear power plant
SB LOCA:	Small break loss-of-coolant-accident
SG:	Steam generator
VVER:	Pressurized water reactor (Russian type).

Acknowledgment

The major part of the work described in this paper was supported by the Tacis Project "Experimental Studies on (a) Bubble Condenser Test Facility (R2.01/99). (b) TKR Test Facility (R2.02/99) at EREC-Electrogorsk."

References

[1] A. M. Bukrinsky, Y. V. Rzheznikov, Y. V. Shvyryaev et al., "Accident Localization System under LB LOCA conditions at NPP with VVER-440," *Thermal Engineering*, no. 4, pp. 47–49, 1978.

[2] "Bubble condenser experimental qualification (PH 2.13/95)," Final Thermal-Hydraulic Test Report BC-D-ER-SI-0028, Rev. 0. Task 2: Deliverable 2.4, 1999.

[3] "Experimental Studies on: A. Bubble Condenser Test Facility (R2.01/99). B. TKR Test Facility (R2.02/99) at EREC-Electrogorsk, Re-mobilization of the BC V-213 test facility and result of comparative experiment," Tech. Rep. BC-TR-01E, 2003.

[4] "Experimental studies on: A. Bubble condenser test facility (r2.01/99). b. TKR test facility (r2.02/99) at EREC-Electrogorsk. modification of the test facility for the Kola NPP tests," Tech. Rep. BC-TR-02E, 2003.

[5] "Bubble condenser experimental qualification (PH 2.13/95)," Test Matrix Development BC-D-ER-SI-0006, Rev. 5. Deliverable 2.2, Part 2 of 6, 1999.

[6] ATHLET Mod 1.2 Cycle D, "User's Manual, GRS-P-1/1," September 2001.

[7] COCOSYS V1.2, "User Manual, GRS-P-3/1," July 2000.

[8] H. Wolff et al., "Pre-and post-test calculations of the EREC experiment SLB G02 Project INT 9142, Task 3.1," Tech. Rep. GRS-V-INT 9142-6/2003, Berlin, Germany, 2003.

[9] "Input Data Base for WWER 440/W213 Systems," Tech. Rep. RF13-TR02, 2000.

[10] "Experimental," Tech. Rep. BC-TR-03E, 2003.

[11] "Experimental studies on: a. Bubble condenser test facility (R2.01/99). B. TKR test facility (R2.02/99) at EREC-Electrogorsk. Test plan and pre-test calculations," Tech. Rep. BC-TR-04E, 2003.

[12] "Experimental studies on: a. Bubble condenser test facility (R2.01/99). B. TKR test facility (R2.02/99) at EREC-Electrogorsk. Results of LB LOCA test 5," type BC-TR-05E, 2003.

[13] "Experimental studies on: a. Bubble condenser test facility (R2.01/99). B. TKR test facility (R2.02/99) at EREC-Electrogorsk. Results of LB LOCA test 1," Tech. Rep. BC-TR-06E, 2003.

[14] "Experimental studies on: a. Bubble condenser test facility (R2.01/99). B. TKR test facility (R2.02/99) at EREC-Electrogorsk. Results of MSLB test 7," type BC-TR-07E, 2003.

[15] "Experimental studies on: a. Bubble condenser test facility (R2.01/99). B. TKR test facility (R2.02/99) at EREC-Electrogorsk. Results of MSLB test 9," Tech. Rep. BC-TR-08E, 2003.

[16] "Experimental studies on: a. Bubble condenser test facility (R2.01/99). B. TKR test facility (R2.02/99) at EREC-Electrogorsk. Results of SB LOCA test 12," Tech. Rep. BC-TR-09E, 2003.

[17] I. E. Idel'chik, *Handbook on Hydraulic Resistances*, Moscow, Russia, 1992.

[18] "Answers to remaining questions on Bubbler Condenser," Activity Report of the OECD NEA Bubbler-Condenser Steering Group NEA/CSNI/R, 2003.

[19] "Experimental studies on: a. Bubble condenser test facility (R2.01/99). B. TKR test facility (R2.02/99) at EREC-Electrogorsk," Tech. Rep., 2005.

Hindawi Publishing Corporation
Science and Technology of Nuclear Installations
Volume 2012, Article ID 780472, 22 pages
doi:10.1155/2012/780472

Research Article

PMK-2, the First Integral Thermal-Hydraulics Tests for the Safety Evaluation of VVER-440/213 Nuclear Power Plants

Gy. Ézsöl, L. Perneczky, L. Szabados, and I. Tóth

Department of Thermohydraulics, MTA KFKI Atomic Energy Research Institute, P.O. Box 49, 1525 Budapest, Hungary

Correspondence should be addressed to Gy. Ézsöl, ezsol@aeki.kfki.hu

Received 20 May 2011; Accepted 5 August 2011

Academic Editor: Klaus Umminger

The PMK-2 facility is a full-pressure thermal-hydraulic model of the primary and partly the secondary circuit of the VVER-type units of Paks NPP. The facility was the first integral-type facility for VVERs. The PMK-2 was followed later by the PACTEL (for VVER-440), the ISB, and PSB for VVER-1000. Since the startup of the facility in 1985, 55 experiments have been performed primarily in international frameworks with the participation of experts from 29 European and overseas countries forming a scientific school to better understand VVER system behaviour and reach a high level of modelling of accident sequences. The ATHLET, CATHARE, and RELAP5 codes have been validated including both qualitative and quantitative assessments. The former was almost exclusively applied to the early phase of validation by integral experiments, while the quantitative assessments have been performed by the Fast Fourier Transform Based Method. Paper gives comprehensive information on the design features of PMK-2 facility with a special respect to the representativeness of phenomena, the experiments performed, and the results of the validation of ATHLET, CATHARE, and RELAP5 codes. Safety significance of the PMK-2 projects is also discussed.

1. Introduction

The PMK-2 projects were initiated in the early 1980's, parallel to the start-up procedures of the units of the Paks nuclear power plant of VVER-440/213 type. The vendor provided the safety report of the plant, however, without details of analyses, and with short information on the computer codes applied to the analyses. Therefore, to perform independent assessment of the safety of the plant in the country, there was an urgent need for tools of plant system analyses, that is, for thermohydraulic system codes and thermohydraulic system experiments to assess the predictive capabilities of codes. In the first part of the 1980's, an early version of the thermohydraulic system code RELAP was available through the IAEA. To get results of system tests for VVER-440/213 type NPPs, the design and construction of the PMK-2 facility were initiated, because, at that time, no integral-type facility existed for VVERs that is, PMK-2 (Paks Model Experiment) was the first and the only facility for VVERs. The facility was put into operation in 1985. The PMK-2 was followed by the PACTEL facility for VVER-440 in Finland (1990) and the ISB and PSB facilities for VVER-1000 in Russia (1992 and 1998, resp.).

This report on the PMK-2 projects contains information providing comprehensive descriptions of the first integral-type research programme organized and conducted for VVER-440/213 nuclear power plants, primarily for the Paks nuclear power plant, to study design basis accidents, performing system experiments and getting expertise in code validation primarily through international standard problems, with the participation of experts of 29 countries from the whole world.

Report contains the description of design features of the PMK-2 facility, modelling of the VVER-440/213-specific design solutions, controls, and actions for safety systems. A description and evaluation is given in the 55 experiments performed, which cover an almost complete spectrum of design basis accidents (DBA) corresponding to the most recent version of the safety analysis report (SAR) of the Paks NPP. The OECD-VVER cross reference matrices are

developed for the PMK-2 tests for large breaks, small and intermediate leaks, and transients, providing internationally accepted methodology for the identification of major phenomena addressed by the tests. Matrices contain test types occurring in transients and accidents.

Major findings of experiments include results of tests having safety significance, identified by the use of OECD-VVER code validation matrices. In these matrices physical/thermohydraulic phenomena are linked to test types or inversely. The main items of phenomena are as follows: break flow, pressuriser thermohydraulics, heat transfer in SG primary and secondary side, single- and two-phase natural circulation, mixing and condensation during injection from ECCSs, loop seal behaviour in hot leg and clearance in cold leg, core heat transfer including DNB, and dryout. Tests are selected from the cross-reference matrices applied to the PMK-2 tests for large breaks, small and intermediate leaks, and transients. Major findings identified give primarily the basis of the evaluation of the code prediction; that is, if an identified phenomenon is well predicted by the code, the assessment for this phenomenon is successful.

An effective way to increase the confidence in the validity and accuracy of computer codes can be provided by international standard problems (ISP), which were organized and conducted by the OECD/CSNI since 1975, and 20 tests for validation purposes had been performed in about 25 years. The IAEA Standard Problem Exercises were initiated in 1986, and four PMK-2 based exercises were conducted. These activities provided wide frameworks to assess the capabilities of computer codes to represent phenomena occurring in plant transients and accidents and offered a floor to exchange modelling expertise among the best specialists of the field.

Other international frameworks were provided by the EU-PHARE and EU-Framework projects, as well as the US NRC CAMP Program. Altogether 19 PMK-2 tests were applied to study the pressuriser thermohydraulics, large break in the hot leg, primary to secondary leaks, accident analysis methodologies, steam generator heat transfer, and the effectiveness of secondary and primary bleed and feed, as well as accident analysis methodologies.

Methodology and practice applied to the PMK-2 projects include qualitative and quantitative activities. The qualitative assessment is based on the engineering judgement, which means the comparison of the results of a test and computer code calculation, evaluating the results by visual observation. In the quantitative assessment, the comparison is made quantitatively. In the PMK-2 projects, the quantitative assessment is performed by the fast fourier transform based method (FFTBM).

The quantitative assessment is made by the Fast Fourier Transform Based Method (FFTBM) developed at the University of Pisa (Italy). The methodology and an FFTBM code had been implemented at the AEKI. This is a powerful technique for the quantification of the error between measured and calculated parameters of the transient processes, occurring in plants or in scaled-down facilities. The code provides the amplitude and weighted frequency of the deviation of measured and calculated quantities.

2. The PMK-2 Facility: The First Integral-Type Facility for VVER-440/213 Plants

The PMK-2 facility is located at the MTA KFKI Atomic Energy Research Institute, Budapest, Hungary. It is a full-pressure thermal-hydraulic model of the primary and partly the secondary circuit of VVER-440/213 type units of Paks NPP. At the start-up time of Paks NPP, PMK-2 was the first and only integral-type facility for VVERs. Modelling of specific design solutions and modelling aspects of PMK-2 are shortly given below. Details were published in [1–3].

2.1. Design Features of VVER-440/213-Type Reactor Systems. A schematic drawing of the primary circuit of the Paks NPP with one main circulating loop is presented in Figure 1. The six-loop primary circuit is equipped with VVER-440 reactors and horizontal steam generators (SGs) in each loop. The active length of the core is 2.5 m; the number of fuel rods is 39,312 in hexagonal rod array with fuel assemblies consisting of 127 fuel rods in closed shrouds. The reactor control is achieved by control assemblies having the dimensions of fuel assemblies. The inner diameter of the reactor vessel is 3.5 m.

It can be seen in Figure 1 that there are loop seals in both hot and cold legs. Like in PWRs, loop seal exists in the cold legs in consequence of the main circulating pumps (MCP), but also in the hot legs, because the six hot and cold legs are connected to the vessel at different elevations, forming U-tubes with a depth of 1.4 m. This specific feature affects the thermohydraulic behaviour of the system.

The steam generators in each loop are large horizontal vessels with a diameter of 3.2 m. The inner diameter of the horizontal heat transfer tubes is 13.2 mm with an average length of 9 m. The total number of tubes is 5536 in 77 rows with an overall height of 1.82 m of the tube bundles resulting in a large water volume in the secondary side of the SG.

The emergency core cooling systems (ECCSs) consist of four safety injection tanks (SITs), three parallel high-pressure injection systems (HPIS), and three parallel low-pressure injection systems (LPIS). The latter is activated at a system pressure of 0.7 MPa. The HPI systems are activated either by low system pressure or low water level in the pressuriser. The original SIT set-point pressure was 5.9 MPa, higher than the secondary pressure of 4.6 MPa. The inlet and outlet temperatures are 540 and 570 K, respectively. The operating pressure is 12.3 MPa, and the core thermal power is 1375 MW.

2.2. Modelling Aspects of PMK-2. In most of the transients and accidents—especially in experiments in support of the development of accident management procedures—it is important to start the experiments from the nominal operating parameters of the plant; therefore, the PMK-2 is a full pressure/temperature facility, and the coolant is water. In the transient processes the control and safety signals of the plant are followed. For the design of the PMK-2 the volume scaling criteria were selected which would require the maintenance of the length, elevation, area, volume, and pressure drop relationships. However, it is not possible to maintain

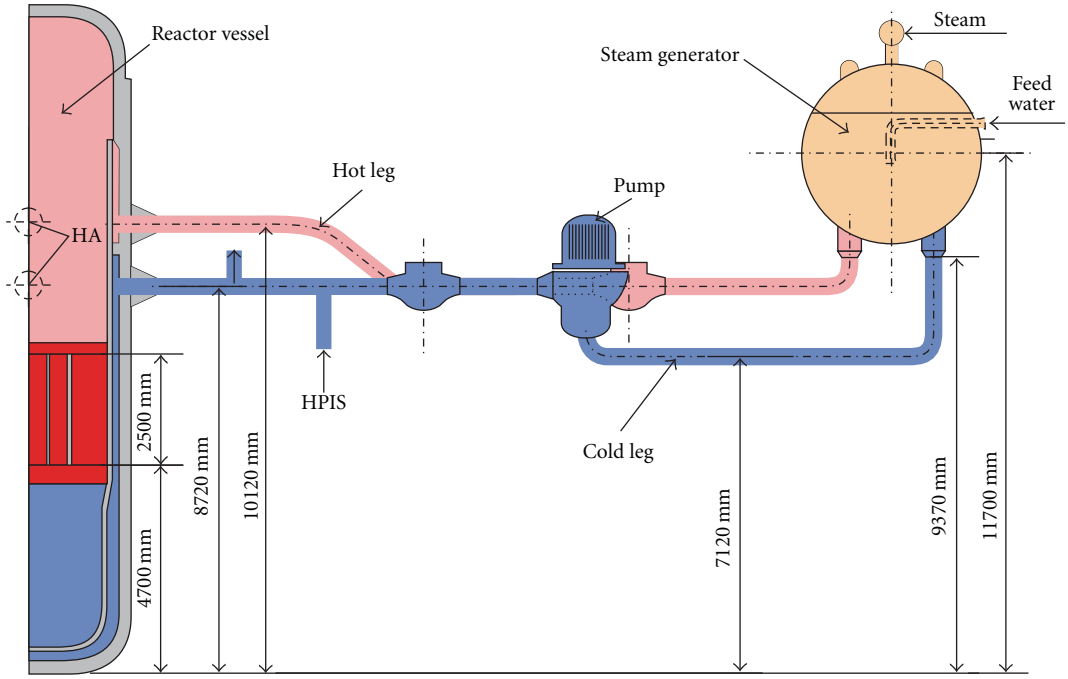

Figure 1: Schematic drawing of the primary circuit of the VVER-440 plant.

the requirements simultaneously; therefore, acceptable compromises are needed.

When the facility was designed in the early 1980s, the range of scaling ratios of integral-type thermohydraulic facilities was, for example, 1 : 48 for ROSA-IV in Japan and 1 : 1705 for SEMISCALE in the USA. Considering the scaling ratio interval and the financial possibilities of the country, a 19-rod core model with 2.5 m heated length was selected which gives the power ratio of 1 : 2070 (39 312/19 ≅ 2070), and, therefore, the overall volume scaling ratio is also 1 : 2070. Due to the importance of gravitational forces in natural circulation, the elevation ratio is 1 : 1. The scaling ratio is near to the SEMISCALE scaling ratio, which facility was successfully used for pretests in the LOFT project.

The six loops of the plant in the PMK-2 facility are lumped into a single loop, and the break is modelled by orifices of suitable sizes at the hot and cold leg elevations in the upper plenum and downcomer. From the component models the main design and similarity features of the core model, the steam generator model, and the hot leg model are presented.

The cross-section of the 19-rod core model is presented in Figure 2. The hexagonal fuel rod array with a fuel rod diameter of 9.1 mm, a pitch of 12.2 mm, and with a heated length of 2.5 m the same as in the reference system. However, the axial power distribution is uniform. In steady state the similarity of thermohydraulic processes in the core is ensured by the same operational parameters and the similar geometry. The similarity of natural circulation is evaluated by the scaling criteria obtained by Ishii and Kataoka [4] from the integral effects of local balance equations along the entire loop. These criteria for both single- and two-phase natural

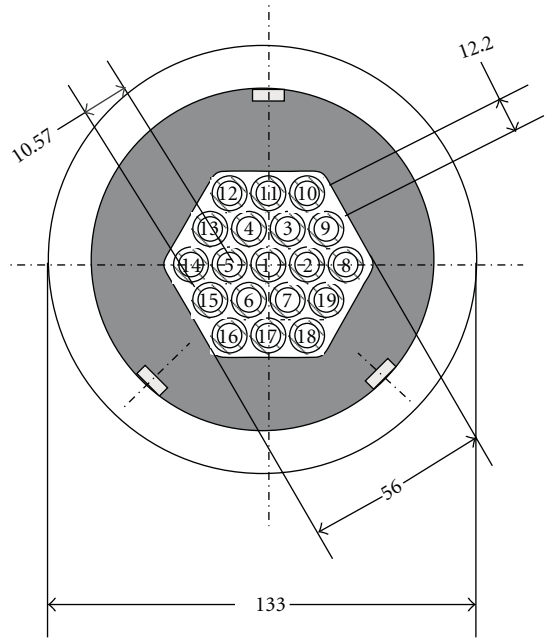

Figure 2: Cross section of the core model.

circulation are almost completely fulfilled for the core, except for the time ratio and Biot numbers due to the different fuel element structure of the model and the reference system.

The cross-section of the steam generator (SG) model is shown in Figure 3 with one of the 82 rows of the horizontal heat transfer tubes between the hot and cold collectors, with a length of 3715 mm. The tube number, diameter, and length

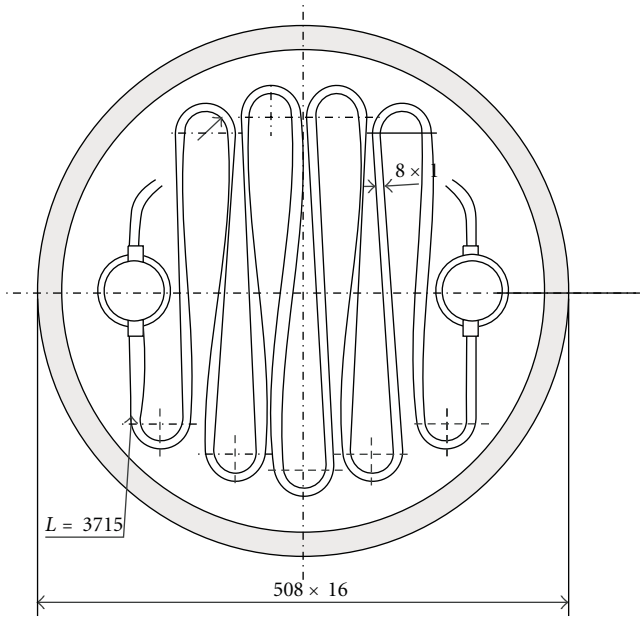

Figure 3: The cross section of the steam generator.

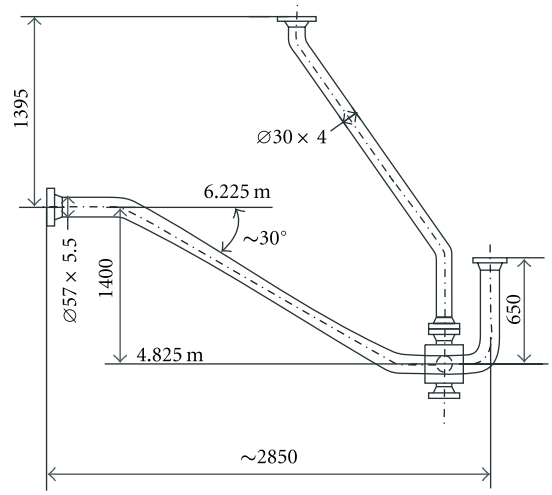

Figure 4: Hot leg with pressuriser surge line.

were determined by the requirement of volume scaling. The elevations of tube rows, the vertical surface distribution of tubes, and the overall heat transfer coefficient between the primary and the secondary side are the same as in the reference system. On the secondary side the coolant temperature, pressure, and the steam to water volume ratio are kept. Geometry of PMK-2 SG model is somewhat different from the full scale SG. Therefore, a question can arise how well SG model in PMK-2 can model SG in the plant. Test results of different transients, especially PHS-TC and OAH-C2 tests dedicated to SG heat transfer study, show that SG behaviour in the plant can be reproduced well enough.

Cold and hot legs are volume scaled, and care was taken to reproduce the correct elevations of the loop seals in both the hot and cold legs. For practical reasons the lengths could not be maintained 1 : 1; therefore, a relatively large tube diameter of 46 mm has been chosen to keep the Froude number which is important to get stratification in two-phase natural circulation. The hot leg with the pressuriser surge line is presented in Figure 4.

The component models discussed above have about the same vertical position in the loop as the components of the primary circuit in the reference system. The main circulating pump is applied to produce the nominal operating flow conditions and flow coast down following pump trip in the transient process. For the pressuriser the volume scaling, the water to steam volume ratio, and the elevation of the water level are kept; however, the diameter and height ratios cannot be realized. For the hydroaccumulators the volume scaling and elevation are kept with N_2 pressure upon the water level as in the plant.

Figure 5 shows the scheme of the PMK-2 facility. After the pump trip the pump is valved off by closing valves PV11 and MV12, while MV11 is open. From the emergency core cooling systems (ECCS) the four SITs of the Paks NPP are modelled by two vessels, and they are connected to the downcomer and upper plenum. The HP and LPI systems are modelled by the use of piston pumps. Figure shows locations of measured parameters, for example, PR21, TE15, LE11, LV21, and so forth, and the elevations of component models. The reference level of 0.0 m is the lower flat of the reactor model.

The nominal parameters of the PMK-2 corresponding to the nominal operating parameters of the reference plant are as follows: primary pressure: 12.3 MPa; coolant temperature at core inlet: 540 K; core power: 664 kW; mass flow rate: 4.5 kg/s; secondary pressure: 4.6 MPa; feedwater temperature: 493 K; steam mass flow rate: 0.36 kg/s; HPIS and LPIS flow: 0.014 and 0.042 kg/s, respectively, for each unit.

Measurement locations are presented in circles as follows: TE: temperature; PR: pressure; LE: (coolant) level; LV: local void. The local void is measured by needle-shaped conductivity probes. The sampling rate of the data acquisition system is 1 s.

3. The PMK-2 Experimental Data Base for VVER-440/213 Plants

The PMK-2 data base, described in detail in [1], covers the list of design basis accidents analysed in the Safety Analysis Report of the Paks plant as well as practically all test types described in the OECD-VVER cross-reference matrices. It consists of 55 tests, which address and help to understand all the important aspects of plant system behaviour in accident conditions. These tests can be divided into five groups as follows: 15 tests with 7.4% cold leg breaks; 10 tests with cold leg breaks of different sizes, covering a range from 0.5% to 30%; 10 tests with hot leg breaks and primary to secondary leaks; 10 tests for natural circulation; 10 tests for plant transients and accidents.

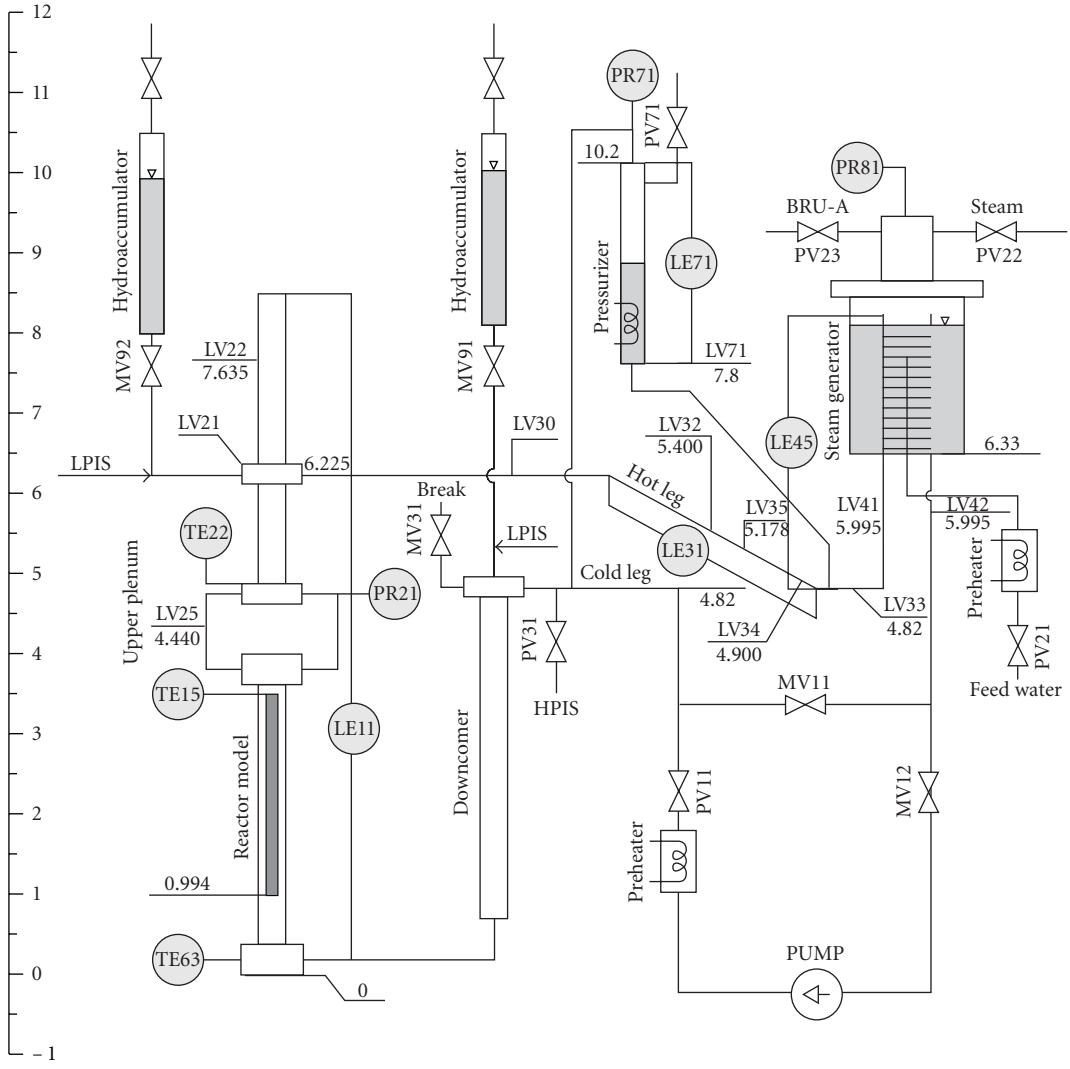

Figure 5: Scheme of PMK-2 facility.

The experimental results are available in digital form on a CD attached to [1].

A complete list of tests is given in Tables 1, 2, 3, 4, and 5.

4. Major Findings of Experiments

The significance of the PMK-2 experiments mainly consists in the creation of a unique, high-quality data base that can be used for code validation, especially for VVER-specific phenomena [3]. The OECD-VVER code validation matrices [5] for the three main groups of transients, namely, large breaks, small/intermediate leaks, and plant transients have been carefully reviewed with respect to what extent the PMK-2 tests represent thermohydraulic phenomena listed there. It was found that the following phenomena are simulated at a level required by the validation matrices: break flow; pressuriser thermohydraulics and surge line hydraulics; heat transfer in SG primary and secondary sides; single- and two-phase natural circulation; mixing and condensation during injection from ECCSs; loop seal behaviour in hot leg and clearance in cold leg; core heat transfer including DNB and dryout.

Besides addressing typical phenomena during transients, an important number of PMK-2 experiments support specific cases of plant performance, like operator actions taken in Emergency Operating Procedures and steam generator tube and header ruptures, system behaviour in a LOCA occurring during plant cooldown, and in an ATWS sequence. These data helped to validate codes for VVER-specific design basis accidents or for beyond design conditions.

Tests addressing the Emergency Operating Procedures of the Paks plant supported the following procedure developments: response to inadequate core cooling, response to degraded core cooling, post-LOCA cooldown and depressurisation, and response to loss of secondary heat sink and of loss of all AC power. The results experimentally supported the qualification of procedures and validation of codes.

Table 1: 7,4% cold leg breaks.

No. of tests	Project identification	Test acronym	Date of tests	ECCS configuration and/or main objectives
(1)	IAEA-SPE	SPE-1	1986	Minimum ECCS configuration: 0 SIT and 1 HPIS
(2)	ATKP-2	SPE-ROV	1987	Without ECCS: 0 SIT, 0 HPIS and 0 LPIS, onset of core dryout
(3)	ATKP-2	PAV-CM	1987	DBA case with ECCS configuration: 3 SITs and 1 HPIS, late SIT actuation
(4)	IAEA-SPE	SPE-2	1987	DBA case with ECCS configuration: 3 SITs and 1 HPIS, nominal initial power, and delayed steam dump
(5)	OKKFT G-11	SP0	1988	DBA case with ECCS configuration: 3 SITs and 1 HPIS, HL/CL connection
(6)	OMFB 00307/91	OM1-BF	1992	ECCS configuration: 3 SITs, 0 HPIS, 1 LPIS
(7)	OMFB 00307/91	OM1-G0	1992	DBA case with ECCS configuration: 3 SITs and 0 HPIS AM actions, reference case, secondary bleed and feed
(8)	OMFB 00307/91	OM1-G1	1992	DBA case with ECCS configuration: 3 SITs and 0 HPIS AM actions, noncondensables, secondary bleed and feed
(9)	OMFB 00307/91	OM1-G2	1992	DBA case with ECCS configuration: 3 SITs, 0 HPIS, 1 LPIS AM actions, noncondensables, secondary bleed and feed
(10)	IAEA-SPE	SPE-4	1993	DBA case with ECCS configuration: 3 SITs, 0 HPIS, 1 LPIS AM actions, secondary bleed and feed
(11)	PHARE SRR3/95	PHS-BF	1999	DBA case with ECCS configuration: 3 SITs, 0 HPIS, 1 LPIS AM actions, primary and secondary bleed and feed
(12)	IMPAM-VVER	IMP-21	2003	ECCS configuration: 0 HPIS, 3 SITs, 1 LPIS AM actions: primary bleed and feed, with low pressuriser level
(13)	IMPAM-VVER	IMP-22	2004	ECCS configuration, 0 HPIS, 3 SITs, 1 LPIS AM actions: primary bleed and feed, early actuation
(14)	IMPAM-VVER	IMP-23	2004	ECCS configuration, 0 HPIS, 3 SITs, 1 LPIS AM actions: primary bleed and feed, a counterpart test to PACTEL, low SIT pressure
(15)	IMPAM-VVER	IMP-32	2004	ECCS configuration: 0 HPIS, 3 SITs, 1 LPIS AM actions: primary bleed and feed, a counterpart test to PACTEL

Table 2: Cold leg breaks of different sizes.

No. of tests	Project identification	Test acronym	Date of tests	Break size %	ECCS configuration and/or main objectives
(1)	OKKFT G-11	G11-35	1989	3.5	Minimum ECCS configuration: 0 SIT, 1 HPIS
(2)	OKKFT G-11	CLB-14A	1990	14.8	Minimum ECCS configuration: 0 SIT, 1 HPIS Core dryout, cladding temperature excursion and cooldown
(3)	OKKFT G-11	CLB-14B	1990	14.8	DBA case with ECCS configuration: 3 SITs and 1 HPIS Core dryout, cladding temperature excursion and cooldown
(4)	OKKFT G-11	CLB-10A	1990	1.0	Minimum ECCS configuration: 0 SIT, 1 HPIS Test with a classical SBLOCA break size
(5)	AEKI	CLB-10B	1994	1.0	Minimum ECCS configuration: 0 SIT, 1 HPIS Test of 1990 (1%CLB) is repeated with local void probes
(6)	OMFB 0881/95	OM5-BF	1995	1.0	Minimum ECCS configuration: 0 SIT, 1 HPIS AM actions, primary bleed and feed
(7)	PHARE SRR3/95	PHS-05	1999	0.5	ECCS configuration: 0 SIT, 3 HPISs Overfeeding by high pressure injection
(8)	OAH-CAMP	OAH-C1	1999	2.0	ECCS configuration: 2 SITs, 0 HPIS AM actions, secondary bleed and feed
(9)	IMPAM-VVER	IMP-1	2003	0.5	ECCS configuration: 3 HPIS, 0 SIT Post-LOCA cooldown, modelling ES-1.2 procedure in Paks NPP
(10)	IMPAM-VVER	IMP-31	2004	30	ECCS configuration: 0 HPIS, 0 SIT, 1 LPIS LBLOCA during cooldown

Table 3: Hot leg breaks and primary to secondary leaks.

No. of tests	Project identification	Test acronym	Date of tests	Break size %	ECCS configuration and/or main objectives
(1)	OKKFT G-11	G11-7A	1989	7.4	ECCS configuration: 0 SIT and 1 HPIS Hot leg break LOCA for comparison
(2)	OKKFT G-11	G11-7B	1989	7.4	DBA case with ECCS configuration: 3 SITs and 1 HPIS Hot leg break LOCA for comparison
(3)	OKKFT G-11	G11-PS	1988	4.7	DBA case with ECCS configuration: 3 SITs and 2 HPISs Study of system behaviour in PRISE conditions
(4)	IAEA-SPE	SPE-3	1989	11.8	DBA case with ECCS configuration: 3 SITs and 3 HPISs PRISE, SG safety valve remains open
(5)	PHARE 4.2.6b	PH4-PS	1996	1.0	DBA case with minimum ECCS configuration: 2 SITs and 1 HPIS Pressuriser thermohydraulics when safety valve opens
(6)	PHARE 4.2.6b	PH4-SLB	1997	32.0	DBA case with minimum ECCS configuration: 2 SITs, 1 HPIS, 1 LPIS Pressuriser surge line break, core dryout, refill, reflood
(7)	PHARE 2.02	PH2-PS	1997	4.5	Maximum ECCS configuration: 4 SITs and 3 HPISs PRISE, SG safety valve stuck open, spray in PRZ, sec. bleed and feed
(8)	PHARE VVER01	PHV-11	1998	4.5	ECCS configuration: 2 SITs and 2 HPISs PRISE, AM actions, spray in PRZ, secondary bleed and feed
(9)	PHARE VVER01	PHV-12	1998	1.5	ECCS configuration: 2 SITs and 2 HPISs PRISE, AM actions, spray in PRZ, secondary bleed and feed
(10)	PHARE VVER01	PHV-13	1998	0.7	ECCS configuration: 1 HPIS and no SITs PRISE, AM actions, spray in PRZ, secondary bleed and feed

Note: There are three types of breaks:
(i) hot leg break in tests no. 1 and 2,
(ii) leak on the pressuriser in tests no. 5 and 6,
(iii) primary to secondary leaks in tests nos. 3, 4, 7, 8, 9, and 10.

Table 4: Tests for natural circulation.

No. of tests	Project identification	Test acronym	Date of tests	Main objectives
(1)	OKKFT G-11	G11-TC	1988	Study of natural circulation, step by step decrease of primary inventory up to crisis
(2)	OMFB 00307/91	OM1-TC	1993	One- and two-phase natural circulation, step by step coolant decrease, N_2 in the system, crisis
(3)	PA Rt.	PAV-GFK	1993	Study of disturbances: shut-down conditions, N_2 in the upper plenum
(4)	PA Rt.	PAV-FET	1993	Study of disturbances: closing of main isolation valve
(5)	PA Rt.	PAV-GKK	1993	Study of disturbances: gas in the SG collectors
(6)	PA Rt.	PAV-HVM	1993	Study of disturbances: cold water injection to the hot leg
(7)	OMFB, 1044/96	OM6-GFK	1998	Effect of gas injection to the upper plenum
(8)	OMFB, 1044/96	OM6-FET	1998	Effect of isolation valve closing in the cold leg
(9)	PHARE SRR3/95	PHS-TC	1998	SG heat transfer study with level decrease, step by step
(10)	OAH-CAMP	OAH-C2	2001	SG heat transfer study with continuous coolant level decrease in the SG secondary side

In the field of primary to secondary leaks the tests are representative for plant response in these VVER-specific accident types and reflect the effectiveness of secondary bleed and feed and of pressure reduction by pressuriser spray and supported the development of effective operator actions to minimize the coolant loss to the atmosphere.

The test investigating the consequences of a LOCA occurring during plant cooldown, when the pressuriser is filled by nitrogen, supplied information on spreading of noncondensable gas along the primary circuit following the cold leg break.

An example on *core heat transfer including DNB and dryout*. The safety significance of these phenomena is the control of the cladding temperature. The core heat transfer is the first step when the heat is transferred from the fuel surface to the coolant; then the steam generator tubes transmit the heat to the secondary side. In the case of large breaks all heat transfer regimes from single phase liquid to single phase (saturated and superheated) steam are relevant, but cladding temperatures are mainly influenced by correct prediction of critical heat flux, heat transfer to steam, precooling by entrained liquid during reflooding and rewetting. The cladding

Table 5: Plant transients and accidents.

No. of tests	Project identification	Test acronym	Date of tests	Main objectives
(1)	AEKI	LOF-66	1986	Study of system behaviour in total loss of flow, minimum value of DNBR
(2)	ATKP	ATK-PC	1987	MCP rotor seizure, minimum DNBR ratio
(3)	ATKP	ATK-FW	1987	Total loss of feedwater, experimental support to system analysis in Paks NPP
(4)	OMFB 00307/91	OM1-FW	1992	Total loss of feedwater, effect of secondary bleed with passive secondary feed
(5)	OMFB 00307/91	OM1-ST	1992	Station blackout, effectiveness of secondary bleed and feed
(6)	OMFB 00307/91	OM1-MSH	1993	Main steam header break, secondary bleed and feed
(7)	OMFB 00881/95	OM5-FW	1996	Total loss of feedwater, secondary bleed, and primary bleed and feed
(8)	OMFB 00881/95	OM5-ST	1997	Station blackout, secondary bleed, and primary bleed and feed
(9)	PHARE VVER02	PHV-21	1999	Station blackout with ATWS, density, and boron concentration feedback
(10)	PHARE VVER02	PHV-22	1999	Station blackout with ATWS, density, and boron concentration feedback

temperatures measured in PMK-2 allow identifying these regimes. The limitations for this phenomenon are in the 1-D representation of the core and the uniform axial power profile.

Quality of measurements strongly depends on the accuracy of measured parameters. In the PMK-2 tests, measurement transducers of temperatures, pressures, differential pressures, levels, local voids, and flow rates are calibrated in accordance with the measurement quality control system. Accuracy estimation includes a calibration constant, absolute maximum error, and standard deviation. In addition, there is a calibration system, and an in-site calibration before each test can be made together with mass and energy balance measurement at operation conditions [1].

Experiments selected to represent phenomena are as follows:

(i) OAH-C1, 2% cold leg break without HPIS, with secondary bleed,

(ii) PHS-BF, 7.4% cold leg break with secondary side bleed and primary side bleed and feed,

(iii) PH4-SLB, 32% break in the surge line at the hot leg connection.

Figure 6 presents the core model with thermocouples to identify thermocouple locations on different rods (from 1 to 19) and at different levels. The identification is given in Table 6 with thermocouples TE10 to TE19, number of rods, where temperatures are measured, and the level from 0.0 m elevation.

Tables 7 and 8 present the heater rod surface temperatures in OAH-C1 and in PHS-05, PHS-BF, and PH4-SLB, respectively. Table 8 includes data from PHS-05 test to show similar results for the test case having the smallest break size in the PMK-2 tests. Table 7 includes cladding temperatures measured at elevations of 2.994 and 3.444 m as follows: TE14 is on rod no. 6 in normal location typical for bundles; TE15 is on rod no. 11 in wall location, TE16 is on rod no. 1 in central location, TE17 is on rod no. 17 in corner location, TE18 and TE19 are on rod no. 2 and 3 in normal locations, respectively, (see also Figure 1). Column "Temperature excursion" shows starting time of temperature excursions (starts), the maximum value of cladding temperatures (max.), and the time when the temperature excursion is ended (end). The other columns are the transient time (Time, s), the coolant level in the reactor model (LE11), and the value of cladding temperatures. There are three maximum values of cladding temperatures (1., 2. and 3. max). These are the maximum temperatures in cases of dryout as it can be seen also in Figures 8, 9, and 10.

Table 6: Thermocouple locations in the core model (see Figure 6), measuring cladding temperatures in different rods and elevations.

Identification	Number of rods	Level from 0.00 m, m	Levels from core inlet, mm
TE10	10	1.044	50
TE11	2	1.494	500
TE12	8	1.994	1000
TE13	9	2.494	1500
TE14	6	2.994	2000
TE15	11	3.444	2450
TE16	1	3.444	2450
TE17	16	3.444	2450
TE18	2	3.444	2450
TE19	3	3.444	2450

The *OAH-C1* test is started from the nominal operating parameters of the plant, with the availability of 2 SITs only and with secondary side bleed. Injection from SITs begins at 159 s and terminates at 2548 s. The secondary bleed is initiated at 1502 s. Though the SIT injection starts at 159 s, it practically stops due to the stagnation of the primary pressure, and it is reinitiated by the secondary bleed at 1502 s.

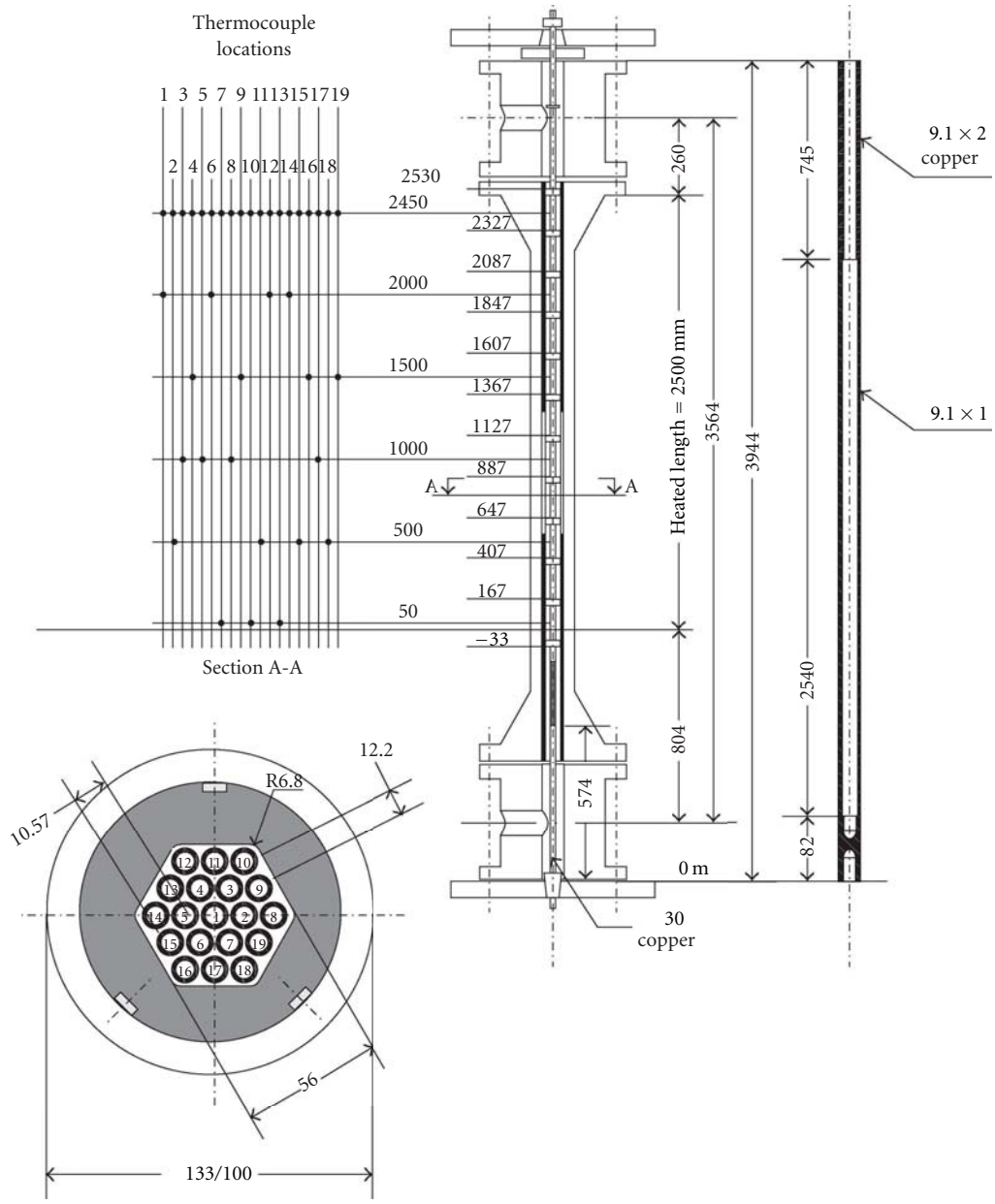

Figure 6: Core model with thermocouple locations for the identification of locations on rods and level (from [1]).

The cold water from the SITs is injected into saturated steam in the downcomer head, causing extensive direct contact condensation.

Results focusing on dryout occurrence in different regions of the core are presented in Table 7 and in Figures 7 to 10. Crisis occurs first at the elevation of 2.994 m, with the maximum value of TE14 temperature in rod no. 6. It is 628 K at 1156 s and at a coolant level of 2.761 m in the reactor model (LE11). At the outlet section (3.444 m) crisis occurs three times in rod no. 11, 1, 16, 2, and 3, in wall position (TE15), central position (TE16), corner position (TE17), and in normal positions (TE18, TE19). The highest temperatures were measured during the third temperature excursion: 718.0 K (wall position), 739.2 K (central position), 713.2 (corner position), 737.7, and 742.0 K (normal positions). The effect of cold channel wall can be seen in the maximum temperatures.

The *PHS-BF test* is started from nominal operating parameters of the plant, with the availability of 3 SITs and 1 LPIS. To cool down the system, secondary side bleed is initiated at 900 s. 2 SITs inject cold water to the downcomer and 1 SIT to the upper plenum from 43.0 to 693 s.

Results obtained are shown in Table 8 and in Figures 11, 12, 13, and 14. Crisis occurs at the three uppermost instrumented elevations (2.494 m, 2.994 m, and 3.444 m). At the outlet level the crisis occurs in the same rods as in test OAH-C1, but earlier in the transient, due to the faster transient process.

Table 7: Cladding temperatures in OAH-C1 test.

Identification	Location rod no./elevation —/m	Temperature excursion	Time s	LE11 m	Temperature K
TE14	6/2.994	Starts	1131	2.774	543.4
	normal	Max.	1156	2.761	628.4
		End	1175	2.696	549.9
TE15	11/3.444	Starts	1118	2.968	544.4
	wall	1. max.	1180	3.232	684.0
		2. max.	1263	3.210	692.7
		3. max.	1515	2.970	**718.0**
		End	1585	2.874	546.0
TE16	1/3.444	Starts	1119	2.947	544.7
	central	1. max.	1179	3.144	697.0
		2. max.	1260	3.145	702.4
		3. max.	1515	2.970	**739.2**
		End	1592	3.141	546.0
TE17	16/3.444	Starts	1115	3.021	544.4
	corner	1. max.	1179	3.144	680.7
		2. max.	1259	3.068	681.7
		3. max.	1514	2.886	**713.2**
		End	1585	2.874	546.0
TE18	2/3.444	Starts	1117	2.985	544.4
	normal	1. max.	1180	3.232	701.0
		2. max.	1261	3.184	708.7
		3. max.	1515	2.970	**737.7**
		End	1590	3.006	546.0
TE19	3/3.444	Starts	1117	2.985	544.4
	normal	1. max.	1179	3.144	711.0
		2. max.	1261	3.145	712.4
		3. max.	1514	2.886	**742.0**
		end	1555	3.007	546.0

The *PH4-SLB test* is started from the nominal operating parameters of the plant, with ECCS configuration as 2 SITs, 1 HPIS, and 1 LPIS. 2 SITs inject cold water to the upper plenum. The reactor model is almost fully empty in the time interval of 220 to 350 s. The HPIS injection begins at 17.0 s, the SIT injection starts at 20 s, while LPIS flow is initiated at 304 s.

Results obtained are shown in Table 8 and in Figures 15, 16, 17, and 18. Crisis occurs at elevations and rods as in the case of PHS-BF test but, due to the large break size, earlier in time and with higher peak temperature. The maximum temperature is 943.6 K in rod no. 1, that is, in the central rod at the outlet level.

5. PMK-2 Test Results in International Code Validation

PMK-2 test results have been continuously applied to the validation of different versions of the ATHLET, CATHARE, and RELAP5 codes, since the first IAEA code validation exercise in 1986. In addition, PMK-2 tests figure in the matrices of developmental assessment of internationally recognised computer codes for safety analysis, like ATHLET and RELAP5.

Three small break LOCA and one primary to secondary leak tests served as a basis for VVER-specific Standard Problem Exercises organised under the umbrella of IAEA in the period 1987 to 1995 [6–9].

A special small break LOCA test was run to investigate the hot leg loop seal behaviour and the effectiveness of secondary side bleed, with the aim to support code validation activities within the US NRC CAMP programme [10].

A large number of tests were conducted in EU-PHARE and EU-Framework programmes covering a wide variety of test types including pressuriser surge line break, large primary to secondary leakage, station blackout with ATWS, and tests supporting accident management strategies in VVER-440/213 plants [3].

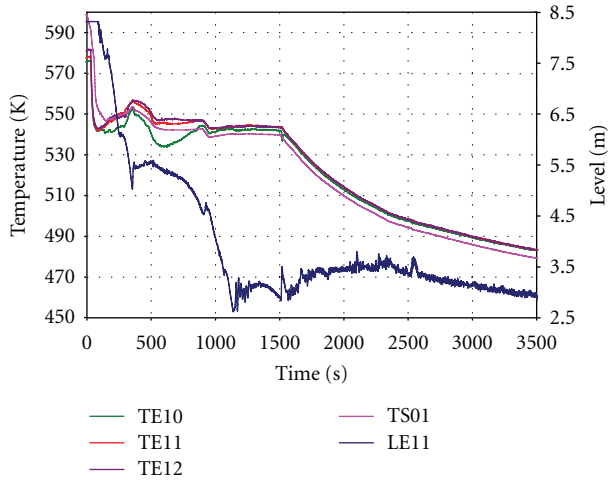

Figure 7: Cladding temperatures TE10, TE11, TE12, saturation temperature (TS01) and coolant collapsed level in the core model (LE11), in OAH-C1, 2% cold leg break without HPIS, with secondary bleed.

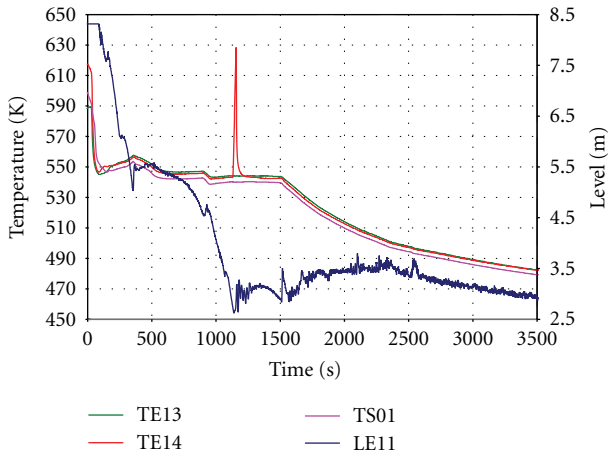

Figure 8: Cladding temperatures TE13, TE14, saturation temperature (TS01) and coolant collapsed level in the core model (LE11), in OAH-C1, 2% cold leg break without HPIS, with secondary bleed.

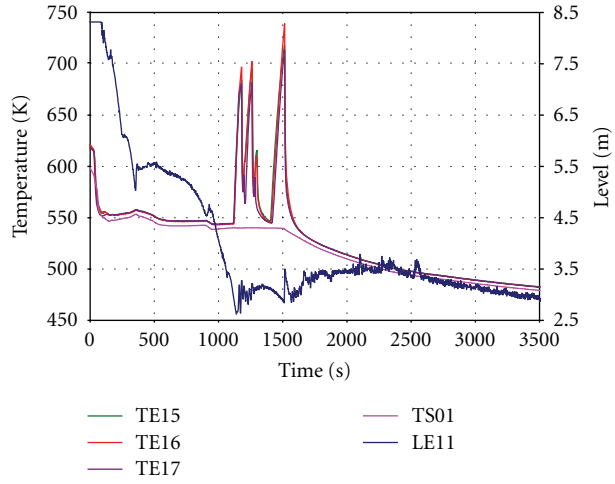

Figure 9: Cladding temperature TE15, TE16, TE17, saturation temperature (TS01) and coolant collapsed level in the core model (LE11), in OAH-C1, 2% cold leg break without HPIS, with secondary bleed.

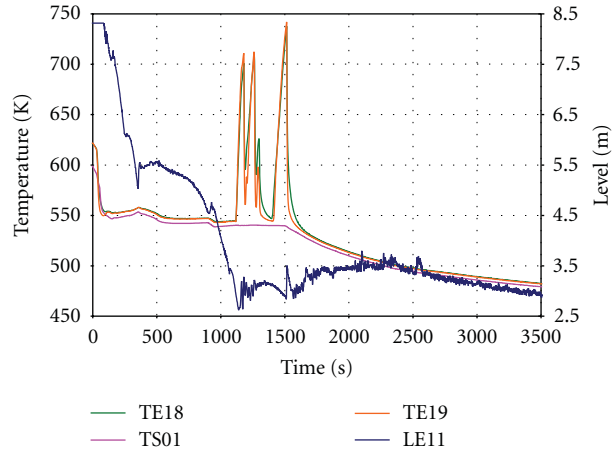

Figure 10: Cladding temperatures TE18, TE19, saturation temperature (TS01) and coolant collapsed level in the core model (LE11), in OAH-C1, 2% cold leg break without HPIS, with secondary bleed.

Twenty-eight PMK-2 tests were applied to different international code validation exercises, and several versions of ATHLET, CATHARE, and RELAP5 have been assessed by foreign and Hungarian experts. The expertise gained in international cooperations—involving experts of 29 countries participating in PMK-2 projects—helped to better understand VVER system behaviour and reach a high level of modelling of accident sequences. Results of these activities are referenced in [1, 3], together with validation results obtained in national projects.

6. Results of Validation of ATHLET, CATHARE, and RELAP5

Since codes applied for safety analysis in Hungary are ATHLET for large break LOCA, RELAP5 for small break LOCA and plant transient analyses, as well as CATHARE, which is used as an independent tool in support of the regulatory authority, validation activity in the country concentrated on these codes [3].

Methodologies of code validation used in PMK-2 projects include both qualitative and quantitative assessments. The former was almost exclusively applied in the early phase of code validation by integral experiments. It is based on visual observation and engineering judgement of the agreement. Also the quantitative assessment methodology includes a qualitative part, which is a prerequisite to the quantitative part. Quantitative assessment results were obtained by the Fast Fourier Transform Based Method, which had extensively been used also in OECD and IAEA standard problems [11–13].

Table 8: Cladding temperatures in PHS-05, PHS-BF, and PH4-SLB tests.

Identification	Location rod. no./elevation	PHS-05 Break size 0.5%		PHS-BF Break size 7.4%		PH4-SLB Break size 32%	
	—/m	Time s	Temp. K	Time s	Temp. K	Time s	Temp. K
TE13	9/2.494	—	—	479	525.4	238	546.7
	wall			717	543.4	406	851.4
			1557	470.6			
TE14	6/2.994	—	—	493	551.2	236	553.4
	normal			733	564.4	419	927.8
			1578	608.2			
TE15	11/3.444	4768	603.4	525	586.7	224	501.2
	wall			749	572.7	444	821.4
			1603	685.7			
TE16	1/3.444	4768	606.7	520	591.7	223	524.0
	central			749	583.0	444	943.6
			1603	725.2			
TE17	16/3.444	4767	598.0	512	593.4	223	503.4
	corner			748	586.4	440	882.0
			1590	667.7			
TE18	2/3.444	4768	609.7	525	598.4	224	512.0
	normal			749	584.4	444	913.0
			1609	725.4			
TE19	3/3.444	4768	613.0	520	604.0	224	517.0
	normal			749	591.4	435	916.0
			1600	717.0			

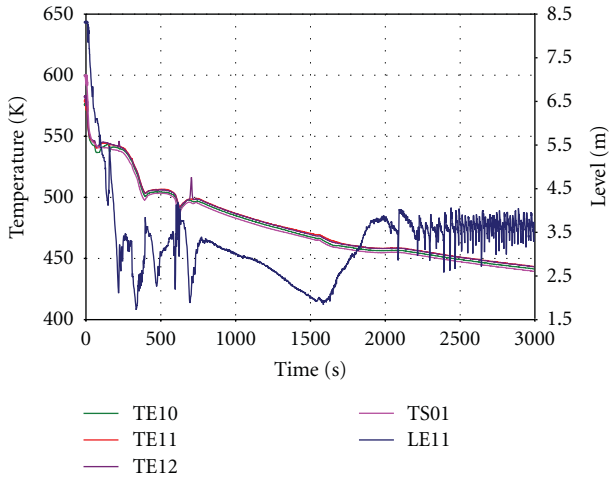

Figure 11: Cladding temperatures TE10, TE11, TE12, saturation temperature (TS01) and coolant collapsed level in the core model (LE11), in PHS-BF, 7.4% cold leg break with secondary bleed and primary side bleed and feed.

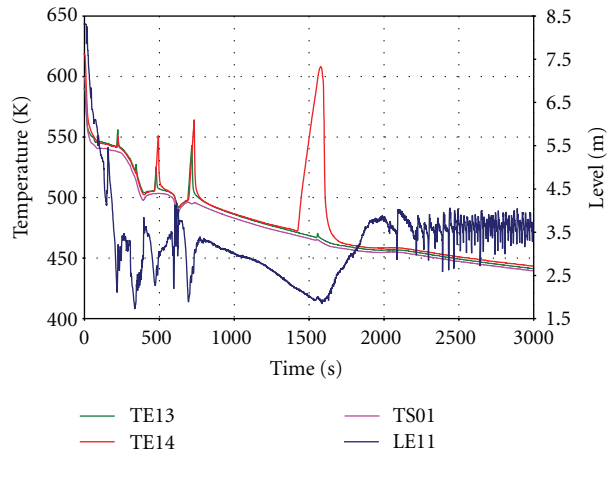

Figure 12: Cladding temperatures TE13, TE14, saturation temperature (TS01) and coolant collapsed level in the core model (LE11) in PHS-BF, 7.4% cold leg break with secondary bleed and primary side bleed and feed.

Results of code validation work in the PMK-2 projects are presented by tests selected in a way to represent major test types of the OECD-VVER code validation matrices: different small break LOCAs, pressuriser leak, steam generator header rupture, large break LOCA showing the three typical phases of blowdown, refill and reflood, and station blackout with ATWS. Results are as follows.

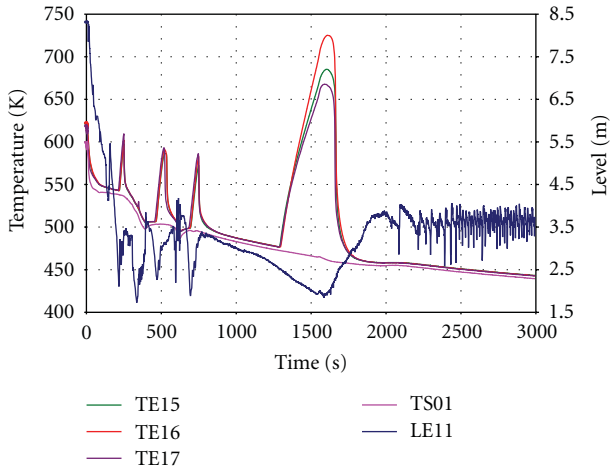

Figure 13: Cladding temperatures TE15, TE16, TE17, saturation temperature (TS01) and coolant collapsed level in the core model (LE11), in PHS-BF, 7.4% cold leg break with secondary bleed and primary side bleed and feed.

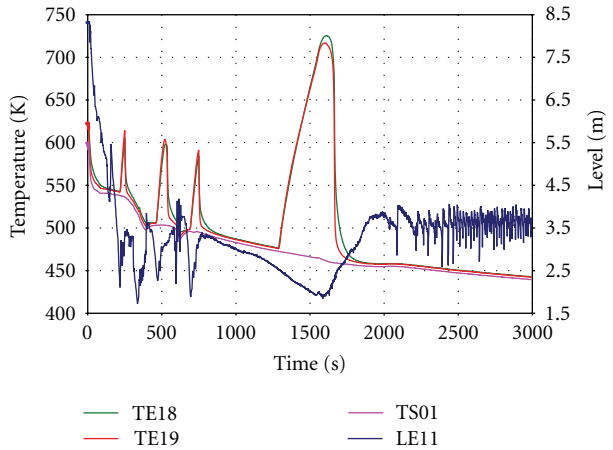

Figure 14: Cladding temperatures TE18, TE19, saturation temperature (TS01) and coolant collapsed level in the core model (LE11) in PHS-BF, 7.4% cold leg break with secondary bleed and primary side bleed and feed.

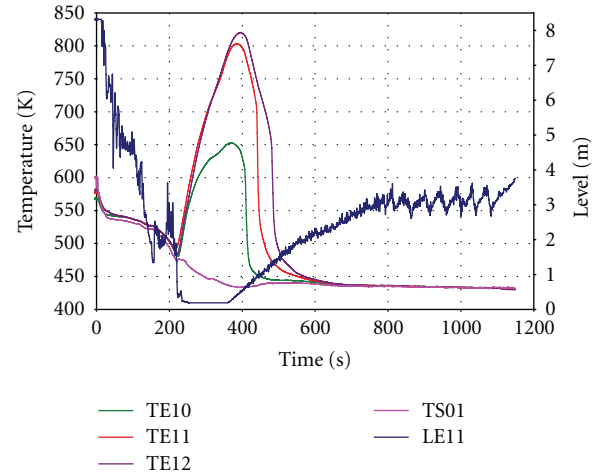

Figure 15: Cladding temperatures TE10, TE11, TE12, saturation temperature (TS01) and coolant collapsed level in the core model (LE11), in PH4-SLB, 32% break in the surge line at the hot leg connection.

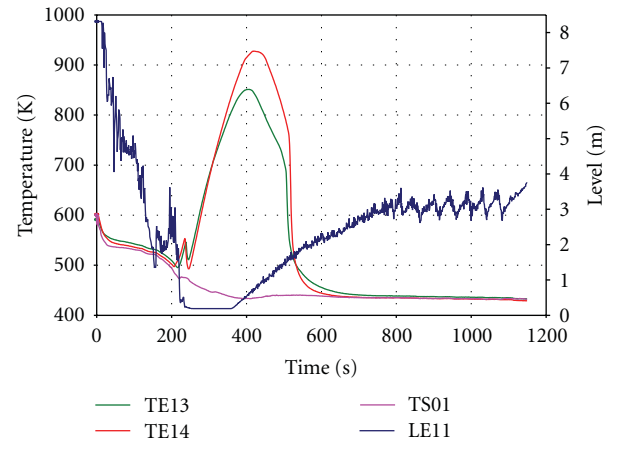

Figure 16: Cladding temperatures TE13, TE14, saturation temperature (TS01) and coolant collapsed level in the core model (LE11), in PH4-SLB, 32% break in the surge line at the hot leg connection.

For small break LOCA, all the three codes are capable of predicting the overall trend of transient and the test-specific phenomena in a "qualitatively correct" way with some quantitative disagreements. Results of the quantitative assessments gave "very good" qualification levels.

Results of the large break LOCA test calculated by the ATHLET code can be qualified to be qualitatively and quantitatively "correct". Results of quantitative assessments for CATHARE and RELAP5 give "very good" qualification level for both codes. In spite of these promising results the codes cannot be regarded as qualified for VVER large break cases, since the PMK-2 data base contains only tests, which lie in the lower part of the large LOCA break size.

The qualitative assessment of RELAP5 *by a plant transient* station blackout with ATWS shows that predictions of key parameters and sequence of events are qualitatively and quantitatively "correct", since the most important test-specific phenomena as pressuriser behaviour during safety valve opening, primary system behaviour during coolant depletion, and refill of the core are well predicted. The qualification level of quantitative prediction is also "good".

Results show that different model approaches applied to the ATHLET, CATHARE, and RELAP5 codes do not influence the quality of predictions in the different types of transients as SBLOCA, LBLOCA, and Transients.

Computer code modelling, development of nodalisations, needs significant users' expertise and experience gained in simulating plant transients, and vice versa, experiences obtained in the development of computer model for facilities can directly be applied to plant models. Nodalisation may also depend on transient type to be simulated. However, users develop, for example, for a facility a "basic"

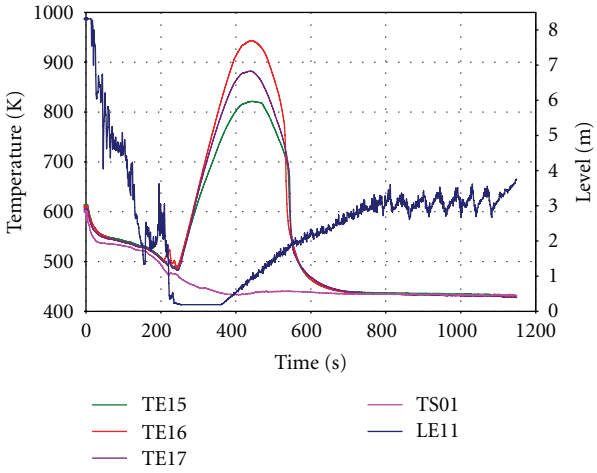

Figure 17: Cladding temperatures TE15, TE16, TE17, saturation temperature (TS01) and coolant collapsed level in the core model (LE11), in PH4-SLB, 32% break in the surge line at the hot leg connection.

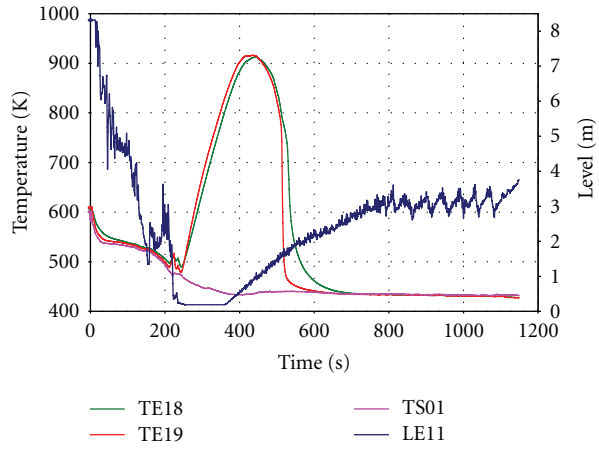

Figure 18: Cladding temperatures TE18, TE19, saturation temperature (TS01) and coolant collapsed level in the core model (LE11), in PH4-SLB, 32% break in the surge line at the hot leg connection.

nodalisation; however, it should be modified in cases when certain phenomena should be described in detail and properly. Methodology for different codes are different. Experts from Germany, France, and USA helped us in developing nodalisation for ATHLET, CATHARE, and RELAP5, respectively. Results of assessment activities in the PMK-2 projects show that similar quality of transient predictions can be achieved by each of the three codes.

6.1. Example for the Qualitative Assessment. The qualitative assessment by engineering judgement refers to the comparison of the results of a test and the results of a computer code calculation, evaluating the results by visual observation. In other words, the qualitative assessment is made by evaluating and ranking the discrepancies between the measured and calculated parameters. In the practice of the qualitative assessment, the comparison by visual observation is limited to the time variations of parameters.

The qualification of qualitative assessment results is as follows.

(i) Calculation falls within experimental data uncertainty band, which means that the code calculation is *qualitatively and quantitatively correct*.

(ii) Calculation does not fall within the uncertainty band but shows correct trend. It means that the code calculation is *qualitatively correct*.

(iii) Calculation lies out of the uncertainty band and does not show correct trend, and the reason is unknown. The result of calculation is *not acceptable*.

The *OAH-C1*, 2% cold leg break test with 2 SITs and 1 HPIS, addresses the study of the effectiveness of the secondary side bleed, to reinitiate the SITs injection and cooldown of the system, after significant loss of the primary coolant, which leads to extensive dryout in the core.

The test is started from the nominal operating parameters of the Paks NPP with availability of 2 SITs, both injecting to the downcomer. After the subcooled blowdown, however, the primary pressure is practically stagnating, and the injection from SITs is initiated by the opening and closing of the BRU-A. Due to the coolant loss, extensive dryout occurs in the core at 1514 s with a maximum temperature of 742 K. The injection from SITs is reinitiated by secondary bleed through the BRU-A to cool down the system. The validation is focused on the phenomena: mixing and condensation during injection from ECCSs; loop seal behaviour in hot leg and clearance in cold leg; core heat transfer including DNB and dryout; heat transfer in covered and partly covered core; core thermohydraulics.

The code, validated by the test, is the RELAP5/mod3.2.2 Gamma, in the framework of the US NRC CAMP program. The computer code model with the nodalisation scheme is presented in Figure 19.

Results of calculations for the initial conditions and boundary conditions fall into the uncertainty bands of the tests; therefore, the code calculation is qualitatively and quantitatively correct. The same is true for the timing of events, except for the generation of scram. However, it does not affect the overall trend of the time variation of parameters, which are shown in Figures 20, 21, 22, and 23.

Results of transient calculation are as follows.

(i) The overall trend of the time variations of parameters presented in Figures 20 to 23 is well predicted. In the calculation, the BRU-A opens three times in the test, however, two times in the calculation with slightly different times.

(ii) Due to the cold water injection from SITs into the downcomer, direct contact condensation occurs in the downcomer head. The more extensive condensation in the calculation results in higher mass loss

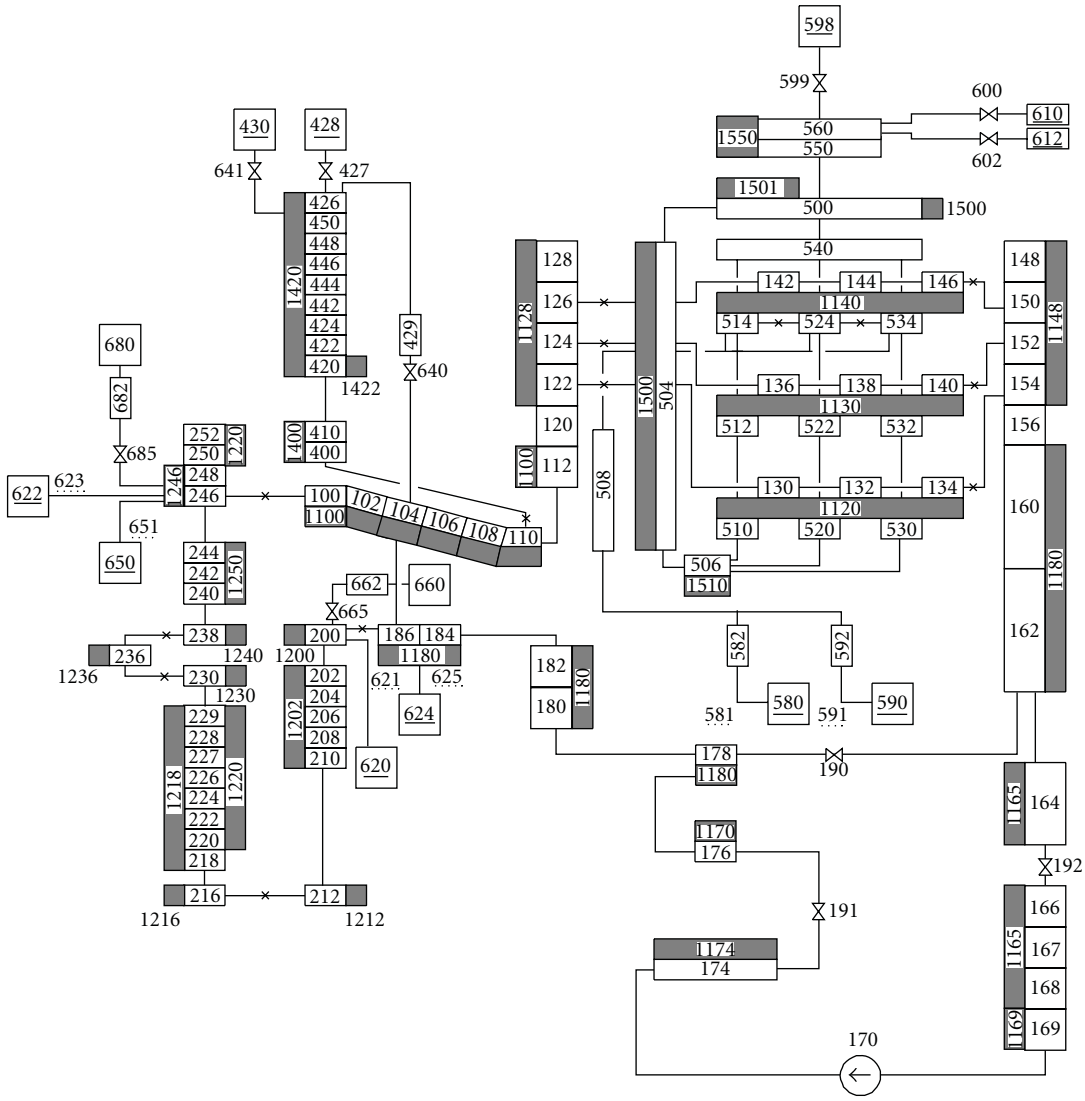

Figure 19: PMK-2 nodalisation scheme for RELAP5/mod3.2.2 Gamma as applied to the OAH-C1 test.

through the break: this indicates that the phenomena mixing and condensation are overpredicted.

(iii) The core heat transfer and especially the timing and value of maximum cladding temperature (1514 s/742 K in the test and 1526 s/726 K in the calculation) are well predicted (Figure 23).

(iv) The hot leg loop seal behaviour is very well predicted as shown in Figure 22. The deviation in the prediction of timing of cold leg loop seal clearing is ~11%.

6.2. Example for the Quantitative Assessment. The methodology for the qualitative and quantitative assessment of computer code accuracy with applications was presented in several papers [14–16]. The FFT-based method includes two phases as the qualitative and quantitative phases. The time variations of the measured and calculated parameters characterizing the transient are the basis in the qualitative phase and input to the quantitative phase, that is, to the FFTBM (Fast Fourier Transform Based Method) code.

The procedure for the *qualitative phase of the assessment* is primarily based on OECD/CSNI and US INEL suggestions [17, 18]. The main steps are as follows:

(i) subdivision of the transient in "phenomenological windows". For each window: specification of key phenomena, identification of "relevant thermal-hydraulic aspects" (RTA), and selection of parameters characterizing the RTAs are given;

(ii) qualitative analysis of the results of the measured and calculated time variations of parameters with the subjective judgments are as follows.

(a) *Excellent*: the code predicts the parameter qualitatively and quantitatively; the calculation falls within experimental data uncertainty band;

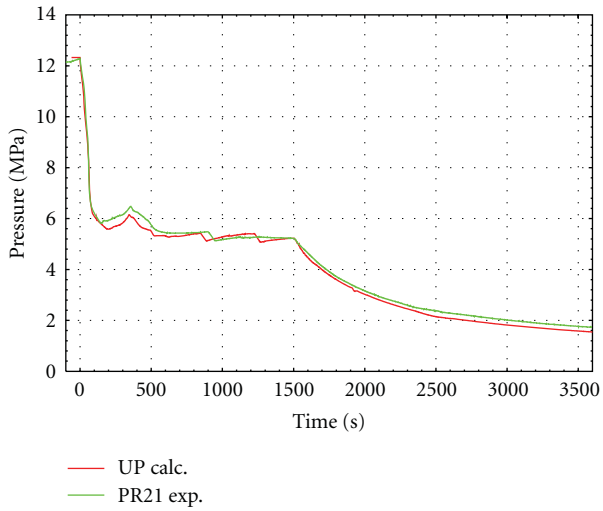

Figure 20: Measured and calculated primary pressures (PR21) in OAH-C1 test. Calculation by RELAP5/mod3.2.2 Gamma code.

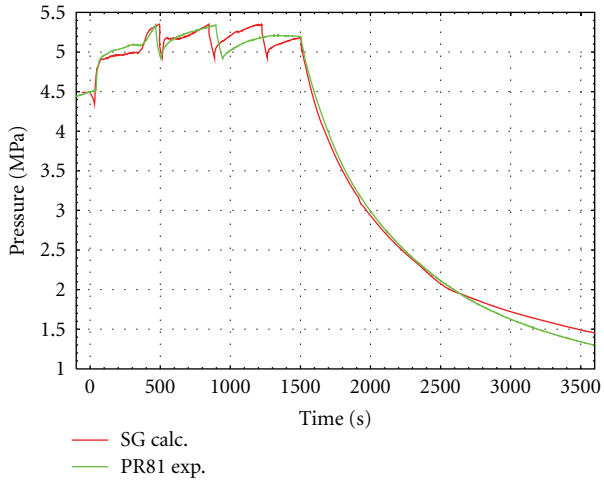

Figure 21: Measured and calculated secondary pressures (PR81) in OAH-C1 test. Calculation by RELAP5/mod3.2.2 Gamma code.

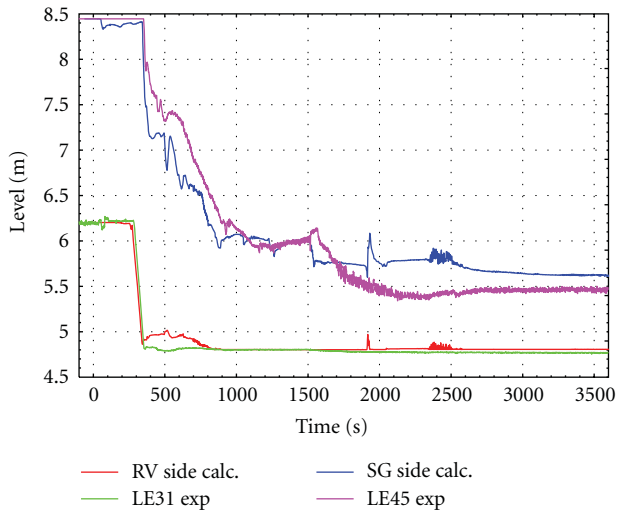

Figure 22: Measured and calculated coolant levels (LE31/LE45) in the hot leg loop seal in OAH-C1 test. Calculation by RELAP5/mod3.2.2 Gamma code.

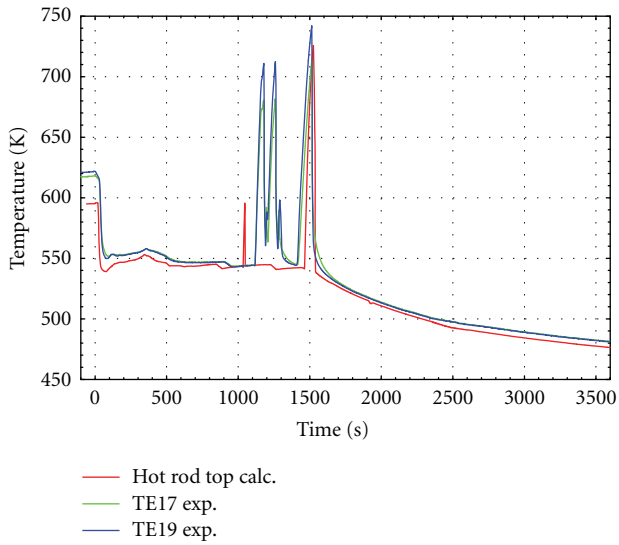

Figure 23: Measured and calculated cladding temperatures (TE17, TE19) in OAH-C1 test. Calculation by RELAP5/mod3.2.2 Gamma code.

the calculation is qualitatively and quantitatively correct.

(b) *Reasonable*: the code predicts the parameter qualitatively but not quantitatively; the calculation is not within experimental data uncertainty band but shows correct behaviour and trends.

(c) *Minimal*: the code does not predict the parameter, but the reason is understood and predictable; the calculation does not lie within experimental uncertainty band and does not show correct behaviour and trends.

(d) *Unqualified*: the code does not predict the parameter, and the reason is not understood; the calculation does not lie within experimental uncertainty band and does not show correct behaviour and trends.

In the qualitative phase of assessment the definition of "phenomenological windows" and corresponding RTA's is highly influenced by the expertise and practice of user.

The quantitative phase of the FFT-based method [13, 15], with the improvements [12], is presented below. The fast Fourier transform (FFT) is an algorithm that rapidly computes the discrete Fourier transform. To apply it, functions must be identified by a number of values that is a power with base equal to 2, and also sampling theorem should be fulfilled. The fulfilment of the sampling theorem is required to avoid distortion of sampled signals due to aliasing occurrence. Thus if the number of points defining the function in the time domain is NVAL $= 2^{m+1}$, then according

to the sampling theorem the sampling frequency, $f_s = 2f_{\max} = \text{NVAL}/T_d$, where T_d is the transient time duration of the sampled signal and $f_{\max}$ is the maximum frequency component of the signal. The sampling theorem does not hold beyond $f_{\max}$. It can be seen that the selection of the number of points is strictly connected to the sampling frequency. The FFT algorithm determines the number of points, equally spaced, which is a power with base 2 (N ranges from 2^9 to 2^{12}). Generally, an interpolation is necessary to satisfy this requirement. The FFTBM application implies analysis window (T_d) selection, the number of points (NVAL) determination through the fixed frequency (FFIX—minimum maximum frequency of analysis) value selection, the cut-off frequency (FCUT) value determination, and the weights selection. The cut off frequency has been introduced to cut-off spurious contributions.

The FFTBM calculates the measurement-prediction discrepancies in the frequency domain. For the calculation of these discrepancies experimental signal ($F_{\text{exp}}(t)$) and error function are needed. The error function in the time domain $\Delta F(t) = F_{\text{cal}}(t) - F_{\text{exp}}(t)$, where $F_{\text{cal}}(t)$ is the calculated signal. The code accuracy quantification for an individual calculated variable is based on amplitudes of discrete experimental and error signal obtained by FFT at frequencies f_n, where $n = 0, 1, \ldots, 2^m$, $N = 2^m$, and m is the exponent $m = 8, 9, 10, 11$. These spectra of amplitudes together with frequencies are used for calculation of average amplitude (AA) and weighted frequency (WF) that are the measures of code accuracy.

Normally 14 to 28 variables are selected for accuracy analysis. The most suitable factor for the definition of an acceptability criterion is the total average amplitude AA_{tot}. With reference to the accuracy of a given calculation, we can define the following acceptability criterion: $\text{AA}_{\text{tot}} < K$, where K is acceptability factor valid for the whole transient and is $K = 0.4$. Previous studies showed that

$\text{AA}_{\text{tot}} \leq 0.3$ characterize very good code predictions,

$0.3 < \text{AA}_{\text{tot}} \leq 0.5$ characterize good code predictions,

$0.5 < \text{AA}_{\text{tot}} \leq 0.7$ characterize poor code predictions,

$\text{AA}_{\text{tot}} > 0.7$ characterize very poor code predictions.

The experiment selected to represent quantitative assessment is the PHS-05 SBLOCA test.

In accordance with the methodology described above, the evaluation of code accuracy needs steps as given below, which are input to the FFTBM code and preliminary, qualitative evaluation of code predictions. Data needed are as follows.

Parameters characterizing the transient are selected from the results of calculations performed by the ATHLET, CATHARE, and RELAP5 codes and shown in Table 9.

Time windows, which are time intervals with characteristic phases of transients, are determined by the qualitative evaluation of the results of calculations performed by the codes. The time windows of the selected transient process are as follows:

(i) primary system subcooled: 0 to 350 s,

(ii) reactor model emptying: 350 to 4720 s,

(iii) core overheating: 4720 to 5000 s,

(iv) primary inventory restoration, overfeeding of pressuriser: 5000 to 6997 s.

Table 9: Selected parameters for comparison in PHS-05 test.

Figure no.	Label	Description
1	TE15	Heater rod surface temperature at core outlet
2	TE63	Coolant temperature at core inlet
3	TE22	Coolant temperature in upper plenum
4	TE41	Coolant temperature at SG inlet
5	TE42	Coolant temperature at SG outlet
6	PR21	Pressure in upper plenum
7	PR81	Pressure in the SG secondary side
8	LE11	Coolant collapsed level in the reactor model
9	LE71	Coolant level in the pressuriser
10	LE31	Coolant level in the hot leg loop seal, reactor side
11	LE45	Coolant level in the SG hot collector
12	LE46	Coolant level in the SG cold collector
13	LE52	Coolant level in the cold leg loop seal, reactor side
14	MA01	Integrated mass flow through the break

Table 10 contains the *Relevant Thermohydraulic Aspects* (*RTA*) and the system parameters characterizing the RTAs for the selected time windows.

(i) *RTA types*:

TSE: Time sequence event,

SVP: Single-value parameter,

IPA: Integrated parameters.

(ii) *Other columns of the table*:

exp: experimental values,

ATHLET: values calculated by ATHLET Mod2.0A,

CATHARE: values calculated by CATHARE2 V1.5,

RELAP: values calculated by RELAP5/mod3.3.

By the use of the data presented above, together with the time variations of parameters of the PHS-05 test, calculated by the ATHLET, CATHARE, and RELAP5 codes, the FFTBM code prepares input forms. The nodalisations applied to the system code calculations are as follows: Figure 24 for ATHLET, Figure 25 for CATHARE, and Figure 19 for RELAP5.

The time windows, which are shown in Table 10, with the relevant thermohydraulic aspects (RTA), are important features of the method. The qualification (Q) based on subjective judgement is as follows: E (excellent), R (reasonable), M (minimal), and U (unqualified). The overall trend of the transient is not influenced by M value (which occurs 2, 3, 4 cases for the codes ATHLET, CATHARE, and RELAP5,

Table 10: RTAs and parameters characterizing RTAs in PHS-05 test for selected time windows: 0 to 350 s, 350 to 4720 s, 4720 to 5000 s, 5000 to 6997 s.

RTAs	Parameters characterizing RTAs	Type	Exp. PHS-05	ATHLET		CATHARE		RELAP5	
				Calc.	Q	Calc.	Q	Calc.	Q
(1) *Primary system subcooled: 0 to 350 s*									
Pressuriser emptying	Pressuriser empty	TSE	350 s	205	M	125	M	222	M
Primary pressure behaviour	Primary pressure at 8.8 MPa	TSE	292 s	284	M	184	M	321	M
	Primary pressure at 350 s	SVP	6.61 MPa	6.36	R	7.42	R	7.57	R
Secondary pressure behaviour	Maximum secondary pressure	SVP	5.34 MPa	5.34	R	5.41	R	5.32	E
	Secondary pressure at 350 s	SVP	5.32 MPa	5.33	R	5.33	E	5.28	E
Pump behaviour	Coast-down begins	TSE	100 s		E	100	E	102	E
	Coast-down ends	TSE	248 s		R	236.7	R	250	E
Primary mass inventory	Average break flow	IPA	0.019 kg/s		M	0.028	M	0.023	R
(2) *Reactor model emptying (LE11): 350 to 4720 s*									
Primary pressure behaviour	Primary pressure at 1300 s	SVP	6.31 MPa	6.04	R	5.42	R	6.14	R
	Primary pressure at 4720 s	SVP	4.79 MPa	5.28	R	5.34	R	4.84	R
Secondary pressure behaviour	Secondary pressure at 4720 s	TSE	4.79 MPa	5.07	R	5.23	R	4.80	E
Loop seal behaviour	Cold leg loop seal clearing	TSE	3182 s	3203	E	2920	R	3155	E
	Hot leg loop seal clearing	TSE	1272 s	1192	R	1473	R	1204	R
Primary mass inventory	Average break flow	IPA	0.011 kg/s		R	0.016	R	0.011	E
Primary temperature behaviour	Coolant temperature at core outlet at 4720 s	SVP	534.7 K	540.5	R	541.2	R	534.9	E
(3) *Core overheating, rewetting (TE15): 4720 to 5000 s*									
Dryout occurrence	Onset of dryout	TSE	4720 s	4260	R	4905	R	5135	R
	Minimum level in reactor model at (s)	SVP	3.05 m 4760 s	3.26 m 4590 s	R	1.89 m 4908 s	R	2.59 m	R
	Time of maximum cladding temperature	STS	4768 s	4360	R	4930	R	5160	E
	Maximum cladding temperature	SVP	613 K	693	R	645.9	R	593	R
Rewetting	HPIS injection initiated	TSE	4751 s		R	4924	R	5150	R
	End of dryout	TSE	5000 s	4380	R	5000	E	5340	R
(4) *Primary inventory restoration (overfeeding of pressuriser): 5000 to 6997 s*									
Primary pressure behaviour	Pressure at 5000 s	SVP	4.61 MPa	5.37	R	4.46	R	4.78	R
Primary temperature behaviour	Coolant temperature at core outlet at 5000 s	SVP	532.1 K	541.3	E	530	E	534.2	E
	Coolant temperature at core inlet at 5000 s	SVP	506.0 K	511.1	R	508.9	E	518.7	R
Primary mass inventory	Average break flow	IPA	0.019 kg/s		R	0.019	E	0.014	R
	Total mass through the break	IPA	94.9 kg	99.0	R	110	R	84.8	R

Q: E = excellent, R = reasonable, M = minimal, U = unqualified.

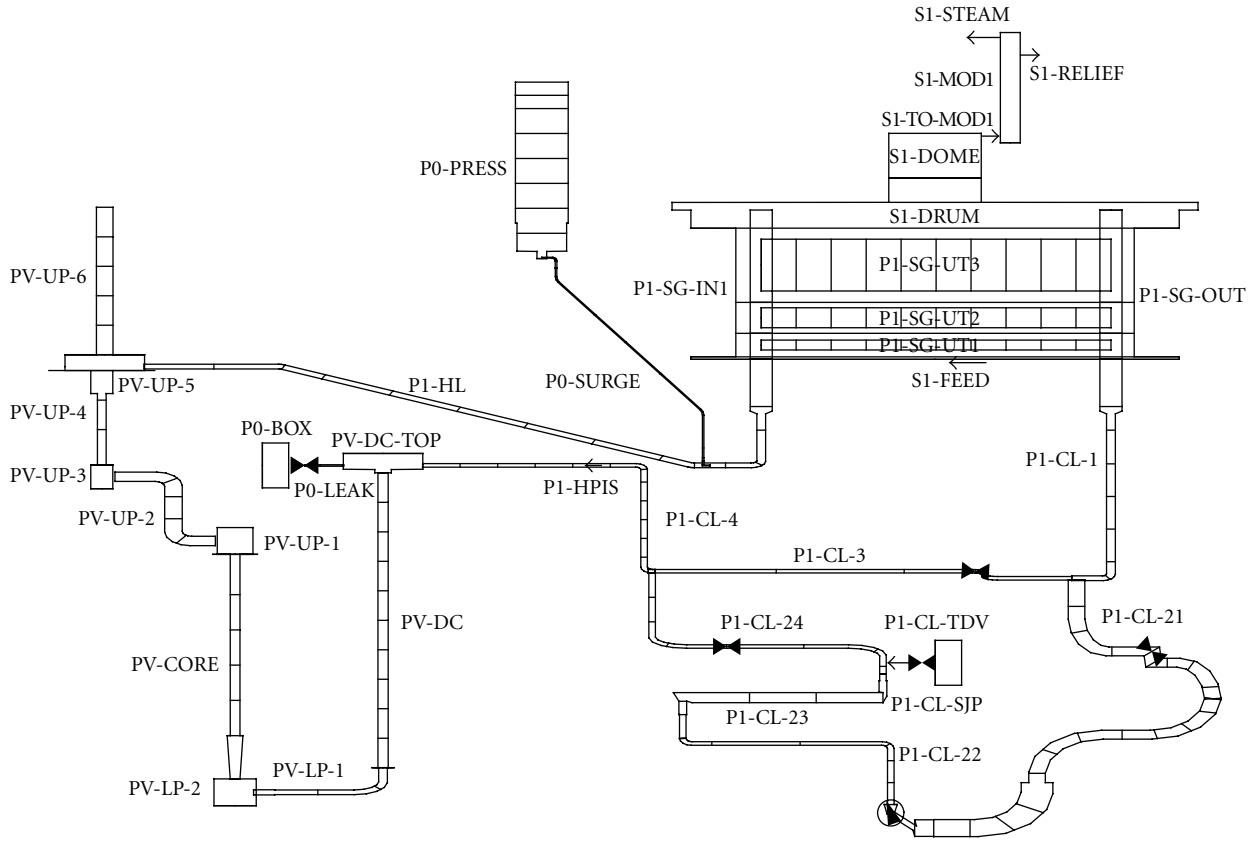

Figure 24: Nodalisation scheme for PMK-2 facility for the ATHLET 2.0A applied to PHS-05 experiment.

resp.). Therefore, the prediction is reasonable for all the three codes. It is because the assessment level M refers only to the "pressuriser empty" and "primary pressure at 8.8 Mpa" and the disagreement does not influence the transient process significantly in the late phase of transient process.

Results of quantitative assessment obtained by the FFTBM code are shown in Table 11. The qualification is "very good".

7. Conclusions

The integral-type facilities have great significance, because they can provide experimental information on transients and accidents anticipated to occur in nuclear power plants. In the 1980s the PMK-2 was the first and the only integral-type facility for VVERs. The PMK-2 was later followed by the PACTEL facility for VVER-440 (Finland 1990) and by the ISB and PSB facilities for VVER-1000 (Russia, 1992 and 1998, resp.).

The PMK-2 facility is a full-pressure thermohydraulic model of the primary and partly the secondary circuit of the Paks nuclear power plant of VVER-440/213 type. The overall scaling ratio is 1 : 2070, the elevation scale is 1 : 1, due to the importance of gravitational forces in natural circulation. The available power is 2 MW that allows establishing nominal conditions of the plant. All the VVER-specific design features are included in the design of the facility. The PMK-2 facility satisfies the criteria of the OECD/CSNI Facility and Test Qualification Matrix.

The first PMK-2 experimental data base covers the list of design basis accidents analysed in the Safety Analysis Report of the Paks NPP, as well as practically all test types described in the OECD-VVER cross-reference matrices. The data base consists of 55 tests which address and help to understand all the important aspects of plant system behaviour in accident conditions. Results are available in digital form at the OECD/NEA data bank.

The significance of the PMK-2 experiments mainly consists in creation of a unique, high-quality data base that can be used for code validation in the three main groups of the OECD-VVER code validation matrices, namely, large breaks, small/intermediate leaks, and plant transients. Phenomena simulated at the level required by the validation matrices are as follows: break flow, pressuriser thermohydraulics and surge line hydraulics, heat transfer in SG primary and secondary sides, single- and two-phase natural circulation, mixing and condensation during injection from ECCSs, loop seal behaviour in hot leg and clearance in cold leg, and core heat transfer in clearing DNB and dryout.

PMK-2 test results had continuously been applied to the validation of different versions of ATHLET, CATHARE, and RELAP5, primarily in international frameworks as: IAEA SPEs, US NRC CAMP programme, EU-PHARE, and EU-Framework programmes. Altogether, 28 PMK-2 tests were

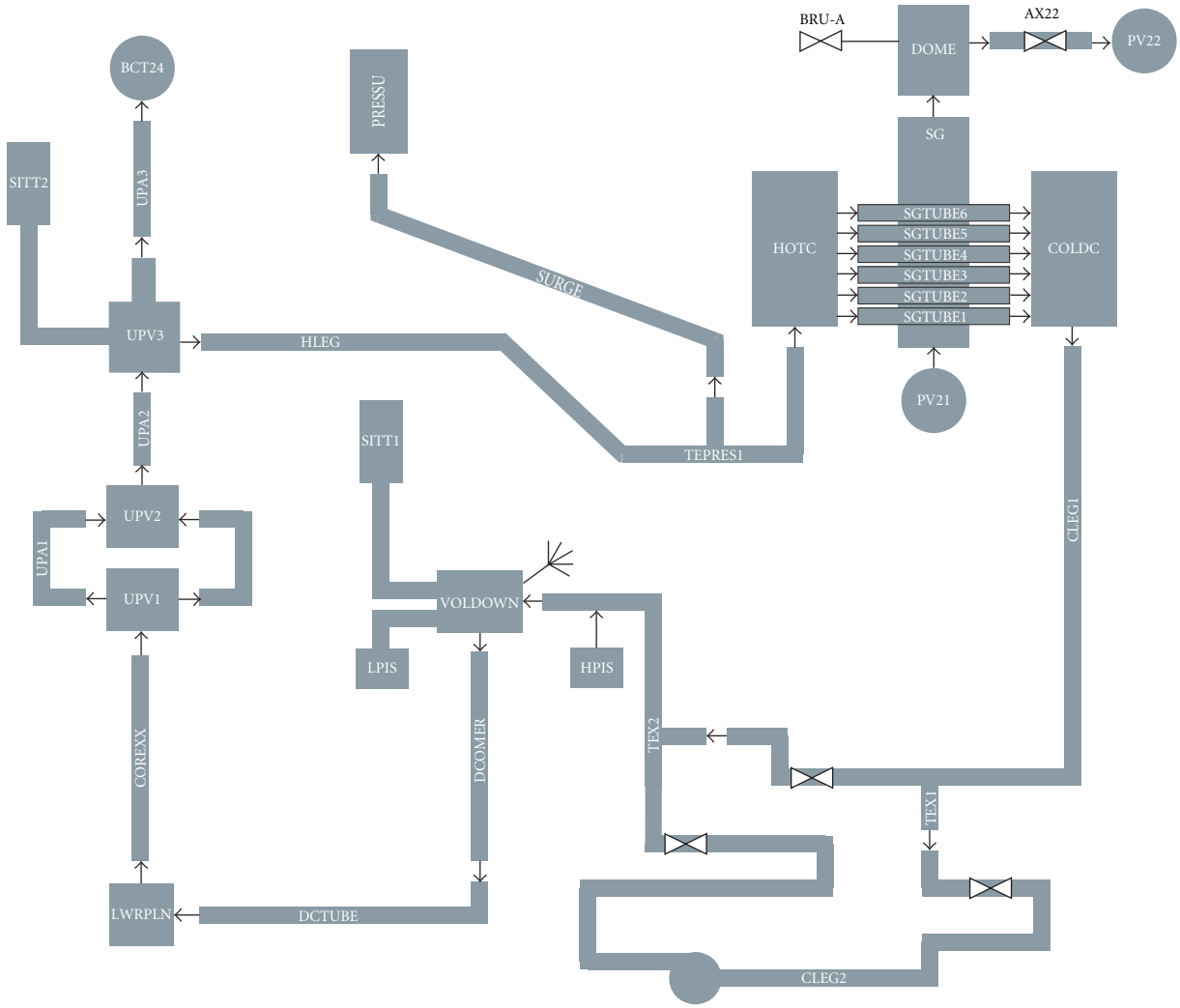

Figure 25: Nodalisation scheme for PMK-2 facility for CATHARE2 V1.5 applied to the PHS-05 experiment.

applied to different international code validations. During the 20-year period of PMK-2 projects a scientific school has been established with the participation of experts from 29 countries.

Since the codes applied for safety analysis in Hungary are ATHLET for LBLOCA, RELAP5 for SBLOCA, and transients, as well as CATHARE which is used as an independent tool to support regulatory authority, validation activities in the country are concentrated to these codes. Methodologies of code validation in the PMK-2 projects include both qualitative and quantitative assessments. The qualitative assessment is based on visual observation and engineering judgement of the agreement. The quantitative assessment results are obtained by the Fast Fourier Transform Based Method. Last version of the codes as ATHLET MOD2.0A, CATHARE2 V1.5, and RELAP5/mod3.3 have been validated, selecting representative tests.

Expertise gained in the PMK-2 projects was essential for the national reassessment of the safety and for the preparation of the Final Safety Analysis Report of the Paks nuclear power plant on a high level and played an important role in all the modifications performed in the plant, for example, for EOP development, increase of power, handling of primary to secondary leak, and others.

Table 11: The total values of AA and WF.

Code	AA_{tot}	WF_{tot}
ATHLET Mod2.0-A	0.25	0.03
CATHARE2 V1.5	0.22	0.03
RELAP5/mod3.3	0.23	0.04

The qualification is "very good".

The PMK-2 projects significantly supported the solution of specific problems encountered during the lifetime of the Paks NPP. They corroborated that there is no need to interconnect the hot and cold legs in the operating plant as it had been proposed by Gidropress; they verified the effectiveness of secondary and primary bleed and feed in a group of EOPS

like post LOCA cooldown and large break LOCA during cooldown; they continuously supported safety improvement activities in the field of SG tube and SG header ruptures and others.

Hopefully, the PMK-2 data base has significant value for the safety evaluation of all VVER-440/213 type reactors in operation and provides valuable source of scientific information to the nuclear community in the world.

Nomenclature

AA: Average amplitude (error function for FFTBM)
AEKI: Atomic Energy Research Institute
AM: Accident management
ATWS: Anticipated transient without scram
BF: Bleed and feed
BRU-A: Steam dump valve
CAMP: Code Assessment and Maintenance Program
CSNI: Committee for Safety of Nuclear Installation
DAS: Data acquisition system
DBA: Design basis accident
DE: Density
DNB: Departure from nucleate boiling
DNBR: Departure from nucleate boiling ratio
DP: Differential pressure
ECCS: Emergency core cooling system
EFW: Emergency feed water
EU: European Union
f_{max}: Maximum frequency component of the signal
f_s: Sampling frequency
FCUT: Cut-off frequency
FET: Valve closure in cold leg
FFT: Fast Fourier transform
FFTBM: Fast Fourier transform based method
FFIX: Minimum-maximum frequency
FL: Flow
GFK: Gas in upper plenum
PAV-GKK: Gas in SG collectors
HA: Hydroaccumulator
HPIS: High pressure injection system
HVM: Cold water injection into hot leg
IAEA: International Atomic Energy Agency
IBLOCA: Intermediate break LOCA
IMPAM: Improved accident management
ISP: International standard problem
KFKI: Central Research Institute for Physics
LBLOCA: Large break LOCA
LE: Level
LOCA: Loss of coolant accident
LOFA: Loss of flow accident
LPIS: Low-pressure injection system
LV: Local void
MCP: Main circulating pump
OM1-MSH: Main steam header—bleed and feed
MTA: Hungarian Academy of Sciences
NEA: Nuclear Energy Agency
NPP: Nuclear power plant
NVAL: Number of points in time domain
NVH: High-pressure water-cooled loop
OAH: National Atomic Energy Authority of Hungary
OECD: Organisation for Economic Cooperation and Development
OKKFT: National Middle-Term Safety Research and Development Program
OMFB: National Committee for Technological Development
PARt: Paks Nuclear Power Plant Company
PM: Pump rotor seizure
PMK: Paks model experiment
PR: Pressure
PRISE: Primary to secondary
RTA: Relevant thermohydraulic aspect
SAR: Safety analysis report
SBLOCA: Small break LOCA
SIT: Safety injection tank
SPE: Standard problem exercise
STB: Station blackout
T_d: Transient time duration of signal
TLF-BF: Total loss of feed water—bleed and feed
TLFW: Total loss of feed water
UP: Upper plenum
US NRC: United States Nuclear Regulatory Commission
WF: Weighted frequency (error function for FFTBM).

References

[1] L. Szabados, G. Ézsöl, L. Perneczky, and I. Tóth, "Final report on the PMK projects. Results of experiments performed in the PMK-2 facility for VVER safety studies," Tech. Rep. vol. I, Akadémiai Kiadó, Budapest, Hungary, 2007.

[2] L. Szabados, "Integral thermal-hydraulics tests for the safety evaluation of VVER-440/213 nuclear reactors and safety code validation," *Nuclear Technology*, vol. 145, no. 1, pp. 28–43, 2004.

[3] L. Szabados, G. Ézsöl, L. Perneczky et al., "Final report on the PMK projects. Major findings of PMK-2 test results and validation of thermohydraulic system codes for VVER safety studies," Tech. Rep. vol. 2, Akadémiai Kiadó, Budapest, Hungary, 2009.

[4] M. Ishii and I. Kataoka, "Scaling criteria for PWR's under single-phase and two-phase natural circulation," in *Proceedings of the Australian Neuroscience Society Annual Conference (ANS '82)*, Sydney, Australia, 1982.

[5] OECD/NEA, "Validation matrix for the assessment of thermal-hydraulic codes for VVER LOCA and transients. A report by the OECD support group on the VVER thermal-hydraulic code validation matrix," Nuclear Energy Agency, NEA/CSNI/R(2001)4, June 2001.

[6] "Simulation of a loss of coolant accident. Results of a standard problem exercise on the simulation of a LOCA," Tech. Rep. IAEA-TECDOC-425, Vienna, Austria, 1987.

[7] "Simulation of a loss of coolant accident with hydroaccumulator injection. Results of the second standard problem exercise on the simulation of a LOCA," Tech. Rep. IAEA-TECDOC-477, Vienna, Austria, 1988.

[8] "Simulation of a loss of coolant accident with a leak on the hot collector of the steam generator. Results of the third standard problem exercise," Tech. Rep. IAEA-TECDOC-586, Vienna, Austria, 1991.

[9] "Simulation of a loss of coolant accident without high pressure injection but with secondary side bleed and feed. Results of the fourth standard problem exercise," Tech. Rep. IAEA-TECDOC-848, Vienna, Austria, 1995.

[10] L. Perneczky, G. Baranyai, A. Guba, G. Ézsöl, and I. Tóth, "Description and RELAP5 assessment of the PMK-2 CAMP-CLB experiment. 2% cold leg break without HPIS with secondary bleed," Tech. Rep. NUREG/IA-0201, U.S. Nuclear Regulatory Commission, 2001.

[11] F. D'Auria, A. Eramo, M. Frogheri, and G. M. Galassi, "Accuracy quantification in SPE-1 to SPE-4 organized by IAEA," in *Proceedings of the 4th ASME/JSME International Conference on Nuclear Engineering (ICONE '96)*, vol. 3, pp. 461–469, March 1996.

[12] A. Prošek, F. D'Auria, and B. Mavko, "Review of quantitative accuracy assessments with fast Fourier transform based method (FFTBM)," *Nuclear Engineering and Design*, vol. 217, no. 1-2, pp. 179–206, 2002.

[13] B. Mavko, A. Prošek, and F. D'Auria, "Determination of code accuracy in predicting small-break loca experiment," *Nuclear Technology*, vol. 120, no. 1, pp. 1–18, 1997.

[14] A. Prošek and B. Mavko, "A tool for quantitative assessment of code calculations with an improved fast Fourier transform based method," *Electrotechnical Review*, vol. 70, no. 5, pp. 291–296, 2003.

[15] R. Bovalini, F. D'Auria, and M. Leonardi, "Qualification of the fast fourier transform based methodology for the quantification of thermohydraulic system code accuracy," DCMN—University of Pisa, NT194 (92), 1992.

[16] F. D'Auria, M. Leonardi, and R. Pochard, "Methodology for the evaluation of thermohydraulic codes accuracy," in *Proceedings of the International Conference on New Trends in Nuclear System Thermohydraulics*, pp. 467–477, Pisa, Italy, 1994.

[17] H. Holmström, "Quantification of code uncertainties," in *Proceedings of the Organisation for Economic Co-operation and Development/Committee on the Safety of Nuclear Installations (OECD/CSNI '92)*, Aix-en-Provence, France, 1992.

[18] R. R. Schultz, "Methodology for quantifying calculational capability of RELAP5/mod3 code for SBLOCAs, LBLOCAs and operational transients," in *Proceedings of the CAMP I Meeting*, Villigen, Switzerland, 1992.

Hindawi Publishing Corporation
Science and Technology of Nuclear Installations
Volume 2012, Article ID 173637, 19 pages
doi:10.1155/2012/173637

Research Article

SPES3 Facility RELAP5 Sensitivity Analyses on the Containment System for Design Review

Andrea Achilli,[1] Cinzia Congiu,[1] Roberta Ferri,[1] Fosco Bianchi,[2] Paride Meloni,[2] Davor Grgić,[3] and Milorad Dzodzo[4]

[1] *SIET S.p.A., UdP, Via Nino Bixio 27/c, 29121 Piacenza, Italy*
[2] *ENEA, UTFISSM, Via Martiri di Monte Sole 4, 40129 Bologna, Italy*
[3] *FER, University of Zagreb, Unska 3, 10000 Zagreb, Croatia*
[4] *Research and Technology Unit, Westinghouse Electric Company LLC, Cranberry Township, PA 16066, USA*

Correspondence should be addressed to Roberta Ferri, ferri@siet.it

Received 11 March 2011; Accepted 27 July 2011

Academic Editor: Alessandro Del Nevo

An Italian MSE R&D programme on Nuclear Fission is funding, through ENEA, the design and testing of SPES3 facility at SIET, for IRIS reactor simulation. IRIS is a modular, medium size, advanced, integral PWR, developed by an international consortium of utilities, industries, research centres and universities. SPES3 simulates the primary, secondary and containment systems of IRIS, with 1:100 volume scale, full elevation and prototypical thermal-hydraulic conditions. The RELAP5 code was extensively used in support to the design of the facility to identify criticalities and weak points in the reactor simulation. FER, at Zagreb University, performed the IRIS reactor analyses with the RELAP5 and GOTHIC coupled codes. The comparison between IRIS and SPES3 simulation results led to a simulation-design feedback process with step-by-step modifications of the facility design, up to the final configuration. For this, a series of sensitivity cases was run to investigate specific aspects affecting the trend of the main parameters of the plant, as the containment pressure and EHRS removed power, to limit fuel clad temperature excursions during accidental transients. This paper summarizes the sensitivity analyses on the containment system that allowed to review the SPES3 facility design and confirm its capability to appropriately simulate the IRIS plant.

1. Introduction

The IRIS reactor, with its integral design, is an advanced engineering solution of the latest LWR technology. Medium-sized, safe, modular, and economic, it provides a viable bridge to generation IV and satisfies the GNEP requirements for grid-appropriate NPPs [1–3].

In the frame of an R&D program on nuclear fission, funded by the Italian Ministry of Economic Development, ENEA, as member of the IRIS consortium, is supporting the design, construction, and testing of the SPES3 ITF at SIET laboratories [4–6].

The SPES3 design was carried out following the subsequent steps: (a) definition of a preliminary facility design, based on specified system geometry; (b) setup of the RELAP5 facility model and DBA simulation; (c) comparison of SPES3 and IRIS results against the same transient; (d) identification of the main differences and understanding of related reasons; (e) FSA application to selected thermo-fluid-dynamic parameters in order to assess and quantify the discrepancies; (f) updating of the SPES3 design to match the IRIS behaviour; (g) final result comparison; (h) final FSA application and assessment of acceptability criteria for considering SPES3 correctly simulating IRIS.

The above-mentioned process allowed to verify the SBLOCA PIRT objectives for the IRIS reactor, as defined by a group of international experts [7]. The Phenomena Identification and Ranking Table put in evidence the thermal-hydraulic phenomena playing an important role in operation of IRIS safety systems. Two figures of merit were considered fundamental for the accident sequence control: containment pressure and reactor vessel mass inventory. Sufficient water in the vessel allows to remove stored energy, and decay heat without fuel clad temperature excursions and adequate heat

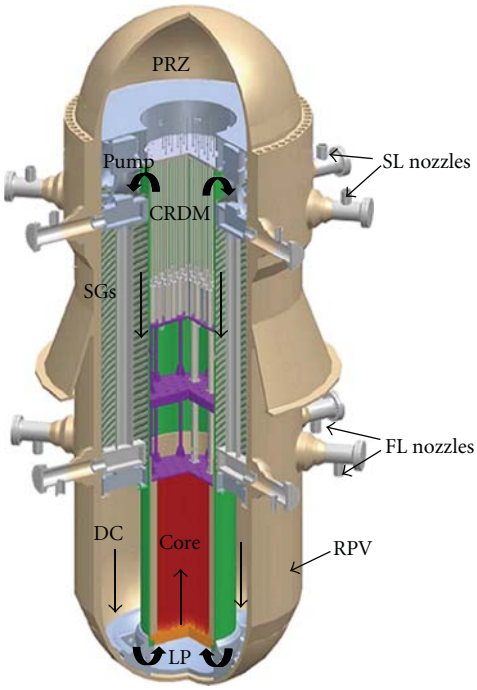

Figure 1: IRIS integral layout.

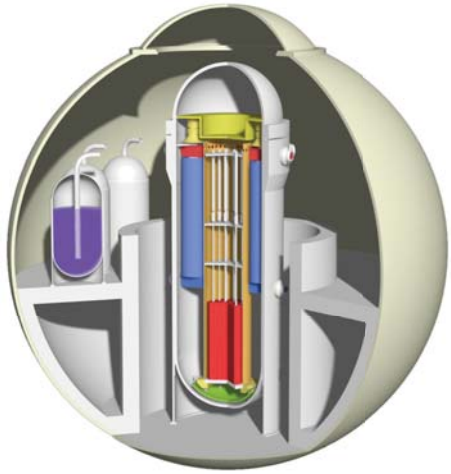

Figure 2: IRIS containment systems.

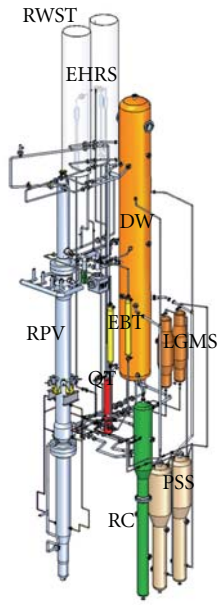

Figure 3: SPES3 facility layout.

rejection to the RWST prevents containment overpressurization and contributes to core cooling also thanks to dynamic coupling between the primary and containment systems.

The DBA simulation on the facility allowed to understand the transient plant behaviour and the mutual system interaction. The comparison with the IRIS results led to running many sensitivity cases that required the SPES3 design review for better matching the IRIS transients.

The SPES3 tests will provide a qualified data base for the assessment of codes to be used in the reactor safety analyses.

The SPES3 facility is under construction, based on the IRIS reactor design. The availability of such a complex plant opens the way to other possibilities of exploitation, and studies are foreseen for using it in a wider field of application for integral layout SMR simulation [8].

2. IRIS Plant and SPES3 Facility Layout and Nodalization

The IRIS pressure vessel and containment are shown in Figures 1 and 2, whereas the SPES3 facility is presented in Figure 3.

The SPES3 facility reproduces all parts and components of the IRIS plant with 1 : 100 volume scaling factor, 1 : 1 elevation scaling factor, and prototypical fluid and thermal-hydraulic conditions. The reactor vessel includes the internals, consisting of the electrically heated core simulator, the riser with control rod device mechanisms, the pressurizer, the pump suction plenum, the helical coil steam generators, the downcomer, and the lower plenum. Three SGs simulate the eight IRIS SGs. A pump, located outside of the RPV, for room reasons, and connected to it by pipes, simulates eight IRIS pumps. Two emergency boration tanks are simulated and connected to the DVI lines, devoted to direct injection of emergency fluid into the vessel. Three secondary loops simulate four IRIS loops. Each secondary loop is simulated up to the main isolation valves and includes the feed line, the SG, the steam line, and the emergency heat removal system with a vertical tube heat exchanger immersed in a refuelling water storage tank. The IRIS spherical containment compartments are simulated by tanks, connected to each other by pipes and to the RPV by break lines [4, 5]. They include dry-well and reactor cavity, representing the dry zone surrounding the RPV, respectively above and below the mid-deck plane; pressure suppression systems representing the wet zone around the lower part

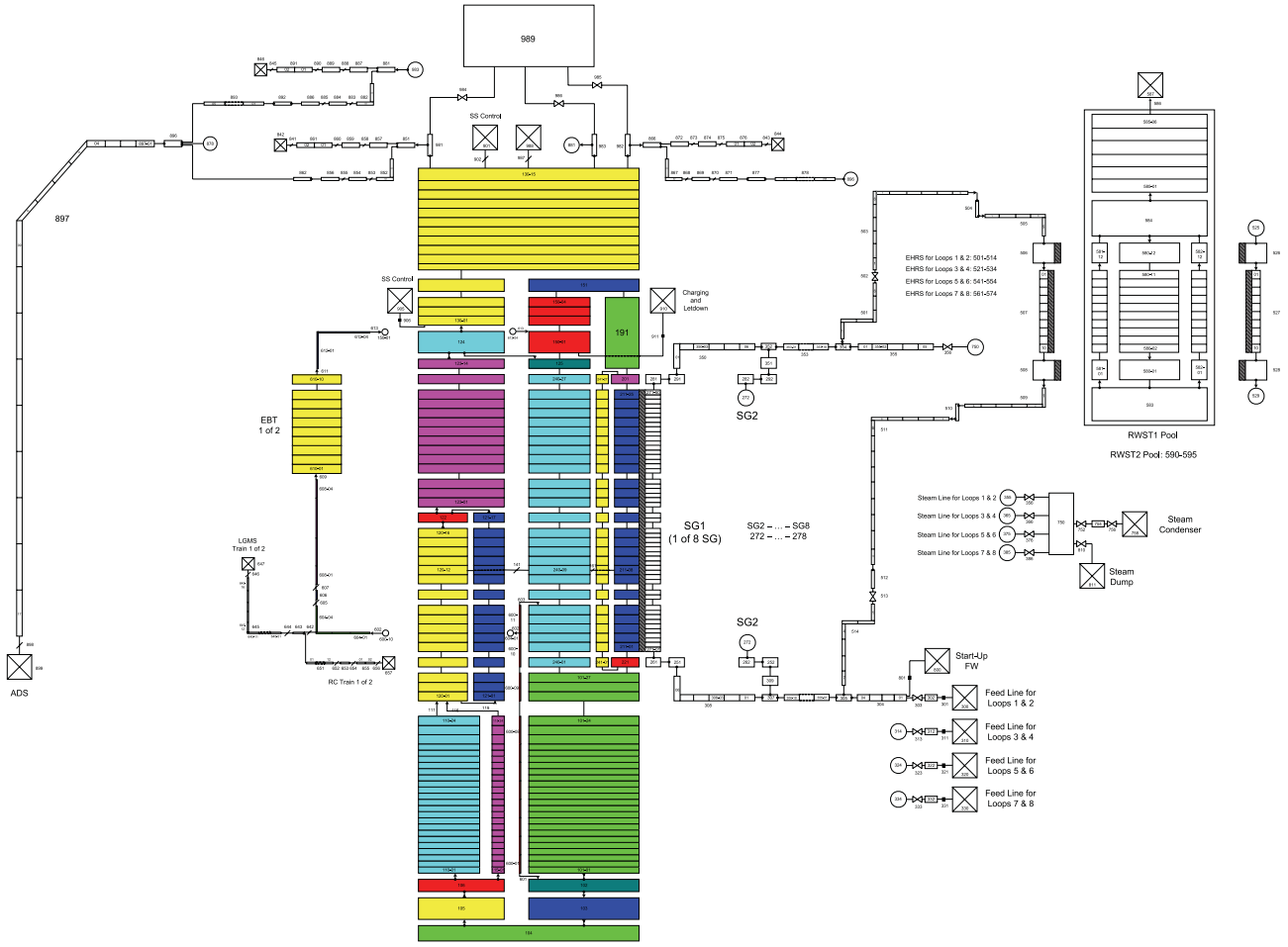

Figure 4: IRIS primary and secondary circuit nodalization for RELAP5 code.

of the RPV, suitable to dump pressure in case of containment pressurization; long-term gravity make-up systems representing the cold water reservoir to be poured into the RPV when depressurized. The two stages of the automatic depressurization system are simulated, connected to the pressurizer top, with stage I discharging into the quench tank and stage II directly connecting RPV and DW at high plant elevation.

The facility allows to test both LOCAs and secondary side breaks (DBA and BDBA) as well as to perform separate effect tests on particular components such as SG-EHRS thermally coupled to RWST.

The IRIS nodalization was developed in two parts: the primary and secondary circuits for the RELAP5 code and the containment system for the GOTHIC code (Figures 4 and 5). The RELAP5 nodalization includes 1845 volumes, and 1940 junctions, 1015 heat structures with 8600 mesh points, while the GOTHIC model includes 85 volumes, 28 junctions, and 57 heat structures.

The SPES3 nodalization was completely developed for the RELAP5 code (Figures 6, 7, and 8). It includes 1499 volumes, 1639 junctions, 1839 heat structures, and 19322 mesh points.

3. Design-Calculation Feedback Process for SPES3 Facility Final Design

The RELAP5 model for SPES3 was initially developed on the basis of the preliminary design of the facility, and the steady-state conditions are based on the actual IRIS nominal operation [9]. Five DBAs were simulated with particular attention to the occurring phenomena and sequence of events. In particular, three SB-LOCAs and two secondary side breaks were simulated, according to the specified test matrix [10].

Once the phenomena occurring in the DBAs were investigated, attention was focused on the most challenging transient scenario, the DVI line DEG break, for a direct comparison of the SPES3 and IRIS results.

WEC, in collaboration with the University of Pisa and Politecnico di Milano, developed the Fractional Scaling Analysis for IRIS and SPES3. The method, based on system and time sequence decomposition, allowed to identify the parameters mostly affecting the transient and to quantify the distortions between IRIS and SPES3 simulations introduced by such parameters (e.g., containment tank metal mass, heat transfer at core side wall, etc.).

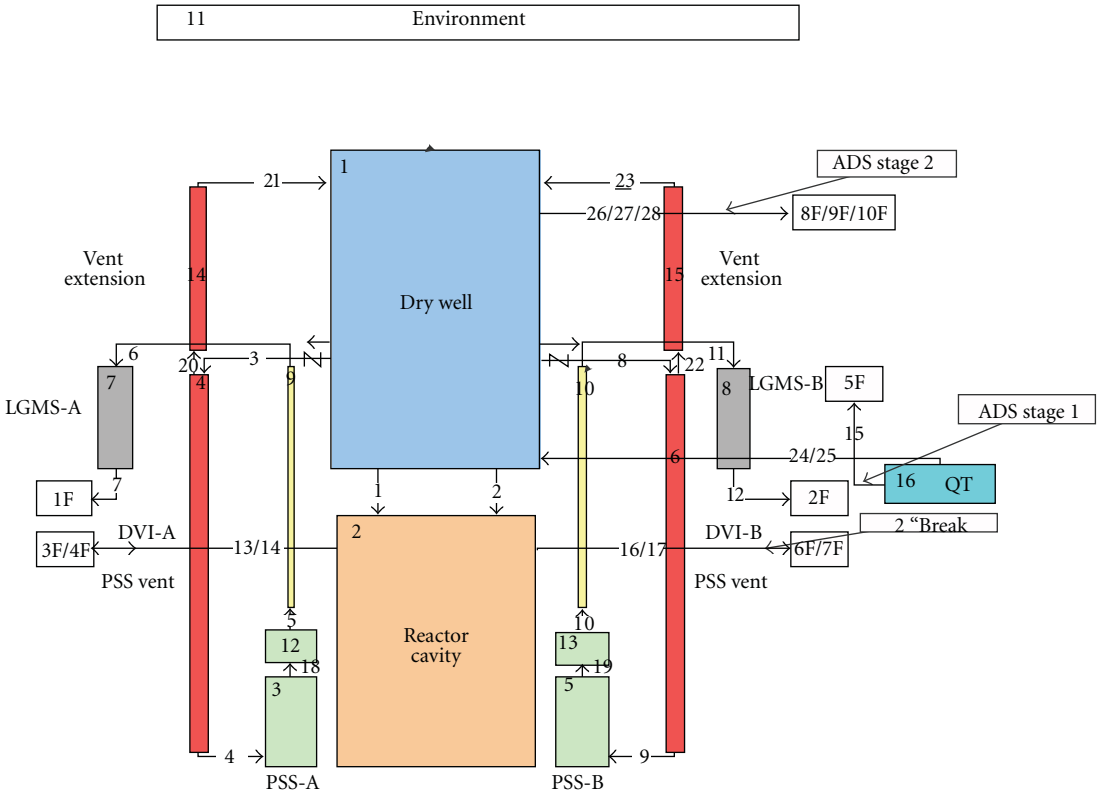

Figure 5: IRIS containment nodalization for GOTHIC code.

The first application of the DVI line DEG break evidenced important differences on containment pressure, especially in early phase of the accident, at pressure peak, and also on the long term.

The need of understanding the reasons and reducing discrepancies led to performing a series of sensitivity cases on SPES3 containment, making SPES3 response closer to reactor one, and finalizing the facility design [11, 12].

The main events, identified in the DVI line break transient, are listed below for better understanding all sensitivity analyses and the design-calculation feedback process. Approximate timing of events is reported too. The long-term phase of the transient was simulated to verify the safe, stable plant operation.

(i) The break opening (0 s) causes the RPV blowdown and depressurization, containment pressurization, steam dumping into PSS with air build-up at PSS top, and consequent pressurization;

(ii) the signal of high containment pressure (~30 s) triggers the reactor scram, the secondary loop isolation, and the actuation of two out of four EHRSs;

(iii) the signal of low PRZ water level (~120 s) triggers the pump coastdown, and the natural circulation in the core is guaranteed through the check valves, connecting riser and downcomer at one-third of the SG height;

(iv) the signal of low PRZ pressure (~200 s) actuates the remaining EHRS and triggers the ADS stage I, to help RPV depressurization, and the EBT intervention, to inject cold water into the primary circuit;

(v) the signal of low differential pressure between RPV and DW (~2250 s) triggers the LGMS injection into the DVI line and opens the valves connecting RC and DVI line to allow water reverse flow from the containment to the primary side;

(vi) when PSS pressurization is sufficiently high, cold water flows from PSS to DW (3500 s), increasing the RC flooding and allowing water to enter the RPV;

(vii) the signal of low LGMS mass (~25000 s) opens the ADS stage II with possible reverse steam flow from DW to RPV;

(viii) on the long term (simulation up to 100000 s), the plant is cooled by EHRSs that reject core decay heat to RWST.

The starting point for the sensitivity analyses was the comparison between cases SPES3-97 and IRIS-HT1 results, which showed qualitatively good agreement in occurring phenomena, but also quantitative discrepancies in containment pressure, affecting the sequence of events and transient evolution (Figure 9).

A series of parameters identifying and potentially affecting containment pressure is: (a) SPES3 containment overvolume of about 10% with respect to 1 : 100 scaled IRIS; (b) SPES3 containment metal mass greater than IRIS for mechanical resistance to the same design conditions; (c)

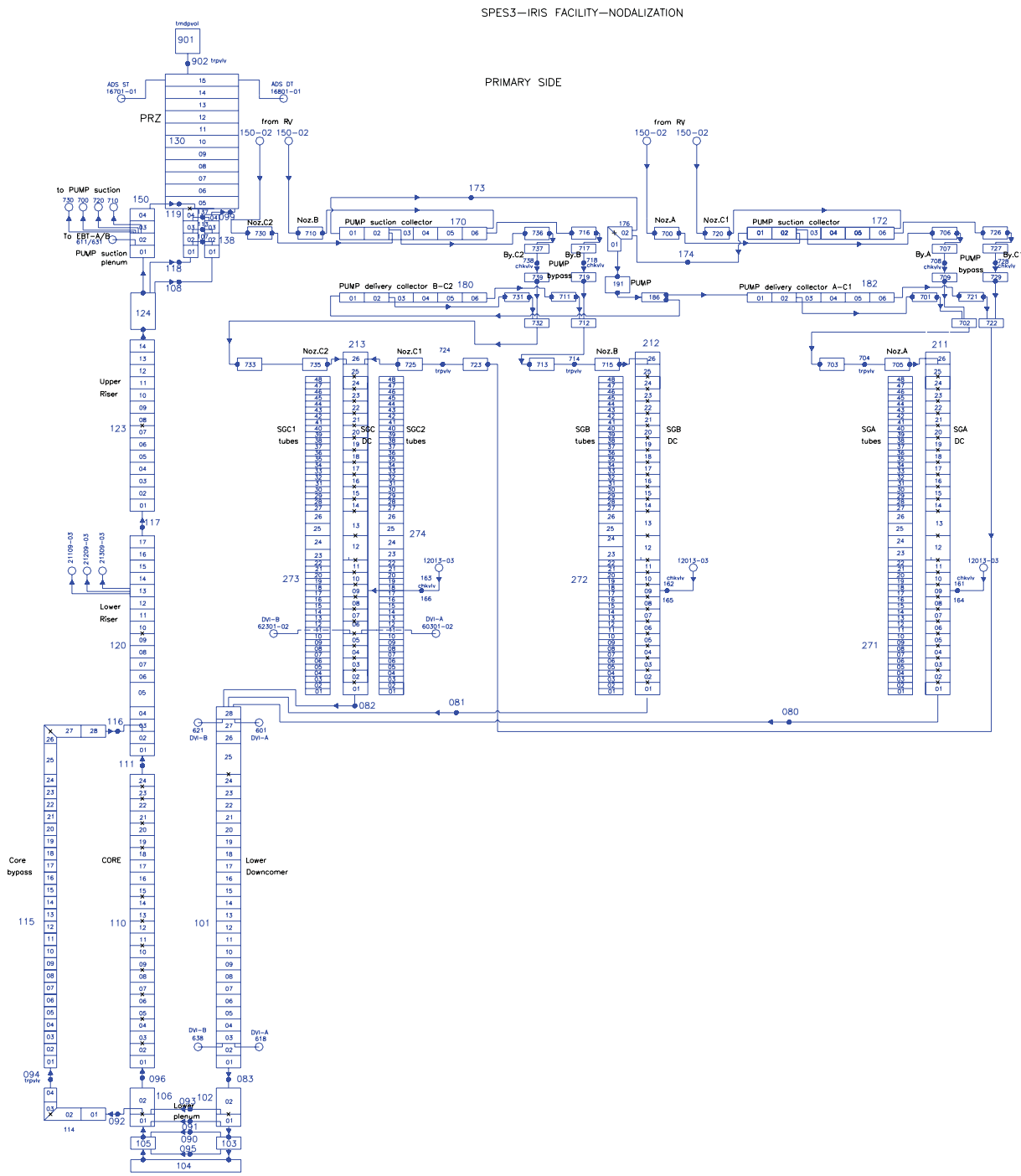

FIGURE 6: SPES3 primary circuit nodalization for RELAP5 code.

SPES3 component surface-to-volume ratio ten times greater than IRIS, due to volume scaling and component height conservation; (d) containment metal structure temperature; (e) containment piping pressure drops; (f) EHRS and RWST modelling and heat transfer coefficients.

A synthesis of the performed sensitivity cases on SPES3 is reported in Table 1, where they are grouped according to the investigated parameters. A synthesis of IRIS cases, utilised for the comparison, is reported in Table 2.

A reduction of DW volume, for correctly scaling IRIS (1 : 100), did not provide great improvements (a few percent) in the containment pressure response. An improvement was observed only in the long term related to lower heat losses to environment due to DW size reduction (Figure 10).

In order to compensate for the extra surface in SPES3, a thermal insulation of DW inner surface was tested with different thickness of Aluminium Silicate Rescor 902. As shown in Figure 11, the introduction of an increasing

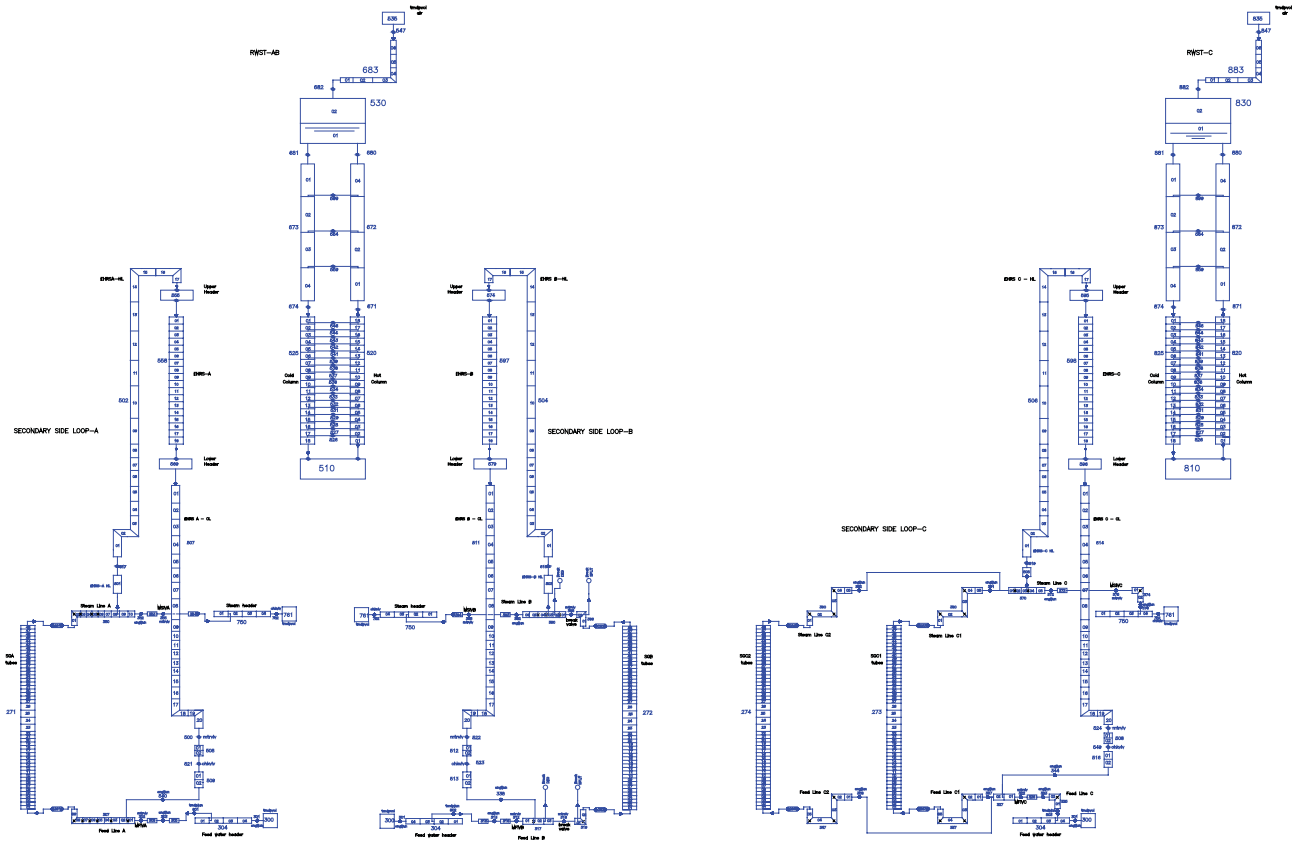

Figure 7: SPES3 secondary circuit and EHRS nodalization for RELAP5 code.

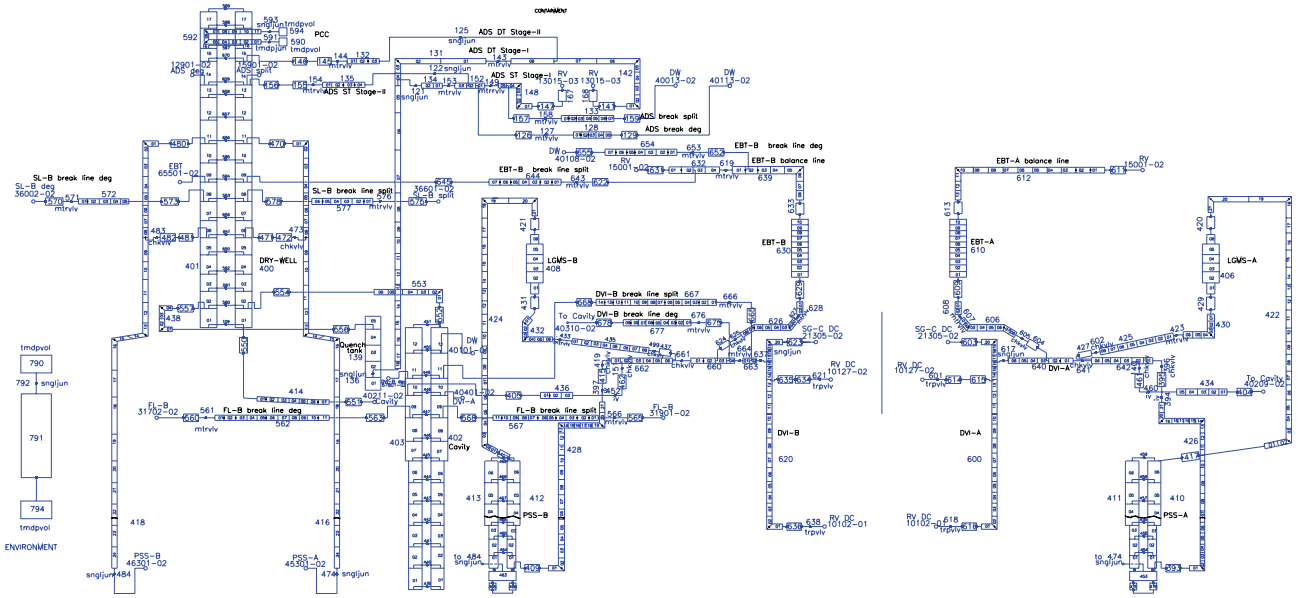

Figure 8: SPES3 containment nodalization for RELAP5 code.

thickness of thermal insulation increased pressure in the very short term, but the additional mass reduced the containment pressure peak. The result was that the DW insulation led to worse effects on pressure than with noninsulated DW, showing that masses have larger effects than surfaces.

The influence of DW heat structure mass on containment pressure response was investigated by reducing DW thickness by 40% (25 mm to 15 mm), approximately corresponding to a design pressure of 1.5 MPa, instead of the original 2 MPa. As shown in Figure 12, pressure increase in the early

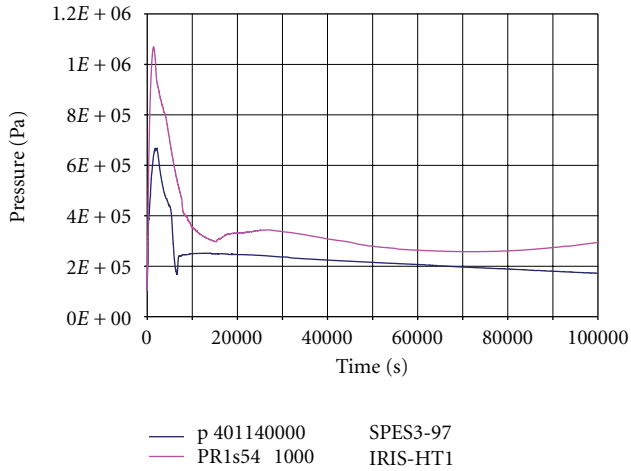

Figure 9: SPES3-97 and IRIS-HT1 DW pressure. Note: The IRIS Drywell Volume was subdivided in 4x4x4 sub-volumes in the three directions, marked 1s1, 1s2... up to 1s64. Pressure from a cell at the top of the model was used as reference.

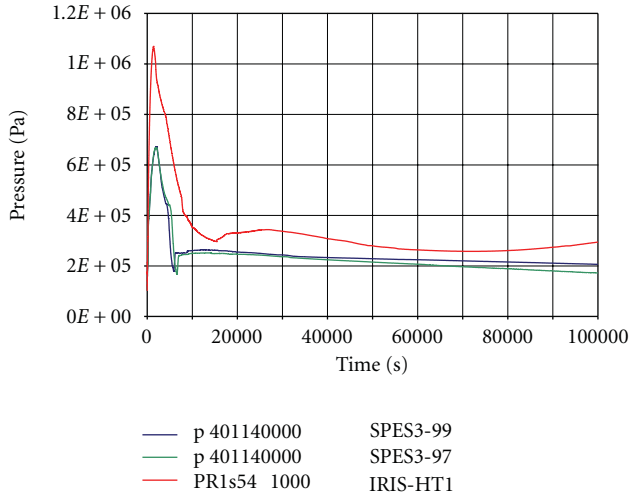

Figure 10: SPES3-97, 99 and IRIS-HT1 DW pressure.

phase of the transient was steeper and pressure peak higher. Containment pressure was still below the IRIS one, showing that such DW metal mass reduction was not enough to have the desired pressure response.

A further DW mass reduction was performed in a theoretical case, where concrete plus carbon steel IRIS DW equivalent mass was distributed on SPES3 DW surface, resulting in a thickness of 10 mm AISI 304. As shown in Figure 13, the further DW mass reduction allowed to get pressure values closer to IRIS both in the early phases of the transient and at the pressure peak, but still below IRIS pressure. That showed that other parameters affected the results.

An attempt to investigate how a greater DW volume reduction affects containment pressure was performed by scaling it 1 : 150 with respect to IRIS. Figure 14 shows a pressure gain only in the early phases of the transient

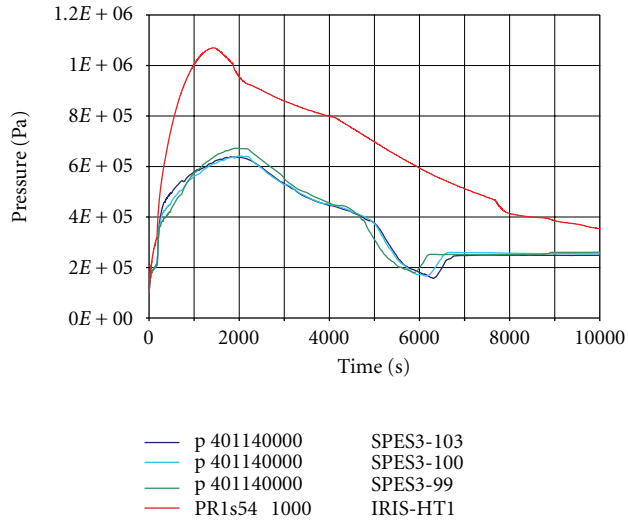

Figure 11: SPES3-99, 100, 103 and IRIS-HT1 DW pressure (short term).

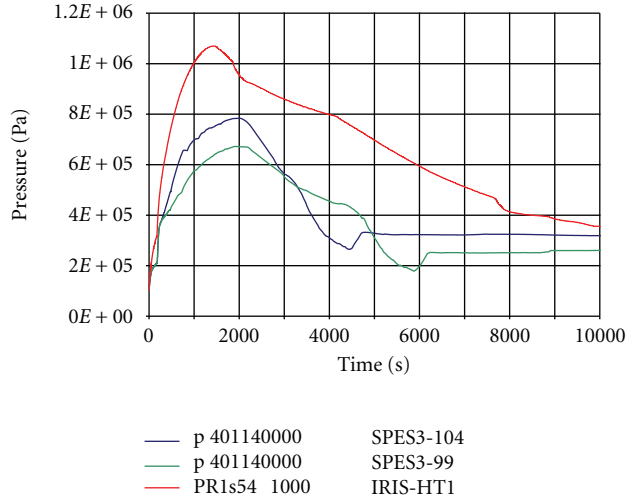

Figure 12: SPES3-99, 104 and IRIS-HT1 DW pressure (short term).

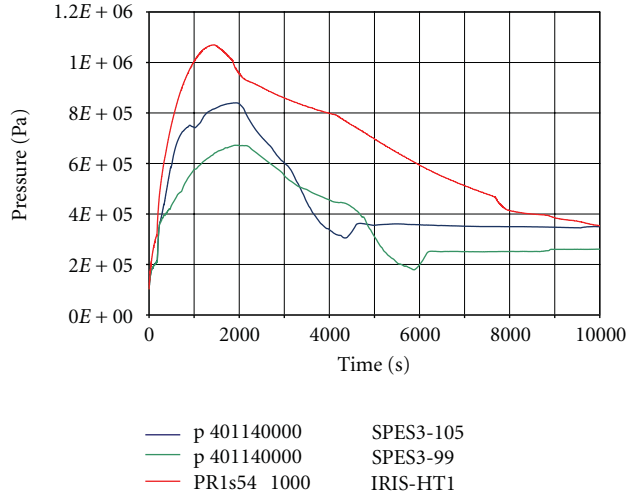

Figure 13: SPES3-99, 105 and IRIS-HT1 DW pressure (short term).

Table 1: Characteristics of the SPES3 cases.

SPES3 cases	Characteristicseffect for mass	Results
SPES3-97	Containment volume ~110% of IRIS volume; DW wall thickness 25 mm for 2 MPa design pressure; Containment metal wall initial temperature 48.9°C.	Starting point for sensitivity analyses.
	Sensitivity on the DW inner surface insulation	
SPES3-94	1 mm Teflon on the DW inner surface	Little improvements in containment pressure, limited to the early phase of transient.
SPES3-100	DW volume correctly scaled on IRIS volume. 1.5 mm Rescor 902 Aluminium Silicate layer on the DW inner surface	Little improvements in containment pressure. Negative effect for mass addition.
SPES3-103	DW volume correctly scaled on IRIS volume. 3 mm Rescor 902 Aluminium Silicate layer on DW inner surface	Little improvements in containment pressure. Negative effect for mass addition.
	Sensitivity on the containment volume	
SPES3-99	DW volume correctly scaled on IRIS volume	Little improvements in containment pressure.
SPES3-106	DW volume scaled 1 : 150 on IRIS volume	Little improvements in containment pressure, limited to the early phase of transient. Modelling due to a component simulation with a different scaling factor.
SPES3-107	Equivalent to SPES3-99 with corrected minor input mistakes	
	Sensitivity on the containment metal structure	
SPES3-104	DW wall thickness 15 mm for 1.5 MPa design pressure	Improvement of containment pressure, but not sufficient.
SPES3-105	DW wall thickness 10 mm (equivalent to 1 : 100 IRIS DW mass distributed on SPES3 surface)	Further improvement of containment pressure, but not sufficient.
SPES3-108	DW heat structure directly scaled 1 : 100 in terms of mass and surface (a one-hundredth slice of IRIS structure attributed to SPES3). DW wall material as in IRIS	Improvement of containment pressure response in early phase of the transient, due to DW surface reduction impact. No improvement in later phases, due to other SPES3 containment structures, not simulated in IRIS.
SPES3-111	DW heat structure initial temperature from 48.9°C to 84°C	Heat structure preheating compensates for the extra mass. Containment pressure response not sufficiently improved as other containment heat structures are non-preheated.
SPES3-112	PSS wall eliminated All containment tanks volume resized to scale IRIS 1 : 100. Thickness reduced to resist 1.5 MPa design pressure. Air space metal structure initial temperature 84°C.	Containment pressure response improved.
SPES3-115	PSS main vent pipe no additional restriction. LGMS to DVI line calibrated orifice from 4 mm to 3.2 mm. ADS stage I ST calibrated orifice from 7.019 mm to 5.637 mm. ADS stage I DT calibrated orifice from 9.927 mm to 7.973 mm. EHRS-A and B CL calibrated orifice from 6 mm to 5 mm. EHRS-C CL calibrated orifice from 12 mm to 8.5 mm	Containment pressure similar in SPES3 and IRIS. ADS stage I mass flow correctly reproducing IRIS. LGMS to DVI line and EHRS CL mass flow not correctly reproduced.

Table 1: Continued.

SPES3 cases	Characteristicseffect for mass	Results
SPES3-119	Containment volume scaled 1 : 100 on IRIS. DW heat structure directly scaled 1 : 100 in terms of mass and surface. PSS, LGMS, RC thickness 1 mm (to get closer to IRIS nonsimulated structure) LGMS to DVI line calibrated orifice from 2.3 mm to 2.5 mm. PSS vent pipe extension orifice from 5.2 to 7.3 mm. RC to DVI line additional calibrated orifice of 1 mm (original valve D = 10.7 mm) EHRS-C CL calibrated orifice from 6.7 mm to 7 mm	Containment pressure very similar in SPES3 and IRIS.Great importance of correct heat structure simulation.
SPES3-122	As SPES3-120. Containment heat structure initial temperature 48.9°C.	For comparison with SPES3-120 to quantify the heat structure preheating influence.
SPES3-132	As SPES3-130. EHRS-A and B tube 2% additional surface thermally insulated with Teflon (originally 0.6 tubes out of 3 insulated to scale 1 : 100 240 IRIS tubes). EHRS-C 0.2 tubes out of 5 insulated to scale 1 : 100 480 IRIS tubes. Additional 2% tube surface thermally insulated with Teflon	EHRS tube heat transfer surface reduced to correctly simulate IRIS surface.
	Sensitivity on the containment piping pressure drops	
SPES3-109	PSS main vent pipe resizing from 2.5″ to 2″ Sch. 40. PSS vent pipe extension resizing from 3/4″ to 1/2″ Sch. 40	PSS to DW mass flow closer to IRIS one.
SPES3-110	PSS main vent pipe additional restriction at the check valve (D_{orifice} 14.19 mm)	Only early steep but limited containment pressure increase.
SPES3-118	Containment volume scaled 1 : 100 on IRIS. LGMS to DVI line calibrated orifice from 3.2 mm to 2.3 mm. EHRS-C CL calibrated orifice from 8.5 mm to 6.5 mm. PSS vent pipe extension additional restriction (D_{orifice} 5.2 mm). Containment heat structure initial temperature 48.9°C	Attempt to match IRIS injection mass flows.
SPES3-120	Containment volume scaled 1 : 100 on IRIS. Thickness to resist 1.5 MPa design pressure. Air space metal structure initial temperature 84°C. QT initial temperature 48.9°C. LGMS to DVI line calibrated orifice from 2.3 mm to 2.5 mm	IRIS injection mass flow reproduced, but different pressure drops in the pipes.
SPES3-124	PSS main vent pipe resizing from 2″ to 2.5″ Sch. 40 PSS vent pipe extension resizing from 1/2″ to 1″ Sch. 40 LGMS to DVI line calibrated orifice from 2.5 mm to 3.6 mm. PSS vent pipe extension orifice from 7.3 to 19 mm. PSS vent pipe extension connection to DW elevation decrease of 1.5 m to match IRIS. PSS sparger elevation decrease of 0.25 m to match IRIS. PSS bottom modelled with a branch. Containment air space metal structure initial temperature 84°C, water space 48.9°C	Mass flow determined by actual piping pressure drops as in IRIS.Containment pressure response qualitatively and quantitatively close to IRIS. The PSS bottom modelling did not affect the PSS vent pipe emptying mode.

Table 1: Continued.

SPES3 cases	Characteristicseffect for mass	Results
SPES3-127	As SPES3-124 PSS bottom modelled with three branches.	The PSS bottom modelling did not strongly affect the PSS vent pipe emptying mode.
SPES3-130	As SPES3-127 RWST top pipe introduction for connection to atmosphere.	Reduced loss of mass at RWST top due to dry air and water contact.
SPES3-135	AS SPES3-132 Completely reviewed the EHRS circuits and RWST model: EHRS-A and B tube 4% surface thermally insulated with Teflon other than the originally insulated 0.6 tubes. EHRS-C 4% surface thermally insulated other than the originally insulated 0.2 tubes. EHRS-A and B HL resized from 2″ to 1.25″ Sch. 80. EHRS-A and B CL resized from 1.25″ to 1.5″ Sch. 80. EHRS-C HL resized from 2.5″ to 2″Sch. 80. EHRS-C CL resized from 1.5″to 3″ Sch. 80. HL-A and B additional orifice $D = 17$ mm. HL-C additional orifice $D = 24$ mm. CL-A and B orifice resized from 5 mm to 5.9 mm. CL-C orifice resized from 7 mm to 8.3 mm. EHRS tube heat structure fouling factor set to 2.9 left and 2.77 right (original values 2.725 left, 3.54284 right) [13]. RWST-AB and C rising slice area resized from 0.491 m^2 to 0.119167 m^2; recirculation slice resized from 1.217 m^2 to 1.601169 m^2 [13]. RWST-AB and C slice side junction area from 0.151 m^2 to 0.135 m^2 [13].	The complete revision of the EHRS piping and heat exchanger parameters led to matching transferred energy.
SPES3-146	As SPES3-135. PSS vent pipe extension orifice from 19 mm to 17.5 mm. SG tube inlet orifice from 12.5 mm to 11.7 mm	Good similarity between SPES3 and IRIS BASE CASE for FSA final application.

Table 2: Characteristics of the IRIS cases.

IRIS cases	Characteristics	Results
IRIS-HT1	Containment heat structures simulated only for the DW.	Starting point for comparison with SPES3.
IRIS-HT5g	Heat structures added to all containment compartments and secondary sidepiping. PSS main vent pipe connection to DW rise of 4 m. PSS sparger set at 0.75 m from PSS bottom. RWST remodelled with parallel slice approach.	Similar containment pressure response with SPES3.
IRIS-HT6_rwstc	SG tubes inner layer removed which simulated the Fouling. ADS stage II actuation signal corrected to intervene on low LGMS mass. RWST remodelling according to PERSEO area ratio and HTC calibration on experimental data. EHRS heat transfer parameters set as in SPES3 (by multiplier fouling factors) [12, 13]. RWST top pipe introduction for connection to atmosphere. Correction of energy transfer parameters at the GOTHIC and RELAP5 code couplings.	Better matching of EHRS long-term energy transfer to RWST.
IRIS-HT6_rwstc1a	Corrected elevation difference between the RELAP5 and GOTHIC parts of the model: the ADS stage I vent pipe end should be 0.5 m from QT bottom (it was connected to QT top); LGMS tanks rise of 0.75 m.	Results very similar to IRIS-HT6_rwstc BASE CASE for FSA final application.

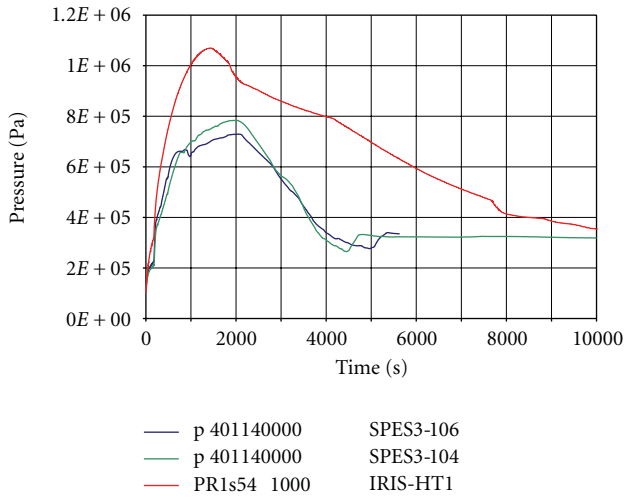

Figure 14: SPES3-104, 106 and IRIS-HT1 DW pressure (short term).

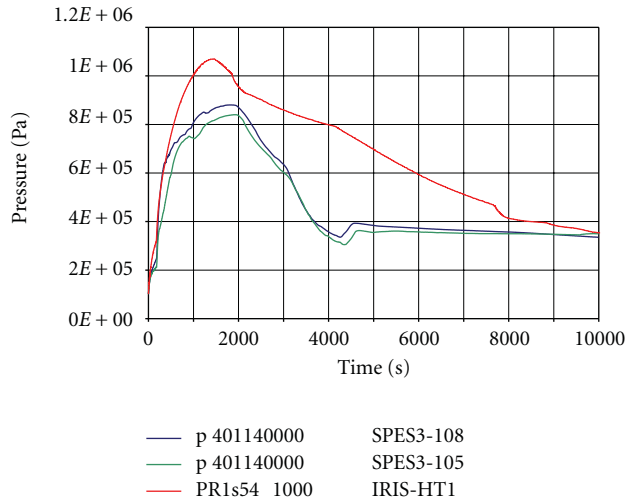

Figure 15: SPES3-105, 108 and IRIS-HT1 DW pressure (short term).

with a lower peak value. No improvement was obtained by overreducing the DW volume with a scaling factor different from 1 : 100.

A theoretical case, where IRIS DW structures were directly scaled 1 : 100 in mass and surface, was investigated. A one-hundredth vertical slice of IRIS DW structures was attributed to SPES3 DW, maintaining the same thickness and material composition. Figure 15 compares two cases with equivalent heat structure masses, but different surfaces and material properties. Pressure increase was similar in IRIS and SPES3, in the early phase of the transient, when surface has a greater impact, but later energy transfer to heat structures prevailed and SPES3 pressure did not increase as expected, with all SPES3 containment structures being completely simulated against the only IRIS DW structure simulation. Moreover, gas space volume at the PSS and LGMS top was about 14% higher in SPES3 than IRIS, so limiting the containment pressure peak. Containment pressure trend showed also differences in the depressurization phase, related to steam condensation in RC and DW due to broken loop LGMS water entering the RC (~2000 s in SPES3) through the DVI break line, containment side, and PSS injection into the DW (~3000 s in SPES3). Injection mass flows are shown in Figures 16 and 17, and they depended on different pipe pressure drops and containment pressurization.

An attempt to make closer SPES3 and IRIS PSS to DW injection mass flows was performed: size of PSS main vent pipe and extension was decreased and the results compared with a base case (SPES3-107) equivalent to SPES-99, where minor input mistakes were corrected. PSS injection results were effectively closer to IRIS with consequent slower containment depressurization (Figures 18 and 19).

The attempt was performed to see how a restriction at the PSS main vent pipe check valve affects the steam-air transfer

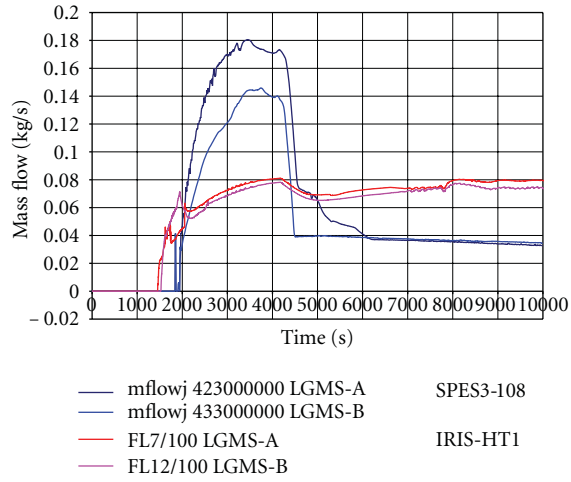

Figure 16: SPES3-108 and IRIS-HT1 LGMS to DVI injection mass flow (short term).

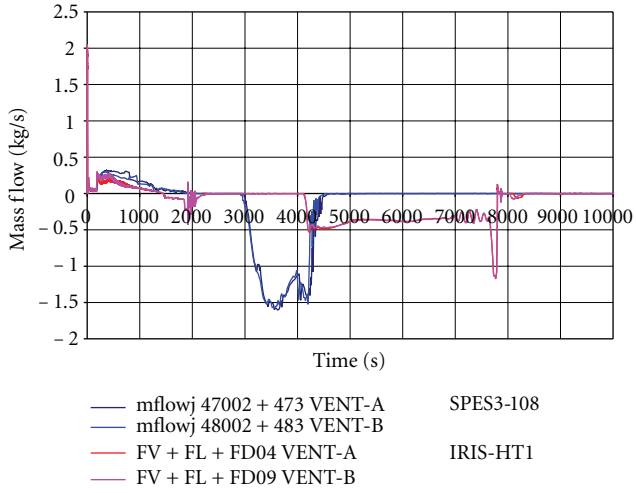

Figure 17: SPES3-108 and IRIS-HT1 PSS to DW injection mass flow (short term). Note: for IRIS, the total mass flow (FL + FV + FD) is obtained by the sum of phasic mass flows (liquid, gas and droplets.

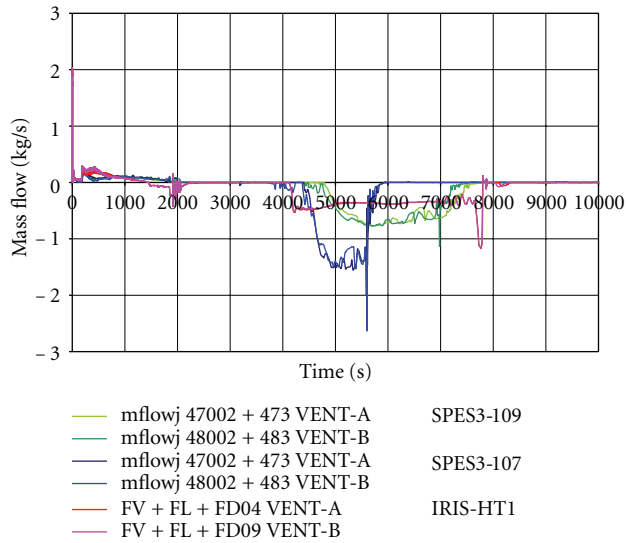

Figure 18: SPES3-109, 107 and IRIS-HT1 PSS to DW injection mass flow (short term).

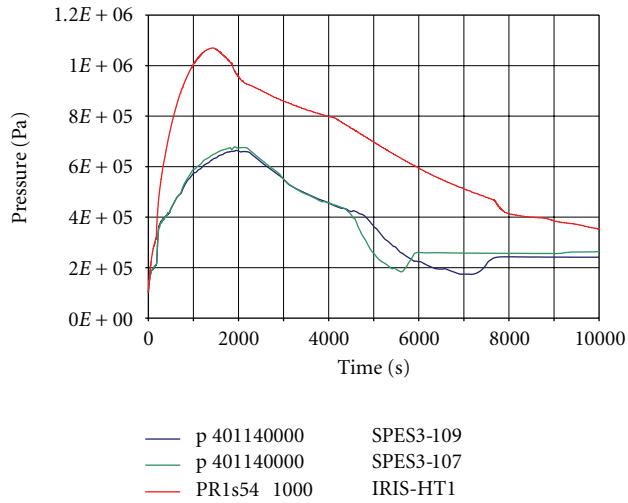

Figure 19: SPES3-109, 107 and IRIS-HT1 DW pressure (short term).

from DW to PSS and eventually rise DW pressure. The result was a steep but limited pressure increase (Figure 20).

The impossibility of reducing the DW thickness under 15 mm, to resist 1.5 MPa design pressure, led necessarily to an excess of mass with respect to IRIS 1 : 100 scaled mass. In SPES3-105 case, the IRIS scaled mass was distributed on the SPES3 DW surface obtaining an equivalent thickness of 10 mm. The possibility of compensating for 5 mm extra mass, by preheating the DW heat structures, was investigated. The preheating temperature of 84°C was estimated by an energy balance between the cases with 10 mm and 15 mm thickness from the specified initial temperature of 48.9°C and regime temperature of 172°C after the heat-up transient. Figure 21 compares the cases with 15 mm (SPES3-104), 10 mm (SPES3-105), and 15 mm (SPES3-111) pre-heated DW thickness. The 10 mm and 15 mm pre-heated DWs are equivalent showing that heat structure preheating compensates for the excess of mass in SPES3. Only DW preheating is not enough to have the same IRIS pressure response.

The comparison between the cases with and without PSS heat structures allowed to quantify the phenomenon of air cooling when steam-air mixture flowed from DW to PSS. The run was interrupted by a nonconvergence error on noncondensable gas properties in the PSS, but available results allowed to evaluate the pressure gain, with respect to the theoretical case with 1 : 100 IRIS DW volume and surface scaled structures, as shown in Figure 22.

In order to reduce distortions on pressure as much as possible, related to scaling mismatching, all the SPES3 containment compartments were scaled 1 : 100 on IRIS volumes and all thicknesses were sized to resist 1.5 MPa

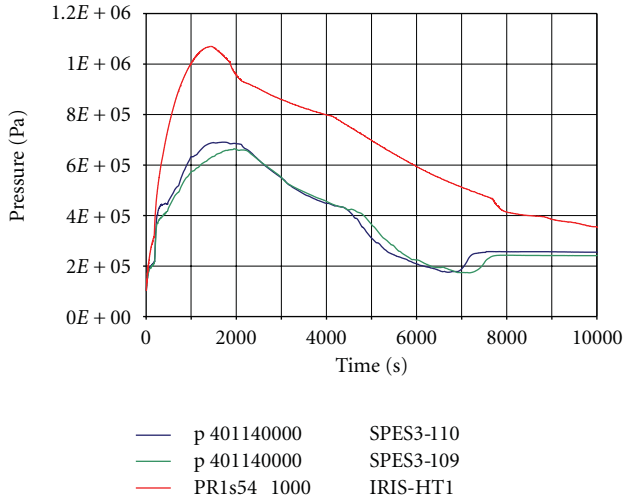

Figure 20: SPES3-110, 109 and IRIS-HT1 DW pressure (short term).

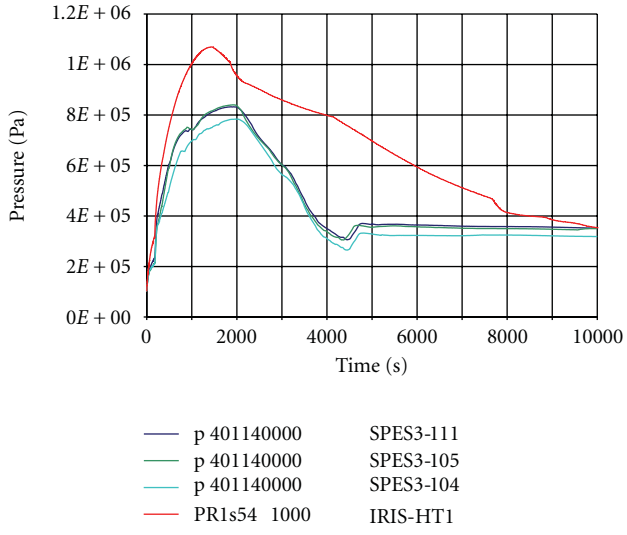

Figure 21: SPES3-111, 105, 104 and IRIS-HT1 DW pressure (short term).

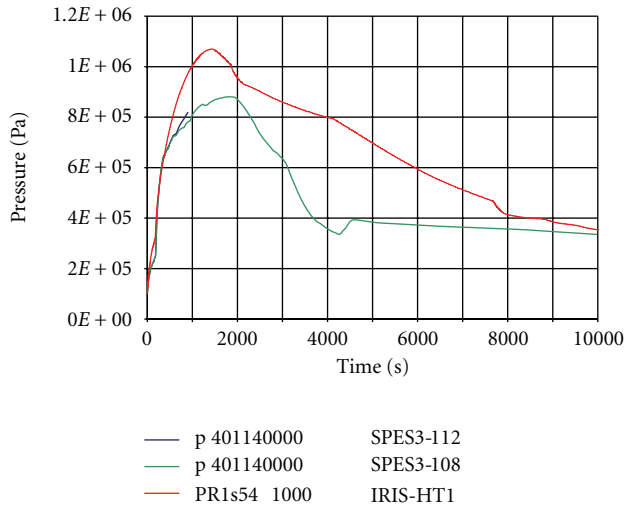

Figure 22: SPES3-112, 108 and IRIS-HT1 DW pressure (short term).

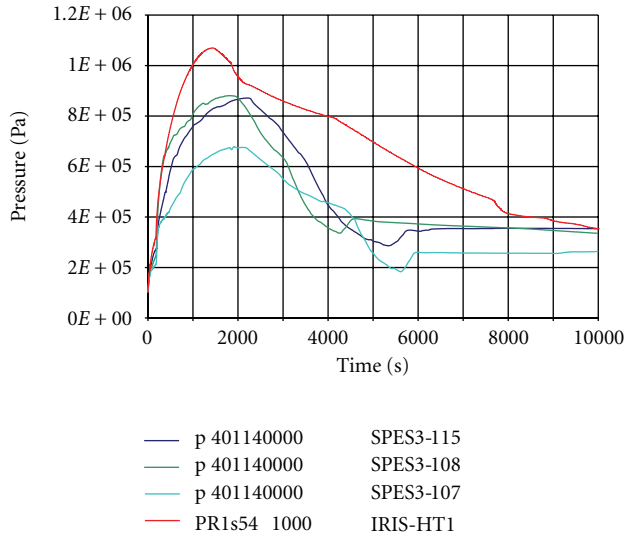

Figure 23: SPES3-115, 108, 107 and IRIS-HT1 DW pressure (short term).

pressure, so limiting the thermal inertia of the metal walls. In particular, the containment air zone heat structures were preheated at 84°C, while those in the liquid zone were kept at 48.9°C. Moreover, the calibrated orifices on the LGMS to DVI lines, the ADS stage I, and EHRS-C CL were resized to match IRIS mass flows. Figure 23 shows that, notwithstanding a slower DW pressure increase, that case is similar to the case with IRIS DW scaled 1 : 100 in mass and surface (SPES3-108), confirming that containment volume resizing and heat structure preheating are good solutions toward IRIS containment pressure response. Orifice resizing was not enough to match the IRIS LGMS to DVI and EHRS-C CL mass flows, while it was correct to scale ADS stage I mass flow (Figure 24), even if a stronger water entrainment was evidenced in IRIS at the second flow peak.

Further calibrations of the injection line orifices were performed that evidenced contact condensation stronger in SPES3 (RELAP5) than in IRIS (GOTHIC).

A case was run where IRIS containment heat structures were reproduced on SPES3 with the DW 1 : 100 scaled in mass and surface and all other tanks with 1 mm thick walls to avoid code convergence errors in case of complete heat structure removal. Figure 25 shows very similar SPES3 and IRIS containment pressure rising phase and a pressure peak only 0.1 MPa lower in SPES3 than in IRIS, demonstrating the importance of a correct simulation of the heat structures.

The containment piping orifice, sized to match IRIS injection mass flows, allowed a direct comparison between the plants, but it did not meet the piping pressure drop scaling criteria. It allowed to understand two important

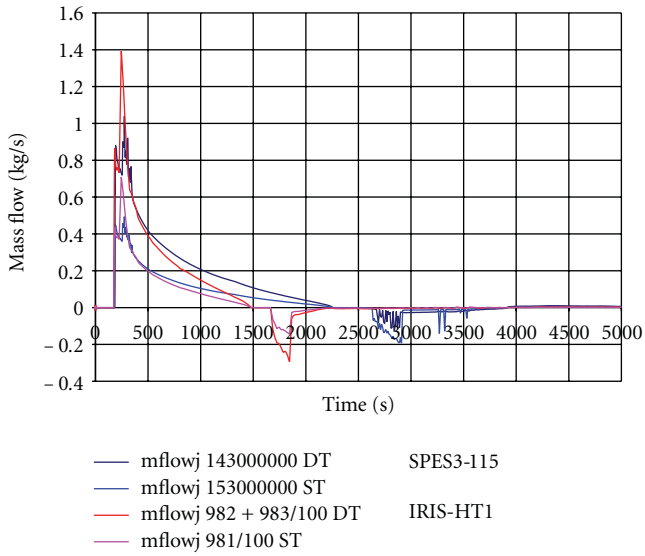

Figure 24: SPES3-115 and IRIS-HT1 ADS stage I ST and DT mass flow (short term).

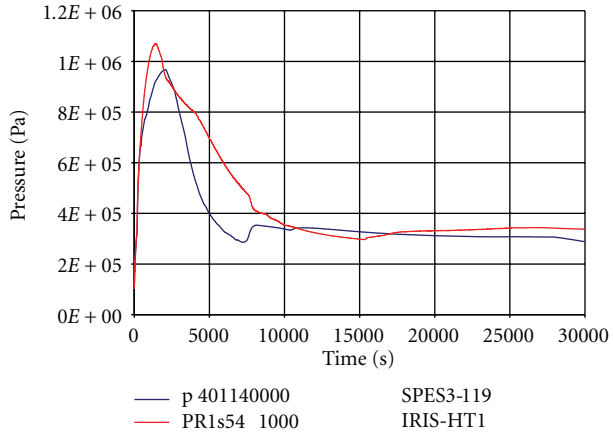

Figure 25: SPES3-119 and IRIS-HT1 DW pressure (short term).

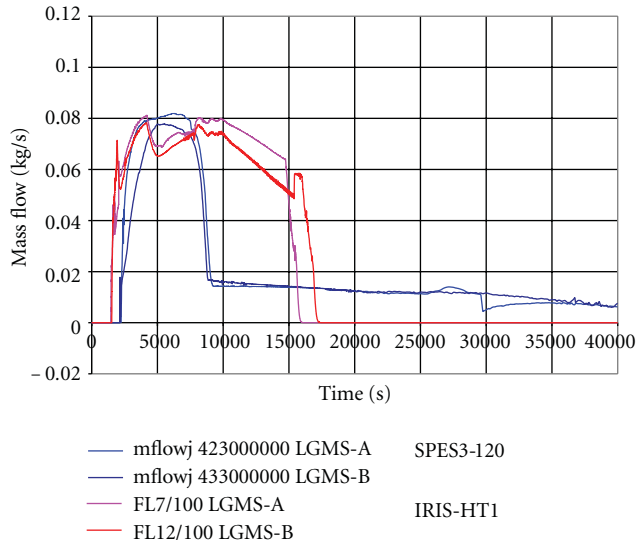

Figure 26: SPES3-120 and IRIS-HT1 LGMS injection mass flow.

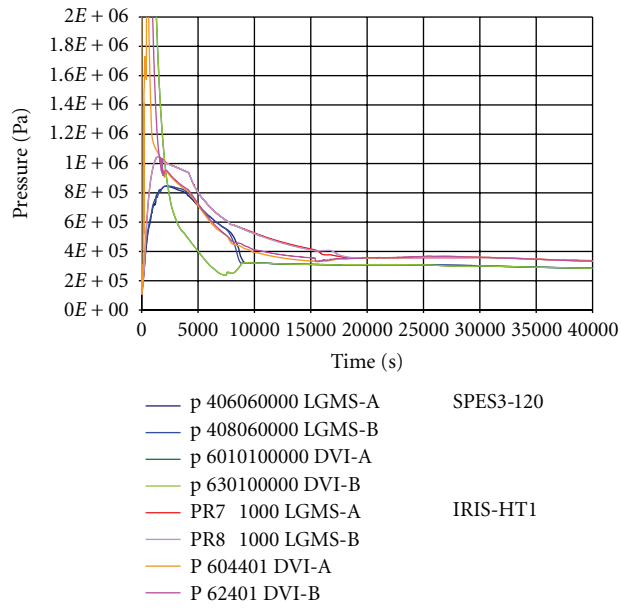

Figure 27: SPES3-120 and IRIS-HT1 LGMS and DVI pressure.

differences related to the injection of LGMS into the DVI lines and of PSS into the DW. As shown in Figures 26 and 27, IRIS LGMS injection into the DVI line is always driven by differential pressure between LGMS and DVI line (until about 18700 s), instead in SPES3, such differential pressure extinguishes earlier (around 9200 s) and later LGMS injection is driven only by gravity with a large mass flow decrease. The reason for such early pressure equalization in SPES3 is related to the PSS injection stop, vent pipe emptying, and gas flow from PSS to DW. That phenomenon did not occur in IRIS, where the vent pipes did not empty avoiding air transfer from PSS to DW, keeping the PSS pressurized with respect to DW and DVI (Figure 28).

The sensitivity cases on containment tank geometry, heat structures, and piping pressure drops led to reviewing both the IRIS and SPES3 models in IRIS-HT5g and SPES3-124. All IRIS containment heat structures were simulated and SPES3 piping geometry was adjusted to match IRIS pressure drops.

Figure 29 compares SPES3 and IRIS containment pressures, showing a good qualitative and quantitative agreement. The LGMS to DVI and PSS to DW injection mass flows are shown in Figures 30 and 31. With the same simulated pressure drops in the piping, different values of mass flow are evidenced due to greater differential pressures in SPES3 between LGMS and DVI and PSS and DW. Various reasons could explain these differences and the most likely is the different code simulation of contact condensation with the consequent different pressurization of containment compartments. Remodelling of IRIS RWST led to similar RWST water temperatures, but greater exchanged power in SPES3 caused faster heat-up (Figure 32).

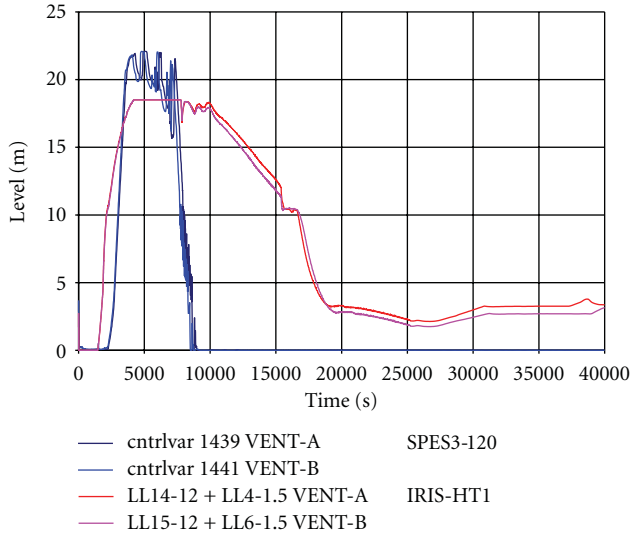

Figure 28: SPES3-120 and IRIS-HT1 PSS vent pipe level.

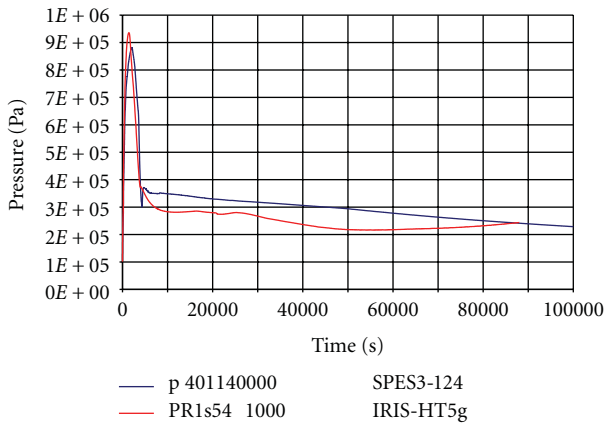

Figure 29: SPES3-124 and IRIS-HT5g DW pressure.

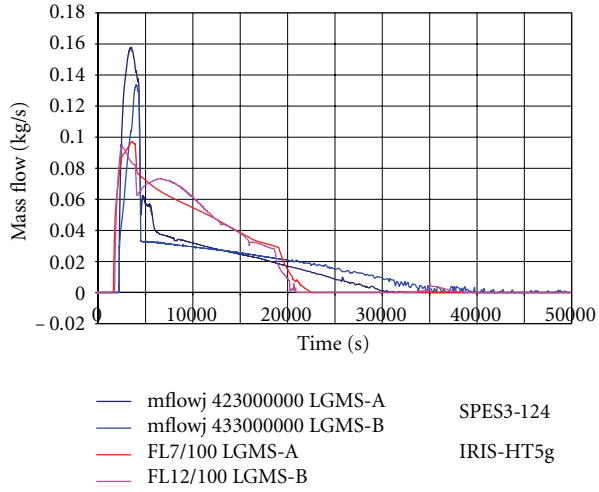

Figure 30: SPES3-124 and IRIS-HT5g LGMS to DVI mass flow (short term).

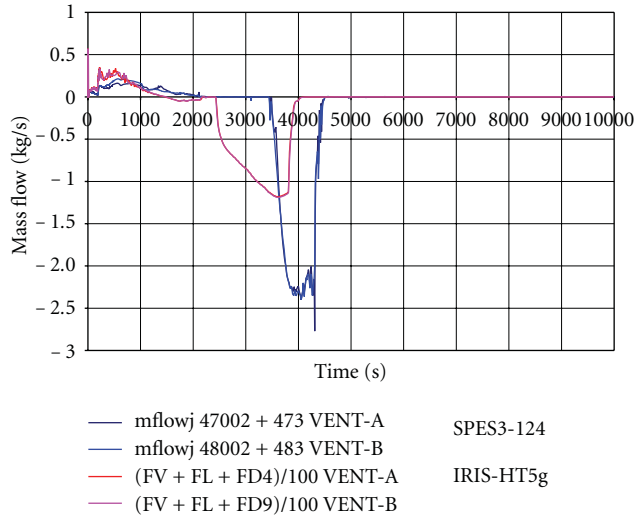

Figure 31: SPES3-124 and IRIS-HT5g PSS to DW mass flow (short term).

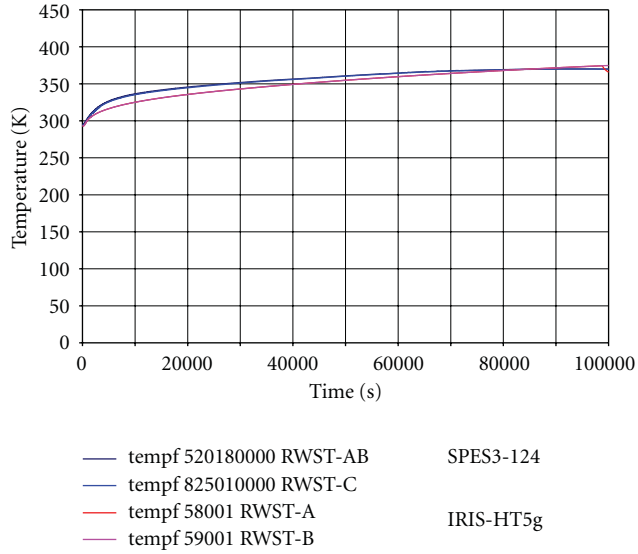

Figure 32: SPES3-124 and IRIS-HT5g RWST temperature.

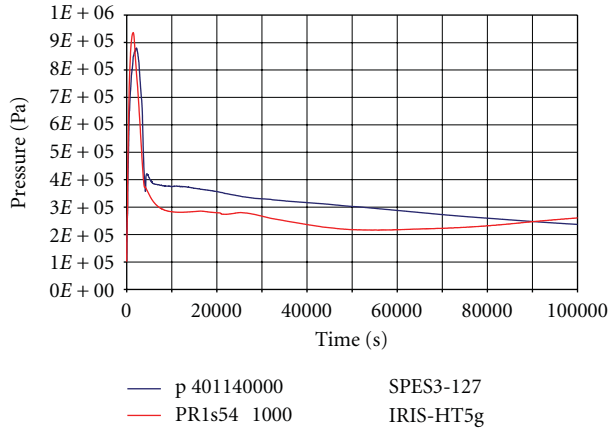

Figure 33: SPES3-127 and IRIS-HT5g DW pressure.

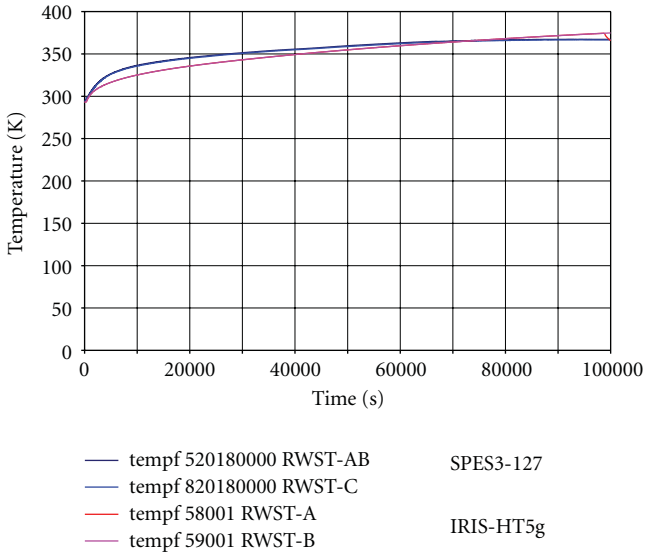

Figure 34: SPES3-127 and IRIS-HT5g RWST temperature.

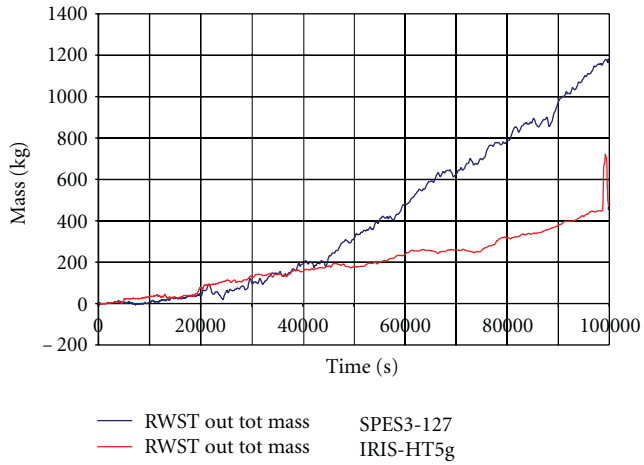

Figure 35: SPES3-127 and IRIS-HT5g RWST top integral mass flow.

The SPES3 PSS bottom remodelling was the further attempt to investigate PSS vent pipe emptying at the end of PSS injection into the DW. No important differences were observed. The SPES3-127 results were used to investigate the EHRS heat transfer to RWST, considered the cause of the different containment pressure trend in the long term, where IRIS increased after 50000 s while SPES3 continued to decrease (Figure 33). RWST temperature in SPES3 did not reach saturation, but established at lower values (Figure 34), due to the direct connection, in the model, of RWST top with the atmosphere control volume, and mass lost through RWST top caused by water solution in dry air with energy removal and temperature limitation (Figure 35).

That phenomenon led to a further modification of the model with the introduction of a discharge pipe at RWST top, limiting the contact surface with air and solving the problem of RWST water temperature that, finally, could

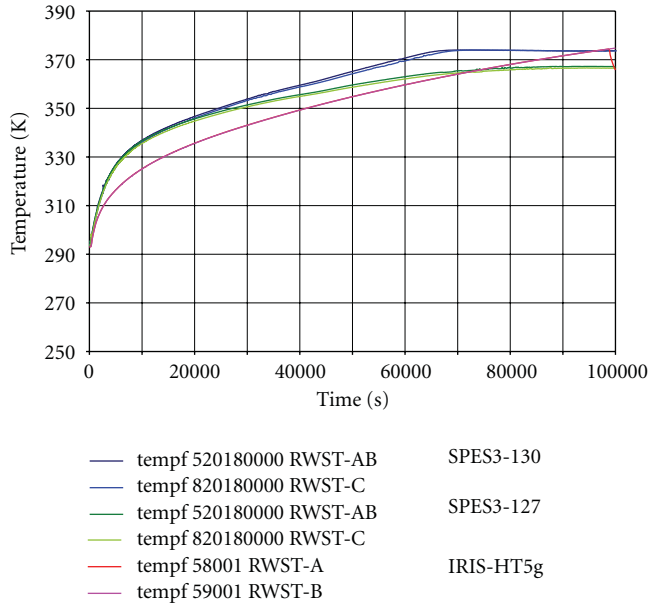

Figure 36: SPES3-130, 127 and IRIS-HT5g RWST temperature.

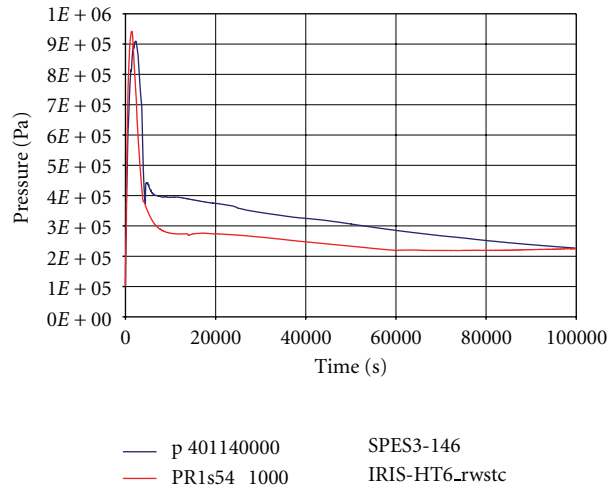

Figure 37: SPES3-146 and IRIS-HT6_rwstc DW pressure.

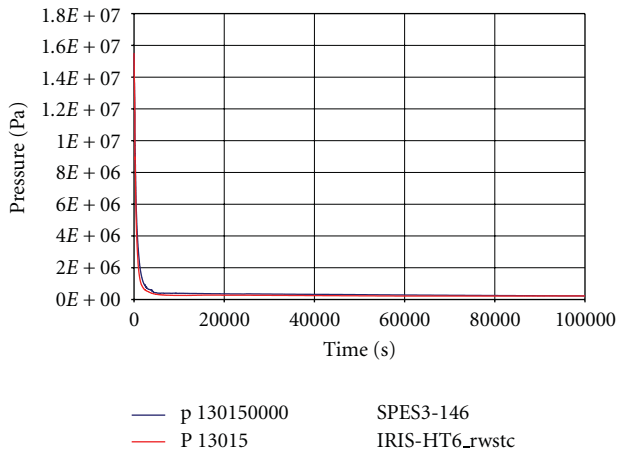

Figure 38: SPES3-146 and IRIS-HT6_rwstc PRZ pressure.

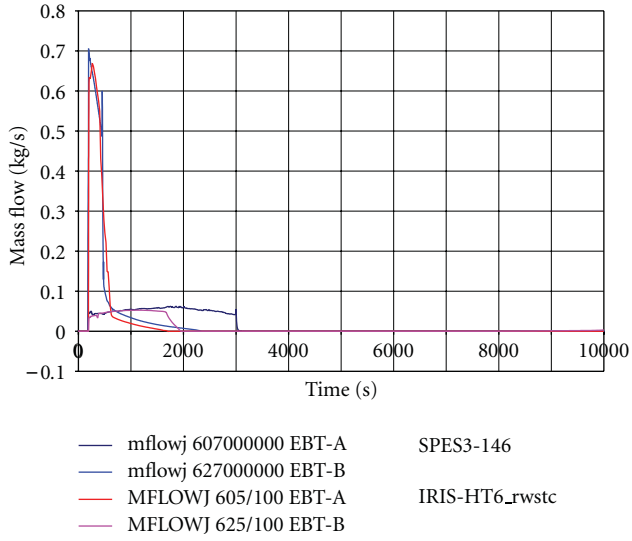

Figure 39: SPES3-146 and IRIS-HT6_rwstc EBT injection mass flow (short term).

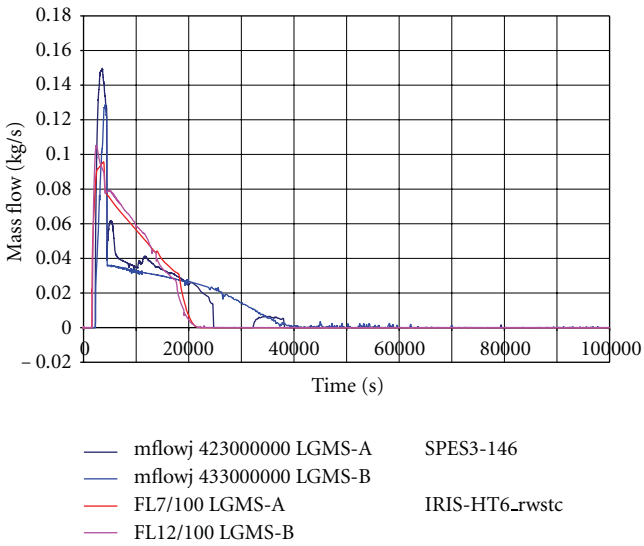

Figure 40: SPES3-146 and IRIS-HT6_rwstc LGMS to DVI injection mass flow.

reach saturation (Figure 36). Faster water heat-up in SPES3 showed that EHRS energy transfer to the RWST is greater than IRIS. That led to a series of sensitivity cases on a stand-alone model of EHRS-RWST that led to investigating the differences between the models and finding a common modelling approach based on experimental data on an in-pool heat exchanger and literature values of the heat transfer coefficients [13]. The method provided proper multiplying factors for the HTC to be applied to tube heat structures, condensing and boiling side, in the form of fouling factors [14] and a criterion to set the area of the pool slice containing the heat exchanger. IRIS EHRS-RWST was modified accordingly in the IRIS-HT6_rwstc case. A stand-alone model was also utilized to calibrate pressure drops in

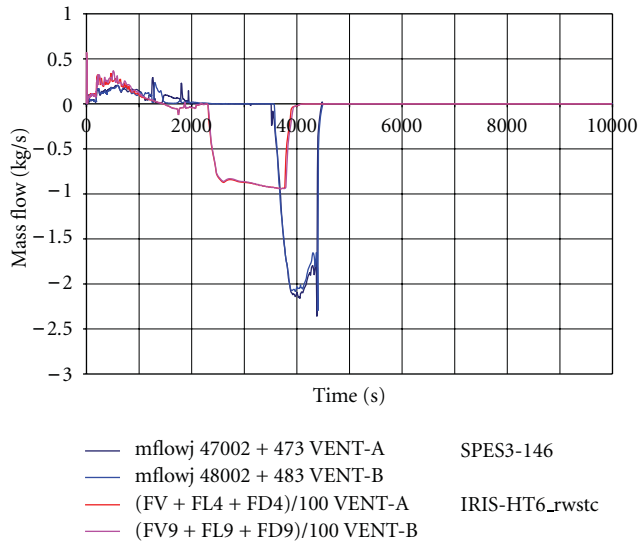

Figure 41: SPES3-146 and IRIS-HT6_rwstc PSS to DW injection mass flow (short term).

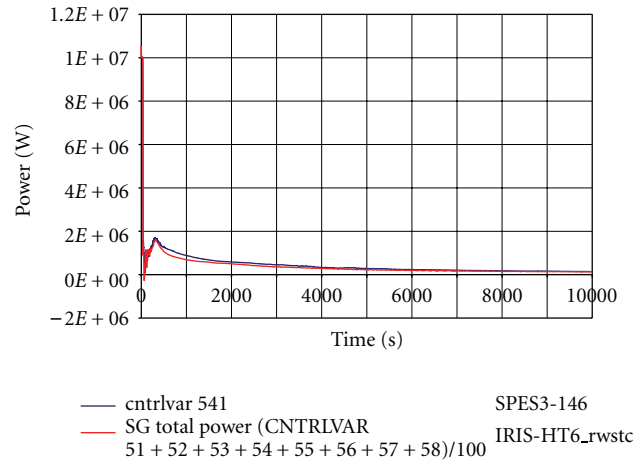

Figure 42: SPES3-146 and IRIS-HT6_rwstc SG power (short term).

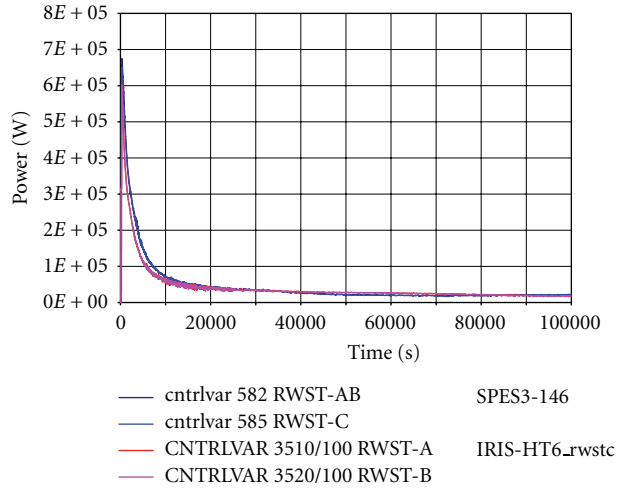

Figure 43: SPES3-146 and IRIS-HT6_rwstc RWST power.

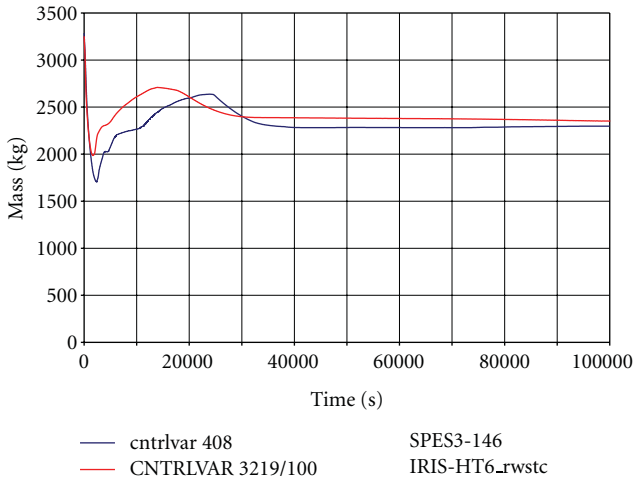

Figure 44: SPES3-146 and IRIS-HT6_rwstc RV mass.

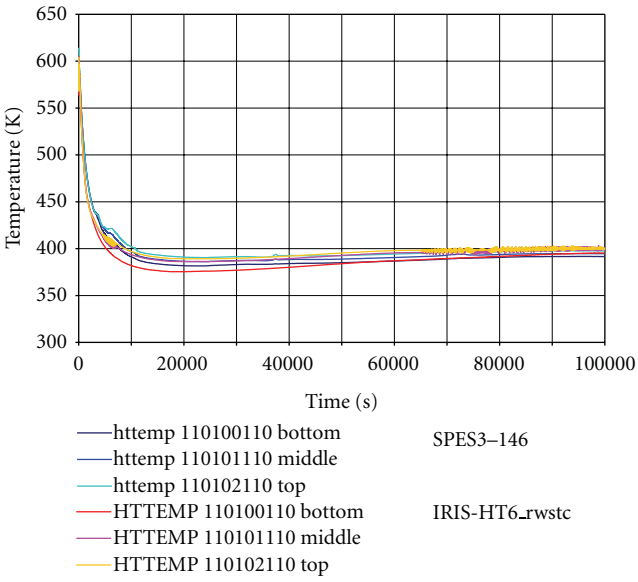

Figure 45: SPES3-146 and IRIS-HT6_rwstc core heater rod outer surface temperature.

EHRS hot legs and cold legs to properly reproduce the IRIS loops with adjustment to calibrated orifices. Moreover, the need of thermally insulating 4% of SPES3 HX heat transfer surface was evidenced to compensate for AISI 304 thermal conductivity greater than IRIS Inconel 600.

The SPES3-146 case included all design and model updates previously described and was considered the base case to compare to IRIS-HT6_rwstc. The main quantities of the transient and those that were objective of the SPES3 facility model and design optimization are shown in Figures 37, 38, 39, 40, 41, 42, 43, 44, and 45.

The last IRIS case was successively run to correct some differences, found in RELAP5 and GOTHIC models, about the end elevations of LGMS and ADS stage I lines. Small differences, compared to IRIS-HT6_rwstc results, were found in LGMS flows as well as some changes in ADS stage I flow, after initial discharge. Such differences do not affect or modify the results of the analysis previously described.

The final FSA is planned to be performed on the SPES3-146 and IRIS-HT6_rwstc1a results.

4. Conclusions

The design of the SPES3 facility was finalized thanks to an iterative calculation-design feedback process that allowed to verify the adequacy of containment pressure and reactor vessel mass inventory simulation, objectives of the SBLOCA PIRT for the IRIS reactor [7].

Since the early simulations, efficiency of IRIS safety systems was demonstrated in coping with SBLOCAs. The comparison with the SPES3 results and the early application of the FSA allowed to identify the main causes of discrepancy between the results and to put in evidence specific phenomena particularly affected by simulation choices. The containment heat structures, the heat transfer from EHRS to RWST, and piping pressure drops were found to be the most affecting parameters in matching the IRIS results. The review of the SPES3 design, in accordance to the above-mentioned parameter optimization, led to demonstrating that the PIRT identified FoMs are satisfied and that the residual discrepancies can be considered conservative: SPES3 RPV mass lower than IRIS mass and SPES3 heater rod temperatures higher than IRIS ones.

Besides the SPES3 design review, the main outcome of this work is the availability of a set of data suitable for the final FSA application, in progress at the moment, and the quantification of SPES3 facility distortions in IRIS simulation.

The SPES3 facility is under construction at SIET laboratories.

Nomenclature

ADS:	Automatic depressurization system
CIRTEN:	Consorzio Interuniversitario per la Ricerca Tecnologica Nucleare (University Consortium for Nuclear Technologic Research)
CL:	Cold Leg
cntrlvar:	(CNTRLVAR) control variable (RELAP5 variable)
CRDM:	Control rod drive mechanism
DBA:	Design basis accident
DC:	Downcomer
DEG:	Double ended guillotine
DT:	Double train
DVI:	Direct vessel injection
DW:	Dry well
EBT:	Emergency boration tank
EHRS:	Emergency heat removal system (EHRS-A, B, C for loops A, B, C)
ENEA:	Agenzia Nazionale per le Nuove Tecnologie, l'Energia e lo Sviluppo Economico Sostenibile (Italian National Agency for New Technologies, Energy and Sustainable Economic Development)

FD: Droplet mass flow rate (GOTHIC variable)
FER: Fakultet Elektrotehnike i Računarstva (Faculty of Electric Engineering and Computing) FL Feed Line
FL: Liquid mass flow rate (GOTHIC variable in the graphs)
FoM: Figure of merit
FSA: Fractional scaling analysis
FV: Gas mass flow rate (GOTHIC variable)
GNEP: Global nuclear energy partnership
GOTHIC: Generation of thermal-hydraulic information for containments
HTC: Heat transfer coefficient
httemp: (HTEMP) heat structure temperature (RELAP5 variable)
HX: Heat exchanger
IRIS: International reactor innovative and secure
ITF: Integral test facility
LGMS: Long-term gravity make-up system
LL: Liquid level (GOTHIC variable)
LOCA: Loss of coolant accident
LP: Lower plenum
LWR: Light water reactor
mflowj: (MFLOWJ) mass flow rate (RELAP5 variable)
NPP: Nuclear power plant
p: (P) Pressure (RELAP5 variable)
PIRT: Phenomena identification and ranking table
PR: Pressure (GOTHIC variable)
PRZ: Pressurizer
PSS: Pressure suppression system
QT: Quench tank
RC: Reactor cavity
RELAP: REactor loss of coolant analysis program
RPV: Reactor pressure vessel
RV: Reactor vessel
RWST: Refueling water storage tank
R&D: Research and development
SB: Small break
SET: Separate effect tests
SIET: Società Informazioni Esperienze Termoidrauliche (company for information and experiences on thermal-hydraulics)
SG: Steam generator
SL: Steam line
SMR: Small and medium-sized reactor
SPES: Simulatore pressurizzato per esperienze di sicurezza (pressurized simulator for safety tests)
ST: Single train
tempf: (TEMPF) liquid temperature (RELAP5 variable)
WEC: Westinghouse Electric Company LLC.

References

[1] M. D. Carelli, L. E. Conway, L. Oriani et al., "The design and safety features of the IRIS reactor," *Nuclear Engineering and Design*, vol. 230, no. 1–3, pp. 151–167, 2004.

[2] M. D. Carelli, B. Petrović, L. E. Conway et al., "IRIS design overview and status update," in *Proceedings of the 13th International Conference on Nuclear Engineering (ICONE13-50442 '05)*, Beijing, China, May 2005.

[3] B. Petrović, M. D. Carelli, and N. Cavlina, "IRIS—international reactor innovative and secure: progress in development, licensing and deployment activities," in *Proceedings of the 6th International Conference on Nuclear Option in Countries with Small and Medium Electricity Grids*, Dubrovnik, Croatia, May 2006.

[4] M. D. Carelli, B. Petrović, M. Dzodzo et al., "SPES-3 experimental facility design for IRIS reactor integral testing," in *Proceedings of the European Nuclear Conference (ENC '07)*, Brussels, Belgium, September 2007.

[5] M. Carelli, L. Conway, M. Dzodzo et al., "The SPES3 experimental facility design for the IRIS Reactor simulation," *Science and Technology of Nuclear Installations*, vol. 2009, Article ID 579430, 12 pages, 2009.

[6] R. Ferri, A. Achilli, C. Congiu et al., "SPES3 facility and IRIS reactor numerical simulations for the SPES3 final design," in *Proceedings of the European Nuclear Conference (ENC '10)*, Barcelona, Spain, May June 2010.

[7] T. K. Larson, F. J. Moody, G. E. Wilson et al., "Iris small break loca phenomena identification and ranking table (PIRT)," *Nuclear Engineering and Design*, vol. 237, no. 6, pp. 618–626, 2007.

[8] IAEA-TECDOC 1536, "Status of small reactor designs without on-site refuelling (IAEA '07)," 2007.

[9] R. Ferri and C. Congiu, SPES3-IRIS facility nodalization for RELAP5 Mod.3.3 code and steady state qualification. SIET 01 423 RT 08 Rev.0, ENEA FPN-P9LU-017, 2009.

[10] R. Ferri and C. Congiu, SPES3-IRIS facility RELAP5 base case transient analyses for design support. SIET 01 489 RT 09 Rev.0., ENEA FPN-P9LU-035, 2009.

[11] R. Ferri and C. Congiu, SPES3-IRIS facility RELAP5 sensitivity analyses of the Lower Break transient for design support. SIET 01 499 RT 09 Rev.0., FPN- P9LU-040, 2009.

[12] R. Ferri, SPES3-IRIS facility RELAP5 sensitivity analyses on the containment system for design review. SIET 01 526 RT 09 Rev.0., ENEA NNFISS-LP2-017, 2010.

[13] R. Ferri and P. Meloni, Approach for a correct simulation of the SPES3-IRIS Emergency Heat Removal System with the RELAP5/MOD3 Code. SIET 01 745 RT 11 Rev.0. Piacenza, Italy, 2011.

[14] RELAP5 code manual. NUREG/CR-5535/Rev.1 Idaho National Engineering Laboratory (USA), 2001.

Hindawi Publishing Corporation
Science and Technology of Nuclear Installations
Volume 2012, Article ID 238019, 16 pages
doi:10.1155/2012/238019

Project Report

The LOBI Integral System Test Facility Experimental Programme

Carmelo Addabbo and Alessandro Annunziato

Commission of the European Communities, Joint Research Centre, Via E. Fermi 1, 21027 Ispra, Italy

Correspondence should be addressed to Carmelo Addabbo, carmelo.addabbo@ec.europa.eu

Received 9 March 2011; Accepted 1 July 2011

Academic Editor: Klaus Umminger

The LOBI project has been carried out in the framework of the European Commission Reactor Safety Research Programme in close collaboration with institutional and/or industrial research organizations of EC member countries. The primary objective of the research programme was the generation of an experimental data base for the assessment of the predictive capabilities of thermal-hydraulic system codes used in pressurised water reactor safety analysis. Within this context, experiments have been conducted in the LOBI integral system test facility designed, constructed, and operated (1979–1991) at the Ispra Site of the Joint Research Centre. This paper provides a historical perspective and summarizes major achievements of the research programme which has represented an effective approach to international collaboration in the field of reactor safety research and development. Emphasis is also placed on knowledge management aspects of the acquired experimental data base and on related online open access/retrieval user functionalities.

1. Background

The LOBI project originated from a reactor safety research and development contract between the European Commission (EC) and the former Bundesminister für Forschung und Technologie (BMFT) of the Federal Republic of Germany. On the basis of contingent and perceived safety requirements, the BMFT decided in 1972 on the need of an integral system test facility for thermal-hydraulic investigations relevant to accident conditions in pressurized water reactors (PWRs) of German design.

A general international consensus of opinions emerged in the early 70s on the need to provide reliable methodologies for a realistic estimate of emergency-core-cooling system (ECCS) performance which was being questioned as large power reactors were being introduced. Due to the limited sophistication of safety codes and to the lack of relevant experimental data for assessing their predictive capabilities, sufficient conservatism was prescribed in the safety evaluations of design basis accidents (DBAs), such as loss-of-coolant accidents (LOCAs), in order to account for worst-case uncertainties. This entailed stringent licensing requirements and undesirable operational constraints on nuclear power plants.

Within this context, reactor safety research and development programmes were formulated at the international level to improve the understanding and modelling capabilities of the thermal-hydraulic phenomenologies governing the course of a LOCA or of any other anticipated abnormal occurrence in water cooled reactors. Emphasis was placed mainly on deterministic methodologies supported, as appropriate, by probabilistic risk assessment studies with the aim to better understand accident progression and to substantiate the request for the eventual relaxation of over-conservatism in some safety analysis acceptance criteria.

The European Commission has been engaged in nuclear safety research activities since the signing in 1957 of the treaties establishing its precursors; that is, the European Atomic Energy Community and the European Economic Community. In line with its institutional role, the action of the Commission has been mainly devoted to a systematic effort in promoting the harmonization of safety practices and methodologies among the member states.

On the basis of its tender of May 1973, the Joint Research Centre was charged by the German BMFT with a R&D contract which envisaged the design, the construction, and the operation of an integral system test facility for the investigation of thermal-hydraulic phenomenologies pertinent to

PWR large break LOCAs. The contractual agreement was signed in December 1973 and was then renegotiated in 1982 extending the original research objectives to the small break LOCA and Special Transients scenarios.

In its final configuration, the LOBI experimental data base consists of 70 tests (Table 2) covering a wide range of accident scenarios relevant to the safety analysis of PWRs.

2. Research Objectives

The LOBI research programme, as initially conceived, has been mainly oriented towards the generation of an experimental data base relevant to risk-dominant accidents and transients in PWRs. Specific research objectives included:

(i) the identification and/or verification of basic phenomenologies governing the thermal-hydraulic response of an integral system test facility for a range of conditions relevant to LOCAs and special transients in PWRs,

(ii) the generation of an experimental data base for the independent assessment of the predictive capabilities of large thermal-hydraulic system codes used in water reactor safety analysis.

The experimental programme has been supported by comprehensive code application and assessment activities. ATHLET (DRUFAN), CATHARE, RELAP4, RELAP5, and TRAC have been largely used either within JRC or by outside organizations for test design and test prediction calculations. Development and application of advanced two-phase flow measurement techniques to support the execution of the experimental programme have constituted an integral part of the overall research strategy. At the time, a considerable effort has also been devoted to the development of an IBM version of the RELAP5 code which, together with various model improvements introduced at the JRC, has been instrumental in enabling the code calculation capabilities of many organisations within and outside the EC.

The most stringent concern in the operation of nuclear power plants is to ensure that its inventory of radioactive material remains safely confined at all times, both during normal and off-normal conditions. In order to satisfy this compelling requirement, nuclear power plants have to comply with a set of design and construction standards, operational constraints, and safety regulations.

The many different safety features which are engineered in each nuclear power plant to compensate for any departure from normal operating conditions should an accident occur, must, irrespective of the cause, provide sufficient safety margins to prevent the release of radioactive material in excess of prescribed limits, and ensure the protection of the operators and the general public.

The emergency core cooling system (ECCS) is the most important safety feature of a water-cooled reactor. Its main purpose is to maintain the reactor in a coolable geometry in the event of loss of coolant caused by a break in the main cooling system or by the operation of the safety relief systems in the case of intact circuit faults. To meet this widely accepted requirement, the ECCS should have the capabilities to

(i) provide sufficient core cooling by removing both residual stored energy and decay heat at a rate such to limit the maximum fuel cladding temperature to a value less than the prescribed limit thereby preventing the cladding from loosing its structural integrity,

(ii) have sufficient capacity, diversity, reliability, and redundancy to provide core cooling under all conceived accident conditions.

The ECCS safety features of a pressurised water reactor consist of a set of independent subsystems which include the high pressure injection system (HPIS), the accumulator injection system (AIS), and the low pressure injection system (LPIS); each subsystem is characterised by redundancy of equipment and flow paths.

At present, PWR safety analysis is based on the evaluation of ECCS performance during design basis accidents (DBAs) which include large break LOCAs, small break LOCAs, and special transients resulting from intact circuit faults.

3. The Experimental Installation

The LOBI test facility was designed to represent a full-power high-pressure integral system test facility 1 : 700 scale model of a 4-loop, 1300 MWe PWR, Figure 1. It incorporates the essential features of a typical PWR primary and secondary cooling system. The test facility was commissioned in December 1979 and was operated until June 1982 in the MOD1 configuration for the investigation of large break LOCAs; it was then extensively modified into the MOD2 configuration which incorporates design and instrumentation features best suited for the characterization of phenomenologies relevant to small break LOCAs and special transients.

The measurement system comprises a total of about 470 measurement channels. It allows the measurement of all relevant thermohydraulic quantities at the boundaries (inlet and outlet) of each individual loop component and within the reactor pressure vessel model and steam generators. A process control system allows the simulation of time- or pressure-dependent parameters such as main coolant pump hydraulic behaviour, core decay heat release, and safety injection flow rates. A fast running data acquisition system complements the experimental installation.

3.1. Mechanical Components. The test facility comprises two primary loops, the intact and the broken loop which represents, respectively, three loops and one loop of the reference PWR. Each primary loop contains a main coolant circulation pump and a steam generator. The simulated core consists of an electrically heated rod bundle arranged in a square matrix inside the pressure vessel model. The primary cooling system which is shown schematically in Figure 2 operates at normal PWR conditions, approximately, 158 bar and 294–326°C pressure and temperature, respectively.

Figure 1: Photographic view of the LOBI test facility.

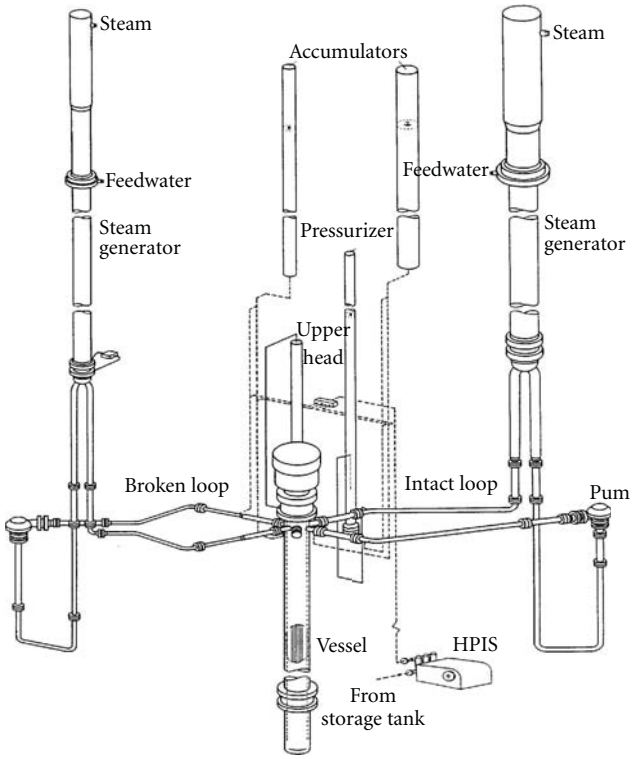

Figure 2: Schematic view of the LOBI test facility.

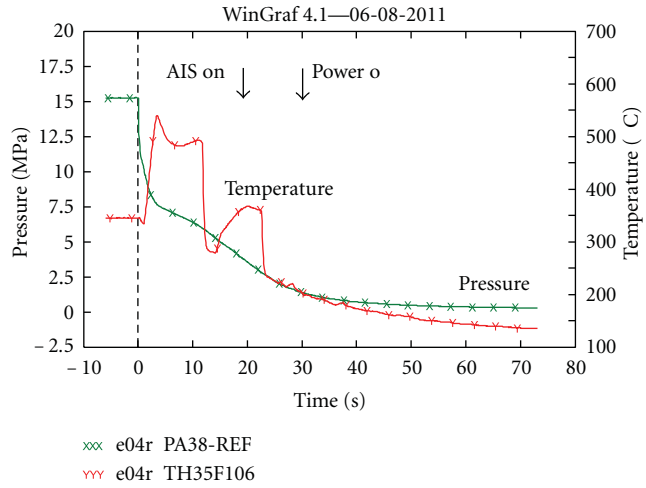

Figure 3: Primary system pressure and heater rod temperature response to a large 200% cold leg break LOCA (Downcomer gap width 50 mm).

Heat is removed from the primary loops by the secondary cooling system which contains a condenser and a cooler, the main feedwater pump, and the auxiliary feedwater system. Normal operating conditions of the secondary cooling system are 210°C feedwater temperature and 64.5 bar pressure.

3.1.1. Reactor Pressure Vessel Model. The reactor pressure vessel model comprises the pressure vessel, the core barrel tube, and the core simulator. Lower plenum, upper plenum, an annular downcomer, and an externally mounted upper head simulator are additional major components of the overall pressure vessel assembly. The reactor core is simulated by an electrically heated rod bundle consisting of 64 rods arranged in an 8 × 8 square matrix inside the flow shroud; heater rod bundle dimensions are reactor typical. The heater rods are directly heated hollow tubes (material 1.4948 DIN 17007), and the rod wall thickness within the heated length is varied in 5 steps to achieve a chopped cosine-shaped axial power distribution.

The upper part of the rod bundle which extends entirely into the upper plenum is formed by hollow nickel tubes connected to the upper power plate. The lower part is formed by nickel rods and flexible nickel braids which extend partially into the lower plenum where they connect to the lower-power connecting ring. The heat dissipated within these "unheated" regions amounts to about 14%.

Nine grid spacers of original design are placed along the heated length; five additional spacers are mounted in the upper unheated part of the rod bundle. Ceramic segments are arranged inside the core barrel tube forming a square flow shroud which extends over the heated length region of the rod bundle.

The upper head is simulated by an external vessel connected to the upper plenum and to the upper downcomer. Volume as well as height and relative elevations of the reference plant upper head are preserved. In the initial MOD1 version of the test facility, the annular downcomer formed by the pressure vessel and the core barrel tube had a gap width of 50 mm which was later decreased to 12 mm to better represent fluid volume distribution.

3.1.2. Steam Generators. The LOBI test facility contains two shell and inverted U-tube type steam generators having a geometrical configuration similar to that of the reference plant. In the MOD1 configuration, the steam generators were designed to preserve heat transfer capabilities without proper

simulation of secondary side fluid distribution. In the MOD2 configuration, the steam generators were designed with the aim to better represent thermal-hydraulic phenomenologies of interest in intact circuit faults.

The overall scaling ratio which required a capacity ratio of 3 : 1 between the intact and the broken loop steam generator led to a heat transfer exchange power of 3.96 MW (24 U-tubes + 1 installed spare) and 1.32 MW (8 U-tubes + 1 installed spare) for the intact and broken loop SG, respectively.

Each steam generator consists of a single cylindrical pressure vessel with an annular downcomer separated from the riser region by a skirt tube. This tube is supported above the tube plate and carries the coarse separator; a fine separator is arranged in the uppermost part of the steam dome. The U-tubes are arranged in a circle within the riser region around an axially mounted filler tube, with the U-bends crossing over one another above it. This design permits cross-flow between cocurrent and counter-current legs of the U-tubes over their entire length and heat and mass transfer between riser and downcomer to account for the recirculation characteristics of the prototypical system. An adjustable throttle device is installed at the lower end of the downcomer to properly set the recirculation ratios.

Feedwater is directed into the downcomer by a "J-nozzle" feed ring sparger and flows downward mixed with the recirculation water returned by the coarse and fine separators. The steam water mixture leaving the bundle region flows upward into the coarse separator where the moisture is partially removed by centrifugal separation and returned to the downcomer. Additional separation is attained in the fine, box-grid type separator from where saturated, practically dry steam flows into the outlet nozzle. On the primary side, fluid enters the U-tubes through an inlet chamber and flows first upward and then downward exchanging heat with the secondary fluid.

3.1.3. Main Coolant Pumps. The main coolant pumps of both loops are centrifugal type pumps having a specific speed of 29.2 (DIN). The two pumps are equal in size and are, therefore, operated at two different speeds such as to yield the two different steady-state mass flows of 21 Kg/s and 7 Kg/s for the intact and broken loop at the same pressure head. A special control and drive system allows variation of the pump speed in the forward and backward directions over a range of ±8500 rpm. Since the locked rotor resistance of the MCPs is less than the equivalent reactor pump, there are provisions for the insertion of an additional flow resistance at the outlet of each pump. To account for the injection of the main coolant pump seal water, a closed loop seal water compensation system is installed.

3.1.4. Pressurizer. The pressurizer design is geometrically similar to that of the reference plant; however, it is scaled in volume but not in height. The surgeline rises within the pressurizer and leaves it radially. The pressurizer is provided with normal and additional heaters; the spray system is simulated with cooling coils placed in the steam region. There

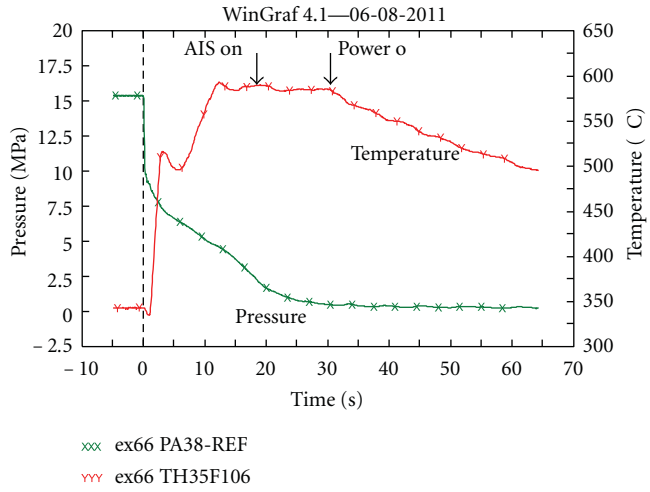

Figure 4: Primary system pressure and heater rod temperature response to a large 200% cold leg break LOCA (downcomer gap width 12 mm).

are provisions for connecting the surgeline to either the intact or broken loop hot legs. The simulation of power-operated relief valves (PORVs) as well as safety relief valves (SRVs) is provided in the pressurizer relief line.

3.1.5. Primary Loop Pipework. The main coolant pipes connecting the major primary loop components have inner diameters of 73.7 mm and 46.1 mm for the intact and broken loop, respectively. Measurement inserts are installed at the inlet and outlet of each major component forming integral part of the main pipework. Since the main coolant pumps are equal in size with an inlet-outlet diameter of 65 mm, special cross-sections adapters are installed at the inlet-outlet of each pump to fit the main loop pipes.

3.1.6. Break Assembly. The break assembly consists of a T-shaped insert with the break orifice housed in a recess machined in the insert. The break assembly can be connected to the main coolant pipe at the selected break location; for example, cold leg, hot leg, or pump seal. Pressurizer breaks or inadvertent opening of the valves are simulated by an orifice inserted in the relief line. A proper connection can be established between primary and secondary systems at the tube plate elevation to simulate steam generator tube rupture (SGTR) sequences.

3.2. Safety Injection Systems. The LOBI-MOD2 emergency-core-cooling system (ECCS) comprises the high-pressure injection system (HPIS) and the accumulator injection system (AIS). As required, the low-pressure injection system (LPIS) could also be simulated. Provisions are made for cold leg, hot leg, or combined cold and hot leg ECC injection in both primary loops. In the MOD1 version of the test facility, only the accumulator system was simulated.

The HPIS water is supplied by a positive displacement pump driven by a variable speed motor. The pump is rated

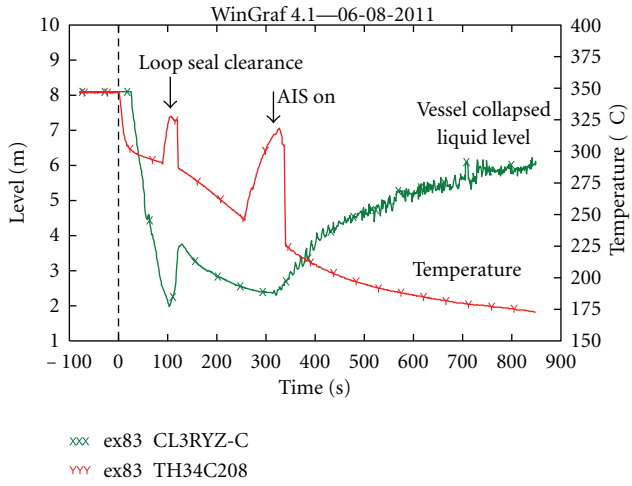

Figure 5: Heater rod temperature and vessel-collapsed liquid level in a small 10% cold leg break LOCA.

for a maximum flow of 0.39 Kg/s at a total head of 200 bars. A special speed control system provides appropriate flow regulation to match the reactor HPIS-expected performance. Properly designed and calibrated throttling devices are installed in the main injection line to provide the required partitioning (depending on particular simulation needs) of the injection rate between the broken and the intact loop.

The AIS is composed of two accumulators, one in each loop. The accumulator of the intact loop has three times the volume and water capacity of that of the broken loop. The total volume of each accumulator is scaled to that of the reference plant having one accumulator for each loop; gas space, water volume as well as height and elevations are preserved. Both accumulators are rated for a maximum pressure of 60 bar and a temperature of 50°C.

Additional safety injection systems consist of the volume control system (VCS) and of the auxiliary feedwater system (AFWS). The VCS consists of a feed pump and a water preheating system which allows the control of the injected water at the prevailing cold leg fluid temperature. Similarly, the AFWS consists of a feed pump an a water preheating system as the injected water is preheated to generally about 130°C to prevent thermal shocks in the SG feed line and J-nozzle feed ring.

3.3. Measurement System. The LOBI test facility in both the MOD1 and MOD2 configurations has been fitted with a comprehensive measurement system. Relevant thermal-hydraulic quantities were measured at the boundaries of each major component and within the reactor pressure vessel model and the steam generators.

Measurement in the primary loop pipework is performed within the measurement inserts at the inlet and outlet of each major component, that is, the reactor pressure vessel model, the steam generators, and the main coolant pumps. The inserts in the horizontal pipework are properly instrumented in the lower and upper part of the flow cross-section to characterize eventual flow and thermal stratification phenomena. Fluid and wall temperatures, absolute and differential pressures, fluid velocities and density as well as flow direction indicators are generally provided at each measurement insert.

Measurement of temperatures, pressures, and differential pressures are extensively made along the downcomer, lower plenum, rode bundle section, and upper plenum flow paths. Fluid velocity and fluid density are measured at the rod bundle inlet box.

Each rod bundle is supplied with three thermocouples brazed into grooves of 0.8 mm depth and 10 mm length machined into the outer surface of the heater rod tubes and then led through the wall to the inside of the tubes; they leave the rods through the open upper end.

The LOBI-MOD2 steam generators are instrumented to provide a maximum of information on both the magnitude and location of the heat transfer process taking place between the primary and the secondary systems. In particular, the instrumentation is concentrated in the region of the lowest U-bend and immediately above the tube plate in order to detect changes in heat transfer regime.

Steam generators measurements include fluid temperatures, U-tube wall temperatures, and differential pressures on both the primary and secondary side. Primary side instrumentation is applied to two representative U-tubes in each steam generator; the highest U-tube is fitted with temperature sensors whereas differential pressures are measured in the shortest U-tube. Special Pitot tubes are installed in the downcomer of the steam generator secondary side to measure fluid velocities at three peripheral positions.

Measurements in the secondary system is concentrated in the feedwater and in the steam lines at the inlet and outlet of each steam generator. Feedwater line measurement includes fluid temperature and velocity whereas in the steam line fluid temperature and volumetric flow is measured. A special spool piece with low-density measurement capability may be mounted at the outlet of the broken loop steam generator for detecting eventual carry-over in those tests involving blowdown of the secondary side. The pressurizer and the surgeline are provided with fluid temperature and differential pressure measurements and a full-flow turbine.

All ECC injection lines are provided with full-flow turbines and fluid temperature measurements. Mass flow measurement is also provided in the main coolant pump seal water injection lines. The break flow measurement system consists of a condenser-catch tank system. Initially, the high energy flow is condensed in the cold liquid pool contained in the catch tank; thereafter, long-term low-flow energy removal is ensured by a small 250 KW condenser. The break flow in its integral form is obtained by the incremental mass of the catch tank.

A special tailored data acquisition system based on state of art information technologies available at that time is used to record all measurement signals; the sampling rate can be varied up to 20000 samples/s as appropriate for the representation of the experimental information especially in fast evolving transients. Selected data are then read back from the

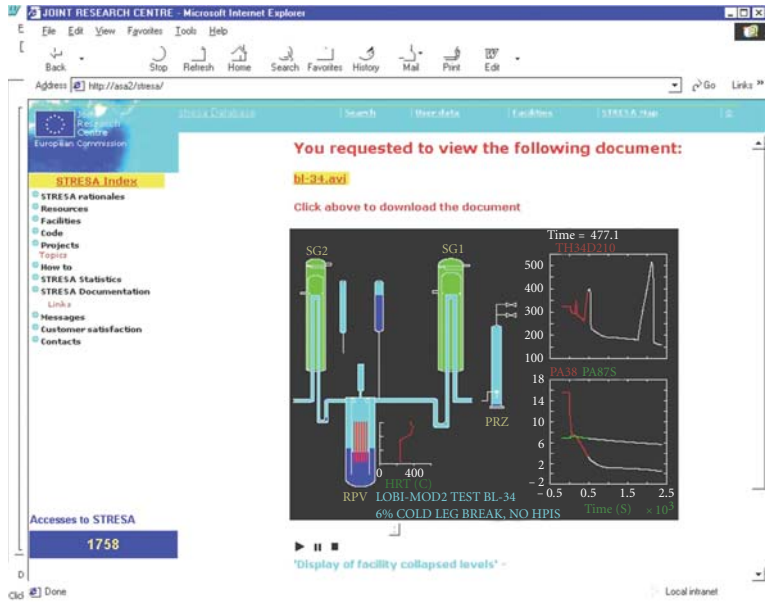

Figure 6: Display of collapsed liquid levels, heater rod temperature, and system pressures at 477 s into a 6% SBLOCA.

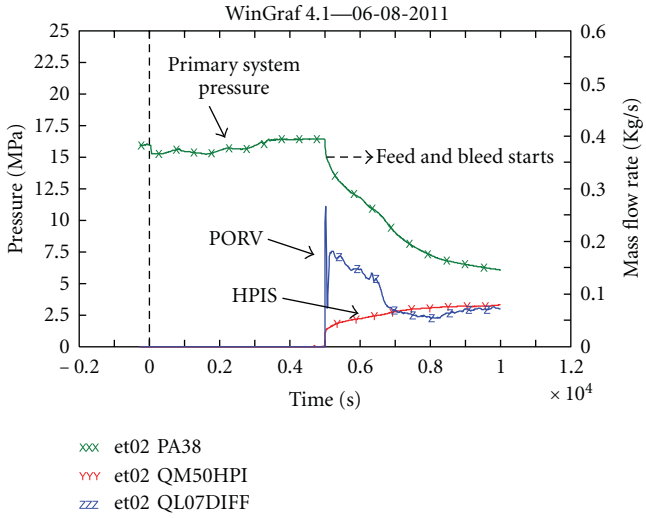

Figure 7: Primary system pressure and HPIS/PORV flow during a loss of feed water with bleed and feed.

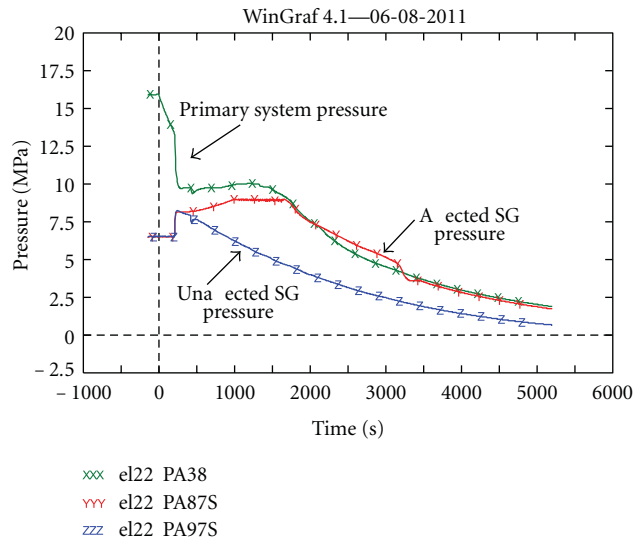

Figure 8: Primary and secondary system pressures in a 0.4% steam generator tube rupture.

analog tape, converted into engineering units and stored on 300 Mbyte disk modules ready for normalization and correction.

The data acquired at very high sampling rate are discretised and reduced to about 1000 data points over the entire experiment time range; each reduced value is simply an average over the time interval between a discrete set of data points. This is required in order to have a manageable set of data for storage and further processing and analysis. The reduced data in its final form are stored on the corresponding normal-time experimental data tape. As appropriate, special selects are made for the analysis of experimental time intervals characterized by fast transients and stored on a related short-time data tape.

A real-time loop control and monitoring system provides defined set of time ordered operations to represent components response during the simulated transient. Control of main coolant pump speed, core heating power, high-pressure injection system flow rate and steam generator level is performed on a real-time basis in response to predefined trip signals.

4. Scaling Criteria

The LOBI test facility was scaled to preserve, insofar as possible or practical, similarity of thermal-hydraulic behaviour

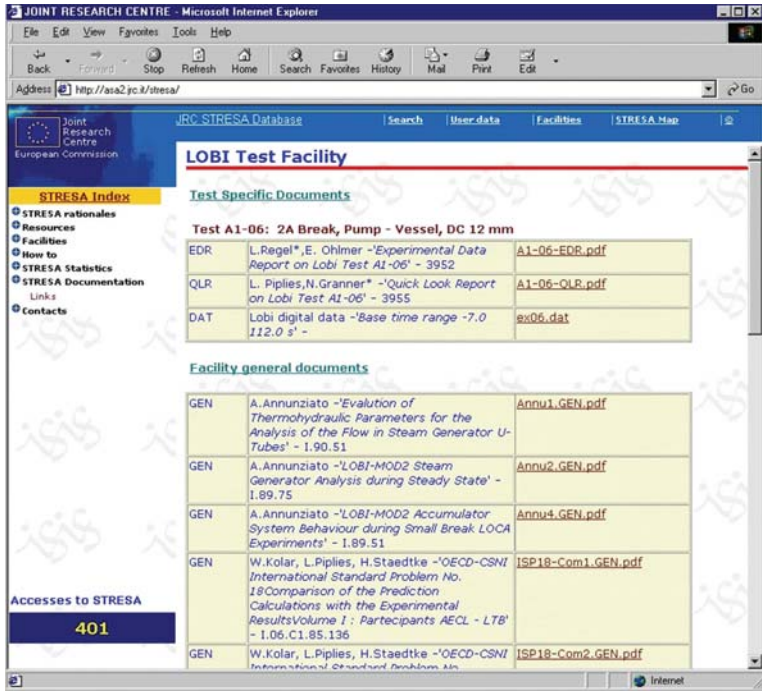

Figure 9: Typical STRESA data set for each LOBI test.

with respect to the reference plant; the German 1300 MWe BIBLIS B power station of Siemens/KWU design commissioned in 1976. It is worth noting that the first commercial nuclear power plant in Germany, the 17 MWe VAK KAHL station of the BWR type, was commissioned in 1960 and that the first unit of the PWR type, the 345 MWe KWO Obrigheim station, was commissioned in 1968.

As general scaling principle, a power-to-volume scaling criterion was adopted in the design of the facility to ensure the preservation of the specific power input into the primary fluid, Table 1. To meet general scaling requirements, the test facility was designed to preserve, taking into account the selected 1 : 700 power to volume scaling ratio, the following main parameters:

(i) core power to system volume ratio,

(ii) volumes and relative volumes of individual components,

(iii) rupture size to primary system volume ratio,

(iv) pressure drop and temperature distribution along main flow paths,

(v) height and elevation of major components, and

(vi) core and steam generators heat transfer surfaces.

The elevation of the major components were maintained at full height with the exception of the pressurizer which, while preserving the total volume and the steam to liquid volume ratios, was somehow shortened to allow increased radial dimensions to accommodate the internal heaters. The core and steam generators heat transfer and flow areas were matched to the scale factor. Strict adherence to the power-to-volume scale factor would have resulted in unacceptably high wall frictional pressure losses in the primary loop pipework which was appropriately shortened to increase the pipe diameter in order to match the expected pressure drop in the reference plant.

In the MOD2 configuration of the test facility, special emphasis was given to the scaling of the steam generator primary and secondary sides due to their importance on the thermal-hydraulic evolution of small break LOCAs and special transients. In particular, volume ratio, heat transfer surface-to-volume ratio, hydraulic resistances and elevations, and height of the shortest U-tube were preserved.

A major exception to the general scaling concept is the design of the reactor pressure vessel model annular downcomer. The test facility has been configured with a downcomer of two different gap widths. Initially, a downcomer gap of 50 mm was installed in the MOD1 configuration to prevent ECC bypass which is largely influenced by hot wall delay and counter-current flow limitation phenomena; this, however, resulted in a 6.3 times too large a downcomer volume and, as a consequence, in an atypical thermal-hydraulic system response during large break LOCAs. The downcomer gap width was later changed to 12 mm which again, was a technical compromise between a 7 mm volume-scaled and a 25 mm pressure drop-scaled downcomer.

The LOBI test facility, as any other scaled test facility, has inherent distortions with respect to the reference plant which may impair the typicality of some results. The power-to-volume scaling concept results in a design which exhibits

Table 1: LOBI test facility design and operational parameters.

Reference plant	Siemens-KWU	Biblis B
	Loops	4
	Power	1300 MWe
Primary system	Loops	2 (1 : 3)
	Total volume	0.6 m^3
	Scaling factor	1 : 700
Core	Power	5.28 MWe
	Length	3.9 m
	Number of rods	64
	Matrix	8 × 8 square
	Heater rod OD	10.75 mm
	Pitch	14.3 mm
	Electrical heating	Direct
Vessel downcomer	Configuration	Annular
	Gap width	MOD1: 50 and 12 mm
		MOD2: 12 mm
Steam generators	Type	U-Tubes
	Number of tubes	1-Loop SG: 8
		3-Loop SG: 24
Main coolant pumps	Type	Centrifugal
	Specific speed (DIN)	29.2
Operational conditions	Primary system pressure	15.8 MPa
	Core temperatures	294/326°C inlet/outlet
	Secondary system pressure	6.4 MPa
	SG temperatures	210/280°C inlet/outlet
Organisation	EC joint research centre	Ispra, Italy

a basically one-dimensional thermal-hydraulic response, components high surface area to fluid volume ratio, and large metal mass to fluid volume ratio. The structural stored energy and system heat losses are important contributors to distortions in those components, such as the reactor pressure vessel and steam generator downcomers, where the coupling between wall heat transfer and fluid flow is at time dominant.

System heat losses may significantly influence primary as well as secondary side energy removal especially during the long-term phase of a small break LOCA or intact circuit fault simulations. The LOBI test facility exhibits larger heat losses relatively to the reference plant due to design (higher surface area to volume ratio of fluid retaining components) and operation constraints (main coolant pump seal and instrument cooling); typically, heat losses in a full size plant account for about 0.05% of the nominal thermal power whereas in the LOBI test facility it accounts for about 1.5%.

All in all, the experimental results acquired in the LOBI test facility cannot be directly extrapolated to full-size plants; they provide, however, a reference data base for the understanding of governing thermal-hydraulic phenomenologies and for the assessment of the predictive capabilities of system codes used in water reactor safety analysis.

5. Project Evolution

The LOBI project has evolved over a time period which has seen a very intensive international effort in reactor safety research and development. In the early '70 s, the level of understanding of LOCA phenomenologies and the attendant computational capabilities were rather primitive. A very limited experimental data base from integral system tests conducted in an initial, very crude configuration of the USNRC semiscale test facility and early one-dimensional versions of system codes such as RELAP were available.

Since then, a very large experimental data base has been gathered in several integral system test facilities, and the computational capabilities have matured encompassing a number of best-estimate codes such as RELAP, TRAC, ATHLET, and CATHARE. In the meantime, two major reactor accidents occurred in TMI-2 (March 1979) and Chernobyl (April 1986) power plants which have had a significant impact on the deployment of nuclear reactor technologies.

5.1. Execution of the MOD1 Programme. The LOBI test facility became fully operational in December 1979 with the execution of the first 200% cold leg break LOCA experiment which was used for an international pretest prediction exercise (PREX). Early in the programme and in response to the TMI-2 accident which occurred in March 1979, new research priorities were formulated to emphasize small break LOCA and special transients tests in the follow-up programme.

After the execution of an initial test series and due to experimental evidences on the atypical influence of the large downcomer (and hence large vessel water inventory) on the system thermal-hydraulic response, the original 50 mm gap width downcomer was replaced with a downcomer having a smaller 12 mm gap width (and hence better scaled vessel water inventory), Figures 3 and 4. In the meantime, while the small downcomer was being procured, an interim test programme was carried out to assess test reproducibility, break geometry, and size effects on the course of a large break LOCA.

The experimental programme with the small 12 mm downcomer was initiated in March 1981 with test A1-66, a 200% cold leg break LOCA with cold leg ECC injection. The LOBI-MOD1 experimental programme was then concluded in June 1982. From December 1979 to June 1982, 28 experiments were carried out including 25 large break LOCA and 3 small break LOCA tests.

5.2. Execution of the MOD2 Programme. After extensive modifications to the test facility, the experimental programme was resumed in April 1984 with the facility in the MOD2 configuration. The first small break LOCA test, a 1% cold leg break LOCA which was used for the OECD-CSNI International Standard Problem 18, was performed in

Table 2: LOBI-MOD1 and LOBI-MOD2 test matrix.

Test	Date	Definition	Objectives	Phenomenologies
LOBI-MOD1: Downcomer width 50 mm				
A1-04	12.12.79	Germany	200% CL break LOCA ECC-AIS in CL, first test in power ascension series, 1.8 FPS, PREX test	DNB, early rewet, dryout, final rewet, system performance at low power
A1-01	29.01.80	Germany	200% CL break LOCA ECC-AIS in CL+ HL, second test in power ascension series, 3.0 FPS	DNB, early rewet, dryout, final rewet, oscillatory refill behaviour, DEGB partially communicative
A1-02	14.02.80	Germany	200% CL break LOCA ECC-AIS in CL + HL, third test in power ascension series, 8.2 FPS	DNB, early rewet, dryout, final rewet, oscillatory refill behaviour
A1-03	19.03.80	Germany	200% CL break LOCA ECC-AIS in CL + HL, fourth test in power ascension series, 8.8 FPS, power off from 3.2 s to 5 s	DNB, early rewet, dryout, final rewet, oscillatory refill behaviour
A1-04R	17.04.80	Germany	200% CL break LOCA ECC-AIS in CL, Counterpart to A1-04 at nominal power 10.2 FPS, baseline CL LOCA	DNB, early rewet, dryout no final rewet before power shutoff, no sustained oscillation during refill
A1-05	06.05.80	Germany	200% CL break LOCA ECC-AIS in CL + HL Counterpart to A1-04R, namely, AIS mode Enhanced AIS injection, 10.2 FPS	DNB, early rewet, dryout No effective improvement of AIS performance, oscillatory refill behaviour
SD-SL-01	04.06.80	Germany	10% CL break LOCA ECC-AIS in CL, first test of the small break LOCA scoping series, instrumentation response to slow transients Link between small and large break LOCAs	No degradation of core heat transfer
SD-SL-02	04.06.80	Germany	1% CL break LOCA ECC-AIS in CL, second test of the small break LOCA scoping series Secondary 100 K/h cooldown	Flow to break mainly from vessel side, flow from pump side impeded due to closure of break valve, no degradation of core heat transfer
SD-SL-03	24.09.80	Germany	0.4% CL break LOCA, ECC-AIS in CL, third test of the small break LOCA scoping series Secondary 100 K/h cooldown,	No degradation of core heat transfer, natural circulation and reflux condenser heat transport detected
A2-59	27.10.80	Germany	100% CL break LOCA ECC-AIS in CL, first test of interim matrix, system response to communicative break	DNB, early rewet, dryout, final rewet, clear bottom-up rewet trend, response similar to DEGB
B-101	26.11.80	France	$2 \times 50\%$ CL break LOCA ECC-AIS in CL, second test of the interim matrix, influence of noncommunicative break configuration	DNB, early rewet Comparison of B-101 with A2-59 precluded by difference in power load
A2-55	19.01.81	Germany	50% CL break LOCA ECC-AIS in CL, third test of the interim matrix, system response to intermediate large break sizes	DNB and early rewet only at core upper levels, thereafter, effective core cooling prevailed over the whole core
A2-59R	11.02.81	Germany	100% CL break LOCA ECC-AIS in CL, fourth test of interim matrix, counterpart to A2-59 with respect to reproducibility	A2-59R and A2-59 system thermal-hydraulic response similar, MOD1 reproducibility confirmed

Table 2: Continued.

Test	Date	Definition	Objectives	Phenomenologies
B-R1M	17.03.81	Germany	25% CL break LOCA ECC-AIS in CL, fifth test of the interim matrix, system response to small large break sizes	Core thermal response followed prevailing system saturation temperature, no core thermal excursions tendency to loop seal formation
LOBI MOD1: Downcomer width 12 mm				
A1-66	03.07.81	Germany	200% CL break LOCA ECC-AIS in CL, baseline test, counterpart to A1-04R with respect to downcomer width	DNB, early rewet at core bottom and top dryout, no conclusive rewet observed, CCFL and hot wall delay effects in downcomer
A1-07	09.07.81	Germany	200% CL break LOCA ECC-AIS disabled System response with no ECCS Baseline test for ECCS injection mode	DNB, early rewet at core bottom and top ends, dryout, rod temperatures high after power shutoff
A1-06	21.07.81	Germany	00% CL break LOCA ECC-AIS in CL + HL System response to combined ECCS injection, Baseline test with respect to ECC injection mode	DNB, early rewet at core bottom and top ends, dryout, heater rod temperature turnaround after ECC injection starts, no clear definite rewet
A1-67	30.09.81	Germany	25% CL break LOCA ECC-AIS in CL + HL System response to intermediate break Break size test series	Delayed dryout at core mid and upper elevations, rewet, response tendency towards small break LOCA features, loop seal formation and clearout
A1-68	28.10.81	Germany	50% CL break LOCAECC-AIS in CL + HL System response to intermediate break Break size test series	DNB, rewet, clear top-down rewet behaviour
A1-10A	25.11.81	Germany	200% HL break LOCA ECC-AIS in HL + CL System response to hot leg break Break location test series, Low core power	DNB, rewet only at core, mid, and upper elevations, hot leg ECC core penetration hindered by sustained positive core flow, CCFL at core exit
A1-10B	10.12.81	Germany	200% HL break LOCAECC-AIS in HL + CL System response to hot leg break Break location test series Nominal core power	DNB, rewet limited at core upper elevations, higher peak cladding temperatures with respect to A1-10A, CCFL at core exit
A1-70	13.01.82	Germany	200% PS break LOCA ECC-AIS in CL + HL System response to pump suction break, Break location test series	DNB, rewet, less severe overall core heat transfer degradation with respect to similar cold and hot leg break DEGB-LOCA
A1-73	04.02.82	Germany	25% HL break LOCA AIS in CL + HL System response to hot leg small large break LOCA Break size and location test series	No core heat transfer degradation, heater rod temperatures at the prevailing system saturation temperature
A1-72	24.03.82	Germany	200% CL break LOCA ECC-AIS in CL + HL influence of pump operation mode, pump countdown delayed off, pump head simulation	DNB, early rewet, dryout, enhancement of initial recovery of positive core flow, lower peak cladding temperatures with respect to A1-06
A1-69	06.04.82	Germany	100% CL break LOCA ECC-AIS in CL + HL System response to intermediate break LOCA, break size effect test series	DNB, early rewet, dryout, final rewet, typical DEGB LOCA blowdown features, preferentially top-down rewet observed

Table 2: Continued.

Test	Date	Definition	Objectives	Phenomenologies
A1-74	21.04.82	Germany	200% CL break LOCA ECC-AIS in CL + HL System response to ECCS injection in both intact and broken loop, counterpart to A1-72	DNB, early rewet, dryout, no discernible impact on overall system response from the addition of ECC injection into broken loop
B-222	05.05.82	France	100% CL break LOCA ECC-AIS in CL Noncommunicative (2 × 50%) CL break configuration, counterpart to B-101 with respect to downcomer size	DNB, early rewet, dryout, limited effectiveness of cold leg ECCS injection
B-302	16.0.82	Italy	100% HL break LOCA ECC-AIS in CL Noncommunicative (2 × 50%) HL break configuration	Dryout at core mid and upper elevations, rewet, positive core flow throughout the whole transient, enhanced refill and effective core cooling
LOBI-MOD2: Downcomer width 12 mm, shell and U-tube steam generators				
A1-76	12.04.84	Germany	SG performance under primary forced circulation, variation of secondary inventory, and core power: (i) flooding of SG coarse separator at nominal core power (ii) flooding of SG coarse separator at 50% core power and reduced secondary water level (iii) boiloff of SG SS at 10% core power	Data on coarse and fine separator efficiency, variation of recirculation ratios, void distribution in the SG riser region, and degradation of SG heat transfer
A2-81	27.09.84	Germany	1% CL break LOCA ECC- HPIS in CL, AIS off Secondary cooldown at 100 K/h First test of the small break LOCA test series, OECD International Standard problem 18 (ISP 18)	Coupling of primary and secondary systems depressurisation, 2 phase NC and reflux condenser heat transport, flow separation and stratification in horizontal pipes liquid holdup in hot legs and SG U-tubes
A1-82	28.09.84	Germany	1% CL break LOCA ECC-HPIS in HL, AIS in HL + CL Secondary cooldown at 100 K/h Counterpart to A2-81 relatively to HPIS location	Coupling of primary and secondary systems, 2 phase NC and reflux condenser heat transport, low subcooling in pressure vessel downcomer, reduced ECC bypass to the break
A1-78	24.10.84	Germany	2% CL break LOCA ECC-HPIS in HL, AIS in HL + Cl Secondary cooldown at 100 K/h Test of the break size effect test series	Decoupling of primary and secondary systems, reverse SG heat transfer, voiding in SG U-tubes and liquid holdup in hot legs, loop seal formation, and core liquid level depression
A2-77A	28.11.84	Germany	Characterization of NC and reflux condenser heat transport mechanisms at a primary system pressure of 90 bar and 70 bar, (i) 90 bar: 1 and 2 phase NC and reflux condenser (ii) 70 bar: 2 phase NC and reflux condenser	NC heat transport mechanisms characterized as function of primary system mass inventory, minimum mass inventory of c. 45% at c. 3% of core power to sustain effective reflux heat transport and prevent core heat transfer degradation, oscillatory transition from 2 phase NC to reflux
A1-83	19.12.84	Germany	10% CL break LOCA ECC-HPIS in HL, AIS in HL + CL Secondary cooldown at 100 K/h, larger of the small break size effect test series	Decoupling of primary and secondary systems, early voiding of SG U-tubes and hot legs, initial core dryout and rewet coupled to loop seal formation and clearout, second core dryout, and rewet coupled to mass inventory boiloff and AIS injection

Table 2: Continued.

Test	Date	Definition	Objectives	Phenomenologies
A2-90	27.03.85	Germany	LONOP-ATWS or "SBO" Anticipated transient caused by loss of offsite and normal onsite electrical power with failure to SCRAM (i) boiloff of SG secondary system down to a level of c 1 m above tube plate, (ii) SG refill and cooldown at 100 K/h	Pressure increase in primary and secondary systems, fluid discharge from pressurizer PORV and SG SRV, pressurizer insurge/outsurge, SG heat transfer degradation, recovery of primary to secondary heat transfer, 1 and 2 phase NC
A1-85	07.05.85	Germany	0.4% pressuriser break LOCA ECC-HPIS in HL, AIS in HL + CL Secondary cooldown at 100 K/h, test of the break location effect series	Coupling of primary and secondary systems depressurisation, pressurizer insurge, primary system overfeeding
BL-00	03.07.85	France	0.4% CL break LOCA ECC- HPIS in CL Secondary cooldown at 57 K/h First test of the EC B test matrix	Primary and secondary systems thermally coupled, liquid holdup in SG U-tubes, stratification in horizontal pipework, Thermal nonequilibrium downstream ECC injection points, 2 phase and reflux condenser heat transport, primary overfeeding and refill, no core dryout
A1-84	14.10.85	Germany	10% HL break LOCA ECC-HPIS in HL, AIS in CL + HL Secondary cooldown at 100 K/h Test of the break location effect test series, counterpart to A1-83	Decoupling of primary and secondary systems depressurisation, early voiding of SG U-tubes and hot legs, holdup and CCFL at core exit, ECC penetration and flow channelling
BT-00	30.11.85	UK	LOFW with primary feed and bleed (i) loss of main feedwater and SG boildown to c. 1 m (ii) loss of auxiliary feedwater and SG dryout (iii) long-term cooldown via primary feed and bleed	SG boil-off and heat transfer degradation, PORV and SRV fluid discharge, pressurizer insurge/outsurge, PORV flow compensation via HPIS flow, primary system refill, verification of *Feed and Bleed* as an accident management procedure
BT-01	24.01.86	Belgium	10% SLB with pressurised thermal shock (PTS) and plant recovery procedure (i) small steam line break transient (ii) establishment of PTS conditions (iii) accident mitigation and recovery	SG secondary blowdown and heat transfer, primary system cooldown rate, pressurizer insurge/outsurge, downcomer temperature stratification, primary depressurization via pressuriser PORV cooling system and mass inventory control via HPIS injection
BL-02	22.03.86	UK	3% CL break LOCA ECC-HPIS in CL, AIS in CL SCS cooldown at 56 K/h Test of the break size effect test series	Primary and secondary systems decoupled, SG heat transfer reversed, formation and clearout of loop seal, no core dryout
A1-79	15.05.86	Germany	1% CL break LOCA HPIS in HL, AIS off Secondary cooldown at 100 K/h Effect of high (4/4) HPIS injection rate	Coupling of primary and secondary systems cooldown, primary system overfeeding, NC heat transport hindered by condensation in hot legs and upper plenum induced by high HPIS rate
A1-88	11.06.86	Germany	0.4% CL break LOCA ECC-HPIS in HL, AIS off SCS cooldown at 100 K/h in IL-SG Asymmetric cooldown of secondary system	Primary system pressure coupled to isolated SG, pressurizing effect of isolated SG, primary system depressurization, break flow compensated by HPIS flow

Table 2: Continued.

Test	Date	Definition	Objectives	Phenomenologies
BL-01	20.09.86	Germany	5% CL break LOCA ECC-HPIS in HL, AIS on secondary cooldown at 100 K/h Test of the break size effect test series	decoupling of primary and secondary systems, SG reverse heat transfer, clearout of intact loop seal, liquid holdup in HL
BC-01	18.10.86	JRC	SG secondary mass inventory determination LOBI-MOD2 characterization test	SG mass inventory determined at various power levels, relationship of SG mass versus downcomer water level determined
BC-02	26.11.86	JRC	SG heat losses determination LOBI-MOD2 characterization test	SG heat losses determined via (i) steady-state method balancing core power (ii) cool-down method SG heat losses unacceptably high: ILSG—24 kW, BLSG—18 kW, need improvement of thermal insulation
BL-21	24.01.87	Italy	steam generator tube rupture (SGTR) break Size 0.4%, ascending side Intentional PCS depressurization through PORV and AIS actuation as recovery procedure	Break and PCS depressurization, natural circulation and reflux condenser heat transport, core uncovery and dryout, PORV discharge, AIS actuation and core rewet
BL-12	19.02.87	France	1% CL break LOCA ECC-HPIS off, AIS in CL SCS cooldown off, system response with degraded safety systems	core uncovery and dryout at high PCS pressure, phase separation and stratification, thermal nonequilibrium downstream AIS location, loop seal formation and clearout, core rewet
BT-02	09.05.87	France	LOFW + LOAF (loss of main and auxiliary feedwater) PCS bleed and feed as recovery procedure	SG boiloff and heat transfer degradation, PCS heatup and pressurization, pressurizer insurge/outsurge, PORV discharge and HPIS compensation, recovery of PCS inventory
BT-12	17.06.87	UK	steam line break (SLB) Break size 100% (orifice limited) SCS break size effect and location test series	Faulted SG depressurization, break flow and steam line carryover, faulted SG heat extraction, reverse heat transfer in unaffected SG, pressurizer behaviour, PCS overcooling and thermal stratification
A1-91	26.09.87	Germany	1% CL break LOCA ECC-HPIS in HL, AIS off Secondary cooldown at 100 K/h Effect of low (1/4) HPIS injection rate	PCS and SCS thermal coupling, core thermal response with reduced HPIS capacity, core liquid level depression, loop seal formation, no core dryout at reduced HPIS capacity
BT-03	24.10.87	Italy	loss of feed water-anticipated transient without SCRAM (LOFW-ATWS) PCS passive recovery procedure	PCS heat up and pressurization, PORV and SRV discharge, voiding and refill of SG, pressurizer insurge/outsurge, intentional PCS depressurization and AIS actuation, core dryout
A1-92	30.11.87	Germany	Characterization of NC and reflux condenser heat transport at a primary pressure of 40 bar, 1 and 2 phase NC and reflux condenser, Counterpart to PKL test AC.1	NC and reflux condenser heat transport mechanisms as function of primary mass inventory, minimum mass inventory to sustain reflux condenser and prevent core heat transfer degradation c. 45%, rather stable transition from 2 phase NC to reflux condenser

Table 2: Continued.

Test	Date	Definition	Objectives	Phenomenologies
BL-16	19.03.88	Germany	0.4% small break LOCA ECC- HPIS in HL, AIS off SCS cooldown in BLSG at 100 K/h, MCPs off and restart	Asymmetric SCS cooldown, pressurizing effect of isolated SG, thermal homogenisation and fluid redistribution following MCPs restart
BC-03	15.04.88	JRC	SG heat losses determination LOBI-MOD2 characterization test	Measurement of SG heat losses after improvement of thermal insulation (ref.: BC-02) ILSG: 6.8 kW, BLSG: 5.0 kW
A1-93	30.04.88	Germany	2% CL break LOCA, HPIS off, AIS on secondary system cooldown at 100 K/h, accident management procedure, pressurizer PORV on high core heater rod temperature	Decoupling of primary and secondary systems, loop seal formation and core level depression, core dryout and AIS injection, enhancement of primary depressurization and AIS actuation through intentional opening of pressurizer PORVs
A1-94	27.05.88	Germany	4% CL break LOCA at 40 bar, HPIS off, AIS on, OBI counterpart to PKL test, secondary system cooldown at 100 K/h, AIS on at high core heater rod temperature	Core uncovery and dryout, AIS injection and core rewetting, verification of PKL-III pressure scaling concept
BC-04	07.02.89	JRC	Core bypass flow measurement LOBI-MOD2 characterization test	Determination of upper plenum to upper downcomer flow bypass: c. 3% of core flow
BL-30	15.04.89	JRC	5% CL break LOCA, HPIS in CL, AIS in CL, SCS cooldown at 100 K/h, test of the break size effect test series	Primary depressurization at a moderate rate, primary and secondary systems thermally decoupled, loop seal formation and clearout
BL-22	17.06.89	Belgium	SGTR: Steam generator tube rupture (0.4%) accident initiation and mitigation phases	Break flow, overfilling of affected SG and SRV discharge, autostabilizing mechanism for break flow when affected SG level reaches U bend elevation, verification of emergency operating procedures
A1-87	11.11.89	Germany	Cooldown transient, LOBI counterpart to PKL-III test	1 phase NC under saturated conditions, upper head steam bubble formation and propagation, SG heat transfer
BT-04	0.02.90	France	Cooldown transient under asymmetric conditions, BLSG isolated, ILSG cooldown at 56 K/h	Reverse heat transfer in isolated SG, pressurizing effect of isolated SG, flow reversal in secondary of isolated SG
BL-34	22.03.90	JRC	6% CL break LOCA, HPIS off, AIS on at 40 bar, initial conditions scaled to low power (10%), SCS cooldown disabled, counter part test to BETHSY, LSTF and SPES	Sequence of 3 core thermal excursions (1) dryout and rewet due to loop seal formation and clearout, (2) dryout due to boiloff and rewet due to AIS, (3) dryout due to depletion of AIS injection and rewet due to LPIS injection
BL-44	26.04.90	JRC	6% CL Break LOCA, HPIS off, AIS on at 40 bar, initial conditions scaled to full power (100%), SCS cooldown disabled, Counter Part Test to BL-34 (full power-low power)	Phenomenologist similar to BL-34, sequence of 3 core dryout/rewet phases, first dryout less extensive due to less pronounced core liquid level depression
BT-56	03.07.90	UK	Multiple failure transient evolving from an original LOFW: isolation of ILSG, MCP power off, SCRAM failure, PCS blowdown through upper plenum due to rupture of the safety disk	PCS heat up and pressurization, pressurizer insurge/outsurge, primary and secondary systems decoupled, dryout at high pressure, blowdown of the PCS through a relatively large break in upper plenum represented by the rupture disk opening

Table 2: Continued.

Test	Date	Definition	Objectives	Phenomenologies
BT-15/16	22.11.90	UK	LOFW: loss of feed water with MCP on (BT-15), SG boiloff and refill with MCPs off (BT-16)	BT-15: SG boiloff and heat transfer degradation with MCPs on, primary system heat up, reestablishment of SG heat transfer following AFW actuation, BT-16: SG boiloff and heat transfer degradation with MCPs off, natural circulation in PCS, SG refill
BT-17	07.02.91	Germany	LOFW; loss of feed water and secondary feed and bleed recovery procedure Intentional PCS depressurization from upper plenum	SG boiloff, PCS heat up and pressurization, pressurizer insurge and PORV discharge, SCS blowdown and PCS depressurization due to condensation in SG U-tubes, PCS depressurization from upper plenum, pressurizer outsurge, core dryout and partial rewet
BT-06	21.03.91	France	FLB: feed line break (10%) MCPs on, AFW on in ILSG MCPs off and asymmetric natural circulation in PCS with a voided SG	Blowdown and heat transfer from faulted SG, break flow fed from different flow paths, residual heat removal by unaffected SG, pressurizer insurge/outsurge
BL-40	16.05.91	Spain	SGTR: steam generator tube rupture in 1-loop PWR (Jose' Cabrera NPP), E-3 emergency recovery procedures	Break flow, PCS natural circulation, PCS depressurization and control of subcooling margin and pressurizer level cycling PORV and HPIS flow
BL-06	21.06.91	UK/France	1% CL break LOCA, HPIS off, AIS on at 40 bar, SCS cooldown as in BL-12, MCPs on, effect of MCP on/off issue	PCS depressurization with MCPs on, core dryout and rewet, PCS pressure stagnation, termination of AIS injection, depressurization from PORV and actuation of LPIS

ATWS: anticipated transient without scram; AIS: accumulator injection system; BL: broken loop; CL: cold leg; CCFL: counter current flow limitation; DEGB: double ended guillotine break; DNB: departure from nucleate boiling; ECC: emergency core cooling system; FLB: feed line break; FPS: full power seconds; HL: hot leg; HPIS: high pressure injection system; IL: intact loop; LPIS: low pressure injection system; LOCA: loss of coolant accident; LOFW: loss of feed water; LONOP: loss of offsite and normal onsite power; MCP: main coolant pump; NC: natural circulation; PCS: primary cooling system; PORV: power operated relief valve; SCS: secondary cooling system; SRV: safety relief valve; SGTR: steam generator tube rupture; SLB: steam line break; SBO: station break out.

September 1984 and the first special transient test case (A2-90) simulating a "Station Blackout" transient was performed in March 1985. The first MOD2 test of the Community programme, a 0.4% cold leg break LOCA specified by the French representatives in the LOCA Programme Task Force was executed in July 1985.

As the LOBI-MOD2 experimental programme was evolving, the catastrophic Chernobyl accident took place in April 1986; this, however, due to the peculiarities of the RBMK reactor type accident had no significant impact on the LOBI-established research priorities.

The last experiment of the BMFT contractual programme was executed in November 1989 with the termination of the CEC-BMFT contract in December 1989. Thereafter, the experimental programme was exclusively dedicated to the execution of tests from the Community matrix. With the execution in June 1991 of test BL-06, a 1% cold leg break LOCA designed to address the pump on-off issue, the execution of the envisaged LOBI experimental programme was successfully concluded. Significant signatures of small break LOCA tests and special transients are depicted in following Figures 5, 6, 7, and 8.

5.3. International Collaboration. The international context in which the LOBI research programme has been carried out has offered an opportunity for a close collaboration among delegates of national research laboratories. It has also provided an independent forum for the exchange of concerns and expertise among the participants contributing thus to the harmonization of national views on reactor safety-related matters.

5.3.1. Counter Part Test Programme. Large system codes used in reactor safety analysis are generally benchmarked against experimental data from scaled integral system or separate effect test facilities; comparison of code-predictive capabilities of simulated accidents or transients in full-size plants would be desirable, but this is, clearly, prohibitive for obvious economic and practical considerations. Controversy, thus, arises when the predictive capability of a system code is scaled up from a small size test facility to the full-size real plant.

It is, therefore, desirable although not strictly required to assess code predictive capabilities against a set of data obtained from different scale test facilities under similar initial and boundary conditions. This, to a certain extent, would

decouple the assessment process from physical assumptions emphasizing, instead, the relevance of the geometrical scaling parameters especially on the qualitative rather than quantitative evolution of the thermal-hydraulic phenomenologies.

Within this context, a number of tests of the MOD1 and MOD2 experimental programmes were defined and executed as counter part to similar tests performed in other test facilities such as Semiscale, PKL, BETHSY, LSTF, and SPES. The collaboration has also been extended to posttest analysis of the results.

5.3.2. International Standard Problems Prediction Exercises. The very first test of the LOBI-MOD1 experimental programme, test A1-04, was used for a special type of blind standard problem exercises, the LOBI preprediction exercise (PREX); 16 participants from various EC member states and the USA submitted calculations using a number of system codes.

The first small break LOCA test of the LOBI-MOD2 experimental programme, test A2-81, was designated by the Committee on the Safety of Nuclear Installations (CSNI) of the Organization for Economic Cooperation and Development (OECD) as International Standard problem 18 (ISP-18); 27 participants from European and North American organizations provided prediction calculations with 12 codes or code versions.

6. Management of the Experimental Data Base

Management of research data is an issue being debated at the national and international levels by industrial, institutional, professional, and academic research organisations; specifically, preservation and archive as well as access and retrieval of research data are seen as underlying principles of good scientific practices especially in the governance of publicly funded research programmes.

The European Science Foundation (ESF) has addressed the issue of data accumulation, handling and storage in its policy briefing on Good Scientific Practices In Research and Scholarship [1] recommending:

> *data are produced at all stages in experimental research and scholarship. Data sets are an important resource, which enable later verification of scientific interpretation and verification. They may also be the starting point for further studies. It is vital, therefore, that all primary and secondary data are stored in a secure and accessible form.*

Archival and dissemination of research data has also been addressed inert alias in the Berlin Declaration [2] promoted by the Max-Planck Gesellschaft (MPG) together with representatives from several international research organisations who have recommended:

> *our mission of disseminating knowledge is only half complete if the information is not widely and readily available to society. New possibilities of knowledge dissemination not only through the classical form but also and increasingly through the open access paradigm via the Internet have to be supported.*

Since the inception of the LOBI project, it was anticipated that a proper data analysis and documentation management system would be of fundamental importance in order to ensure that over time the investment of public resources would be beneficial for the nuclear community at large. In view of the continuous advancement of computer hardware and software technologies that are making storage/retrieval techniques rapidly obsolete, particular attention has been placed on conversion of old format onto new media and machines enabling potential users to access and retrieve the data. Currently, the LOBI analytical and experimental data base can be accessed via Internet at http://asa2.jrc.it/. Each experimental data set comprises the digital data file, the Quick look Report (QLR), the Experimental Data Report (EDR) and as appropriate the Test Prediction Report (TPR). As appropriate AVI or MPEG files showing temporal evolution of collapsed liquid levels are also available. The overall data base is complemented by Test Facility Description Reports and components as built drawings (Figure 9).

7. Conclusions

The LOBI Project has represented an important contribution to reactors thermal-hydraulic safety research. A comprehensive data base relevant to the understanding of governing phenomenologies expected in PWR accident conditions and to the assessment of system codes used in water reactors safety analysis has been provided. As structured, the LOBI project has represented an effective approach to international collaboration in the field of reactor safety research and development. In addition, the EC-JRC context, in which the research programme has been carried out, has provided an independent forum for a systematic exchange of technical and scientific information among experts from EC member states and for sharing best practices in the field of water-cooled reactor safety analysis.

References

[1] European Science Foundation, "Policy briefing on good scientific practice in research and scholarship," 2000.

[2] Max-Plank-Gesellschaft, "Open access to knowledge in the sciences and humanities," 2003.

Hindawi Publishing Corporation
Science and Technology of Nuclear Installations
Volume 2012, Article ID 282987, 17 pages
doi:10.1155/2012/282987

Research Article

Trace Code Validation for BWR Spray Cooling Injection and CCFL Condition Based on GÖTA Facility Experiments

Stefano Racca[1] and Tomasz Kozlowski[2]

[1] *San Piero a Grado Nuclear Research Group (GRNSPG), University of Pisa, Pisa 56100, Italy*
[2] *Division of Nuclear Power Safety, Royal Institute of Technology, 100 44 Stockholm, Sweden*

Correspondence should be addressed to Stefano Racca, stefano.racca@dimnp.unipi.it

Received 10 March 2011; Accepted 22 June 2011

Academic Editor: Alessandro Del Nevo

Best estimate codes have been used in the past thirty years for the design, licensing, and safety of NPP. Nevertheless, large efforts are necessary for the qualification and the assessment of such codes. The aim of this work is to study the main phenomena involved in the emergency spray cooling injection in a Swedish-designed BWR. For this purpose, data from the Swedish separate effect test facility GÖTA have been simulated using TRACE version 5.0 Patch 2. Furthermore, uncertainty calculations have been performed with the propagation of input errors method, and the identification of the input parameters that mostly influence the peak cladding temperature has been performed.

1. Introduction

The development of thermal-hydraulic system codes (THSCs) began between the sixties and the seventies when conservative approaches have been used to demonstrate the safety margins necessary for the licensing and operation of a nuclear power plant (NPP). During these years, the improvements in computer technology and in computational methods have led to a new generation of THSC that can provide more realistic results without the need for conservative assumptions.

Nevertheless, the results of these advanced system codes are still affected by several kinds of uncertainties derived from many sources, for example, the modelling of the facility, the nonperfect understanding of some thermal-hydraulic phenomena, the approximation in numerical solution, the nodalization effect, and so on [1].

Therefore, it is necessary to perform a series of procedures for the code validation, using data deriving from integral test facility (ITF) or separate effect tests facility (SETF). Moreover, many methods for the evaluation of uncertainties have been developed in order to evaluate the reliability of any thermal-hydraulic code calculations, taking into account the possible sources of errors [1].

The aim of this work consists of validation of the U.S. NRC code TRACE for the spray cooling injection in a BWR reactor. The data from the Swedish GÖTA separate effect test facility are used and compared with the results derived from the modelling of the facility with the code. The study of the countercurrent flow limiting (CCFL) phenomenon and how it is modelled in the code is analysed with particular attention.

Furthermore, the propagation of input errors (PIEs) method is used to perform an uncertainty analysis on the code, and to identify which input parameters have the strongest influence on the figure of merit (peak cladding temperature).

2. Description of the Facility

The GÖTA test facility was located at the Studsvik Thermal Engineering Laboratory during the 70s. From 1975 to 1977, this facility was used to investigate the thermal hydraulics of typical ASEA-ATOM 8×8 BWR fuel bundles subjected to spray cooling from the top and reflooding from the bottom.

The layout of the test loop is schematically described in Figure 1. It consists mainly of two pressure vessels: a test vessel (left side of the figure) and a pressurizer (right side of

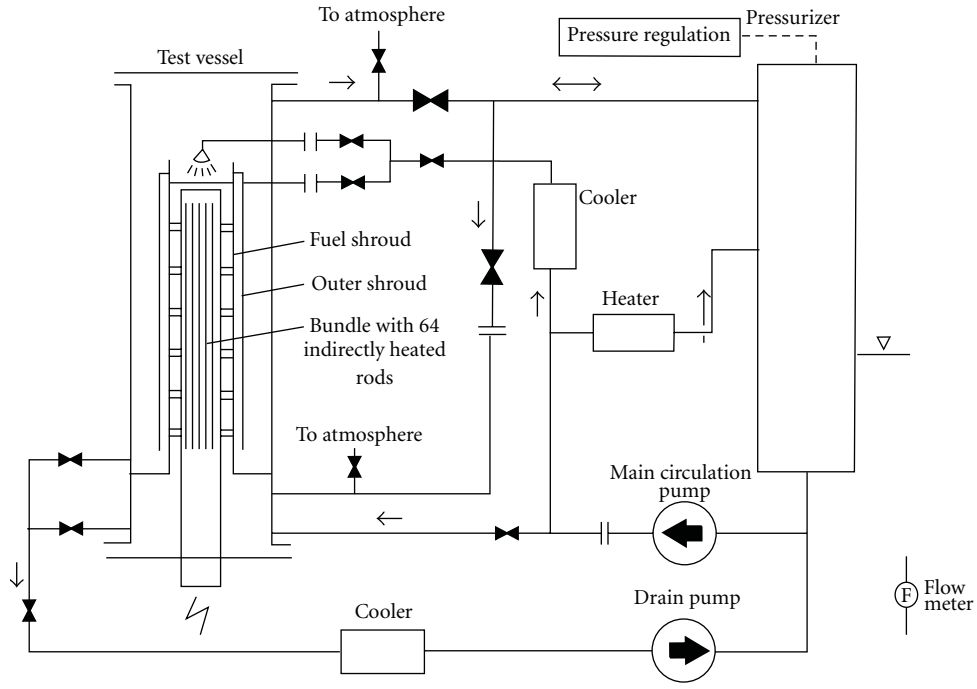

Figure 1: The GÖTA test loop.

the figure), which also form a water reservoir for the spray system in the loop.

The pressure was regulated by the injection of subcooled water into the steam present in the upper part of the pressurizer. The steam produced in the electrically heated evaporator was used to raise the pressure in the pressurizer.

The main circulation pump drove the water from the pressurizer vessel to a water cooler, which regulated the temperature of the water, and then to the spray injection systems in the test vessel. Before being injected, the water passed through two separate mass flow measuring devices, one for each spray system. One of the two spray systems injected water through a nozzle into the fuel bundle, while a spray ring delivered water equally to all the four sides of the square bypass channel.

The temperature of water was regulated by varying the water flow on the secondary line of the water cooler. However, any variation of the secondary flow affects the performance of the cooler, so it was quite difficult, in practice, to perform the experiments with the exact prescribed water temperature.

The water collected in the lower plenum below the bundle and the water outside the bundle canister was drained back directly to the pressurizer by two separate lines that operated automatically and independently.

The pressure regulation system was not used for experiments at atmospheric pressure. In these tests, steam produced was vented directly to the atmosphere. This significantly simplified the experimental procedure. The entire test loop has been design for a maximum pressure of 7 MPa, but most of the experiments have been conducted at atmospheric pressure [2].

In this paper, only the test bundle has been modelled and simulated with the TRACE code, and no attempt has been made to model the pressurizer and the other components of the loop. The system pressure and the water temperature in the spray lines have been set as the boundary conditions for the bundle.

2.1. The Test Bundle. The test bundle is located in the test vessel. It consists of 64 rods assembly positioned by spacers in a bundle channel (inner shroud or canister). The lower, nonheated part of the rods is extended out of the channel to a bottom flange where they are fixed. Forty rods have 5 thermocouples each, mounted on the inner side of the rod cladding.

The bundle channel is mounted "leak proof" in a flange in the pressure vessel. The flange separates the upper and the lower plenum; the water falling outside to the bundle is collected in the upper plenum, while the water moving down through the channel arrives in the lower plenum of the vessel. Two schemes of the test bundle are reported in Figure 2 in order to show the characteristic dimensions of the components and their position inside the test vessel.

Outside the bundle, there is an outer channel (Figure 2(e)) that simulates the bypass region in the reactor. The outer channel is also mounted on the flange that divides the lower and the upper core, but there are openings that allow the passage of water from the gap between the inner and the outer shroud to the remaining part of the upper plenum.

The bypass channel is cooled by the spray ring (Figure 2(a)) on the top of the vessel, and it is maintained in its position by 8 space supports mounted 100 mm below the bundle midplane (Figure 2(b)). The spray ring tube has 92

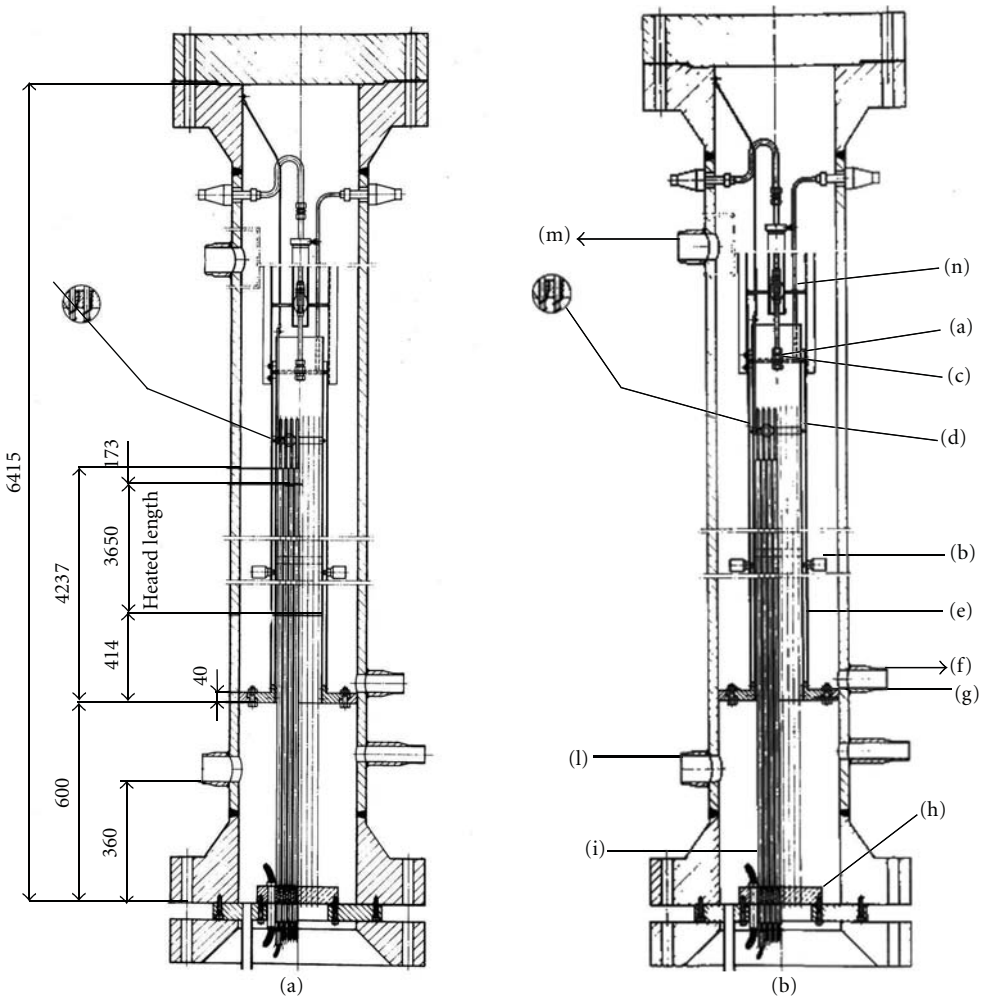

(a) Spray ring
(b) Space supports
(c) Spray nozzle
(d) Top grid
(e) Outer shroud
(f) Bypass channel outlet
(g) Flange separating upper and lower plenum
(h) Lower support plate
(i) Graphite seals for TC channels
(l) Internal channel outlet
(m) Steam vent
(n) Inner shroud (canister wall)

Figure 2: Section of the test bundle.

holes with 0.35 mm diameter drilled in various downward direction angles.

The spray nozzle (Figure 2(c)) for the injection in the bundle is mounted inside the inner shroud, and it ends 170 mm above the top grid (Figure 2(d)).

The inner channel is made of Zr-4 and has 40 thermocouples mounted on its four sides, placed in pockets drilled from the outside. The outer shroud is made of stainless steel and has 10 thermocouples mounted on two of its four sides.

The 64 heated rods are arranged in the original ASEA-ATOM spacers. The 7 spacers are mounted at a distance of 561 mm, with one spacer at the lower end of the channel. As the test bundle was dismantled after all the experiments, it was discovered that the spacers had moved during the test series.

The heaters, designed by Watlows Mfg Co, used an Inconel-600 clad and an inner coil (80% Ni and 20% Cr) embedded in a boron nitride matrix. Five thermocouples were drawn inside the cladding. The heater rod outer diameter is 12.25 mm, except for the three rods in each corner which have an outer diameter of 11.75 mm. A cross-section of the bundle, together with the cross-section of the heater rods, is shown in Figure 3.

The test bundle power supply is provided by two DC-converters coupled in series to achieve the necessary voltage. In order to guarantee the prescribed rod-to-rod power distribution, the heaters are divided in four groups. One of these groups is fed directly by the DC source, while the others are arranged in series with electrical resistances, one for each group. As preresistances, water cooled tubes are used. In this way, the net power supplied to the test bundle is limited to somewhat over 350 kW.

The experiments were run with time-dependent power in the bundle. The power decay curves were chosen to

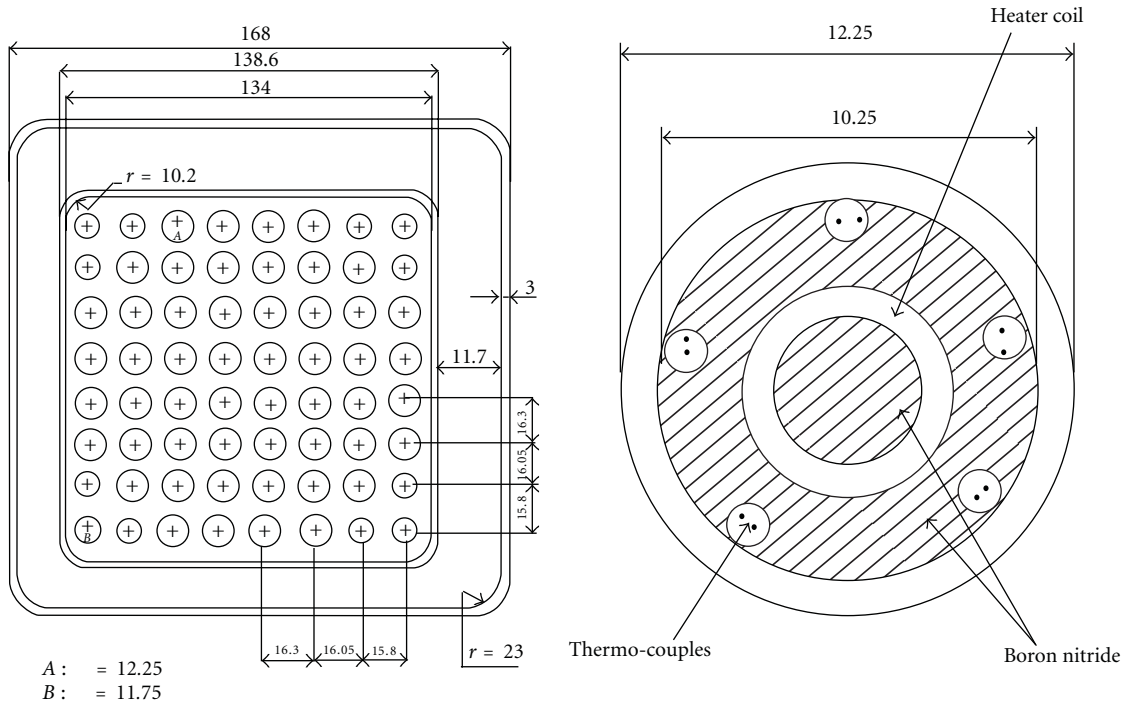

Figure 3: Cross-sections of the bundle and the heater rod.

correspond to the power decay in BWR during the spray cooling injection following a postulated LB-LOCA (large break loss of coolant accident). For a guillotine break on a recirculation line, this phase is calculated to occur approximately 15 seconds after the LOCA. The portion of the power generated by fission products has been calculated according to ANS 1971 decay heat standard plus 20%.

The power inside the channel is delivered in such a way that five different groups of rods can be distinguished. Each group presents a different power peaking factor with respect to the average value and a fixed axial power shape. The internal rod-to-rod power distribution is reported in Figure 4 (highlighting the various groups) together with the axial power profile and the location of the level where the experimental data are available.

2.2. The Test Number 78. Several tests have been carried out in this facility, with different initial conditions and with different configurations of the test loop. In these tests, one or two parameters were varied, while all the others were kept constant. In this paper, only the results of test number 78 will be considered, and compared with the TRACE code calculations.

The test number 78 was conducted on December 10, 1975. The test was started by adjusting the venting valves, the pressure, the spray flow rates, and the water temperature to their prescribed values. After closing the spray injection system, the rods were heated with a low constant power in order to dry all the surfaces (at around saturation temperature). Then, the bundle power was increased according to a predefined power curve until the prescribed initial peak cladding temperature (PCT) at the nominal power was reached. The physical parameters at the beginning of the experiment are listed in Table 1.

The spray system was then activated, and the power was decreased according to the ANS 1971 decay heat standard plus 20%. The water collected in the lower plenum and in the lower part of the bypass channel was drained by two separate lines in short and frequent periods, whenever the void fraction in these volumes fell below fifty percent [3].

The experimental data extracted from test number 78 were the temperatures for each rod group at five different heights. For each rod group and level, a range of temperatures and an average value of all the rods in the group are reported. It is important to note that this is a significant limitation for the correct understanding of the experiment and for the code simulation as it is not possible to identify the temperature evolution of one single rod. Furthermore, at certain levels and for certain groups the gap between the maximum and minimum measured temperature may be more than six hundred Kelvin, even if the cross section of the assembly is symmetrical in the radial direction.

However, the evaluation of an average temperature will be useful for the comparison with the TRACE code, because the TRACE results will be presented as an average temperature of all the rods in a group.

For the purpose of this work, it will be particularly important to verify the capability of the TRACE code to simulate the correct temperature behaviour in the midplane of each rod group (where the temperature reaches its maximum), in order to predict the peak cladding temperature

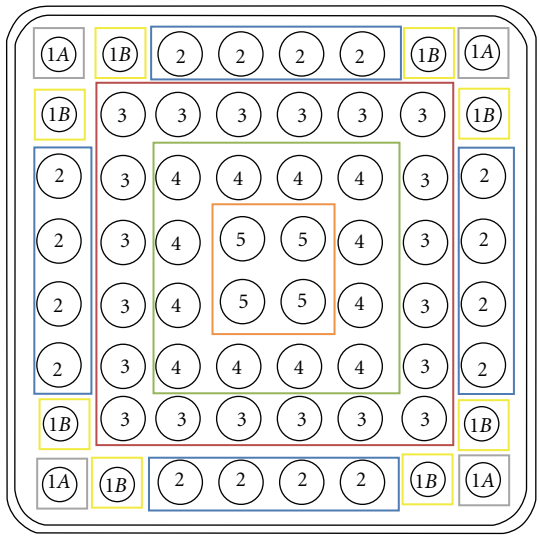

	Rod group	Peak factor
	1*A*	1.2
	1*B*	1.1
	2	1.1
	3	0.92
	4	0.9
	5	0.9

(a)

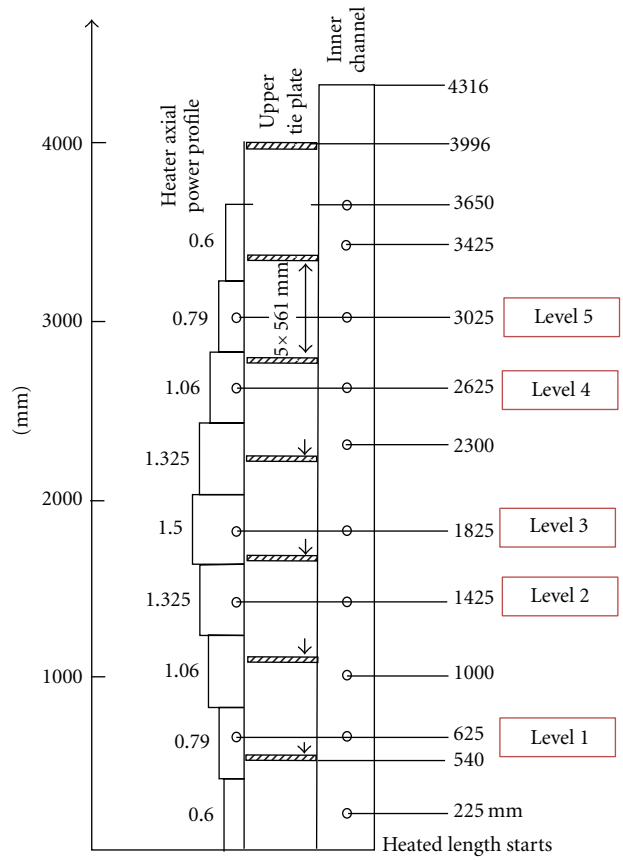

(b)

Figure 4: Internal rod- to-rod power distribution (a) and axial power shape (b).

Table 1: Test number 78 initial parameters.

Parameter	Nominal	Actual
Initial bundle power (kW)	300	303
Spray flow rate in the bundle (kg/s)	0.12	0.12
Fraction of the spray flow rate in the bypass (kg/s)	20%	20%
Pressure (MPa)	0.1	0.11
Initial peak cladding temperature (°C)	700	736
Spray water temperature (°C)	60	60
Steam venting	Top	Top

of the entire assembly, and the position where this value is reached.

3. Description of the Model

The simulation of the experiment has been carried out with the U.S. NRC code TRACE, version 5.0 Patch 2. The graphical SNAP interface has then been used to build the nodalization and to prepare model of the GÖTA experiment.

Two different models with different components have been tested. The first one uses two PIPE components to simulate the fuel assembly and the bypass channel, and eight heat structures (HTSTR component) representing the six rod groups (shown in Figure 4), the inner and outer walls.

The second model tested uses the CHAN component for the simulation of the fuel assembly (rods and canister wall) and a PIPE component for the bypass channel. The CHAN component has been designed with the specific purpose of simulating BWR fuel assembly. The nodalization diagrams of both models are shown in Figure 5.

The other elements of the GÖTA facility have been modelled using the same components for both models.

In particular, two FILL components have been used to represent the coolant spray injection system, which operates

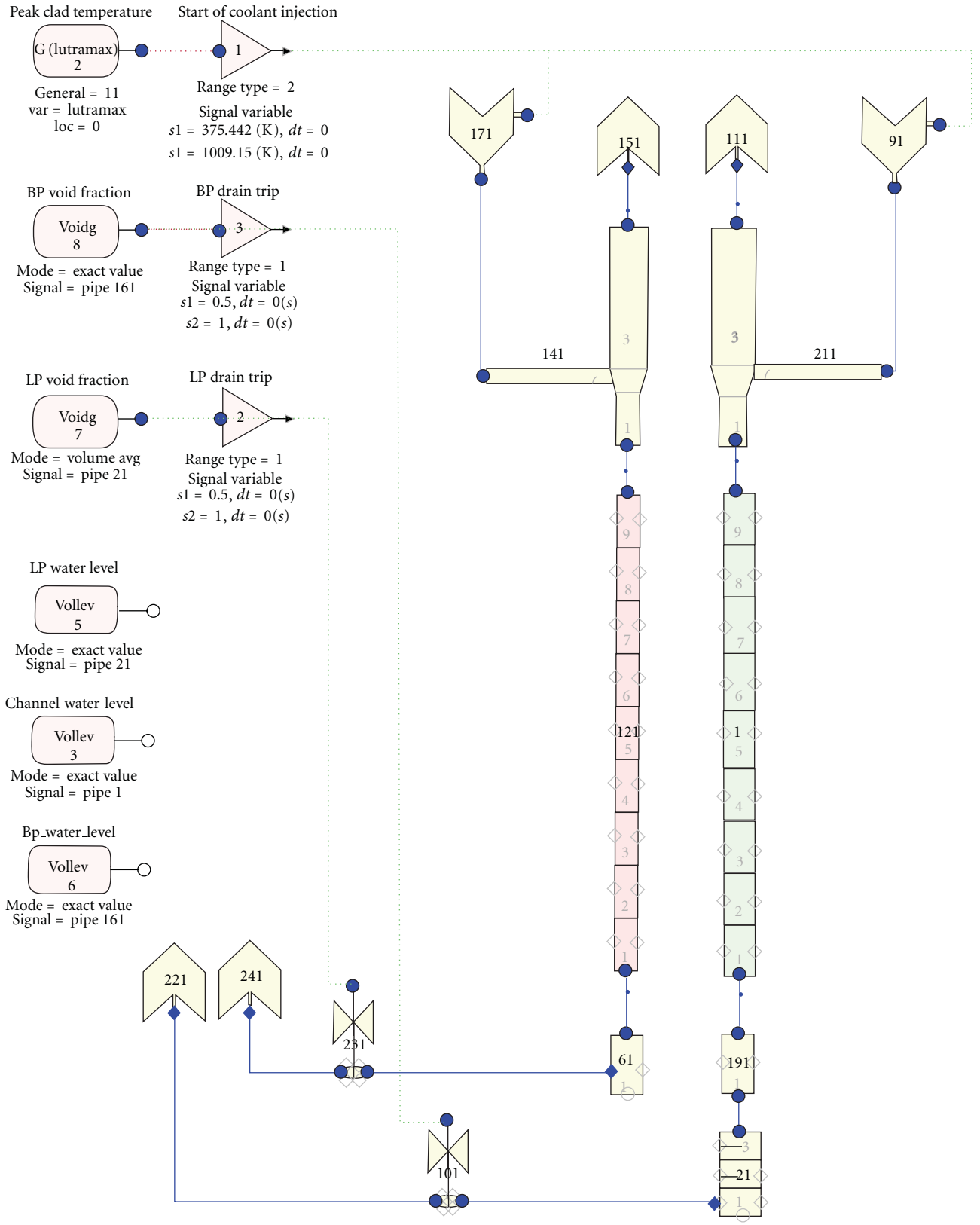

(a)

Figure 5: Continued.

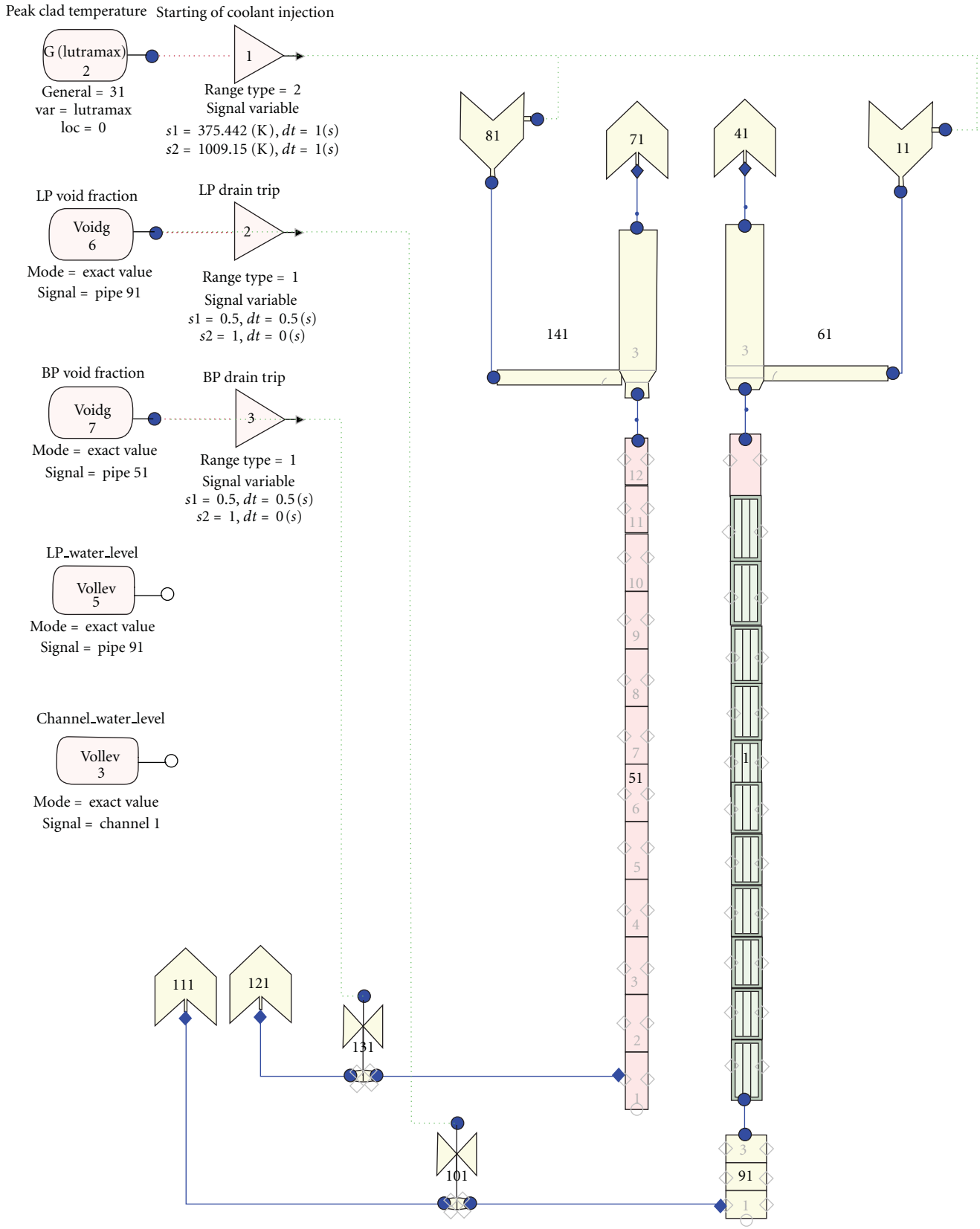

(b)

Figure 5: Nodalization diagrams for PIPE (a) and CHAN (b) models.

separately for the main channel and for the bypass channel, with two different values of the mass flow rate. The beginning of the spray injection is controlled by a TRIP block, which activates the coolant injection as soon as the peak cladding temperature (measured by another control block) reaches the prescribed value reported in Table 1.

The upper part of the bundle has been modelled using two BREAK components for the steam vent (one per each channel) and two TEE components that simulate the steam line and the spray cooling line.

A PIPE component has been used to simulate the lower plenum of the bundle. In the "PIPE model," another PIPE component has been used also for the simulation of the lower, unheated part of the channel, while in the "CHAN model," this section of the assembly is included directly in the CHAN component.

The water draining from the bottom of the test vessel has been modelled using two BREAK components. Two VALVE components connect the lower plenum and the lower part of the bypass channel to the BREAK components, respectively.

The opening and closing of the valves is controlled by two TRIP blocks. Each valve is initially closed, and it opens whenever the void fraction in the corresponding section of the test vessel falls below fifty percent.

Other control and signal blocks are added in order to check the behaviour of certain important parameters. In the nodalization diagrams shown in Figure 5, some signal blocks have been added to visualize the collapsed water level in the main channel, in the lower plenum, and in the lower part of the bypass channel.

3.1. Closure Models and Code Options. In order to improve the simulation, several code options and special models have been tested. TRACE code allows great flexibility in the modelling procedure, by allowing including or excluding certain code features by the user.

3.1.1. Fine Mesh Reflood and Axial Heat Conduction. As specified in the TRACE manual, the fine mesh reflood option has to be turned on whenever the calculation results in a significant dryout and heatup of the fuel rods. When this option is active, the HTSTR component has the capability to dynamically add or remove axial nodes during the TRACE calculation. This option produces more accurate prediction of the axial gradient at a quench front moving through a fuel assembly or a fuel rod.

Since this option increases the temperature gradients in the axial direction, the user should consider the activation of the "axial heat conduction" option. If this option is turned off, only heat conduction in the radial direction will be calculated.

The activation of these two options significantly improves the temperature prediction at most of all the axial levels. Turning off these options results in an excessive increase in the temperatures and absence of quench phenomena.

Nevertheless, two important issues related to these features have been found:

(1) increase in the computational time that can vary from few minutes to more than two hours;

(2) very fast quenching in the lower part of the channel (Level 1), which is not confirmed by the experimental data.

3.1.2. Radiation Model. The simulation of radiation heat transfer is very important for the correct representation of the GÖTA experiments. TRACE offers different possibility for the construction of the radiation model, and there are also differences depending on the model (PIPE or CHAN) used. In both cases, the TRACE radiation model requires the definition of all the surfaces involved, and for each surface, the emissivity, the view factors, and the beam lengths with respect to the other surfaces have to be defined.

However, the CHAN component gives a possibility to set the "radiation model" option, which allows the code to evaluate the view factors and beam lengths between all the rods in the channel automatically (through a Monte Carlo simulation). The advantage of this option is the high accuracy in the calculation of all the parameters within the channel. The disadvantage is that this option prevents the user to define a radiation model (RADENC component) that includes the outer surface of the canister wall and the inner face of the bypass channel wall.

This limitation affects the results in a nonnegligible way. Previous investigators [3] found that 20%–25% of the heat radiated from the heated rods to the canister's inner side was reradiated from the canister's outer side to the shroud. The lack of canister wall radiation in the TRACE CHAN model results in a higher temperature of the canister wall than measured experimentally.

In order to reduce this effect, a very low value of the emissivity for the inner side of the canister wall has been chosen. In this way, the canister wall absorbs less heat by radiation, keeping its temperature similar to the experimental data.

The values of emissivity used for the simulations have been chosen performing a sensitivity study. It was verified that using 0,3 for the canister wall and 0,67 for the fuel rods lead to a better prediction of the PCT compared to the experimental data. In addition, it has been found that wall emissivity larger than 0,3 prevents the wall to quench resulting in a very high temperature.

On the other hand, no view factors or beam length calculation is provided for the PIPE component, and the user has to define these parameters manually. The radiation model is then implemented by acting directly on the RADENC component. From the point of view of modelling flexibility, this gives the possibility to model the heat exchange between the outer side of the canister wall and the bypass channel wall.

The view factors are input as a matrix, with row index surface connected to column index surface. TRACE requires zero values on the diagonal (which connect the surface to itself) which means that a heat structure cannot "see" itself.

Since the rods have been modelled in a way that a single heat structure represents the entire rod group, it is clear that when the PIPE model is used, it is not possible to simulate

Table 2: View factors from the GÖTA documentation [3].

	Rod group 1	Rod group 2	Rod group 3	Rod group 4	Rod group 5	Canister wall
Rod group 1	0,1932	0,1010	0,2033	0,0130	0,0000	0,4895
Rod group 2	0,0727	0,1899	0,3334	0,0257	0,0024	0,3759
Rod group 3	0,1170	0,2667	0,3026	0,2498	0,0143	0,0496
Rod group 4	0,0125	0,0342	0,4164	0,3353	0,1913	0,0103
Rod group 5	0,0000	0,0096	0,0716	0,5739	0,3386	0,0063
Canister wall	0,4189	0,4470	0,0736	0,0092	0,0018	0,0495

Table 3: View factors used in TRACE.

	Rod group 1*A*	Rod group 1*B*	Rod group 2	Rod group 3	Rod group 4	Rod group 5	Canister wall
Rod group 1*A*	0,0000	0,1932	0,1010	0,2033	0,0130	0,0000	0,4189
Rod group 1*B*	0,1932	0,0000	0,1010	0,2033	0,0130	0,0000	0,4189
Rod group 2	0,1010	0,1010	0,0000	0,3334	0,0257	0,0024	0,3759
Rod group 3	0,2033	0,2033	0,3334	0,0000	0,2498	0,0143	0,0496
Rod group 4	0,0130	0,0130	0,0257	0,2498	0,0000	0,1913	0,0103
Rod group 5	0,0000	0,0000	0,0024	0,0143	0,1913	0,0000	0,0063
Canister wall	0,4189	0,4189	0,3759	0,0496	0,0103	0,0063	0,0000

the heat exchange by radiation between two rods of the same group. Tables 2 and 3 shows the view factors from the test documentation [3] and the values actually used in the TRACE simulation, respectively.

Values in Table 3 are obtained applying the constraints imposed by TRACE to the values reported in Table 2. In particular, zero values on the diagonal have been set, and the same value of the emissivity for elements (i, j) and (j, i) has to be used.

The deficiencies in the modelling of the view factors with TRACE appears evident from the two tables. For example, observing the rod group 3, it can be noticed that instead of a view factors of 0,3026 TRACE imposes the value of zero. That means that an important part of radiation heat transfer cannot be modelled correctly with TRACE.

Regarding the canister wall, the same issue has been found in the PIPE model as in the CHAN model. The wall emissivity larger than 0,3 prevents the wall to quench resulting in a very high temperature.

3.1.3. CCFL Model. The countercurrent flow limitation is a very important phenomenon from the point of view of the emergency core cooling both in PWR and in BWR. In case of this work, it can occur during the spray injection phase, preventing the cooling of the rods and the wall.

It is a local phenomenon, limiting the liquid flow from the upper part of the channel to the lower region due to the steam flow in the opposite (countercurrent) direction. Any increase in the vapour flux leads to a reduction in the liquid counterflow, until eventually it becomes zero.

In TRACE code, it is possible to evaluate CCFL through three types of correlations: Wallis, Kutateladze, and Bankoff. The Wallis correlation [4] uses the dimensionless superficial velocity to express the CCFL model, while the Kutateladze correlation [5] expresses the CCFL in terms of Kutateladze number. The Bankoff correlation [6] interpolates the two previous correlations. Equation (1) shows the Wallis, Kutateladze and Bankoff correlations, respectively,

$$\begin{aligned} j_g^{*1/2} + m_W j_f^{*1/2} &= C_W, \\ K_g^{1/2} + m_K K_f{}^{1/2} &= C_K, \\ H_g^{1/2} + m_B H_f^{1/2} &= C_B, \end{aligned} \tag{1}$$

where m and C are the constants determined from the experiment, j_i^*, K_i, and H_i^* are the dimensionless superficial velocity, the Kutateladze number, and the dimensionless flux of phase i, and they have the form

$$\begin{aligned} j_i^* &= j_i \left[\frac{\rho_i}{gd\left(\rho_f - \rho_g\right)} \right]^{1/2}, \\ K_i &= j_i \left[\frac{\rho_i^2}{g\sigma\left(\rho_f - \rho_g\right)} \right]^{1/2}, \\ H_i^* &= j_i \left[\frac{\rho_i}{gw\left(\rho_f - \rho_g\right)} \right]^{1/2}. \end{aligned} \tag{2}$$

In the above equations, j_i and ρ_i are the superficial velocity and the density of phase i, d is the diameter, σ is the

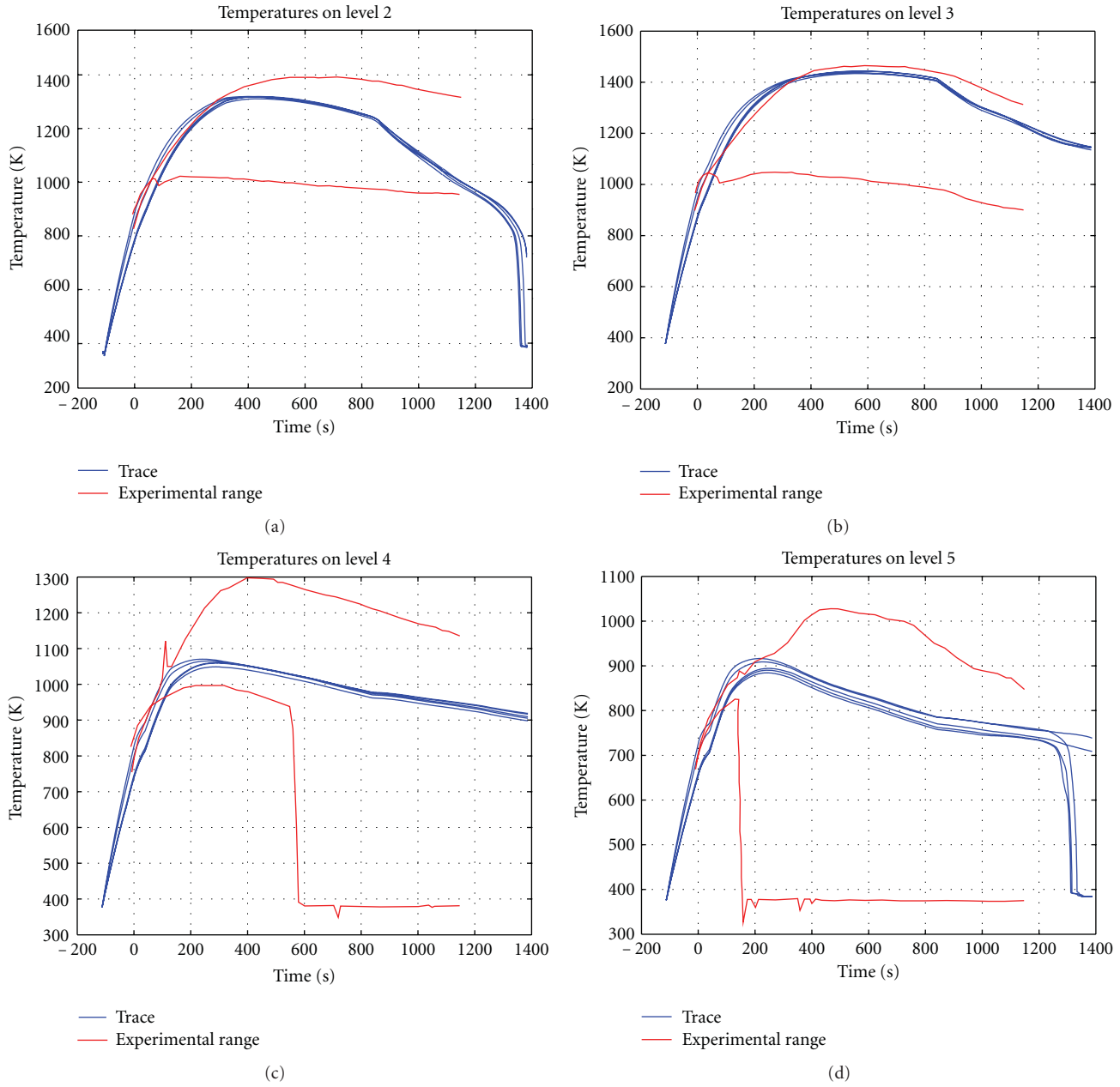

Figure 6: Results of the PIPE model.

surface tension, g is the gravitational constant and w is the interpolative length scale determined from,

$$w = d^{1-\beta} L_1^{\beta}, \quad (0 \le \beta \le 1),$$
$$L_1 = \left[\frac{\sigma}{g\left(\rho_f - \rho_g\right)}\right]^{1/2},$$
$$\beta = \tanh(\gamma k_c d), \tag{3}$$
$$k_c = \frac{2\pi}{t_p},$$

where L_1 is the Laplace capillarity constant, β is the scaling constant between 0 and 1, k_c is the critical wave number, γ is the perforation ratio, and t_p is the plate thickness.

Bankoff also developed a correlation for the parameter C_B based on the Bond number (L^*),

$$L^* = n\pi d\left[\frac{g\left(\rho_f - \rho_g\right)}{\sigma}\right]^{1/2}, \tag{4}$$

such that,

$$C_B = \begin{cases} 1,07 + 0,00433L^*, & \text{for } L^* \le 200, \\ 2, & \text{for } L^* > 200, \end{cases} \tag{5}$$

where n is the number of holes in the tie plate.

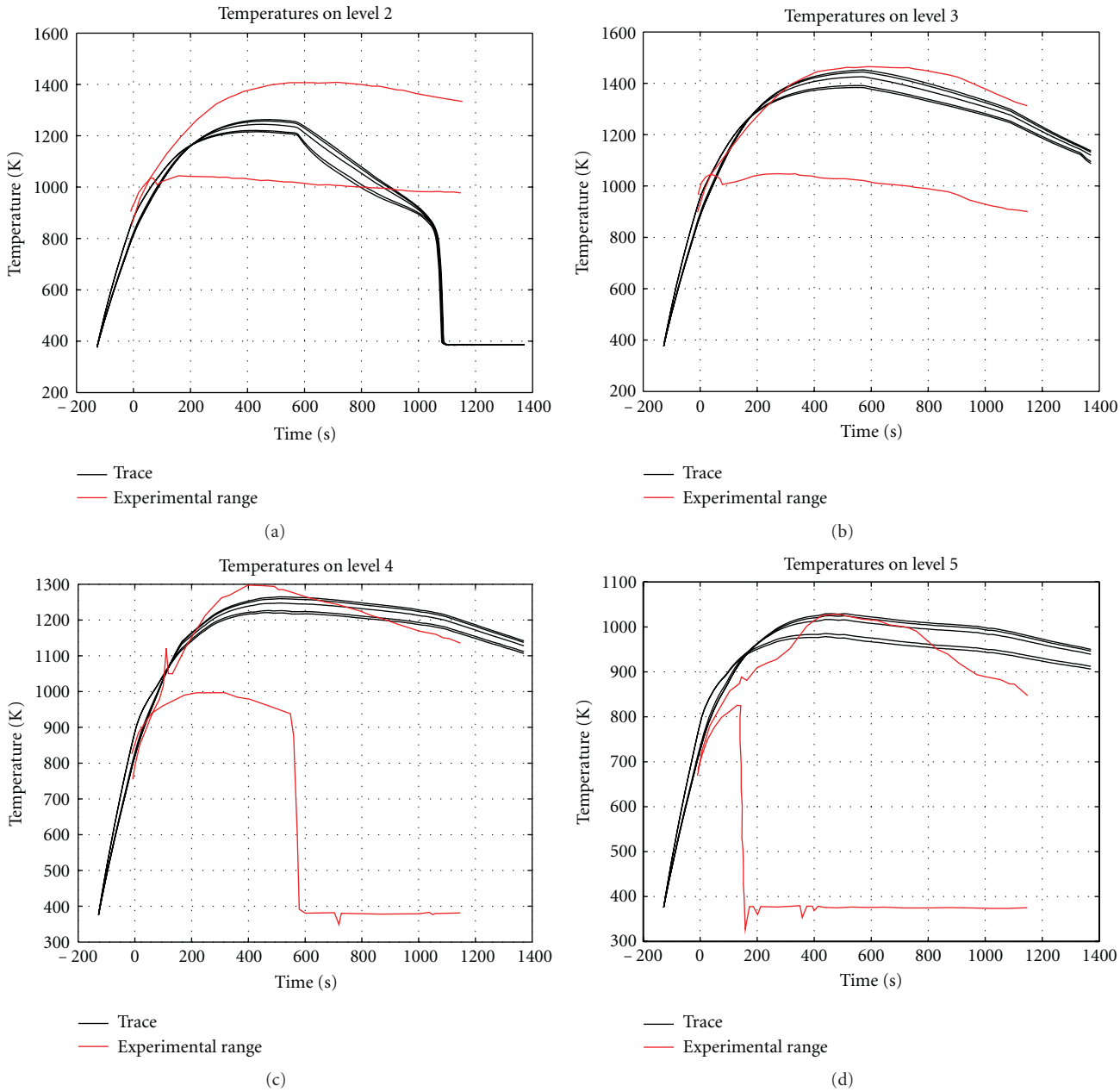

Figure 7: Results of the CHAN model.

The CCFL model is activated by specifying the location in the component where the phenomenon is expected to occur.

Three parameters have to be set in TRACE in order to define which model the code should use:

(1) the interpolation constant CBETA: the value zero means that the Wallis model will be used, 1 is for the Kutateladze model, and the value between 0 and 1 defines the interpolation constant for the Bankoff model;

(2) the CCFL slope m;

(3) the CCFL intercept C.

If the Bankoff model is used, the geometrical data of the tie plate has to be defined.

These models have been tested, in particular Bankoff model for the upper tie grid (above the channel) and Wallis and Kutateladze models for the fuel channel. The implementation of the Bankoff model showed no influence on the prediction of the PCT, so it has not been considered for the final calculations. On the contrary, different results have been found with the Wallis and the Kutateladze correlations. Previous studies [7] have shown that the Wallis correlation is preferable if the hydraulic diameter of the pipe is relatively small (2.5 mm to 50 mm), so this correlation has been selected to model the CCFL in the GÖTA test bundle.

4. Results

The experimental data used for the comparison are the temperatures measured at different levels in the channel. The data are presented in the test documentation [3] as a range of temperatures where the maximum, the minimum, and an average value are shown for each rod group at each level. In order to simplify the visualization, all the experimental temperatures in each level are shown in one plot, and only the maximum and the minimum values are reported together with all the computed temperatures for that axial level.

The comparison between the calculated and experimental data is shown on Figure 6 for the PIPE model and Figure 7 for the CHAN model. Each line represents the cladding temperature evaluated at each group for one particular axial level.

The results reported in Figure 6 show that the computed temperatures are always within the range of the experimental data. In the upper part of the bundle (Level 4 and 5), the TRACE results follow an average temperature between the maximum and the minimum in the level. In the lower part of the bundle (Level 2 and Level 3), the calculated results are closer to the maximum. In particular, at the Level 3 where the peak cladding temperature is located, TRACE code predicts the evolution of the maximum temperature very well.

It is important to understand the reason for the large difference between the distribution of the calculated and experimental data. In addition to the inaccuracies regarding the modelling of the radiation that have been already described, there is another important issue related to the physics of the experiment.

During the tests in the GÖTA facility, it has been observed that the water injected from the spray in the top of the channel flows downward mainly in the region closer to the canister wall, while the central part of the channel is mainly occupied by the vapour that moves upward. This phenomenon causes a large temperature difference between the rods, because the rods in the peripheral region are cooled significantly more than the inner rods. This effect, together with the fact that the outer rods are facing the canister wall which is at a lower temperature, leads to a large difference between the minimum and the maximum temperature showed in Figures 6 and 7, even if the maximum radial power peaking factor is located in the corner rods (see Figure 4).

It is not possible to simulate this multidimensional phenomenon in PIPE and CHAN component, because of the 1D approximation used to solve the conservation equations in these components. This inherent limitation of the TRACE code explains the very low temperature differences in the radial direction; the difference between the various rod groups is only due to the radiation model.

The results of the CHAN model (Figure 7) show some differences in the temperature behaviour relative to the PIPE model. The temperatures in the upper part of the bundle (Levels 4 and 5) are slightly overpredicted in the CHAN Model. Even if Levels 4 and 5 maximum cladding temperature is well predicted, the general evolution of the transient shows a much slower temperature decrease with respect to the experiment.

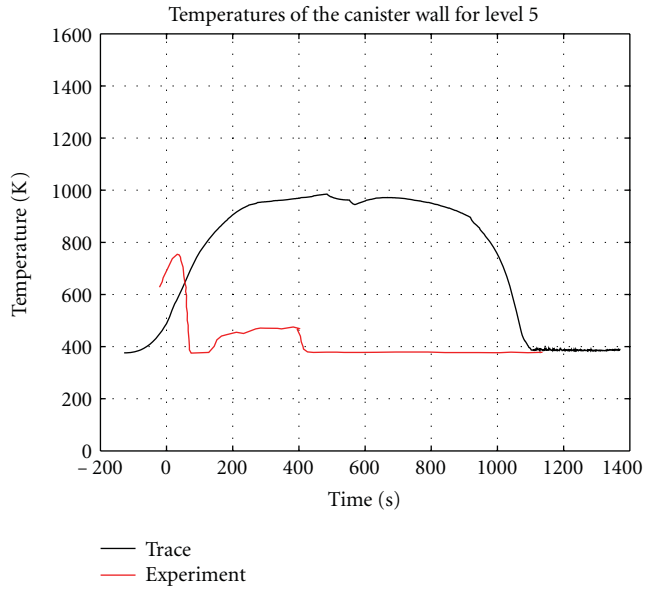

Figure 8: Temperature on the canister wall midplane.

On the other hand, the results in the midplane and in the bottom of the channel (Levels 2 and 3) show that the quenching is predicted earlier than in the experiment, even if the PCT (Level 3) is higher than in the PIPE model.

Similarly as the PIPE Model, the inability of the code to model 2D phenomena strongly affects the temperature distribution within each level. On the other hand, the identified weakness in the radiation model, present also in the CHAN component, results in an unjustified increase in the temperature of the canister wall mid-plane shown in Figure 8, which is not present in the PIPE model. As has been explained in Section 3.1.2, the code prevents the user to model the heat exchange by radiation from the outer side of the canister wall to the bypass channel, which results in an increase of the wall temperature and a delay in the quench.

Finally, the temperature calculated in the bottom of the channel (Level 1) is reported in Figure 9 in order to show how the fine mesh reflood and axial heat conduction options affect the behaviour of the temperature at the bottom of the channel. A more reasonable solution that fits better the experimental data can be obtained by deactivating those options, but this would cause worse prediction of temperatures on the mid-plane. Since it is more important to predict correctly the peak cladding temperature, we have decided to maintain these options, accepting the error deriving from the code calculation.

5. Sensitivity and Uncertainty Analysis

The last part of the experiment analysis consists of the application of a sensitivity and uncertainty analysis. In the past, the licensing has always been done using conservative values for the computations in order to demonstrate the safety margins imposed by the regulations. Nowadays, it is

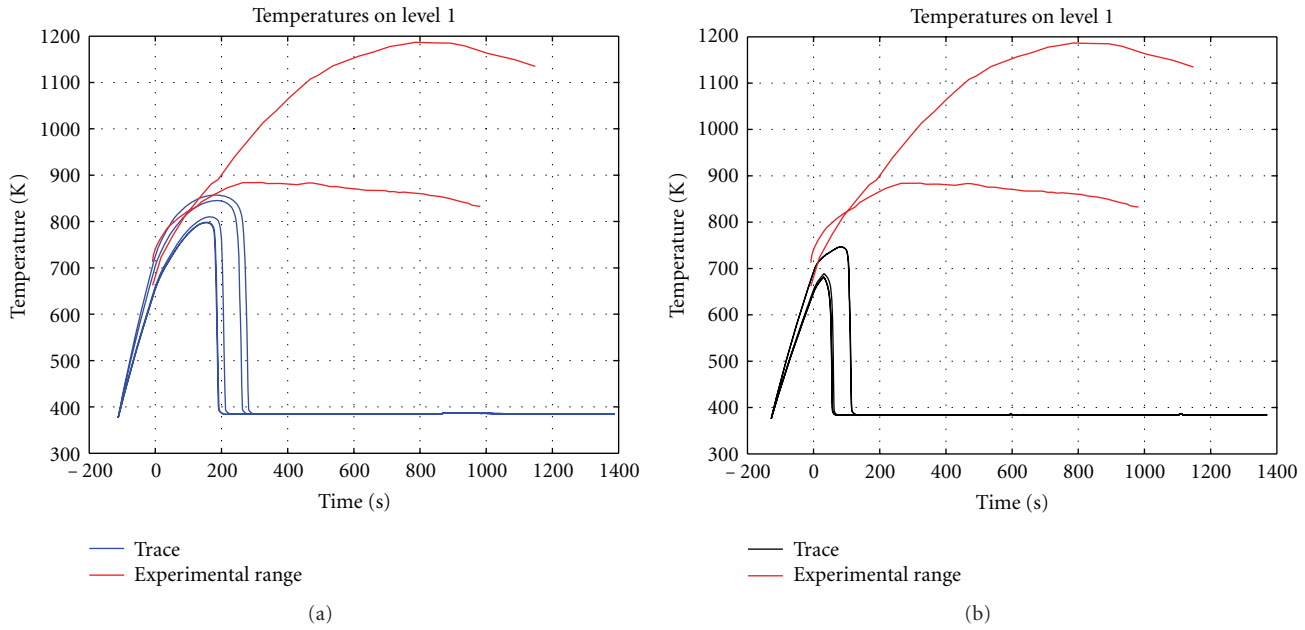

Figure 9: Temperatures computed from the PIPE model (a) and CHAN model (b) at Level 1.

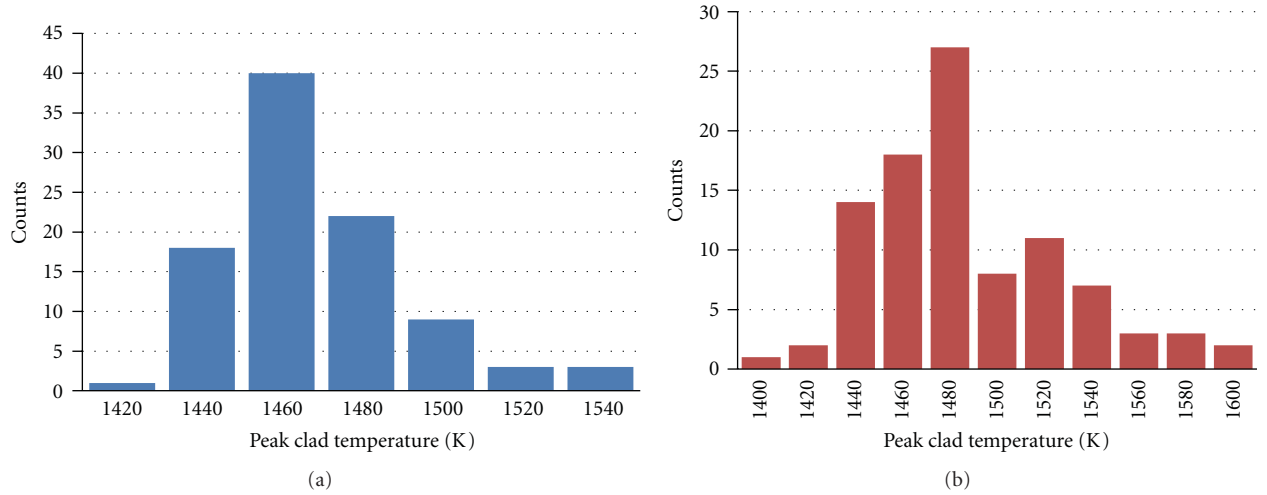

Figure 10: PCT distribution for the PIPE (a) and the CHAN model (b).

possible to estimate certain parameters with best-estimate calculations with the complement uncertainty evaluation, and these calculations can be used for licensing as well. Several methods have been developed for the uncertainty evaluation of system codes. In this work, only propagation of input errors (PIEs) is considered [8].

5.1. Propagation of Input Errors Evaluation. The PIE approach consists of the statistical variation of the input parameters together with their uncertainties, in order to reveal the propagation of errors through the code. Instead of using the input parameters as discrete values, they are varied according to a probability density function (PDF), and a certain number of calculations are performed in order to evaluate distribution and uncertainty of the output parameters.

The PDFs for the various input parameters are derived from the literature and from experts judgment, while the required number of calculations is given by the Wilks formula [9],

$$1 - \left(\frac{\alpha}{100}\right)^N \geq \frac{\beta}{100}, \tag{6}$$

which means that N calculations are required to be β% confident that at least α% of the combined influence of all the characterized uncertainties is below the tolerance limit.

Table 4: Uncertain parameters.

	Parameter	1-σ uncertainty	Type of distribution	Reference
		T/H initial parameters		
1	Initial power	0.75%	Normal	[10, page 21]
2	Decay heat power table	0.75%	Normal	Own judgment
3	Water drain temperature	5K	Uniform	Own judgment
4	Water drain pressure	0.01 MPa	Uniform	Own judgment
5	Steam vent temperature	5 K	Uniform	Own judgment
6	Steam vent pressure	0.5%	Uniform	Own judgment
7	Spray system pressure	5%	Uniform	Own judgment
8	Spray system temperature	0.5 K	Uniform	Own judgment
9	Spray system mass flow	0.5%	Uniform	[10, page 21]
		Vessel-related parameters		
10	Tee roughness	30%	Normal[a]	[10, page 3.32]
11	Bundle wall roughness	30%	Normal[a]	[11, page 3.32]
12	Bypass channel wall roughness	30%	Normal[a]	[11, page 3.32]
13	Length of main channel	1 mm	Uniform	Own judgment
14	Length of the bypass channel	1 mm	Uniform	Own judgment
15	Length of the main channel tee	1 mm	Uniform	Own judgment
16	Length of the bypass tee	1 mm	Uniform	Own judgment
		Bundle-related parameters		
17	Bundle flow area	0.5%	Uniform	Own judgment
18	Bundle hydraulic diameter	0.5%	Uniform	Own judgment
19	Bypass channel Flow Area	0.5%	Uniform	Own judgment
20	Bypass hydraulic diameter	0.5%	Uniform	Own judgment
21	Spacers friction	5%	Uniform	[8, page 35]
22	Rod emissivity	15%	Uniform	Own judgment
23	Bundle wall emissivity	15%	Uniform	Own judgment
24	CCFL slope	10%	Uniform	Own judgment
25	CCFL constant	10%	Uniform	Own judgment
		Timing		
26	Spray injection trip	1 s	Uniform	Own judgment
27	Drain valve trip delay	0.5 s	Uniform	Own judgment

[a] The distribution was approximated with normal.

The formula for the two-sided statistical tolerance intervals is given as

$$1 - \left(\frac{\alpha}{100}\right)^{N} - N\left[1 - \left(\frac{\alpha}{100}\right)\right]\left(\frac{\alpha}{100}\right)^{N-1} \geq \frac{\beta}{100}, \quad (7)$$

where α and β have the same meaning as the previous equation. The level of coverage/confidence used for the uncertainty calculation on the TRACE models of the GÖTA is 95%/95%. The two-sided formula has been used which means that 93 calculations are required.

Table 4 shows all the input parameters that have been taken into account in this study. The references are reported for parameters found in the literature; while for those which no literature has been found, the PDF is based on our own judgment.

No rigorous methodology is used to select the parameters listed in Table 4. The considered parameters, as well as their uncertainties, are rather illustrative than precise. For this reason, the uncertainty study reported here should be considered as an example of uncertainty calculation used to demonstrate the feasibility of this procedure.

The PIE method has been applied for both the PIPE and the CHAN models, using exactly the same uncertainty parameters (Table 4) and the same number of calculations (93). The output parameter chosen for the PIE evaluation is the PCT, and the distribution of this parameters obtained from the PIE calculations is reported for both models in Figure 10.

The results of the uncertainty evaluation of the PIPE model show that the spread of the output parameter (PCT) can be approximated with the normal distribution, and the peak of the distribution is located on the interval 1440–1460 K, which is in a good agreement with the experimental data.

The distribution of the CHAN model output parameter (PCT) differs in the location of the peak and the distribution. The peak of the PCT distribution is located on the interval 1460–1480 K, it has larger spread (standard deviation), and

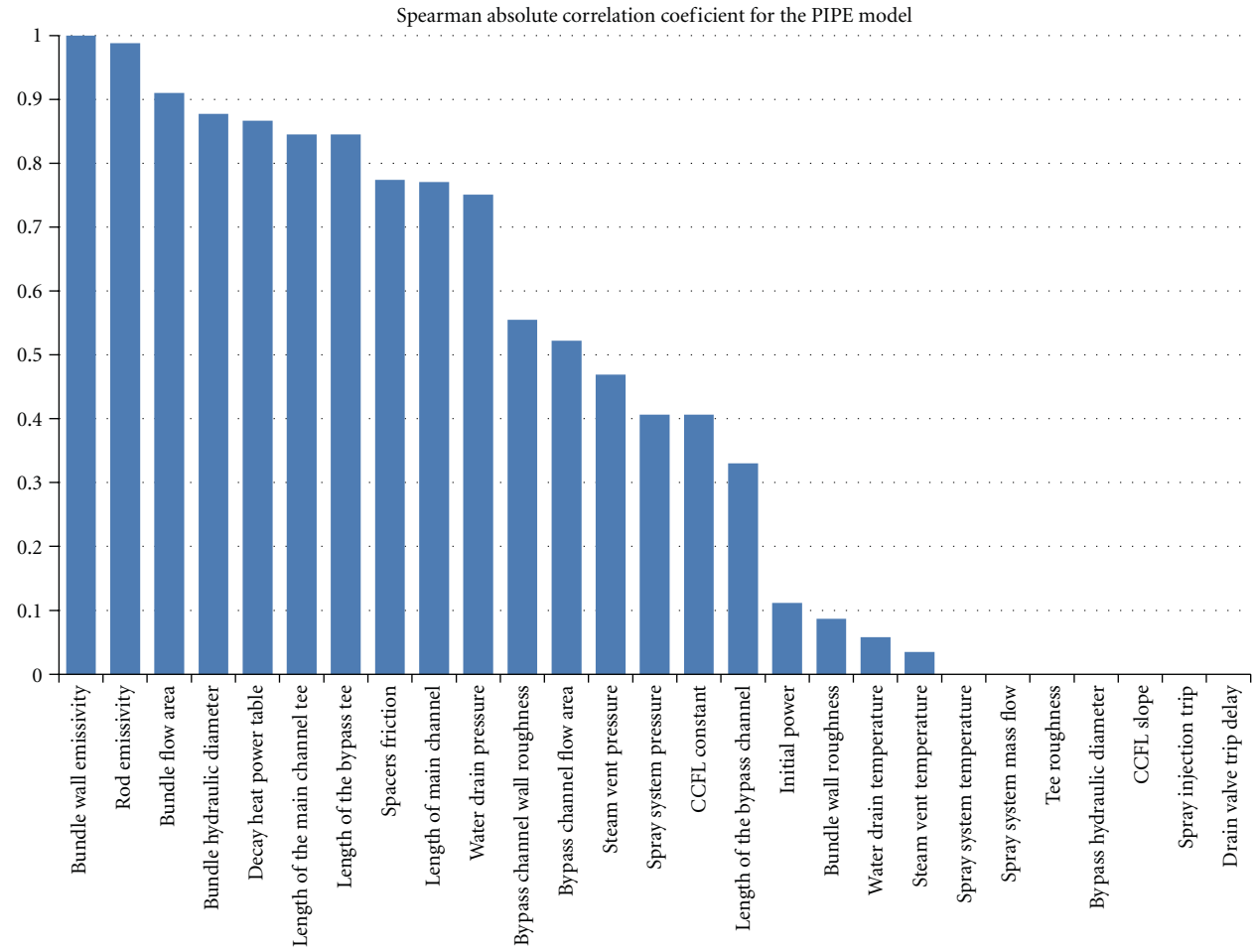

Figure 11: Absolute Spearman correlation coefficient for the PCT for the PIPE model.

it does not fit the normal distribution. This implies that the CHAN model results have larger uncertainty than the PIPE model results.

5.2. Sensitivity Analysis. A sensitivity study has been performed on all the parameters in Table 4, in order to define the most influential input parameter on the figure of merit (PCT).

The Spearman correlation is used to obtain the correlation coefficient between the input parameter and the output. This coefficient provides a quantitative measure of effect the input parameter has on the output figure of merit (PCT) [8].

If n variation of the parameters is done, the n raw scores X_i and Y_i are converted to ranks x_i and y_i, and the differences $d_i = x_i - y_i$ between the ranks of each observation on the two variables are calculated. If there are no tied ranks, the Spearman correlation coefficient is defined as follows [12]:

$$\rho = 1 - \frac{6 \sum d_i^2}{n(n^2 - 1)}. \quad (8)$$

In Figures 11 and 12 the absolute value of the Spearman correlation coefficient is reported for each parameter for PIPE and CHAN models, respectively.

The results from the PIPE model show that the two most influential parameters are the rod and the wall emissivity. This confirms that the radiation heat transfer plays a very important role in the cooling of the bundle, especially the interactions between the rods and the canister wall. Other important parameters are the one related to the geometry of the channel, that is, the flow area and the hydraulic diameter. These parameters influence the mass flow rate of water and steam through the channel which determines the "coolability" of the rods.

The results from the CHAN model show that the most influential parameter is the CCFL constant. The CHAN model is much more sensitive to the CCFL phenomenon than the PIPE model. Nevertheless, the Spearman correlation coefficient for the bundle wall emissivity shows that radiation model still plays a very important role in the evolution of the transient.

These results should be considered keeping in mind that the CHAN model overestimates the temperature at the top of the bundle, and it has been identified that the CCFL model has a significant contribution in this overestimation.

It is also important to note that the geometrical parameters that played a nonnegligible role in the PIPE model are

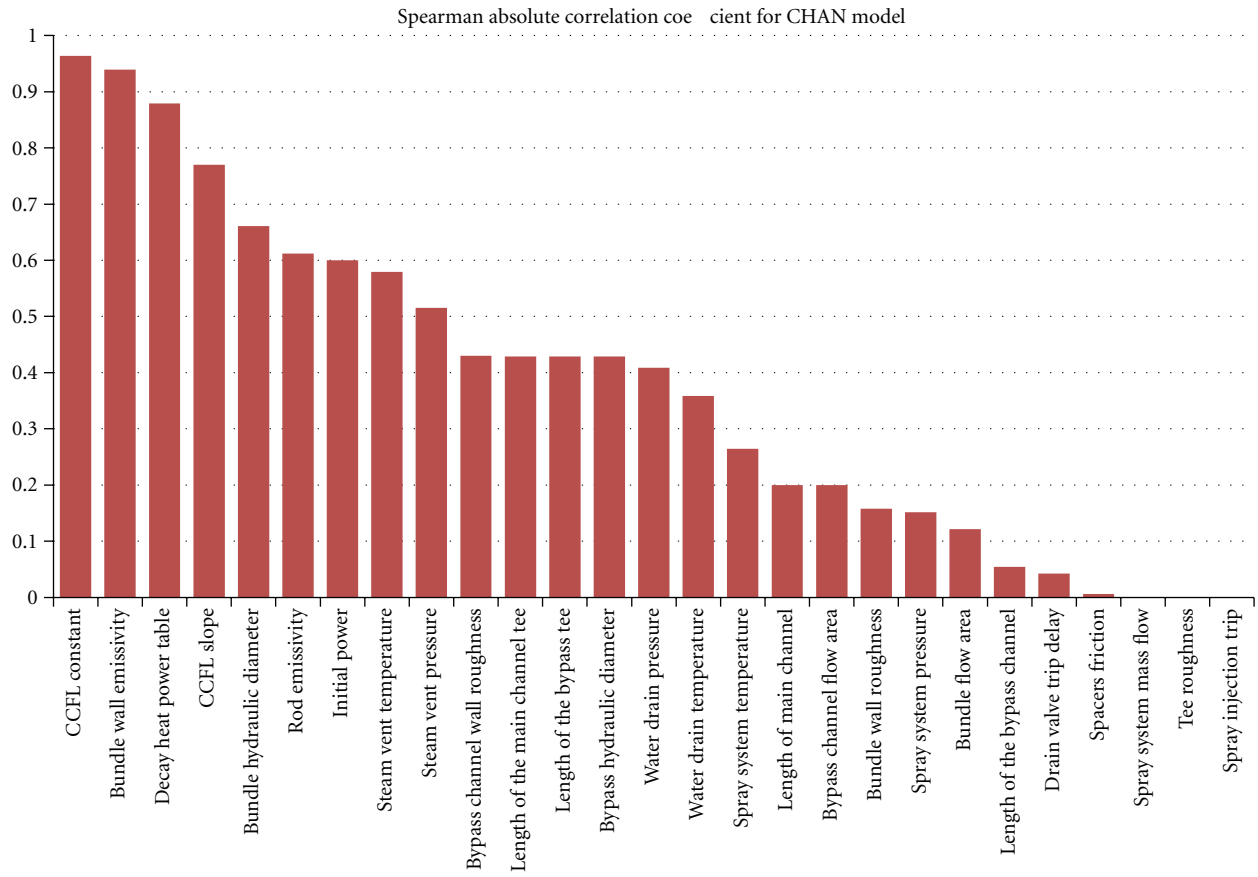

Figure 12: Absolute Spearman correlation coefficients for the PCT for the CHAN model.

less important for the CHAN model, while the boundary conditions, that is, pressure and temperature at the FILL and BREAK components, affect more the results of the CHAN model.

6. Conclusion

In this paper, the results derived from two different TRACE models of the GÖTA test facility have been analysed and compared. An uncertainty study has been performed, and the most influential parameters have been determined.

First, the results clearly show that the inability of the PIPE and CHAN components to model 2D phenomena does not prevent the code from a reasonable prediction of the PCT and its evolution in time, which is very important from the safety point of view. Only the trend of the best-estimate results for the PCT is captured.

It was found that for the considered experiment, the PIPE model provides a slightly better prediction of the PCT than the CHAN model. However, both models predict an incorrect behaviour in the lower part of the channel (Level 1), where the activation of the axial heat conduction option results in a strong underestimation of the temperatures for all the rod groups.

These results suggest that for the simulation of such kind of facility, it is better to use a more flexible component that allows the user to set more input parameters. For instance, the PIPE component has a possibility to create the fuel heat structures separately and to set different value of emissivity in each one of them. This is not possible with the CHAN component, since only one value of emissivity is used for all the rods. Moreover, the possibility to set own value of the view factors represents additional degree of freedom for the PIPE component.

Finally, the results of the uncertainty calculations show that the PIPE model has a smaller uncertainty in the figure of merit (PCT). In fact, Figure 10 (a) shows how most of the computed PCTs are in the same interval as the experimental data (1440–1460 K). On the other hand, it can be noticed that the CHAN model overestimates the PCT.

On the basis of the uncertainty analysis performed, the most influential parameters for the PIPE model are the wall and the rod emissivity. These results highlight the importance of radiation heat transfer in a fuel assembly when the cladding temperature in the core is high (i.e., close, or above 1000 K). These results also emphasize the need of improving the radiation model in TRACE both in the CHAN and PIPE components.

On the other hand, the most influential parameter for the CHAN models is the CCFL correlation constant. This explains the overprediction of the temperature on the top of

the bundle, which is due to an overestimation in the CCFL phenomenon.

Abbreviations

1-D, 2-D: One dimensional, two dimensional
ANS: American Nuclear Society
BWR: Boiling water reactor
CCFL: Counter current flow limiting
ITF: Integral test facility
LB-LOCA: Large break loss of coolant accident
NPP: Nuclear power plants
PCT: Peak cladding temperature
PDF: Probability density function
PIE: Propagation of input errors
PWR: Pressurized water reactor
SETF: Separate effect tests facility
SNAP: Symbolic nuclear analysis package
THSC: Thermal-hydraulic system codes
TRACE: TRAC/RELAP Advanced Computational Engine
U.S. NRC: United States Nuclear Regulatory Commission.

References

[1] F. D'Auria, A. Bousbia-Salah, A. Petruzzi, and A. Del Nevo, "State of the art in using best calculation tools in nuclear technology," *Nuclear Engineering and Technology*, vol. 38, no. 1, 2006.

[2] S. O. Eriksson, R. Harju, and R. Pettersson, "BWR emergency core cooling investigations: spray cooling heat transfer experiment in a full scale BWR bundle mock-up," DSF Project No 1—STUDSVIK/E4-78/64, Studsvik, 1978.

[3] D. L. Caraher and Ö. Rosdahl, "Assessment of RELAP5/MOD2 Radiation and Quench Model Using GÖTA Spray Cooling Test 78 Data," SKY Project 13.3-917/84 - STUDSVINK/NP-87/43, Studsvik, 1987.

[4] G. B. Wallis, *One Dimensional Two-Phase Flow*, McGraw-Hill, New York, NY, USA, 1969.

[5] S. S. Kutateladze, "A hydrodynamic theory of changes in the boiling process under free convection," *Izvestia Akademii Nauk, USSR, Otdelenie Tekhnicheski Nauk*, vol. 8, p. 529, 1951.

[6] S. G. Bankoff, R. S. Tankin, M. C. Yuen, and C. L. Hsieh, "Countercurrent flow of air/water and steam/water through a horizontal perforated plate," *International Journal of Heat and Mass Transfer*, vol. 24, no. 8, pp. 1381–1395, 1981.

[7] Y. H. Cheng, J. Rwang, C. Shih, and H. T. Lin, "A study of steam-water countercurrent flow model in TRACE code," in *Proceedings of the 17th International Conference on Nuclear Engineering*, Brussels, Belgium, 2009.

[8] I. Gajev, *Sensitivity and uncertainty analysis of BWR stability*, Licentiate Thesis in Energy Technology, KTH Engineering Sciences, Stockholm, Sweden, 2010.

[9] H. Glaser, "GRS method for uncertainty and sensitivity evaluation of code results and application," *Science and Technology of Nuclear Installation*, vol. 2008, Article ID 798901, 7 pages, 2008.

[10] B. Neykov, F. Aydogan, L. Hochreiter et al., "OECD-NEA/US-NRC/NUPEC BWR Full-size Fine-Mesh Bundle Test (BFBT) Benchmark," Volume I: Specifications, OECD 2006, NEA No. 6212, NEA/NSC/DOC, 2005.

[11] T. Wickett, F. D'Auria, and H. Glaeser, "Report of the uncertainty method study for advanced best estimate thermal-hydraulic codes applications," page 14, Vol. I OECD/CSNI Report NEA/CSNI R (97) 35, Paris, France, 1998.

[12] J. L. Mayers and A. D. Well, *Research Design and Statistical Analysis*, Lawrence Erlbaum, 2002.

Hindawi Publishing Corporation
Science and Technology of Nuclear Installations
Volume 2012, Article ID 950389, 10 pages
doi:10.1155/2012/950389

Research Article

CATHARE Assessment of Natural Circulation in the PKL Test Facility during Asymmetric Cooldown Transients

Anis Bousbia Salah and Jacques Vlassenbroeck

Bel V (Subsidiary of the Belgian Federal Agency for Nuclear Control), Walcourtstraat 148, 1070 Brussels, Belgium

Correspondence should be addressed to Anis Bousbia Salah, anis.bousbiasalah@belv.be

Received 1 March 2011; Accepted 25 May 2011

Academic Editor: Alessandro Del Nevo

Results of the CATHARE code calculations related to asymmetric cooldown tests in the PKL facility are presented. The test under consideration is the G2.1 experiment performed within the OECD/NEA PKL-2 project. It consists of carrying out a cooldown under natural circulation conditions in presence of two (out of four) emptied Steam Generators (SGs) and isolated on their secondary sides. The main goal of the current study is to assess the impact of a chosen cooldown strategy upon the occurrence of a Natural Circulation Interruption (NCI) in the inactive (i.e., noncooling) loops. For this purpose, three G2.1 test runs were investigated. The calculation results emphasize, mainly, the effect of the cooldown strategy, and the conditions that could lead to the occurrence of the NCI phenomenon.

1. Introduction

After the reactor trip, several cooldown procedures can be followed in order to bring the primary side temperature and pressure to the Residual Heat Removal System (RHRS) operating conditions. For example, the primary cooldown can be carried out by a linear or stepwise temperature decrease, with a coincident or delayed depressurization. Generally, the Emergency Response Guidelines (ERG) impose a limit on the cooldown rate in order to prevent steam bubble formation under the reactor vessel head during the depressurization phase. Furthermore, Natural Circulation Interruption (NCI) has also to be avoided during the cooldown phase as pointed out by [1]. Indeed, the interruption of natural circulation in one or more inactive primary loops could stop the cooldown in these loops and lead to degradated states [1, 2].

Up to now, the NCI phenomenon has not yet been deeply investigated analytically and experimentally as well. The issue was addressed by the OECD/NEA PKL-2 project [3] in order to assess the impact of different cooldown strategies on the occurrence of the flow stagnation in the inactive loops where the corresponding SGs are emptied and isolated. Former studies, on the PKL facility, made by Dubiel and Mandl [4] showed that NCI could occur in the loop with isolated and filled SGs if a (stepwise) cooldown at 50°C/h, with a mean value around 10°C/h, is performed. Recently, Vlassenbroeck et al. [1] investigated the NCI in a typical 2-loop NPP using a thermal-hydraulic system code. The latter study emphasised the fact that a linear cooldown rate larger than 14°C/h could lead to NCI.

In the current study, three experimental runs performed in the 4-loop PKL facility are considered. They concern three cooldown strategies under natural circulation conditions where 2 out of 4 SG are emptied and isolated on their secondary sides. The objective was to check if natural circulation is maintained in all loops at a continuous cooldown rate of 50°C/h and if not, whether natural circulation can be maintained by a stepwise cooldown rate at 50°C/h.

The test simulation was carried out using the advanced thermal-hydraulic system code CATHARE 2/V2.5_1/mod8.1 developed by CEA, EDF, AREVA, and IRSN [5]. The current study allows drawing conclusions about the NCI occurrences under some specific conditions and also about the capabilities of the current computational tools in predicting the NCI phenomenon, to better understand the interaction between the key parameters expected during the transient.

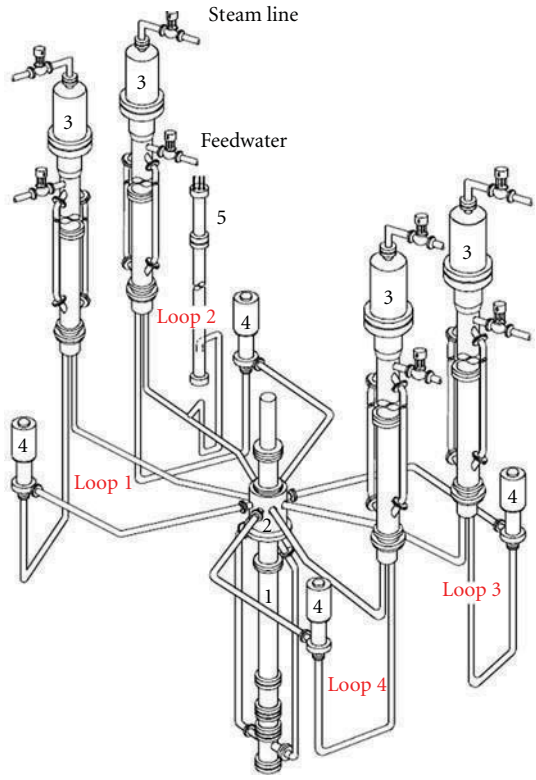

1 Reactor pressure vessel
2 Downcomer
3 Steam generator
4 Pump
5 Pressurizer

Figure 1: Layout of the PKL test facility [6].

2. PKL Facility Description

The PKL (Primaer KreisLauf) facility [6] has been built in order to perform experimental investigations related to different integral behaviour of a typical 4-loop 1300-MW Siemens pressurized water reactor (PWR) plant under normal and accident conditions. The layout of the PKL facility (Figure 1) shows the primary side and the most significant components of the secondary side. The scaling ratios of the facility are 1 : 1 elevation ratio and 1 : 145 for the power, volumes, and the cross section areas. However, the maximum operating primary pressure is 45 bar.

The primary side is represented by 4 identical and symmetric loops arranged around the reactor pressure vessel. For each loop, a secondary side is associated, as well as all the significant interface and auxiliary systems.

3. CATHARE Model for PKL

The adopted CATHARE nodalization for the current study is a full 1D model. In total, the nodalization contains almost thousand of hydraulic nodes and heat structures distributed on the primary and the secondary side.

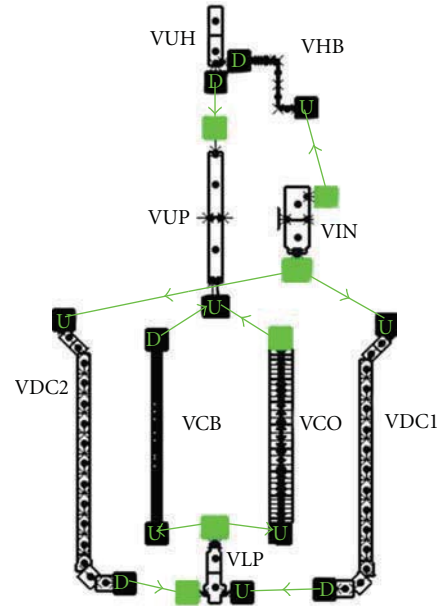

Figure 2: CATHARE modelling of the PKL reactor vessel components.

3.1. PKL Reactor Vessel. The PKL vessel model as modelled by the CATHARE code is composed by the upper downcomer ring (VIN), the 2 downcomer pipes (VDC1 & VDC2), the lower plenum (VLP), the heated core zone (VCO) and the core bypass (VCB) zone, the upper plenum (VUP), the upper head (VUH), and the upper head bypass (VHB). In Figure 2, the aforementioned components are shown, more details are provided in Table 1.

The downcomer consists of an upper downcomer ring where the flows coming from the different cooling loops are mixed up. The descending part of the downcomer consists of 2 pipes connecting the downcomer ring to the core lower plenum. The rod bundle consists of 314 uniformly disposed heated rods. The latter were lumped into one equivalent heating channel with a uniform axially distributed power. The CATHARE nodalization was chosen to fit the spacer's position. The geometry of the core upper plenum includes the connections to the 4 hot legs and the lower part of the upper head. The upper head is connected to the core upper plenum through 9 holes that simulate the guided tubes zone, and also to the upper part of the downcomer through 4 upper head bypass pipes.

3.2. Steam Generators (Primary Side). The SG zone is composed of an inlet zone, SG U-tubes, and an outlet zone. The total number of U-tubes in each SG is 28, distributed in 7 elevations having 4 tubes each (see Figure 3(a)). In the CATHARE model, for each elevation, the 4 tubes are lumped into one representative tube as shown in Figure 3(b). Each lumped tube is divided into 36 nodes in order to get a detailed representation of the heat transfer between the primary and secondary side.

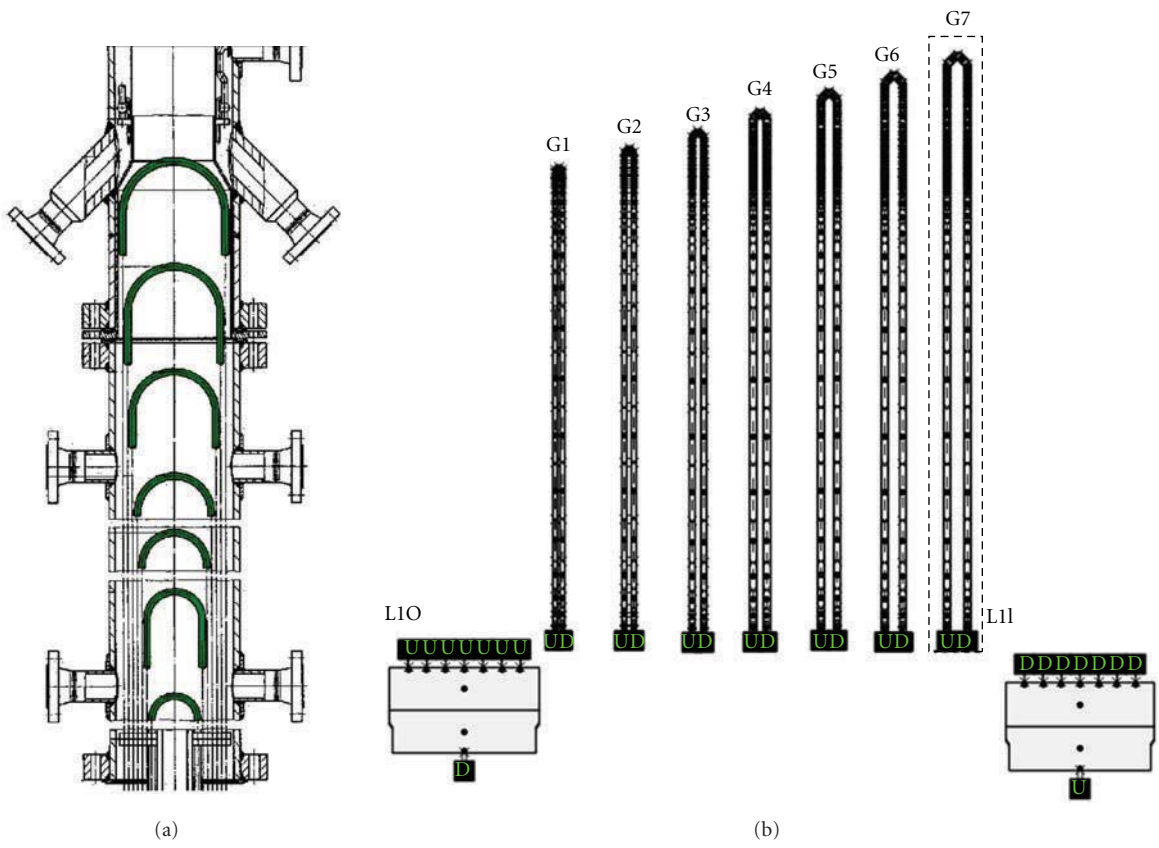

Figure 3: (a) The 7 U-tubes elevation geometry [6]. (b) U-tubes CATHARE model for the PKL configuration.

Table 1: Main components of the PKL reactor vessel.

Component	CATHARE component	CATHARE element
Lower plenum	VLP	VOLUME
Core bundle	VCO	AXIAL
Core bypass	VCB	AXIAL
Core upper plenum	VUP	VOLUME
Vessel upper head	VUH	VOLUME
Upper downcomer	VIN	VOLUME
Downcomer pipes	VDC1, VDC2	AXIAL
Upper head bypass	VHB	AXIAL

3.3. Secondary Circuit Description and Modelling. The main components of the secondary circuit are summarized in Table 2. The CATHARE model of the secondary circuit is shown in Figure 4, in which the upper annular downcomer of the steam generator is represented by a VOLUME component. The latter is connected to the feedwater line, the two downcomer pipes, and the recirculation line (the carry-under of the steam separator of the SG). The downcomer is represented by one AXIAL component that lumps the 2 real pipes. The riser nodalization is chosen to cope with the primary side nodalization of the U-tubes in order to satisfy the CATHARE code rules concerning the heat exchange between the primary and secondary sides. The steam dome volume is modelled by the VOLUME component. The dryer or the separator option was not activated since in the real PKL configuration no special features exist for the phase separation.

3.4. Nodalization Assessment. The single-phase pressure losses of the PKL facility correspond to a large extent to the values encountered in a PWR. Under steady-state conditions, the pressure drop across the primary side was checked against measured data provided in [7], taking into account the butterfly valve (located downstream of each primary coolant pump) pressure drops that simulate the frictions of the locked rotor of the primary pumps. On the other hand, the heat losses of the main primary components were also tuned in the CATHARE model in order to match the measured heat

Table 2: Main components of the PKL secondary side.

Component	CATHARE component	CATHARE element
Feed water line	FWn*	Axial
Annular downcomer	SnDW*	Volume
Downcomer pipes	DCnP*	Axial
Lower plenum	SnLP*	Volume
Riser	SnU*	Axial
Steam generator	SnD*	Volume
Steam lines	SLn*	Axial

*n is the loop number 1 to 4.

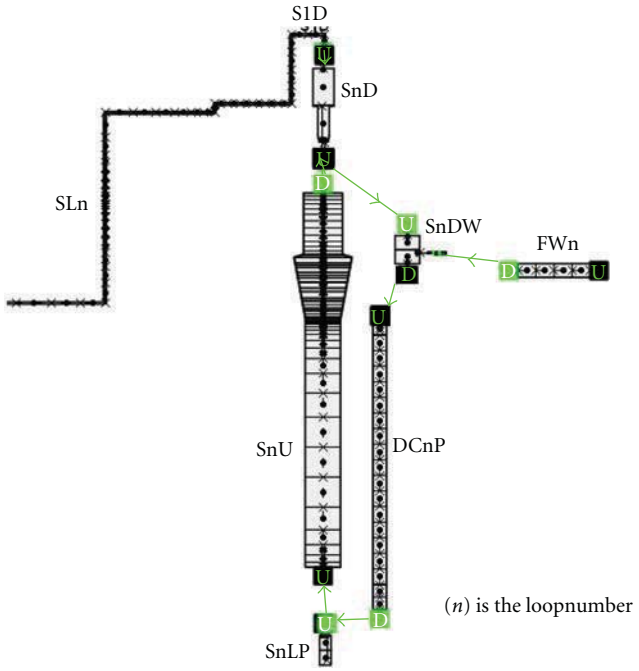

Figure 4: PKL secondary side view of the steam generator.

losses as documented in [8]. It should also be mentioned that some unknown cross section of some loop components were tuned in order to match the measured volumes as reported in [9].

The assessment of the nodalization is therefore carried out through a comparative study between the measured and calculated steady-state PKL operating conditions. This study is detailed in the following sections, and the main key parameters are outlined in Tables 6 and 7.

4. G2.1 Test Description

The PKL-2 G2.1 test consists of 3 runs in which 3 different cooldown procedures are followed. They concern three cooldown strategies under natural circulation conditions where 2 out of 4 SG are emptied and isolated on their secondary sides. The objective is to check if natural circulation is maintained in all loops at a continuous cooldown rate of 50°C/h and if not, whether natural circulation can be maintained by a stepwise cooldown rate at 50°C/h.

In Run-1 and Run-2, a continuous cooldown with different way of decreasing the primary pressure is carried out, while for Run-3 a stepwise cooldown procedure is performed.

4.1. NCI Phenomenon. NCI can occur under single- or two-phase flows due to several initiating events. Under two-phase flow, NCI can result from a loss of primary mass inventory as in the case of a small SBLOCA, or when a steam bubble is formed in the SG U-tubes.

On the other hand, during single-phase flow, NCI can occur progressively as the heat sink, in a loop, is gradually lost. The process is generally slow and can be described by the following single-phase momentum static governing set (1) under natural circulation conditions and negligible acceleration losses:

$$\oint_{\text{Vessel}} \rho g dz + \oint_{\text{SG}(n)} \rho g dz + \oint_{\text{Hotleg}-\text{Coldleg}(n)} \rho g dz = \Delta P_{f-\text{Vessel}} + \Delta P_{f-\text{Loop}(n)} \quad (1)$$

with $n = 1, 2, 3, 4$.

Indeed, when the heat sink is lost in loop 1 for instance, the second term of the left-hand side of (1) becomes null. Therefore, the flow in the inactive loop will decrease gradually and may stop when the driving force in the reactor pressure vessel minus the friction in the vessel are counterbalanced by the driving force in the inactive loop

$$\oint_{\text{Hotleg}-\text{Coldleg}(1)} \rho g dz \approx \oint_{\text{Vessel}} \rho g dz - \Delta P_{f-\text{Vessel}}. \quad (2)$$

4.2. Conditioning Phase. During the G2.1 test, the rod bundle power was fixed at 642 kW in which 100 kW was added to compensate the heat losses in the loops. This power level corresponds to a scaled decay heat power of 1.7%.

The initial conditions of each of the individual test runs were adjusted through the so-called conditioning phases during which the secondary sides of SG-1 and SG-3 were emptied and isolated afterwards. The main test phase starts when the temperature level of the secondary side of the isolated SGs reaches the primary side temperature.

Table 3: Main events for PKL2 G2.1 Run-1.

Time [s]	Measures/Events
0	Start of Run-1
360	End of heat-up phase, Start of continuous cooldown at 50°C/h by SG-2 and SG-4
535	PRZ heater switched off
2820	Spraying in PRZ by volume control system switched on (Subcooling at core outlet maintained)
5300	Flow stagnation in loop-1
6770	Flow stagnation in loop-3
8680	End of Run-1

Table 4: Main events for PKL2 G2.1 Run-2.

Time [s]	Measures/Events
0	Start of Run-2. Continuous cooldown initiated: continuous cooldown at 50°C/h by SG-2 and SG-4
80	PRZ heater switched off
2240	Spraying in PRZ by volume control system switched on (positive subcooling in the SGU-tubes is maintained)
6140	Flow stagnation in loop-1
7310	End of Run-2

4.3. Test Phase. For Run-1, the test consists in carrying out a continuous cooldown at 50°C/h and primary depressurization by spraying in the pressurizer. The pressure decrease is controlled in order to ensure a subcooled margin at the core outlet. The main events for Run-1 are outlined in Table 3. It should be mentioned here that only for Run-1 a heat-up phase of 360 s was performed.

For Run-2, the test consists in carrying out a continuous cooldown rate of 50°C/h but with controlled primary depressurization that ensures subcooling in the apex of the SG U-tubes. The main events for Run-2 are outlined in Table 4.

And finally for Run-3, a stepwise cooldown, during which subcooling in the SG U-tubes is maintained, is performed. The primary temperature is decreased successively after a short stabilization time by 20°C, 30°C, and 40°C following a cooldown rate of 50°C/h. The main events for Run-3 are outlined in Table 5.

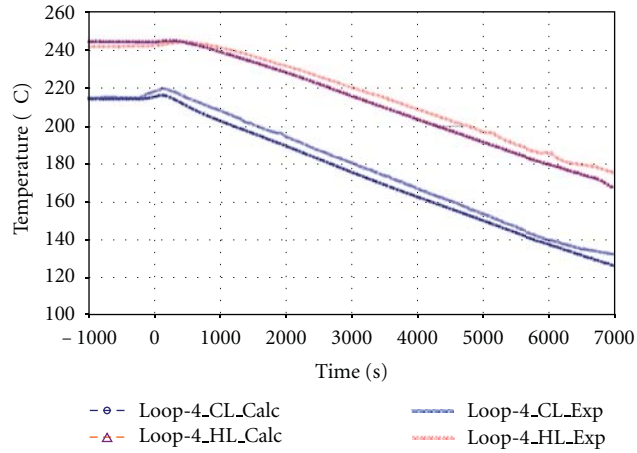

Figure 5: Run-1: Cold and hot leg temperature evolution in the active loops.

5. Calculation and Experimental Results

The simulation of each run covers the conditioning and the test phases. The results at the end of the conditioning phase are summarized in Tables 6 and 7 for the primary and secondary side, respectively. On the whole, good agreement between the calculation and the experimental results is obtained. This constitutes a good qualitative indicator for the representativeness of the developed CATHARE model for PKL as well.

5.1. G2.1 Run-1. The first run starts with the isolation of the secondary side of the active SG-2 and SG-4 from the steam header. A heat-up period in the primary side follows during 360 s approximately. The cooldown through the discharge valves begins afterwards.

At the beginning of the cooldown phase, as illustrated in Figure 5, the calculated hot-leg temperature in the active loops is overestimated by 2.0°C. On the other hand, as illustrated in Figure 6, the flow in the active loops is underestimated by about 10%, and overestimated by 20% in the inactive loops. This observation can be explained by the difference between the calculations and the measurements at the end of the conditioning phase. As can be seen in Figure 7, the heat sink in the experiment is almost lost, while it is not the case in the calculation results. This is more probably due to an underestimated calculated value of the secondary pressure. On the whole, at the beginning of the cooldown phase, the total primary flow agrees rather well with the experimental one.

Through the cooldown phase, the experimental and the calculated coolant temperature evolutions in loop-2 and loop-4 follow well the linear 50°C/h rate. This cooldown rate is obtained by controlling the atmospheric dump valve (ADV) opening on both steam lines, calculated as reported in Figure 8. The subsequent secondary pressure decreases are

Table 5: Main events for PKL2 G2.1 Run-3.

Time [s]	Measures/Events
0	Start of Run-3. Cooldown step-1 initiated: 50°C/h cooldown gradient by SG-2 and SG-4; temperature decrease by 20°C
90	PRZ heater switched off
1460	Cooldown step-1 finished
3270	Cooldown step-2 initiated: 50°C/h cooldown gradient by SG-2 and SG-4; temperature decrease by 30°C
5490	Cooldown step-2 finished
7750	Cooldown step-3 initiated: 50°C/h cooldown gradient by SG-2 and SG-4; temperature decrease by 40°C
14870	Cooldown step-3 finished
17520	End of Run-3

Table 6: Primary side steady-state results versus measurements for all runs.

Primary circuit	EXP.RUN-1	CALC.RUN-1	EXP.RUN-2	CALC.RUN-2	EXP.RUN-3	CALC.RUN-3
Pressure (bar)	40	40	40	40	40	40
Bundle power (kW)	642	642	642	642	642	642
Core outlet Temp (°C)	243	244.0	241.5	244.5	241.1	244.5
Cold leg Temp 1–3 (°C)	239–243	235	240. 0	237.5	213.0	237.5
Cold leg Temp 2–4 (°C)	215.	222.2	213. 0	215.1	213.0	215.1
Subcooling at core outlet (°C)	5	6	6	7	7	7
Loop 2–4 mass flow rate (kg/s)	1.35–1.45	1.3	1.41–1.38	1.38–1.39	1.4	1.38–1.39
Loop 1–3 mass flow rate (kg/s)	0.73–0.8	1.0	0.72–0.77	0.73–0.74	0.75	0.73–0.74
Pressurizer water level (m)	4.0	4.15	4.1	4.15	4.1	4.15

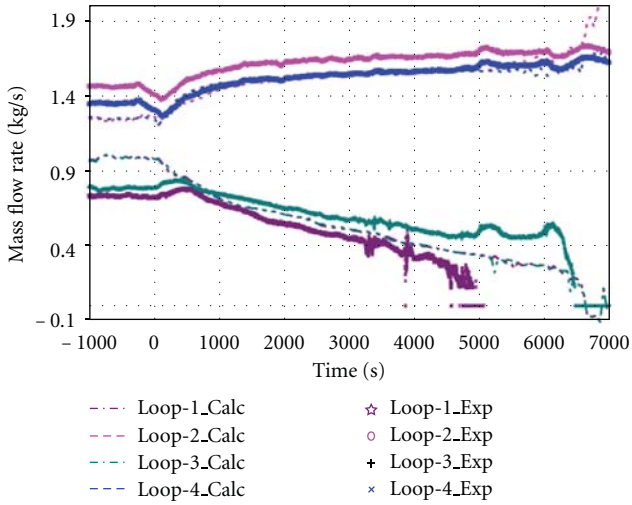

Figure 6: Run-1: Loops flow rate evolutions.

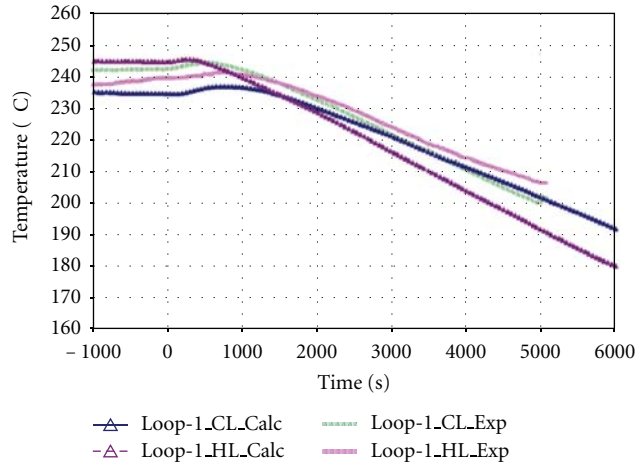

Figure 7: Run-1: Cold and hot leg temperature evolution in the active loops.

shown in Figure 9. The agreement between the calculations and the measurement is less good in this case.

In Figure 6, the flow rate evolutions in loop-2 and loop-4 agree well with the experimental trends but the agreement is less good in the inactive loops. In fact, differences exist between the measured flow rates in loop-1 and loop-3 and become more pronounced later on. Indeed, the flow interrupts first in loop-1, at around 5300 s, and later in loop-3 after 1500 s. This difference could be explained by the fact that loop-1 and loop-3 may have different pressure and heat losses. This is not the case in the CATHARE PKL model; the inactive loops are modelled identically and thus the calculated flow rates are the same, as well as the predicted flow interruption time occurrence (at about 7000 s). It should however be noted that the NCI in Run-1 is the consequence of steam formation in the U-tubes, due to continuous depressurization of the primary side.

According to the experimental and calculation results, the flow interruption process follows in some manner a chaotic trend. It does not start in the longest tube and end in the shortest one, as it could be expected. As can be seen in Figure 10(a), the flow for loop-1 is first interrupted in

Table 7: Secondary side steady-state results versus measurements for all runs.

Secondary circuit	EXP.RUN-1	CALC.RUN-1	EXP.RUN-2	CALC.RUN-2	EXP.RUN-3	CALC.RUN-3
Pressure SG-1 and SG-3 (bar)	24–24.7	24	31–32	32	31–32	32
Pressure SG-2 and SG-4 (bar)	21	21	20	21	20	21
Water level in SG-1 and SG-3 (m)	0	0	0	0	0	0
Water level in SG-2 and SG-4 (m)	12.1	12.1	12.1	12.1	12.1	12.1
Feedwater temperature (°C)	50	50	47	47	47	47

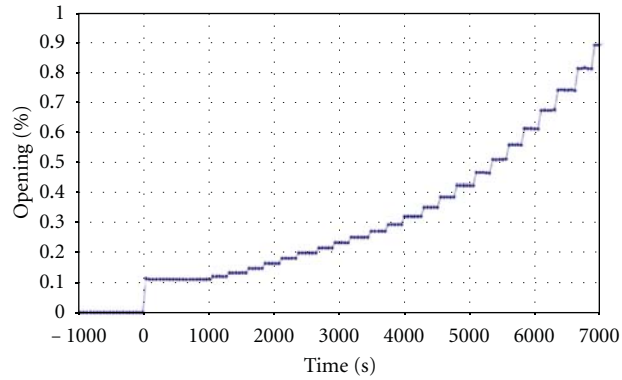

Figure 8: Run-1: Calculated atmospheric discharge valve opening evolution in the active SG.

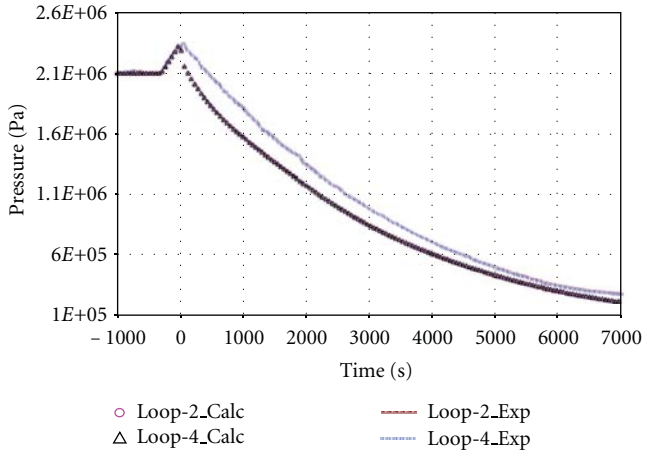

Figure 9: Run-1: Secondary side pressure evolution in the active loops.

the middle tube (Tube-19), then in the longest tube (Tube-29), and finally in the shortest tube (Tube-1). While for loop-3 (see Figure 10(b)), the flow stops first in the longest tube (Tube-29), then in the shortest tube (Tube-2) and later in the middle tube (Tube-19). This behaviour is obviously governed by the void growth, the temperature and flow redistribution in the U-tubes.

This trend is also observed in the CATHARE predictions (see Figure 11), where the flow is interrupted first in the middle length tube, then in the longest tube, and finally, in the shortest tube.

5.2. G2.1 Run-2. The second run is more or less identical to the first one, except for the fact that the primary pressure is kept high enough to preclude any void formation in the U-tubes. Unlike the case in Run-1, the NCI is the result of the driving force balance in the different loops of the tests facility. The test starts by the isolation of the secondary side of the active SG from the steam header. The cooldown via the corresponding ADV is activated immediately at the end of the conditioning phase; there is no heat-up period in this run.

At the beginning of the cooldown phase, as can be seen in Figure 12, the calculated hot leg temperature in the active loops is overpredicted by 2.0°C. This difference was already observed in Run-1 case. On the other hand, unlike the first run, the coolant flow in all loops is well predicted (see Figure 13); the final state of the conditioning phase of Run-2 is well simulated.

Throughout the cooldown phase, the calculated coolant temperatures (see Figure 12), the flow rate evolutions (see Figure 14), and the secondary pressure decrease (see Figure 13), in the active loop-2 and loop-4, match well the experimental trends. As it was the case for Run-1, the agreement is less good in the inactive loop-1 and loop-3. Indeed, there are differences between the measured flow rates in loop-1 and loop-3. This leads to a flow interruption in loop-1, and a flow restart in loop-3 at around 5500 s. This flow restart, as can be seen in Figure 12, is most probably due to the fact that at the end of the test (beyond 5000 s) the cooldown rate of 50°C/h can no longer be ensured. Its mean value, after 5000 s, is less than 25°C/h.

In the CATHARE model, the flow interrupts in both loops at the same time as a consequence of the driving forces balances in loop-1 and loop-3 and the driving force in the vessel. The code predicts an NCI time that corresponds with the experimental NCI observed in loop-1.

5.3. G2.1 Run-3. During the third run, a stepwise cooldown procedure is performed. As in Run-2, the primary pressure is kept high enough to preclude any void formation in the U-tubes. In the first step, the active loops temperature is decreased by 20°C following a linear cooldown rate of 50°C/h. After a stabilization period of 1800 s, the active loop temperature is reduced by 30°C according to a cooldown rate of 50°C/h. Then, after stabilization period of 2260 s, the third and last step is initiated. The temperature is decreased by 40°C during 7120 s instead of 2880 s. Indeed, during this step the cooldown rate of 50°C/h could not be reached at the end

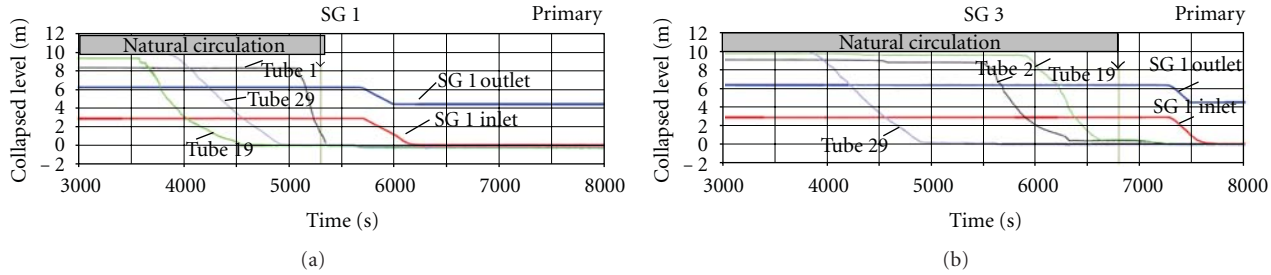

Figure 10: (a) Run-1: Measured collapsed levels in the U-tubes of the inactive loop-1. (b) Run-1: Measured collapsed levels in the U-tubes of the inactive loop-3.

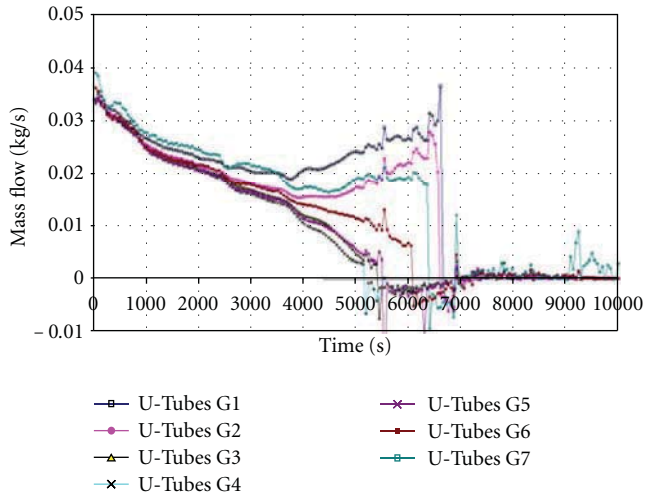

Figure 11: Run-1: Predicted mass flow rate evolution in the U-tubes of the inactive loops.

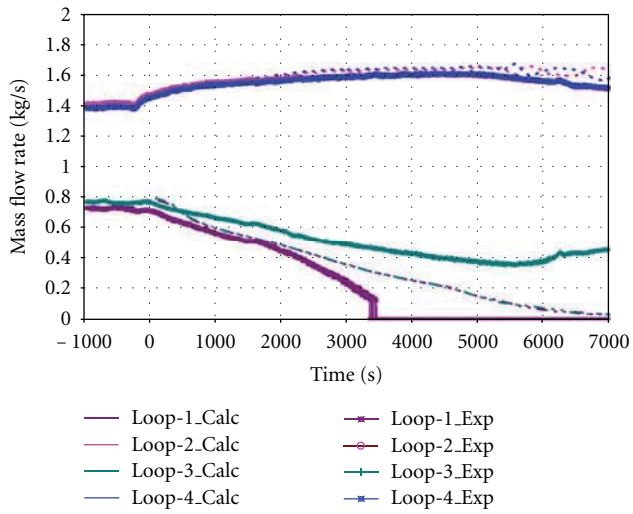

Figure 13: Run-2: Loops flow rate evolutions.

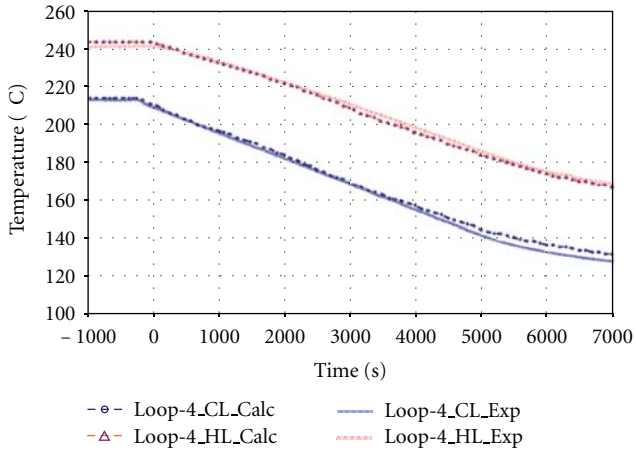

Figure 12: Run-2: Cold and hot leg temperature evolution in the active loops.

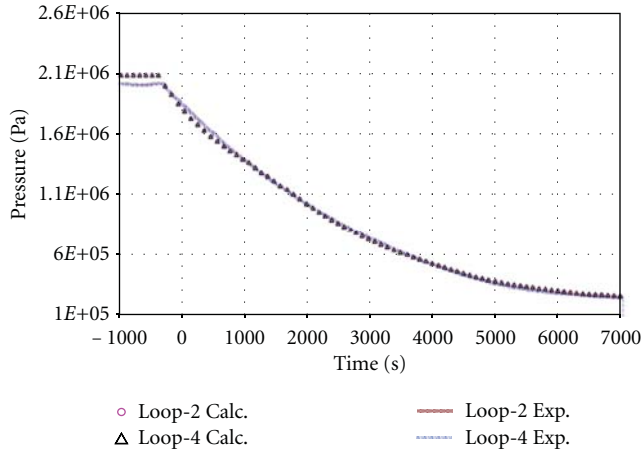

Figure 14: Run-2: Secondary side pressure evolution in the active loops.

of the test due to the fact that the secondary side pressure is almost at atmospheric levels.

As shown in Figure 15, the calculated cold and hot-leg temperatures in the active loops are well predicted. The coolant flow in all loops is also well predicted (see Figure 16). This trend is kept throughout the entire test time span. The secondary pressure decrease is also well predicted by the calculation (see Figure 17). As it is the case for the former runs, the agreement between the calculated and measured mass flow rate in the inactive loops is less good. This is mainly

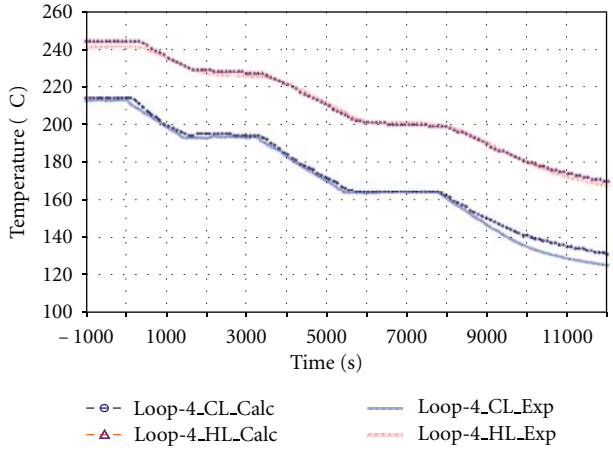

Figure 15: Run-3: Cold and hot leg temperature evolution in the active loops.

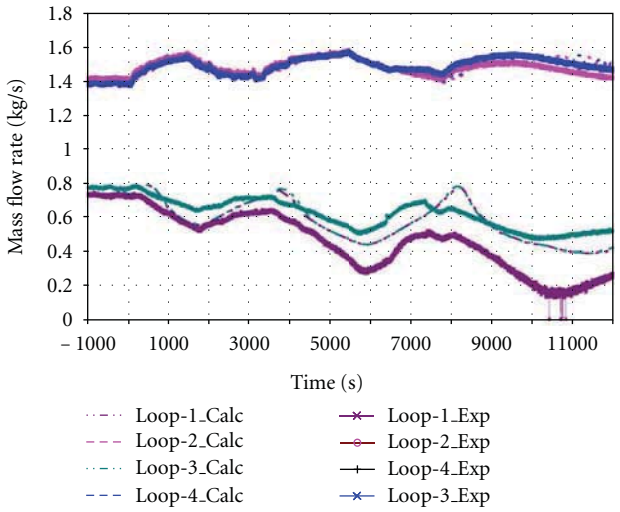

Figure 16: Run-3: Loops flow rate evolutions.

due to the differences in the measured flow rates that exist between loop-1 and loop-3. This difference is most probably due to geometric differences between loop-1 and loop-3, and also to some mixing effect in the upper part of the downcomer that are not modelled in the CATHARE model. However, the predicted values lie between the measured mass flow rates in loop-1 and loop-3.

Unlike Run-1 and Run-2, no flow interruption in the inactive loops is observed experimentally for Run-3. The flow rate in these loops decrease with decreasing temperatures of the active loops. In loop-1, the flow rate reaches 15% of its initial value during the third cooldown step. However, as already mentioned above, the cooldown rate of 50°C/h during the third step was not ensured; the mean cooldown rate during the last step is around 36°C/h. Therefore, if during this period the cooldown rate of 50°C/h would have been ensured, the flow rate in loop-1 would probably have been interrupted. Furthermore, if shorter periods

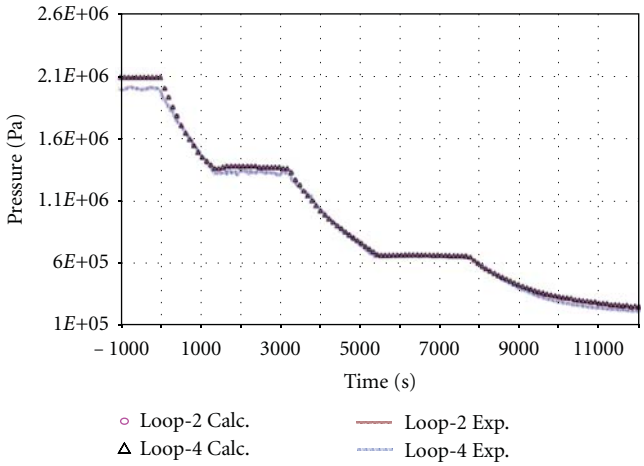

Figure 17: Run-3: Secondary side pressure evolution in the active loops.

between the temperatures decrease of the stepwise cooldown procedure were considered, NCI would also occur.

6. Conclusions

In the current study, asymmetric cooldown tests with empty and isolated SGs in the 4-loop PKL facility are investigated. The impacts of several cooldown strategies on the NCI occurrence are assessed experimentally and simulated numerically with the CATHARE code. According to the calculation results, it can be concluded that:

(i) NCI occurs when high linear value of the cooldown rate (i.e., 50°C/h) is performed. The NCI occurs in Run-1 and Run-2 due to steam formation in the apex of the U-tubes, and due to driving forces balance in the loops, respectively;

(ii) a stepwise cooldown procedure allows avoiding NCI, as far as the temperature steps are rigorously chosen in relation to the decay heat level and the time interval between successive cooldown steps;

(iii) the experiments show that slight configuration differences between inactive loops could have an important impact on the NCI occurrence;

(iv) the CATHARE computer code can accurately simulate the NCI phenomenon. However, deeper investigation and assessment of broader conditions could impact the NCI occurrence, as the power level, the cooldown rate and strategy, and the 3D mixing effect in the vessel downcomer.

Nomenclature

ΔP_f : Friction pressure drop (N/m^2)
ρ: Density of the fluid (kg/m^3)
G: Acceleration due to gravity (9.81 m/s^2)
z: Vertical coordinate (m).

Acronyms

ADV: Atmospheric discharge valve
NC(I): Natural circulation (interruption)
NPP: Nuclear power plant
PRZ: Pressurizer
PWR: Pressurized water reactor
RCS: Reactor coolant system
RHRS: Residual heat removal system
SG: Steam generator.

Acknowledgments

The authors would like to express their thanks to the entire PKL-2 group and more particularly to Dr. K. Umminger.

References

[1] J. Vlassenbroeck, A. B. Salah, and A. Bucalossi, "Assessment of natural circulation interruption during asymmetric cooldown transients," *Nuclear Technology*, vol. 172, no. 2, pp. 179–188, 2010.

[2] K. Umminger, W. Kastner, J. Liebert, and T. Mull, "Thermal hydraulics of PWRS with respect to boron dilution phenomena. Experimental results from the test facilities PKL and UPTF," *Nuclear Engineering and Design*, vol. 204, no. 1–3, pp. 191–203, 2001.

[3] http://www.oecd-nea.org/jointproj/pkl.html.

[4] K. D. Dubiel and R. M. Mandl, "Abfahren eines DWR ohne Hauptkühlmittelpumpen nach Dampferzeuger-Heizrohrbruch mit Erreichen der Notkühlkriterien," Private Communication, 1994.

[5] Equipe CATHARE, DRN/DTP/SMTH/LMDS, "CATHARE-2 V2.5_1/mod8.1 Dictionary," SMTH/LMDS/EM/2002_067, 2008.

[6] R. Guneysu and H. Kremin, "Description of the PKL Test Facility," NTCTP-G/2007/en/0010, 2007.

[7] S. P. Schollenberger and K. Umminger, "Determination of Pressure Losses in the PKL III test Facility for Mass Flows of 0.8 to 25.0 Kg/s per Loop," NTT1-G/2006/en/0066, 2006.

[8] S. P. Schollenberger and T. Mull, "Determination of Heat Losses in the PKL III Test Facility for Temperature Levels from 25 to 250°C," NTT1-G/2006/en/0067, 2006.

[9] R. Guneysu and H. Kremin, "Determination of Individual Volumes and of Total Volume in the PKL Test Facility," NTCTP-G/2007/en/0011, 2007.